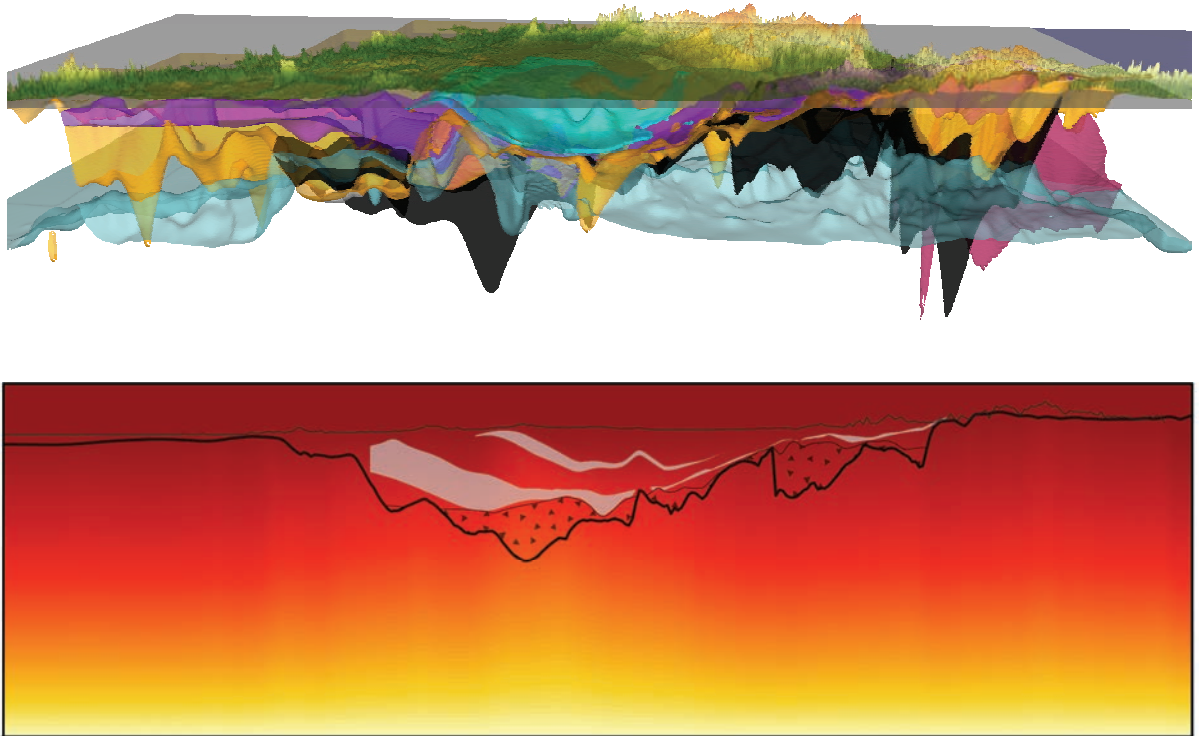


# THE THERMAL STRUCTURE OF THE SYDNEY GUNNEDAH BOWEN BASIN EASTERN AUSTRALIA



**Cara Danis**

Department of Earth and Planetary Sciences

Macquarie University



A thesis submitted to Macquarie University in the fulfilment of the requirements for  
the degree of Doctor of Philosophy

September, 2011

# TABLE OF CONTENTS

ABSTRACT	5
DECLARATION AND CERTIFICATION	6
PREAMBLE AND NOTES ON THESIS FORMAT	7
ACKNOWLEDGMENTS	11
<b>CHAPTER 1. INTRODUCTION</b>	<b>13</b>
1.1 Background on Geothermal in Australia	15
1.2 Research Aims	16
1.3 Research Approach and Outcomes	16
<b>CHAPTER 2. BACKGROUND MATERIAL</b>	<b>18</b>
2.1 The evolution of the east coast of Australia: Ordovician to Permian	19
2.1.1 The Lachlan Fold Belt	20
2.1.2 The New England Fold Belt	22
2.1.3 Thomson Fold Belt	24
2.1.4 Summary	24
2.2 The evolution of the east cost of Australia: Permian to Cretaceous	29
2.2.1 Tectonic Overview	30
2.2.2 The Sydney Basin – Stratigraphy and Structure	31
2.2.3 The Gunnedah Basin – Stratigraphy and Structure	35
2.2.4 The Bowen Basin – Stratigraphy and Structure	38
2.3 Geophysics	42
2.3.1 Gravity	42
2.3.2 Magnetics	44
2.3.3 Seismic Reflection Profiles	46
2.4 Geothermal Exploration in Australia and the Geothermal Potential of the Sydney-Gunnedah-Bowen Basin System	52
2.4.1 History and Development 1994 to 2008	53
2.4.2 Data gaps and problems in geothermal exploration	56
2.4.3 Geothermal potential of the Sydney-Gunnedah-Bowen Basin system	56
<b>CHAPERT 3. PREVIOUS WORK AND DATABASES</b>	<b>59</b>
3.1 Previous Work	60
3.2 Databases and Information	61
3.2.1 Boreholes	61
3.2.2 Interactive Resources	61
3.2.3 Pre-compiled Data Packages	62

<b>CHAPTER 4. METHODOLOGY</b>	<b>63</b>
4.1 Borehole Data	<b>64</b>
4.1.1 Coal Percentage Calculations	<b>65</b>
4.1.2 Temperature Measurement and Logging	<b>66</b>
4.2 Climate Correction	<b>69</b>
4.3 Temperature Extrapolation	<b>70</b>
4.4 Density Measurement	<b>71</b>
4.5 Gravity Measurement and Modelling	<b>74</b>
4.6 Surface Contouring and 3D Geological Model	<b>77</b>
4.7 Data Distribution and Analysis	<b>82</b>
4.8 Numerical Thermal Modelling in Underworld	<b>85</b>
4.8.1 Ellipsis	<b>85</b>
4.8.2 Underworld 2D	<b>87</b>
4.8.3 Underworld 3D	<b>88</b>
 <b>CHAPTER 5. SUBSURFACE STRUCTURE</b>	 <b>90</b>
Gunnedah Basin 3D architecture and upper crustal temperatures	<b>91</b>
Deep 3D structure of the Sydney Basin using gravity modelling	<b>114</b>
Building 3D geological knowledge through regional scale gravity modelling for the Bowen Basin	<b>140</b>
 <b>CHAPTER 6. 3D GEOLOGICAL MODEL</b>	 <b>158</b>
Sydney-Gunnedah-Bowen Basin deep 3D structure	<b>159</b>
 <b>CHAPTER 7. GEOTHERMAL ASSESSMENT TECHNIQUES</b>	 <b>169</b>
Geothermal state of the Sydney Basin: assessment of constraints and techniques	<b>170</b>
 <b>CHAPTER 8. IMPLICATIONS OF DISTURBANCE AND THERMAL RECOVERY FOR GEOTHERMAL MEASUREMENTS</b>	 <b>196</b>
The implication of fluid disturbance and thermal recovery on bottom-hole temperatures for the collection of equilibrated measurements and the need to understand borehole history: a case study on PZ14A, Ulan Coal Mine, NSW Australia.	<b>197</b>
 <b>CHAPTER 9. UNCERTAINTY IN 3D GEOTHERMAL MODELS</b>	 <b>205</b>
An assessment of subsurface temperatures and uncertainty in 3D geothermal models of the Sydney-Gunnedah basin system	<b>206</b>
 <b>CHAPTER 10. THERMAL STRUCTURE AND GEOTHERMAL POTENTIAL</b>	 <b>226</b>
10.1 Thermal Structure of the of the SGBB	<b>228</b>
10.2 Geothermal Potential	<b>240</b>
10.3 Summary	<b>246</b>

## **CHAPTER 11. CONCLUSIONS**

**247**

## **REFERENCES**

**251**

### **APPENDIX (Digital)**

- A. Equilibrated Temperature Measurements
- B. Ultimate Borehole Database
- C. Coal Percentage Intervals and Calculations
- D. Climate Correction
- E. Temperature Extrapolation Graphs
- F. Density Calculation
- G. Gravity Model Profiles and Model Vision Files
- H. Geological Model Layer Files
- I. dDAS Map
- J. Underworld 2D Thermal Models
- K. Ellipsis 2D Thermal Models
- L. Underworld 3D Surfaces
- M. Conference Abstracts and Non Peer Reviewed Articles



## **ABSTRACT**

The Earth's upper crust hosts many important economic resources and understanding its geometry and thermal structure is critical for resource development and management, and scientific research. In Australia subsurface structure is currently understood through deep seismic reflection surveys, gravity profiles and small scale integrated geological models and the subsurface thermal profile from extrapolated borehole temperature measurements and heat flow measurements. This style of approach has inherent limitations, including the inability to account for 3D effects on subsurface temperatures and heat flow.

The Sydney-Gunnedah-Bowen Basin (SGBB) system is the largest sedimentary basin on the east coast of Australia, and is host to many energy rich resources. Thermal structure is controlled principally by geology and basin architecture, which is characteristic of an extensional rift origin. Through integrated geophysical methods and a novel approach to 3D thermal modelling both the geometry and thermal structure of the upper crust of the SGBB is characterised. The ability to calibrate and constrain thermal models with real world observables is critical to understanding uncertainties and providing representative estimates of temperature. By constructing the thermal model on an upper crustal scale the thermal field is self consistent with detailed 3D geological structures and physical rock properties. This model is also scalable and able to focus on smaller, detailed areas.

The 3D geological and thermal model of the SGBB provides the first integrated framework from which to assess the thermal structure and build the next generation of detailed models for future research. By characterising the thermal structure new resource exploration in geothermal energy is possible, with the estimated temperature at depth over 150°C in most parts of the Sydney and Bowen basins.

## **DECLARATION**

This thesis is based on work carried out in the Department of Earth and Planetary Sciences at Macquarie University and in other institutions in collaboration with Macquarie University over the period between July 2008 and September 2011. I hereby declare that all data and interpretations presented in this study are my own work, except information from published and unpublished works of others that has been fully acknowledged.

## **CERTIFICATION**

I certify that this thesis has not been submitted for a higher degree to any other university or institution. I further certify that this thesis is an original piece of research and any assistance in the preparation of the thesis itself has been appropriately acknowledged.

Cara Danis

Submitted 27 September, 2011.

Accepted 8 August 2012

## **PREAMBLE AND NOTES ON THESIS FORMAT**

This thesis is presented in the form of “Thesis by Publication”, with Chapters 5 to 9 being papers which are either published or suitable for publication in peer-reviewed journals. The constant theme of thermal structure, basin architecture and geothermal potential is presented in the papers. The papers are formatted to the publication style of the journal submitted to or published in, and as such formatting and reference style may vary. Figures, tables and references for each individual paper are included within the relevant paper.

In all chapters, with the exception of those of published papers, the figures and tables included within are placed in-text and labelled so that Chapter 1 figures increase sequentially as follows: 1.1, 1.2, 1.3 etc, followed by Chapter 2 figures labelled 2.1, 2.2 etc and the same for tables. Figure and table numbers are in bold and the caption text is italicised to differentiate captions from main text. In chapters which are published papers, the figures and tables are included in-text and labelled according to the journal style.

Pagination begins with the Title Page and continues sequentially throughout the thesis. The introduction, which forms the first chapter, outlines the background of the thesis and presents the research aims. The introduction also outlines the study area and discusses the approach taken to address these aims.

### **Chapter 2: Background Material**

This chapter is devoted to the geological history of the Sydney-Gunnedah-Bowen Basin and relevant background information on the geophysics and geothermal potential of the basin system. This material is in parts detailed, and often summarised in many of the papers presented in this thesis, and is included as it forms the material consulted for the gravity modelling and construction of the geological model. The geological history is presented as an overview from the Ordovician to Early Cretaceous time with specific emphasis on the formation and composition history of the rocks which constitute the basement of the geological model and of the three sedimentary basins.

### **Chapters 3 and 4: Previous Work, Information Databases and Methodology**

The third chapter presents previous work relevant to techniques of this project, e.g. gravity modelling, and an overview of all the databases of where information has been gathered. The fourth chapter outlines the various different methodologies, most of which are covered in associated papers, but in different levels of detail depending on the journal requirements. This chapter is structured to characterize the overall project workflow.

### **Chapter 5: Subsurface Structure**

This chapter presents three papers on the subsurface structure of each basin in the Sydney-Gunnedah-Bowen Basin system. The first two papers, focusing on the Gunnedah and Sydney basins have been published in the Australian Journal of Earth Sciences. The third, on the Bowen Basin, has

been published in Exploration Geophysics. These papers focus on regional scale gravity modelling to determine depth to basement and basal volcanics with constraint from borehole records and seismic reflection profiles. The subsurface structure developed in this work feeds into the creation of a 3D geological model.

### **Chapter 6: 3D Geological Model**

The development of a detailed 3D geological model of the Sydney-Gunnedah-Bowen Basin system is the fundamental framework for research to understand the thermal structure. By combining data from the surfaces determined by gravity modelling, i.e. depth to basement and basal volcanics, with borehole data basic lithological layers are created. These lithological layers represent units with similar thermal properties which are incorporated into detailed thermal models. The 3D geological model builds confidence in the knowledge and understanding of the subsurface architecture of the Sydney-Gunnedah-Bowen Basin whilst also providing a framework of geological layers which have a wide variety of applications. This paper has been published in Exploration Geophysics.

### **Chapter 7: Geothermal Assessment Techniques**

This chapter presents a paper which has been published in the Australian Journal of Earth Sciences and discusses the limitations of temperature extrapolation and the impact this method has on geothermal exploration in the Sydney Basin. The past method of using temperature extrapolation to assess the thermal structure of the upper crust, and its geothermal potential, have inherent problems which are often not considered or understood. This paper comments on the extrapolation method and the quality of the data used and compares the estimates of temperature at depth with those of numerical thermal modelling. The paper also presents the collection of new equilibrated temperature data which is critical to the 3D thermal modelling of chapter nine.

### **Chapter 8: Implications of Disturbance and Thermal Recovery for Geothermal Measurements**

This chapter presents a short paper, prepared for submission to the Australian Journal of Earth Sciences, on the aquifer mixing, thermal recovery and implications for geothermal temperature measurements. The effect of fluid disturbance on a temperature measurement is often not considered during the collection of measurements for geothermal purposes. A three year study of a thermal recovery in a groundwater monitoring piezometer highlights the importance of understanding the history of a borehole in order to gather meaningful data.

### **Chapter 9: Uncertainty in 3D Geothermal Models**

The typical Monte Carlo style stochastic assessment, i.e. sampling of thousands of models, to understand uncertainty is not appropriate or practical for large scale models. This chapter presents a manuscript on how the uncertainty of large scale 3D geothermal models is assessed and the process by which parameters are optimised to 'best-fit' values. By using an incremental approach to evaluating model uncertainty unknown model parameters are tuned such that they match, as closely as possible, to real world observables. It focuses on the Sydney-Gunnedah Basin thermal model in Underworld and uses the equilibrated temperature measurements from chapter seven as the real world observables to optimise the thermal properties for each model material to 'best-fit' values. This

manuscript has been formatted to the style of the Australian Journal of Earth Sciences and will undergo stylistic and structural re-formatting for submission to an appropriate journal. These 'best-fit' values are applied to the high resolution 3D model of the complete Sydney-Gunnedah-Bowen Basin model, for an assessment of the thermal structure and geothermal potential in Chapter Ten.

## **Chapter 10: Thermal Structure and Geothermal Potential**

This chapter is a discussion of the thermal structure and geothermal potential of the Sydney-Gunnedah-Bowen Basin from the results of high resolution 3D thermal modelling in *Underworld* using 'best-fit' parameters.

## **Chapter 11: Conclusions**

This final chapter presents an overview of the five project research aims, a discussion on the main outcomes and limitations with concluding remarks.

## **Appendix**

There are thirteen separate appendix parts for this thesis representing databases, spreadsheets, conference abstracts and non-peer reviewed medial articles. These are presented in digital form and discussed below.

- A) Contains two spreadsheets: Equilibrated Measurements (Raw).xls which is all the raw temperature data from the equilibrated boreholes and Complete Equilibrated Measurements List.xls which is the climate corrected equilibrated temperature data.
- B) Contains the Ultimate Borehole Master Spreadsheet.xls which holds all the location, depth and reference information and stratigraphy for the boreholes used in this work.
- C) Contains two spreadsheets: Coal Percentage Intervals.xls which is the raw data from borehole logs for each basin and the thickness of stratigraphic units. Coal Percentages.xls is the calculation sheet for the coal percentages as described in Chapter 4.
- D) Contains the Climate Correction.xls spreadsheet which contains the calculations for each borehole temperature for both the equilibrated and non-equilibrated boreholes.
- E) Contains two spreadsheets: Equilibrated extrapolation graphs.xls and Non Equilibrated extrapolation graphs.xls. These contain the graphs used in Section 4.3 and Chapter 7.
- F) Contains the Density.xls spreadsheet of all the density calculations for each sample.
- G) Contains the Model Vision .ses files for each gravity profile, subdivided into the basins. A TIF image is also included of the profile.
- H) Contains two folders: Grid Surface Files which contains all the Surfer .grd files for the model layers and subfolders of the .csv files uploaded into Underworld and .xls files showing dual coordinates of Latitude/Longitude and MGA for the points. The Grid Surface Spreadsheets folder contains the raw data used to grid each Surfer grid surface file.
- I) Contains the code information file CRAPMap.sln, the input file alllines.csv source file main.cpp and the CRAPMap.vcproj file used in making the dDAS map.
- J) Contains the *Ellipsis* thermal model input files .in and results .dat for the Gunnedah Basin.

- K) Contains the *Underworld* 2D thermal model information in two sub folders, Input Files which is the .xml files for each profile in the Sydney Basin, and Output Files which are in subfolders for each line and contain a profile image .jpg and the output data.
- L) Contains the .csv files for each surface in the Sydney Gunnedah Bowen Basin model for input into *Underworld* 3D and a subfolder of the dual coordinates of Latitude/Longitude and MGA for the points.
- M) Contains published conference abstracts and extended abstracts for the Australian Society of Exploration Geophysics (ASEG) and Australian Geothermal Energy Conference (AGEC) and two non peer reviewed publications in Namoi Energy.

### **Contributions to Works**

My contributions to the papers presented in this thesis are as follows:

- In Chapter 5, paper one I was responsible 100% for the modelling of the gravity data, 100% in the measurement of density values, 95% in the fieldwork collection of rock samples (5% fulfilled by colleagues), 95% of the thermal modelling (5% was undertaken by supervisor) and 80% of the preparation of the manuscript and figures for publication with the remaining 20% fulfilled by supervisors.
- In Chapter 5, paper two I was responsible for 100% of the modelling of the gravity data, 100% in the measurement of density, 95% in the collection of rock cores from the Core Library (5% assistance from the core library technician with the extraction of samples), 95% of the thermal modelling (5% fulfilled by supervisor), 50% in the CRAP map work (50% fulfilled by co-author A. Danis), 60% in the preparation and editing of the 3D geological model and surfaces (40% fulfilled by co-author L. Twigg) and 90% in the preparation of the manuscript and figures for publication (the remaining 10% fulfilled by supervisors and co-authors).
- In Chapter 5, paper three I was responsible 100% for the modelling of the gravity data and 95% in the preparation of the manuscript and figures for publication with the remaining 5% fulfilled by supervisors.
- In Chapter 6 I am the sole author and responsible for 100% of the 3D geological compilation and preparation of the manuscript and figures for publication.
- In Chapter 7 I was responsible for 80% of the fieldwork collection of down-hole temperature data (10% fulfilled by field assistants and 10% fulfilled from co-author J. Lee), 100% in the temperature extrapolation and thermal models and 95% in the preparation of the manuscript and figures for publication (5% fulfilled by supervisor).
- In Chapter 8 I am the sole author and responsible for 95% of the collection of field temperature measurements (5% fulfilled by field assistants), and 100% responsible in the preparation of the manuscript and figures for publication.
- In Chapter 9 I was responsible 100% for the construction of the geological surfaces for the model, 20% responsible for the thermal modelling process (20% fulfilled by co-author J. Mansour and 60% fulfilled by co-author S. Quenette) and 40% responsible for the preparation of the manuscript and figures for publication with the remaining 60% fulfilled by co-authors.

As primary author on all papers I am responsible for the geological model used and, in addition to consultation with co-authors, am ultimately responsible for the data interpretation.

## ACKNOWLEDGEMENTS

I would like to acknowledge the contributions of the following people, and organisations, who provided guidance, encouragement, time and finance throughout the duration of this research:

- First and foremost I am indebted to the support and advisement of my supervisors, Craig O'Neill and Mark Lackie. Both have been consistently available and their support, expert advice, guidance and patience over the course of my studies have been invaluable. I am incredibly grateful for their support and encouragement during some very tough times. They have graciously reviewed my research and provided much valued and constructive feedback leaving the quality of my work greatly improved.
- Secondly I would like to thank my co-authors and colleagues, Luke Twigg, Steve Quenette, Adrian Danis, John Mansour, Louis Moresi, Owen Kaluza, Ben Mather and Adam Beall who have assisted in many ways and done fantastic work. To Luke, who tirelessly helped with creating and editing the 3D model surfaces of the Sydney-Gunnedah basin in AutoCAD and 3D StudioMax. His contribution saved many months of often tedious editing. To Steve, from eResearch at Monash, although this isn't your area of expertise your assistance and ability to apply Underworld to this problem has been invaluable. You solved many little program issues, worked tirelessly to get the models up and running and came up with many great ideas. Also without the help of John, Owen, Ben and Adam from Monash Uni and the AuScope simulation and modelling project this seriously large scale model would not have been completed. To Owen, thank you for extracting data and making fantastic images. Credit must also go to Louis Moresi who developed Underworld and without this program the ability study thermal structure at such a large scale with highly representative models would be difficult.
- I must thank Steve Quenette and Owen Kaluza especially for going above and beyond in the last few weeks of this thesis to get the final data ready for me. I am very grateful for the late nights and significant amount of effort you have contributed.
- Thirdly I must acknowledge the many field hands I had who helped me in all weather to collect data from many interesting and beautiful places. My thanks to Katrina Fyfe, Maureen Danis and Greg Jacques who I dragged to many a place to take a temperature measurement on the promise of coffee. To Greg Russell (NSW Office of Water), Tony Paull (Sydney Catchment Authority) and Cheryl Henriques (Ulan Coal Mines) who helped out and allowed me access to boreholes. To my work colleagues Dot Sheehan (ALS Environmental), Ben Rotter (Coffey Geotechnics) and Corinna De Castro (Coffey Geotechnics) who spent extra time during the 'Coffey' work jobs to help me collect extra temperature measurements.
- I must also acknowledge the following companies who allowed me access to their sites for data collection; Ulan Coal Mines Ltd, Sydney Catchment Authority, NSW Office of Water and Barton Golf Driving Range. I also must thank Coffey Geotechnics for allowing me to use their equipment and granting client access.
- Special thanks to John Lee from Hydroilex Pty Ltd for providing me with over 10 years worth of drilling and temperature information in the Sydney Basin.
- I want to thank my fellow colleagues and all the staff in the Department of Earth and Planetary Sciences for their support, feedback and assistance over the course of my studies. To my

fellow students, Ellen, Sarge, Raj, Elyse, Mel and Kath, thanks for all the encouragement, coffees and good times. Best wishes in your projects.

- I also acknowledge that I was the recipient of an Australian Postgraduate Award for my time as a postgraduate student and this funding was gratefully received.
- I have been supported and encouraged unwaveringly by my parents during the course of my candidature. I am overwhelmingly indebted to their support over the last few years and especially for all of my time studying. To my family and friends, who I often saw very little of, thank you for your patience, support, encouragement and understanding during this period. To my wonderful soon to be husband Greg you have offered amazing support, help in the field, patience and love.

Over the course of my 3.5 years as a PhD student I have enjoyed the challenges that research brings and I have learnt that it is not something that can, or should, be done alone. The friends I have made and the experiences I have gained I will long remember. My goal has always been to do something that would be of benefit to humanity and be true to the science and I feel I have achieved this goal with this project. May my work bring all glory and honour to the Lord My God.

*The important thing is to not stop questioning.*

Einstein



# CHAPTER 1

## INTRODUCTION



*Jamison Valley, Wentworth Falls NSW*

## INTRODUCTION

The Earth's upper crust hosts many important economic resources, from minerals and groundwater, to energy, but the subsurface structure is generally poorly understood. Around the world, the resources of the upper crust are experiencing rapid rates of development as demand increases. This has led to the need for an integrated framework from which to maximise resource return, as well as monitor potential interplays, e.g. between groundwater and resources development, by understanding the subsurface structure in three dimensions (3D), the geological processes giving rise to this structure, and thermal nature of the upper crust. Heat from the interior of the Earth is the major driving force behind plate tectonics and therefore is ultimately responsible for the subsurface and surface structure of the Earth.

The development of multiple resources in Australia's energy rich sedimentary basins i.e. minerals, energy (coal, coal seam gas, natural gas, geothermal), groundwater and carbon sequestration has highlighted the lack of subsurface information, especially in the vast Sydney-Gunnedah-Bowen Basin (SGBB) (Figure 1.1). In this basin system the understanding of the architecture and thermal structure has primarily been confined to the extrapolation of borehole temperature measurements, and localised 3D structural models or continental scale crustal estimates of temperature at depth and heat flow.

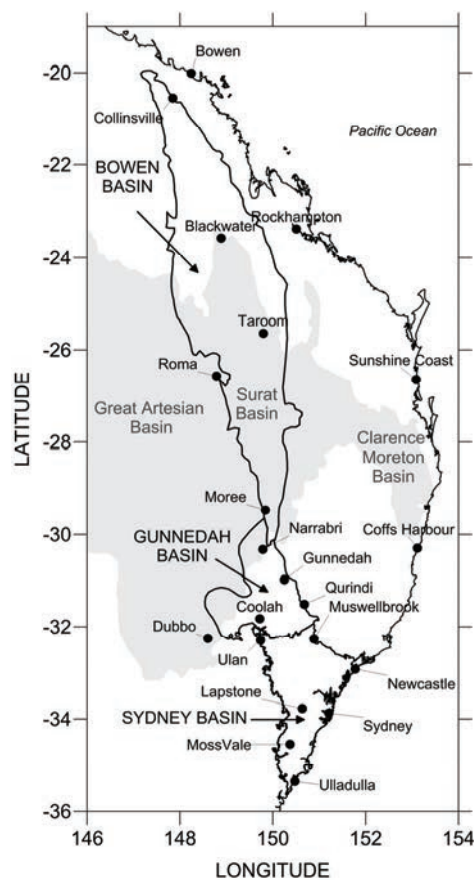


**Figure 1.1** The east coast of Australia and the extent of the Sydney-Gunnedah-Bowen Basin. Outline of the Great Artesian Basin, Surat Basin and Clarence Moreton Basin modified from Krassay et al. (2009).

An enhanced understanding of the thermal structure of the SGBB does not only substantially benefit the development of geothermal resources; it also offers additional information to explain the occurrence of other important mineral deposits. Heat flow and tectonic setting play a vital role in the occurrence of mineral deposits, petroleum accumulations, the formation of metallogenic provinces and geothermal anomalies.

The aim of this research is to examine the thermal structure of the Sydney-Gunnedah-Bowen Basin system through an integrated approach of modelling and calibration with measured temperature data. To achieve the primary aim of this research requires a 3D geological model on a scale of 10 to 1000s of times larger than the most detailed resource models available. The development of a self consistent geological model, suitable for incorporation into thermal models, will function as the framework from which to build the next generation of detailed thermal models for future research. Small scale integrated geological models are available for parts of the system, i.e. Sydney Basin OzSEEBASE™ model (FrOG Tech 2006) but these have defined scopes, lack transparency and are for commercial purposes.

### **1.1 Background on Geothermal in Australia**

Around the world the exploitation of geothermal fluids for energy has long been established in the conventional systems associated with waters heated by volcanic magmas. In Australia early geothermal exploitation used hydrothermal systems (shallow hot aquifers) for spas and water-source heat pumps for air conditioning buildings. With conventional geothermal resources absent, Australia turned to more unusual geothermal deposits which are associated with hot dry crystalline rocks and hot sedimentary aquifers buried at depth under thick insulating sedimentary cover.

Renewed investigation of sustainable renewable energy sources, like geothermal, as part of the Australia Federal Government's Energy Initiative Program, resulted in the re-examination of geothermal potential in sedimentary basins, including the vast 1600 km long SGBB. Australia's vast hydrothermal and hot rock energy resources have the potential to become a significant source of safe, secure and competitively priced emission free renewable power (Goldstein *et al.* 2008). Early work in the 1990's by government led collaborations resulted in the first quantitative assessment of Australia's geothermal potential. Huge potential geothermal resource areas were identified in central Australia, the north-eastern part of South Australia and the south-western part of Queensland. Early estimates of the geothermal resource base suggested 22 million petajoules of stored heat energy. Even a small percentage of that heat energy could supply Australia's energy demands for many years.

Although there are many technological and engineering challenges to overcome in the development of geothermal power in Australia, an objective of this research is to improve the resources available for locating prospective geothermal areas.

## 1.2 Research Aims

The research aims of this project are:

- 1) To create a detailed 3D geological model, based on distinctive density and thermal properties, of the Sydney-Gunnedah-Bowen Basin system, with specific emphasis on depth to basement, sediment thickness and thermally insulating layers such as coal, for use in the *Underworld* platform.
- 2) Assess the limitations of extrapolated temperature maps as a sole geothermal resource exploration tool.
- 3) Collect equilibrated down-hole temperature measurements to calibrate the *Underworld* thermal models.
- 4) Through the specialist geodynamic modelling framework of *Underworld* develop a high resolution 3D thermal model to assess thermal structure of the Sydney-Gunnedah-Bowen Basin.
- 5) To create an estimated temperature at 5 km depth below the surface map, from the 3D thermal model, for the Sydney-Gunnedah-Bowen Basin as a geothermal exploration tool.

## 1.3 Research Approach and Outcomes

This thesis aims to develop a detailed 3D geological model from which to undertake numerical thermal modelling to assess the thermal structure, and subsequently the geothermal potential, of the SGBB. The detailed geological model is developed from integrated gravity modelling and structural depth information, i.e. borehole records and seismic reflection profiles, as surfaces for depth to basement and key lithological boundaries. Regional scale gravity modelling, of the Bouguer gravity anomaly, is the primary tool for understanding the deep crustal structure of the SGBB as borehole records and seismic data allow tight constraints of depth and many architectural features. With a consistent density contrast between the basin sediments and older basement modelling of representative packages of lithologies, i.e. sediment, volcanics and basement which have different but measureable densities, achieves a model of the entire SGBB system. In essence, the model consists of basement, defined as the pre extensional rifting phase Palaeozoic rocks, a basin sedimentary package containing Permian to Triassic (and in some places Jurassic) sediments and coal bearing layers between which is basal rift related volcanics. These representative lithology packages also have distinctive thermal properties allowing easy application of the 3D geological model into the thermal model.

The geodynamic modelling code *Underworld* offers a platform to integrate the detailed 3D geology with thermal properties on an upper crustal scale. By constructing a model at this scale the thermal field is self consistent with the geological structures and physical rock properties. To determine model parameters, i.e. material thermal properties and subsurface temperature boundaries, published averages are utilised with measured temperature data to optimise these parameters to the 'best-fit'. Current measured temperature at depth information cannot be used in the thermal models because it includes data from non-equilibrated boreholes. Part of this research is the collection of new equilibrated temperature at depth measurements. With a thermal model that correlates with 'real world observables', estimates of uncertainty and confidence in the model

parameters are possible, which ensures representative estimates of the thermal structure of the SGBB.

With representative estimates of temperature at depth the geothermal potential of the SGBB system can be assessed based on the key industry indicator; the 150°C temperature contour. An assessment of the depth of this contour and the maximum temperatures reached at 5 km depth below ground surface, the limit of economic drilling, will highlight potential geothermal anomalies and areas for further exploration.

The outcomes of this research are in two areas. Firstly the development of a detailed 3D geological model of the upper crustal structure of the SGBB provides not only the framework required for the thermal modelling of this project, it can also provide a framework for many other research applications and a resource management tool. Secondly an understanding of the thermal structure of the resource rich SGBB provides important new insight into the occurrence of resource deposits as well as a new exploration tool for the emerging geothermal industry.



# CHAPTER 2

## BACKGROUND MATERIAL



*Empress Falls, Wentworth Falls NSW*

## **BACKGROUND MATERIAL**

There is a vast amount of information published on the Sydney-Gunnedah-Bowen Basin system and although this review aims to be comprehensive it is by no means exhaustive. The background material relevant for the research undertaken in this project is separated into four main sections. The first section looks at the evolution of the east coast of Australia from the Ordovician to the Early Cretaceous time, specifically the material which forms the substrate of the basin system, with a summary collated in Table 2.1. This section describes the evolution of the Tasmanides (i.e. Lachlan Fold Belt, New England Fold Belt and Thomson Fold Belt) which form the substrate to the SGBB in terms of tectonic cycles to encompass the depositional/magmatic as well as contractional and deformation histories of rock packages from the work of Glen (2005). Collision is used to reflect accretion on to an arc to the developing Gondwana landmass, not continent to continent collision. The second section looks at the inception of the basins of the SGBB system with regards to tectonic cycles, geology and structure. The third section reviews the available geophysical databases, with a brief assessment, of gravity, magnetic and seismic reflection data in the SGBB. The final section provides a brief history of the development of geothermal energy and exploration in Australia from 1994 to 2008; with an assessment of data gaps and problems in geothermal exploration and a review of the assessment of the geothermal potential of the SGBB system.

### **2.1. The evolution of the east coast of Australia: Ordovician to Permian**

The Tasmanides is the name given to a collection of orogenic belts along the eastern part of Australia (Figure 2.1) which records: the break-up of the Meso-proterozoic supercontinent, the formation of a passive margin, the establishment of convergent margin orogenic belts (from the Middle Cambrian), the collision of Gondwana with Laurussia to form Pangaea (320 to 330 Ma) (Veevers 2000) and the beginning of the Gondwana Pangaea break-up (227 Ma) (Glen 2005). They comprise five major orogenic belts, the Delamerian, Lachlan, Thomson, New England and North Queensland with the internal rift-foreland basin of the Sydney-Gunnedah-Bowen Basin. The Tasmanides of eastern Australia represent one sector of the Pacific margin of Gondwana that stretched 20,000 km through New Zealand, Antarctica and into South America (Glen 2005). The history reflects extension or rifting in a convergent margin setting along the proto-Pacific plate. The phases of extension and rifting are separated by deformation events that occupy short intervals (Glen 2005).

Three orogenic belts; the Lachlan, New England and Thomson have been identified as the substrate and sediment source to the Sydney-Gunnedah-Bowen Basin system. Their development and tectonic evolution, from the Ordovician to Early Permian, provides valuable background information on lithologic composition and geological structure. The key deformation events; the Delamerian Cycle, Lachlan Super Cycle and Hunter-Bowen Super Cycle, which are comprehensively described in the work of Scheibner & Veevers (2000), Veevers (2000) and Glen (2005), are summarized below for the three orogenic belts. Refer to Table 2.1, at the end of the section, for a comparative simplified evolution history.

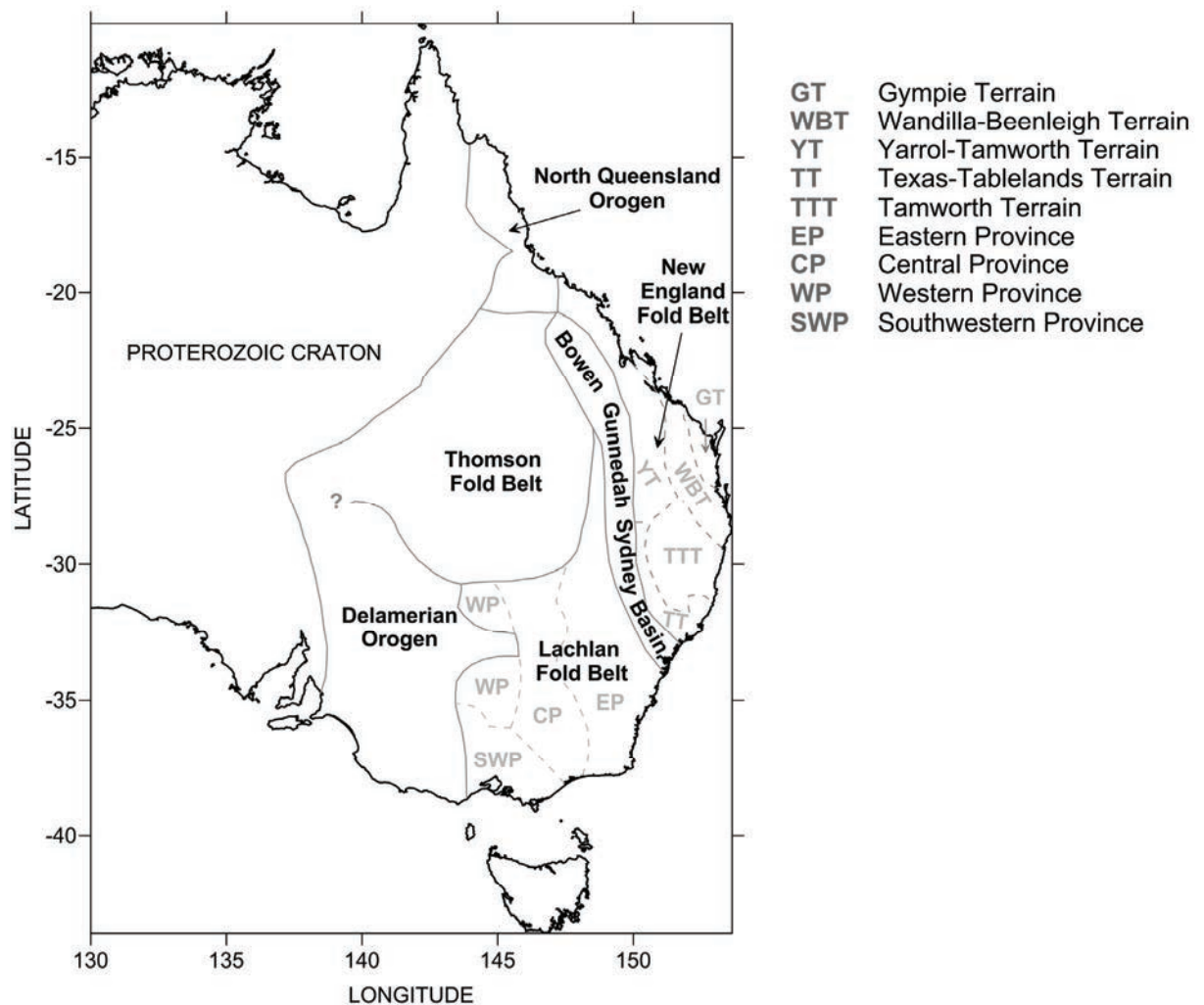


**Figure 2.1** Subdivision of the Tasmanides. Adapted from Leitch (1974) Scheibner & Veevers (2000) and Glen (2005).

### 2.1.1 The Lachlan Fold Belt

The Lachlan Fold Belt (LFB), also known as the Lachlan Orogen, extends northwards from eastern Tasmania through Victoria and New South Wales into the central west of Queensland. In north-western NSW and in Queensland the LFB is covered by the extensive Jurassic-Cretaceous Great Artesian Basin (Figure 1.1). The LFB is comprised of predominantly early Ordovician through to Late Carboniferous rocks which record the three major deformation events (Branagan & Packham 2000) of the Lachlan Supercycle (Glen 2005) and parts of the earlier Delamerian Cycle (Table 2.1). The Lachlan Super Cycle is comprised of three events; the Benambran Cycle (Ordovician-Silurian boundary), Tabberabberan Cycle (late Early to Middle Devonian boundary) and Kanimblan Cycle (in the Early Carboniferous) with the events observed also in the North Queensland Orogen and New England Orogen (Benambran and Tabberabberan only) (Glen 2005).

The LFB is subdivided into four main provinces (Figure 2.1) based on major faults and differences in geology. Glen (2005) identifies that there have been a variety of possibilities put forward for the substrate of the LFB; continental (e.g. Rutland 1976; Chappell & White 1974), oceanic (e.g. Crook 1980), mixed oceanic and continental (e.g. Scheibner 1973) and oceanic in Victoria with subsequent



major under thrusting of continental material (e.g. Crawford *et al.* 1984). In the Southwestern and Central provinces the conformable relationships between Cambrian volcanic and sedimentary rocks and the overlying Ordovician turbidites are used to infer that the turbidites were deposited on oceanic igneous substrate (Crawford *et al.* 1984; Gray & Willman 1991).

The palaeogeography of the Ordovician, particularly in NSW, is interpreted as a series of volcanic islands, thought to be part of an island arc, surrounded by oceanic crust formed at the time of rifting of the old continent margin (Branagan & Packham 2000). The orogenic processes, which began in the Ordovician, progressively thickened the crust from a deep oceanic environment where turbidities were deposited, through the middle Silurian to Early Devonian where magmatism and granitoid emplacement was widespread, to a continental environment with broad fluvial plains and a shallow sea by the Late Devonian.

Convergence in the Delamerian Cycle is only represented by small areas of Cambrian mafic and ultramafic rocks in the Southwestern subprovince (Glen 2005). In the Benambran Cycle, the first event of the Lachlan Super Cycle (Table 2.1), the convergent phase, resulted in the deposition of quartz-rich, craton derived turbidites, basalts with a MORB-like tholeiitic chemistry and cherts. The subsequent compression phase firstly deformed the Ordovician turbidites by folding, thrusting and faulting in response to east-west and north-south shortening and then extension produced basin and platform areas where shallow-water limestone, shale, sandstone and volcanics and deep-water turbidites were deposited.

In the second event of the Lachlan Super Cycle, the Tabberabberan Cycle is characterized by major basin formation and emplacement of granitoids during rifting (Glen, 2005) (Table 2.1). Granites are prevalent in the Eastern and Central subprovinces of the LFB and occupy up to 36 % of the surface area (Chappell *et al.* 1988). I-type granites occur in the east and a mixed component of I-type and S-type granites occur in the west. Some granites were emplaced into the extending upper crust, where they are co-magmatic with and overlain by Late Silurian and Early Devonian felsic volcanics erupted from extensional basins (Wyborn & Chappell 1986) whilst others were emplaced into the mid crust and exhumed by thrusting (Glen 2005). Based on the geochemistry of the granites Chappell & White (1974) considered the boundary where the I-type granites changed to S-type reflected the eastern limit of thin Proterozoic continental crust containing continental sediments underneath the LFB. Alternative models have been used to explain the origin of the granite types, i.e. mixing basaltic magma and Ordovician sediments (Collins 1998), a mafic substrate underlying the Ordovician turbidites (Keay *et al.* 1997; Collins 1998) or tonalites (Chappell & Stephens 1988; Williams & Chappell 1998). The major basin formation in the late Early-Middle Devonian (Table 2.1) reflects localized strike slip tectonics, though there are differing views as to whether these deformations were part of a longer-lived deformation prograding from the west (i.e. Gray & Foster 1997; Gray *et al.* 1997) or related to oblique strike-slip collision (Glen 2005). Silurian-Devonian granites reflect Middle Devonian deformation with N-S elongate shapes, solid state foliations, S-C fabrics and mylonite zones (Glen 2005). The last stage of the Tabberabberan Cycle is marked by brittle conjugate NE- and NW- trending faults and east-west shortening.

The Kanimblan Cycle (Table 2.1), the last in the Lachlan Super Cycle, contains a brief rifting and loading phase, which produced A-type volcanics and granites and rift related sediments and a deformation phase of east-west shortening (Glen 2005) during the Carboniferous. A post collisional phase followed with granite emplacement (Pogson & Watkins, 1998), such as in the north-eastern part of the LFB with the Bathurst and Gulgong Granites, generated by the melting of underlying Ordovician volcanic rocks (Watkins 1998).

### **2.1.2 The New England Fold Belt**

The most easterly component of the Tasmanides is the New England Fold Belt (NEFB), also known as the New England Orogen, which occupies much of coastal Queensland, and extends south into north-eastern NSW underneath the Mesozoic cover of the Clarence-Moreton and Surat basins (Figure 1.1). The NEFB forms the basement to the eastern part of the Sydney Basin (Glen, 2005) and extends offshore as the Currarong Orogen (Jones & McDonnell 1981; Jones *et al.* 1984) or 'offshore uplift' (Bradley 1993; Alder *et al.* 1998) as represented in seismic data (see Figure 2.2). The NEFB has an inferred thrust contact with the Eastern subprovince of the LFB (Glen 2005).

The NEFB is divided into several structural subprovinces by Leitch (1974) and terrains by Scheibner & Veevers (2000) which have been combined in Figure 2.1. The southern province contains the Texas and Tablelands Terrain and Tamworth Terrain. The northern province consists of an external fold-thrust belt, the Yarrol – Tamworth Terrain, with intrusive granites in the north and an internal part with accretionary complex rocks that are deformed, metamorphosed and intruded by granitoids (Glen 2005), the Texas-Tablelands, Wandilla-Beenleigh and Gympie Terrains. The subdivision reflects the development of a Late Devonian-Carboniferous convergent margin (Hunter Bowen Supercycle 1, Table 2.1) consisting of arc, forearc basin and accreted terranes (Glen 2005).

The substrate to the NEFB has been inferred by Glen (2005) to be oceanic, east of the Peel-Manning and Yarrol Fault Systems (i.e. the Texas-Tablelands, Wandilla-Beenleigh and Gympie Terrains) and mixed oceanic and continental to the west (i.e. the Yarrol-Tamworth Terrains). However there is evidence, from fault-bounded outcrops of Neoproterozoic – Devonian material, which points to the presence of older substrate indicating the persistence of old lithosphere (Glen 2005).

The rocks of the NEFB record the major deformation events of the Delamerian and the four part Hunter-Bowen Supercycle (Table 2.1). In the Delamerian Cycle (530 Ma) the rift phase is represented by an ophiolite, with a depleted MORB-like signature that suggests formation as oceanic crust at a Neoproterozoic ocean ridge (Bruce *et al.* 2000), and indicates the existence of a proto-Pacific Ocean east of the Delamerian Orogen after supercontinent break-up (Glen 2005). Convergence, the second part of the Delamerian Cycle, is represented by the exhumation of eclogite blocks in the serpentinite – lubricated Peel-Manning Fault and indicate Cambrian subduction (Glen 2005).

The Hunter-Bowen Super Cycle, divided into four cycles, records the Middle Devonian to Triassic (376 to 227 Ma) convergent margin development of East Gondwana which is expressed in the evolution of the NEFB and the SGBB system. The elements of this classic margin have been studied by numerous

authors including Leitch (1974), Day *et al.* (1978), Cawood (1982), Cawood & Leitch (1985), Aitchison & Flood (1992) and Cawood *et al.* (2011) and are from west to east, an arc, a forearc basin and subduction complexes together with accreted terrains. The four cycles of the Hunter-Bowen Super Cycle are briefly described below from Glen (2005).

Cycle 1, in the Late Devonian, is characterised by an east facing continental or intra-oceanic arc dominated by intermediate volcanism, a forearc basin along the Yarrol-Tamworth trough bounded by the Yarrol and Peel-Manning Fault system, and subduction complexes with accreted terrains. The Late Devonian strata consists of volcanoclastic sandstone and conglomerates derived from the andesitic arc of the west, interbedded with sediments, some limestone and the presence of minor andesitic lavas, dacites and rhyolitic ignimbrites.

Cycle 2, in the Carboniferous, is characterised by an east-facing Andean-type arc dominated by felsic ignimbrites and granites. In the northern NEFB, the Carboniferous continental margin is represented by the granitic and mafic to silicic rocks noted by Day *et al.* (1978) of the Connors and Auburn arches. The major pulses of granite formation on these arches occurred between 324 Ma and 305 Ma (Glen 2005) prior to uplift. In the southern NEFB an approximately 400 km belt of NW-trending Carboniferous volcanic rocks represent the outboard parts of the continental margin that was developed on the crust of the LFB (Glen 2005). There is major segmentation of the Tamworth trough by cross-cutting faults as a result of the forearc basin development. The cessation of subduction in the southern NEFB is followed by major deformation, around 311 to 300 Ma (Glen 2005), which resulted in uplift and the emplacement of granite suites e.g. Hillgrove (Dirks *et al.* 1992; Cawood *et al.* 2011) and Bundarra (Flood & Shaw, 1977; Cawood *et al.* 2011) (Table 2.1). The Carboniferous and Devonian rocks of the northern part of the Tamworth trough were deformed into a west-vergent foreland fold thrust belt (Glen 2005) (i.e. Tamworth Terrain).

Cycle 3, in the Early Permian, is characterised by crustal extension associated with the inception of the SGBB. In the northern NEFB Granites were intruded into the Carboniferous accreted terrains during regional extension that led to generation of major low-angle normal faults. In the southern NEFB, uplift occurred in metamorphic complexes (e.g. Dirks *et al.* 1997) and emplacement of serpentinite along the Peel-Manning Fault (Leitch 1969). The Early Permian SGBB rift basin and other smaller rift basins, developed above the deformed rocks of the forearc basins, the accretionary complexes and on top of the rocks of older basement of the Lachlan, Thomson and North Queensland fold belts (Glen 2005).

Cycle 4, the Permian to Triassic, is characterised by arc magmatism and the foreland basin stage of development in the SGBB. Renewed convergence in the late Early Permian to Triassic was accompanied by the extrusion of ignimbrites and the emplacement of major I-type granites (Table 2.1) of the New England Batholith (Glen 2005) in the southern NEFB, and some also in the northern NEFB. Shaw *et al.* (1991) notes that some granites, and their associated volcanic rocks, occur in NNE-trending grabens or rifts. Foreland loading of the southern NEFB commenced in the late Early Permian and volcanic detritus and uplifted detritus feed the developing foreland basins where crustal

loading was synchronous with active volcanism and granite formation (Glen 2005). In the Early Triassic uplift between 244 Ma and 235 Ma (Fielding *et al.* 2001) led to the shedding of large amounts of craton-derived detritus into the SGBB (Table 2.1). Cycle 4 ends at the time of the collision of the Gympie Terrane with Gondwana causing a major crustal loading event and widespread thrusting and folding. Thrusting in the offshore part of the NEFB was west directed and Glen (2005) suggests it could be responsible for the formation of major N-S folds and blind faults in the main part of the Sydney Basin.

### **2.1.3 Thomson Fold Belt**

The Thomson Fold Belt (TFB), also known as the Thomson Orogen, underlies much of central and western Queensland and a small portion of north-western NSW, where it is concealed by the Mesozoic cover of the Great Artesian Basin. Drill data indicates that rocks range in age from Precambrian through to Late Devonian (Murray 1994; Scheibner & Veevers, 2000). West of the Bowen Basin, of which the TFB could form part of the basement, Cambrian or older rocks deformed by the Delamerian Cycle occur along the margin (Glen 2005), particularly in the Anakie Inlier (see Figure 2.2), which is thought to extend south in the subsurface towards the Nebine Ridge (Withnall 1995). Drilling has shown concealed igneous rocks along the southern boundary but the age of these is unknown (Glen 2005). With little outcrop of the TFB exposed the discussion on the development and tectonic history is limited. The Delamerian Cycle and parts of the Hunter-Bowen Super Cycle deformation events are recorded in the exposed rocks.

In the western part of the TFB the rift cycle of the Delamerian is represented by continent-derived sandstones and mudstones (Glen 2005). In the east, the Anakie Inlier shows evidence of rifting with alkaline and tholeiitic volcanic rocks, with the presence of quartz sandstone suggesting an intracontinental setting (Withnall 1995). The ages of these rocks have been suggested by Withnall *et al.* (1996) to be Neoproterozoic or, according to Fergusson *et al.* (2001), late Neoproterozoic to Middle Cambrian. A volcanic belt, largely concealed, along the southern margin of the TFB reflects the convergent phase of the Delamerian. Cycle 1, of the Hunter-Bowen Super Cycle, is represented by volcanism and granite intrusion in the Anakie Inlier (Glen 2005). In Cycle 3, in the Early Permian, extension of the TFB occurred during the inception of the SGBB.

### **2.1.4 Summary**

From the development and tectonic evolution of the three orogenic belts, the Lachlan, New England and Thomson, an assessment of their composition is derived. In summary the LFB is comprised of multiply deformed turbiditic sediments, Silurian-Devonian volcanics, numerous periods of granitic intrusion and large plutonic suites. The NEFB is similarly comprised, with multiply deformed accretionary terrain sediments, Devonian-Carboniferous volcanics and numerous granitic intrusions including large plutonic suites. The TFB is more difficult to define due to limited outcrops, but contains deformed sediments, volcanics and granite intrusions. Overall the orogenic belts, which form the basement to the Sydney-Gunnedah-Bowen Basin system, have similar compositions, development and tectonic histories.

**Table 2.1** A simplified evolution history of the LFB, NEFB and SGBB Tasmanides. Compiled from Schiebner & Basden (1998), Schiebner & Veevers (2000) Branagan & Packham (2000), Glen (2005) and Cawood et al. (2011).

	Timing Ma	Location	Orogenic Stage	Tectonic Environment	Comments / Details
<b>JURASSIC - CRETACEOUS</b>	65 to 200	Tasman Epicratoni c Province		Uplift and erosion	Breakup and dispersal of Pangea and east Gondwanaland, development of passive continental margins around Australia bordered by oceanic lithosphere. Development of the Great Dividing Range. Formation of epicontinental basins with potential fluid hydrocarbon sources.
<b>TRIASSIC</b>	200 to 227	NEFB and SGBB	Mesozoic Rifting	Right lateral transtensional rifting, subsidence	Deposition confined to the intramontane half grabens of the Clarence-Moreton Basin. Initiation of the Great Artesian Basin in the sump of the lowlands between the western-central craton and the NEFB. By 200Ma quartzose sediment encroached and crossed in places the eroded foreland basin and orogen. Maar volcanic diatremes (200 to 190 Ma) in Sydney Basin. The Garrawilla Volcanics (basalt) (221 to ~160 Ma) and other Jurassic igneous rocks in the Surat Basin.
	227 to 235	NEFB	Hunter-Bowen Super Cycle 4	Collision	Minor plutonic activity confined to Demon Fault, regarded as the transpressional conduit of the magma. Right lateral movement (~6 km) on Demon Fault – Venus Fault.
	227 to 235	SGBB	Hunter-Bowen Super Cycle 4	Collision, uplift	Basins converted into fold-thrust belts as deformation fronts migrate westwards. Thrusting (233 Ma) of Tamworth Belt westward over Middle Triassic and unconformably overlying Early Jurassic rocks of the Surat Basin. High angle reverse faults terminate at the unconformity between the Gunnedah and Surat Basins. Vitrinite reflectance data confirm the removal of up to 2 km of Triassic and Permian sediments during the Late Triassic Period of erosion in Gunnedah Basin. Compression and left lateral strike slip movement on the Hunter-Mooki Fault have result in a number of high relief anticlines in front of the main thrust. Movement on Lapstone Monocline-Nepean Fault system (en echelon high angle reverse faults, some wrenching and sinistral transpressive motion) may be during Late Triassic.

**Table 2.1 (Continued)**

	Timing Ma	Location	Orogenic Stage	Tectonic Environment	Comments / Details
<b>TRIASSIC</b>	242	NEFB	Hunter-Bowen Super Cycle 4	Collision	Cycle 4 was terminated by the collision of Gympie Terrane / Province with Gondwana in the Early to Middle Triassic. This deformation is inferred to have caused the Bowen phase of the Hunter-Bowen Super Cycle, a major crustal loading event.
	235 to 250	SGBB	Hunter-Bowen Super Cycle 4	Convergence, relative uplift from 244 to 235 Ma	Environmental change above the Permian Triassic boundary coincided with the end of tuff and coal deposition and the onset fluvial sedimentation. In the Sydney Basin this was especially derived from the NEFB and synchronous with major periods of volcanism and granite emplacement. Uplift led to shedding of large amounts of craton derived detritus in to the Bowen, Gunnedah and Sydney Basins forming the Clematis and Lower Napperby formations and Hawkesbury sandstone respectively. Final filling (235 to 230 Ma) of the basins dominated by detritus shed from the NEFB but finer grained suggesting lesser topographic expression and reduced thrusting.
<b>PERMIAN</b>	250 to 258	NEFB	Hunter-Bowen Super Cycle 4	thrusting	Intense folding/faulting and metamorphism in southern NEFB (255 Ma), moderate folding in adjacent basins.
	250 to 258	SGBB	Hunter-Bowen Super Cycle 4	Convergence, crustal loading	All basins converted to coal bearing foreland basins, fed in pulses from volcanic detritus and uplifted detritus (~253 Ma) from NEFB. Crustal loading synchronous with active volcanism and granite formation. Marine regression ~253 Ma. Broad folding after coal deposition associated with sinistral transcurrent faults.
	258 to 264	SGBB	Hunter-Bowen Super Cycle 4	Compression	Conversion of rift basins in the Sydney-Gunnedah-Bowen Basin system to foreland basins
	264	NEFB	Hunter-Bowen Super Cycle 4	Convergent magmatic arc	Extrusion of widespread ignimbrite sheets and emplacement of major I-type granites of the New England Batholith
	265	NEFB	Hunter-Bowen Super Cycle 3		Un-roofing of Barrington Tops Granodiorite. Deposition of Greta Coal Measures in Sydney Basin, Maules Creek Coal Measures in the Gunnedah Basin and Reid Dome Beds in the Bowen Basin.
	267 to 268	NEFB	Hunter-Bowen Super Cycle 3	Compression, large scale folding	N-S deformation into the Permian Basins. Formation of oroclines. Intense folding / faulting in north NEFB and Bowen Basin (265 Ma).

**Table 2.1 (Continued)**

	Timing Ma	Location	Orogenic Stage	Tectonic Environment	Comments / Details
	268 to 300	SGBB	Hunter-Bowen Super Cycle 3	Extension, detachment faulting	Extensional or transtensional rifts that are floored by volcanics or underlain by intrusive rocks. Rift volcanics at the base of the SB include the 292 Ma Rylstone Volcanics and 270 Ma Werrie Basalt. Interpretation of the Early Permian extension include subduction of a spreading ridge, slab break-off and changes in the plate boundary configuration form retreating to advancing.
CARBONIFEROUS	268 to 300	NEFB	Hunter-Bowen Super Cycle 3	Extension (rifting 300 to 280), N-S compression, dextral transtension	Emplacements of granites and serpentinites and formation of rift sedimentary basins. Inception of the Bowen-Sydney Basin. From 302 Ma deposition of glacial sediments. Dextral transtension produced orocline related pull-apart basins and widespread volcanism. Marine transgression at 288 Ma.
	300 to 310	NEFB	Hunter-Bowen Super Cycle 2	Uplift, strike/slip faulting, crustal block rotation, extension	Erosion during glaciation, development of Sydney-Gunnedah basin by extension (~302 Ma). Thick extensional volcanics (Rylstone Volcanics) and voluminous plutons (Hillgrove, Wongwibinda, Bundarra) erupted in an intra-montane setting
	320	LFB	Lachlan Super Cycle <i>Kanimblan</i>	Deformation, uplift	Arc widens by emplacement of high level I type granitoids generated by melting of underlying Ordovician volcanic rocks. Granite emplacement i.e. Bathurst Batholith (330 to 315 Ma), Gulgong Plutonic Suite and other granites along a 600 km long belt to the SSE and in the subsurface to the NNW.
	330 to 350	LFB	Lachlan Super Cycle <i>Kanimblan</i>	Shallow subduction, E-W shortening (340 Ma)	Kanimblan upland mountain building. N-S thrusts. Intrusion of S and I type granites and A type volcanics.
DEVONIAN	362	NEFB	Hunter-Bowen Super Cycle 2	Convergence	Subduction and extensional granites
	376	NEFB	Hunter Bowen Super Cycle 1	Convergence	East facing continental or intra-oceanic arc dominated by intermediate volcanism, forearc basin and subduction complexes with accreted terranes.
	382 to 394	LFB	Lachlan Super Cycle <i>Tabberabberan</i>	Contraction, strike/slip	Major basin inversion, growth faults undergoing varying degrees of reverse/oblique reactivation and development of basin inversion structures. Brittle conjugate NE and NW trending faults offsetting major plutons and producing small amount of extension.

**Table 2.1** (*Continued*)

	Timing Ma	Location	Orogenic Stage	Tectonic Environment	Comments / Details
<b>SILURIAN</b>	415 to 430	LFB	Lachlan Super Cycle <i>Tabberabberan</i>	Rifting	Horst and grabens in wide back-arc region. Basin formation and granitoid emplacement. Some granites emplaced into extending upper crust, co-magmatic with and overlain by felsic volcanic rocks erupted in extensional basins. Other foliated granites were emplaced into the middle crust at depths of 10 km then exhumed by thrusting a further 1 to 2 km.
<b>ORDOVICIAN</b>	435 to 450	LFB	Lachlan Super Cycle <i>Tabberabberan</i>	Convergent	Intra-oceanic arc
	443 to 490	LFB	Lachlan Super Cycle <i>Benambran</i>	Convergence E-W compression (495 Ma)	Westward subduction beneath fore-arc basin, volcanic arc and marginal sea. Turbidite deposition.
<b>CAMBRIAN</b>	530	NEFB	Delamerian Cycle	NE subduction, convergence	Eclogite blocks exhumed in Peel-Manning Fault system. Closure of basin margin.
	530	LFB	Delamerian Cycle	NE subduction, convergence	Mafic and ultramafic rocks exposed as fault slices in the hanging walls of major thrust faults



## 2.2. The evolution of the east coast of Australia: Permian to Cretaceous

The SGBB is a major north-south Permian to Triassic structural basin, approximately 1600 km long (Glen 2005), that extends from the south coast of southern NSW, near Ulladulla, to near Bowen on the coast of northern Queensland (Figure 1.1 and Figure 2.2) and covers an area of over 260,000 km<sup>2</sup> (Cadman & Pain 1998).

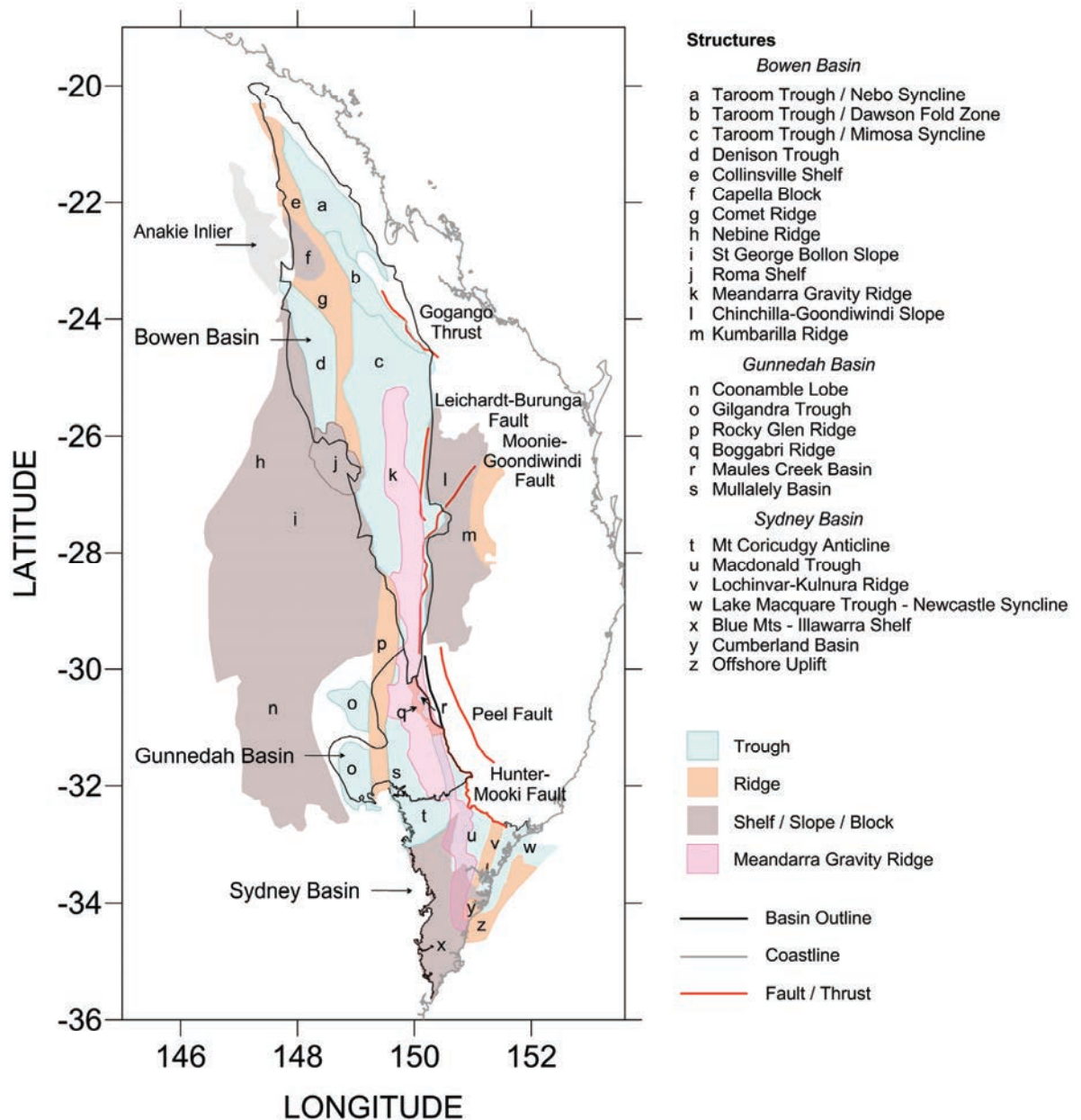


**Figure 2.2** Structural element subdivisions of the Sydney-Gunnedah-Bowen Basin system. Structural elements modified from Adler *et al.* (1998) and Krassay *et al.* (2009).

This section provides a summary of the development, tectonic history, stratigraphy and structure of the Sydney-Gunnedah-Bowen Basin system. Although numerous authors have studied many aspects of the SGBB for its stratigraphy, structure and evolution, several key compilations of information and ideas have been made by Herbert & Helby (1980) for the Sydney Basin, Tadroz (1993) for the Gunnedah Basin and a thematic issue of the Australian Journal of Earth Science (2009, vol 55, issue 3) on the evolution of the Bowen Basin. This material, along with the work of Fielding *et al.* (1995,

2000), Murray (1994), Cadman & Pain (1998), Branagan & Packham (2000) and Langford & Patchett (2005), form the basis of this review.

### **2.2.1 Tectonic Overview**

The SGBB originated in the Early Permian, during Cycle 3 of the Hunter-Bowen Super Cycle (Table 2.1), as extensional (or transtensional) rifts floored by volcanics or underlain by intrusive rocks (Glen 2005). Rift volcanics rocks at the base of the Sydney Basin include the Rylstone Volcanics, near the western margin (i.e. Shaw *et al.* 1989) and the Werrie Basalt in the north-east, which also underlies the Gunnedah Basin (i.e. Leitch 1993; Tadroz 1993; Caprarelli & Leitch 2001). The silicic flows and ignimbrites of the Boggabri Volcanics, which floor parts of the Gunnedah Basin, outcrop near the eastern margin and extend westwards under the basin (i.e. Leitch 1993; Tadroz 1993). The volcanic rocks at the base of the Bowen Basin include the Rookwood, Lizzie Creek, Bulgonnuna, Connors, Combarngo and Camboon Volcanics (Fielding *et al.* 1995; Glen 2005).

The substrate of the SGBB system is considered by Glen (2005), for the Bowen Basin, to be the TFB in the west and the NEFB in the east. Korsch *et al.* (2002) notes the Gunnedah Basin is built over crust of the LFB, whilst the substrate of the Sydney Basin is inferred to be LFB in the west (O'Reilly 1990) and NEFB in the east (Roberts & Engel 1987). There are several interpretations for the Early Permian extension including, subduction of a spreading ridge (Murray *et al.* 1987), slab break off (Caprarelli & Leitch 1998) and changes in the plate boundary configuration from retreating to advancing (Jenkins *et al.* 2002).

A combination of post-rift subsidence and the cessation of loading in the late Early Permian created marine conditions. In Cycle 4 of the Hunter-Bowen Super Cycle, foreland loading of the southern NEFB is recorded in the deposition of coal measures, Greta Coal Measures in Sydney Basin and Maules Creek Coal Measures in Gunnedah Basin (Table 2.1), mixed with volcanic detritus. In The Bowen Basin the earliest deposits of coal interbedded with volcanics are recorded in the Reid Dome Beds of the Denison Trough (Fielding *et al.* 1995). Glen & Beckett (1997) note syn-sedimentary thrusting in the north-east Sydney Basin led to the formation of growth anticlines and westward propagating thrust fronts. Glen (2005) notes that in the Bowen Basin, thrusting produced the Gogango Thrust Zone.

By the end of the Late Permian (250 Ma) the SGBB system had been converted to a coal bearing foreland basin, fed with pulses of volcanic detritus and uplifted detritus from the NEFB (Table 2.1), where crustal loading was synchronous with active volcanism and granite formation (Glen 2005). At the Permian-Triassic boundary a major environmental change coincided with the end of tuff and coal deposition and the onset of fluvial sedimentation, derived from the NEFB, and synchronous with major periods of volcanism and granite emplacement. By the Middle to Late Triassic the SGBB converted into fold-thrust belts in response to westward migrating thrust fronts (Glen 2005). Crustal shortening is observed in the SGBB system, with Glen (2005) suggesting greater amounts in the Bowen Basin than the Gunnedah and Sydney basins. Tadroz (1993) notes that the western part of the Gunnedah Basin

still retains elements of its early rift geometry by being divided into north-south blocks by major cross-faults.

### **2.2.2 The Sydney Basin – Stratigraphy and Structure**

The Sydney Basin is a north-south trending basin, containing generally flat lying Permian-Triassic sequences, approximately 250 km long, averages 100 km in width and covers an area of approximately 37,000 km<sup>2</sup> onshore and 15,000 km<sup>2</sup> offshore (Bembrick & Lonergan 1976; Adler *et al.* 1998). The structural framework (Figure 2.3) is described by Herbert & Helby (1980) and comprises eleven onshore structural elements; the Hunter Valley Dome Belt, Hornsby Plateau, Blue Mountains Plateau, the Cumberland Basin with Fairfield, Penrith and Botany sub-basins, Woronora Plateau, Illawarra Plateau, Sassafras Plateau and Boyne Mount Plateau and four offshore principle elements; the Offshore Syncline, the offshore extension of the Newcastle Syncline, an offshore extension of the New England Fold Belt and the Offshore Uplift of the Currarong Orogen.

The Hunter-Mooki thrust system is generally considered the north-eastern boundary and the north-western boundary is the Mt Coricudgy Anticline. The Sydney Basin extends offshore to the margin of the continental shelf (Mayne *et al.*, 1974) and is difficult to define. It developed as a foreland basin in front of the deforming New England Fold Belt, with a series of north-trending grabens and half grabens formed in response to limited crustal extension in an east-west direction during the Late Carboniferous to Early Permian.

Branagan & Packham (2000) note that the basin basement is marked by a number of faults which were active during sedimentation, and produced broad folds, monoclines and faults in the sedimentary succession. Sedimentation in the Sydney Basin can be divided into many distinct depositional episodes related to marine transgression and regression and terrestrial sedimentation. A simplified stratigraphy of the Sydney Basin is shown in Table 2.2 and a schematic cross-section is shown in Figure 2.4.

In the Sydney Basin the total thickness of the sedimentary package ranges on average from 2 to 3 km over much of the basin, thickens near the Hunter-Mooki Fault to 5 km and reaches up to 6 km offshore (Veevers 1984). During the Late Carboniferous, cratonic rocks of the LFB were emergent and stood elevated at more than 600 m (Herbert 1972). Extensive volcanism took place in a rift zone, extending from the Hunter Valley area northwards into Queensland, and huge volumes of coarse volcanic debris were deposited to the east of the rift. This was followed by alpine and valley glaciers depositing thick fluvioglacial conglomerate, diamictite and varves and the deposition of the Talaterang Group conglomerates in eroded valleys of LFB Palaeozoic basement. Volcanism continued into the Early Permian with thick basaltic and rhyolitic sequences such as the Lochinvar Formation of the Dalwood Group in the Sydney Basin and the Boggabri Volcanics and Werrie Basalt in the Gunnedah Basin.

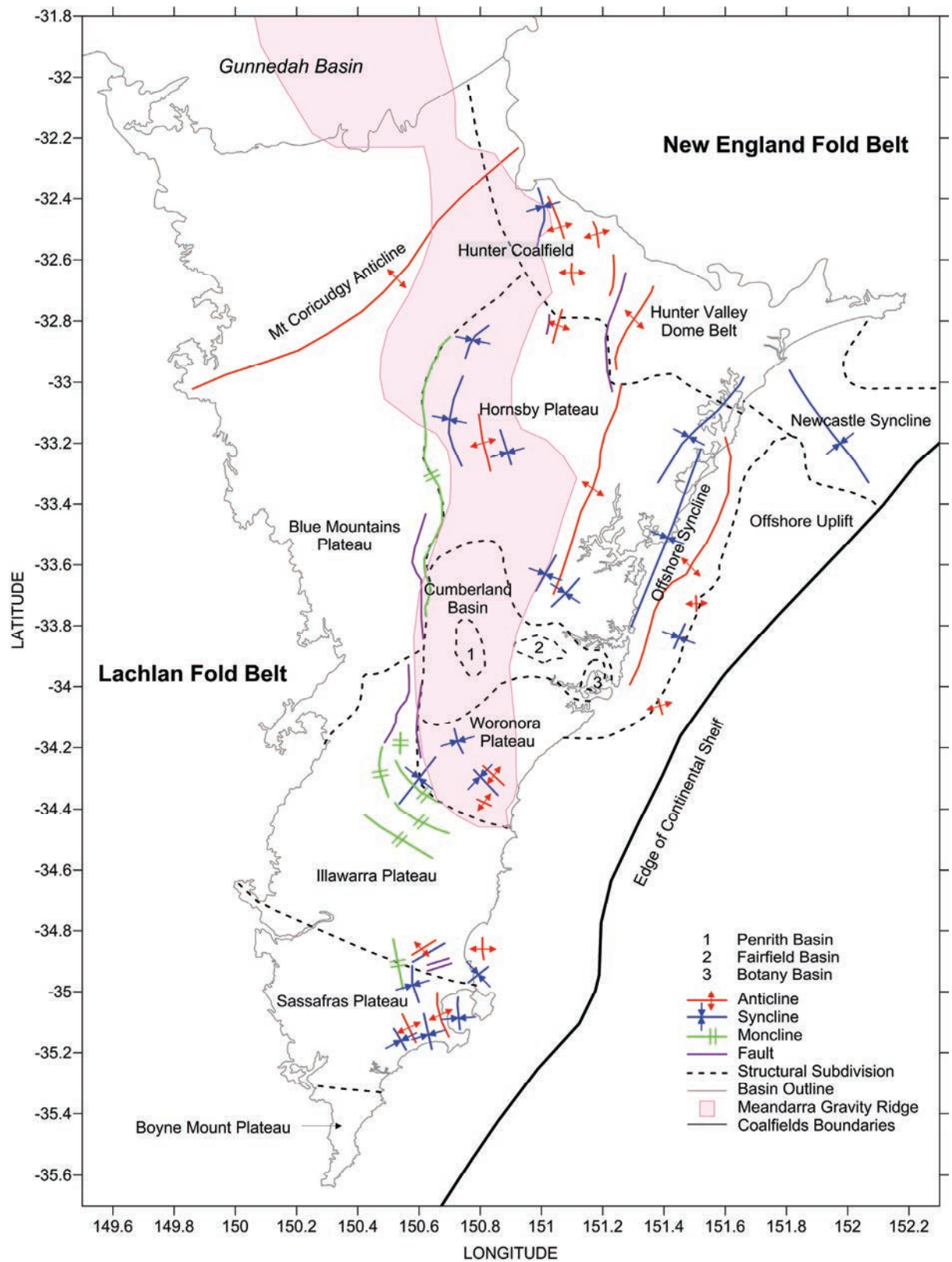



**Figure 2.3** Structure and tectonic map of the Sydney Basin. Compiled from Herbert & Helby (1980), Shepherd & Huntington (1981), and NSW 1:250 000 scanned geological maps Sydney SI56-5, Wollongong SI56-9, Newcastle SI56-2, Ulladulla SI56-13 and Singleton SI56-1.



**Table 2.2** A simplified stratigraphy of the Sydney Basin. Modified from Herbert & Helby (1980).

			SYDNEY BASIN			
			HUNTER COALFIELD	NEWCASTLE COALFIELD	WESTERN COALFIELD	SOUTHERN COALFIELD
PERMIAN	TRIASSIC	EARLY TO MIDDLE				Wianamatta Group
			Hawkesbury Sandstone			Hawkesbury Sandstone
			Terrigal & Newport Formation			
		Narrabeen Group	Narrabeen Group	Narrabeen Group	Narrabeen Group	
	LATE	Singleton Supergroup	Newcastle Coal Measures			
			Dempsey FM	Baal Bone FM	Bargo Claystone	
			Tomago Coal Measures	Illawarra Coal Measures	Illawarra Coal Measures	
			Kulnura Marine Tongue	Marrangaroo Conglomerate	Erins Vale FM	
		Bulga FM				
					Gerringong Volcanics	
		Maitland Group	Maitland Group	Shoalhaven Group		
	EARLY	Greta Coal Measures	Greta Coal Measures		Shoalhaven Group	
Gyarran Volcanics		Dalwood Group	Metasediments & Granite			
LATE CARBONIFEROUS			Seaham Formation Conglomerates	Seaham Formation Conglomerates/ Kuttung Volcanics		Clyde CM   Wasp Head FM
						Talaterang Group Conglomerates

 Unconformity    FM = Formation    CM = Coal Measures

— Unconformity FM = Formation CM = Coal Measures

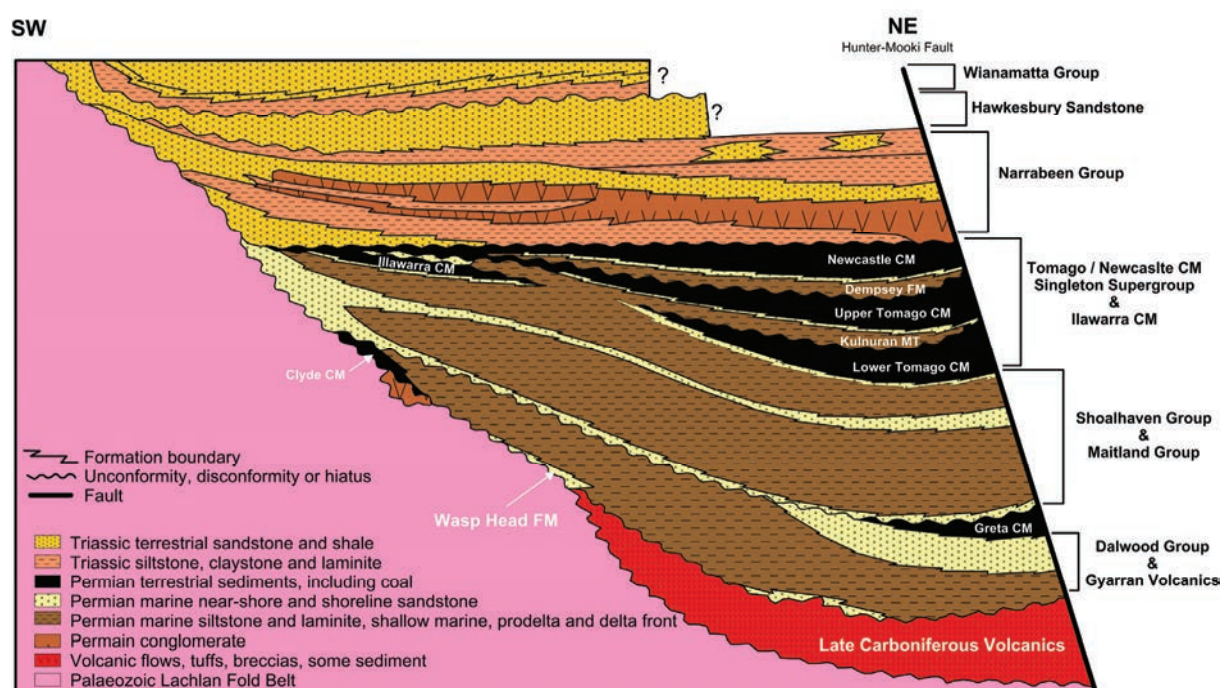


**Figure 2.4** A NE-SW schematic cross-section of the Permian to Triassic stratigraphy in the Sydney Basin. Adapted from Herbert & Helby (1980).

As volcanism waned, subsidence and marine deposition became characteristic. Several volcanic centres became islands which shed debris into the surrounding transgressive Early Permian sea. Herbert & Helby (1980) note that the defined structural outline of the Sydney Basin has not yet evolved and as such sedimentation occurred across a broad continental shelf and over the continental slope into an adjacent trench. In the southern Sydney Basin, beach and near-shore sands of the Wasp Head Formation were transgressing the Lachlan Fold Belt. Extensive marine transgressions produced the thick blanket of sand and silt of the Dalwood Group as well as the deposition of the Greta Coal Measures (Figure 2.4) along a terrestrial wedge.

Basin wide subsidence followed and resulted in a transgression which expanded the area of marine deposition. In the northern Sydney Basin, the base of the Maitland Group (Branxton Formation) was deposited from reworked material derived from the underlying fluvio-deltaic sediments. In the southern part of the basin the base of the Shoalhaven Group (Snapper Point Formation) was deposited, sourced from eroding hard rock Late Devonian quartzite headlands and spread extensively over the southern and western parts of the basin. As the Early Permian sea moved westward over the Lachlan Fold Belt considerable quantities of boulders and pebbles were eroded from coastal cliffs. Another regressive-transgressive episode occurred prior to the mid Permian finalising the deposition of the Maitland Group and upper parts of the Shoalhaven Group (Berry Siltstone).

After the mid Permian, Hunter-Bowen Super Cycle 4 (Table 2.1), uplift of the NEFB led to rapid subsidence of the adjacent Sydney Basin, erosion and deposition. During three major regressive episodes as much as 2000 m of terrestrial and marine sediments were deposited (Herbert & Helby 1980). These sediments, forming the Tomago Coal Measures, Illawarra Coal Measures and the Singleton Super Group contain the most important coal in the Sydney Basin (Figure 2.4). The bulk of the sediment in the deltaic environment is derived from the NEFB, with maximum thickness adjacent to the Hunter-Mooki thrust fault. Following this, in the northern eastern part of the basin, prodelta and delta front laminated sand and silt were deposited seawards of a shoreline comprising a barrier island-estuarine channel sand complex (lower Newcastle Coal Measures) and can be correlated with the Bargo Claystone in the southern part of the Basin and with the upper part of the Singleton Super Group (Denman Formation) in the north.

The Narrabeen Group, comprising up to 800 m of lithic conglomerate, quartz-lithic sandstone, and shale (red, green and grey) was deposited in the Late Permian to Middle Triassic when major alluvial systems prograded and sediment was deposited from the New England Fold Belt. Overlying the Narrabeen Group is the Middle Triassic Hawkesbury Sandstone, up to 250 m thick, and is dominantly a coarse quartz sandstone. Overlying this is the Wianamatta Group (comprising the Ashfield Shale, Minchinbury Sandstone and Bringelly Shale), up to 300 m thick and dominantly shale with sporadic thin lithic sandstones. The Narrabeen Group was deposited in three episodic environments; estuarine/alluvial, fluvial and fluvial-deltaic. Subsidence caused limited transgression and an upward transition to fluvio-deltaic deposits of the upper Narrabeen Group in the Newport and Terrigal Formations.

Uplift of the Lachlan Fold Belt to the southwest of the Sydney Basin tilted and led to the erosion of Late Permian and Early to Middle Triassic sediments in the southern part of the basin. The deposition of the Hawkesberry Sandstone occurred in an alluvial environment that has been compared by Conaghan & Jones (1975) with the huge Brahmaputra River system in India. The sand was probably derived from upper Devonian quartzites in the LFB and graphite, commonly found throughout the sandstone, may have been derived from Victorian Ordovician graphitic slates (Herbert & Helby 1980).

The Wianamatta Group was the last phase of sedimentation directly related to the tectonic development of the Sydney Basin, with sediments deposited in a continuous succession of environments grading upward from subaqueous, to shoreline and ultimately to alluvial during a single major regression (Herbert & Helby 1980). Mid-Triassic deformation terminated deposition in the Sydney Basin. Jurassic sedimentation is not evident in the Sydney Basin, only Jurassic volcanic breccia pipes (diatremes). According to Herbert & Helby (1980) it is possibly that an unknown, but not great, thickness of early Jurassic sediments may have extended from the Great Artesian Basin unconformably over the Sydney Basin but have since been completely eroded.

### **2.2.3 The Gunnedah Basin – Stratigraphy and Structure**

The Gunnedah Basin is a structural trough in north-eastern NSW, which forms the middle part of the SGBB system (Figure 2.5). It is bounded by a regional unconformity surface over the LFB in the west and by the NEFB to the east along the Hunter-Mooki Fault. The basin appears continuous with the Bowen Basin in the north and the Sydney Basin in the south, however boundaries are generally drawn between the Bowen and Gunnedah around Moree and between the Gunnedah and Sydney south of Coolah from near Ulan to south of Quirindi (Tadroz 1993) (Figure 1.1). Bembrick *et al.* (1973) defines the northern boundary along a transverse structural high north of Narrabri and the southern boundary along the Mount Coricudgy Anticline. Subsequent modification to these structural subdivisions is based mainly on aspects of stratigraphy and sedimentation within the basins and not on the structures which influence the deposition of the Permian and Triassic sediments (Tadroz 1993).

In the Gunnedah Basin, marine and non-marine Permian and Triassic sediments rest unconformably upon the Late Carboniferous to Early Permian silicic and mafic volcanics of the Boggabri Volcanics (Figure 2.6). The northerly orientated Boggabri Ridge divides the Gunnedah Basin into two parts, the Maules Creek Basin and Mullaley Basin (Figure 2.5). Sedimentation in the basin follows similar distinct depositional episodes, related to marine transgression and regression and terrestrial sedimentation, as in the Sydney Basin. A simplified stratigraphy of the Gunnedah Basin is shown in Table 2.3.

In the Early Permian sedimentation in the Gunnedah Basin closely reflected conditions that prevailed during the earliest stages of basin development (Tadroz 1993). Fluvial processes redistributed weathering from the dormant volcanic terrane. The extensional tectonic regime initiated several half-graben-like structures which received sediment from neighbouring highlands (Tadroz 1993). Basin fill localised in small rapidly subsiding troughs, separated by highlands and ridges consisting of silicic and mafic volcanics.

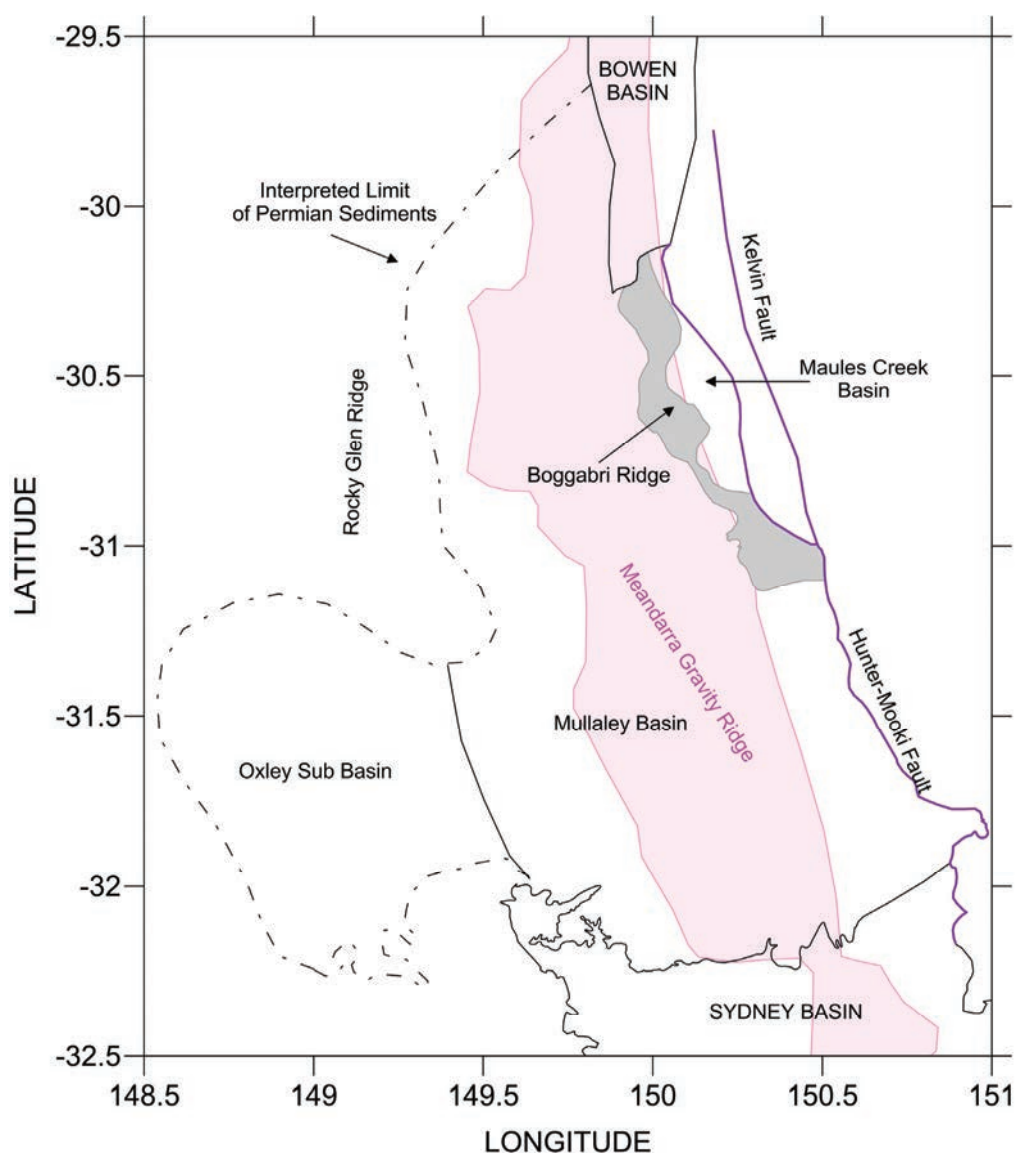


**Figure 2.5** Structure and tectonic map of the Gunnedah Basin. Modified from Tadroz (1993).

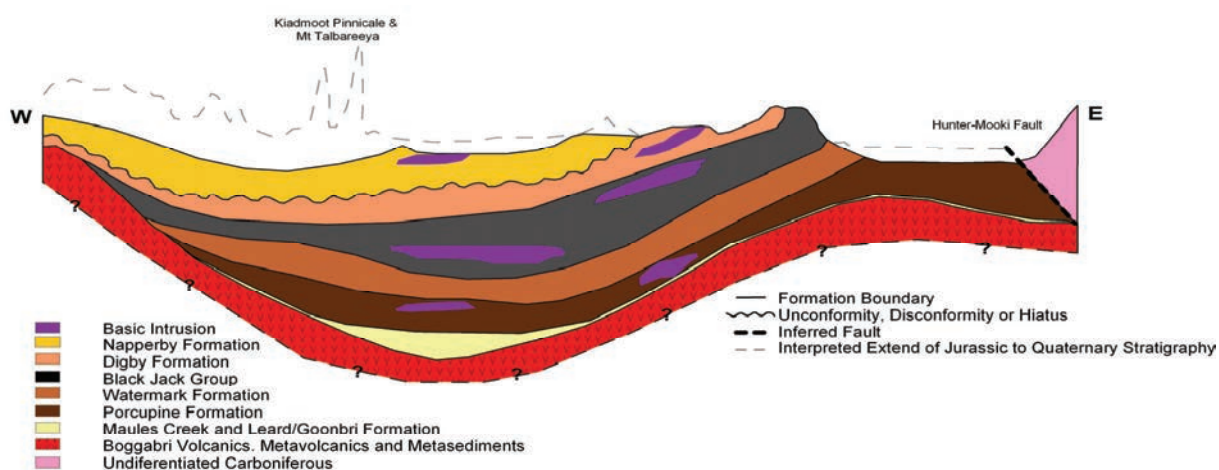


**Figure 2.6** An E-W schematic cross-section of the Gunnedah Basin showing Carboniferous to Triassic stratigraphy. The approximate extent of Jurassic to Quaternary stratigraphy shown as dashed line. Modified from Tadroz (1993).



**Table 2.3** *Simplified stratigraphy of the Gunnedah Basin. Modified from Tadroz (1993).*

JURASSIC	EARLY	Surat Basin Sediments
TRIASSIC	LATE	Garrawilla Volcanics
	EARLY	Deriah Formation
		Napperby Formation
		Digby Formation
	PERMIAN	LATE
Arkarula Sandstone		
Watermark Formation		
Porcupine Formation		
EARLY		Maules Creek Formation
		Leard & Goonbri Formation
		Boggabri Volcanics & Werrie Basalt
		Metavolcanics & Metasediments
LATE CARBONIFEROUS		

The fine-grained lacustrine sediments of the Leard and Goonbri Formation accumulated in the most rapidly subsiding areas in the troughs but were soon inundated by coarse braided river deposits of the Maules Creek Formation as humid alluvial fan systems in-filled the evolving troughs. The northerly orientated Boggabri Ridge acted as the principal sediment source and effectively divided the Gunnedah Basin into two basins. The Maules Creek Formation attains a thickness in excess of 800 m in the Maules Creek Basin and possibly thicker adjacent to the Mooki Fault. West of the Boggabri Ridge the formation is less than 100 m thick.

In the early part of the Late Permian deposition the marine shelf sediments of the Porcupine Formation occurred. These sediments are equivalent to the Snapper Point Formation (base of the Shoalhaven Group) and Braxton Formation (base of the Maitland Group) in the Sydney Basin. The Porcupine Formation ranges in thickness from 0 to 10 m along the western margin of the Mullaley basin, 20 to 60 m in the north and from 30 to >170 m in the south and south-east. The Watermark Formation gradationally overlies the Porcupine Formation and is characterised by siltstone and claystone. It represents the maximum extent of Late Permian marine regression in the Gunnedah Basin and ranges in thickness from 175 m to 230 m in the Quirindi area. Deposition of the lower Black Jack Formation in the middle Late Permian is characterised by a south-westerly progradation of deltas, sourced from the NEFB region, followed by regional inundation and shallow marine sedimentation. Lowering of the sea level during the deposition of the lower Black Jack Formation provided appropriate conditions for widespread peat accumulation. Two marine incursions interrupted terrestrial sedimentation for short periods during this main coal forming interval. The first, caused by

tectonic subsidence, which deposited the Kulnura Marine Tongue and Bulga Formation in the Sydney Basin and Arkarula Sandstone in the Gunnedah Basin.

The second marine incursion, which deposited the Dempsey Formation, Baal Bone Formation and Bargo Claystone in the Sydney Basin, did not reach the Gunnedah Basin but some lateral equivalents are represented by the upper Black Jack Formation in the eastern half of the Mullaley basin. Coal measure sedimentation then resumed with the southward progradation of major fluvial/deltaic systems from the north of the Sydney Basin, resulting in the deposition of the upper Black Jack Formation. The deposition of the upper Black Jack Formation in the latest Late Permian represents the last phase in the Permian depositional history of the Gunnedah Basin. Sedimentation was influenced by the encroachment of conglomeratic braided fluvial systems and an abundance of tuff and pyroclastic detritus (Tadroz 1993).

In the Late Permian a major depositional break and a period of structural re-adjustment, uplift and erosion are evident in the northern Gunnedah Basin. An angular unconformity is present between the Permian sediments of the Black Jack Formation and the Triassic Digby Formation. Deposition resumed in the Early Triassic when major alluvial systems prograded southwards and south-westwards over the eroded surfaces of the coal measures or the underlying sediments (Tadroz 1993). Thick conglomerate sequences in the form of large alluvial fans and outwash sediments were introduced from the NEFB region across the Hunter-Mooki Fault system to the south-eastern Gunnedah Basin as the lower part of the Digby Formation. Renewed subsidence resulted in the deposition of the Napperby Formation, a sequence of siltstone/claystone, interbedded sandstone/siltstone to sandstone, derived from the NEFB and represent progradation of lacustrine deltas.

The Deriah Formation, a distinctive green sandstone, at the top of the Triassic sequence in the Gunnedah Basin is thought to be a response to the contemporaneous volcanic activity in the NEFB or possibly the appearance of the Nandwear Igneous Complex north east of Gunnedah. Equivalent lithologies to the Hawkesbury Sandstone are not present in the Gunnedah Basin, as the NEFB remained the dominate source of sedimentation. A major mid-Triassic episode of deformation cause reverse faults and uplifted small blocks form which the upper part of the Napperby Formation was removed. Jurassic sedimentation in the Gunnedah Basin is represented by deposition of sediments from the overlying Jurassic-Cretaceous Great Artesian Basin.

#### **2.2.4 The Bowen Basin – Stratigraphy and Structure**

The Bowen Basin is an elongate, north-south trending, asymmetrical basin extending from northern NSW through central QLD covering an area of approximately 200,000 km<sup>2</sup>. It is the largest part of the SGBB system and is divided into 13 main structural areas (Figure 2.2) with the major structural features shown in Figure 2.7. The eastern boundary of the basin is marked by a series of north-south orientated thrust faults (Moonie-Goondiwindi and Leichardt-Burunga) extending south from the Connors-Auburn Arch.

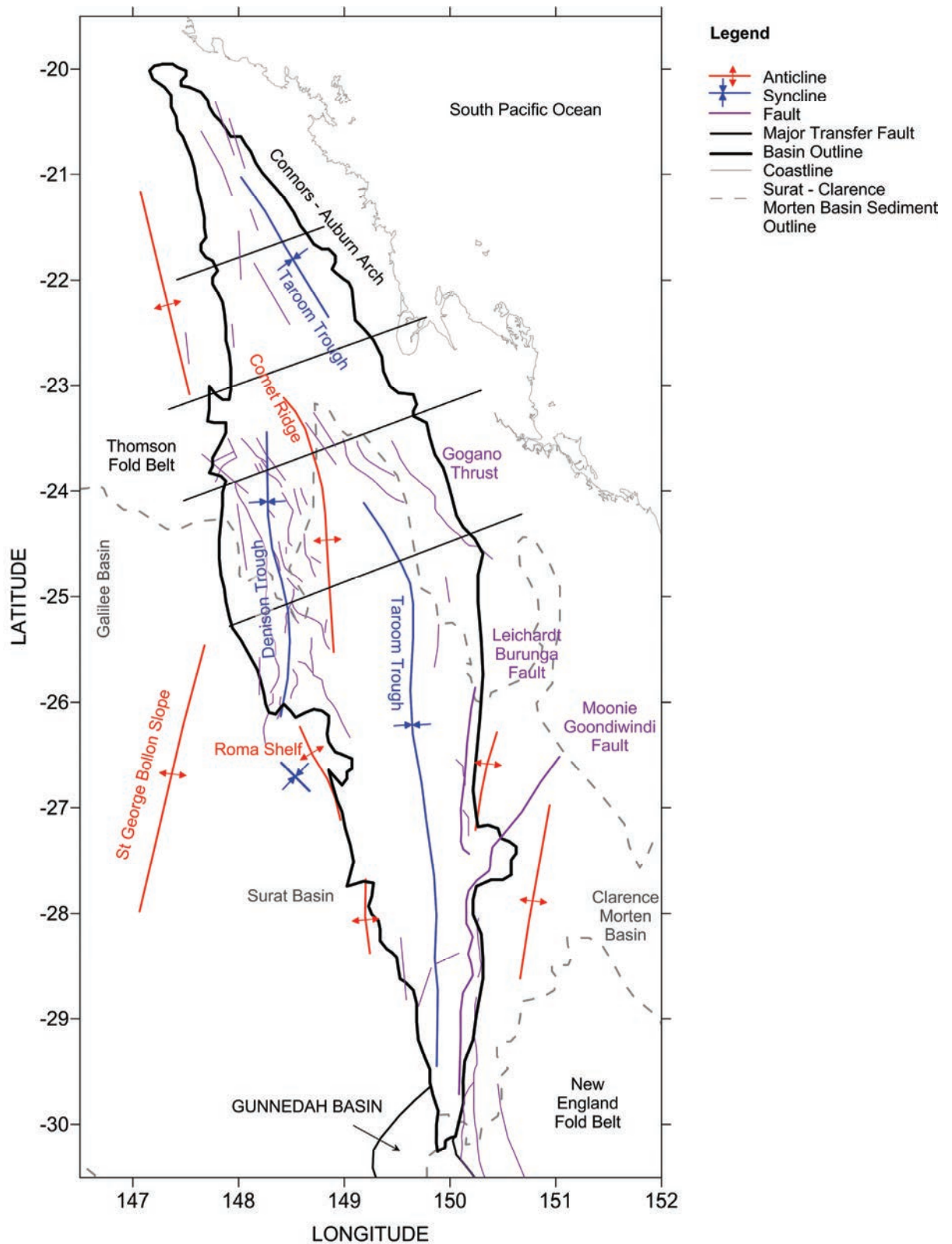


**Figure 2.7** Structure and tectonic map of the Bowen Basin. Compiled from Baker et al. (1993), Tadroz (1993), Fielding et al. (1995) and Cadman & Pain (1998).

The western margins are less well defined, with sediments deposited on the Saint George-Bollon Slope thinning and inter-fingering with sediments of the Galilee Basin. The Comet platform separates the two major depositional centres of the Denison and Taroom Trough (Cadman & Pain 1998). A

simplified stratigraphy is presented in Table 2.4 and Figure 2.8 is schematic cross-section through the central part of the Bowen Basin.

**Table 2.4** *Simplified stratigraphy of the Bowen Basin. Modified from Day et al. (1983), Cadman & Pain (1998) and Fielding et al. (1995).*

		DENISON TROUGH / COMET RIDGE	ROMA SHELF / ST GEORGE – BOLLON SLOPE	CENTRAL AND SOUTHERN TAROOM TROUGH
TRIASSIC	MIDDLE			
		Moolayember Formation	Moolayember Formation	Moolayember Formation
			Snake Creek Mudstone Member	
		Clematis Group	Showgrounds Sandstone	
PERMIAN	EARLY	Rewan Group	Rewan Group	Rewan Group
	LATE	Backwater Group	Backwater Group	Backwater Group
		Black Alley Shale		Back Creek Group
		Mantuan Formation	Mantuan Formation	
		Peawaddy Formation		
		Catherine Sandstone		
		Ingelara Formation		
		Freitag Formation		
		Upper Aldebaran Sandstone		
		Lower Aldebaran Sandstone		
		Cattle Creek Formation		
		Reids Dome Beds	Reids Dome Beds	Camboon Volcanics
CARBONIFEROUS			Combango Volcanics Roma Granite	
DEVONIAN		Timbury Hills Formation	Timbury Hills Formation	

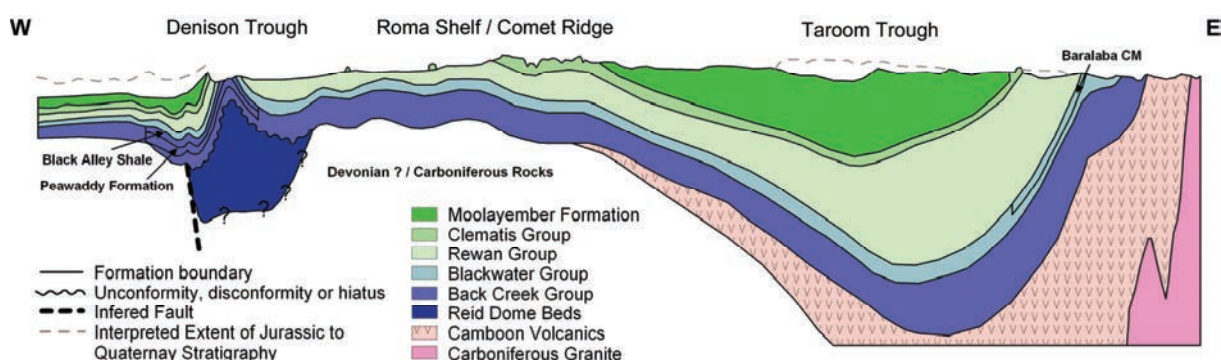


**Figure 2.8** *E-W schematic cross-section of the central Bowen Basin showing Carboniferous to Triassic stratigraphy. Approximate extent of Jurassic to Quaternary stratigraphy shown as dashed line. Adapted from Malone et al. (1967).*

Four basin phases have been identified in the Bowen Basin, with the earliest phase being basin development in the Late Carboniferous to Early Permian, involved a series of grabens and half grabens from crustal extension (Cadman & Pain 1998; Elliott 1989). Sediments comprising fluvial and lacustrine facies with locally thick coal bodies (Reid Dome Beds) were deposited in the Denison Trough (Fielding *et al.* 1995; Brakel *et al.* 2009) and volcanics were laid down on the eastern flank of the Roma Shelf and in the Taroom Trough (Figure 2.8) (Murray 1994; Cadman & Pain 1998). The top of the Reid Dome Beds and the early volcanics is a strongly diachronous surface, representing the gradual flooding of the basin by the sea (Fielding *et al.* 1995).

Rift development in the Denison Trough and volcanism in the Taroom Trough was succeeded by a period of thermal subsidence, followed by a phase of subsidence driven by foreland loading (Brakel *et al.* 2009). Modest volumes of quartz rich sediment continued to be shed eastwards from uplifted basement into the western part of the Denison Trough. In the Denison Trough, subsidence is characterised by four marine to marginal-marine transgressive-regressive cycles producing the Cattle Creek Formation, Aldebaran Sandstone, Freitag Formation and Peawaddy Formation. In the Taroom Trough subsidence produced the marine volcanoclastic sediments at the top of the Camboon Volcanics (Brakel *et al.* 2009) and the lower Back Creek Group.

The effects of thrust loading on the eastern margin of the basin in the Late Permian limited the volumes of volcanic detritus entering the basin and lead to the deposition of the upper part of the Back Creek Group. A resurgence of the volcanic arc on the eastern margin of Gondwana in the late Late Permian coincided with the onset of more severe, broadly westward-directed compression and the initiation of thrusting (Fielding *et al.* 1995). The depocentre was located, according to Brakel *et al.* (2009) close to the present eastern margin of the basin, and the thickest sediments are preserved along the axis of the Taroom Trough.

The residual marine basin, now isolated from the palaeo-Pacific ocean, was infilled by three southward progradational pulses of the Blackwater Group such that by the end of the Permian alluvial plain conditions were established across the entire basin. As thrust loading proceeded the basin became overfilled and coal-bearing facies gave way to the reddened alluvial strata of the Rewan group, shortly before the Permian-Triassic boundary (Fielding *et al.* 1995). The Rewan Group consists of interbedded red, gray-green and dark grey shales, siltstones and lithic sandstone with minor amounts of conglomerate (Cadman & Pain 1998) approximately <300 m thick. Deposition was greatest in the southwest, with maximum subsidence in the area of the Taroom Trough. Sediments were derived from elevated source areas to the south, east and north and were distributed by meandering streams (Day *et al.* 1983). Arc derived sediment continued to accumulate in the Bowen Basin at least until latest Middle Triassic, interrupted by a massive influx of quartzose, craton-derived sediment of the Clematis Group (Fielding *et al.* 1995).

Renewed subsidence of the Taroom Trough was marked by the accumulation of sediments from the Middle Triassic Moolayember Formation (lithic sandstone, mudstone, shale and conglomerate <1650m thick) in a fluvio-lacustrine environment (Day *et al.* 1983) with sediment sourced from areas in

the north and east. Closure of the Bowen Basin around the Hunter-Bowen Orogeny in the latest Middle to early Late Triassic is bracketed by the youngest preserved sedimentary rocks of the Moolayember Formation. Beeston (1986) estimated that up to 3000 m of strata may have been removed by erosion during the Late Triassic compressive climax, which marked the final act of the Tasman Orogenic System in eastern Australia. Uplift, erosion and folding of the Bowen Basin during Late Triassic times preceded deposition of the unconformably overlying Early Jurassic basal units of the Great Artesian Basin.

### **2.3. Geophysics**

The geophysical databases used in this project provide the key information from which the structure of the Sydney-Gunnedah-Bowen Basin system is derived. Regional gravity data was used for the 2.5D modelling of structure whilst the magnetic intensity maps aid in determining surface volcanic features from deeper structures and seismic reflection profiles show geometry. All these datasets are available for download from Geoscience Australia (GA). This review section is divided into three parts, gravity, magnetics and seismic reflection, and provides a brief overview of the dataset (not the technique itself) and a preliminary assessment of features. A more detailed discussion of the features, and detailed maps, are provided in Chapter 5 for each basin. For gravity, Wynne & Bacchin (2009) provide information with regards to history, coverage and resolution, which is summarised below. There are numerous seismic reflection profiles located in the SGBB so this section is limited to five representative profiles of the basin structure, which are described below.

#### **2.3.1 Gravity**

In Australia, gravity data is available as detailed map sheet surveys, special interest surveys or national grids with a variety of station spacings, ranging from 10 m to over 11 km. Prior to 1990 most surveys had a station spacing of 10 km or more, with most conducted by the Bureau of Mineral Resources as part of the first pass reconnaissance gravity survey of Australia. Since then, surveys have usually been conducted with station spacings of 4 km or less. In the Australian National Gravity Database (ANGD) there are more than 1700 gravity surveys which together contain more than 1.4 million gravity stations.

In August 2008 a new national gravity grid over continental Australia was released by GA, using the new Australian Absolute Gravity Datum 2007, derived from onshore observations from the gravity stations in the ANGD. The gravity units of the new grid are micrometres per second squared ( $\mu\text{ms}^{-2}$ ) with  $1 \mu\text{ms}^{-2}$  equivalent to 0.1 milligals (mGal). The gravity grid has a basic station coverage of 11 km, with South Australia, Tasmania and parts of New South Wales covered at spacing of 7 km and Victoria at approximately 1.5 km. Areas of scientific or economic interest have station spacings of 2 km, 2.5 km or 4 km. The spherical cap Bouguer gravity anomaly, over continental Australia, is the data of interest and is calculated using a density of  $2.67 \text{ t/m}^3$ . GA grids the data using a variable density gridding technique, in the INTREPID Geophysics software package, to a cell size of 0.5 minutes of arc =  $0.0083333^\circ$  (approximately 800 m) for the geodetic grid in the latitude longitude datum of GDA94. In June 2009 a revised version of the continental onshore gravity grid was released, incorporating the results of the September 2008 recent heli-grav survey over the southern Gunnedah Basin. Figure 2.9



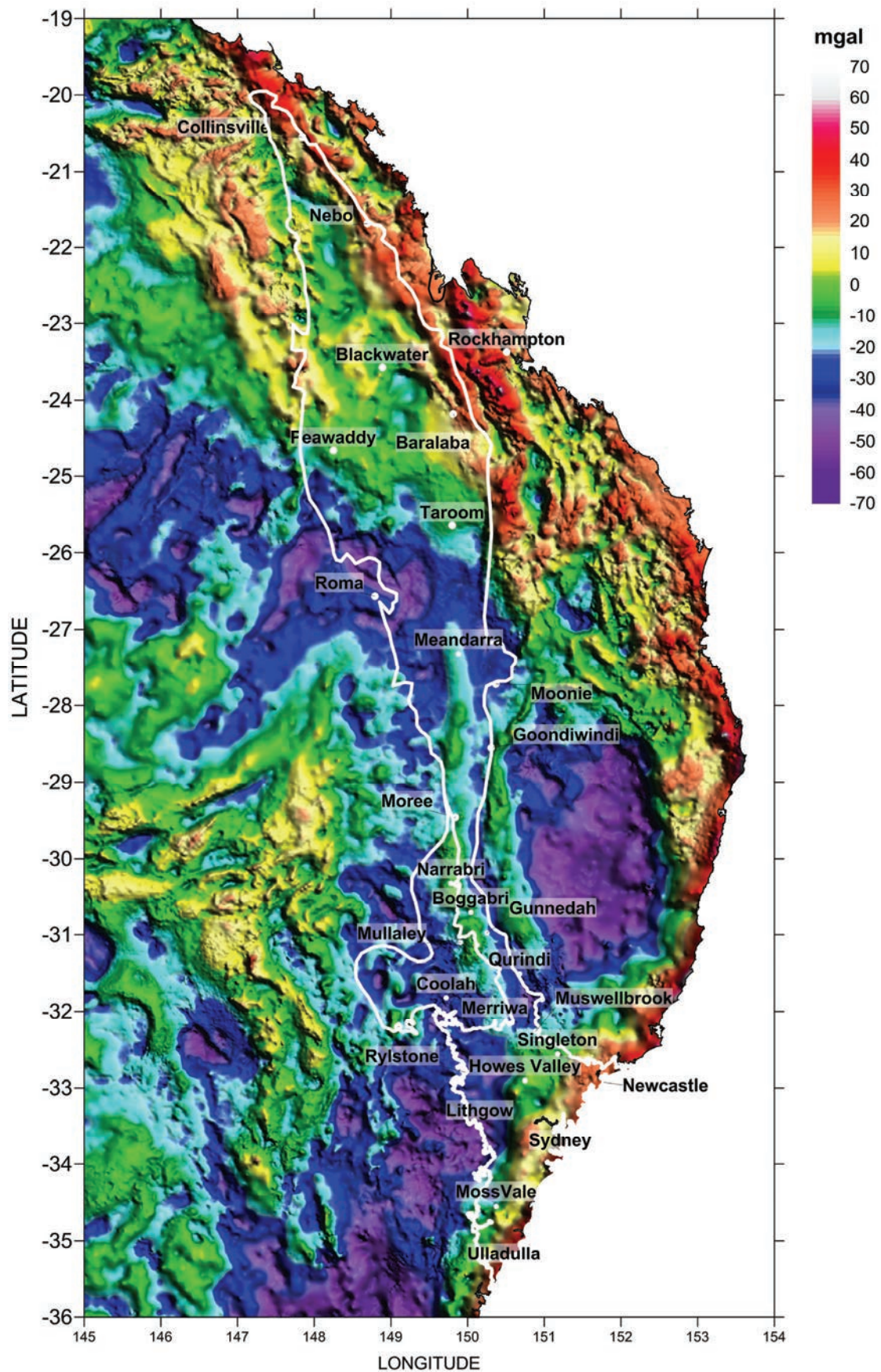


**Figure 2.9** Spherical cap Bouguer anomaly map of the Sydney-Gunnedah-Bowen Basin. Data sourced from the ANG2 0.5 minute onshore gravity grid June 2009 available from Geoscience Australia.

presents the spherical cap Bouguer anomaly map, from the ANG2 0.5 minute onshore gravity grid June 2009, for the Sydney-Gunnedah-Bowen Basin showing illumination from the NE. Gravity anomaly lows are shown as blues to greens and highs are shown as yellow to reds. The known areas of large granite intrusions, such as the New England Batholith (centred around 152°E -30°S), Bathurst Batholith (centred around 149.5°E -33.5°S) and Roma Granites (centred around 149°E -27.5°S) show as distinctive purple gravity lows. Features like the Meandarra Gravity Ridge described by Qureshi (1989) Guo *et al.* (2007) and Krassay *et al.* (2009) appear as a blue to green moderate gravity high in the Gunnedah Basin and southern Bowen Basin between latitude -32°S to -27°S, but is not well defined in the Sydney Basin. Gravity lows in the western part of the Gunnedah Basin and west of Lithgow in the Sydney correspond to exposed mapped granites.

There are several areas of gravity lows that are of interest for the 2.5D gravity modelling as they could represent potential buried plutons. In the Sydney Basin these are north and west of Sydney, north and west of Moss Vale, west of Howes Swamp and around the Muswellbrook – Singleton area. In the Gunnedah Basin areas of interest occur east of Gunnedah and Narrabri. In the Bowen Basin gravity lows are not as prevalent in the northern part of the basin as they are in the central and southern parts. West of Nebo, north-west of Taroom and south of Blackwater are potential areas of interest. The central part of the Bowen Basin, around Roma and Taroom contains the deepest sediment thickness, thus the extent of buried granites around the Roma area are also of interest.

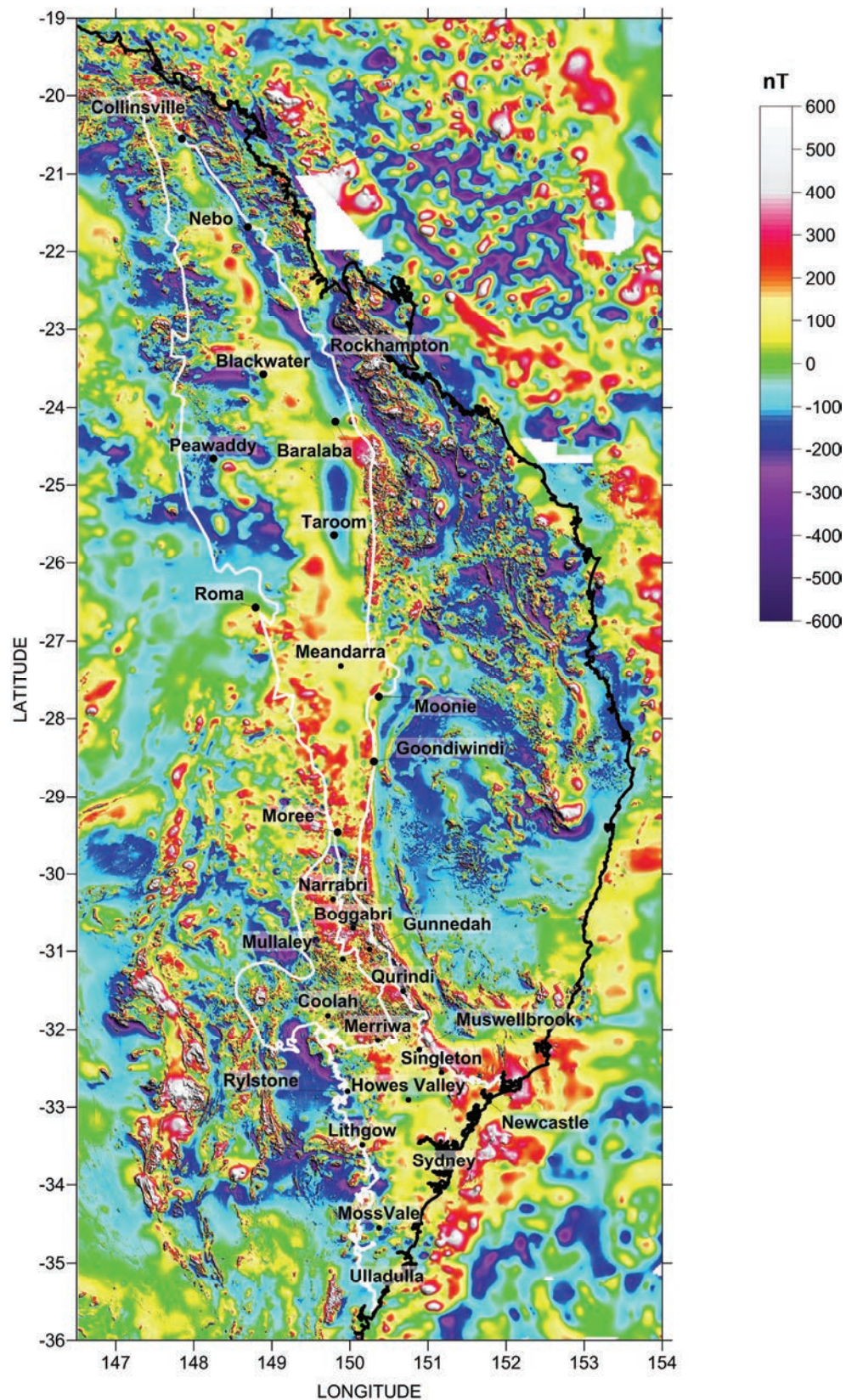
### 2.3.2 Magnetism

Figure 2.10 presents the Total Magnetic Intensity (TMI) map for the Sydney-Gunnedah-Bowen Basin from the 2004 Fourth Edition Total Magnetic Anomaly Grid of Australia. The TMI map is in nanoteslas (nT) with a grid cell spacing of 0.004 seconds of arc (approximately 400 m) and contains onshore and near shore data. Figure 2.10 is a reproduction of the TMI image available for download from GA using the same data set. No additional processing has been undertaken. On the TMI map, areas of low intensity are shown in blue to purple and areas of high intensity are shown in reds to white.

In the Gunnedah Basin many high intensity anomalies are predominantly in response to surface volcanics, i.e. Tertiary and Jurassic volcanics. Exposed basal volcanics, i.e. Boggabri Volcanics along the Boggabri Ridge, also show as high intensity anomalies but their full subsurface extent at depth is ambiguous. In the Sydney Basin some magnetic anomalies correspond to surface volcanics, e.g. the Gerringong Volcanics exposed near Wollongong, south of Sydney, whilst others could relate to deeper features, e.g. Lapstone (east of Lithgow towards Sydney). Qureshi (1984, 1989) and Leaman (1990) model the high intensity anomaly at Lapstone as a dense mafic body at depth, presumed related to the basal volcanics. Offshore of the Sydney Basin, high intensity anomalies may relate to volcanic sea mounts. In the Bowen Basin, the anomalies of interest are the low intensity anomalies around Roma, where there is known buried granites, and around Taroom and Peawaddy where sediments are thick. Exposed volcanics in the northern most part of the Bowen Basin are represented by high intensity anomalies. The resolution of the TMI map is clearer in delineating the shape of anomalies than the gravity map, as areas of magnetic anomalies similarly occur in areas of gravity lows. The exceptions



are the area north of Moss Vale, south of Sydney and around Gunnedah, Narrabri, Peawaddy and Taroom.



**Figure 2.10** Total Magnetic Intensity (TMI) anomaly map for the Sydney-Gunnedah-Bowen Basin. Data sourced from the 2004 Fourth Edition Total Magnetic Anomaly Grid of Australia available from Geoscience Australia.

### 2.3.3 Seismic Reflection Profiles

The seismic reflection method is considered a powerful means of obtaining information on the geometry and structure of the crust and upper mantle as well as sedimentary layers in the upper parts of the crust. Since the late 1950's reflection surveys have been conducted in the Sydney-Gunnedah-Bowen Basin system, initially by the Bureau of Mineral Resources and private survey companies. Results and interpretation of deep seismic reflection profiles have been undertaken by many authors, including R. Korsch, K. Wake-Dyster, D. Johnstone, D. Finlayson, S. Mayne and P. Arditto. Some seismic reflection profiles are available in the Onshore Deep Seismic Survey dataset (Kilgour 2002) from GA, whilst others can be accessed through State Government department archives such as DIGS. Seismic reflection profile interpretations have been done on the following profiles which are of interest to this project;

- BMR84 (Finlayson *et al.* 1990; Korsch *et al.* 1992; Krassay *et al.* 2009),
- BMR91.G01 (Korsch *et al.* 1993, 2009b; Waschbush *et al.* 2009, Krassay *et al.* 2009),
- BMR78.06 (Korsch *et al.* 1992) BMR78.02 (Brakel *et al.* 2009; Korsch *et al.* 2009a),
- BMR 89.B01 (Korsch *et al.* 1992; 2009b; Waschbusch *et al.* 2009),
- AAR 79-S3 (Brown *et al.* 1983),
- SY81-20, SY81-24 (Arditto 2003),
- SY81-26, SY81-34 (E.S.P. Exploration 1982),
- SS04-C (Moffitt 1961),
- SS021-P, SS021-AT (Burbury 1986),
- T4-M41S, M4S (Sesimograph Service Ltd 1965),
- DPI 4, 5, 6 (Minfo 2008),
- SY91-15A (Maung *et al.* 1997; Causebrook 2005),
- CD87-115b, SY91-02, SY91-08, SY91-14 (Blevin *et al.* 2007),
- CD87-112, 118, 119, 122 (Herbert 1989; Blevin *et al.* 2007),
- SS048-U20 (Herbert 1989),
- SY91-01, SY91-12, SY91-14, SY91-16 (Adler *et al.* 1998),
- MAC-22BJ (Korsch *et al.* 2009b; Totterdell *et al.* 2009),
- C83-T-04, 80-P11 (Korsch *et al.* 2009b; Brakel *et al.* 2009),
- P4, 85-B1-G, AD91-17, 84-E413, 83-M231, S784, S785, HIS-1223, 87B-011, 83-52/8, A82-LT-26, HT82-T-109, A82-LT-24, P81-112, B81-2, TH85-273, S78-6 (Korsch *et al.* 2009b),
- SH85-902, A82-LT-26, 86-P4, 85-H1, 87-WD23, 83-R9 (Hoffmann *et al.* 2009),
- 88-Q108, S80-11, 85-B1-G, 85-NGN-6, S86-300, S88-403 (Totterdell *et al.* 2009),
- S84-CT-05, 92-BW-16, 83-52/8, S84-BM-01, C83-GL-02, 79-E12, AD91-03, S78-2, 79-S3, 87-WD24, 84-E413 (Brakel *et al.* 2009), and
- 80-LR1, 81-12, 87-WD22, 87WD24, 87WD-26, R83-81, AD91-12, AD92-02 (Korsch *et al.* 2009a).

Of this extensive list of seismic reflection profiles, this section looks at five key profiles, one from the Gunnedah Basin and two from both the Sydney and Bowen basins (Figure 2.11).

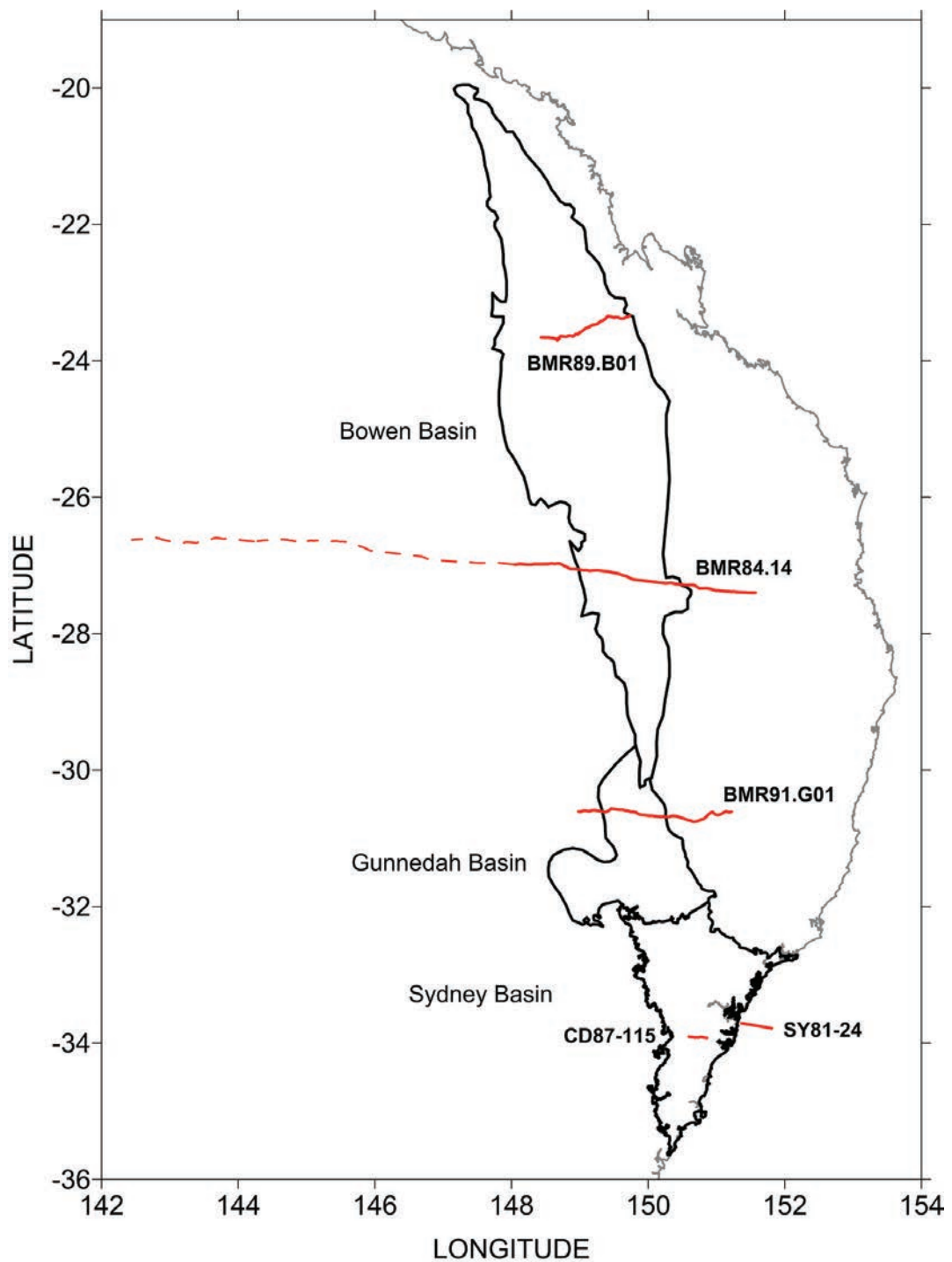


**Figure 2.11** Location map of selected seismic reflection profiles in the Sydney-Gunnedah-Bowen Basin. Profiles shown as red lines. Dashed red line shows the full profile length of BMR84.

In the Sydney Basin, the east-west profile CD87-115 from the Camden area, has been interpreted by Blevin *et al.* (2007) for section CD87-115b (Figure 2.12) and shows a generally flat lying Permian to Triassic sediments, which appear to thicken towards the east. Blevin *et al.* (2007) interprets high-angle, low-to-moderate displacement normal faults offsetting the flat laying sediments. Based on the two-way travel time conversion of Blevin *et al.* (2007) (Figure 2.13) the interpretation suggests basement begins at ~1.75 km on the western end of the profile and deepens to ~2.3 km at the eastern end.



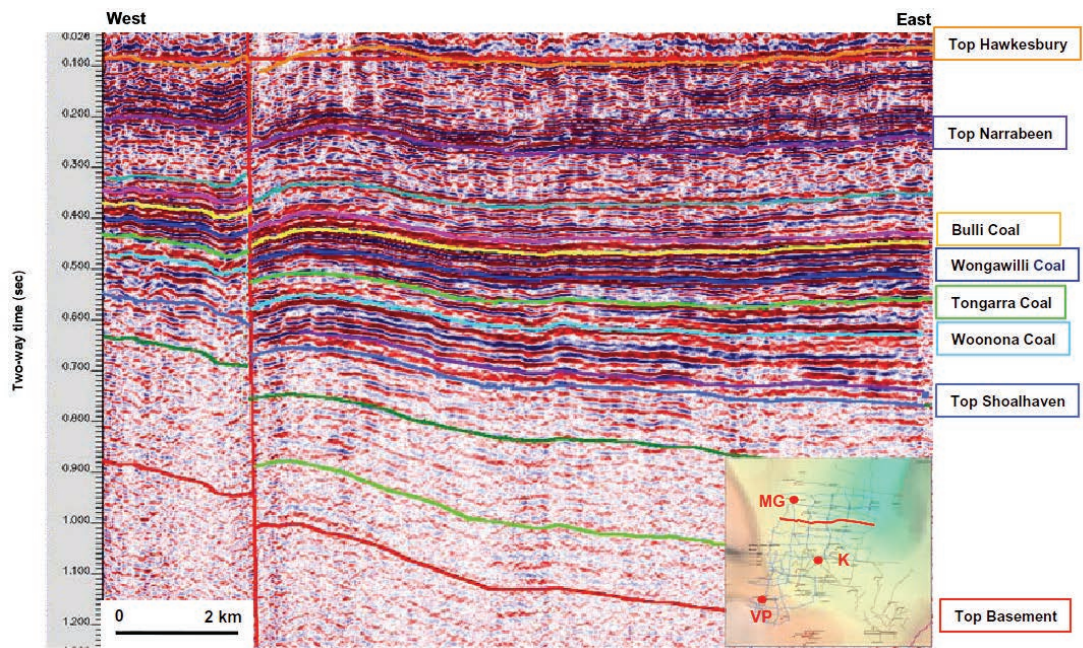


**Figure 2.12** Seismic reflection profile line CD87-115b from Blevin et al. (2007). Map insert shows nearby boreholes MG = Mulgoa 1, KH = Kirkham 1 and VP = Victoria Park 1.

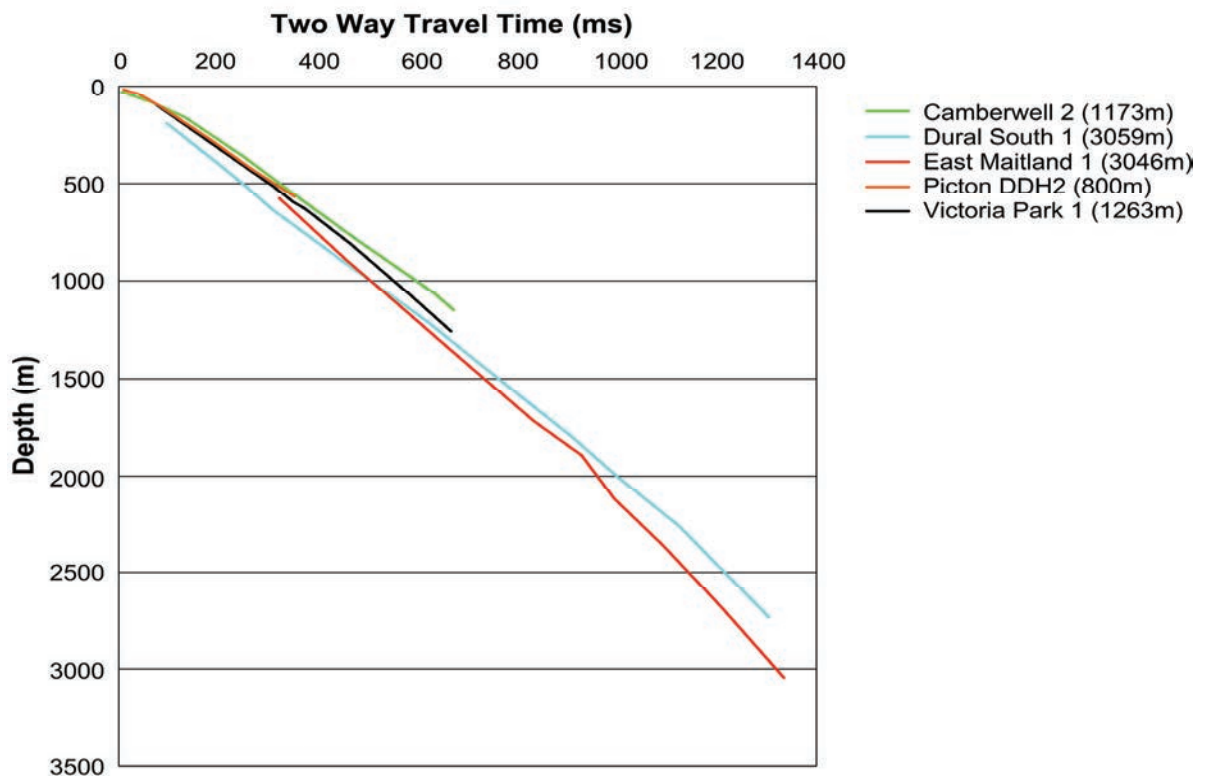


**Figure 2.13** Down-hole plot of well velocity data using check shots, measured in milliseconds two way travel time, against well depth in metres to used to convert seismic reflection profile travel times into depth. Modified from Blevin et al. (2007).

Offshore of the Sydney Basin, profile SY81-24 (Figure 2.14) has been interpreted by Arditto (2003) for economic basement (i.e the dept to the base of petroleum and or coal bearing units as shown by the blue line), the top of the Gerringong Volcanics (green line) and the base of the Narrabeen Group (light

blue line). Numerous faults (red lines) are also interpreted. In this profile, near the coast (SP 0) the basement is deepest and then shallows towards SP 800, associated with the structure of the offshore uplift (Figure 2.3). Using the two-way travel time conversion (Figure 2.13), basement depth is estimated at ~3 km close to the coast, shallowing to ~2 km over the offshore uplift before deepening to ~3.5 km near the continental shelf.

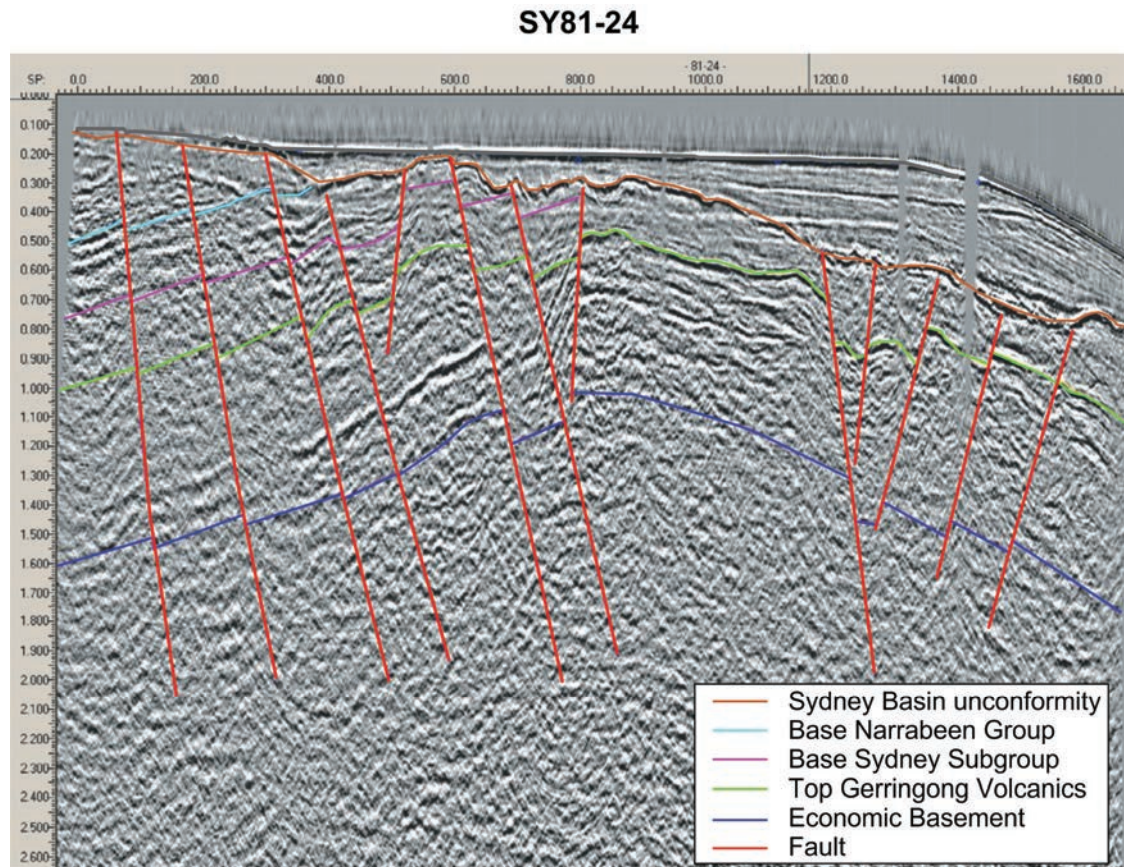


**Figure 2.14** *Interpreted seismic reflection profile SY81-24. Modified from Arditto (2003).*

In the Gunnedah Basin, profile BMR91.G01 (Figure 2.15) shows the geometry and structure through the northern part of the basin. Korsch *et al.* (1993) provides an interpretation of the seismic reflection profile and a detailed interpreted geological cross-section through the Gunnedah Basin (Figure 2.15b). The profile shows the Lachlan Fold Belt exposed on the surface in the west at the Rocky Glen Ridge and then extending underneath the sediments of the Gunnedah Basin to be truncated by the Tamworth Belt at the Kelvin Fault and the New England Fold Belt at the Peel Fault. A closer look of the profile across the Gunnedah Basin shows the basal Permian Volcanic unit (of the Boggabri Volcanics and Werrie Basalt) is underneath the sediments of the Gunnedah Basin and truncated by the Kelvin Fault. The basal volcanics interpreted at the surface, in the centre of the Gunnedah Basin, are correlated with the exposed Boggabri Ridge. On the edge of the Gunnedah Basin the geometry of the major faults is clearly observable. Sediments from the Gunnedah Basin are interpreted to extend some distance down the Mooki Fault before being truncated at the base of the Kelvin Fault. Korsch *et al.* (1993) interprets a large amount of volcanics at the base of the Gunnedah Basin at depths of 1 km or less (based on the two-way travel time conversion in Figure 2.13).



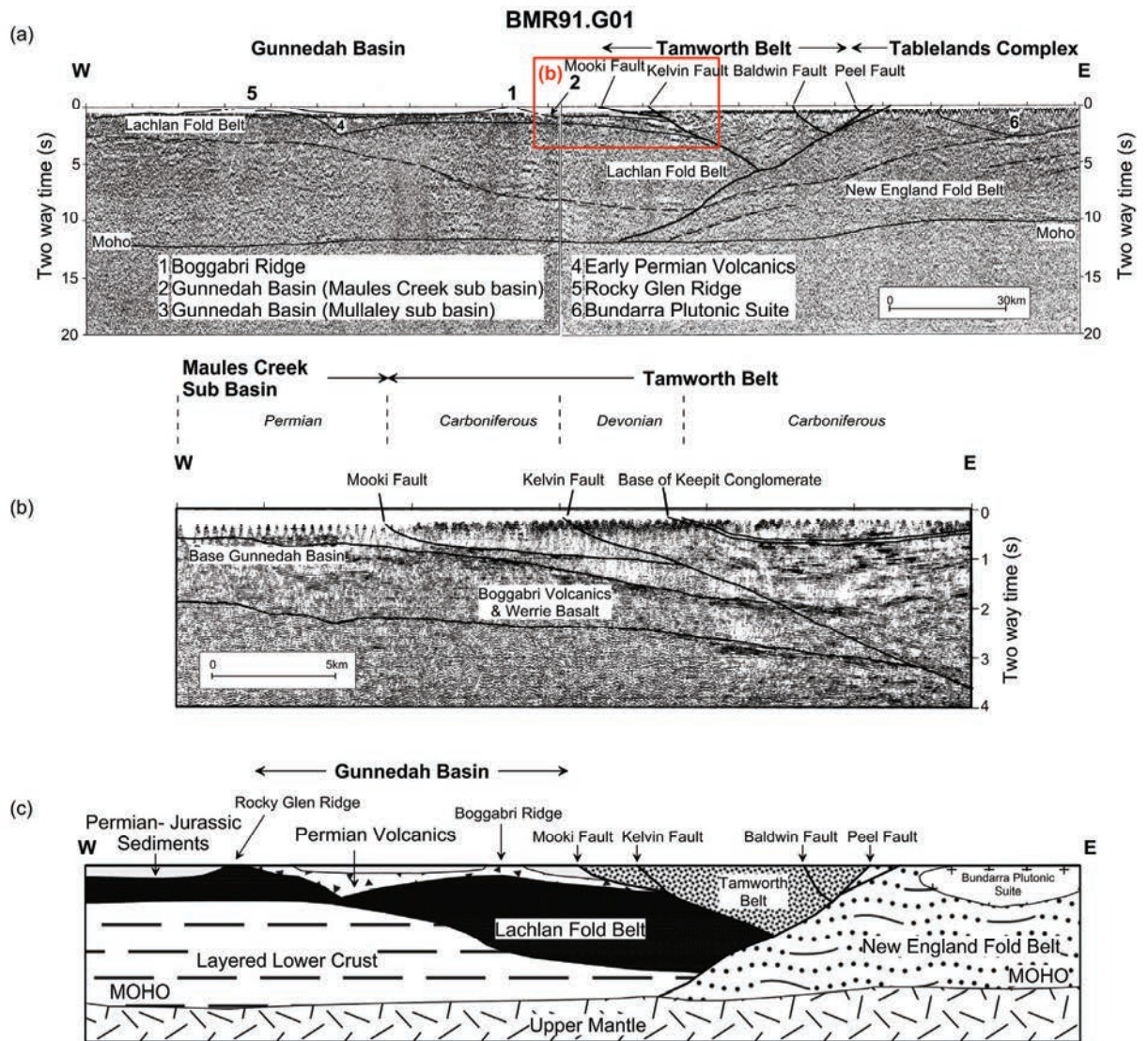


**Figure 2.15** (a) Interpreted deep seismic reflection profile BMR91.G01 of the Gunnedah Basin with (b) close up of the Gunnedah Basin near the Mooki Fault and (c) an interpreted geological cross-section. Modified from Korsch *et al.* (1993).

In the central Bowen Basin, the east-west deep crustal profile of BMR84.14 (Figure 2.16a) highlights the complete geometry of the basin with a typical extensional rift basin, Early Permian volcanics and deep thick sediments bounded on each side by shallower basement (Figure 2.16c). A separate BMR survey was conducted across the Taroom Trough (Figure 2.16b) and has been interpreted by Kilgour (2002). This profile, although it does not entirely match BMR84.14, because the location of overlap is approximate only, it shows a similar basement structure with the boreholes used to pick stratigraphic horizons marked. Using the two-way travel time conversion (Figure 2.13) depth to basement in the Taroom Trough is estimated at approximately 6 km.

In the north-eastern part of the Bowen Basin seismic reflection profile BMR89.B01 (Figure 2.17) shows the geometry over the eastern edge of the basin is a highly faulted area. In the interpreted geological cross-section (Figure 2.17b) Korsch *et al.* (1993) suggest the basement is the Thomson Fold Belt, which extends under the Jellinbah Thrust before truncating on the New England Fold Belt.

Basement in the Blackwater Zone is estimated by Korsch *et al.* (1993) to be approximately 3 km deep and almost 6 km deep under the Yarrabee Thrust.

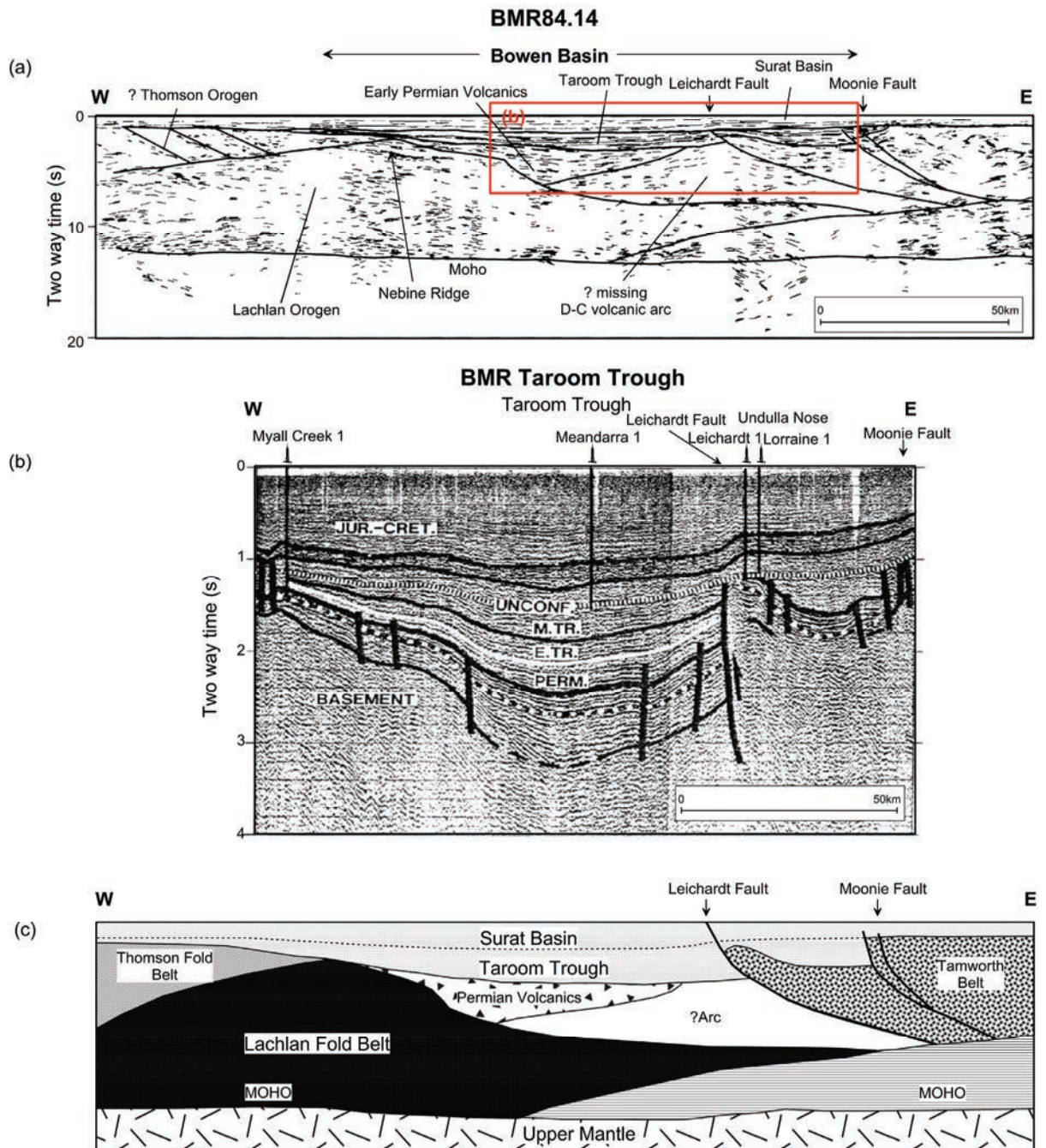


**Figure 2.16** (a) Interpreted deep seismic reflection profile BMR81.14 of the Bowen Basin with the red box the approximate location of (b) a BMR profile across the Taroom Trough with boreholes (modified from Kilgour 2002) and (c) the interpreted geological cross-section of BMR81.14 (modified from Korsch *et al.* 1993).



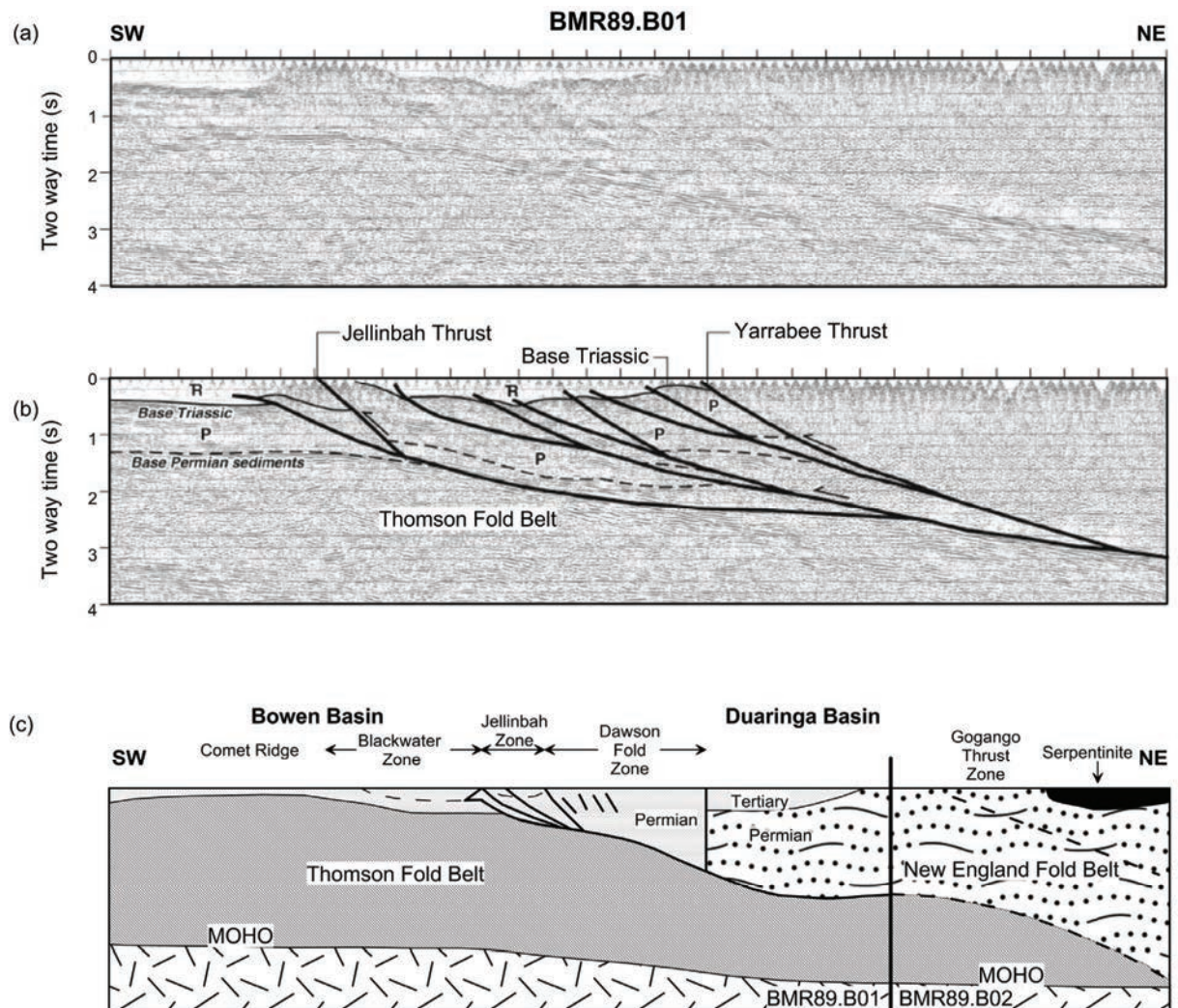


**Figure 2.17** Deep seismic reflection profile BMR89.B01 north-eastern Bowen Basin (a) unmigrated profile, (b) interpreted structure (Korsch et al. 2009b) and (c) interpreted geological cross-section of BMR89.B01 and extension BMR89.B02 (modified from Korsch et al. 1993).

#### 2.4. Geothermal Exploration in Australia and the Geothermal Potential of the Sydney-Gunnedah-Bowen Basin System

Geothermal resources generally fall into two categories, the conventional hydrothermal systems associated with volcanic magmas fields i.e. New Zealand, and the non-conventional hot rock resources. In Australia, geothermal resources are generally considered non-conventional and are categorized into three systems; engineered geothermal systems (EGS), hot sedimentary aquifers (HSA) and shallow warm aquifers. EGS and HSA are currently being explored in Australia, as the main future for potential geothermal power, because of vast resource estimations. Terms like hot fractured rock (HFR) or hot dry rock (HDR) in EGS are commonly used to describe subsurface rocks which are abnormally hot but lack significant water for extraction. The purpose of this review is not to describe in detail the mechanics of EGS or HSA, but rather to provide a brief understanding of the methods and identify key requirements for exploration in Australia. Figure 2.18 compares the typical conventional volcanic geothermal system with the EGS and HSA in terms of geological system and temperature requirements.



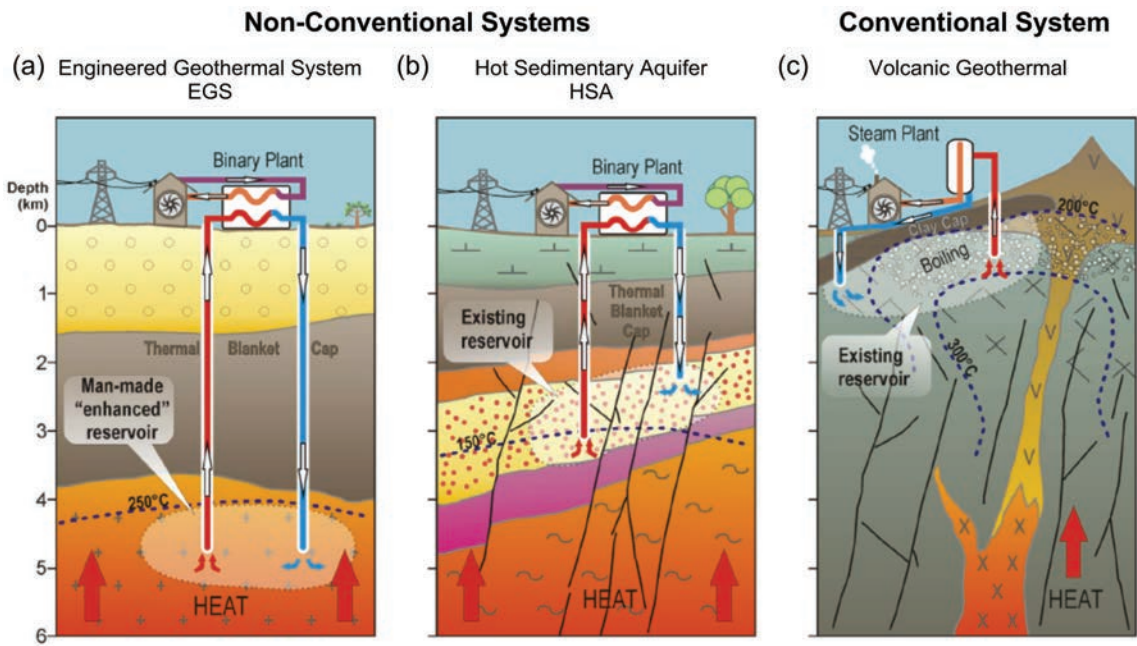


**Figure 2.18** Conceptual models of conventional and non-conventional geothermal systems (a) Engineered Geothermal System (EGS), (b) Hot Sedimentary Aquifer (HSA) and (c) Volcanic Geothermal. Modified from Hot Rock Ltd (2009).

In both EGS and HSA, cold water is pumped down an injection well under pressure, flows through the medium, is heated and returned to the surface through a production well. The EGS system is essentially a closed loop system using the trapped heat from the radioactive decay of heat producing elements whilst HSA uses groundwater aquifers which are heated from a deeper source. Both these techniques require the heat source to be buried under several kilometres of insulating sediments. Shallow warm aquifers, similar to HSA but to a shallower depth, are currently the only geothermal resource exploited in Australia. At Birdsville, Queensland, a small binary power station sources hot (98°C) groundwater from the Great Artesian Basin producing 120 kW of power for the town (Goldstein *et al.* 2008).

For non-conventional geothermal systems in Australia to be successful there needs to be anomalous hot temperatures, i.e. greater than 150°C, at depth with the source, either granite or aquifer, under insulating rock cover to trap the generated heat (Goldstein *et al.* 2008). Current drilling technology limits economic development, and therefore exploration, to targets within about 5 km (Budd *et al.* 2008) depth.

#### 2.4.1 History and Development 1994 to 2008

Research aimed at evaluating Australia's resources of hot rock geothermal resources started in 1994 (Burns *et al.* 2000) with a collaboration of groups headed by the Australian Geological Survey Organisation. They began by creating the continental dataset GEOTHRDD, which contained the bottom-hole temperatures of over 3000 boreholes, and produced an extrapolated temperature at 5 km depth map of the continent (Figure 2.19a). This map, produced by Somerville *et al.* (1994), allowed the first assessment of temperature a depth and resource potential. The total Australian resource base was estimated at around 22 million petajoules, with a surface area of almost 230,000 km<sup>2</sup> and a rock

volume of around 344,000 km<sup>3</sup> (Burns *et al.* 2000). Almost 80% of the resource was found to be concentrated in central Australia, the north-eastern corner of South Australia and the south-western corner of Queensland.

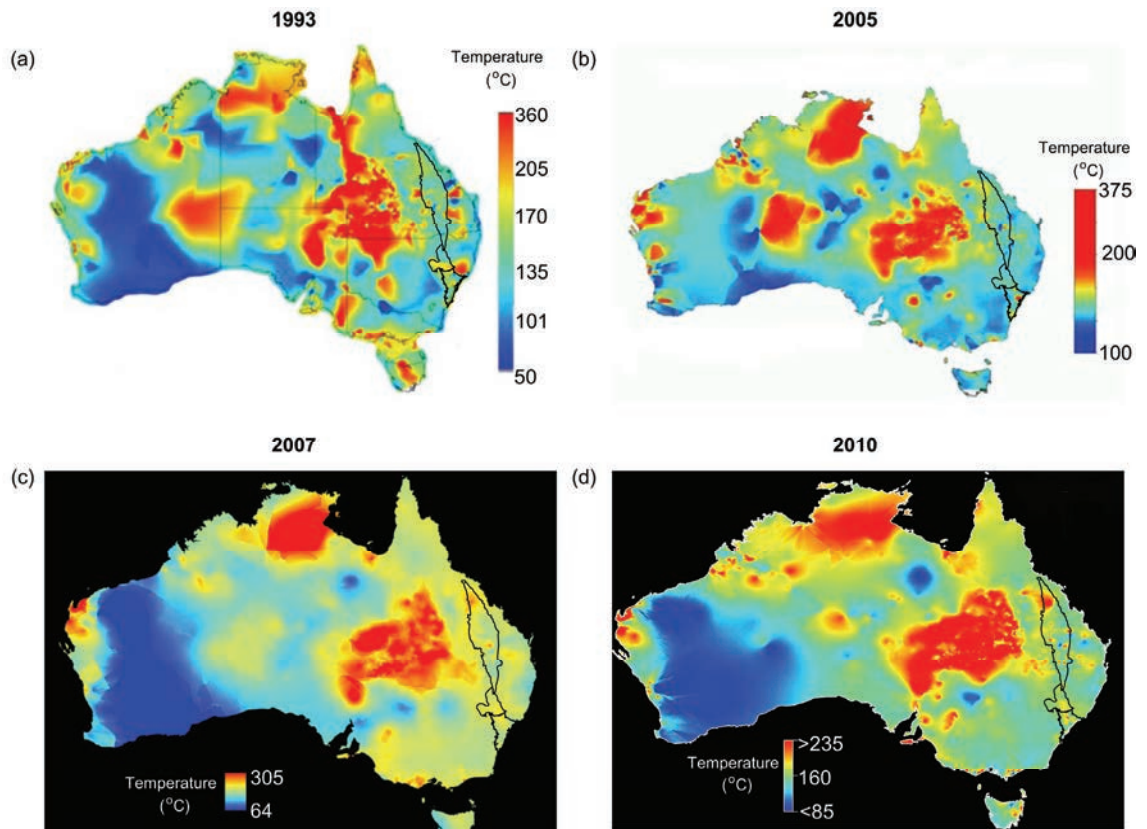


**Figure 2.19** Extrapolated temperature at 5 km depth over continental Australia with the Sydney-Gunnedah-Bowen Basin outlined (a) the 1993 estimate (modified from Deep Energy 2009), (b) the 2005 estimate (modified from Deep Energy, 2009), (c) the 2007 estimate using the Austherm07 database (modified from Budd *et al.* 2007) and (d) the 2010 OzTemp estimate (Gerner & Holgate 2010).

Prior to 1997, development of geothermal resources in Australia consisted primarily of under-utilised hydrothermal systems, water source heat pumps and feasibility of deep-seated Hot Dry Rock studies in the Cooper Basin (Burns *et al.* 2000). Around 1998 the New South Wales Department of Mineral Resources recognised the status of hot rocks as a 'Group 8' mineral, meaning the resource may be explored under the mineral rights of the Crown and development cannot be resisted by individual owners of surface property rights (Burns *et al.* 2000). This led to the first competitive exploration licences and the beginning of geothermal resource companies. Hot Rock Energy Pty Ltd and Pacific Power Corporation were the first companies to begin geothermal exploration in Australia. Since 2001, 33 companies have begun exploring for geothermal resources with 283 licence application areas covering approximately 231,000 km<sup>2</sup> (Goldstein *et al.* 2008), predominately in South Australia in the resource areas identified on the map of Somerville *et al.* (1994).

Chopra & Holgate (2005) combined over 1000 new bottom-hole temperature measurements with the continental dataset to create a new database called Austherm05 and a new extrapolated temperature

at depth map (Figure 2.19b). In 2006 Geoscience Australia (GA) started the Geothermal Energy Project as part of the Onshore Energy Security Program (Budd *et al.* 2008). GA identified that the greatest geological need was an improved understanding of the distribution of temperature in the upper crust of Australia and the existing datasets that map temperature and heat distribution both suffered from insufficient data points compounded by poor data distribution. Improvements began with GA collecting more bottom hole temperature measurements and heat flow measurements, purchasing the Austherm05 database, utilising the OzSEEBASE™ crustal sediment thickness work of FrOG Tech (2006) and created the Austherm07 database and extrapolated temperature at depth map (Figure 2.19c). In Figure 2.19 the evolution of estimated temperature at 5 km depth can be seen between 1993 and 2010. As more data is added and the extrapolation process refined, temperature anomalies become more defined and new anomalies appear.

Around late 2006 the Australian Geothermal Energy Group (AGEG) formed (Goldstein *et al.* 2008), representing a mix of industry, government and academic researchers, and created technical interest groups to deal with the issues emerging in the geothermal industry. AGEG is the body formed to provide support for Australia's membership in the International Energy Agency's Geothermal Implementing Agreement (IEA-GIA) and has overlapping membership and aims with the Australian Geothermal Energy Association (AGEA) (Beardsmore & Hill 2010). AGEA, formed in 2007, is the national association of the geothermal industry, whose primary members are exploration, development and service companies, and its mission is to accelerate the development and commercialization of Australia's geothermal energy resources.

In the mean time, geothermal companies were drilling wells and building trial plants to try and demonstrate their geothermal energy potential. Geodynamics completed its first demonstration well in 2003, Habanero 1, and since this time, up until early 2008, over 40 geothermal wells have been drilled by 8 major companies (Goldstein *et al.* 2008). The significant players in the geothermal industry in Australia are; Geodynamics, Petratherm, Green Rock Energy, Panax, Geothermal Resources Ltd, Torrens Energy, Eden Energy, Pacific Hydro and KUTh Energy Ltd.

Five principle focus topics of research in the geothermal industry in Australia have been identified by Goldstein *et al.* (2008) as:

- 1) identification and targeting of locations with high potential for geothermal development;
- 2) reserve and resource definitions;
- 3) assessment of technologies;
- 4) environmental impacts; and
- 5) modelling future energy supply.

This research project aims to address the needs of the first research topic by using numerical thermal modelling as a more effect tool in geothermal exploration target identification than temperature extrapolation maps.

#### **2.4.2 Data gaps and problems in geothermal exploration**

Reviewing the history and development of geothermal exploration and information in Australia highlights what the main data gaps are; the sparse coverage of measured temperatures, the limited heat flow measurements, the limited knowledge of granite chemistry, the limited measurements of the thermal properties of sedimentary rocks and the limited models of sediment thickness. GA is putting considerable effort into collecting this necessary information as part of their geothermal energy project but this review has detected several issues in the data.

The first problem is the use of bottom-hole temperature information for temperature extrapolation maps. Very little of the temperature data collated in the Austherm04 database was collected specifically for geothermal exploration, the majority is sourced from petroleum, mineral exploration and groundwater bores (Chopra & Holgate 2005) at the time of drilling. These measurements taken immediately after the cessation of drilling, or up to a few days later, do not represent the thermal equilibrium of the surrounding geology. They are non-equilibrated and as a result when extrapolated these temperatures may not reflect an accurate estimate at depth. Although corrections for non-equilibrated measurements can be done, generally by the old traditional method of Horner plots, they have been shown by authors like Deming (1989), to depend strongly on assumptions that may not be justified, and critically, most empirical corrections seem to only work within the geothermal field in which they have been derived.

The second major problem is the use of extrapolated temperature maps for geothermal resource assessment. Extrapolation maps require a 1D linear 2 layer model (e.g. Chopra & Holgate 2005) of sediment overlying basement and use the geothermal gradients derived from the bottom-hole temperatures to estimate temperature at 5 km depth. Extrapolation maps poorly account for the structure of sedimentary basins and the important thermal effects of their geology and architecture.

Musson *et al.* (2009) identified that the ability of geothermal resources to be accurately assessed in Australia is limited by scarce/inaccurate thermal datasets (extracted mostly from shallow drill-holes), oversimplified interpretations and under-constrained thermal models. In reviewing the development and history of geothermal exploration in Australia, this project identifies that the ability to accurately assess and estimate temperature at depth is the key to successful geothermal exploration and resource development.

#### **2.4.3 Geothermal potential of the Sydney-Gunnedah-Bowen Basin system**

With interest predominantly in the north-eastern part of South Australia, central Australia and south-western Queensland the geothermal potential of the Sydney-Gunnedah-Bowen Basin is not well considered. The extrapolated temperature map of Somerville *et al.* (1994) and the Austherm07 map (Figure 2.19c) shows the SGBB has predominantly a moderate temperature (yellow) of approximately 240°C. There are a few areas of high temperature (red) but they are small and isolated and not nearly as attractive for geothermal exploration as the extensive high temperatures in the Great Artesian Basin. Looking at the distribution of wells (Figure 2.20a) the majority of temperature measurements are concentrated in the Great Artesian Basin and there is sparse data in the SGBB. The number of down-

hole heat flow measurements are also limited, with approximately 200 (Budd *et al.* 2007), as shown in Figure 2.20b, and with such sparse coverage a meaningful continental scale heat flow map is not possible. Heat flow in the southern part of the Sydney Basin has been measured between 66 to 113  $\text{mWm}^{-2}$  and 66 to 84  $\text{mWm}^{-2}$  in the Gunnedah Basin. In the Bowen Basin heat flow measurements range from 26 to 65  $\text{mWm}^{-2}$ .

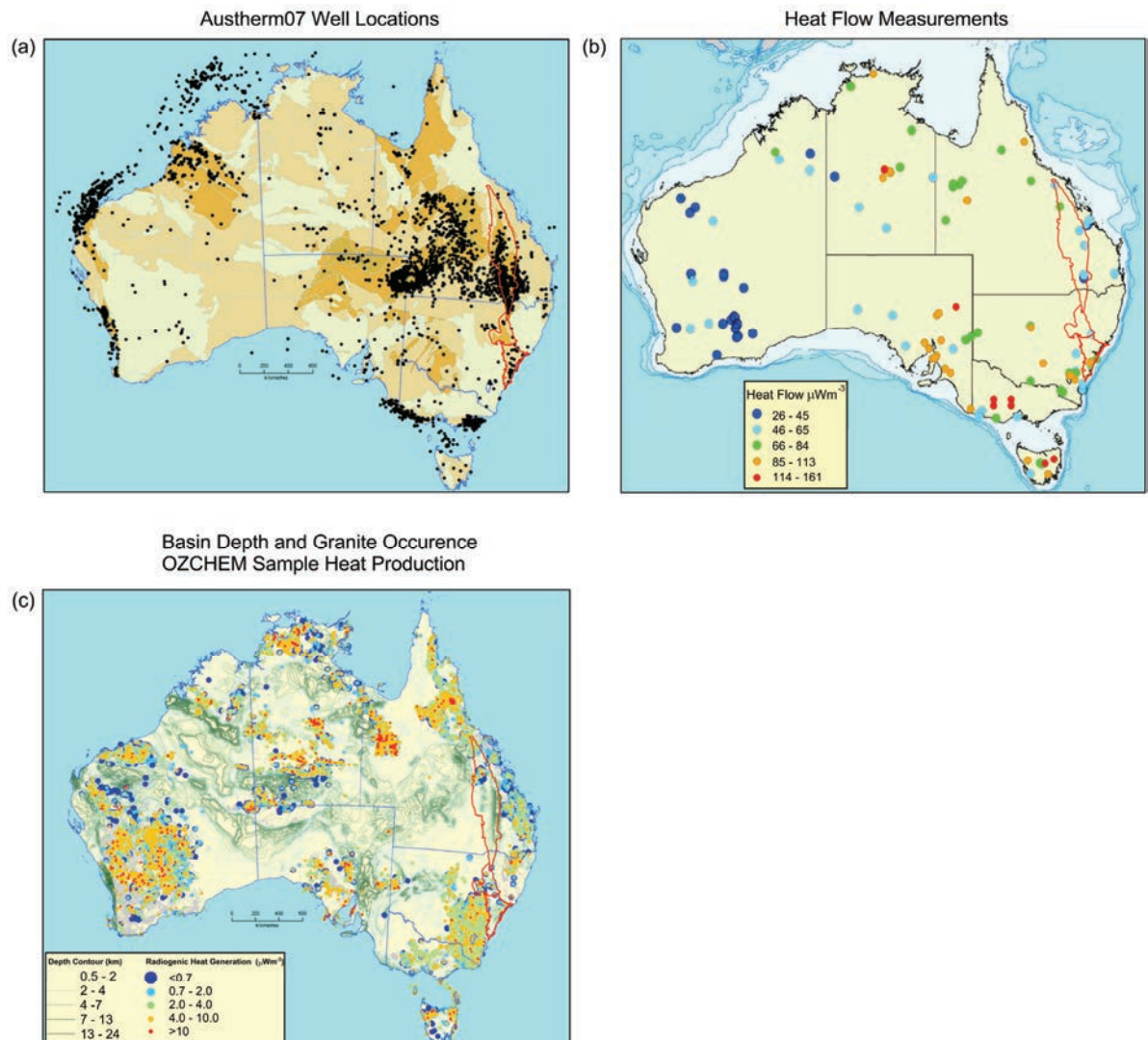


**Figure 2.20** Key database distributions and results for continental Australia with Sydney-Gunnedah-Bowen Basin outline in red (a) location of Austherm07 wells (modified from Budd 2007), (b) heat flow measurement values and location (modified from Barnicoat & Ernst 2010) and (c) OZCHEM samples for heat production with basin depth contours (modified from Budd 2007).

Granite is essential for producing the heat source and surface samples provide an understanding of chemistry and radiogenic heat output that can be used when mapping deeply buried granites. Figure 2.20c shows the location of OZCHEM samples for which radiogenic heat production values have been calculated. In the SGBB samples record on average radiogenic heat production values of 0.7  $\mu\text{Wm}^{-3}$  to 4.0  $\mu\text{Wm}^{-3}$ . Two samples in the western Gunnedah Basin and one in the northern Bowen Basin have a radiogenic heat production values greater than 10  $\mu\text{Wm}^{-3}$ .

Despite the limited data coverage in the SGBB there does appear to be good geothermal potential yet to be explored. The extrapolated temperature map, even with its limitations, suggests temperature at 5 km depth is close to the critical levels required for EGS and well within range of the temperature levels required for HSA. The surface granites have moderate to high radiogenic heat production values, therefore the expectation is, that buried granites could also be similar.

The next chapter, Chapter 3, discusses the previous work in the Sydney-Gunnedah-Bowen Basin which is relevant to the proposed work of this project, as well as outlining the available information databases.



# CHAPTER 3

## PREVIOUS WORK AND DATABASES



*Hands on Rock, Ulan NSW*

## PREVIOUS WORK AND INFORMATION DATABASES

### 3.1 Previous Work

This section provides a brief discussion of relevant previous studies in the Sydney-Gunnedah-Bowen Basin, with a specific emphasis on research that determines basin structure through modelling. The Sydney-Gunnedah-Bowen Basin has been a focus of ongoing exploration for many years and as such, a wealth of information has built up regarding its structure, history and resource distribution. There have been many early basin reservoir style studies, primarily by private exploration companies, with the principle purpose of determining reservoirs suitable for oil and gas production. These are not discussed here. The primary works that are relevant to this project are the gravity modelling of Krassay *et al.* (2009) and Guo *et al.* (2007) in the Gunnedah Basin and gravity modelling of Qureshi (1984, 1989) and gravity and magnetic modelling of Leaman (1990) in the Sydney Basin. These works show that gravity modelling is a fundamental tool for mapping the extent and depth of sedimentary basins and provide a basic understanding of the structure of the SGBB.

In the Sydney Basin, Leaman (1990) was the first to conduct basin-scale gravity and magnetics modelling, with 13 north-west south-east orientated profiles and 2 south-west north-east orientated profiles, to assess the structure and depth of the basin. He suggests, from gravity modelling that on the onshore segment of the Sydney Basin has sediment thickness up to 4 km thick, and notes the magnetic data does not help much other than to show that the gravity estimates are not wildly erratic. Qureshi (1984, 1989) earlier modelled a single regional-scale gravity profile east-west through the Sydney Basin over a significant gravity high. He models sediments of the Sydney Basin, up to 4 km thick, overlying a dense mafic body, over 10 km in thickness, which he suggests could be to be part of the Meandarra Gravity Ridge.

This Meandarra Gravity Ridge is further studied by Krassay *et al.* (2009) and is interpreted to be rift related volcanics which formed at the inception of the SGBB. The work of Krassay *et al.* (2009) primarily looks at the asymmetric nature of the Meandarra Gravity Ridge and his model profiles, which transect the Gunnedah Basin and Bowen Basin, provide a preliminary estimate on sediment thickness and basin geometry. His gravity models showed that low density granites in the Lachlan Fold Belt basement are needed to fit the observed gravity data and in general the geometry represents an extensional rift origin for the basins. Guo *et al.* (2007) took Krassay's work in the Gunnedah Basin a step further with the collection of 5 new east-west gravity profiles to model the basin's profile. He showed that with forward gravity modelling the anomalies can generally be explained using the densities of the presently exposed rock units. In the Gunnedah Basin Guo *et al.* (2007) modelled a mafic volcanic body with a thickness of 4.5 to 6 km under a sediment thickness of 1 to 4 km associated with the Meandarra Gravity Ridge. He shows it is possible to produce a good match between the observed gravity data and the calculated gravity profile with a rift configuration, though slight adjustments to the shape of the mafic volcanic body and the thickness of the sediments is required for the best fit per profile.

Both Krassay *et al.* (2009) and Guo *et al.* (2007) use seismic reflection profile data as constraints on their gravity models, but make no attempt to incorporate any nearby borehole information as a constraint. Qureshi (1984, 1989) and Leaman (1990) use both, although Leaman (1990) does note



that there can be some discrepancy between modelled depths and borehole depths, sometimes around 500 m, but he considers it acceptable. The work of these four authors provides a good background on the geometry of the SGBB and the effectiveness of gravity modelling in determining structure. What is lacking is a compiled 3D depth to basement structure which incorporates the geological constraints of exposed geology and boreholes with the constraints of seismic reflection profiles.

The Sydney Basin reservoir prediction study by FrOG Tech (Blevin *et al.* 2007) is the first attempt at a 3D basin scale model. It uses gravity and magnetic modelling, seismic reflection profiles and borehole information to develop the OZ SEEBASE™ depth to economic basement map. Economic basement is defined as the base of coal and petroleum bearing units and therefore excludes the sedimentary sequences of the lower Sydney Basin as well as the mafic volcanics and basement rocks. The OZ SEEBASE™ model shows a relatively flat surface for economic basement, with average sediment thicknesses of 3 to 5 km, but does not provide any information on the geometry of the deep basin structure, as a result of modelling to economic basement. As a commercial product the transparency of the model is difficult to gauge and as such it's not considered an adequate guide for the modelling work in this research project.

### **3.2 Databases and Information**

There is a vast amount of data available for the SGBB in the published research, Government databases and private company reports. The compilation works, such as those of Herbert & Helby (1980) on the Sydney Basin and Tadroz (1993) on the Gunnedah Basin provide a wealth of knowledge and information. The main other sources of information come from boreholes, interactive resource maps and data packages.

#### **3.2.1 Boreholes**

Stratigraphic information from boreholes is essential in calibrating the gravity models and creating 3D surface interpolation. Two major databases are available online to search. DIGS <<http://digsopen.minerals.nsw.gov.au/>> is the NSW Governments online report database, where non confidential borehole completion reports, mining reports, exploration reports, maps etc are available to download for free. The Queensland Government has digital exploration reports online through QDEX <<http://www.dme.qld.gov.au/mines/index.cfm>> which requires membership for access. Appendix B presents a compilation of all boreholes used in this project, gathered from these online databases and other sources, in both a spreadsheet and Google Earth™ file.

#### **3.2.2 Interactive Resources**

Interactive resources include online maps which provide link to databases where specific information is stored. They show a visual distribution of data, generally in a GIS style interface, making it easy to query and access. The following interactive resources were used in this project:

- Geoscience Australia: Petroleum Wells Database  
<<http://dbforms.ga.gov.au/www/npm.well.search>>
- NSW Department Primary Industries: MinView  
<<http://www.minerals.nsw.gov.au/mv2web/mv2>>

- QLD Department Employment Economic Development and Innovation: Interactive Resource Data and Tenure Maps  
<[http://www.dme.qld.gov.au/mines/interactive\\_resource\\_data.cfm](http://www.dme.qld.gov.au/mines/interactive_resource_data.cfm)>  
<[http://www.dme.qld.gov.au/mines/tenure\\_maps.cfm](http://www.dme.qld.gov.au/mines/tenure_maps.cfm)>
- Geoscience Australia: MapConnect  
<[http://mapconnect.ga.gov.au/MapConnect/?site=Geology&accept\\_agreement=on](http://mapconnect.ga.gov.au/MapConnect/?site=Geology&accept_agreement=on)>
- United States Geological Survey: SRTM  
<[http://dds.cr.usgs.gov/srtm/version2\\_1/SRTM3/Australia/](http://dds.cr.usgs.gov/srtm/version2_1/SRTM3/Australia/)>

### **3.2.3 Pre-compiled Data Packages**

The following pre-compiled database packages have been obtained from the NSW Department of Primary Industries for use in this research:

- Bowen and Surat Basins petroleum data package (2002),
- Sydney Basin Reservoir Prediction Study (September 2007),
- Sydney Basin Geothermal Data Package (August 2008), and
- Hunter-Mooki Seismic Survey (September 2007).

The next chapter, Chapter 4, presents the methodologies of this research in the context of an overview of the development of the project workflow.

# CHAPTER 4

## METHODOLOGY



*Wombeyan Caves Road, Bullio NSW*

## METHODOLOGY

This chapter provides a detailed description of the methodology and techniques used in this project and an overview of the workflow development. The majority of methodologies described here as also stated within their relevant papers, but to a detail suitable for publication. Where necessary, in this section, the detail and rational of the methodologies has been expanded.

This chapter has been structured to show a logical progression of workflow beginning with gathering data from boreholes, including coal percentage calculations, temperature measurements and temperature logging and leading into climate corrections and temperature extrapolation. Following this, are the geophysical techniques of density sampling and calculation and gravity measurement and gravity modelling. Then next is the construction of surfaces for the 3D model followed by an evaluation of the 3D model in a data distribution and analysis system (dDAS) map and lastly the numerical thermal modelling techniques.

### 4.1 Borehole Data

Borehole data forms part of the essential core of information required in this project. From the various data packages and interactive resources outlined in Chapter 3, numerous borehole logs were accessed for stratigraphic and other useful information as presented in the master spreadsheet of Appendix B.

The first major information requirement is stratigraphy depth. Without this, calibration of gravity models could not be achieved. The majority of borehole records, especially those prior to the early 1970s and 1980s, were recorded in feet and required conversion to metres. Positioning information varied depending on the year of drilling and has been converted, as best as is possible, to the current Geodetic Datum of Australia 1994 (GDA94). Ground elevation data is available for some of boreholes whilst others are relative to the Kelly Bushing (KB), which is the height of the rotary table from the ground. This height is relatively standard, between 1 to 4 metres depending on the rig and is considered accurate to use as ground elevation, when no ground elevation is recorded. Where no elevation data is available an approximation has been made from SRTM data.

The next key information to extract from the borehole records is the average percentage of coal in the major coal bearing strata, as outlined in section 4.1.1. This information is essential for numerical thermal modelling, as individual coal layers are too small to input into a basin scale model, requiring representative coal interval with an appropriate percentage of coal, shale and sandstone, the major lithologies.

Down-hole temperature information is another valuable dataset and is required both for temperature extrapolation and thermal modelling. Temperature information, if recorded, is primarily from drill stem test results and geophysical logging. Section 4.1.2 outlines the types of temperature measurements available from the databases and the field collection of new down-hole temperature measurements.

#### 4.1.1 Coal Percentage Calculations

The percentage of coal in the sediments of a coal interval is calculated from detailed drilling logs in each basin. Only logs which have detailed core descriptions or composite logs are of use. In order to ensure the entire coal bearing sequence is assessed only boreholes which contain a representative amount of stratigraphy and reach either basement, basal volcanics or in the case of the Sydney Basin the coal free lower Permian units can be used. This is problematic as few boreholes reach basement and on the edges of the basin if they reach basement they start mid way through the Permian sequence. 104 boreholes satisfied the criteria and the calculations and strata percentages are shown in Appendix C.

In the Bowen Basin there are three distinctive coal bearing intervals, the Jurassic Walloon coal measures, the upper Permian coal measures and the lower Permian Reid Dome Beds. In the case of the Reid Dome Beds coal interval it is considered to only be present in the Denison Trough. Coal percentages are calculated for each interval from 26 boreholes. In the Gunnedah Basin, 10 representative boreholes were used to calculate the coal percentage of the Permian coal interval. 41 boreholes were used in the Sydney Basin to cover the four main coalfield areas. Although two coal intervals are present in the Sydney Basin, the upper Permian and the lower Permian Greta / Clyde coal measures, so few boreholes reach basement that percentages could only be calculated for the upper Permian interval.

To determine the percentage of coal in each borehole, the percentage composition of the core was recorded (Equation 4.1) from the start of the Permian until the last recorded incidence of coal in the log (see Coal Percentage Intervals spreadsheet Appendix C). The total amount, in metres, of coal and other sediments was determined with:

$$C = \frac{i}{100} \times p$$

Eq.4.1

where C = amount of coal (m) in the logging interval,  $i$  = logging interval (m) generally 3 metres, and  $p$  = percentage of coal recorded in the logging interval. For example a 3 m core interval is logged as 20% coal, 40% sandstone and 40% siltstone which means of this 3 m, 0.6 m is coal. By adding the amount of coal per logging interval for the total logged length of the borehole the total amount of coal, in meters is determined. Using Equation 4.2 the percentage of coal is calculated for each borehole:

$$Coal(\%) = \frac{TC}{TL} \times 100$$

Eq.4.2

where TC= total amount of coal in meters and TL= total logged length of the borehole (m).

From the boreholes the range and average percentage of coal overall in the Bowen, Gunnedah and Sydney basins is shown in Table 4.1 as well as for specific units or basin areas.

**Table 4.1** Coal percentage calculations for the Sydney-Gunnedah-Bowen Basin.

Basin	Min	Max	Average	Standard Deviation	N° Samples
BOWEN	0.83	38.43	13.68	9.61	26
<i>Jurassic</i>	1.60	20.00	9.94	7.37	5
<i>Permian</i>	0.83	38.13	15.95	10.38	18
<i>Reid Dome Beds</i>	6.04	9.70	7.57	1.91	3
GUNNEDAH	3.72	25.14	12.48	8.26	10
SYDNEY	2.38	16.61	6.66	2.92	41
<i>Central Coalfield</i>	2.38	7.52	4.20	1.71	7
<i>Hunter-Newcastle Coalfield</i>	4.26	9.85	7.25	2.25	5
<i>Southern Coalfield</i>	2.89	16.61	7.33	3.67	11
<i>Western Coalfield</i>	3.75	8.68	7.65	1.75	7

The average coal percentage for the Permian coal interval across all three basins is 10.8% and for the Jurassic and Reid Dome Beds the average is 9.9% and 7.5% respectively. In the coal, shale and sandstone ratio the ratio between shale and sandstone lithologies over most borehole logs was fairly even. Therefore, for the purpose of thermal modelling a percentage ratio of 10% coal, 45% shale and 45% sandstone is applied as the best representation for any coal bearing interval.

#### 4.1.2 Temperature Measurement and Logging

The direct measurement of underground temperature requires a temperature measuring device to be lowered down a borehole to measure the temperature of the bores groundwater. In order to obtain meaningful and useful estimates of the temperature of the surrounding rock formation the borehole must be in a state of thermal equilibrium. Down-hole temperature results from borehole drilling records, e.g. drill stem tests, are collected when a borehole is not in a state of thermal equilibrium. Temperature measurements in equilibrium were extremely difficult to find in publicly accessible databases, therefore as part of this project new measurements were acquired (presented in Appendix A).

The most effective process for collecting temperature measurements is to use a high resolution thermistor (0.01°C or better) and hold the sensor stationary at each measurement depth until no significant drift is observed (Beardsmore & Cull, 2001). However, in the commercial world, this is generally not done due to time constraints and equipment expense, so most systems of wire-line logging run continuous temperature logs that need to be corrected for the depth of the measurement, which is related to the speed of the logging tool and the response time of the thermistor. Logging speeds of 5 m to 10 m per minute produce results with an absolute error of less than 0.5°C and a relative error of less than 0.05°C (Houseman *et al.* 1989) but in general the absolute error is not within the accuracy of the temperature thermistor.

To overcome this problem this project uses an adaption of the commercial wire-line logging technique, with temperature logging units. These units are less expensive than a geophysical temperature probe but do not have the same high resolution. However with the fixed logging speed this static method of temperature measurement allows the full response time of the thermistor to be achieved making it highly repeatable and accurate to within the error of the thermistor. In this method the logging unit is

lowered down a borehole, into the water column, and allowed to remain stationary at the specific depth for the total length of the thermistor response time, about 20 minutes, before proceeding to the next depth. In this technique boreholes must always be logged from the surface to the total depth, to avoid disturbance to the groundwater column, and the thermistor must be within the groundwater column for maximum thermal coupling. It is also important that the cable used not stretch to keep the logging unit stationary for the required period of time. In this project a groundwater dip meter tape, which is designed not to stretch, or special stretch resistant rope was used. The temperature logging units used are HOBO™ U20 and U12 data loggers, supplied by Onset Computer Corporation Ltd, which contain the temperature thermistor in a sealed stainless steel unit and have the following manufacturers specifications: an operating range of -20 to 50°C and an accuracy of 0.37°C, a resolution of 0.1°C and response time of 3.5 minutes, operating in water at 20°C.

Measurements were collected in 27 boreholes using one of two methods, with the choice of method related to the number of logging units available and or the amount of access at each borehole. Figure 4.1 outlines the equipment set up for the two methods used.

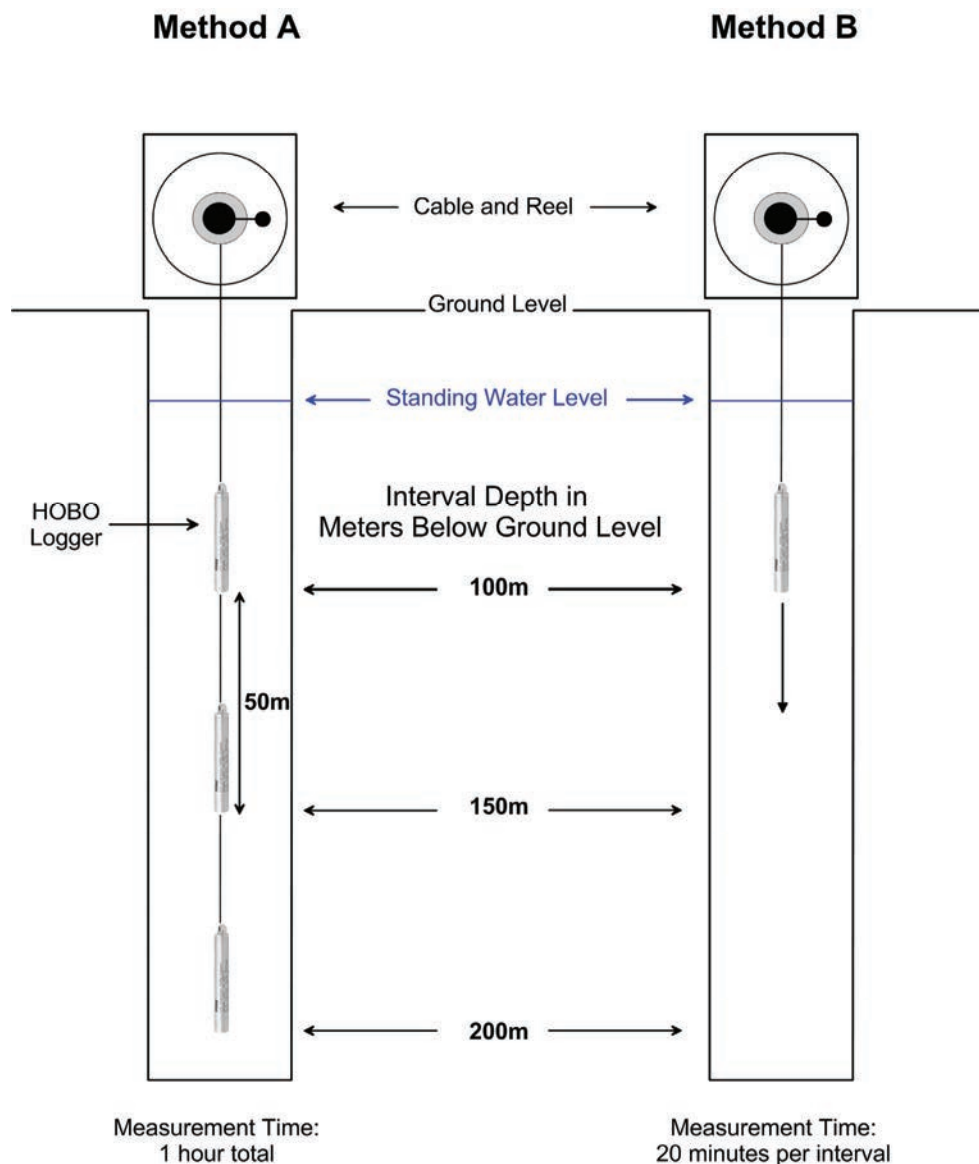


**Figure 4.1** Example of equipment setup for static temperature logging of Method A and Method B.



In Method A several loggers are required and attached at set intervals, generally 25 m or 50 m apart, on a cable which is then slowly lowered to the bottom of the borehole and left undisturbed for at least 1 hour. In Method B a single logger is attached to the end of the cable which is slowly lowered to the first depth then held stationary for 15 to 30 minutes before being lowered to the next depth. The process is repeated until the bottom of the borehole is reached. In each method the smallest logging interval of 1 second is used. Once the loggers are removed and downloaded, the temperature logs are analysed for the stable temperature at each depth interval. The stable temperature is determined by the flat-lining of the temperature, as shown in Figure 4.2. The resulting raw temperature measurements require correction for climate variation.

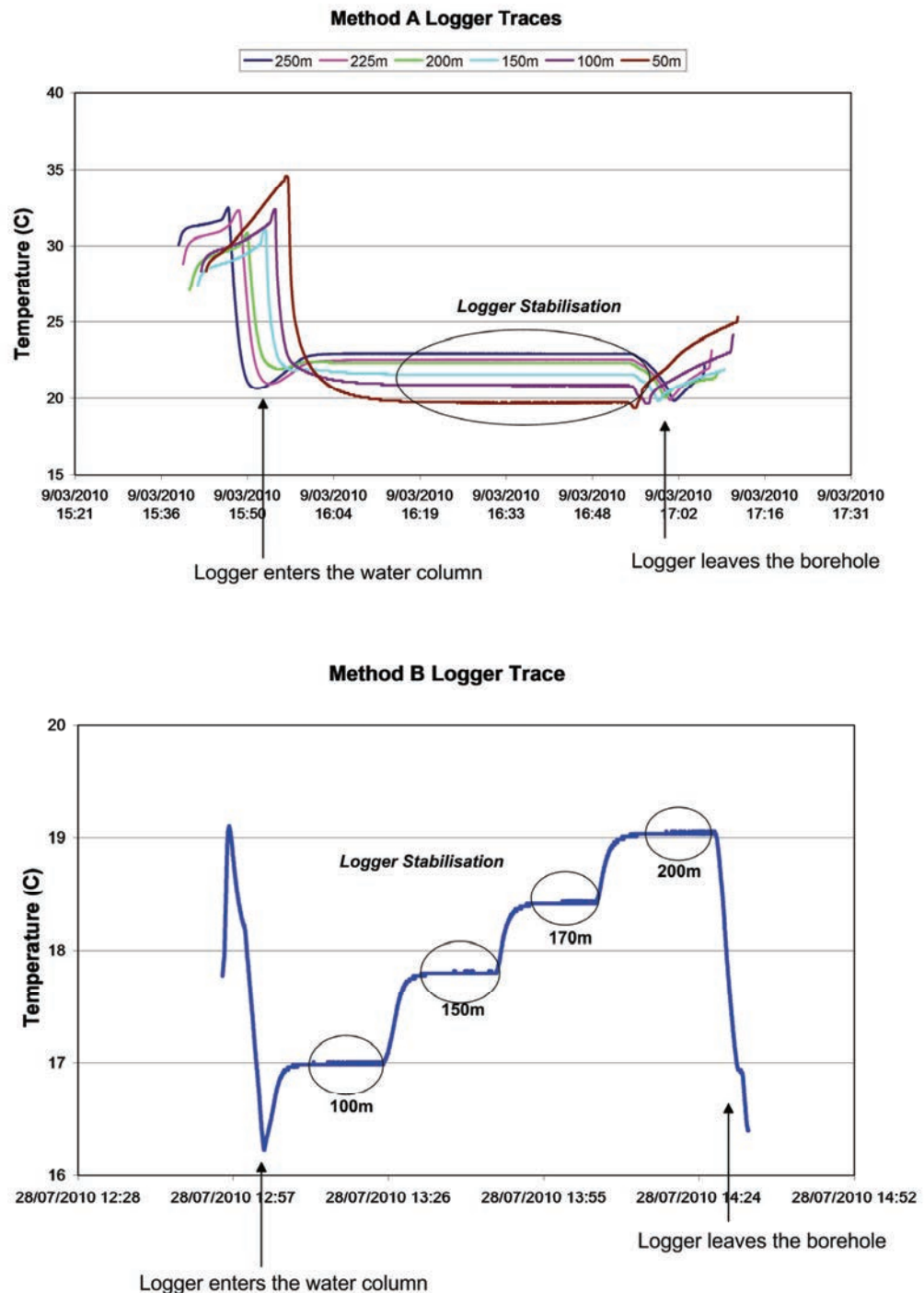


**Figure 4.2** Example of raw logger traces from Method A and Method B with the circled areas showing stable temperature.



## 4.2 Climatic Correction

A climate correction needs to be applied to all measured down-hole temperatures to correct for perturbations in the geothermal gradient caused by recent glaciation. Based on the work of Cull (1979), using data from Broken Hill (Figure 4.3), Equation 4.3 is applied to determine the temperature correction relative to the depth of measurement ( $D_x$ ) and Equation 4.4 is used to calculate the corrected temperature.

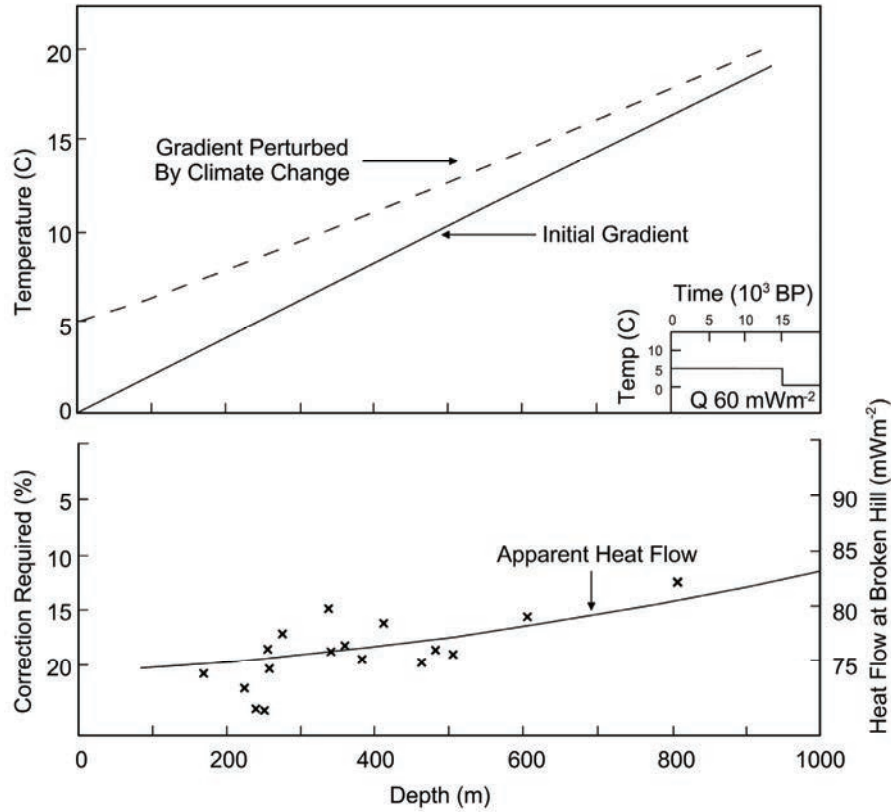


**Figure 4.3** Temperature perturbations associated with representative climatic model causing increases in heat flow consistent with data from Broken Hill. Adapted from Cull (1979).

$$dT_1 = T_s \times \text{ERFC} \left( \frac{D_x}{2 \times \sqrt{0.000001 \times G_1 \times 365.25 \times 24 \times 60 \times 60}} \right)$$

$$dT_2 = T_g \times \text{ERFC} \left( \frac{D_x}{2 \times \sqrt{0.000001 \times G_2 \times 365.25 \times 24 \times 60 \times 60}} \right)$$

Eq. 4.3

where ERFC = complementary error function (see Appendix D),  $T_s$  = present surface temperature of 15°C,  $T_g$  = 5°C, representing the difference between the present surface temperature and the ice age glacial surface temperature of 10°C (note the SGBB was not glaciated hence the higher glacial surface temperature),  $G_2$  = 12000 years, time glaciation started and  $G_1$  = 8000 years, time glaciation ended.  $dT_1$  accounts for temperature at the start of glaciation and  $dT_2$  accounts for temperature change at the end of glaciation.

$$T(D_x)_{\text{Corrected}} = T(D_x) + dT_1(D_x) + dT_2(D_x)$$

Eq. 4.4

Where  $dT_1$  and  $dT_2$  are from Equation 4.3 (in °C) and  $T$  is the raw temperature measurement (°C).

### 4.3 Temperature Extrapolation

As discussed in Chapter 2.4 the geothermal potential of the Sydney-Gunnedah-Bowen Basin system is primarily based on a series of extrapolated temperature maps (Figure 2.19) to a depth of 5 km. To compare any new extrapolated map with the existing map a comparable methodology of extrapolation is required. In this project the 1D two layer extrapolation model method of Chopra & Holgate (2005) is applied, as per the basis of the existing extrapolated map, but with some differences to estimate the temperature at 5 km depth in the Sydney Basin. In the method of Chopra & Holgate (2005) the geothermal gradient of the sedimentary cover is determined by a straight-line interpolation between the surface temperature and the measured temperature at depth. This gradient is extrapolated to the estimated basement depth, below which they apply a uniform geothermal gradient of 25°C/km, due to the absence of specific data (Chopra & Holgate, 2005), for the basement rock to the total required depth. This 25°C/km gradient appears based on the average continental geothermal gradient. The estimate of basement depth, i.e. sediment thickness, in the existing extrapolated map is derived from the crustal sediment thickness model OZ SEEBASE™ developed by FrOG Tech (2006).

In this method a temperature extrapolation map is created from the calculation of the geothermal gradient of the sedimentary package, using boreholes with down-hole temperature measurements, and the geothermal gradient of the basement package using the uniform geothermal gradient, as per Chopra & Holgate (2005) of 25°C/km to a depth of 5 km. Figure 4.4 provides an example of how this is achieved with the temperature data from a borehole.

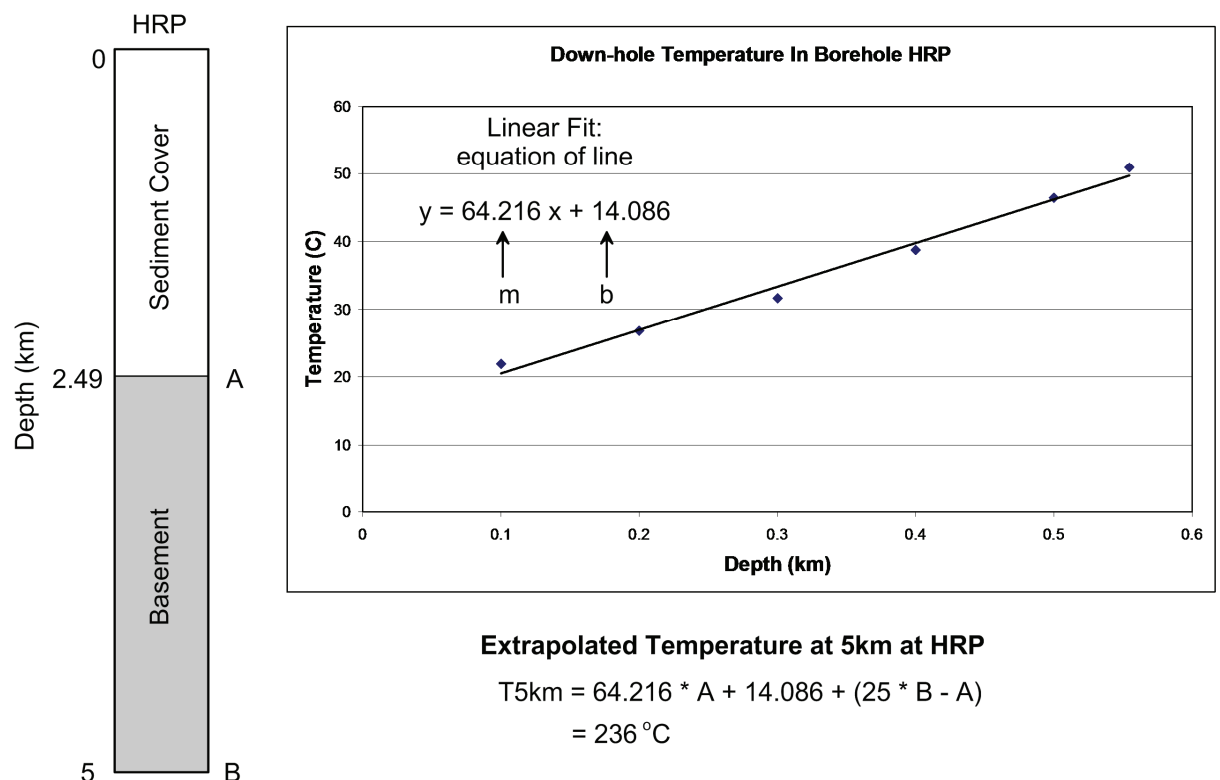


**Figure 4.4** An example of the linear fit and 1D model used to extrapolate temperature at borehole HRP to calculate estimated temperature at 5 km.

In calculating the geothermal gradient of the sedimentary package, the climate corrected temperatures at depth are graphed (see Appendix E) to determine the linear fit, as shown in Figure 4.4. When plotting the measured temperatures from different depths, the potential effect of diurnal and or seasonal variations are minimised by only using measurements from below 100 m beneath the ground surface, when possible.

If only one temperature measurement is available, i.e. bottom-hole measurement from drill stem test, a surface temperature average of 15°C (based on the yearly average surface temperature for the Gunnedah Basin; Cull 1979) is added in order for the measurement to be graphed.

A linear fit is applied, as illustrated in Figure 4.4, to obtain the temperature gradient (m) and the intercept temperature (b) for Equation 4.5, which calculates the extrapolated temperature at a given depth.

$$T = m \times A + b + 25 \times (B - A)$$

Eq. 4.5

where  $T$  = temperature at extrapolation depth in degrees

$m$  = is the temperature gradient from the equation of the linear fit (°C/km)

$A$  = thickness of sediment cover (km)

$b$  = intercept (surface) temperature from the equation of the linear fit (°C)

$B$  = extrapolation depth (km)

25 = geothermal gradient of crystalline basement (°C/km).

Unlike the existing extrapolated temperature map, which uses OZ SEEBASE™ to determine sediment thickness, this project applies the 3D geological model developed as part of the research. With this 3D geological model a more comprehensive and detailed estimate of sediment thickness is achieved for the Sydney Basin than the national scale OZ SEEBASE™ model. The results of this extrapolation work are discussed in Chapter 7.

#### 4.4 Density Measurement

The measurement of the density of specific rock lithologies is necessary for both gravity and thermal modelling. It is the density contrast between key stratigraphic units that allows the 3D structure of the Sydney-Gunnedah-Bowen Basin to be modelled. In this project it was not possible to collect samples from all different stratigraphic units in all three basins, instead representative samples are used.

Samples were collected from 14 field locations around Ulan, Coolah and Merriwa and from the cores of four boreholes; Belford 1, Dural South 1, East Maitland 1 and RDH Kurrajong Heights, held at the NSW Londonderry Core Library (Figure 4.5). 185 core samples were drilled from the hand samples collected from the field locations and 36 were cut from the core samples.

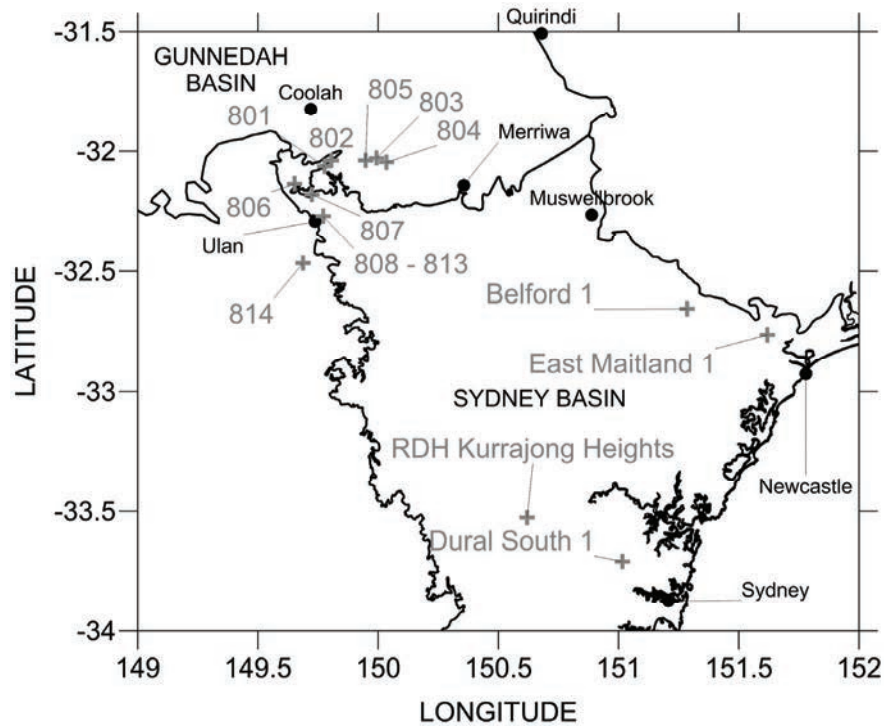


**Figure 4.5** Location of field sample sites and location of boreholes. Werrie Basalt samples were collected from near Quirindi, individual sample locations not specified.

9 drilled core samples of Werrie Basalt, collected for palaeomagnetism and held at Macquarie University, were also measured. Where possible, samples in the field were collected from fresh outcrops to minimise the effect of weathering on the calculations. If weathering was present the resulting density measurements would be considered as absolute minimum values to apply to the gravity modelling.

Density calculation is performed on 226 samples with the AG204 Delta Range Mettler Toledo scale using Equation 4.6 taken from the scale handbook (Mettler-Toledo AG 1994). Samples are firstly measured in a dry state before being soaked for 1 week to 1 month in distilled water in a sealed container. This is done to remove as much air out of the sample as possible for a more representative density. The samples are then weighed wet and the temperature of the distilled water recorded at the time of measurement. The density is calculated using:

$$D = \left[ \frac{(A \times \partial_L)}{(A - B)} \right] + C$$

Eq. 4.6

where  $D$  = density ( $\text{t/m}^3$ ),  $A$  = dry weight (g),  $B$  = wet weight (g),  $\partial_L$  = liquid density and  $C = 0.0012$  (air buoyancy constant). The liquid density is determined from density table for distilled water, in the Mettler Toledo density determination kit, using the measured temperature.

Table 4.2 summarises the average, minimum and maximum density is determined for the key rock lithologies whilst Table 4.3 provides the average, minimum and maximum density determined for each sample location. The density calculation spreadsheet is supplied in Appendix F.

**Table 4.2** Summary of the calculated density of the key rock lithologies measured.

Rock Type	Min	Max	Average	Standard Deviation	N° Samples
<i>Hand Samples</i>					
Tertiary Basalt	2.84	2.98	2.89	0.03	33
Jurassic Sandstone	2.12	2.68	2.31	0.14	24
Triassic Sandstone	2.32	2.44	2.39	0.03	33
Permian Sediments without coal	2.12	2.73	2.37	0.14	53
Permian Sediments with coal	1.40	2.73	2.22	0.37	63
Coal	1.40	1.50	1.43	0.04	10
All sediments without coal	2.12	2.73	2.36	0.13	116
Werrie Basalt	2.74	2.89	2.82	0.05	33
Gulgong Granite	2.51	2.62	2.59	0.03	13
<i>Core Samples</i>					
Permian Sediments	2.53	2.73	2.62	0.07	6
Weathered Basal Volcanics (<2500 m)	2.44	2.89	2.66	0.14	54
Less Weathered Basal Volcanics (2500-300 m)	2.82	2.97	2.88	0.06	9
Least Weathered Basal Volcanics (>3000 m)	2.87	2.97	2.92	0.04	5

**Table 4.3** Calculated density of samples collected for the representative lithologies.

Rock Type	Sample ID	Min	Max	Average	Standard Deviation	N° Samples
Granite	814	2.51	2.62	2.59	0.03	13
Tuff Ash Fall	813	2.49	2.55	2.54	0.02	15
Basalt	807	2.93	2.98	2.95	0.03	3
Basalt	803	2.85	2.91	2.89	0.02	13
Basalt	804	2.84	2.89	2.87	0.01	17
Permian Sediments: Sandstone	812	2.42	2.47	2.45	0.02	13
Triassic Sandstone	806	2.32	2.44	2.39	0.03	21
Jurassic Sandstone	805	2.40	2.68	2.46	0.08	10
Rylstone Tuff	810	3.01	3.39	3.24	0.09	13
Permian Sediments	809	2.12	2.22	2.18	0.03	15
Permian Sediments	811	2.30	2.47	2.38	0.04	19
Coal	808	1.40	1.50	1.43	0.04	10
Jurassic Sandstone	802	2.13	2.28	2.20	0.04	8
Jurassic Sandstone	801	2.12	2.27	2.22	0.05	6
Werrie Basalt	Werrie Basalt	2.74	2.89	2.82	0.05	11
Tuff	Dural South Core 9	2.87	2.94	2.91	0.03	3
Breccia	Belford No.1	2.44	2.64	2.52	0.06	12
Basalt and Tuffs	East Maitland	2.82	2.97	2.79	0.13	11
Permian Sediments: Sandstone	East Maitland	2.53	2.63	2.58	0.04	4
Permian Sediments	Kurrajong Heights	2.65	2.73	2.69	0.06	2
Volcanics – basalt / rhyolite / tuff	Kurrajong Heights	2.63	2.67	2.65	0.02	6

#### 4.5 Gravity Measurement and Modelling

Much of the previous work in the Sydney-Gunnedah-Bowen Basin system has involved gravity modelling to assess basin structure and sediment thickness. This has been achieved through using existing regional gravity measurements, i.e. Qureshi (1984, 1989), Leaman (1990) and Krassay *et al.* (2009) or from collecting detailed gravity profiles, i.e. Guo *et al.* (2007).

For this project the acquisition of detailed gravity profiles across the SGBB would be ideal but currently impractical. Therefore the gravity modelling draws on data from the latest regional gravity grid of Australia, the spherical Bouguer anomaly grid of the Gravity Anomaly Grid of the Australian Region 2008, available from Geoscience Australia. The details of this grid are outlined in Chapter 2 section 2.3.1 and summarised here. The gravity anomaly grid is a 0.5 minute / 0.0083 degree (~800 m) grid, derived from a non-homogenous station spacing which ranges from 2 km to 11 km, to which this project has applied no additional corrections.

To create the gravity profiles for modelling in the interactive potential field modelling package of ModelVision Pro, supplied by Pitney Bowes Business Insight®, slices of data were extracted from the regional grid using the grid slice function in Surfer, supplied by Golden Software®. For each slice the station spacing is on average 1600 m, though depending on the interpolation of the line through the gravity grid the station spacing may in places be less (generally in profiles not along a true east-west or north-south orientation). Model profiles were created in east-west and approximate north-south orientations, as shown in Figure 4.6. In total 39 profiles were created, 16 in the Bowen Basin, 8 in the Gunnedah Basin and 15 in the Sydney Basin. Profiles in the Gunnedah Basin are located in the same orientation as the profiles of Guo *et al.* (2007) whilst profiles in the Sydney Basin were located to pass through areas of interest and as many deep boreholes as possible. In the Bowen Basin east-west profiles were placed along the major latitude intervals, with the exception of Line 200, which was shifted south to model the tip of the basin, and the Ridge and Trough profiles. The Ridge and Trough profiles were constructed to provide interpolation points between the east-west profiles for the 3D surface contouring.

Gravity models of each profile are constructed in ModelVision as an assembly of polygonal bodies, from which the strike length of the bodies perpendicular to the profiles is limited, generally to the approximate geological extent, forming a 2.5D model (see Appendix G for ModelVision files). The background density parameter in ModelVision is set to 2.65 t/m<sup>3</sup>, based on the average bulk density of continental crust, and for each model a data calculated regional correction was applied. The Sydney-Gunnedah-Bowen Basin is an approximate north-south orientated basin, with a relatively flat sedimentary structure. East-west profiles are generally perpendicular with the main geological strike and the strike length for all polygonal bodies, excluding some shallow bodies associated with surface volcanics or alluvials, was set to approximately 100 km in the Bowen Basin and 40 km in the Sydney and Gunnedah basins. This provided a consistent model approach which is considered a representative average of the known mapped geology and the buried or obscured geology in the basins.

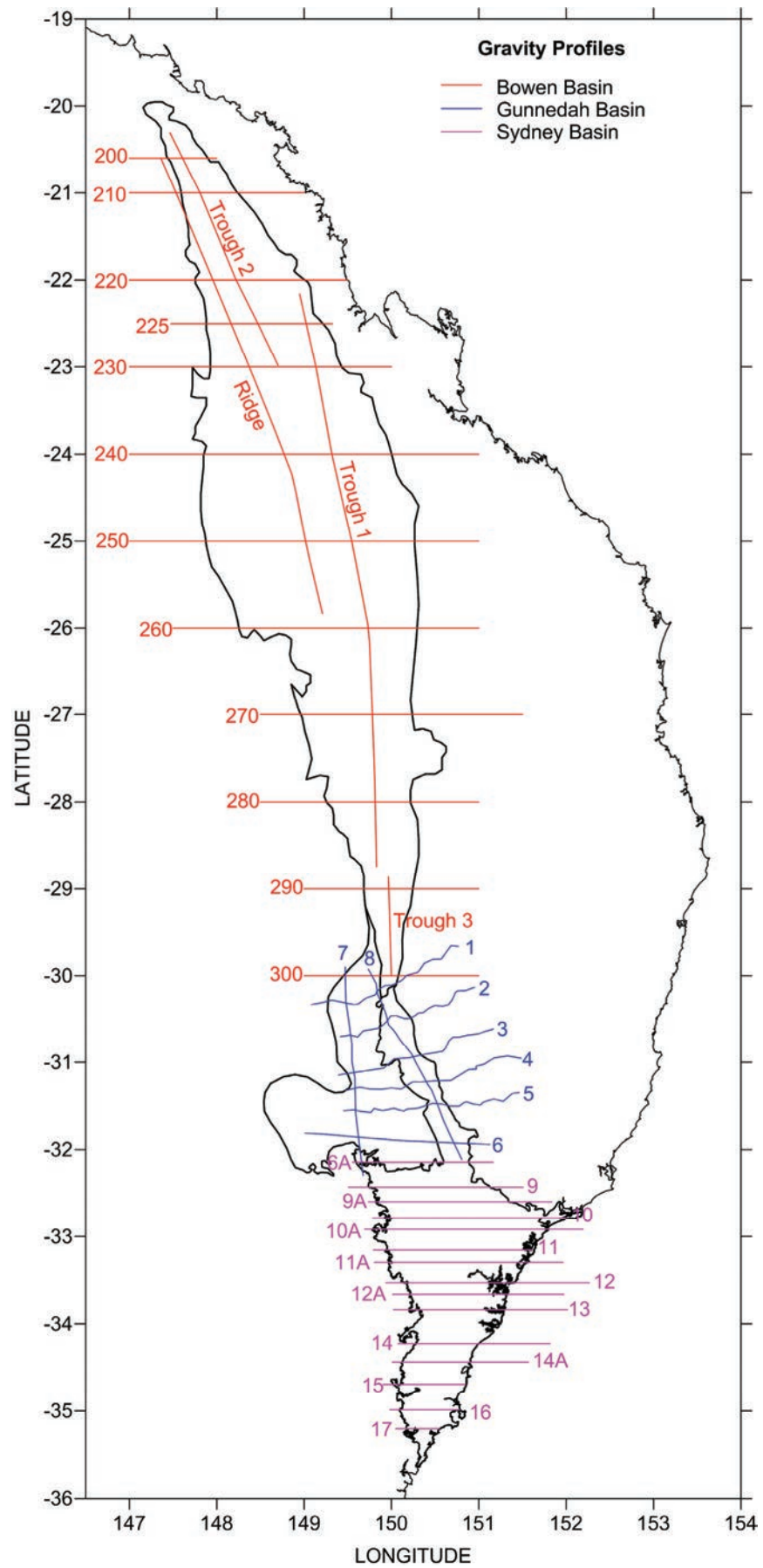


**Figure 4.6** Location of gravity profile lines in the Sydney-Gunnedah-Bowen Basin system.



All profiles are modelled in Map Grid of Australia (MGA), in coordinate Zone 55 for the Bowen and Gunnedah basins and Zone 56 for the Sydney Basin, to a depth of 15 km and extended beyond the basin boundary to minimise edge effects. The density of bodies in the model profiles for each basin is kept consistent to allow a continuous model to be created. The density of bodies is derived from measured and published values and applied as the best representation of the key lithologies or geological packages, as shown in Table 4.4. This was done, as it is not practicable to measure samples from all the lithologies in each basin. It should be noted that the representative density values may not reflect the true density of every lithological body modelled in each part of the SGBB. The lithologies, which form model bodies, are; Jurassic, Triassic and Permian sediments, basal volcanics, basement, granite intrusions, Tertiary volcanics, alluvial sediments and saturated sediments.

For features where a specific density has not been measured an average material density, from Reynolds (2003), is applied. For example for shallow surface features such as alluvial deposits and large river systems, which are predominantly sand, the average density of sand ( $2.00 \text{ t/m}^3$ ) is used and for irrigated floodplains, lakes and harbours a density of  $1.50 \text{ t/m}^3$  is used which is the average density of water ( $1.00 \text{ t/m}^3$ ) and sand ( $2.00 \text{ t/m}^3$ ).

**Table 4.4** *The density of key lithologies.*

<b>Lithology</b>	<b>Density (<math>\text{t/m}^3</math>)</b>
Tertiary / Exposed Carboniferous Volcanics	2.88
Gerringong Volcanics	2.88
Mesozoic to Quaternary Sediments	2.31
Surat Basin Sediments (<300m)	2.35
Upper Sediments (<300m)	2.38
Lower Sediments (>300m)	2.54
Basal Volcanics	2.95
Exposed Basal Volcanics	2.88
Granite	2.59 or 2.65
Basement	2.60 or 2.70

The gravity models consider the effect of increased density with depth by dividing the sedimentary package into sediments of the upper 300 m and sediments below 300 m. This was done after analysis of the density of core samples from Quirindi No 1 which showed a distinctive change in the density of sandstones and siltstones and shale after 300 m, probably related to compaction after this depth. For the upper 300m the density chosen relates strongly to the predominant lithology.  $2.38 \text{ t/m}^3$  is used for Triassic sediments,  $2.35 \text{ t/m}^3$  is used for Surat sediments (the average of the Jurassic and Triassic sediments) and  $2.31 \text{ t/m}^3$  is used for Jurassic sediments. Sediments greater than 300m depth use a density of  $2.54 \text{ t/m}^3$  based on the average density of siltstone from Guo *et al.* (2007), as it is the more dominant lithology in the lower sedimentary packages. The average density of the bulk sedimentary package is therefore  $2.46 \text{ t/m}^3$ , and is consistent with the previous calculated bulk average of Qureshi (1984, 1989), Krassay *et al.* (2009), and Guo *et al.* (2007). A two layer sediment model is more effective in modelling increasing density with depth than a bulk average density, especially in areas where sediments are relatively thin.

The basal volcanics are assigned a density of  $2.95 \text{ t/m}^3$  after the work of Krassay *et al.* (2009), and Guo *et al.* (2007) who interpret the basal volcanics as the source of the Meandarra Gravity Ridge. Density testing of the basal volcanics from 4 boreholes was undertaken to evaluate the estimated density of Krassay *et al.* (2009) and showed a comparable average density of  $2.92 \text{ t/m}^3$ .

For the basement, which consists of Lachlan, New England and Thomson Fold Belt rocks, a representative average density of  $2.70 \text{ t/m}^3$  (Qureshi 1984; Direen *et al.* 2001) is applied, given the generally similar composition of these fold belts. Changes to the density of the basement, to  $2.60 \text{ t/m}^3$ , were made where long-wavelength features, generally gravity lows, could not be achieved with mapped or interpreted shallow geology. The previous work of Krassay *et al.* (2009) also highlighted this. When a granite body is identified, via borehole records or mapped geology, the average granite density of  $2.59 \text{ t/m}^3$  is applied, with the exception of granites in the New England Fold Belt where representative densities of Guo *et al.* (2007) were used. Where New England Fold Belt is exposed on the eastern margin of the SGBB, representative densities from Guo *et al.* (2007) are used.

At depths of 10 km in most model profiles, on the western and eastern margins, a body defined as mid crust with a density of  $2.71 \text{ t/m}^3$  to  $2.72 \text{ t/m}^3$  is modelled as per the work of Guo *et al.* (2007). In the Sydney Basin the depth to the top of this body on the eastern margin is shallower to represent the thinning continental crust at the oceanic crust boundary. Appendix G shows the complete gravity model profiles from the Sydney-Gunnedah-Bowen Basin system. It should be noted that by extending the profiles outside of the basin boundary this reduces the edge effect, however modelled bodies outside the basin boundary may not fit as well with the measured data compared to inside the basin. Profile 2, from the Gunnedah Basin, in Appendix G is the corrected version as a mistake in the density of the sediments under the Mooki Fault was found with the version published.

Most model profiles are constrained from the stratigraphic depths of boreholes along the profile line or depths interpolated or projected from nearby boreholes. 33 seismic reflection profiles are used to provide structural information for model geometry and estimates of depth when borehole information is limited. There are over 1000 boreholes in the SGBB and 200 were used to constrain the gravity model profiles.

#### **4.6 Surface Contouring and 3D Geological Model**

To create the 3D geological framework required for numerical thermal modelling the complex geology of the Sydney-Gunnedah-Bowen Basin system needed to be simplified. Simplification removes the need to model every distinctive stratigraphic unit in the basin system and focus on groups of units that have similar thermal properties. In the gravity modelling, bodies with similar densities were grouped together and these groups are translated into surfaces which are contoured for the 3D geological model because they have distinctive thermal properties. In addition the coal bearing intervals, which cannot be modelled effectively from gravity, are created from the numerous borehole records and a surface elevation is interpolated from 90m elevation data from the Shuttle Radar Topography Mission (SRTM) available from the United States Geological Survey.

Sixteen surfaces were created, from the interpolated gridding of gravity model points and borehole stratigraphy and represent the five main lithology types; sediment, coal bearing sediment, volcanics and basement. These surfaces are:

- Elevation
- Top Jurassic Coal
- Base Jurassic Coal
- Top Permian Coal
- Base Permian Coal
- Top Maules Creek Coal
- Base Maules Creek Coal
- Top Greta Coal
- Base Greta Coal
- Top Reid Dome Beds Coal
- Base Reid Dome Beds Coal
- Top Denison Trough Volcanics Northern
- Top Denison Trough Volcanics Southern
- Onshore Volcanics
- Offshore Volcanics
- Basement

The depth to the volcanics and basement modelled in the gravity model profiles is extracted and converted to metres relative to the Australian Height Datum (mAHD) by subtracting the depth from the mAHD elevation of the ground surface. These points are combined with stratigraphic depths from borehole logs, also converted to mAHD, and gridded in Surfer to create a series of x,y,z points at a 0.05° grid spacing. These surfaces form the upper and lower boundaries of the geological units in the 3D model but can only be visualised in Surfer in 2.5D. The point of intersection between two geological surfaces is determined, either in Surfer or in AutoCAD, in order that the surface is 'blanked' to its approximate geological extent. Where no intersection is possible with underlying units, i.e. Jurassic Coal, the presence / absence of coal in borehole records was used to create an approximate boundary. Editing of the grid surfaces was required to remove spurious points from gridding interpolation and ensure surfaces of lower stratigraphic status were not intruding the upper surfaces unless evidenced by borehole records. Appendix H contains spreadsheets, grid files and xyz files for each surface. Figure 4.7 shows stacked 2.5D profile images of the geological surfaces for each basin.

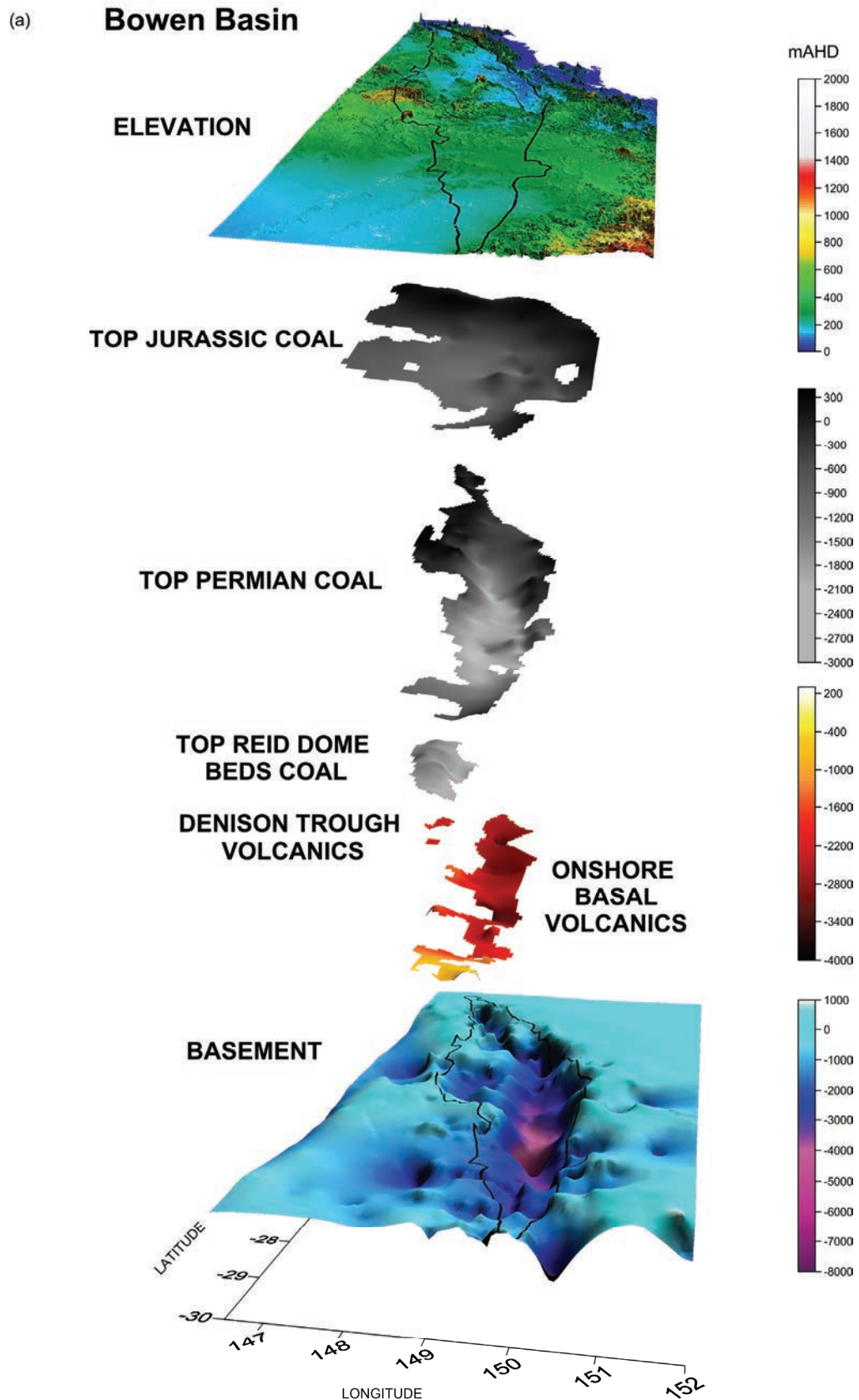


**Figure 4.7** Stacked 2.5D model profiles for the 3D geological model of the Sydney-Gunnedah-Bowen Basin system showing the basement, basal volcanics, top of coal layers and surface elevation for a) Bowen Basin, b) Gunnedah Basin and c) Sydney Basin. Profiles are shown with the same vertical scale but different horizontal scales depending on basin size.

(b)

## Gunnedah Basin

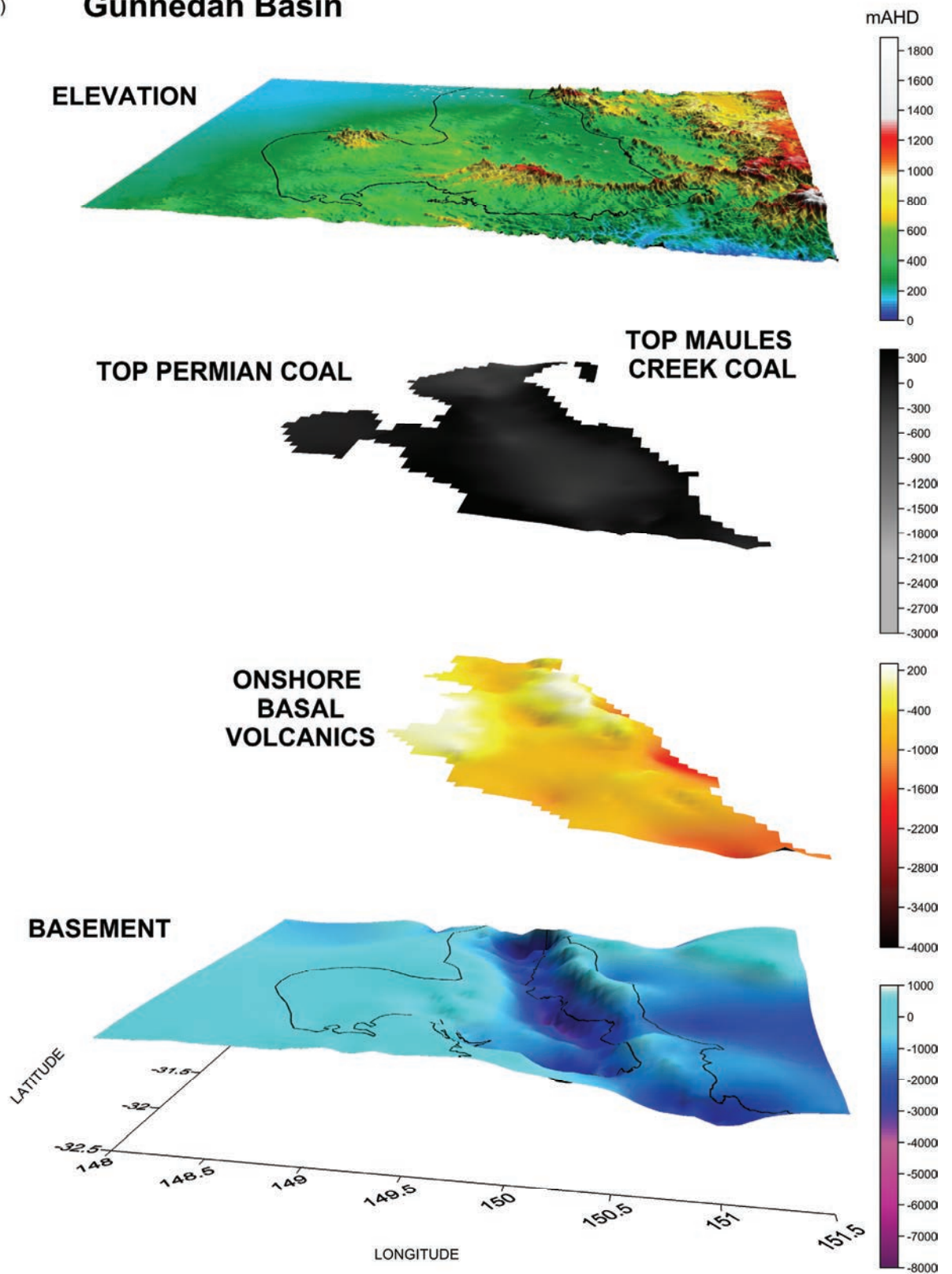
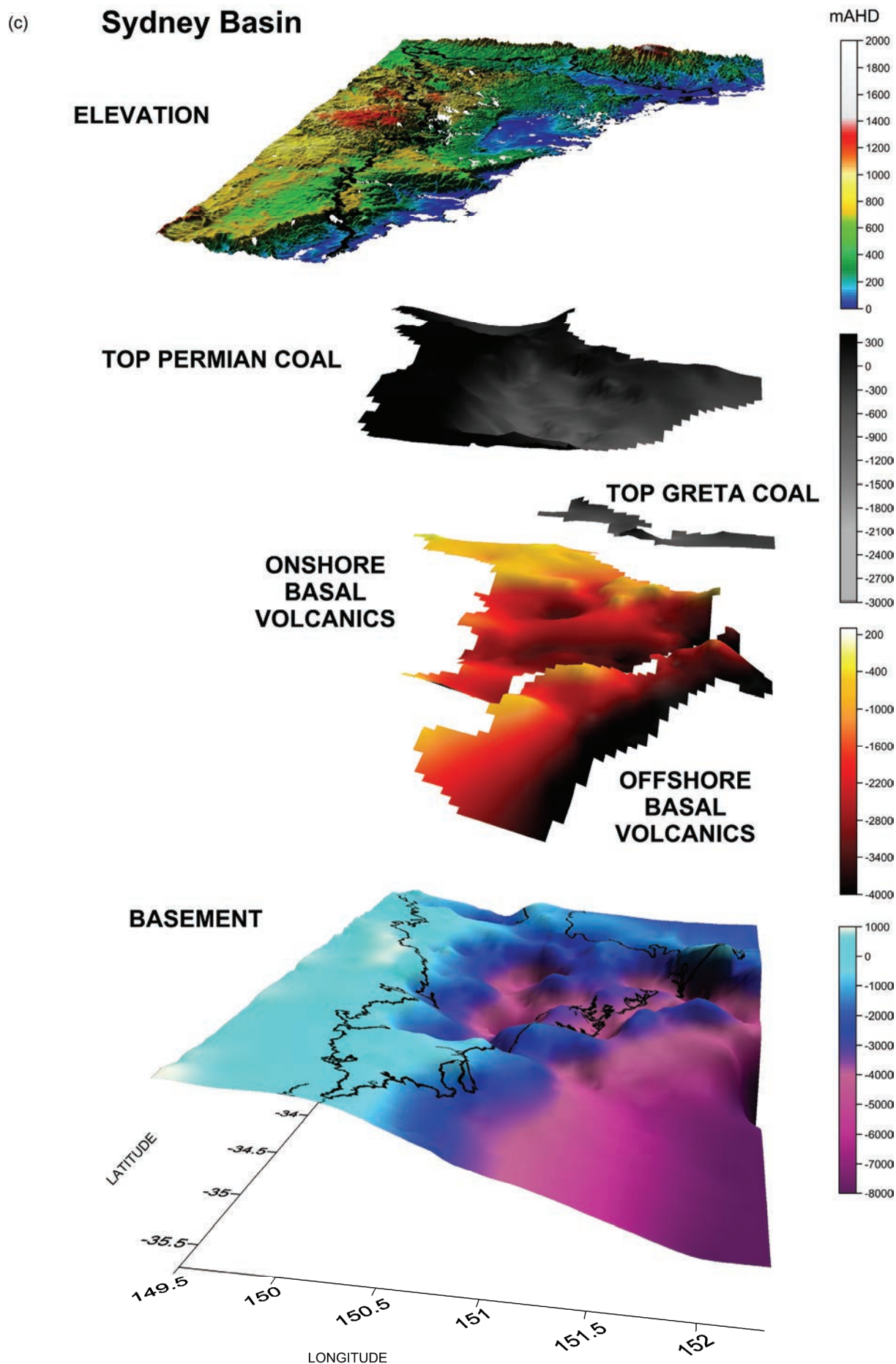


Figure 4.7 (Continued)





**Figure 4.7** (Continued)

#### 4.7 Data Distribution and Analysis

The data Distribution and Analysis System map (dDAS) aims to present a quantitative assessment of the overall 3D geological model of the SGBB, based on the datasets used in construction. This map is designed to be a quick evaluation tool for the confidence and reliability as it highlights areas where large amounts of data have been used compared to those with less, which are therefore more interpretive.

FrOG Tech (2006) introduced the concept of a Confidence Reliability Accuracy and Precision map, as part of the OzSEEBASE™ model of the Sydney Basin. For this project the basic method of the FrOG Tech (2006) map has been adapted for this research and Equation 4.7 was created. With this equation specific criteria, which are the model input databases, are assigned weighting factors and distance of influence constraints (Table 4.5) to produce a numerical value.

**Table 4.5** *Input datasets, maximum distance of influence and arbitrary weighting factor for dDAS.*

Input Dataset	Max Distance of Influence (km)	Weighting Factor
Gravity Model – Basement Surface	20	50
Gravity Model – Volcanics Onshore Surface	20	2
Gravity Model – Volcanics Offshore Surface	20	1
Boreholes – Basement	5	120
Boreholes – Volcanics	5	20
Boreholes – Coal	10	25
Structure Contours from Seismic or Borehole Data	1	5
Surface Geology	5	5
Surface Elevation	4	2
Seismic Reflection Profiles	5	5
Interpolated Points	5	5

The weighting factor is an arbitrary number related to the type of assigned input data and designed to value its quality, reliability and or quantity. It is designed to convert the input datasets into a mathematical value which encompasses all the geological, spatial and qualitative information. Borehole data is considered highly reliable but its overall quantity is low, therefore the weighting factor is high. To incorporate discrimination of the varying depths of the drilling data the stratigraphy influences the weighting factor value. Shallow boreholes, which are more numerous, provide limited information on deep structure thus their weighting factor is less than the deeper boreholes, which reach basement. Gravity modelling and seismic reflection profiles produce numerous points of data for input into the model but their depth of penetration is subject to personal interpretation. The weighting factor is significantly lower than for borehole information, primarily to ensure the dataset doesn't unnecessarily dominate the results, due to the volume of points, but also to incorporate the interpretive nature of this type of data. The maximum distance of influence (Table 4.5) of a particular dataset is related to its type and the level of confidence for interpolating this information away from the point of origin. For example, structural information from borehole data is very location specific and should only be interpreted as applicable to areas very close to the borehole. Gravity modelling, on the other hand, is on a regional scale and could be applied to a greater radius because of the already inherent level of interpretation.

Equation 4.7 gives a value at the centre of the grid cells over the 3D geological model domain.

$$p ( X , Y ) = \sum_{i=0}^n V_i - \frac{d_i^3}{D^3} \times V_i$$

Eq. 4.7

where  $V_i$  is the assigned weighting factor of the data point  $i$  and  $d_i$  is the distance to data from  $(X,Y)$  and  $D$  is the maximum distance of influence. A cubic function is used to give due emphasis to closer data whilst more distant data is weighted appropriately less and if  $d_i > D$  the data is ignored.

The dDAS map (Figure 4.8) is created from gridding the values derived in Equation 4.7 using a  $0.5^\circ$  cell size. The aim is to visually present the complex information contained within the model as areas of confidence ranging from low to moderate to high. This requires a level of subjectivity when determining the values for each confidence range in order to best present the information contained within the SGBB model. For Figure 4.8 the values have been divided between low (0 to 90), moderate (90 to 250) and high (>250) for best visual presentation.

The map presents an overall combined value of confidence, which includes the reliability of the data, the distribution density of the data, depth of data and the quality of the data, for the 3D SGBB model. High confidence areas (green) represent parts of the model with good physical control, i.e. lots of boreholes, seismic profiles, gravity profiles, mapped geology, for which there is confidence that the model is well constrained. Low confidence areas (red) show areas of limited data and represent the more interpretive areas of the model. Outside of the basin boundary for the model the area is shown as low, due partly to limited data, and is outside the area of interest. In the Sydney and Gunnedah basins the overall confidence is high due to a large database of boreholes and seismic reflection profiles. In the Bowen Basin areas of overall high confidence are along the gravity profile lines and clustered around areas of numerous boreholes. Appendix I contains the dDAS map script, input and output files.

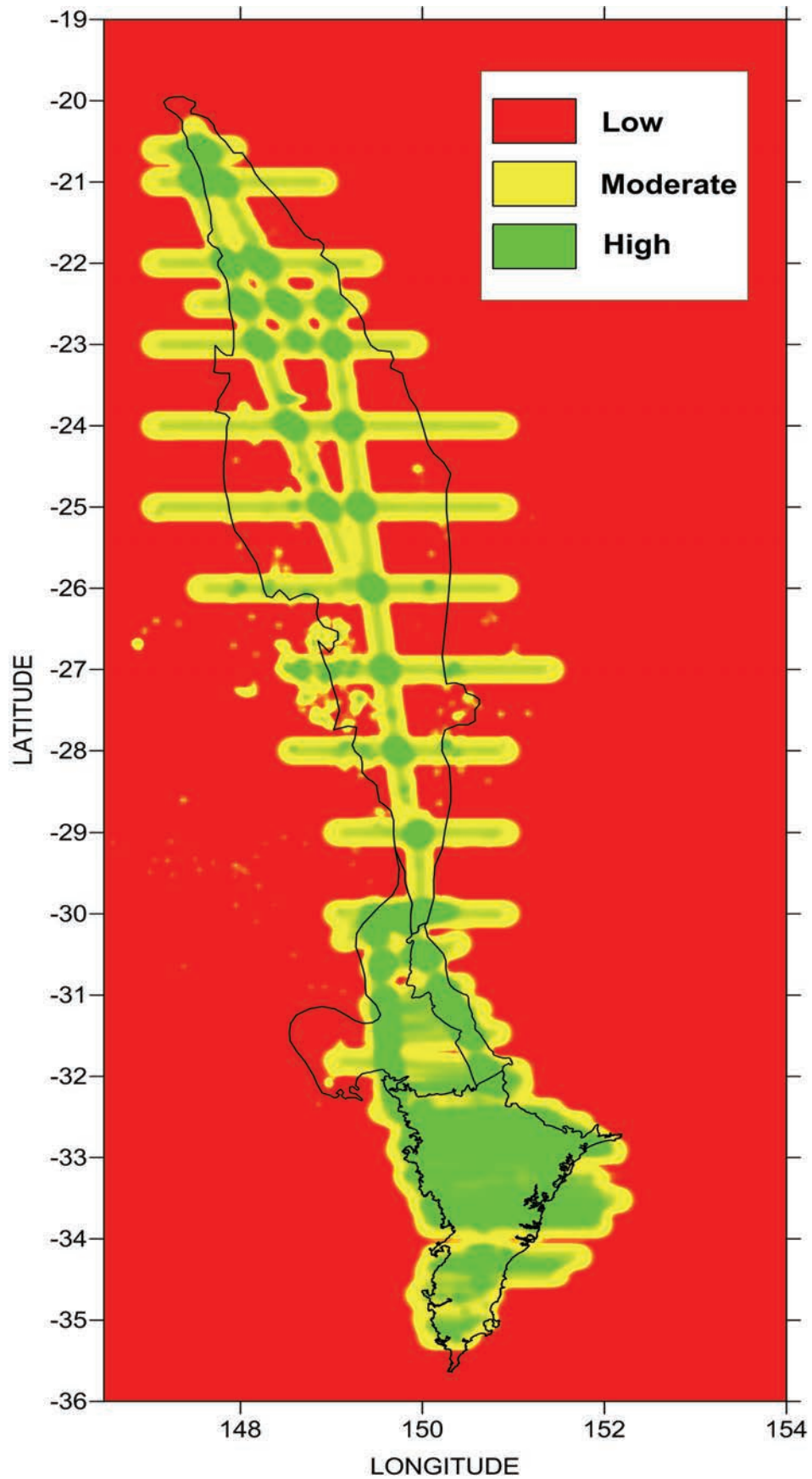


**Figure 4.8** Data Distribution and Analysis System (dDAS) map for the Sydney-Gunnedah-Bowen Basin 3D geological model. This map is an evaluation tool of the overall confidence of the model from the various datasets used in construction and considers all structural layers.

#### 4.8 Numerical Thermal Modelling in *Underworld*

Multi-dimensional numerical thermal modelling is the most efficient way of assessing the thermal structure of the SGBB system. There is an increasing use of 'forward' heat flow assessments constrained by geological models which allow the assignment of meaningful material properties, such as conductivities and heat production, across the entire model domain. The *Underworld* platform (Moresi *et al.* 2007) captures this at the scale of the problem and the rheological complexity required for the SGBB.

Firstly, 2D numerical thermal models were created for the Sydney-Gunnedah Basin system using the finite-element codes *Ellipsis* (Moresi *et al.* 2003) and its successor *Underworld* (Moresi *et al.* 2007) for which the parameters; density ( $\text{t/m}^3$ ), conductivity ( $\text{W/m}^\circ\text{K}$ ) and heat production ( $\mu\text{W/m}^3$ ) are assigned from published material averages (i.e. Wollenberg & Smith 1987; Swaine 1990; Clauser & Huenges, 1995; Herrin & Deming 1996; Forster & Merriam 1999; and Turcotte & Schubert 2002), when no information specific to the SGBB was available, and measured data (OZCHEM database; Budd 2007) specific to the SGBB. The models are not designed take into account advective effects, they are based on conduction only. A detailed description of the 2D models from each platform is provided in section 4.8.1 and 4.8.2. The location and geometry of these 2D models is the same as the 2D gravity model profiles as shown in Figure 4.9.

The boundary conditions of these models require constant top and bottom temperature with reflecting sides. The constant top temperature is  $15^\circ\text{C}$ , based on the yearly average surface temperature for the Gunnedah Basin from Cull (1979) and the basal temperature is a free parameter defined differently, discussed below, for each model type. To ensure the reflecting side boundaries do not create edge effects within the models area of interest, models are created with a minimum 10 km extension at either end. Models start with an initial linear temperature profile between the top and bottom boundary and evolve until the temperature field and surface heat flow reach a steady-state, defined by the heat flux across the system and the internal heat production in each section.

A high resolution 3D model of the SGBB was created using the *Underworld* platform and *Underworld-GT* toolbox. This model covers a volume of over 1600 km by 200 km by 12 km and is on the order of 10 to 100 times bigger than typical reservoir scale 3D models. It includes a temperature dependent conductivity which requires a non-linear approach to the heat flow solution. Through testing of the sensitivity of each model parameter in a small scale model of the Sydney-Gunnedah the uncertainties in the model were assessed and the best fit material parameters and subsurface temperatures derived for application in the high resolution SGBB model.

##### 4.8.1 *Ellipsis*

*Ellipsis*, the prototype to *Underworld*, was used for the 6 2D model profiles in the Gunnedah Basin (Figure 4.9a). These models focused on assessing the effect of basin architecture and coal layers on thermal structure, therefore the thermal properties and boundary conditions were based on published values. Table 4.6 shows the thermal properties of each model material which are based on published



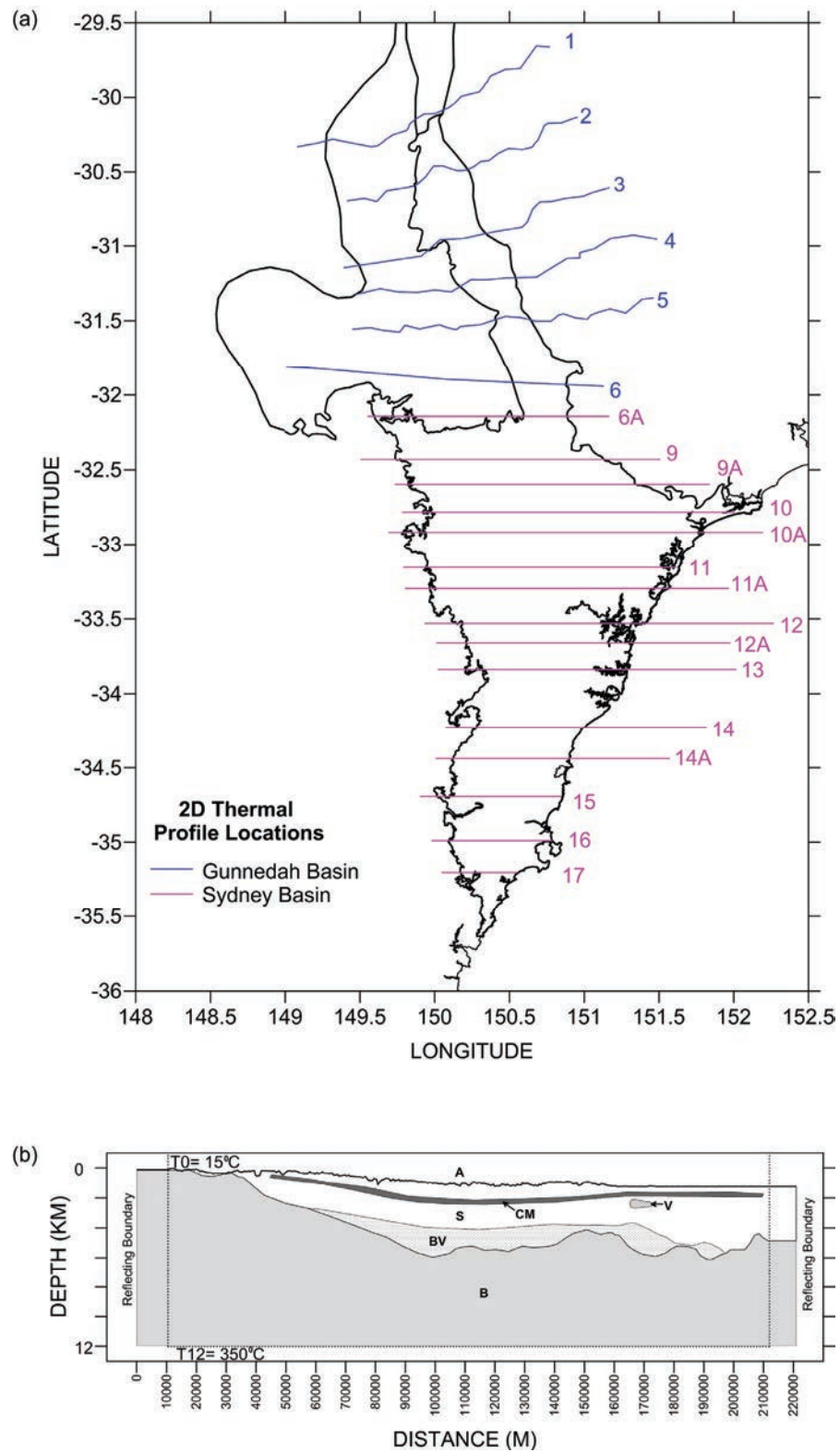


**Figure 4.9** (a) Location of 2D thermal model profiles in the Sydney and Gunnedah basins and (b) a schematic of 2D thermal model setup, where the top boundary condition  $T_0 = 15^\circ\text{C}$ , the basal boundary condition  $T_{12} = 350^\circ\text{C}$  and the side boundary conditions are reflecting. The dashed line represents the limit of the geological model, after which an addition 10 km is added to avoid any edge effects. The model is constructed with the following materials A (air), S (sediment), CM (coal measures), V (volcanics), BV (basal volcanics) and B (basement) for which thermal properties are applied as per Table 4.6 and 4.7.

**Table 4.6** *Thermal properties for Ellipsis model.*

Rock Type	Density (t/m <sup>3</sup> )	Conductivity (W/m-K)	Heat Production (μW/m <sup>3</sup> )
Sediments	2.50	2.00	1.25
Coal Measures	1.50	0.30	1.25
Basal Volcanics	2.90	3.00	0.50
LFB Basement	2.70	3.00	2.00

average measurements, with the exception of density which is determined from the density determinations and gravity modelling of this project. Boundary conditions were specified as 15°C at the surface (based on Cull 1979) and 180°C at 5 km estimated from the National Temperature at 5km map (Budd *et al.* 2008).

The files containing the boundary coordinates, as distance along the profile (m), of the geometry of each discrete polygonal body (see Appendix J); sediment, coal, basal volcanics and Lachlan Fold Belt basement, were loaded into the code platform with a maximum model depth of 5 km and run until steady-state was achieved.

#### 4.8.2 Underworld 2D

2D profile models were constructed along the east-west gravity model profiles in the Sydney-Gunnedah Basin (Figure 4.9a), 15 in the Sydney Basin and 6 in the Gunnedah Basin. Polygonal bodies were created for each discrete material; sediment, coal, Gerringong Volcanics, onshore volcanics, offshore volcanics, Lachlan Fold Belt basement and air with the boundary coordinates, to a depth of 12 km, input into the .xml code file. Each model profile is run for 20,000 time steps to achieve steady-state conditions. Appendix K contains the input .xml files, output .txt files and output .jpg profile images.

The thermal properties of each material are shown in Table 4.7. The density values of the sediments and basal volcanics are based on the values used in the gravity modelling. The density of the coal is based on the average coal:shale:sandstone ratio (0.1:0.45:0.45) derived from coal percentage calculations in section 4.1.1. The model temperature boundary condition at the surface is 15°C and the basal temperature at 12 km is set at 350°C, based on the extrapolation of the geothermal gradient from the Ellipsis model. The basal temperature parameter is an estimate, as no specific data exists, which can be varied. In this 2D modelling to check the validity of this basal temperature boundary estimate the results are compared to measured down-hole temperature data (Figure 4.10) which in general show a good correlation but suggest further optimisation is still required.

**Table 4.7** *Thermal properties for 2D Underworld model.*

Rock Type	Density (t/m <sup>3</sup> )	Conductivity (W/m-K)	Heat Production (μW/m <sup>3</sup> )
Sediments	2.46	2.00	1.25
Coal Measures	1.90	0.30	1.25
Basal Volcanics	2.95	3.00	0.50
LFB Basement	2.70	3.00	2.00

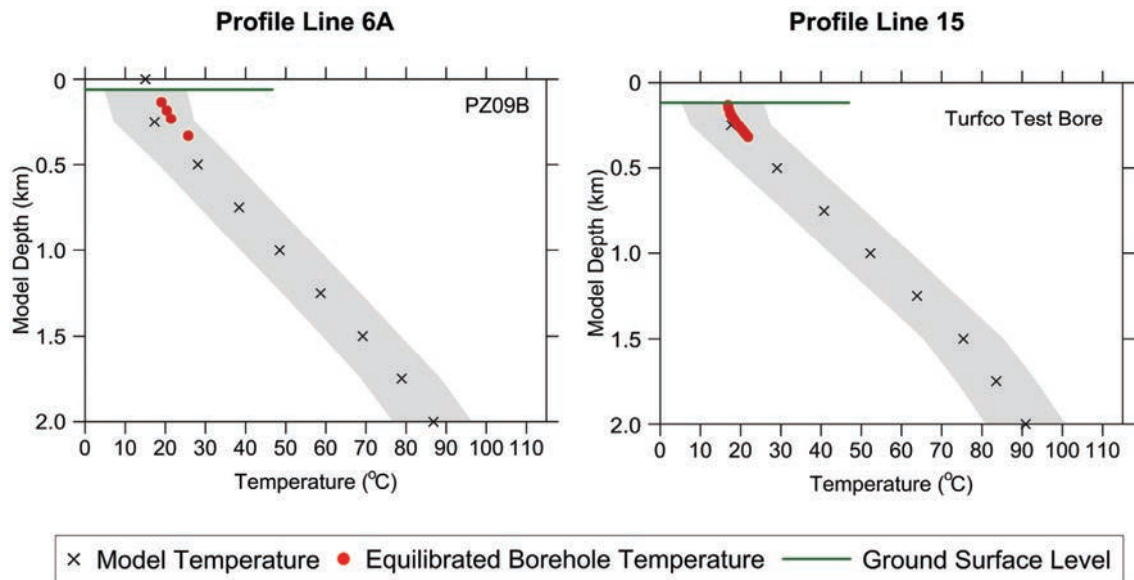


**Figure 4.10** Example of geotherm calibration checks using equilibrated borehole temperatures using Profile Line 6A and Line 15 in the Sydney Basin. Ground surface (green line) varies from model depth zero depending on topography. Equilibrated borehole temperatures shown as red dots, model geotherm temperatures shown as crosses. Gray shaded area represents  $\pm 10^{\circ}\text{C}$  of uncertainty.

#### 4.8.3 Underworld 3D

The 3D thermal models of Underworld are the best avenue for parameter testing and high resolution models to assess thermal structure. The 3D models use surfaces for each model material, rather than polygons, and are created from the 3D geological model which covers the area between Latitude -36 to -19 and Longitude 146.5 to 152.5 at a  $0.05^{\circ}$  grid. Underworld required the surface coordinates in meters, thus all points are converted from Lat Long GDA94 to MGA Zone 55. Ten surfaces represent the four major material types; basement, volcanics, sediments and coal, and are contained within .csv files (see Appendix L). They are imported in stratigraphic order to create unit volumes and a consistent method, based on Smooth Particle Hydrodynamics (SPH) is used to interpolate between the surface points to create the surface geometry at a chosen resolution.

The parameter testing to derive 'best-fit' was undertaken using a 3D model of the Sydney-Gunnedah Basin. To derive the 'best fit' material parameters and subsurface temperature an incremental approach to forward modelling was applied, calibrated by equilibrated temperature logs. The basal temperature was a free parameter which was allowed to vary through the iterations, beginning at  $350^{\circ}\text{C}$  and allowed to converge on the optimal value. This work was undertaken by Steve Quenette from Monash University's eResearch Centre, the results of which is presented in Chapter 9. The approach allows the constraint of uncertainties in the 3D models and an accurate assessment, for a given confidence, of the subsurface temperature over the basin. A model of the Sydney-Gunnedah Basin was loaded into *Underworld* and run from low resolution to high resolution whilst changing the material parameters until the optimum values of Tables 4.8, 4.9 and 4.10 were achieved, which satisfied the thermal constraints imposed by over 300 temperature at depth observation points across the basin. The Sydney-Gunnedah model reached a resolution of 192 by 252 by 348, which is equivalent to

approximately 1400 m x 14 m x 1420 m, with the basal temperature boundary condition best as 345°C at 12 km (the surface temperature boundary remains at 15°C).

**Table 4.8** *Best-Fit thermal properties for 3D Underworld Model 1.*

Rock Type	Density (t/m <sup>3</sup> )	K <sub>0</sub> (W/m·K)	K <sub>Crit</sub> (W/m·K)	T <sub>Crit</sub> (°C)	Heat Production (μW/m <sup>3</sup> )
Sediments	2.46	2.00	1.50	300	1.25
Coal Measures (Jurassic, Reid Dome, Greta, Maules Creek)	1.90	0.30	0.20	300	1.25
Coal Measures (Permian)	1.90	1.20	0.20	300	1.25
Basal Volcanics	2.95	3.00	2.25	300	0.50
Basement (under fault)	2.70	3.00	2.25	300	2.00
Basement	2.70	3.00	1.50	300	2.00

**Table 4.9** *Best-Fit thermal properties for 3D Underworld Model 2.*

Rock Type	Density (t/m <sup>3</sup> )	K <sub>0</sub> (W/m·K)	K <sub>Crit</sub> (W/m·K)	T <sub>Crit</sub> (°C)	Heat Production (μW/m <sup>3</sup> )
Sediments	2.46	2.00	1.50	300	1.25
Coal Measures	1.90	1.20	0.20	300	1.25
Basal Volcanics	2.95	3.00	2.25	300	0.50
Basement (under fault)	2.70	3.00	2.25	300	2.00
Basement	2.70	3.00	1.50	300	2.00

**Table 4.10** *Best-Fit thermal properties for 3D Underworld Model 3.*

Rock Type	Density (t/m <sup>3</sup> )	K <sub>0</sub> (W/m·K)	K <sub>Crit</sub> (W/m·K)	T <sub>Crit</sub> (°C)	Heat Production (μW/m <sup>3</sup> )
Sediments	2.46	2.00	1.50	300	1.25
Coal Measures (Jurassic, Reid Dome Beds, Greta, Maules Creek)	1.90	2.00	0.20	300	1.25
Coal Measures (Permian)	1.90	1.20	0.20	300	1.25
Basal Volcanics	2.95	3.00	2.25	300	0.50
Basement (under fault)	2.70	3.00	2.25	300	2.00
Basement	2.70	3.00	1.50	300	2.00

These values are different from previous parameters in Table 4.7 as a result of the application of temperature dependent conductivity. Clauser & Huenges (1995) compiled a large database of thermal conductivity measurements on various rocks under different temperature conditions and demonstrated that there is a significant decrease in thermal conductivity for when temperature are increased. The thermal conductivity decreases linearly between the surface (K<sub>0</sub> at T<sub>0</sub> of 15°C) to the point where the conductivity stays at a constant value (K<sub>Crit</sub> at T<sub>Crit</sub>). The best-fit thermal properties and subsurface parameters were applied in the complete SGBB model. The model used a resolution of 3000 m by 17 m by 3000 m and the resulting thermal structure is discussed in Chapter 10.

The methodologies presented here in Chapter 4 characterise the workflow of this project and many will be repeated, at various levels of detail, in the research papers presented in Chapters 5 to 9.

# CHAPTER 5

## SUBSURFACE STRUCTURE



*Kanangra Walls, Kanangra NSW*



# Gunnedah Basin 3D architecture and upper crustal temperatures

C. DANIS\*, C. O'NEILL AND M. A. LACKIE

GEMOC ARC National Key Centre, Department of Earth and Planetary Sciences, Macquarie University, NSW 2109, Australia.

The Gunnedah Basin in New South Wales has long been an important coal and gas resource, but limited information exists on the temperature structure or crustal architecture at depth to enable development of its geothermal potential. Here we combine gravity modelling, seismic-reflection surveys and borehole drilling results to develop a 3D depth to basement structural map and geological model of the basin. The 3D structure of the Gunnedah Basin is characteristic of a typical intracontinental rift basin. Gravity modelling of the Lachlan Fold Belt basement, using borehole and seismic-reflection controls, shows a 2–3.5 km-deep approximately north–south-oriented channel between the basement highs of the Rocky Glen Ridge in the west and Boggabri Ridge in the east. Extensional basal volcanics during the Late Carboniferous–Early Permian fill this channel. Borehole data and gravity modelling show up to 1 km of Permian to Jurassic sedimentary rocks overlying the rift volcanics. Preliminary thermal modelling, incorporating the geological model and limited deep borehole temperatures, indicates temperatures at the top of basement are in the range 105–165°C.

**KEY WORDS:** 3D structure, basement temperature, gravity modelling, Gunnedah Basin, thermal modelling.

## INTRODUCTION

The sedimentary basins of eastern Australia host some of Australia's most important economic resources. Historically, the extensive coal and natural gas resources of the regions have been the focus of exploration and extraction. However, the thermal blanketing effect of thick sedimentary successions, in particular low thermal conductivity sediments such as coal and shale, can in some cases lead to significantly elevated temperatures at depths in these basins, making them a target for geothermal energy exploration. With the development of geothermal resources in the Cooper Basin, South Australia, interest in the more accessible east coast sedimentary basins for geothermal resources has intensified.

The Gunnedah Basin is part of the Sydney–Gunnedah–Bowen Basin (Figure 1), a major economic sedimentary basin ~1600 km long. A number of previous studies have addressed aspects of the Gunnedah Basin's deep architecture. The literature describing the geological structure and evolution history of the Gunnedah Basin is extensive (Tadros 1993). Deep seismic-reflection surveys have been carried out by Geoscience Australia (BMR91-G01: Korsch *et al.* 1997), as well as by the New South Wales Department of Mineral Resources' Hunter–Mooki Seismic Survey 2007 (DPI NSW 2008) and numerous private exploration companies (available online through the DIGS database <<http://digsopen.minerals.nsw.gov.au>>) which provide insight on the deep structure of the Gunnedah Basin. Bramall & Qureshi (1984) gave a qualitative interpretation of the regional gravity data while Guo *et al.* (2007) and Krassay *et al.* (2009) undertook gravity modelling of the upper crustal structure of parts of the Gunnedah Basin.

While these previous studies have addressed aspects of the Gunnedah Basin's architecture, none have compiled available geological, geophysical and borehole data into a self-consistent model for the deep Lachlan Fold Belt basement structure of the basin. Understanding the basin's deep structure is critical to modelling its thermal state from limited temperature information, and thus understanding the geothermal potential of the Gunnedah Basin. In the most recent gravity modelling of the Gunnedah Basin (Guo *et al.* 2007; Krassay *et al.* 2009) none of the extensive drilling information was considered or included. The aim of this contribution is to construct a 3D depth to basement model of the Gunnedah Basin, based on the latest regional gravity data, which simultaneously satisfies all available coal and petroleum borehole data, seismic profiles, and surface geological constraints. While commercial basement models exist, these do not have the transparency in their construction required to address the fundamental science questions concerning the thermal, mechanical and hydrogeological state of the upper crust. We then use this basin architecture model to calculate a

\*Corresponding author: [cdanis@science.mq.edu.au](mailto:cdanis@science.mq.edu.au)



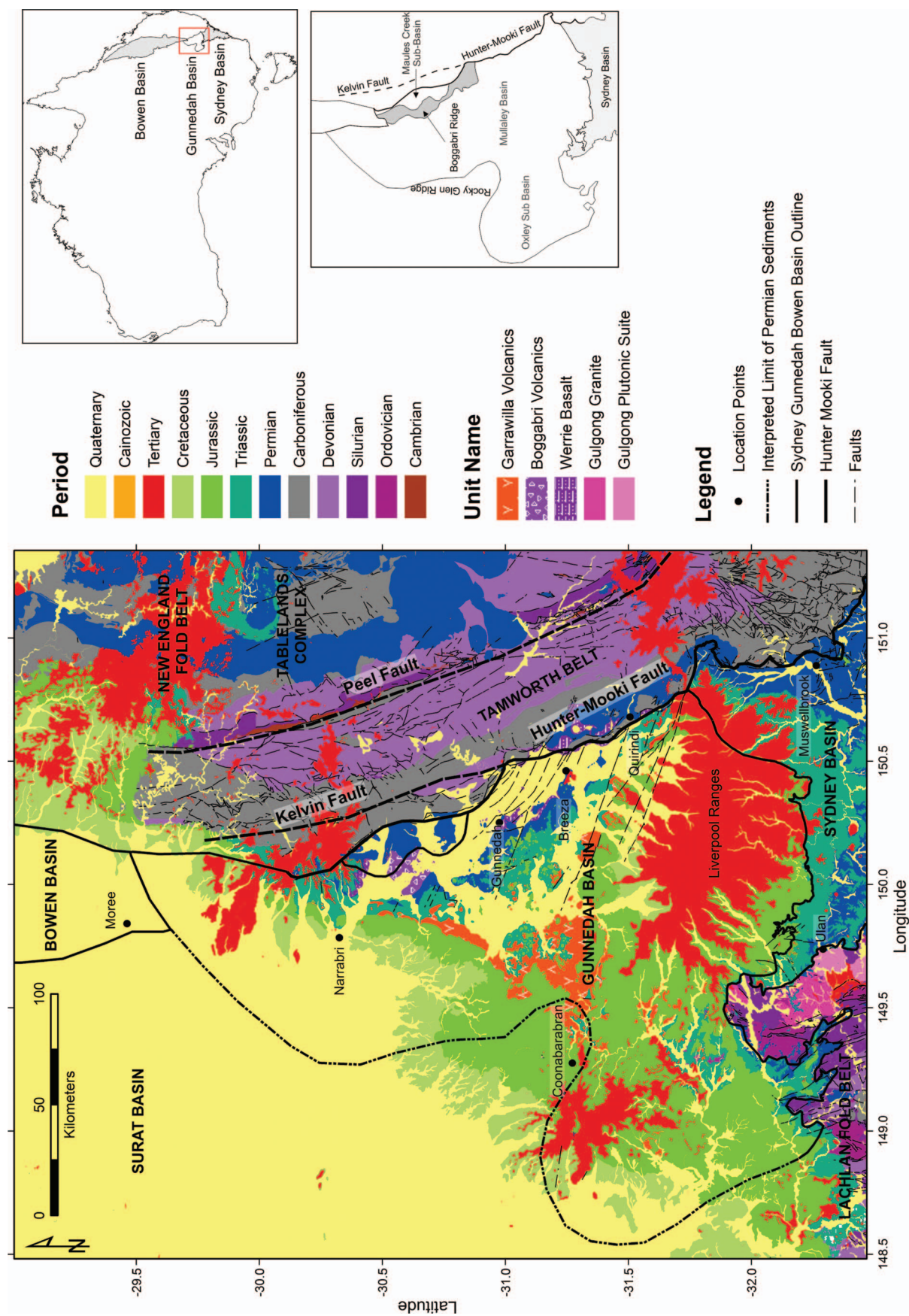


**Figure 1** Geological map of the Gunnedah Basin. Units are coloured according to time period. The key outcrops of the Garrawilla Volcanics, Boggabri Volcanics, Werrie Basalt, Gulgong Granite and Gulgong Plutonic suite are also shown.

3D thermal model of the Gunnedah Basin system to understand its geothermal potential.

## GEOLOGICAL SETTING

The Gunnedah Basin (Figure 1), part of the Sydney–Gunnedah–Bowen Basin system, started development towards the end of the Hunter–Bowen Supercycle in the extensional environment that followed the convergent environment of the Devonian and Carboniferous (Glen 2005). The extensional tectonic regime initiated basaltic and rhyolitic rift volcanics (Boggabri Volcanics and Werrie Basalt) which unconformably overlie the meta-sediment and metavolcanic basement rocks of the Lachlan Fold Belt (Figure 2). Rifting produced half-graben-like structures that received sediment from neighbouring highlands (Tadros 1993). Basin fill localised in small rapidly subsiding troughs separated by highlands and ridges consisting of silicic and mafic

JURASSIC	EARLY	Surat Basin Sediments
TRIASSIC	LATE	Garrawilla Volcanics
	EARLY	Deriah Formation
		Napperby Formation
		Digby Formation
PERMIAN	LATE	Black Jack Group
		Arkarula Sandstone
		Watermark Formation
		Porcupine Formation
		Maules Creek Formation
	EARLY	Leard & Goonbri Formation
		Boggabri Volcanics & Werrie Basalt
		Metavolcanics & Metasediments
LATE CARBONIFEROUS		

**Figure 2** Simplified stratigraphy of the Gunnedah Basin (modified from Tadros 1993).

volcanics. The lacustrine sediments of the Leard and Goonbri Formations accumulated in the most rapidly subsiding areas but were soon inundated by the coal-bearing alluvial fan deposits of the Maules Creek Formation. The north-oriented Boggabri Ridge effectively acted as the principle sediment source and divided the Gunnedah Basin into two sub-basins, the Maules Creek Sub-basin and the Mullaley Sub-basin (Figure 1). At the end of the Hunter–Bowen Supercycle in the Late Permian the Sydney–Gunnedah–Bowen Basin developed into a foreland basin as subduction began again further in the east (Glen 2005). In the early part of the Late Permian, marine shelf sediments of the Porcupine Formation were deposited and gradually overlain by the Watermark Formation, characterised by siltstone and claystone. Deposition of the coal-bearing Black Jack Formation in the middle Late Permian occurred during a lowering of the sea-level. Sedimentation was interrupted by a marine incursion, caused by tectonic subsidence and resulting in the deposition of the Arkarula Sandstone. The upper Black Jack Formation is characterised by conglomeratic sandstone and an abundance of tuff and pyroclastic detritus (Tadros 1993).

In the Late Permian, convergence resulted in major basin tilting and uplift, evident particularly in the northern Gunnedah Basin, the termination of coal sedimentation and the erosion of a thick section of Permian rocks. A regional angular unconformity exists between the Permian of the Black Jack Group and the overlying Triassic Digby Formation. Intense folding/faulting of the southern New England Fold Belt (255 Ma) resulted in east–west compressional movements, mostly accommodated by the Hunter–Mooki Fault system and structural readjustments in the basin (Tadros 1993). Renewed subsidence resulted in the deposition of the Napperby Formation, characterised by siltstone/claystone and interbedded sandstone/siltstone to sandstone, derived from the New England Fold Belt. The Deriah Formation is a distinctive green sandstone at the top of the Triassic sequence. Final filling of the Gunnedah Basin (235–230 Ma) was dominated by the detritus shed from the New England Orogen (Glen 2005). Between 235 and 227 Ma, in the Late Triassic, vitrinite-reflectance data suggest the removal of up to 2 km of Triassic and Permian sediments (Tadros 1993). Compressional and left-lateral strike-slip movement on the Hunter–Mooki Fault resulted in a number of high-relief anticlines (Glen 2005). During the Jurassic–Cretaceous and the breakup and dispersal of Pangea and east Gondwanaland, epicontinental basins (Surat Basin) developed, resulting in Jurassic sedimentation and volcanism (Garrawilla Volcanics) in the northern and western parts of the Gunnedah Basin.

The Gunnedah Basin is bounded by a regional unconformity surface over the Lachlan Fold Belt to the west and by the southern New England Fold Belt to the east along the east-dipping Hunter–Mooki Fault (Tadros 1993). The basin appears continuous with the Bowen Basin in the north and the Sydney Basin in the south, although boundaries are generally drawn in the north across the Moree ‘high’ and in the south as a line from Coolah to Dunedoo and eastward over the Liverpool Range to Quirindi (Tadros 1993).



## METHODOLOGY

### Regional Bouguer and magnetic intensity anomaly maps

Bouguer anomaly and magnetic intensity anomaly maps of the study area (Figure 3) were derived from the Gravity Anomaly Grid of the Australian Region 2008 and Magnetic Anomaly Grid of the Australian Region 2002 available for download from Geoscience Australia (<<http://www.ga.gov.au>>). The gravity data are a 0.0083 degree ( $\sim 800$  m) grid, derived from station spacing's of 7–11 km and 2–4 km over areas of scientific or economic interest, based on the current Australian Absolute Gravity Datum 2007 scale and a reduction density of 2.67 t/m<sup>3</sup>. The magnetic data are a  $\sim 0.01^\circ$  ( $\sim 1$  km) grid. In this study no corrections have been applied to the data prior to gridding in Surfer v9 supplied by Golden Software<sup>®</sup> with kriging at 0.01°.

### Density measurement

A total of 185 core samples for density measurement were drilled from hand samples of the geological units considered to be representative of the Gunnedah Basin, collected from around Ulan, Colah Tops and Merriwa. Samples were measured both dry and wet using an AG204 Delta Range Mettler Toledo Scale and density was calculated using the formula:

$$D = [(A\partial_L)/(A - B)] + C$$

where  $D$  is density (t/m<sup>3</sup>),  $A$  is dry weight (g),  $B$  is wet weight (g),  $\partial_L$  is the liquid density, and  $C = 0.0012$  (air buoyancy constant). Table 1 provides a summary of the measured density.

### Gravity profiles

In order to enable accurate 2.5D gravity modelling of the subsurface of the Gunnedah Basin eight gravity profiles (Figures 3, 4) were extracted from slices of the Bouguer anomaly grid supplied by Geoscience Australia. Profiles 1–5 were taken along the same gravity profile lines modelled by Guo *et al.* (2007) and profiles 6–8 were created to extend coverage across the Gunnedah Basin. Modelling of the gravity data was performed with the interactive potential-field modelling package Model-Vision Pro v8.0 supplied by Pitney Bowes Business Insite<sup>®</sup> (formerly Encom Technology). Models were constructed as an assembly of polygon bodies, forming a 2.5D model, for which the strike length of the bodies perpendicular to the profiles is limited to their approximate geological extent. All profiles are modelled in Map Grid of Australia coordinate Zone 55. Our model profiles use similar density values, body-strike length and lower (7–15 km depth) model geometry to those of Guo *et al.* (2007).

The upper 5 km of the profile is constrained by borehole information from over 60 drillholes (see Figure 3 for locations and Appendix 1 and Figure 4 for details) for the depth of sediment cover, top of basal volcanics and where available, the top of Lachlan Fold

Belt. Boreholes directly on or adjacent to the gravity lines are considered to provide tight structural control for the model layers, while interpolated depths from projected boreholes are used as a guide for the layers between the points of tight control. This limits the variables to model to primarily being the top of the Lachlan Fold Belt. Increasing density with depth was taken into account with a change in density for sediments at >300 m depth.

In this study the gravity profiles (Figure 4) are modelled to 15 km but the upper 5 km is presented to emphasise the delineation of the top of the Lachlan Fold Belt and basin structure. Boreholes used for calibration are shown on the profile and stratigraphic sections of those boreholes are provided in Figure 5. The western Gunnedah Basin boundary is defined by the inferred limit of the Permian sediments. Preliminary investigations, from limited borehole information, indicated shallow Lachlan Fold Belt basement overlain by Permian sediments with sparse coal beds and Jurassic sediments and volcanics. For the purpose of our model we define the Rocky Glen Ridge as the western boundary of the Gunnedah Basin and gravity modelling under the 'Oxley Sub-basin' was not carried out.

### 3D basement structure

The 3D basement structure of the Gunnedah Basin was interpreted from the gravity modelling and the stratigraphic data of over 140 additional boreholes (Figure 3, Appendix 1). First, the depth information from the gravity modelling for the top of the Lachlan Fold Belt and top of basal volcanics was converted to a relative level in metres, with reference to the Australian Height Datum (mAHD). Second, these levels are combined with additional point data from borehole stratigraphy levels and, third, gridded in Surfer using 0.05 degree grid resolution to produce a contoured 3D surface (Figure 6).

Surface elevation from 90 m-resolution Shuttle Radar Topography Mission (SRTM) data, available from the US Geological Society (<<http://dds.cr.usgs.gov/srtm>>), was used to convert all model layer depths to mAHD. Surfaces were created for the top and base of the Mullaley and Maules Creek Coal intervals, base of Jurassic sediment as well as the surface elevation. During gridding it was necessary to use interpolated points, a point value average between two known values, to produce smoother surfaces.

### Thermal models

We use an established finite-element code (Ellipsis: Moresi *et al.* 2003; O'Neill *et al.* 2006), which maps material properties to particle tracers to solve for the thermal field for a 2D conduction problem. This lets us define the boundaries of a large number of materials and set the relevant material thermal properties, such as thermal conductivity and internal heat production.

The code has been extensively benchmarked previously (O'Neill *et al.* 2006), and we have also tested for convergence for a simple conduction problem with a known analytical solution for the dimensions of the problem explored here. For this problem we are purely

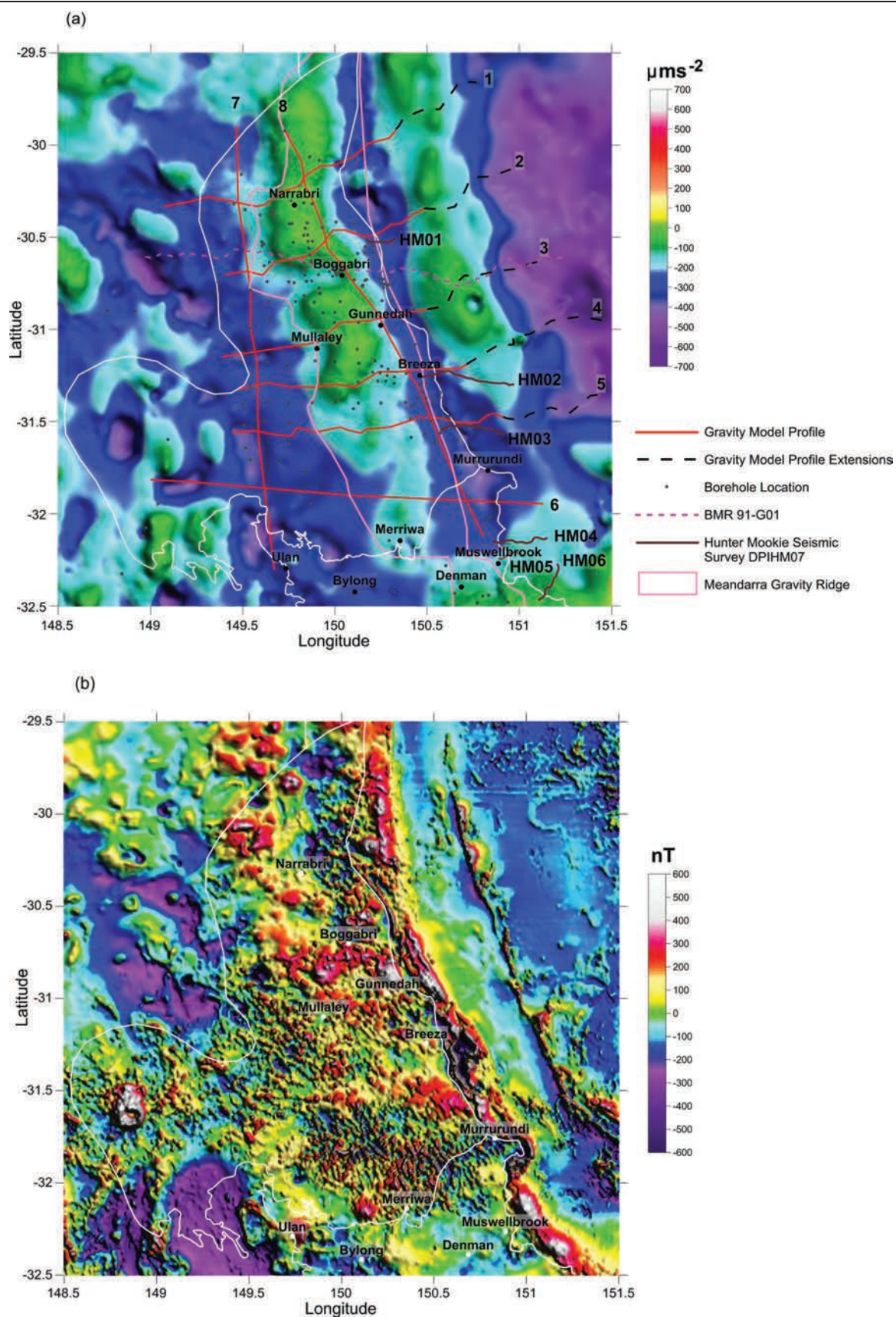


**Figure 3** (a) Bouguer gravity anomaly map of the Gunnedah Basin (white outline), overlain with gravity model profiles (red line and black numbers) and extension lines (black dashed line), borehole and place locations and seismic lines. The location of the Meandarra Gravity Ridge is also shown. The numbered New South Wales Department of Primary Industries' Hunter-Mookie Seismic Lines have the prefix HM. (b) Total magnetic intensity anomaly map of the Gunnedah Basin (white outline).



**Table 1** Summary of density data for the rock samples representative of the Gunnedah Basin.

Lithology	Density (t/m <sup>3</sup> )			
	Range	Mean	SD	<i>n</i>
Jurassic sandstone	2.12–2.68	2.31	0.14	24
Triassic sandstone	2.32–2.47	2.38	0.03	21
Permian sediments	2.12–2.47	2.34	0.11	47
Permian sediments with coal	1.40–2.47	2.18	0.36	57
All sediments	2.12–2.47	2.35	0.10	68
Tertiary basalt	2.84–2.98	2.88	0.03	33
Werrie Basalt	2.74–2.89	2.82	0.05	11
Gulgong Granite	2.51–2.62	2.59	0.03	13

solving the energy equation, and we do not consider deformation or fluid advection. The basic setup of the problem and material properties used are outlined in Table 2.

The new additions to the software capability in the models presented here are the ability to import 2D polygon files containing the boundaries of each discrete material. We consider four materials; sediment, coal, basal volcanics and Lachlan Fold Belt (Table 2), and one quasi-material called ‘air.’ This top air layer has a very large conductivity, and its purpose is to allow direct thermal coupling of the varying topographic surface with the top boundary condition, which is imposed at the top of the rectangular box. The side boundary conditions are reflecting. The bulk material properties of the layers are composites taken from borehole data. For example, the sediment layer has a density and thermal conductivity consistent with the shale:sandstone ratio of the entire sedimentary unit, and the coal similarly has a thermal conductivity appropriate for the entire coal measures, based on the average coal:shale:sandstone ratio (0.1:0.45:0.45) derived from core data, calculated at its average subsurface temperature.

Over the temperature range considered (15–180°C), the thermal conductivity of intrusive crystalline rocks varies to about 80% of their surface value (Clauser & Huenges 1995), that of sedimentary rocks ~67%. We model this by assuming all intrusive rocks at temperatures above 100°C have conductivities 85% of their surface values (Table 2), while all sedimentary above 100°C have a conductivity of 75% their surface value. Clauser & Huenges (1995) did not observe a systematic changes in the conductivity of volcanic rocks over this temperature range.

The 3D basement structure model derived from the gravity modelling was imported, in 2D slices, into the thermal modelling software Ellipsis. The models started with an initial linear temperature profile between the top boundary temperature of 15°C (near the yearly average surface temperature for the Gunnedah Basin: Cull 1979), and the basal boundary temperature at 5 km of 180°C. This basal temperature has been adopted from the average Gunnedah Basin temperature at 5 km, from the Austherm07 model (Budd 2007), and constitutes the biggest uncertainty in the modelling. The material properties are outlined in Table 2, and are derived from

published values for each lithology or composite lithology.

The heat-production values for the basement terrain are taken from representative Lachlan Fold Belt granites immediately adjacent to the Gunnedah Basin (OZCHEM database <<http://www.ga.gov.au/oracle/index.jsp#geochem>>; Budd 2007). Other heat production values are taken from average values for each lithology (Table 2) (Wollenberg & Smith 1987; Swaine 1990; Turcotte & Schubert 2002). We have constructed six cross-sections (same as Lines 1–6 in the gravity section), and solved for the 2D thermal field in each. The models evolve from the initial conditions until the temperature field and surface heat flow reach a steady-state defined by the heat flux across the system, and internal heat production in each section.

### Field temperature measurement and climate correction

Existing temperature constraints from the Gunnedah Basin come primarily from northern end of the basin, in the vicinity of Narrabri, and are presented by Othman & Ward (2002) (Table 3). It should be noted that these temperature estimates are almost entirely from unequilibrated borehole measurements generally within 12 h from the cessation of drilling, and do not constrain particularly well equilibrium borehole temperatures. As a result, we have also taken a number of downhole equilibrated temperature measurements (Table 4), to provide shallow thermal constraints on our models.

Field temperature measurements were carried out in four deep groundwater monitoring piezometers in the Ulan Coal Mines Ltd mining lease area, in March and June 2009, using Hobo<sup>®</sup> U2 water level loggers with an inbuilt temperature sensor. The operating range of the temperature sensor is –20°C to 50°C with an accuracy of 0.37°C at 20°C, a resolution of 0.1°C at 20°C and a drift of 0.1°C per year. The loggers were taped to the cable of a 300 m electronic dipmeter at 0 m, 100 m, 150 m and 200 m and lowered down each piezometer to near the base of the hole. The logging units were set to record at 1 s intervals for 30 min and then removed and downloaded. The stabilised temperature at each interval was determined and then graphed against depth below ground. Temperatures from three additional piezometers with installed logging units were also downloaded. The raw temperatures were climate-corrected based on Cull (1979 figure 9) assuming a present surface temperature of 15°C, a glacial surface temperature of 10°C (and thus a difference in surface temperatures of 5°C), and that glaciation ended 8000 ago.

## RESULTS

### Density testing

The average measured density of representative sediments for Gunnedah Basin from Table 1 are generally comparable to the sediments in the Gunnedah Basin measured by Guo *et al.* (2007). The Gunnedah sediments

are dominated by sandstone in the Triassic and inter-bedded sandstone/siltstone/claystone/tuff and coal in the Permian. Jurassic sandstone has quite a large density range and is strongly influenced by the weathered and friable nature of many samples. The average density is  $2.31 \text{ t/m}^3$  and is considered reasonable to represent the weathered nature of the Jurassic sediments over the Gunnedah Basin. The average measured density of Tertiary basalt is  $2.88 \text{ t/m}^3$ . The Garrawilla Volcanics are basaltic but were not sampled therefore the Tertiary basalt density is considered reasonable and used in the gravity modelling. By analysing the density measurements taken on drillcore from Quirindi 1 (Guo *et al.* 2007) at depth, a distinctive change in composition and density is observed at 300 m. Not only does sediment density increase with burial depth within the basin, but also the ratio of siltstone and shale becomes much greater in the core log. Therefore, to represent increasing density with depth, the model incorporated sediments 0–300 m at  $2.38 \text{ t/m}^3$  based on the average measured density of Triassic sandstone, and sediments >300 m depth at  $2.54 \text{ t/m}^3$  based on the average density of Triassic Siltstone of Guo *et al.* (2007).

This density was chosen as siltstone is the more dominate rock type in the lower sediments and the average falls midway between the average density previously calculated for the Gunnedah sediments  $2.45 \text{ t/m}^3$  (Qureshi 1984, 1989) and the highest density Guo *et al.* (2007) measured for all sandstone/siltstone/shale of  $2.66 \text{ t/m}^3$ . The average of density of the bulk Gunnedah sediments package is therefore  $2.46 \text{ t/m}^3$  and is consistent with previous calculated bulk averages of Qureshi (1984, 1989), Guo *et al.* (2007) and Krassay *et al.* (2009). However, increasing density with depth is better taken into account using a two-layer model with the above stated densities. A density of  $2.54 \text{ t/m}^3$  is also considered representative for the sediments of the Surat Basin, which are expected to be similar in composition at comparable depths.

The density of the Lachlan Fold Belt is  $2.70 \text{ t/m}^3$ , as selected by Guo *et al.* (2007) from the work of Direen *et al.* (2001). However, when required, we use a lower density (which presumed association with either a more granitic composition Carboniferous volcanics or more weathered metasediments): a density of  $2.60 \text{ t/m}^3$  is based on the measured density of the Gulgong Granite (Table 1). Werrie Basalt has a measured density of  $2.82 \text{ t/m}^3$ . This basalt is exposed on the eastern side of the Hunter–Mooki Fault and on the Boggabri Ridge and is weathered. Samples measured were highly vesicular and some samples were significantly weathered, therefore the measured density is expected to be lower than the actual density of Werrie Basalt at depth under the Gunnedah sediments. A density of  $2.95 \text{ t/m}^3$  is considered by Guo *et al.* (2007) to be representative of the mafic volcanics under the Gunnedah Basin and is used in this study.

The densities of established structural units for the gravity model are based mainly on measurements of samples obtained in this study and incorporated the density values used by Guo *et al.* (2007) where no outcrop was observed (i.e. Lachlan Fold Belt) or sampled (i.e. Tamworth Belt). Therefore, the densities are Jurassic

sediments  $2.31 \text{ t/m}^3$ , Tertiary volcanics  $2.88 \text{ t/m}^3$ , Gunnedah sediments <300 m  $2.38 \text{ t/m}^3$ , Gunnedah sediments >300 m  $2.54 \text{ t/m}^3$ , Surat Basin sediments  $2.54 \text{ t/m}^3$ , granite  $2.59 \text{ t/m}^3$ , Lachlan Fold Belt  $2.60 \text{ t/m}^3$  and  $2.70 \text{ t/m}^3$ , and basal volcanics  $2.95 \text{ t/m}^3$ .

## Gravity modelling

The profiles were first modelled using the geometry derived by Guo *et al.* (2007) and from the interpretation of BMR91-G01 seismic line by Korsch *et al.* (1997). Profiles Bingara, Barraba, Manilla, Tamworth and Quirindi are located in the same location as those of Guo *et al.* (2007). The easterly extensions of profiles 1 to 6 into the New England Fold Belt are not presented in Figure 4, but were included in the modelling to avoid edge effects. The modelled outcomes fit well with the observed gravity and are considered structurally consistent with extensional rift-basin formation.

The final structural models were adjusted to fit the observed gravity and control boreholes. The Gunnedah Basin is bounded on the east by the east-dipping Hunter–Mooki Thrust Fault. North of Murrurundi the Hunter–Mooki Fault trends north-northwest and dips  $43\text{--}48.5^\circ\text{NE}$  (Carey 1934) and further north, in the Maules Creek area, Ramsay & Stanley (1976) estimated dips of around  $25^\circ\text{E}$ . The shallowing dip of the Hunter–Mooki Fault was incorporated into the profile. East of the Hunter–Mooki Fault, in the northern part of the Gunnedah Basin, is the Kelvin Fault which is also an east-dipping thrust (Liang 1991). The Kelvin Fault is modelled in the Bingara, Barraba and Manilla profiles. The Rocky Glen Ridge is assessed in this study as the structural control for the western extent of rift volcanics, with no rift volcanics observed in boreholes in the Rocky Glen Ridge area or to the west. Lower density ( $2.60 \text{ t/m}^3$ ) portions of Lachlan Fold Belt were required to help fit the observed long-wavelength gravity lows. The alternative of increasing sediment thickness and/or changes in density instead of the Lachlan Fold Belt lows did not produce a modelled response which satisfied the borehole information and was considered geologically reasonable. These lower density areas of Lachlan Fold Belt often are required where the basement is shallower, suggesting either using a uniform density for the Lachlan Fold Belt may be ineffective or these areas compositionally different, more weathered or contain granitic intrusions. Large dolerite intrusives (100–200 m thick) recorded in several boreholes were initially modelled with a density of  $2.77 \text{ t/m}^3$  in the Bingara and Barraba profiles, although as the response of the bodies did not influence the calculated gravity anomaly they were not included in any of the final models.

## LINE 1 BINGARA PROFILE

The Bingara Profile (Figure 4a) is the most northern profile, with boreholes used for calibration for the base of the Jurassic, basin sediments and top of basal volcanics west of the Boggabri Ridge. To the east of the Boggabri Ridge there are no borehole data available to delineate the thickness of sediments and volcanics



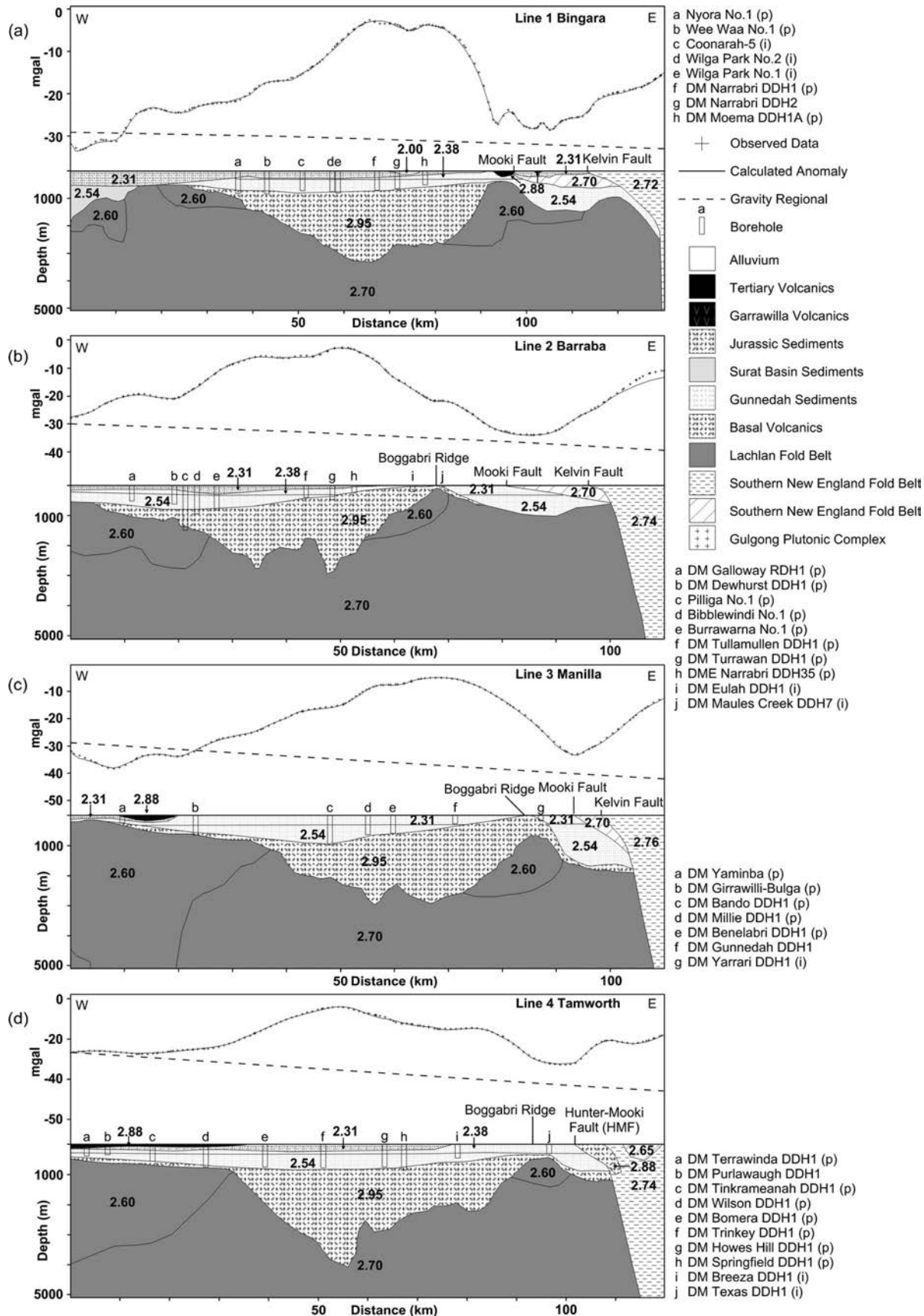


**Figure 4** Gravity model profiles with observed gravity points (crosses), regional correction (dashed line), modelled response (solid line) and key structural features. Density of units in  $\text{t/m}^3$ . Calibration boreholes (Figure 5) shown as rectangles. (a) Line 1 Bingara. (b) Line 2 Barraba. (c) Line 3 Manilla. (d) Line 4 Tamworth. (e) Line 5 Quirindi. (f) Line 6 Liverpool. (g) Line 7 Rocky Glen. (h) Line 8 Boggabri. See Figure 3a for location of lines.

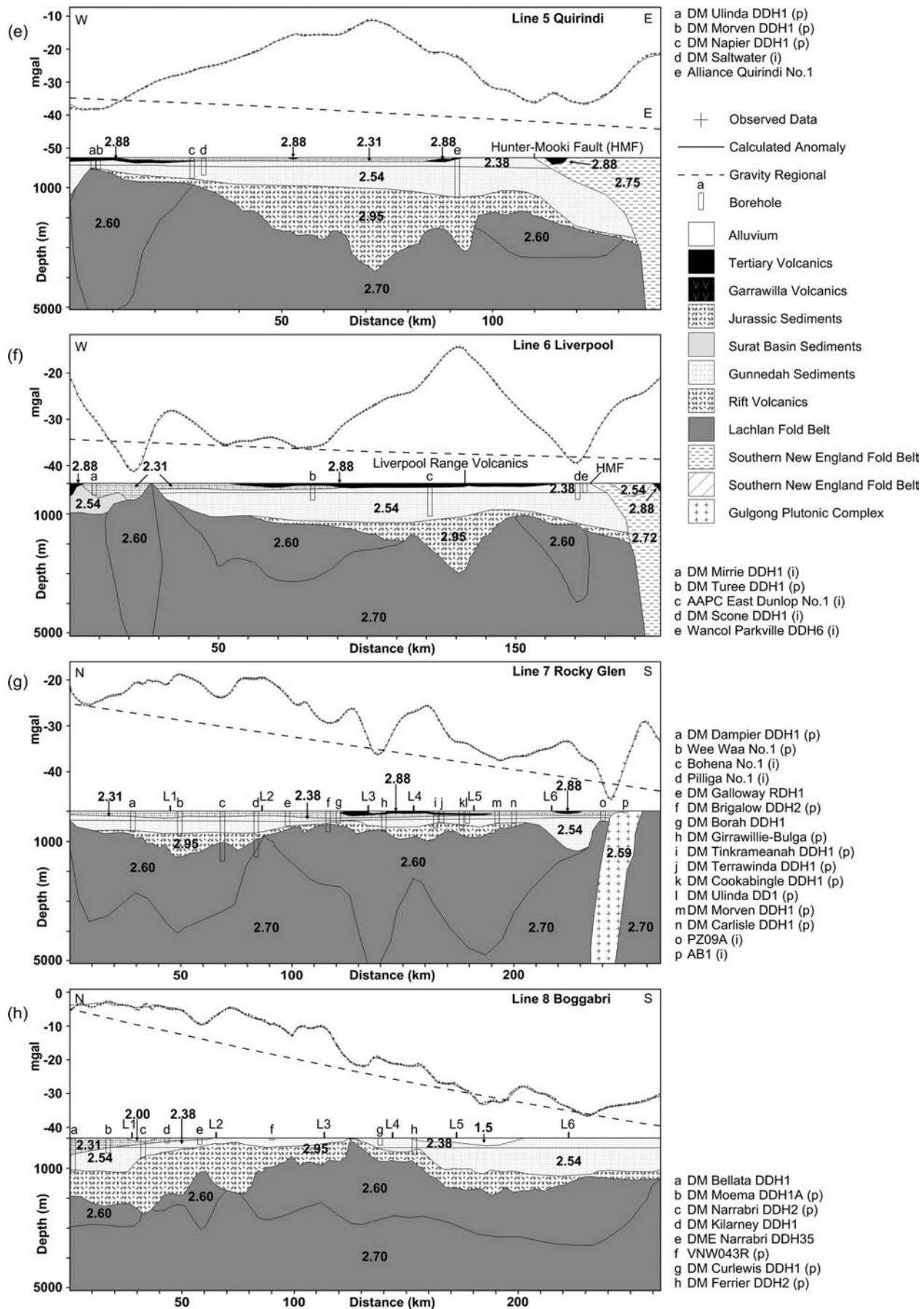


Figure 4 (Continued).

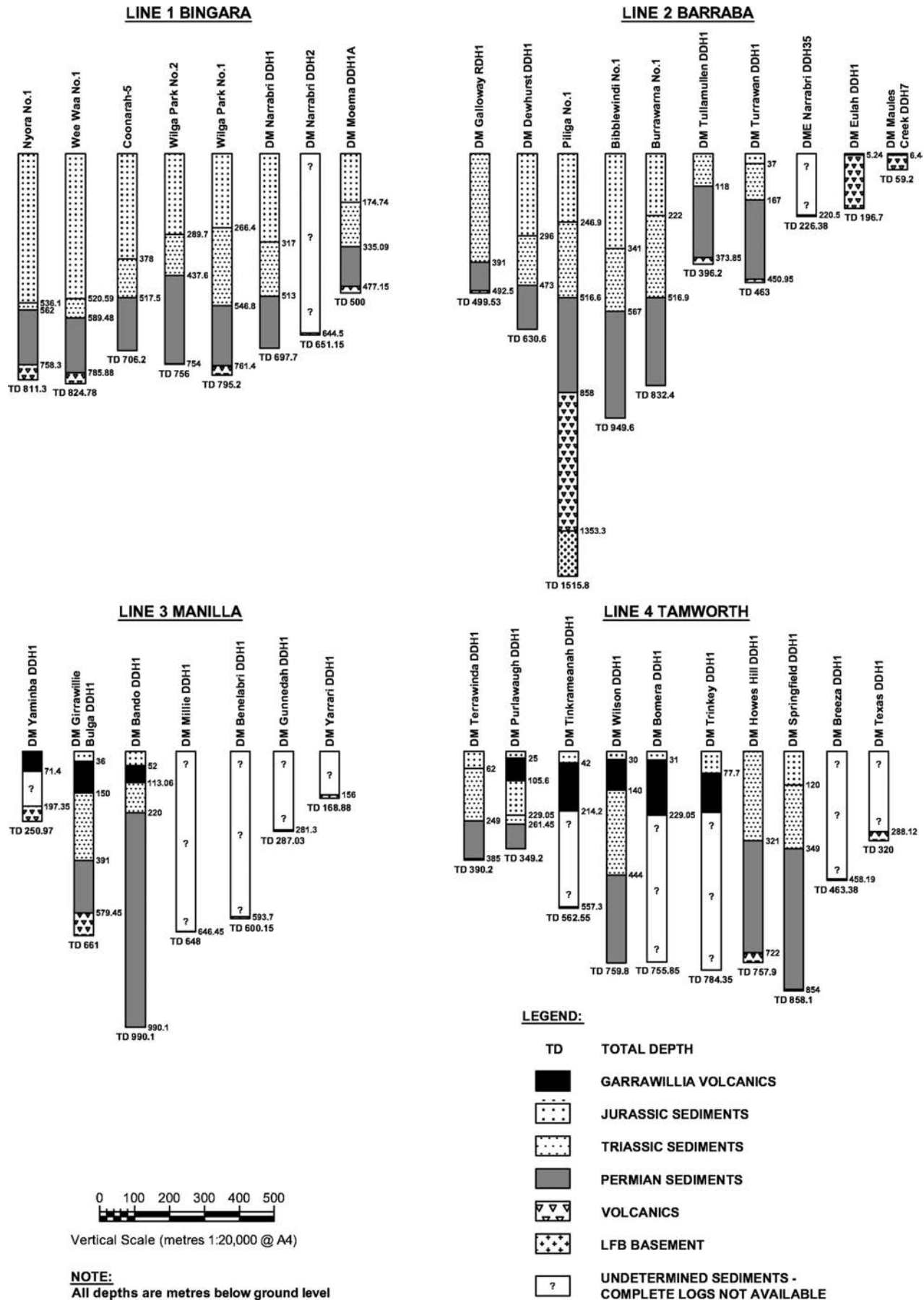


Figure 5 Stratigraphic sections of boreholes in Lines 1-7. LFB, Lachlan Fold Belt.



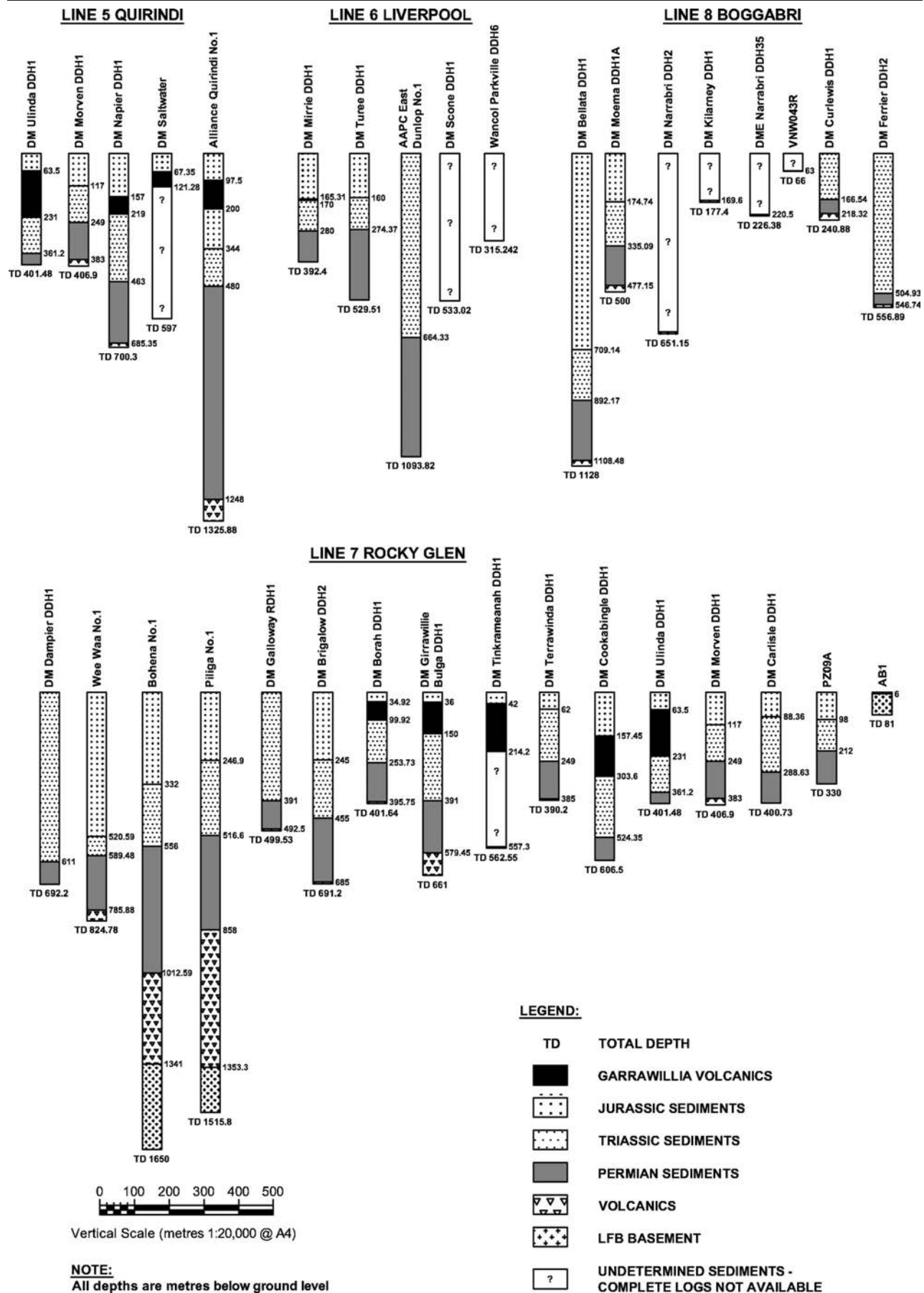
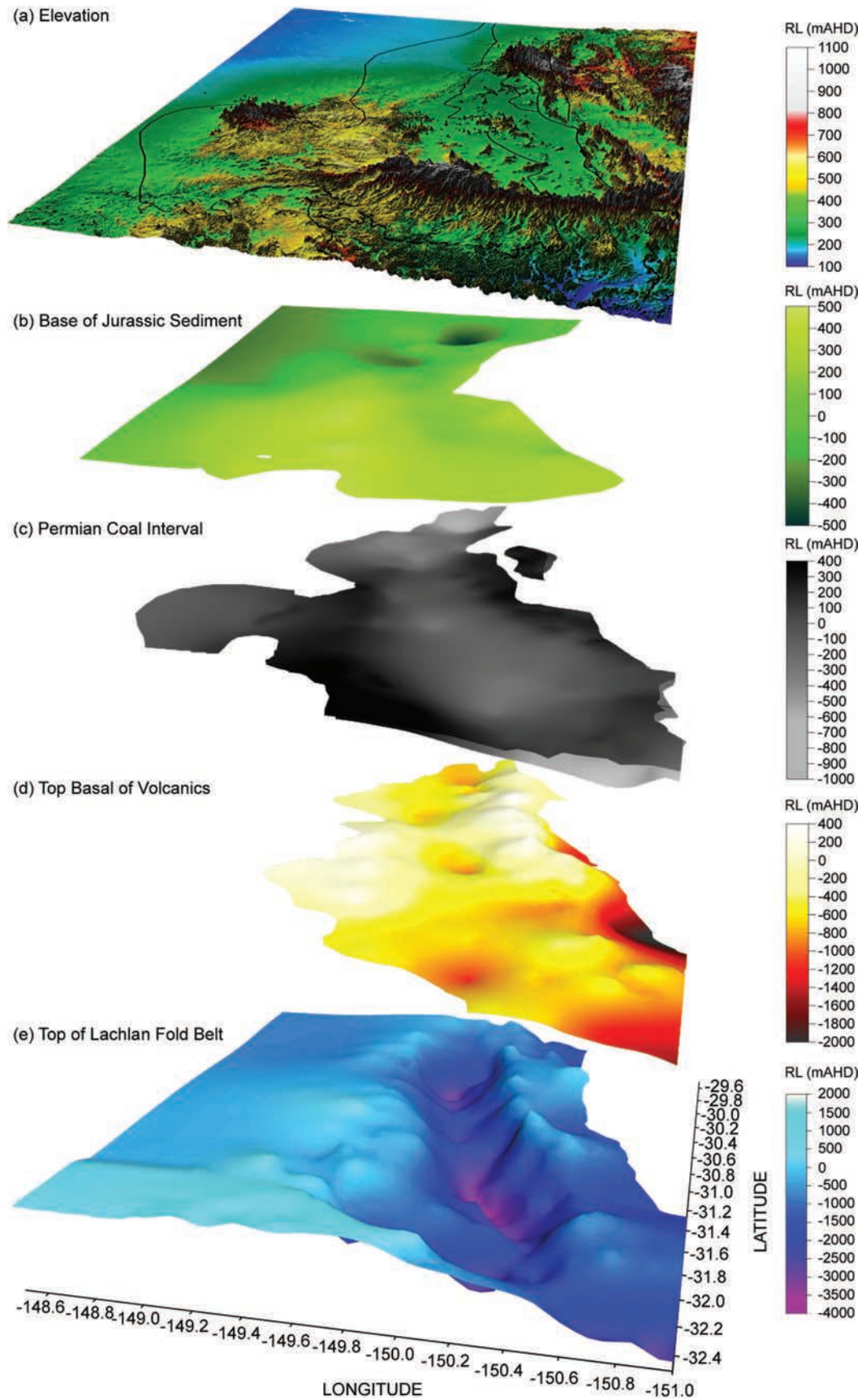


Figure 5 (Continued).



**Figure 6** Stacked model 3D surfaces of the Gunnedah Basin in mAHD, shown to their approximate extent. (a) Elevation with basin outline. (b) Base of Jurassic sediment. (c) Top and base of the Permian coal interval in the Mullaley Basin and Maules Creek Sub-basin. (d) Top of basal volcanics. (e) Top of Lachlan Fold Belt basement with Gunnedah Basin outline. Basement on the western side outside the basin outline should be considered as representative only due to limited borehole controls.

**Table 2** Thermal properties of rock types used in Ellipsis.

Rock type	Density (t/m <sup>3</sup> )	Conductivity (W/m-K)	Heat production ( $\mu$ W/m <sup>3</sup> )
Sediments	2.50	2.00	1.25
Coal Measures	1.50	0.30	1.25
Basal volcanics	2.90	3.00	0.50
LFB basement <sup>a</sup>	2.70	3.00	2.00

<sup>a</sup>LFB, Lachlan Fold Belt.Values derived from Wollenberg *et al.* (1987), Swaine (1990), Clauser & Huenges (1995) and Turcotte & Schubert (2002).**Table 3** Northern Gunnedah Basin temperatures at depth, raw and corrected.

Borehole	Depth (m)	Uncorrected T (°C) <sup>a</sup>	Corrected T (°C)
Coonarah 1A	650.00	37.00	46.75
Wilga Park 1	795.00	63.89	75.81
Nyora 1	811.37	44.50	56.67
Wee Waa 1	824.78	45.00	57.37
Bohena 1	1650.00	60.00	84.75

<sup>a</sup>Uncorrected data as per Othman & Ward (2002).**Table 4** Corrected temperatures at depth measured in selected monitoring piezometers Ulan, New South Wales.

Depth <sup>a</sup>	PZ07A	PZ08C	PZ09B	PZ26A	R755A	R753A
30	–	–	–	23.07	–	–
50	18.94	–	–	–	–	–
80	–	–	19.01	24.21	–	–
90	–	–	–	–	24.06	24.35
100	19.75	–	–	–	–	–
120	–	23.90	–	–	–	–
130	–	–	20.39	–	–	–
140	–	–	–	24.98	–	–
150	20.37	–	–	–	–	–
180	–	–	21.39	–	–	–
230	–	–	–	30.02	–	–
250	27.13	–	–	–	–	–
280	–	–	25.74	–	–	–

<sup>a</sup>metres below ground level

near the Hunter–Mooki Fault. The model indicates ~1 km-thick Permian–Jurassic sedimentary rocks of low density (2.31–2.54 t/m<sup>3</sup>) overlying the basal volcanics (2.95 t/m<sup>3</sup>) in the central part of the profile and the Lachlan Fold Belt (2.60–2.70 t/m<sup>3</sup>) to the east and west. The basal volcanics are deepest (up to 2.5 km thick) west of the Boggabri Ridge. At 70 km along the profile a small low-density body (2.00 t/m<sup>3</sup>) is introduced to represent the alluvial sediments of the Namoi River which have been recorded up to 200 m thick in some boreholes. The Gunnedah sediments are modelled extending underneath the Hunter–Mooki Fault to the Kelvin Fault overlying the Lachlan Fold Belt basement to achieve the observed low at the Hunter–Mooki Fault. The orientation of the Kelvin Fault is determined by best fit of the gravity data.

## LINE 2 BARRABA PROFILE

The Barraba Profile (Figure 4b) is the only profile in the Gunnedah Basin which transects the Maules Creek Sub-basin. The geometry of the basin at this location is similar to that of the model solution developed for the Bingarra Profile. The model indicates ~700 m of Permian–Jurassic sediments overlying basal volcanics in the west and 1–1.5 km of Permian sediments in the Maules Creek Sub-basin under the Hunter–Mooki Fault. A lack of boreholes in the northern part of the Maules Creek Sub-basin makes it difficult to determine the thickness of sediments and the extent of the basal volcanics. Tadros (1993) indicated, based on borehole KCC Maules Creek DDH 19 (projected to be located just east of Maules Creek DDH7), that sediments are at least 800 m thick. The Boggabri Ridge, which is exposed at the surface in this profile, comprises basal volcanics overlying a low density (2.60 t/m<sup>3</sup>) Lachlan Fold Belt basement high. The thickness of the volcanics on the Boggabri Ridge is modelled at less than a few hundred metres. The base of the volcanics in this area has not been reached despite the numerous boreholes in the area. Pilliga 1 is the only borehole on in this profile that delineates the thickness of the basal volcanics and penetrates the top of the Carboniferous volcanics of the Lachlan Fold Belt.

## LINE 3 MANILLA PROFILE

The Manilla Profile (Figure 4c) is the centre profile of the Gunnedah Basin and shows consistent model geometry to the previous profiles but with an increasing dip on the Hunter–Mooki Fault. DM Arrarownie DDH1, located off the western end of the profile, indicates basement begins to shallow with the Rocky Glen Ridge and basal volcanics are absent. Therefore, at the start of this profile the basal volcanics are shown truncated by basement. There is no Jurassic sediment present east of the Garrawilla Volcanics, based on surface geology. BRM91-G01 provides a good structural guide for the sediment depth under the Hunter–Mooki Fault east of the Boggabri Ridge. In this model sediments extend almost 2 km beneath the Hunter–Mooki Fault and overlie a thin layer of basal volcanics.

## LINE 4 TAMWORTH PROFILE

The Tamworth Profile (Figure 4d) shows similar model geometry to the previous profiles, but without the Kelvin Fault. East of the Hunter–Mooki Fault, Werrie Basalt is modelled exposed at the surface, as shown on the geological map. This profile was initially extended further west under the Oxley Sub-basin to explore the possible extent of basal volcanics but the dominance of the Rocky Glen Ridge basement high was noted. In the final model, the extent of basal volcanics ends at the start of the profile, with the basement high of the Rocky Glen Ridge acting as an effective control in limiting the western extent. The depths of volcanics in two of the projected boreholes (DM Howes Hill DDH1, DM Breeza DDH1; Figure 4d) are slightly shallower than the actual modelled top of volcanics. Four boreholes



show ~100–200 m of Jurassic Garrawilla Volcanics at the western end of the profile which have been included because their significant response to the modelled gravity.

#### LINE 5 QUIRINDI PROFILE

The Quirindi Profile (Figure 4e) model indicates ~1 km of Permian–Jurassic sediment overlying the basal volcanics in the central and western part of the profile and Permian sediments 2.5 km underneath the Hunter–Mooki Fault. A large gravity low at the start of the profile is modelled as low density Lachlan Fold Belt and could represent a buried granitic pluton. The Boggabri Ridge, which has been a prominent structure in the previous modelled profiles, is significantly less pronounced in the east on the Quirindi Profile. As with the Tamworth Profile the modelled response of the Garrawilla Volcanics is significant enough to be included and their extent is determined from boreholes and surface geology.

#### LINE 6 LIVERPOOL PROFILE

The Liverpool Profile (Figure 4f) is the southernmost profile in the Gunnedah Basin and transects across the Liverpool Range Volcanics. The purpose of this profile was to model an area of the basin with very limited borehole control to assess the suitability of the previously modelled geometry and therefore the ability to define a continuous basin structure. A high-amplitude gravity anomaly occurs 90–160 km along the profile, presumed to be the Liverpool Range Volcanics, and a strong gravity low occurs 20–30 km along the profile and is here presumed to be the response of the exposed Ordovician Tuklen beds of the Lachlan Fold Belt and Gulgong Granite mapped by North Limited (Kenny 1997).

The volcanics at the base of DM Scone DDH1 and Wancol Parkville DDH6 have previously been interpreted as the basal volcanics, although assessment of these logs and other nearby boreholes indicates these two boreholes appear to terminate in an intrusion interbedded with sandstone rather than basal volcanics. Therefore, they are used in this profile to define minimal thickness of sediments in the eastern part of the profile and not basal volcanics. The model indicates ~1 km of Permian–Jurassic sediments overlying the basal volcanics. The Liverpool Range Volcanics are modelled ~150 m-thick based on estimates from surface relief as the profile crosses the edge of the range. Adjusting the thickness of the Liverpool Range Volcanics requires minor adjustment to the thickness of the basal volcanics. Thickness of the Gunnedah sediments is comparable to the Quirindi Profile as is the geometry of the Hunter–Mooki Fault. This indicates the overall east–west geometry of the Gunnedah Basin is reasonably consistent.

#### LINE 7 ROCKY GLEN PROFILE

The Rocky Glen Profile (Figure 4g) is oriented north–south along the Rocky Glen Ridge, the western structural boundary of the Gunnedah Basin. The best-fit gravity models shows a shallow (<1000 m) Lachlan Fold Belt

basement overlain by a thin undulating layer of basal volcanics and generally <700 m of Permian–Jurassic sediments, with the exception of the southern end near the Gulgong Granite where sediments are modelled up to 1.5 km thick. The east–west profiles tie points are shown on Figure 4g and consistency between the different model directions is well maintained.

#### LINE 8 BOGGABRI PROFILE

The Boggabri profile (Figure 4h), oriented north–south, extends through the gravity high of the Boggabri Ridge and down the eastern edge of the Gunnedah Basin towards Muswellbrook. The best-fit gravity models shows a slightly deeper (1–1.5 km) low-density Lachlan Fold Belt basement overlain by a moderate layer of basal rift volcanics, exposed at the surface in the central part of the profile. Surface exposed Boggabri Volcanic are shown on the geology map to a lesser extent than those modelled in the Boggabri profile as Quaternary alluvial sediments are quite extensive. Modelling of these sediments, estimated from borehole logs as <100 m did not produce a significant response in the calculated gravity anomaly, although it can be modelled by adjusting the base of the basal volcanics by less than 100 m. Limited borehole data are available for the southern part of the profile to constrain sediment thickness and basal volcanic extent and depth. The model indicates a shallowing basement is likely with a thinning basal volcanics layer and ~1.5 km of Permian–Triassic sediments.

### 3D basement structure

Using the gravity profile models and available borehole information the 3D basement structure of the Gunnedah Basin can be interpolated (Figure 6). Also derived from gravity and borehole data are a surface representing the top of the basal volcanics. Using borehole information the Mullaley and Maules Creek coal interval, which is where coal in the Permian Coal Measures first appears and then ends and includes all sediments in between, can be interpolated. The base of the Jurassic sediment is interpolated from borehole information. In the north, northwest and far-western parts of the Gunnedah Basin borehole data are sparse and interpolation points between boreholes is required for smoothing of the surface. The extensive nature of the Liverpool Range Volcanics has limited the amount of exploration in the area and as such borehole information is also limited.

The interpolation of the extent of the coal measures interval was undertaken primarily to aid the thermal modelling. Limited borehole information, primarily in the south around the Liverpool Ranges required some interpretation to produce the surface. Using the gravity models and borehole information the shape of the coal interval shows a gentle dip towards the centre of the Gunnedah Basin allowing extrapolation of the interval where borehole information was limited.

### Thermal structure

Six cross-sections (same as Lines 1–6 in the gravity section) were constructed. To counteract the

uncertainties in these models, we compare results from forward models to available thermal constraints from heat flow and downhole temperature data. Unfortunately, very little reliable heat-flow data exists for the Gunnedah Basin. Available data (Cull 1982) suggested heat fluxes in the range 50–80 mW/m<sup>2</sup> are appropriate for the Gunnedah Basin, although this estimate was made from only two data points. The heat flux predicted in these models is around  $70 \pm 10$  mW/m<sup>2</sup> (depending on profile specifics such as basin thickness and thus total internal heat production, integrated thermal conductivity etc), which is entirely consistent with observed values.

Many coal or petroleum borehole logs in the Gunnedah Basin contain temperature information, although often the temperature measurements are taken within 12 h of drilling so the boreholes have had no time to equilibrate. As such, they are of limited value, as we have no way of reconstructing what the actual equilibrium temperatures are. For example, Othman & Ward (2002) collated some thermal data from the northern Gunnedah Basin from older well completion reports supplied by the Department of Primary Industries, New South Wales (Table 3). Inspection of the well completion reports suggests most temperature measurements were made within 4–12 h after the cessation of drilling. Corrections for non-equilibrium borehole temperatures have been studied (Deming 1989; Zschocke 2005), and older traditional methods (such as Horner plots) have been shown to depend strongly on assumptions that may not be justified, and most empirical corrections seem to only work within the geothermal field in which they have been derived (Deming 1989). The forward modelling of Zschocke (2005) suggested that, for plausible conductivity structures, the magnitude of the temperature perturbation increases almost linearly with depth (assuming a linear geotherm and constant temperature drilling mud), and at 1 km depth may be almost 20°C immediately after the cessation of drilling. In a similar vein we apply an empirical temperature correction to

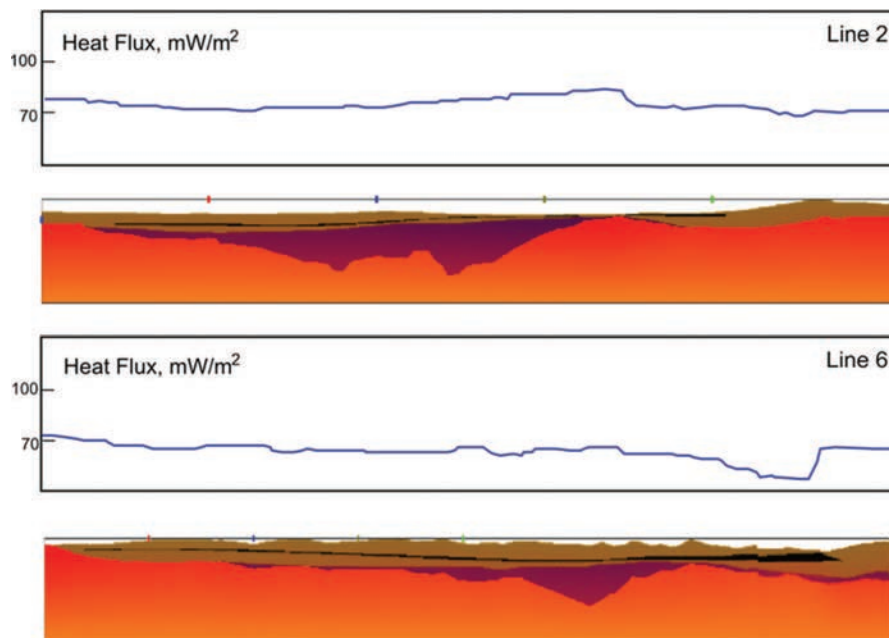
the northern Gunnedah temperature data (Table 3), assuming a short term perturbation which increases linearly to 15°C/km.

We have also taken our own temperature logs of the Ulan region, and the climate-corrected temperature data are shown in Table 4. While the data are at a much shallower depth and lower temperatures than elsewhere, they are at equilibrium conditions and were repeatable, and thus represent the only available data on the thermal state of the southern Gunnedah Basin.

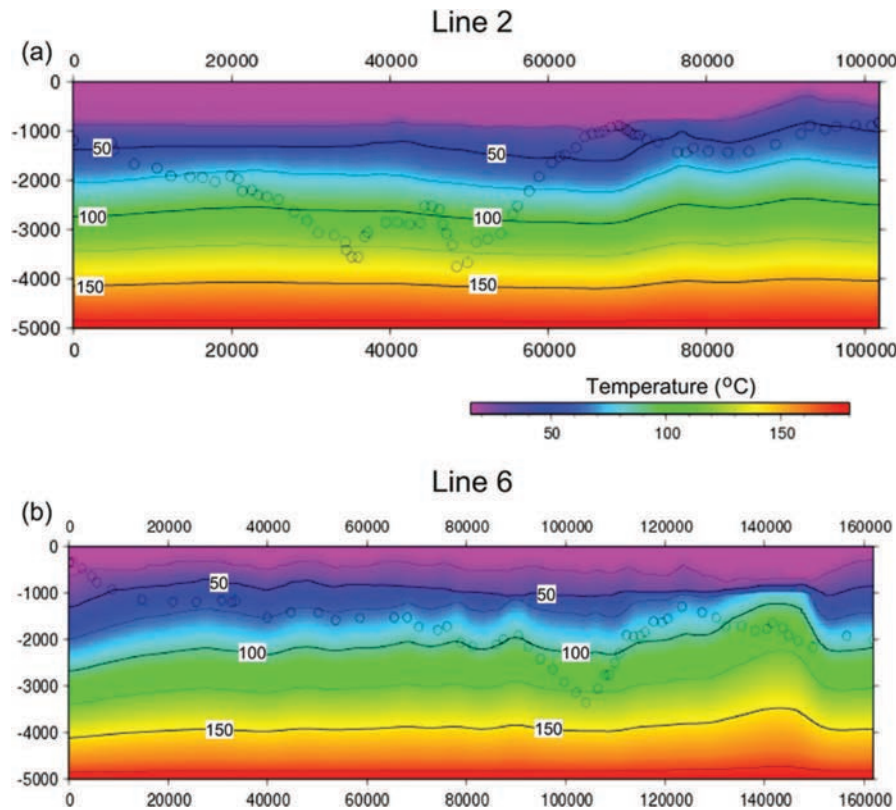
Figure 7 shows the setup of two thermal models for Lines 2 and 6, which were taken as representative of the northern and southern Gunnedah regions, respectively. The lithology is based on the gravity models in Figure 4b and f, and the thermal properties listed in Table 2. The surface heat flux of both of these models is also plotted. The heat flux is strongly influenced by the distribution of the insulating coal measures in these models, with heat being refracted around the thicker coal seams into adjacent, non-insulated areas. The basement topography, and thus the thickness of the overlying sediments, also exerts an important influence on the surface heat flux.

Figure 8 shows the subsurface temperature field for the two models in Figure 7. The surface topography clearly plays an important part in determining the temperature structure of the upper 500 m. However, this effect does not penetrate the thicker coal measures and temperatures beneath the coal measures are largely controlled by the basin topography, and the topology of the coal layer. The net result is we see variations of up to 500 m in the depth of the 150°C isotherm across different lines (e.g. Line 6), which has important implications for geothermal prospecting in the area. We should reiterate, though, that these temperature fields are purely conductive, and do not include the effect of advection of heat due to aquifers.

In order to baseline the models it is important to compare the predicted temperatures to measured



**Figure 7** Representative model configurations of the northern (Line 2) and southern (Line 6) Gunnedah Basin and surface modelled heat flux.



**Figure 8** Subsurface isotherms of representative models of the (a) northern (Line 2) and (b) southern (Line 6) Gunnedah Basin. Basement surface level shown as circles.

subsurface temperatures. Unfortunately, measured temperatures are scarce, and we have data from only two areas, Narrabri (Line 1) and Ulan (Line 6). As mentioned previously, these data have individual problems; the Ulan measurements are limited in depth, and the Narrabri data are from unequilibrated wells to which we have had to apply an empirical correction. These data, along with modelled geotherms from each of the regions, are presented in Figure 9. The depths here are from the surface (i.e. not the relative levels plotted in Figure 8). In all, the modelled geotherms give a good fit to the data within their limitations, and support the use of 180°C at 5 km as an appropriate bottom temperature condition in this region. The range in predicted heat flux ( $\sim 70\text{--}80\text{ mW/m}^2$ ) are also within the range calculated for the Gunnedah Basin.

We have also stacked and gridded the 2D sections to create a 2.5D thermal model of the basin, which is shown in Figure 10 as temperatures draped across the basement topography. Here the temperatures at the top of the basement were sampled for each profile, then gridded and draped across the basement architecture. Somewhat unsurprisingly, the highest basement temperatures occur in the deepest portions of the basin, where the overlying sediment/mafic package is the thickest. The temperature at the top of the basement range from  $\sim 105$  to  $165^\circ\text{C}$ : the highest temperatures occur in the northern and southernmost parts of the basin.

## DISCUSSION

Previous modelling of the Gunnedah Basin, and associated Meandarra Gravity Ridge (which is a gravity

response presumed from an underlying mafic source), have been undertaken by Guo *et al.* (2007) and Krassay *et al.* (2009). Krassay *et al.* (2009) tested the Qureshi model (shallow dense source: Qureshi 1984) and the Leaman model (granitic terrain: Leaman 1990) for modelling the Meandarra Gravity Ridge, concluding that a modified Qureshi-type model with a dense mafic source solely in the upper crust with rift-like geometry produces a good approximation of the gravity data. Guo *et al.* (2007) reached a similar conclusion in modelling the Gunnedah Basin. Principally both Krassay *et al.* (2009) and Guo *et al.* (2007) concluded that the Meandarra Gravity Ridge was produced by high-density mafic volcanic rocks ( $2.95\text{ t/m}^3$ ) that were located immediately below the sedimentary rocks of the Gunnedah Basin, with a thickness of 5–9 km. Krassay *et al.* (2009) suggested that the Meandarra Gravity Ridge is linked to the origin of the Sydney–Gunnedah–Bowen Basin system and is composed of extensional mafic melt.

We have taken this conclusion and the gravity models of Guo *et al.* (2007) and re-tested them, but this time we have included structural and stratigraphic controls from borehole drilling, seismic-reflection survey line BMR91.G01 as well as additional density testing. Geological interpretations of the deep seismic profile based on Korsch *et al.* (1997) suggest that beneath the base of the Permian sedimentary rocks is a reflective unit that corresponds very closely to the shape of the mafic body defined by previous gravity modelling and is the basal volcanics of our modelling.

Given the constraints imposed by borehole information on the depth to the top of basal volcanics, the sensitivity to the base of the basal volcanics is dependent therefore on the density of the basement.

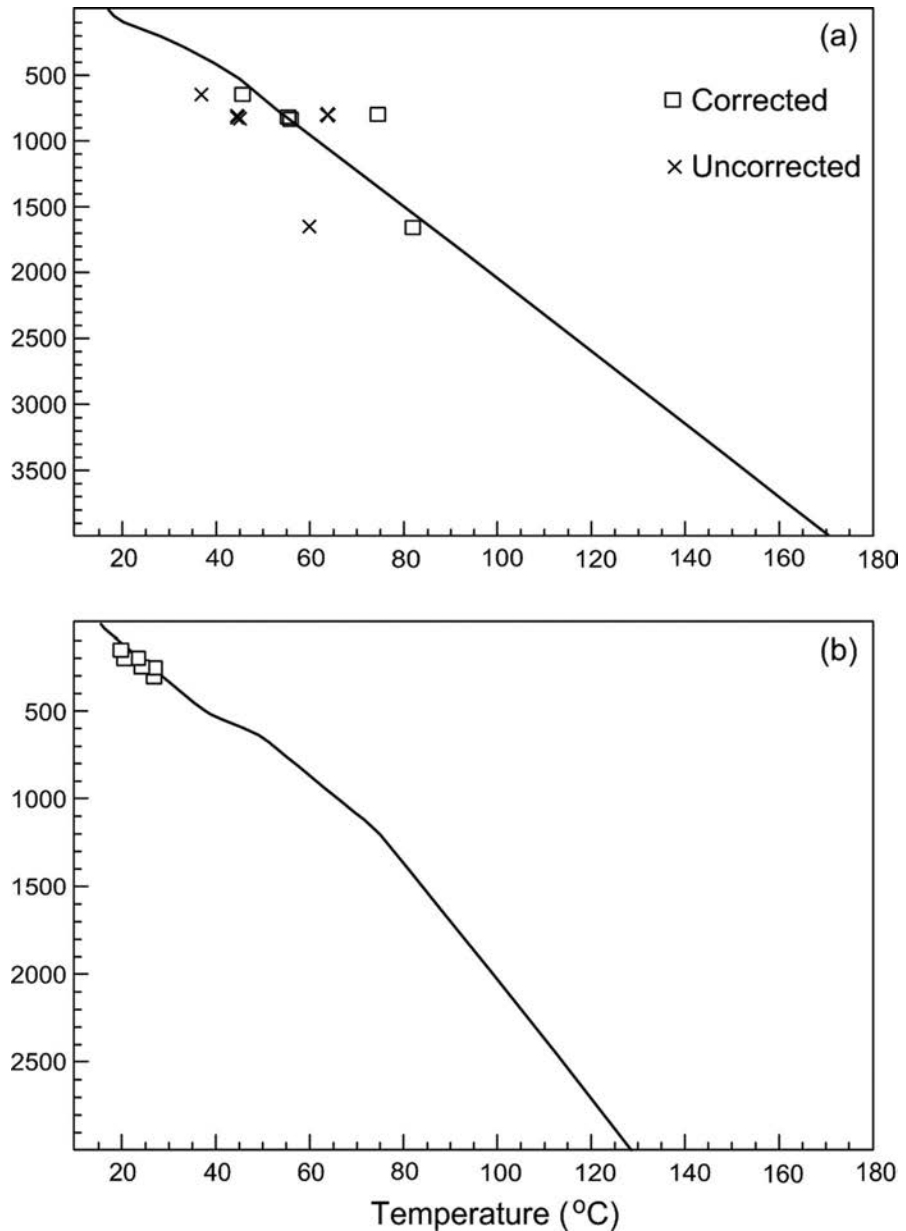


**Figure 9** (a) Uncorrected and corrected borehole temperatures at depth from near Narrabri (Line 2) with geotherm (solid line). (b) Borehole temperatures at depth from Ulan (Line 6) with geotherm (solid line).

Both Krassay *et al.* (2009) and Guo *et al.* (2007) also used a density of  $2.70 \text{ t/m}^3$  for the Lachlan Fold Belt. Krassay *et al.* (2009) also showed that densities  $> 2.74 \text{ t/m}^3$  were inconsistent with the regional gravity field. In addition, we have added a lower density ( $2.60 \text{ t/m}^3$ ) portion to the basement in order to meet the model constraints. This basement heterogeneity was essential to meet borehole constraints and probably represents an increased granitic component. A change in the density of the basement by  $\pm 0.01 \text{ t/m}^3$  results in an  $\sim 390 \text{ m}$  change to the base of the basal volcanics. Where we have borehole constraints on the thickness of the basal volcanics, changes in basement density greater than  $\pm 0.015 \text{ t/m}^3$  result in an unacceptable degradation of fit, and density changes  $> \pm 0.03 \text{ t/m}^3$  result in models that do not satisfy either borehole or seismic data.

The gravity models (Figure 4) indicate a channel-like feature in the Lachlan Fold Belt basement that is filled with basal volcanics. This thick pile of dense material

forms a distinctive gravity high predominately corresponding to the location of the approximately north-south-oriented Meandarra Gravity Ridge (Figure 3), and is consistent with mafic volcanic fill in a channel-like feature. When the gravity modelling and borehole information is interpolated into 3D surfaces (Figure 6) the inferred rift is apparent, running approximately north-south through the centre of the Gunnedah Basin and contains 2.5–3 km of basal volcanics. During decompression melting of the rift basin, horst-graben fault-bounded blocks would have acted as magma conduits for the basal volcanics to extrude and fill the rift valley.

In the west, the gravity low of the Rocky Glen Ridge is modelled containing numerous granitic plutons. This ridge parallels the Meandarra Gravity Ridge in the Gunnedah Basin and appears to extend southwards beside the Sydney Basin, as is evident by the numerous plutonic intrusions around Ulan and Mudgee. The



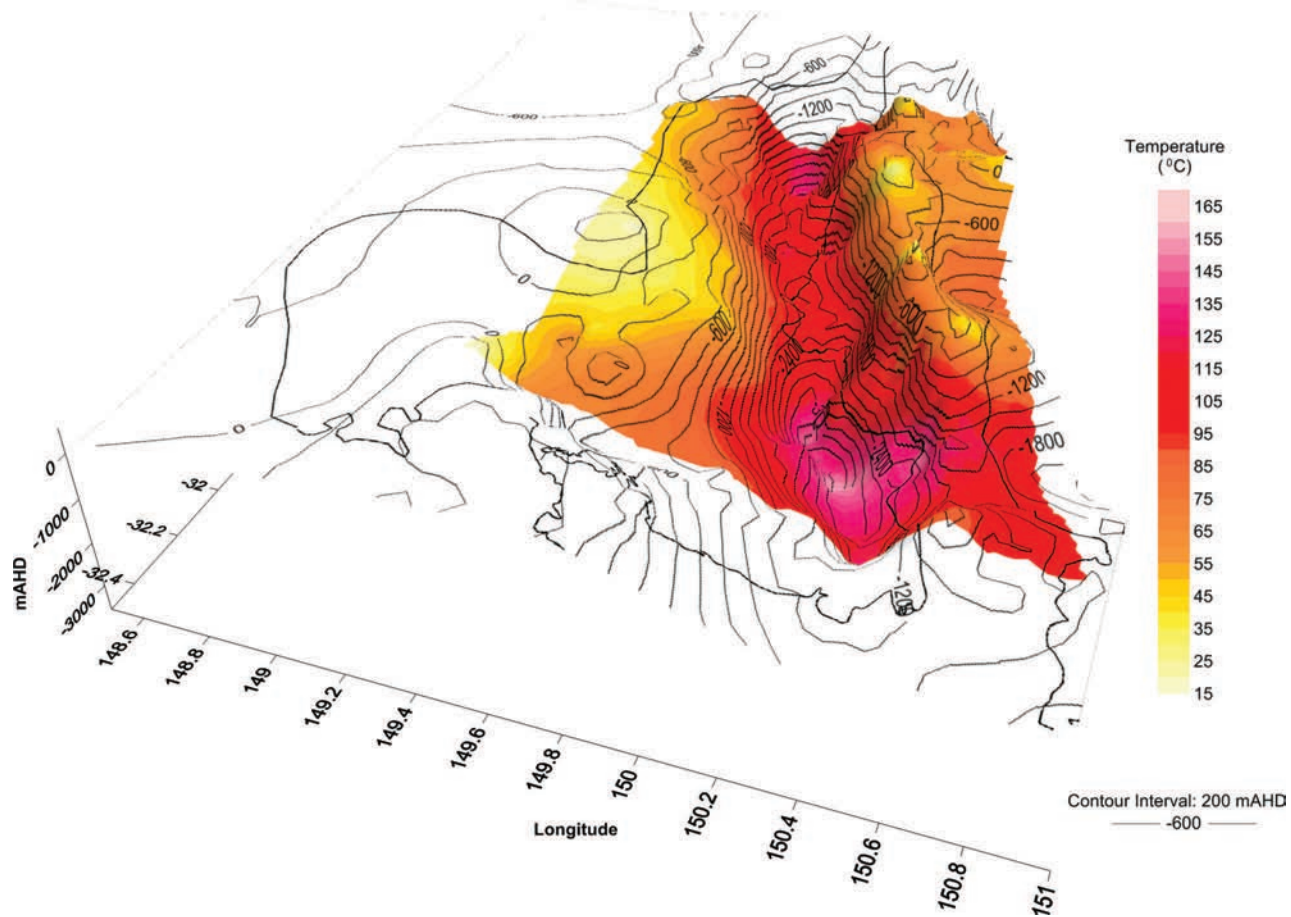


**Figure 10** Temperature of the top of Lachlan Fold Belt basement draped over basin architecture.

Carboniferous rhyolitic volcanics (of the Kuttung Series) occur mainly on the eastern part of the Rocky Glen Ridge (DM Arrarownie DDH1, Bohena No.1 and Pilliga No.1). Rhyolites of the Boggabri Volcanics are more commonly found along the Boggabri Ridge on the eastern side of the basin (from the analysis of drillhole data).

In the northwest, the top of the Lachlan Fold Belt appears to deepen on the western side of the Rocky Glen Ridge. In this area borehole control is very limited and gridding artefacts are present as the limit of the mapped area is approached. It is interpreted that the basement should deepen in this location given borehole logs north, in the Surat Basin, indicate 3–5 km of sediment, and the surface topography is considerably flat at 100 mAHd or less. To the east of the Boggabri Ridge in the northern part of the basin is the small Maules Creek Sub-basin which is a shallow fault-bounded basin. Due to limited coal exploration in the area the structure of the sub-basin is difficult to determine, although drilling does indicate that it deepens in its south with a minor amount of basal volcanics. The basement high in the north and central parts may limit the basal volcanics reaching the Hunter–Mooki Fault, as has been modelled in the Bingarra (Figure 4a) and Barraba (Figure 4b) gravity profiles.

The interpolated surface of the top of the basal volcanics (Figure 6) shows to the west, that the Rocky

Glen Ridge strongly controls the extent of the volcanics while to the east they are exposed in parts along the Boggabri Ridge before being truncated by the Hunter–Mooki Fault. The northern and southern extents of the basal volcanics appear continuous into the Sydney and Bowen Basins. The top of the basal volcanics ranges from 300 mAHd to –900 mAHd and attain a thickness of 1.8–3.2 km. The top of the basal volcanics surface appears to show the effects of later tectonic deformation, with some deep lows probably related to horst–graben blocks, while a general low along the centre of the basin is related to sagging during cooling and sediment loading.

The interpolation of the extent of the coal measures interval was undertaken primarily to aid the thermal modelling. Limited borehole information, primarily in the south around the Liverpool Ranges, required some interpretation to produce the surface. Using the gravity models and borehole information the shape of the coal interval shows a gentle dip towards the centre of the Gunnedah Basin allowing extrapolation of the interval where borehole information was limited.

The geological history of the area indicates a time break between sedimentation at the end of Triassic and the beginning of the Jurassic. During the time break significant erosion of Triassic and Permian sediments in the basin occurred, up to 2 km according to Tadros (1993). Jurassic sedimentation covers a significant area

of the Gunnedah Basin, with the exception of small area between Narrabri and Breeza, and is generally <500 m thick. Towards the north and northwest of the basin the thickness of the Jurassic sediments increase to ~700 m (~400 mAHD).

The surface topography of the Gunnedah Basin ranges from <100mAHD in the northwest to over 1100 mAHD in south along the Liverpool Ranges, in the northeast at Mt Kaputar in the Nandewar Ranges and in the west at the Warrumbungles. The central part of the Gunnedah Basin is relatively flat and of low relief (200–400 mAHD).

Both the denudation history and topography are likely to affect subsurface temperatures. The topographic variations were explicitly incorporated in the thermal calculations here. However, the denudation (or deposition for that matter) was not significant for most of the Cenozoic, and so the basin has equilibrated from the Mesozoic events.

The basal temperature was a variable in this modelling, to be altered in order to fit available downhole temperature constraints. Thus, it is surprising our initial estimate of 180°C, based on the Austherm extrapolated value at 5 km, worked so well. Varying this, by say 10%, results in an unacceptable misfit to the downhole data. Of course this could be compensated by changing the basement heat production or conductivity of the overlying sediments, but such changes are *ad hoc* and would move our estimates away from laboratory-derived values.

One major limitation of the thermal modelling here is that we considered a purely conductive configuration, and did not model advection of heat by aquifers. For slow flow rates this approximation is valid. While the shallow aquifers of the Gunnedah Basin are widely studied (and utilised), the nature, extent, volume and flow rate of deeper aquifer systems are largely unconstrained. Given the decrease in permeability of rocks with pressure, the thermal effects of aquifer heat transport at depth is mitigated, but this is still an area which deserves further attention in future geothermal studies of the Gunnedah Basin.

Finally, the geometry of the Hunter–Mooki Fault was surveyed by the New South Wales Department of Primary Industries (see Figure 3 for line locations) with the results released in DPI NSW (2008), after the modelling in this study was completed. The geometry determined from this survey relative to our gravity models shows some differences in unit interpretation (e.g. DPIHM01 and Line 2) and structure (e.g. DPIHM03 and Line 5). However for the case of DPIHM02 and Line 4 Tamworth and DPIHM04 and Line 6 Liverpool the interpretation of geometry and depth is similar to that of our models.

## CONCLUSIONS

The 3D structure of the Gunnedah Basin is characteristic of a typical intracontinental rift basin. Extension initiated during the Late Carboniferous–Early Permian developed the rift structure in the centre of the Gunnedah Basin where up to 2–3.5 km of volcanics have accumulated. Following thermal subsidence and sedimentation, the Gunnedah Basin shifted to a foreland

basin during the Late Permian. After erosion during the Triassic and Jurassic sedimentation our models indicate up to ~1 km of sediments overlie the basal volcanics with pockets of deeper sedimentation under the Hunter–Mooki Fault. Preliminary thermal modelling, based on limited deep borehole temperatures, indicates top-of-basement temperatures of 105–165°C. Further deep temperature constraints from the Gunnedah Basin are required to better assess its geothermal potential.

## ACKNOWLEDGEMENTS

We would like to thank Ulan Coal Mines Ltd for permission to collect temperature readings in the company's piezometers. We also acknowledge the New South Wales Department of Primary Industries in providing the Hunter–Mooki Seismic Survey data and would like to thank Luke Twigg for creating the stratigraphic columns. Critical reviews by Frances Holgate and Tony Meixner improved an earlier version of this manuscript. This is contribution no. 633 from the Australian Research Council National Key Centre for the Geochemical Evolution and Metallogeny of Continents (<<http://www.gemoc.mq.edu.au>>). CO acknowledges Discovery Project DP0880801 and Auscope simulation and modelling.

## REFERENCES

- BRAMALL A. M. & QURESHI I. R. 1984. A preliminary investigation of the gravity anomalies in the Gunnedah–Tamworth area. *Geological Society of Australia Abstracts* **12**, 74–76.
- BUDD A. R. 2007. *Australian radiogenic granite and sedimentary basin geothermal hot rock potential map (preliminary edition) 1: 5 000 000 scale*. Geoscience Australia, Canberra.
- CAREY S. W. 1934. Note on the implications of the irregular strike-lines of the Mooki Thrust System. *Proceedings of the Linnean Society of New South Wales* **59**, 375–379.
- CLAUSER C. & HUENES E. 1995. Thermal conductivity of rocks and minerals. In: *Rock physics and phase relations, a handbook of physical constants*, pp. 105–126. American Geophysical Union Reference Shelf **3**.
- CULL J. P. 1979. Climatic corrections to Australian heat-flow data. *BMR Journal of Australian Geology & Geophysics* **4**, 303–307.
- CULL J. P. 1982. An appraisal of Australian heat-flow data. *BMR Journal of Australian Geology & Geophysics* **7**, 11–21.
- DEMING D. 1989. Application of bottom-hole temperature corrections in geothermal studies. *Geothermics* **18**, 775–786.
- DIREEN N. G., LYONS P., KORSCH R. J. & GLEN R. A. 2001. Integrated geophysical appraisal of crustal architecture in the eastern Lachlan Orogen. *Exploration Geophysics* **32**, 141–153.
- DPI NSW 2008. Hunter–Mooki Seismic Survey 2007. *MINFO* **88**, 20–21. <<http://www.dpi.nsw.gov.au/aboutus/news/minfo>>
- GLEN R. A. 2005. The Tasmanides of eastern Australia. In: Vaughan A. P. M., Leat P. T. & Pankhurst R. J. eds. *Terrane processes at the margins of Gondwana*, pp. 23–96. Geological Society of London Special Publication **246**.
- GUO B., LACKIE M. A. & FLOOD R. H. 2007. Upper crustal structure of the Tamworth Belt, New South Wales: constraints from new gravity data. *Australian Journal of Earth Sciences* **54**, 1073–1087.
- KENNY P. M. 1997. 1st Annual Report for the period ending November 14, 1997 on Exploration Licences 5154 and 5155. Report Number NE51541a, North Limited. (Digs Report No. GS1999-150\_R.00020780. <<http://digsopen.minerals.nsw.gov.au>>)
- KORSCH R. J., JOHNSTONE D. W. & WAKE-DYSTER K. D. 1997. Crustal architecture of the New England Orogen based on deep seismic reflection profiling. In: Ashley P. M. & Flood P. G. eds. *Tectonics and metallogenesis of the New England Orogen*, pp. 29–51. Geological Society of Australia Special Publication **19**.



- KRASSAY A. A., KORSCH R. J. & DRUMMOND B. J. 2009. Meandarra Gravity Ridge: symmetry elements of the gravity anomaly and its relationship to the Bowen–Gunnedah–Sydney basin system. *In: Korsch R. J. & Totterdell J. M. eds. Evolution of the Bowen, Gunnedah and Surat Basins, eastern Australia*, pp. 355–379. Australian Journal of Earth Sciences **56**.
- LEAMAN D. E. 1990. Geological Note. The Sydney Basin: composition of basement. *Australian Journal of Earth Sciences* **37**, 107–108.
- LIANG T. C. K. 1991. Fault-related folding: Tulcumba Ridge, western New England. *Australian Journal of Earth Sciences* **38**, 349–355.
- MORESI L., DUFOUR F. & MUHLHAUS H.-B. 2003. A Lagrangian integration point finite element method for large deformation modeling of viscoelastic geomaterials. *Journal of Computing Physics* **184**, 476–497.
- O'NEILL C., MORESI L., MÜLLER R. D., ALBERT R. A. & DUFOUR F. 2006. Ellipsis 3D: a particle-in-cell finite element hybrid code for modelling mantle convection and lithospheric deformation. *Computers and Geosciences* **32**, 1769–1779.
- OTHMAN R. & WARD C. R. 2002. Thermal maturation pattern in the southern Bowen, northern Gunnedah and Surat Basins, northern New South Wales, Australia. *International Journal of Coal Geology* **51**, 145–167.
- QURESHI I. R. 1984. Wollondilly–Blue Mountains gravity gradient and its bearing on the origin of the Sydney Basin. *Australian Journal of Earth Sciences* **31**, 293–302.
- QURESHI I. R. 1989. Positive gravity anomaly over the Sydney Basin. *Exploration Geophysics* **20**, 191–193.
- RAMSAY W. R. H. & STANLEY J. M. 1976. Magnetic anomalies over the western margin of the New England fold belt, northeast New South Wales. *Geological Society of America Bulletin* **87**, 1421–1428.
- SWAINE D. J. 1990. *Trace elements in coal*. Butterworth, London.
- TADROS N. Z. (Editor) 1993. The Gunnedah Basin, New South Wales. *Geological Survey of New South Wales Memoir Geology* **12**.
- TURCOTTE D. L. & SCHUBERT G. 2002. *Geodynamics*. Cambridge University Press, Cambridge.
- WOLLENBERG H. A. & SMITH A. R. 1987. Radiogenic heat production of crustal rocks: an assessment based on geochemical data. *Geophysical Research Letters* **14**, 295–298.
- ZSCHOCKE A. 2005. Correction of non-equilibrated temperature logs and implications for geothermal investigations. *Journal of Geophysical Engineering* **2**, 364–371.

Received 1 October 2009; accepted 23 March 2010

## APPENDIX 1: BOREHOLE DETAILS (COORDINATES IN GDA94 DATUM)

Borehole	Reference or DIGS Report number	Latitude GDA94	Longitude GDA94
AAPC Big Adder Hill No. 1	WCR272.R00042090	–32.47871522	150.77487861
AAPC East Dunlop No. 1	WCR267.R00042081	–32.14063712	150.29764616
AAPC Goulburn River No. 1	WCR289.R0004286	–32.42522356	150.65230444
AAPC Wybong No. 1	WCR264.R00042080	–32.27502500	150.60367789
AB1	Coffey Geoscience Report Z60/4AA (1980)	–32.27458479	149.75299124
Alliance Mirrabooka No. 1	Tadros 1993 (GS1985_005.R00014146, WCR088.R00017982)	–31.59526249	150.66393894
Alliance New Windy No. 1	Tadros 1993 (GS1985_005.R00014146)	–31.58120556	150.41642093
Alliance Quirindi No. 1	Tadros 1993 (WCR121.R00017958, GS1985_005.R00014146)	–31.47981673	150.41253209
Alliance Waverton No. 3	Tadros 1993 (GS1985_005.R00014146)	–31.53620409	150.58336177
Alliance Waverton No. 1	Tadros 1993 (GS1985_005.R00014146)	–31.36564796	150.57308145
Alliance Waverton No. 2	Tadros 1993 (GS1985_005.R00014146)	–31.55731533	150.57447340
AOG Belford Dome No. 1	WCR100.R00055477	–32.65480844	151.28586436
AOG Camberwell 1	WCR114.R00055478	–32.54008744	151.10364411
AOG Loder 1	WCR068.R00055476	–32.63369847	151.13447761
AOG Martindale No. 1A Well	WCR125.R00017882	–32.51596468	150.61529459
AOG Sedgfield 1	WCR091.R00031587	–32.51369723	151.25336419
ASV4	CR_98_4095.R00031683 (CR_95_3880.R00017790)	–30.75199279	150.26227050
Ballimore Hill No. 2 Bore	MF06984.R00056840 (GS1982_314.R00010673)	–32.11640000	148.96610000
Baradine West No. 1	MF21528.R00056889 (WRC074.R00021211)	–30.89982429	148.92396402
Baradine West No. 2	WCR706.R00021209	–30.89538073	148.77088833
BD–Belford Dome No. 1	WCR021_WCR026.R00055474	–32.64730840	151.28753097
BD–Belford Dome No. 2	WCR021_WCR026.R00055474	–32.66286405	151.28447552
Bibblewindi No. 1	GS2001_049.R00031795	–30.63442691	149.64978556
Bohena No. 1	WCR073.R00021212	–30.52398721	149.60781044
Bohena No. 2	WCR280.R00031547	–30.52827244	149.61123842
Bohena No. 2D	WCR285.R00042082	–30.52831746	149.61133235
Bohena No. 3	WCR281.R00031548	–30.54572830	149.61056782
Bohena No. 4	WCR282.R00031549	–30.53700886	149.61090133
Bohena No. 6	WCR284.R00031551	–30.53684327	149.62127475
Bohena No. 7	GS2000_069.R00031635	–30.53300940	149.61392710
Burrawarna No. 1	GS20002_380.R00031966	–30.57042378	149.69083630
Coonarah-5	GS2002_805.R00046866	–30.37788056	149.59885278
DM Arrarownie DDH1	Tadros 1993	–30.74280908	149.37085137
DM Bando DDH1	Tadros 1993 (MF31477.R00055034)	–31.16848334	149.89724458
DM Bellata DDH1	WCR225.R00021279	–29.92412577	149.73249814
DM Benelabri DDH1	Tadros 1993 (MF28628.R00055037)	–30.96009506	150.00177737
DM Benelabri DDH2	Tadros 1993 (MF28628.R00055037)	–30.90824653	149.93981181
DM Benelabri DDH3	Tadros 1993 (MF28628.R00055037)	–30.90540095	150.00285967
DM Blake DDH1	Tadros 1993 (GS1985_005.R00014146)	–30.42566959	149.76965458
DM Boggabri DDH1	Tadros 1993	–30.68379128	149.97361450
DM Boggabri DDH2	Tadros 1993	–30.69559369	150.02269410

(continued)

**Appendix 1: (Continued)**

Borehole	Reference or DIGS Report number	Latitude GDA94	Longitude GDA94
DM Boggabri DDH3	Tadros 1993	–30.69057292	150.00648904
DM Boggabri DDH4	Tadros 1993	–30.70233084	150.01246455
DM Boggabri DDH5	Tadros 1993	–30.71147144	149.99057449
DM Bomera DDH1	MF268631.R00056400	–31.39487477	149.88136884
DM Booyamurna DDH1	Tadros 1993	–31.76426520	149.84744447
DM Borah DDH1	Tadros 1993	–30.99205937	149.54331591
DM Breeza DDH1	Tadros 1993	–31.24751921	150.28606104
DM Breeza DDH2	Tadros 1993	–31.23518679	150.38965282
DM Brigalow DDH 2	Tadros 1993 (GS1985_005.R00014146)	–30.94736498	149.64549730
DM Brothers DDH1	Tadros 1993 (MF31484.R00056406)	–31.27500000	150.23600000
DM Brown DDH1	MF31485.R00055330	–31.19669132	150.25602606
DM Brown DDH2	MF31485.R00055330	–31.23040323	150.20871808
DM Bylong DDH1	MF28659.R00055040	–32.34850000	150.03510000
DM Carlisle DDH1	MF28673.R00056416	–31.70225018	149.54535600
DM Caroonna DDH1	Tadros 1993	–31.40818185	150.42310765
DM Caroonna DDH2	MF28651.R00055022	–31.46936099	150.57918252
DM Caroonna DDH3	Tadros 1993	–31.33708208	150.47597860
DM Caroonna DDH4	Tadros 1993	–31.38893250	150.54121654
DM Caroonna East DDH9	GS2000_238.R00031643	–31.33862777	150.57365118
DM Cliff DDH2	Tadros 1993 (GS1985_005.R00014146)	–31.25468966	150.32693239
DM Cliff DDH4	Tadros 1993	–31.28956987	150.32387001
DM Clift DDH1	Tadros 1993 (GS1985_005.R00014146)	–31.27665798	150.27979345
DM Coogal DDH1	MF28828.R00056417	–30.96289651	149.87428137
DM Cookabingie DDH1	Tadros 1993	–31.49180096	149.62948857
DM Coolanbilla DDH1	Tadros 1993	–31.39562241	150.13128408
DM Coolanbilla DDH2	MF28832.R00055350	–31.42606324	150.10400420
DM Curlewis DDH1	Tadros 1993 (MF31495.R00055375)	–31.17249849	150.35412723
DM Dampier DDH1	Tadros 1993 (GS1985_005.R00014146)	–30.16010065	149.49686225
DM Denison DDH1	Tadros 1993 (GS1985_005.R00014146)	–30.85056294	149.89038467
DM Denison West DDH1	MF28847.R00056428	–30.84706282	149.79034810
DM Dewhurst DDH1	Tadros 1993 (GS1985_005.R00014146)	–30.73997687	149.63609023
DM Digby DDH1	Tadros 1993 (GS1985_005.R00014146, MF31496.R00056430)	–31.16820033	150.21975663
DM Dight DDH2	Tadros 1993	–31.08040446	150.43816963
DM Doona DDH1	Tadros 1993 (GS1985_005.R00014146)	–31.39299761	150.38712035
DM Doyles Creek DDH11	MF08748.R00055111	–32.69390000	151.00570000
DM Emerald Hill DDH1	Tadros 1993 (MF30064.R00055044)	–30.84706943	150.03245772
DM Eulah DDH1	Tadros 1993 (MF31501.R00056434)	–30.41673403	150.01084687
DM Ferrier DDH1	MF31502.R00056435	–31.28734035	150.50321500
DM Ferrier DDH2	Tadros 1993	–31.29774426	150.46611681
DM Galloway RDH1	Tadros 1993 (MF31504.R00056437)	–30.78539842	149.54585924
DM Girrawille – Bulga DDH1	Tadros 1993 (GS1985_005.R00014146)	–31.17691594	149.63914425
DM Goran DDH1	Tadros 1993 (GS1985_005.R00014146, MF31505.R00055387)	–31.18035219	150.13414811
DM Goran DDH2	MF31505.R00055387	–31.17388966	150.00154284
DM Gorman DDH1	Tadros 1993 (GS1985_005.R00014146)	–30.52771823	149.77901864
DM Goulburn Valley DDH2	MF25139.R00055005	–32.41620000	150.32610000
DM Gunnadilly DDH1	Tadros 1993 (GS1985_005.R00014146)	–31.49428486	150.52281148
DM Gunnedah DDH1	Tadros 1993	–30.95911976	150.13266457
DM Howes Hill DDH1	Tadros 1993 (GS1985_005.R00014146)	–31.28571123	150.12911097
DM Killarney DDH1	Tadros 1993 (MF31509.R00056451)	–30.31817449	149.87957625
DM Maules Creek DDH2	Tadros 1993 (GS1976-252.R00022059)	–30.58374579	150.16767176
DM Maules Creek DDH3	Tadros 1993 (GS1976-252.R00022059)	–30.55059914	150.16744194
DM Maules Creek DDH4	Tadros 1993 (GS1976-252.R00022059)	–30.58714395	150.12765130
DM Maules Creek DDH5	Tadros 1993 (GS1976-252.R00022059)	–30.58030048	150.21072127
DM Maules Creek DDH6	Tadros 1993 (GS1976-252.R00022059)	–30.54134933	150.20650409
DM Maules Creek DDH7	Tadros 1993 (GS1976-252.R00022059)	–30.42301993	150.10973668
DM Millie DDH1	Tadros 1993 (MF29573.R00056459)	–31.05075182	150.01838779
DM Mirrie DDH1	MF29572.R00056461 (GS1982_314.R00010673)	–31.94267901	149.04626844
DM Moema DDH1A	Tadros 1993 (GS1976_422.R00007375)	–30.06509715	149.86780239
DM Morven DDH1	Tadros 1993 (GS1985_005.R00014146)	–31.63715170	149.52122783
DM Napier DDH1	Tadros 1993 (GS1985_005.R00014146, MF31511.R00056471)	–31.60812699	149.75728258
DM Narrabri DDH1	GS1985_005.R00014146	–30.29900000	149.76500000
DM Narrabri DDH2	Tadros 1993	–30.22273169	149.81207506
DM Nea DDH1	MF31514.R00056473	–31.21256081	150.29191786
DM Nea DDH2	MF31514.R00056473 (Tadros 1993)	–31.23329472	150.24867505

(continued)

**Appendix 1: (Continued)**

Borehole	Reference or DIGS Report number	Latitude GDA94	Longitude GDA94
DM Nombi	MF29489.R00056474	-31.19309049	149.74323819
DM Parkes DDH1	MF29555.R00055356	-30.74035460	149.75420010
DM Parkes DDH2	Tadros 1993 (GS1985_005.R00014146, MF29555.R00055356)	-30.74608807	149.78222243
DM Parkes DDH3	MF29555.R00055356	-30.65086560	149.77260743
DM Parsons Hill DDH1	MF29554.R00055391	-31.61037956	150.54480540
DM Pibbon DDH1	Tadros 1993 (MF29553.R00056481)	-31.59234939	149.09934924
DM Purlawaugh DDH1	Tadros 1993 (MF29552.R00055326)	-31.30928362	149.54717307
DM Queensborough DDH1	MF29551.R00055327 (Tadros 1993)	-31.70861787	149.68561168
DM Saltwater DDH1	Tadros 1993	-31.50309523	149.75689559
DM Springfield DDH1	Tadros 1993 (GS1985_005.R00014146)	-31.39651032	150.25356061
DM Terrawinda DDH1	Tadros 1993 (GS1985_005.R00014146)	-31.39919194	149.50295610
DM Texas DDH1	Tadros 1993 (MF31519.R00056493)	-31.17756844	150.47973732
DM Tinkrameanah DDH1	Tadros 1993	-31.39353229	149.63915063
DM Trinkey DDH1	Tadros 1993	-31.38899913	150.00669561
DM Tullamullen DDH1	Tadros 1993 (GS1985_005.R00014146)	-30.62775753	149.87621759
DM Tunmallallee DDH1	Tadros 1993	-30.86042302	149.45368599
DM Turrawan DDH1	Tadros 1993 (GS1985_005.R00014146)	-30.52181281	149.88190256
DM Turrawan DDH2a	Tadros 1993 (GS1985_005.R00014146)	-30.42238655	149.85491646
DM Ulinda DDH1	Tadros 1993 (MF29549.R00056499)	-31.51673836	149.51033747
DM Walla Walla DDH1	Tadros 1993 (GS1985_005.R00014146)	-30.73643385	149.87850462
DM Wallala DDH1	Tadros 1993	-31.37052338	150.45132566
DM Wallala DDH2	Tadros 1993	-31.36852427	150.49607514
DM Wallala DDH3	Tadros 1993	-31.40222652	150.50204586
DM Weetaliba DDH1	Tadros 1993	-30.84619389	149.64607336
DM Wilson DDH1	Tadros 1993 (GS1985_005.R00014146)	-31.39723771	149.75152264
DM Wondobah DDH1	MF30093.R00055318	-31.10464953	150.12523508
DM Worigal DDH1	Tadros 1993	-30.96024512	149.13247699
DM Yaminba DDH1	Tadros 1993 (MF25106.R00056502)	-31.17174945	149.49466916
DM Yarrari DDH1	Tadros 1993	-30.84208452	150.25994627
DME Narrabri DDH01	Tadros 1993	-30.81499333	149.83648643
DME Narrabri DDH03	Tadros 1993	-30.73756087	149.84902913
DME Narrabri DDH04	Tadros 1993	-30.70407124	149.83958724
DME Narrabri DDH05	Tadros 1993	-30.67017868	149.83544555
DME Narrabri DDH06	Tadros 1993	-30.63821013	149.83814263
DME Narrabri DDH11	Tadros 1993	-30.59434597	149.86770045
DME Narrabri DDH12	Tadros 1993	-30.55853912	149.86272150
DME Narrabri DDH13	Tadros 1993	-30.52049332	149.85891478
DME Narrabri DDH14	Tadros 1993	-30.48663180	149.85535255
DME Narrabri DDH17	Tadros 1993	-30.80375814	149.92208972
DME Narrabri DDH18	Tadros 1993	-30.77397455	149.91801142
DME Narrabri DDH20	Tadros 1993	-30.70143436	149.91523816
DME Narrabri DDH28	Tadros 1993	-30.31328546	149.83486579
DME Narrabri DDH30	Tadros 1993	-30.48846062	149.83597129
DME Narrabri DDH35	CR_99_4138.R00042033	-30.44737864	149.93533030
DME Narrabri DDH37	Tadros 1993	-30.45074820	149.84311556
DME Narrabri DDH41	Tadros 1993	-30.08303590	149.91745751
Elecom Hunter Llanillo DDH1	WCR244.R00002545	-32.43602501	150.83653553
Elecom Hunter Randwick Park DDH1	WCR243.R00002555	-32.43969555	150.80266672
Esso Jerry Plains No. 1	WCR138.R00017224	-32.47314477	150.94114531
EVK001	CR_98_4095.R00031683 (CR_95_3880.R00017790)	-30.75287312	150.26663776
EVK002	CR_98_4095.R00031683 (CR_95_3880.R00017790)	-30.75361583	150.27209733
EVK04	CR_98_4095.R00031683 (CR_95_3880.R00017790)	-30.75506091	150.28241577
EVK05	CR_98_4095.R00031683 (CR_95_3880.R00017790)	-30.75574235	150.28756314
EVK06	CR_98_4095.R00031683 (CR_95_3880.R00017790)	-30.75637035	150.29227753
EVK07	CR_98_4095.R00031683 (CR_95_3880.R00017790)	-30.75710052	150.29720253
EVK08	CR_98_4095.R00031683 (CR_95_3880.R00017790)	-30.72285845	150.24287617
EVK12	CR_98_4095.R00031683 (CR_95_3880.R00017790)	-30.72582688	150.26344495
EVK17	CR_98_4095.R00031683 (CR_95_3880.R00017790)	-30.75322096	150.26923152
EVK18	CR_98_4095.R00031683 (CR_95_3880.R00017790)	-30.75399329	150.27487693
Jacks Creek No. 1	GS2002_382.R00031965	-30.42689214	149.75718017
Kelvin No. 1	WCR111.R00017965	-30.84092719	150.31613548
Morandini No. 1	WCR055.R00021222	-32.32000000	148.85000000
NTM Quirindi DDH3	Tadros 1993	-31.51995634	150.62317153
NTM Quirindi DDH6	GS1971_197.R00026503 (Tadros 1993)	-31.46688311	150.61946535

(continued)

**Appendix 1: (Continued)**

Borehole	Reference or DIGS Report number	Latitude GDA94	Longitude GDA94
NTM Qurindi DDH2	GS1971_197.R00026503 (Tadros 1993)	−31.56238266	150.49105405
NTM Qurindi DDH5	GS1971_197.R00026503 (Tadros 1993)	−31.59970160	150.54673503
NTM Qurinidi 1	GS1971_197.R00026503 (Tadros 1993)	−31.54044140	150.58072217
Nyora No. 1	WCR226.R00017086	−30.31894656	149.45688648
Pilliga No. 1	MF21527.R00056888 (WCR097.R00017974)	−30.65398720	149.62058948
PZ09A	Coffey Geosciences Report S21754.03 (2006)	−32.12471273	149.74263531
Sandy Camp No. 1	WCR070.R00021215	−30.86094225	147.74006752
Scone DDH1	MF21429.R00055366	−32.02876376	150.81980979
Soda-1	MF43967.R00056550	−32.07104553	148.98092471
DM Turee DDH1	MF29407.R00056496	−31.94039512	149.87158440
Union-Kern-A.O.G. Goondiwindi No. 1	WCR094.R00017977	−28.63870829	150.19223083
VNW026R	CR_95_3878.R00031276	−30.76549042	150.15232657
VNW033R	CR_95_3878.R00031276	−30.73144276	150.16965743
VNW040R	CR_95_3878.R00031276	−30.73320308	150.16664187
VNW043R	CR_95_3878.R00031276	−30.72993993	150.10723244
VNW060R	CR_95_3878.R00031276	−30.73231616	150.16813495
VNW26	CR_95_3878.R00031276	−30.76549042	150.15232657
VNW33	CR_95_3878.R00031276	−30.73144276	150.16965743
VNW43	CR_95_3878.R00031276	−30.72993993	150.17232444
VNW50	CR_95_3878.R00031276	−30.76285924	150.15441826
VNW60	CR_95_3878.R00031276	−30.73231616	150.16813495
VNW62	CR_95_3878.R00031276	−30.75875253	150.15436224
VNW63	CR_95_3878.R00031276	−30.76033537	150.15429566
VNW71	CR_95_3878.R00031276	−30.76432921	150.15317132
VWN30	CR_95_3878.R00031276	−30.72833330	150.17484461
Wacol Parkville DDH6	MF08878.R00055216	−32.01508661	150.84270453
Wee Waa No. 1	WCR078.R00021207	−30.35065449	149.51836625
Wilga Park No. 1	WRC219.R00017088	−30.36220821	149.67335982
Wilga Park No. 2	WRC287.R0042084	−30.35736432	149.66677801
Wilga Park No. 3	GS2000_063.R00031629	−30.36368119	149.66471226
Wilga Park No. 4	GS2000_064.R00031630	−30.37306210	149.66373231
Wilga Park No. 5	GS2000_65.R00031631	−30.36780989	149.65693591
WVK095	CR_98_4095.R00031683 (CR_95_3880.R00017790)	−30.77192007	150.26674089



## Deep 3D structure of the Sydney Basin using gravity modelling

C. DANIS<sup>1\*</sup>, C. O'NEILL<sup>1</sup>, M. LACKIE<sup>1</sup>, L. TWIGG<sup>2</sup> AND A. DANIS<sup>3</sup>

<sup>1</sup>GEMOC ARC National Key Centre, Department of Earth and Planetary Sciences, Macquarie University, NSW 2109, Australia.

<sup>2</sup>Groundwork Plus Pty Ltd, Brisbane, Queensland 4064, Australia.

<sup>3</sup>CSE, University of New South Wales, Sydney, NSW 2052, Australia.

A detailed deep 3D geological model is an important basis for many types of exploration and resource modelling. Renewed interest in the structure of the Sydney Basin, driven primarily by sequestration studies, geothermal studies and coal seam gas exploration, has highlighted the need for a model of deep basin geology, structure and thermal state. Here, we combine gravity modelling, seismic reflection surveys, borehole drilling results and other relevant information to develop a deep 3D geological model of the Sydney Basin. The structure of the Sydney Basin is characteristic of a typical intracontinental rift basin, with a deep north–south orientated channel in the Lachlan Fold Belt basement, filled with up to 4 km of rift volcanics, and overlain with Permo-Triassic sediments up to 4 km thick. The deep regional architecture presented in this study will form the framework for more detailed geological, hydrological and geothermal models.

**KEY WORDS:** Sydney basin, gravity modelling, deep 3D structure.

### INTRODUCTION

The Sydney Basin is part of the Sydney–Gunnedah–Bowen Basin system, which was a major extensional rift basin that formed in the Late Carboniferous to Early Permian, with basement comprised of middle to lower Paleozoic Lachlan Fold Belt (LFB) and deformed New England Fold Belt (NEFB) material (Glen 2005). Renewed interest in the deep structure of the Sydney Basin, driven by geothermal exploration, sequestration studies and coal seam gas exploration, has highlighted the need for clear understanding of deep basin geology, structure and thermal conditions.

A detailed 3D geological model is an important basis for many types of exploration and resource modelling. It allows the visualisation of subsurface geological structures and can be used as a regional exploration and targeting tool and form a basis for thermal/hydrogeological model simulations. A variety of tools exist to construct such models, ranging from map-based interpolation of structures (2D methods i.e. depth to basement maps from interpolated drill hole data) to full 3D geological modelling considering complicated structures using structural mapping, drill hole data, seismic data and gravity and magnetic modelling.

Our aim in this paper is to develop a 3D model of the deep Sydney Basin geology, including the basement and basal volcanic unit, developed from available coal and petroleum borehole data, regional gravity modelling and seismic reflection. This follows on from similar

modelling work completed for the Gunnedah Basin (Danis *et al.* 2010). Previous studies have addressed aspects of the Sydney Basin's architecture, but none have compiled all available geological, geophysical and borehole data into a self-consistent model for the deep LFB basement structure.

A Structurally Enhanced view of Economic BASEment model (SEEBASE) has been compiled for the Sydney Basin Reservoir Prediction Study (Blevin *et al.* 2007). This model is drawn from the OZ SEEBASE<sup>TM</sup> study of FrOG Tech (2006) and uses magnetic and gravity data, calibrated with wells and seismic interpretations to defined magnetic basement or economic basement, generally defined as the base of petroleum or coal bearing sediments. A detailed explanation of the methodology of the SEEBASE model is available in the OZ SEEBASE Study 2005 report and is not discussed here. However, this model lacks transparency in compilation and significant detail below petroleum and coal bearing units to enable an assessment of the thermal state of the upper crust in the Sydney Basin, which is the main purpose of developing our model. Herbert & Helby (1980) presented a compilation of previous work on the geology and structure of the Sydney Basin. Previous models of the Sydney Basin structure have generally been geological, focused on the stratigraphy of coal and petroleum prospective units, with only broad estimates on basin sediment thickness and structure. No previous models constrain the extent of rift volcanics or the depth to the top of the LFB

\*Corresponding author: cara.danis@mq.edu.au



basement—information that is critical for understanding upper crustal structure.

Rather than replicate the available detailed geological and structural information for the Sydney Basin, we instead combine regional-scale gravity modelling, with geological, borehole and seismic constraints, to develop a regional geological model. Here we present our 3D basement and structural model of the Sydney Basin, which incorporates a simplified structure and lithology and is consistent with all available geological, borehole and seismic information.

## Geological setting

A detailed understanding of the geology and history of the Sydney Basin is essential for understanding and modelling the deep structure of the basin. Here, we present an in depth assessment of the stratigraphy and structure as reviewed from the literature to interpolate and model deep structure in areas with limited physical data.

The Sydney Basin, part of the Sydney–Gunnedah Basin (Figure 1) is a north–south-trending, generally flat lying Permo–Triassic sequence in eastern New South Wales, centred around Sydney. It is 250 km long, averages 100 km in width and covers an area of approximately 37 000 km<sup>2</sup> onshore and approximately 15 000 km<sup>2</sup> offshore (Bembrick & Lonergan 1976; Adler *et al.* 1998). The Sydney Basin developed as a foreland basin in front of the deforming NEFB, with a series of north-trending grabens and half grabens formed in response to limited crustal extension in an east–west direction during the Late Carboniferous to Early Permian. A simplified stratigraphy of the Sydney Basin is shown in Table 1. Sedimentation in the Sydney Basin is a repeated sequence of marine and terrestrial deposits resulting in the formation of sandstones, shales, claystones and coal intermingled with extrusive volcanics and the intrusion of some late plutons (Figure 1). Onshore, the Sydney Basin sediments have been estimated to attain thicknesses of 4800 to 9000 m and offshore, 5000 to 5900 m (Bembrick & Lonergan 1976; Adler *et al.* 1998).

The structural framework for the Sydney Basin (Figure 2) comprises 11 onshore structural elements, described by Herbert & Helby (1980) from north to south as the Hunter Valley Dome Belt, Hornsby Plateau, Blue Mountains Plateau, the Cumberland Basin with Fairfield, Penrith and Botany sub-basins, Woronora Plateau, Illawarra Plateau, Sassafras Plateau and Boyne Mount Plateau and four offshore principle elements; the Offshore Syncline, the offshore extension of the Newcastle Syncline, an offshore extension of the NEFB and the Offshore Uplift of the Curranrong Orogen.

During the Late Carboniferous the Sydney Basin did not exist as a structural entity (Herbert & Helby 1980). The rocks of the LFB were emergent and stood elevated at more than 600 m (Herbert 1972). Extensive volcanism took place in a rift zone, extending from the Hunter Valley area northwards into Queensland, and huge volumes of coarse volcanic debris were deposited to the east of the rift. Sediments within the newly forming Sydney Basin comprised thick fluvio-glacial conglomer-

ates, diamictites and varves of the Talaterang Group in eroded valleys of LFB Paleozoic basement in the southern part of the Sydney Basin, and Seaham Formation Conglomerates in the northern part.

Volcanism continued into the Early Permian with the thick basaltic and rhyolitic sequences of the Lochinvar and Allendale Formations of the Dalwood Group, but as it waned, subsidence and marine deposition became characteristic (Herbert & Helby 1980). Several volcanic centres became islands that shed debris into the surrounding transgressive Early Permian sea. In the southern Sydney Basin, beach and near-shore sands of the Wasp Head Formation were transgressing the LFB. During the Early Permian, the NEFB and the eastern margin of the LFB slowly subsided creating a broad continental shelf (Herbert & Helby 1980) where, as a result of extensive marine transgressions, thick sequences of sand and silt of the Dalwood, Lower Shoalhaven and Lower Maitland groups were deposited on the inner continental shelf. The Greta and Clyde coal measures were also deposited during this time.

Basin wide subsidence followed, resulting in a transgression and the deposition of the base of the Maitland Group (Branxton Formation) from reworked material derived from the underlying fluvio-deltaic sediments in the northern Sydney Basin and the base of the Shoalhaven Group (Snapper Point Formation), sourced from eroding hard rock Late Devonian quartzite headlands spread extensively over the southern and western parts of the basin. Another regressive-transgressive episode occurred prior to the mid-Permian, finalising the deposition of the Maitland Group and upper parts of the Shoalhaven Group (Berry Siltstone). As the Early Permian sea moved westward over the LFB, considerable quantities of boulders and pebbles were eroded from coastal cliffs.

Latites and volcanoclastic sediments of the Gerringong Volcanics advanced towards the north-north-west, north and south-west from an emergent island volcano or volcanic archipelago that developed offshore south-southwest of Kiama (Campbell *et al.* 2001) and marked the onset of a major phase of shoshonitic volcanism and associated reorganisation of the sedimentary provenance (Tye *et al.* 1996; Carr 1998; Arditto 2003). Five latite members are identified in the Broughton Formation of the Shoalhaven Group and four in the Lower Pheasants Nest Formation of the Illawarra Coal Measures in the Southern Sydney Basin. They attain an approximate maximum thickness of 440 m (Packham 1969). Veevers *et al.* (1994) indicate that the Gerringong marine volcanic sands were part of a sedimentary apron about a vent on a magmatic arc of the Curranrong Orogen occurring in the Early to Late Permian. The Gerringong Volcanics can be traced north of Kiama to Garie Beach, just south of Sydney, and may extend offshore up to 150 km north of Kiama (Veevers *et al.* 1994), as is also indicated by the offshore magnetic signature and strong offshore seismic reflectors. The Gerringong Volcanics may also be related to sporadic occurrences of magmatism elsewhere in the region, including the Milton Mozonite, Termeil Essexite, Stockyard Moun-

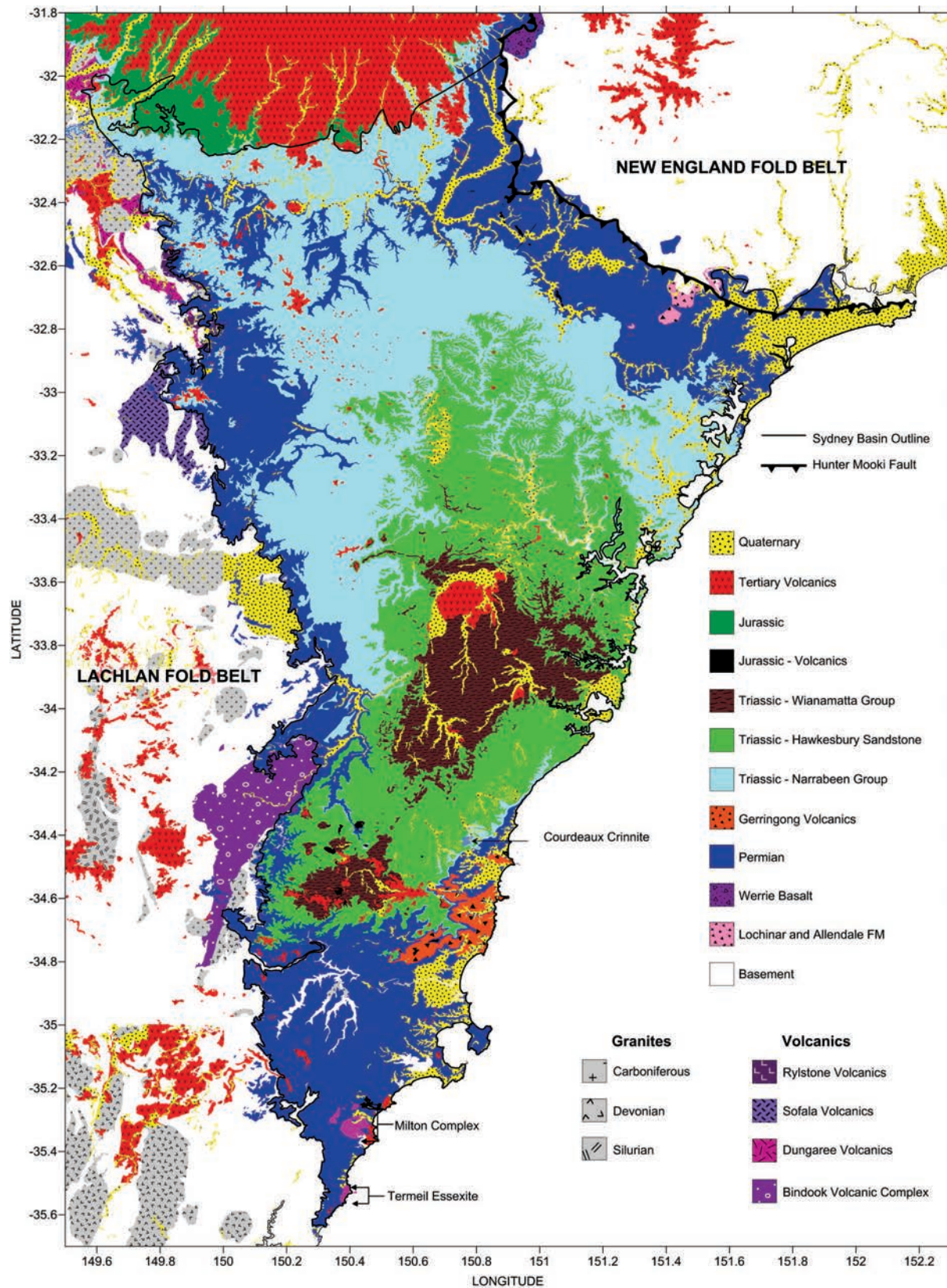


**Figure 1** Geology map of the Sydney Basin. Carboniferous, Devonian and Silurian granites are shown along with Late Carboniferous and Early Permian Volcanics.

tain Basalt, Coonemia Complex and Towradgi Dolerite in the southern Sydney Basin (Veevers *et al.* 1994; Carr 1998). Leitch (1969) suggests the Gerrigong

Volcanics extruded around the same time as the granitic plutons of the Hillgrove Plutonic Suite, *ca* 300 Ma (Kent 1994).



**Table 1** Simplified stratigraphy of the Sydney Basin (modified from Herbert & Helby 1980).

				SYDNEY BASIN						
				HUNTER COALFIELD	NEWCASTLE COALFIELD	WESTERN COALFIELD	SOUTHERN COALFIELD			
TRIASSIC	EARLY TO MIDDLE						Wianamatta Group			
				Hawkesbury Sandstone		Hawkesbury Sandstone				
				Terrigal & Newport Formation						
			Narrabeen Group	Narrabeen Group	Narrabeen Group	Narrabeen Group				
	LATE	Singleton Supergroup		Newcastle Coal Measures						
				Dempsey FM		Baal Bone FM		Bargo Claystone		
				Tomago Coal Measures		Illawarra Coal Measures		Illawarra Coal Measures		
				Kulnura Marine Tongue		Marrangaroo Conglomerate		Erins Vale FM		
		Bulga FM								
		Maitland Group		Maitland Group		Shoalhaven Group				
	EARLY	Greta Coal Measures		Greta Coal Measures		Shoalhaven Group				
		Gyarran Volcanics	Dalwood Group	Dalwood Group						
				Metasediments & Granite						
LATE CARBONIFEROUS				Seaham Formation Conglomerates		Seaham Formation Conglomerates/ Kuttung Volcanics		Clyde CM	Wasp Head FM	Talaterang Group Conglomerates

Unconformity

FM = Formation

CM = Coal Measures

After the deformation of the mid-Permian period, uplift of the NEFB and rapid subsidence of the adjacent Sydney Basin stimulated extensive erosion, the creation of the Hunter-Mooki Thrust system and subsequent deposition. Moderate folding occurred in the northern Sydney Basin, adjacent to the Hunter-Mooki Thrust system, but diminished in intensity towards the southwest where sediments onlap stable parts of the LFB. Minor folding within the Sydney Basin, especially in the Hunter Valley Dome Belt, continued until at least the end of the Permian, and possibly into the Triassic (Herbert & Helby 1980).

Visher (1965) considered that stratigraphic sequences accumulated dominantly by regressive sedimentation, for which the Sydney Basin is no exception. Sedimentation can be divided in to many distinctive depositional episodes, with regressive and transgressive characteristics. In the Sydney Basin regressive sedimentation is commonly associated with coal bearing formations (Herbert & Helby 1980). During three major regressive episodes, as much as 2000 m of terrestrial and marine sediments were deposited (Herbert & Helby 1980) form-

ing the Tomago Coal Measures, Illawarra Coal Measures and the Singleton Super Group, which contains the most important coal in the Sydney Basin. The bulk of the sediment in the deltaic environment is derived from the NEFB, with a maximum thickness in the Hunter Valley adjacent to the Hunter-Mooki Thrust. Following this, in the lower Hunter Valley, prodelta and delta front laminated sand and silt were deposited seawards of a shoreline comprising a barrier island-estuarine channel sand complex (lower Newcastle Coal Measures). This event can be correlated with the Bargo Claystone in the southern part of the basin and in the upper Hunter Valley with the upper part of the Singleton Super Group (Denman Formation).

The Narrabeen Group, comprising up to 800 m of lithic conglomerate, quartz-lithic sandstone, and shale (red, green and grey) was deposited in the Late Permian to Middle Triassic when major alluvial systems prograded and sediment was intruded from the NEFB. Overlying is the Middle Triassic Hawkesbury Sandstone, up to 250 m thick, which is a dominantly coarse quartz sandstone. Overlying the

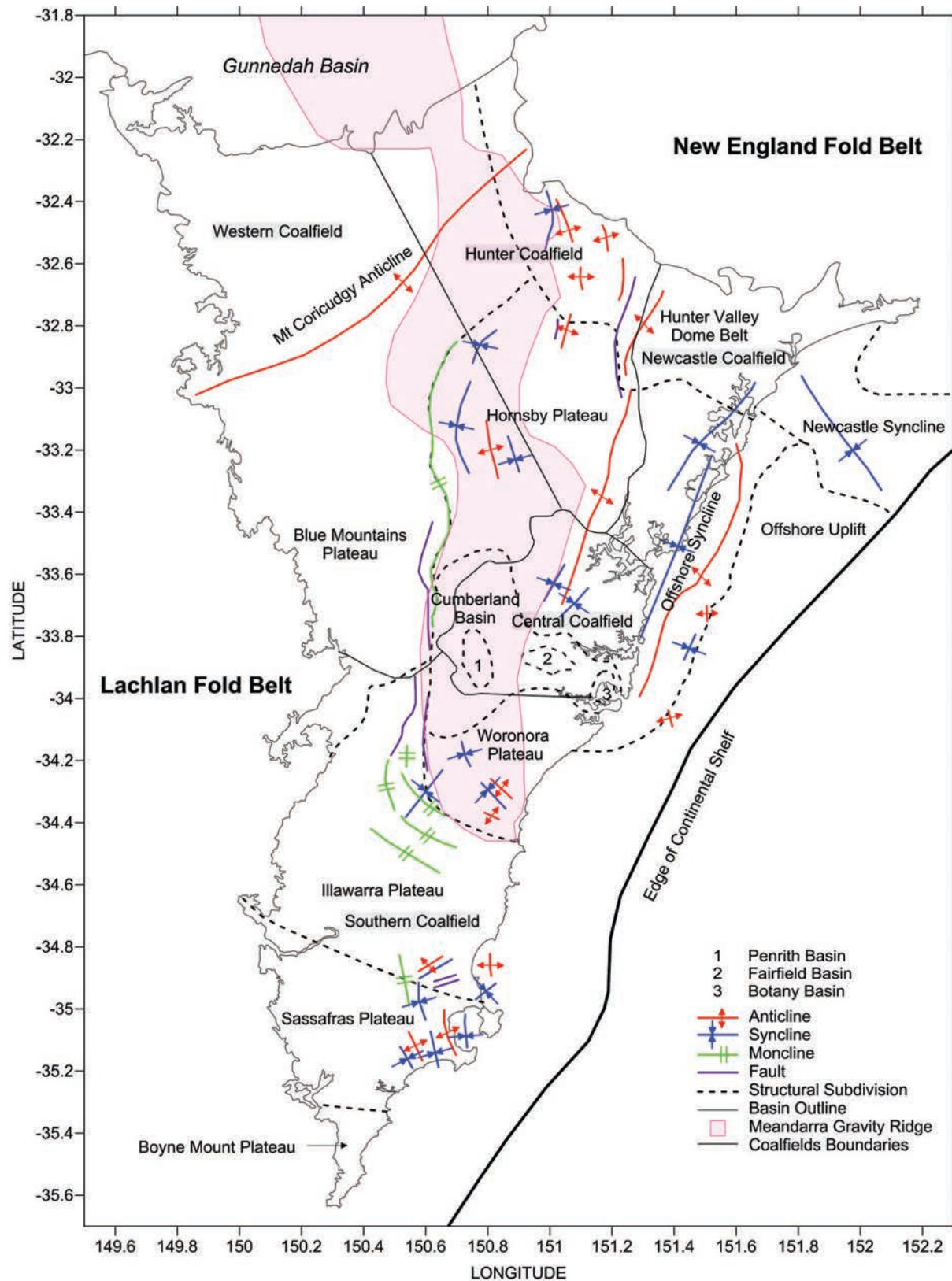


**Figure 2** Structural and tectonic map of the Sydney Basin. Compiled from Herbert & Helby (1980), Shepherd & Huntington (1981), NSW DPI (2005) and NSW 1:250 000 scanned geological maps Sydney SI56-5, Wollongong SI56-9, Newcastle SI56-2, Ulladulla SI56-13 and Singleton SI56-1.

Hawkesbury Sandstone is the Wianamatta Group (comprising the Ashfield Shale, Minchinbury Sandstone and Bringelly Shale), up to 300 m thick and

dominantly shale with sporadic thin lithic sandstones. The Narrabeen Group was deposited in three episodic environments; estuarine/alluvial, fluvial and fluvial-

deltaic. Subsidence caused limited transgression and an upward transition to fluvio-deltaic deposits of the upper Narrabeen Group in the Newport and Terrigal Formations.

Uplift of the LFB to the southwest of the Sydney Basin tilted Late Permian and Early to Middle Triassic sediments in the southern part of the basin, and led to their erosion. The source of the Hawkesbury Sandstone is presumed to be the Upper Devonian quartzites of the LFB and the graphite commonly found within the Hawkesbury Sandstone may have been derived from Victorian Ordovician graphitic slates (Herbert & Helby 1980). The deposition of the Hawkesbury Sandstone occurred in an alluvial environment that has been compared by Conaghan & Jones (1975) with the huge Brahmaputra River System in central Asia, suggesting that the ultimate sediment source area could be quite distant.

The Wianamatta Group was the last phase of sedimentation directly related to the tectonic development of the Sydney Basin, with sediments deposited in a continuous succession of environments grading upward from subaqueous, to shoreline and ultimately to alluvial during a single major regression (Herbert & Helby 1980). Mid-Triassic deformation terminated deposition in the Sydney Basin. Jurassic sedimentation is not evident in the Sydney Basin, where the only Jurassic lithologies are volcanic breccia pipes (diatremes). According to Herbert & Helby (1980) it is possible that an unknown, but not great, thickness of early Jurassic sediments may have extended from the great Artesian Basin unconformably over the Sydney Basin, but if so, these have since been completely eroded.

### Basement composition

Sydney Basin sediments unconformably overlie and onlap LFB sequences. Early gravity modelling (Qureshi 1984; Leaman 1990a) along with drilling information suggested that the basement to the Sydney Basin is an extension of the LFB, as exposed to the south and west of the basin, comprising Ordovician to Devonian sediments, Devonian granites (Blevin *et al.* 2010) and Carboniferous acid volcanics and plutons. Basement rocks have densities ranging from 2.6 to 2.8 t/m<sup>3</sup> with most granitoids in the range of 2.62 to 2.65 t/m<sup>3</sup> (Leaman 1990b).

Further evidence of basement composition is the presence of xenoliths entrained from ~5 km depth observed in diatremes in the Sydney Basin (i.e. Mogo Hill diatreme 50 km north of Sydney), which comprise quartz-rich greywackes distinctive from the Permian coal-measure sediments and are interpreted to represent Siluro-Devonian strata (Emerson & Wass 1980; O'Reilly 1990).

The southern NEFB extends southwards beneath the offshore uplift in the northeastern part of the Sydney Basin, based on similarities of seismic character and magnetic anomaly response (Adler *et al.* 1998). It consists of sequences deposited as a result of Carboniferous subduction related processes, incorporating a subduction complex, fore-arc basin and dacitic to andesitic volcanic arc material.

## METHODOLOGY

### Regional Bouguer and magnetic intensity anomaly maps

The Gravity Anomaly Grid of the Australian Region 2008 and Magnetic Anomaly Grid of the Australian Region 2002, acquired from Geoscience Australia (URL: <<http://www.ga.gov.au>>) have been gridded to produce the spherical Bouguer anomaly and magnetic intensity anomaly map of the Sydney Basin (Figure 3). The gravity data constitute a 0.0083° (~800 m) grid derived from a non-homogenous station spacing, which ranges from 2 to 4 km over areas of special interest and elsewhere averages ~11 km. The gravity data as supplied are based on the current Australian Absolute Gravity Datum 2007 scale and a reduction density of 2.67 t/m<sup>3</sup>.

The magnetic data constitute an approximate 0.01° (~1 km) grid. No corrections have been applied in this study to the downloaded data and the data are gridded in Surfer v.9 supplied by Golden Software® with kriging at 0.01°. Additional gravity data collected during field surveying (Danis 2010) have been used to assist in the gravity modelling but are not included in Figure 4 owing to the different spherical corrections applied between the GA dataset and that from field surveying.

### Density measurement

A total of 36 core samples were collected from the cores of four boreholes; Belford 1, Dural South 1, East Maitland 1 and RDH Kurrajong Heights, held at the NSW Londonderry Core Library. Core samples were cut from the basal volcanic units and Permian Sediments. The samples were measured both dry and wet using an AG204 Delta Range Mettler Toledo Scale, and density was calculated using the formula:

$$D = [(A \times \partial_L) / (A - B)] + C \quad (1)$$

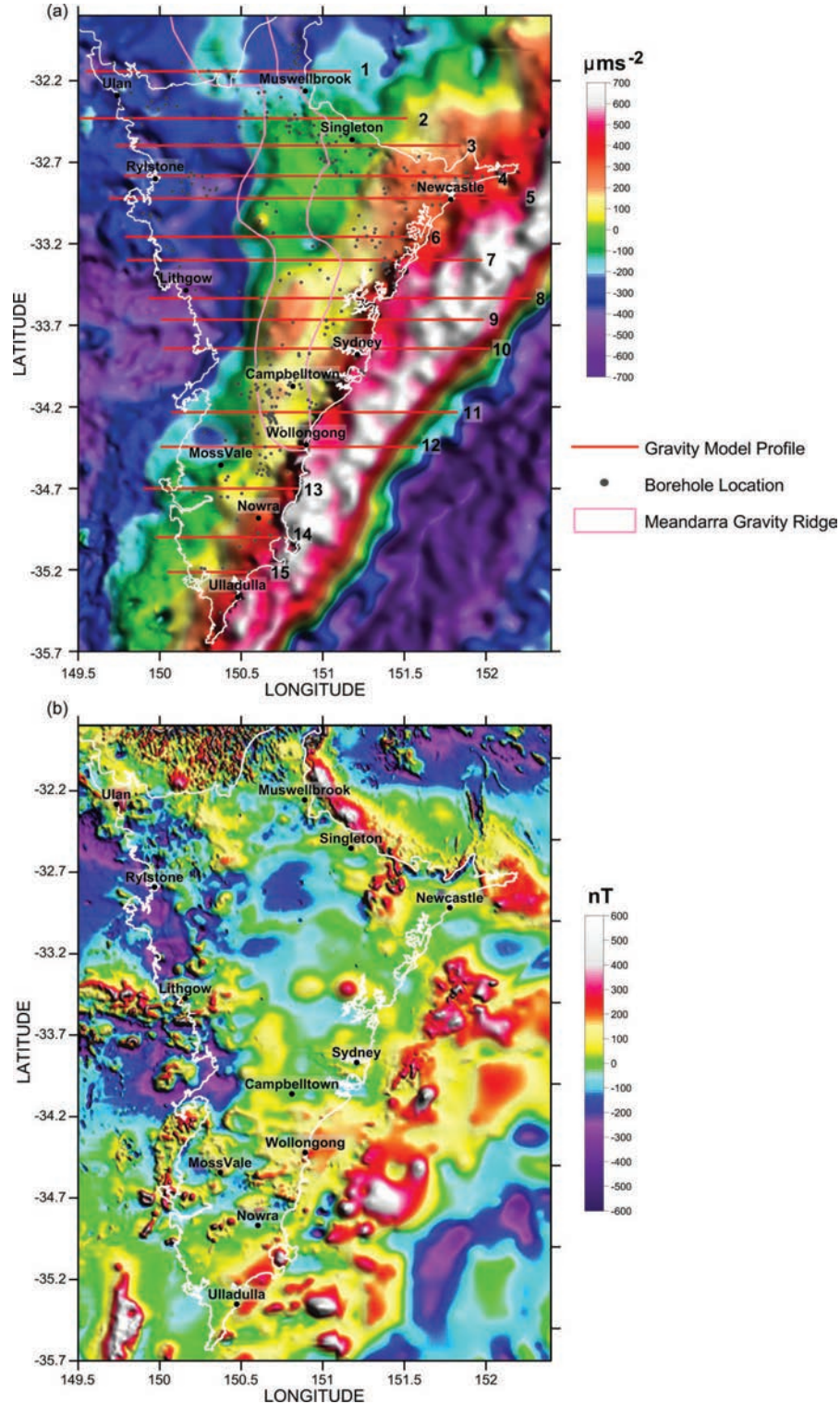
where  $D$  = density (t/m<sup>3</sup>),  $A$  = dry weight (g),  $B$  = wet weight (g),  $\partial_L$  = liquid density and  $C$  = 0.0012 (air buoyancy constant). The results are shown in Table 2 along with a summary of the measured density of samples collected from Guo *et al.* (2007) and Danis *et al.* (2010).

### Gravity profiles

Fifteen east-west gravity profiles were extracted from the spherical Bouguer anomaly grid, each with a station spacing of up to 1600 m depending on the resolution of the data in the grid. Modelling of the gravity data was performed with the interactive potential field modelling package ModelVision Pro v.9.0 supplied by Pitney Bowes Business Insight®. Models were constructed from an assembly of polygonal bodies, from which the strike length is limited to their approximate geological extent, forming a 2.5D model. All profiles are modelled in Map Grid of Australia coordinate Zone 56.

The Sydney Basin model is an extension of previous modelling in the Gunedah Basin (Danis *et al.* 2010), and

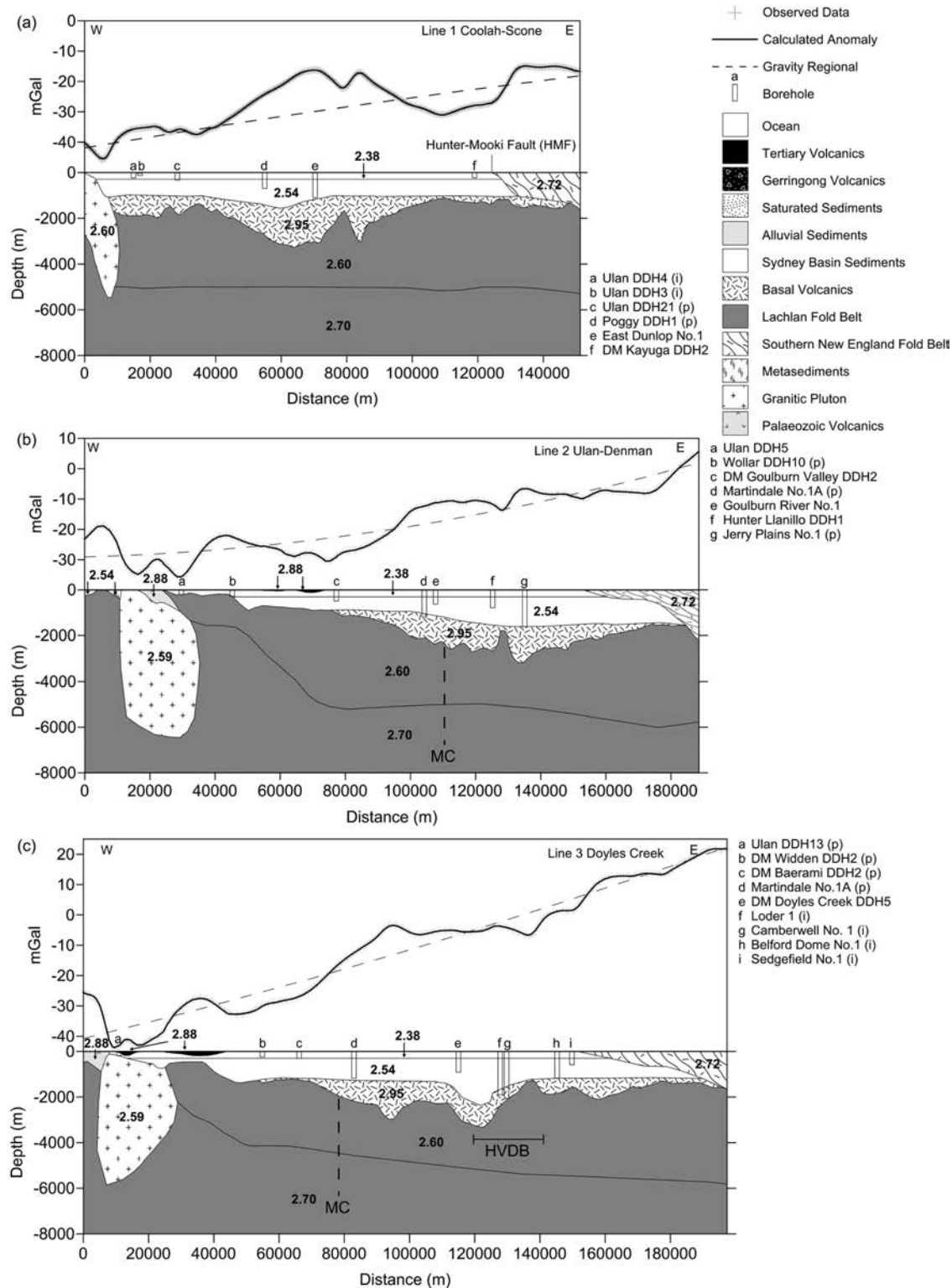




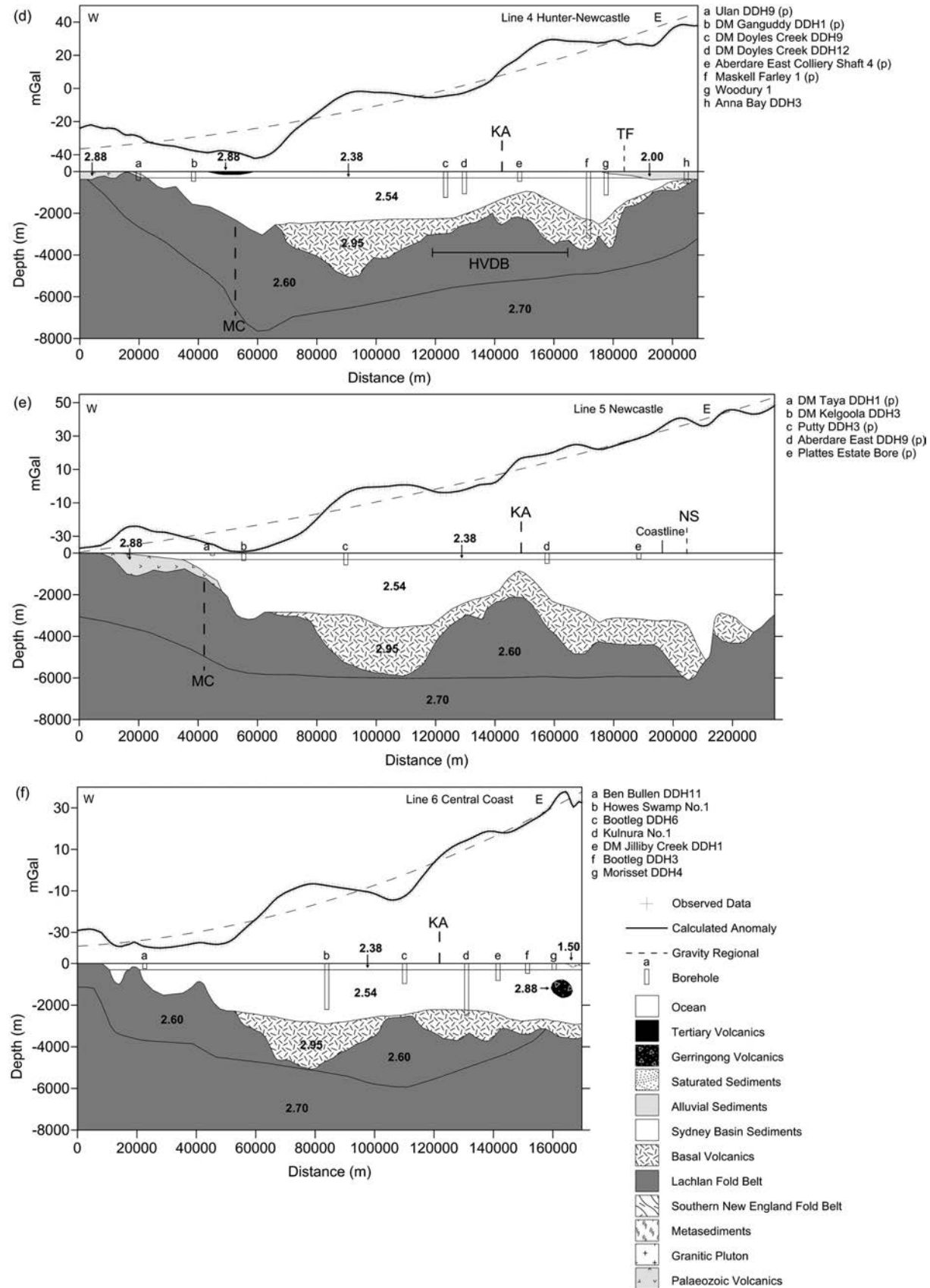
**Figure 3** (a) Spherical Bouguer Gravity Anomaly map of the Sydney Basin (white outline), overlain with gravity model profiles (red line and black numbers), borehole and place locations. The location of the Meandarra Gravity Ridge is also shown. (b) Total magnetic intensity anomaly map of the Sydney Basin (white outline).

therefore for consistency we have chosen to use the same model density values, which are outlined in Table 3. These model density values are derived from Table 2. For shallow surface features, such as thick surficial alluvial deposits and larger rivers, the average

density of sand at  $2.00 \text{ t/m}^3$  (Reynolds 2003) is used. For irrigated floodplains, lakes and harbours, a representative density of  $1.50 \text{ t/m}^3$ , which is the average of the density of water and sand, is applied for saturated sediments/water.



**Figure 4** Gravity model profiles with observed gravity points (crosses), regional correction (dashed line), modelled response (solid line) and key structural features. Density of units in  $\text{t/m}^3$ . Calibration boreholes shown as rectangles (see Appendix B for details). i, interpreted borehole location; p, projected borehole location; MC, Mt Coricudgy Anticline; HVDB, Hunter Valley Dome Belt; TF, Targon Fault; NS, Newcastle Syncline; KA, Kulnura Anticline; TL, Tuggerah Lake; OS, Offshore Syncline; OU, Offshore Uplift; KF, Kurrajong Fault; LM, Lapstone Monocline; YS, Yarramalong Syncline; WR, Woronora Reservoir; WG, Woronora Granite; LA, Lockersleigh Adamellite; UGG, Uringalla/Glenrock Granite; MM, Milton Monzonite. (a) Line 1 Coolah-Scone. (b) Line 2, Ulan-Denman. (c) Line 3, Doyles Creek. (d) Line 4, Hunter-Newcastle. (e) Line 5, Newcastle. (f) Line 6, Central Coast. (g) Line 7, Wolgan. (h) Line 8 Kurrajong. (i) Line 9 Riverstone. (j) Line 10, Sydney. (k) Line 11, Wollongong. (l) Line 12, Nepean. (m) Line 13, Moss Vale. (n) Line 14, Ulladulla. (o) Line 15, Clyde River. Note vertical exaggeration as indicated by the depth and distance scales.





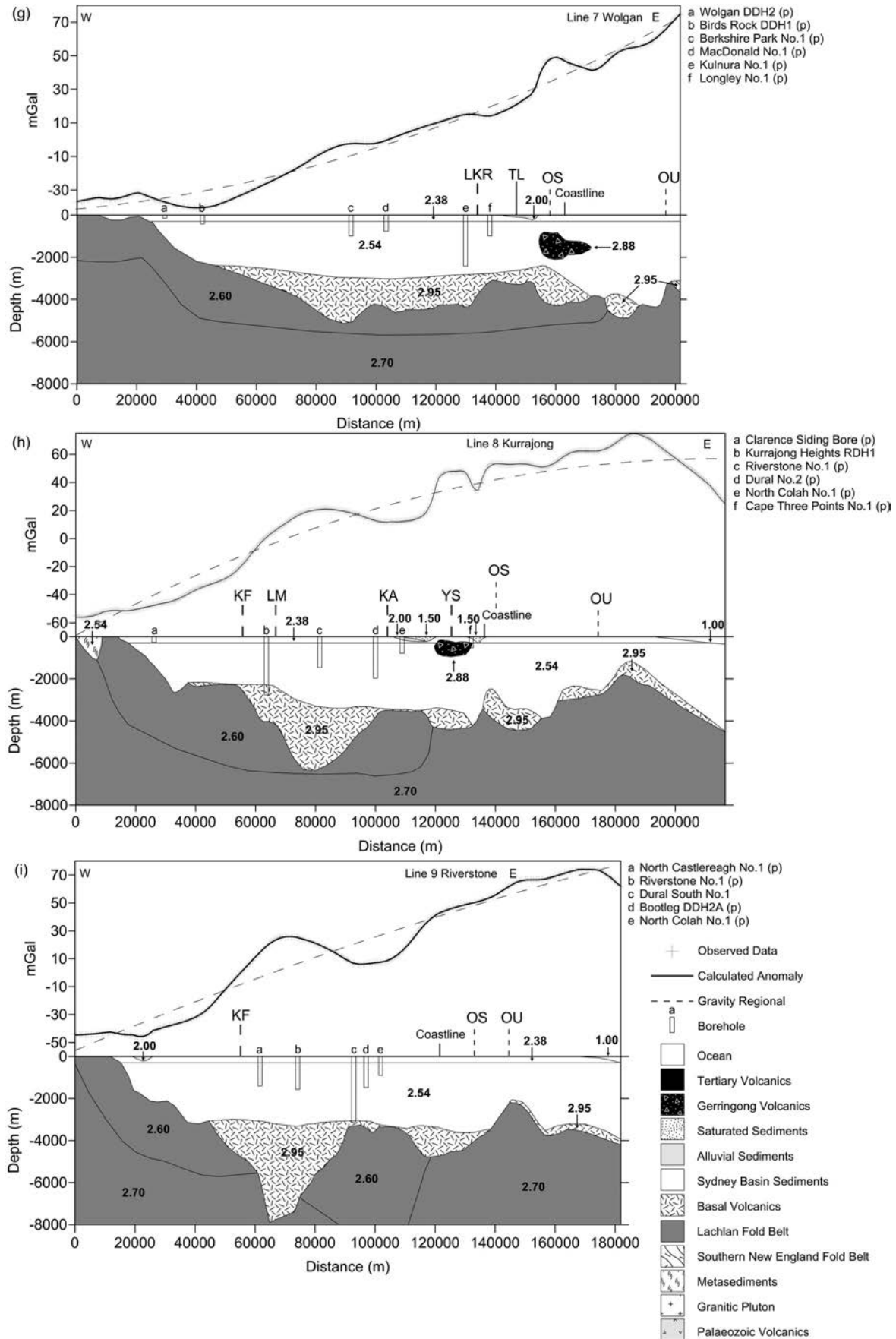


Figure 4 (Continued).

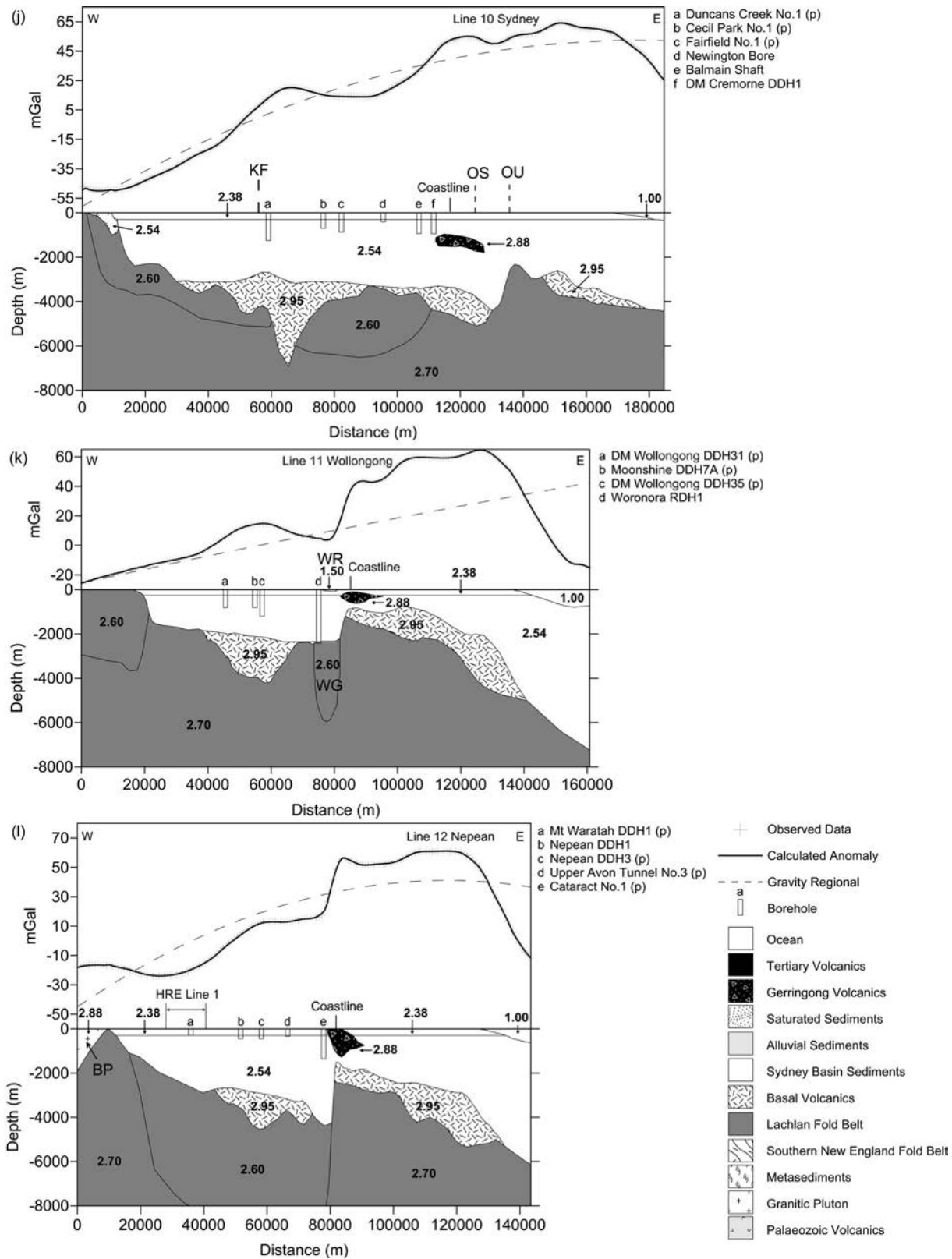


Figure 4 (Continued).



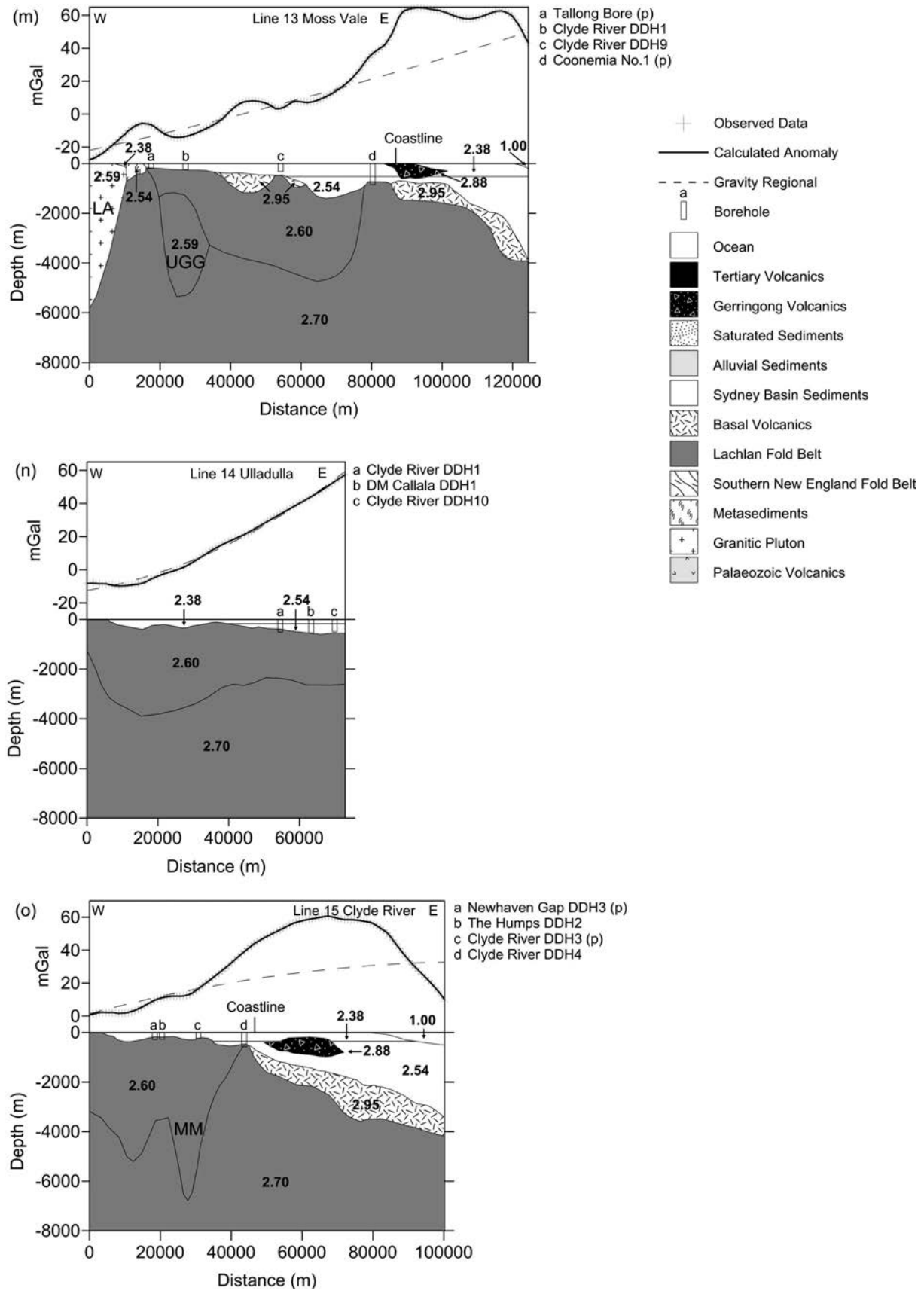


Figure 4 (Continued).

**Table 2** Summary of density data for the rock samples representative of the Sydney Basin.

Lithology	Density (t/m <sup>3</sup> )			
	Range	Mean	SD	<i>n</i>
Jurassic Sandstone	2.12–2.68	2.31	0.14	24
Triassic Sandstone	2.32–2.47	2.38	0.03	21
Permian Sediments	2.12–2.73	2.37	0.14	53
Permian Sediments with Coal	1.40–2.73	2.18	0.36	63
All Sediments	2.12–2.73	2.37	0.11	74
Tertiary Basalt	2.84–2.98	2.88	0.03	33
Werrie Basalt	2.74–2.89	2.82	0.05	11
Gulgong Granite	2.51–2.62	2.59	0.03	13
Basal Volcanics > 3000 m	2.87–2.97	2.92	0.04	5
Basal Volcanics 2500–3000 m	2.82–2.97	2.88	0.06	9
Basal Volcanics < 2500 m	2.53–2.73	2.62	0.07	21

**Table 3** Summary of density values using the gravity modelling of the Sydney Basin.

Lithology	Density (t/m <sup>3</sup> )
Tertiary & Gerringong Volcanics	2.88
Upper Sediments (< 300 m)	2.38
Lower Sediments (> 300 m)	2.54
Basal Volcanics	2.95
Granite	2.59
Lachlan Fold Belt Basement	2.60 or 2.70

In this study, the gravity profiles are modelled to 15 km depth (see Appendix A), and the upper 8 km are presented in Figure 4 to emphasise the delineation of the top of the LFB and the basin structure.

To help constrain the upper 5 km of the model, information was collected from borehole logs, seismic reflection profiles, formation contour maps (defined from seismic reflection surveys), existing gravity and magnetic models, and geological maps. The profiles are constrained by borehole information from over 90 drill holes (see Figure 4 for locations and Appendix B and Figure 5 for stratigraphic details) for depth of sediment cover, top of basal volcanics and, where available, the top of the LFB. The offshore parts of the model lines are constrained from seismic reflection profile and contour maps only, no offshore drilling information is available. Figure 6 shows the location of boreholes (details in Appendix B) and seismic reflection profiles (outlined in Table 4) used in this study. All seismic profiles are used to guide structure and depth in the gravity modelling. Where possible, the most recent profile available is used as the data quality and reliability of some early seismic work are commonly questionable.

Seismic reflection profiles travel times have been converted to depth based on the down-hole seismic shots of seven boreholes, presented in the Sydney Basin Reservoir Prediction Study (Blevin *et al.* 2007), where one second of two way travel time equals approximately 2 km. The structural contour maps of Mayne *et al.* (1974) for the top of Basal Volcanics/Dalwood Group, Greta Coal Measures and base of Triassic, have been digitised

**Table 4** Seismic reflection profile details of Figure 5.

Map reference no.	Seismic line name	Reference/DIGS report no.
1	CD 87-115	Blevin <i>et al.</i> (2007)
2	CD87-112, 118, 119, 122	Herbert (1989), Blevin <i>et al.</i> (2007), SS163
3, 4, 5	DPI 4, 5, 6	MINFO (2008)
6	M4S	SS083
7	SY81-20	Arditto (2003)
8	SY81-24	Arditto (2003), PGR1990_3
9	SY81-26	SS16
10	SY81-34	SS16
11	SY91-01	Adler <i>et al.</i> (1998)
12	SY91-02	Blevin <i>et al.</i> (2007)
13	SY91-08	Blevin <i>et al.</i> (2007)
14	SY91-12	Adler <i>et al.</i> (1998)
15	SY91-14	Adler <i>et al.</i> (1998), Blevin <i>et al.</i> (2007)
16	SY91-15A	Maung <i>et al.</i> (1997), Causebrook (2005)
17	SY91-16	Adler <i>et al.</i> (1998)
18	SS04-U20	Herbert (1989), SS148
19	SS04-C	SS004
20	SS021-P	SS148
21	SS021-AT	SS148
22	T4-M41S	SS083

and converted from feet to metres. These contour maps provide good structural information where boreholes are limited, and correlate well with recent drilling results.

Boreholes directly on or adjacent to gravity profiles provide strong structural control for the model layers, while seismic reflection profiles and nearby boreholes provide interpolated depths which are used as a guide between tight control points. The seismic reflection profiles across the Hunter-Mooki Fault, collected by the NSW Department of Primary Industries (MINFO 2008) have been used to guide the geometry of the fault in the gravity models, where appropriate. Table 5 presents the gravity modelling profiles, the number of boreholes (see Figures 4 and 5 for borehole name), seismic lines and/or other information used for calibration.

### 3D basement structure and lithological layers

The 3D structure of the Sydney Basin was created from the extraction of modelled depths and the stratigraphic data of over 320 boreholes, as presented in Figure 7. Depth information from the gravity models and borehole logs is converted to metres relative to the Australian Height Datum (mAHD) using topographic surface elevations interpolated from 90 m elevation contour data available from the Shuttle Radar Topography Mission (SRTM) at the United States Geological Survey website (URL: <<http://www2.jpl.nasa.gov/srtm/cband-dataproducts.html>>). From this, interpolated surfaces were created for the following; LFB basement (Figure 8), top of Basal Volcanics, the top and base of the Greta Coal Measures (called the Greta Coal Interval), the Permian Coal Interval (which is the interval between the top of the Permian where coal first appears and the base where

coal is no longer present in the Permian stratigraphy) and ground surface elevation. The aim of the 3D structure is to provide the critical geological framework for thermal modelling. Additional geological layers, such as individual strata, are not part of this model but can be added to the basic framework of the geological model.

All the layers, except the ground surface, were imported into AutoCAD and edited to remove several spurious points that result from over interpolation during gridding. A vertical exaggeration of 10:1 is used to view and process the data. AutoCAD prefers to work in a Universal Transverse Mercator project format for XYZ with Eastings, Northings and elevation. Since the Sydney Basin model is quite large it crosses two projection zones, making it difficult to work in metres, so it was preferable to work in degrees. To convert the Z elevation metres into degrees, when displaying

surfaces with latitude and longitude coordinates, elevations were multiplied by a factor of 1/9500. AutoCAD provides viewing functionality in 3D perspective with wireframe and solid surface modes to help identify spurious points. The associated data file is then edited and the model surface rebuilt to display the corrected surface. The point of intersection between two geological layers is calculated in AutoCAD to produce smooth boundaries and transitions between model surfaces. Geological layers were then exported from AutoCAD in .dwg format (a native format for CAD used for storing two- and three-dimensional design data and metadata) and imported into 3D Studio Max where the surfaces were contoured and smoothed for the addition of the colour contour images. The surfaces were rendered and outputted to the stacked profile shown in Figure 7. The elevation surface is contoured separately in Surfer and combined with the stacked profile in a graphics editing

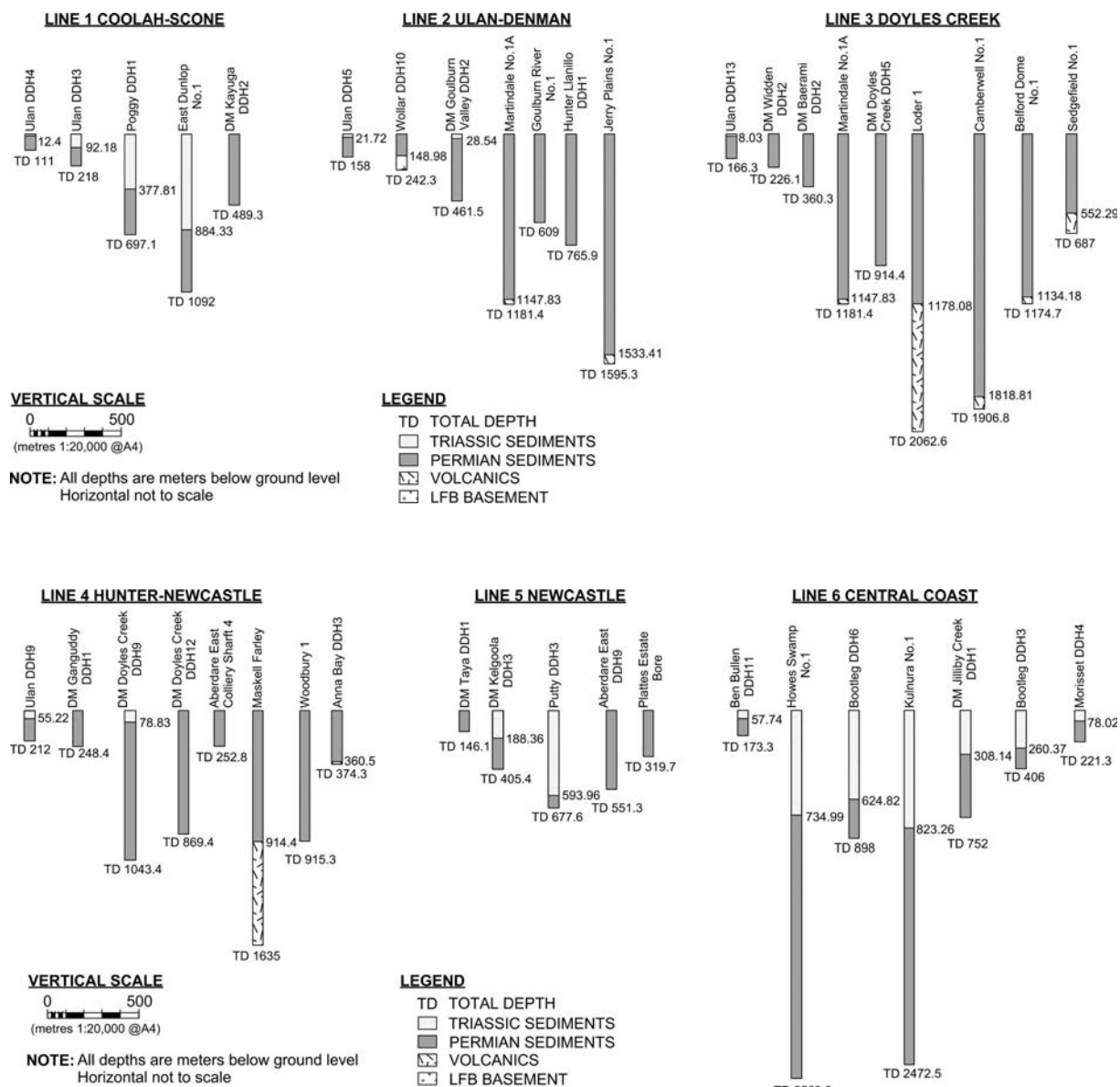


Figure 5 Stratigraphic sections of boreholes in Lines 1 to 15.

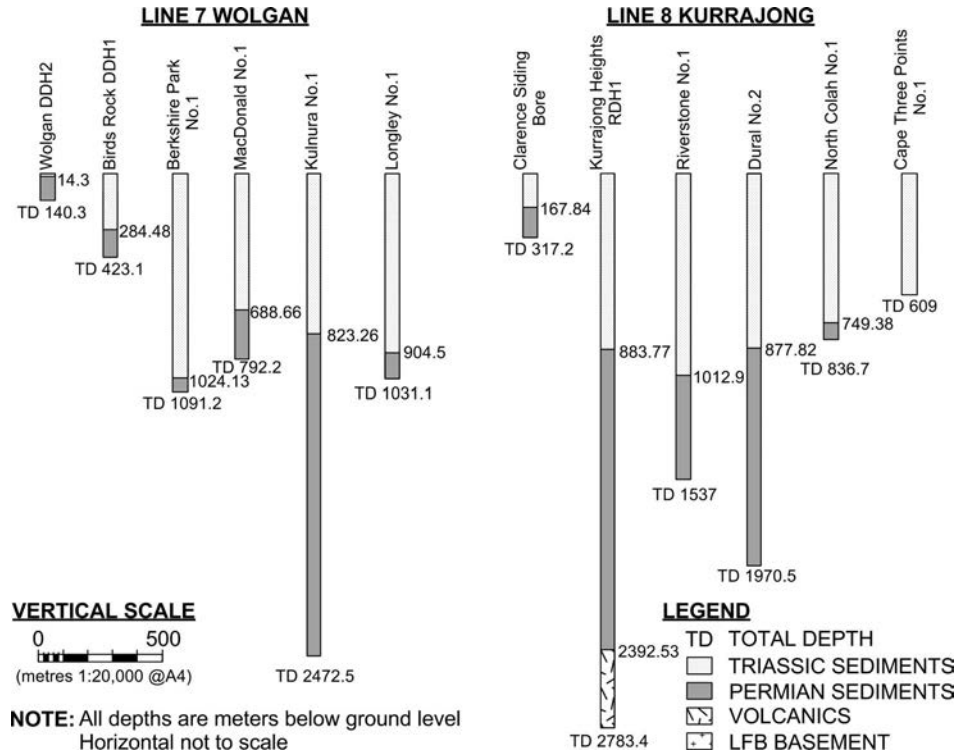


Figure 5 (Continued).

program. The final 3D geological model consists of geological layers in simple XYZ format that can be imported into numerous visualisation, animation, GIS and geophysical programs.

### Confidence reliability accuracy and precision map

The Confidence, Reliability, Accuracy and Precision (CRAP) Map (Figure 9) aims to communicate an evaluation of the various datasets used in supporting the development of the 3D geological model. A CRAP map for the OZ SEEBASE model of the Sydney Basin has been produced by Frog Tech Pty Ltd and this work applies a similar methodology to produce a CRAP map for our 3D geological model. The map is a resulting maximum confidence value at any X, Y location within the Sydney Basin from the following input datasets shown in Table 6. The value of a point in the weighted grid is calculated with the following formula (Equation 2):

$$p(X, Y) = \sum_{i=0}^n V_i - \frac{d_i^3}{D^3} \times V_i \quad (2)$$

where  $V_i$  is the assigned weighting factor of the data point  $i$ ,  $d_i$  is the distance to data from  $(X, Y)$ , and  $D$  is the maximum distance considered relevant. We use a cubic function to give due emphasis to closer data, while more distant data are weighted appropriately less, and if  $d_i > D$ , the data are ignored. The points  $p(X, Y)$  are chosen to be the centre of the cells forming a  $0.05^\circ$  grid over the Sydney Basin. The total confidence value of each cell is the addition of the weighting factors of each nearby dataset. Because of this, the confidence value is

an arbitrary number related to the type of assigned input data. Datasets with multiple points close together receive smaller weighting factors (i.e. seismic and structure contours) than those of more discrete points (i.e. boreholes) (see Table 5). Values of 0 to 20 are considered low, 20 to 40 moderate and greater than 40 high. The map represents an overall combined value of confidence and reliability, from the different types of data used in each geological layer, for the complete 3D model of the Sydney Basin. Areas of high confidence generally represent parts of the model with good physical data control for which the 3D geological model is more constrained, while areas of low confidence show parts of the model for which there is very limited data; thus the 3D geological model is more interpretive.

## RESULTS

### Density testing

The measured densities of the core samples from the Belford 1, Dural South 1, East Maitland 1 and RDH Kurrajong Heights 1 (Table 2) are divided into three groups of basal volcanics, based on depth. The samples were dominated by tuffs and breccias, which were often highly weathered, and basalt and rhyolite. Core samples from the bottom of Dural South 1 and East Maitland 1 (greater than 3000 m depth) were the least weathered of all the samples and comprised both tuffs and basalt. The average density of  $2.92 \text{ t/m}^3$  is comparable to the  $2.95 \text{ t/m}^3$  proposed by Krassay *et al.* (2009) for deep dense bodies that they interpret as the source of the Meandarra Gravity Ridge.



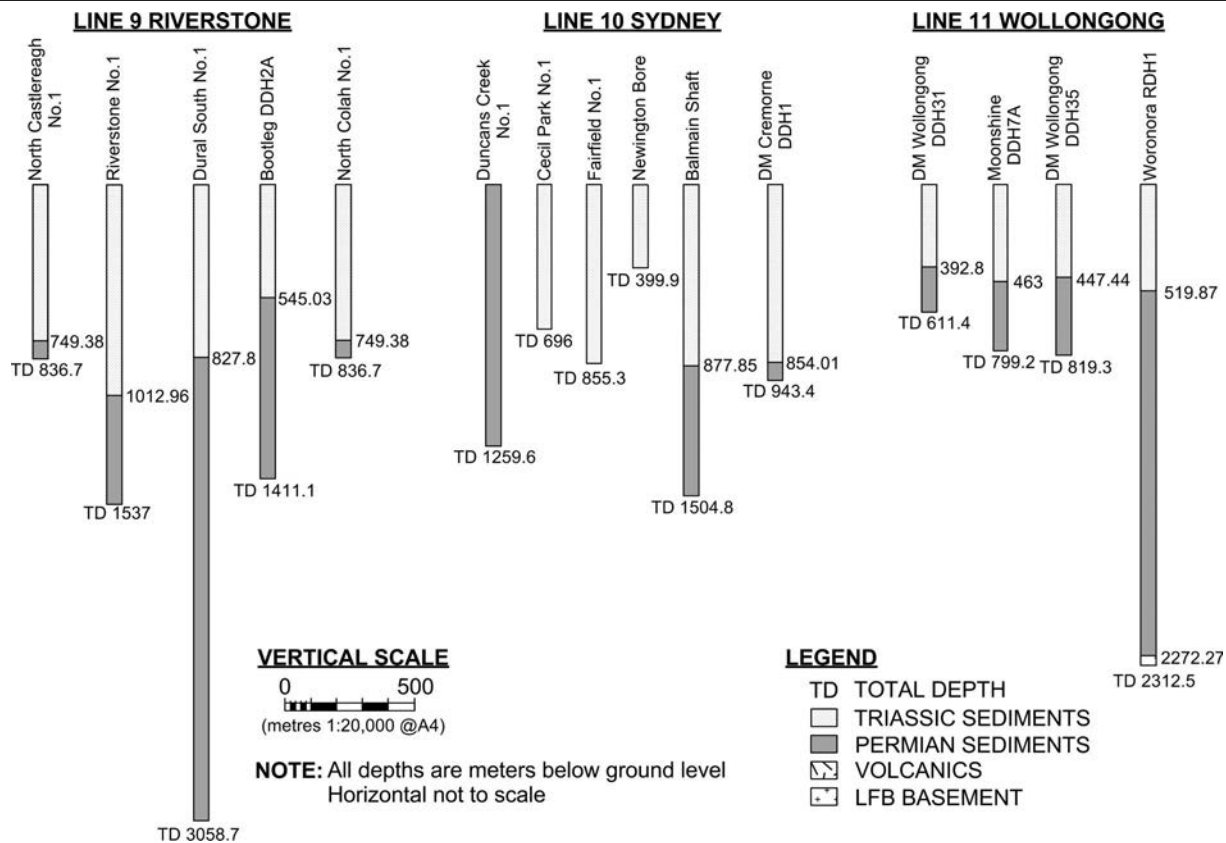


Figure 5 (Continued).

### Gravity modelling

The modelled outcomes for the Sydney Basin fit well with the observed gravity (Figure 4). The geometry of the models is considered consistent with both extensional rift basin formation and the geometry observed from our previous work in the Gunnedah Basin (Danis *et al.* 2010). The Sydney Basin is bounded to the west by a structural basement high, composed of numerous granitic plutons, many of which outcrop on the basin margin. This structural basement high appears continuous with the western basement high of the Rocky Glen Ridge in the Gunnedah Basin. To the north-east, the basin is truncated by the Hunter-Mooki Fault. In the south, thin sediments of the Sydney Basin overlie the structural basement high of the Boyne Mount and Sassafras Plateaus (Figure 2). At the coast, the boundary of the basin is harder to define. Seismic reflection data suggest possible continuation of the basal volcanics and sediments to the offshore uplift towards the edge of the continental shelf. Structurally, the offshore uplift appears to be a controlling factor in sedimentation; therefore for the purposes of this study we consider the offshore uplift to be the eastern boundary of the Sydney Basin.

A lower-density portion ( $2.60 \text{ t/m}^3$ ) of the LFB was required to fit the observed long-wavelength gravity lows for the majority of models. The alternative of increasing sediment thickness and/or changes in density did not produce a modelled response which satisfies the borehole information and was considered geologi-

cally reasonable. We chose not to change the density of the basal volcanics, so as to be consistent with previous models, however decreasing the density would lead to an increase in the thickness of basal volcanics required in some parts of the model. This lower-density portion of the LFB may be related to, but not limited to, a more granitic-rich basement or metasediments. The seismic structure contour maps of Mayne *et al.* (1974) provide good controls on the depth to the top of the basal volcanics where borehole information is absent. Where boreholes have reached the top of the basal volcanics, the depths are comparable with those indicated by the seismic structural map of Mayne *et al.* (1974). Basal volcanics have been added over the top of the basement on the offshore uplift to achieve the observed gravity highs. It is not possible to determine whether the observed gravity high is related fully, or in part, to a contribution of the early rift volcanics, shoshonites related to the Gerringong Volcanics or basalt seamounts, as their seismic velocities and densities are quite similar. It was also necessary in most profiles that extend offshore (as shown in Appendix A) to add a small wedge of denser mid crust, at 12 km depth, to produce the observed gravity high on the offshore eastern end of the profile. This is considered appropriate if we assume thinning of the continental crust with the approach of the ocean-continental crust boundary.

The profiles Lines 1 to 3 (Figures 4a–c) show similar model geometry of exposed LFB granites, metasediments or volcanics in the west, thick sediments of the Sydney Basin with basal volcanics and minor surface



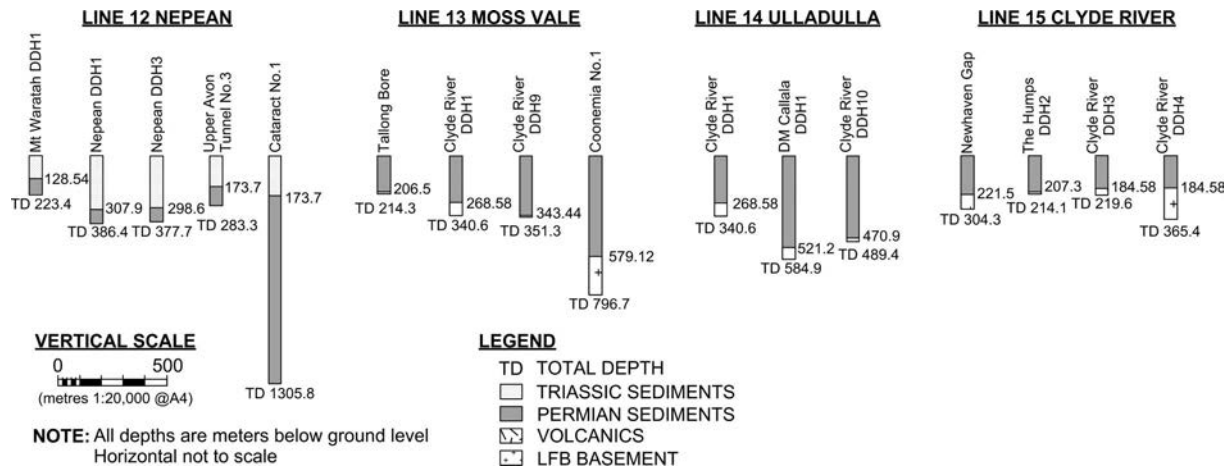


Figure 5 (Continued).

Triassic volcanics and truncation in the east by the Hunter-Mooki Fault. The strong gravity high in the middle of Line 1 is in response to the thickening of basal volcanics which form part of the Meandarra Gravity Ridge high. This high is continued through in Lines 2 and 3, despite the overall trend of increase in the observed gravity from west to east. For each line, the inferred position of the Hunter-Mooki Fault is generally a good fit with the geometry of the seismic reflection profiles collected by the New South Wales Department of Primary Industries (NSW DPI) (MINFO 2008). Sediment thickness is generally less than 1.5 km, and the basal volcanics are thicker in Line 1 than in Lines 2 and 3. Lines 2 and 3 were positioned near or over the structural basement high of the Mt Coricudgy Anticline. The model's geometry reflects the shallowing of the basement to the west, and Line 3 shows the truncation of the basal volcanics by the basement high (Figure 4c).

The profile of Line 4 (Figure 4d) shows a geometry consistent with an extensional rift origin and an increase in sediment thickness compared with the northern three lines. The geological map indicates that Rylstone Volcanics are present at the western end of the line, and therefore a small pocket of surface volcanics was included in the model, with a density of  $2.88 \text{ t/m}^3$ . On the eastern end of the profile are the Stockton Sands for which an approximate thickness of 300 m is modelled based on nearby borehole logs. Underneath the Stockton Sands, the Targon Fault is presumed to truncate and uplift the basement and volcanics to a depth of less than  $\sim 300 \text{ m}$ . The fault-bounded domal structures of the Belford and Loder Domes, which are interpreted to be related granitic plutons, fit the observed gravity well when using a low-density LFB basement and match with the seismic structure contour maps. The top of the basal volcanics is constrained in Line 4 by Maskell Farley 1 and Anna Bay DDH3, which reached basal volcanics at 914 and 360 m, respectively.

The anticline/syncline structures of the Hunter Valley Dome Belt are well represented by both Lines 4 and 5 (Figure 4e). The Newcastle profile Line 5 is the northernmost profile to go offshore into the Newcastle Syncline. Offshore seismic reflection profiles (i.e. SY91-

14) indicate a horst and graben-like basement structure with the top of the basal volcanics at  $\sim 3.6 \text{ km}$  at their shallowest and deepening to over 5 km. The seismic structure contour map of Mayne *et al.* (1974) infers two fold axes offshore, which occur just west of the two gravity highs. The structure at the eastern end of the profile could be related to uplift and reactivation of basement faults. In the central part of the profile, sediments are over 3 km thick, and almost 2 km of basal volcanics overlie basement. The basement high at 140 km along the profile is related to the Belford/Loder Dome.

Profile Lines 6 and 7 (Figure 4f-g) show a similar model geometry, with shallow LFB basement in the west, deepening in the central part under the basal volcanics before rising for the structural high of the Kulnura Anticline. At the end of Line 6, near the coastline, a subsurface portion of the Gerringong Volcanics is modelled. A subsurface portion of Gerringong Volcanics is also modelled at the coastline for profile Line 7. The exact thickness, depth and extent of the Gerringong Volcanics are not constrained by mapping or borehole data in this area, but as suggested by Campbell *et al.* (2001), they may be present this far north and could act as the source of the localised gravity high on the eastern end of Line 6. The localised gravity low which follows this high is modelled with a small amount of low-density saturated sediment (most likely related to Quaternary dune or river material). In Line 7, a small amount of alluvials is modelled to account for the localised gravity low near Tuggerah Lake. Although no boreholes in profile Line 7 reached basal volcanics, Kulnura 1 shows at least 2.4 km of sediment, and in profile Line 8, Kurrajong Heights RDH1 shows basal volcanics at 2.3 km. Maximum sediment thickness in profile Lines 6 and 7 is approximately 3 km onshore and over 4 km offshore.

The Kurrajong profile (Line 8, Figure 4h) is one of three profiles through the deepest part of the Sydney Basin. Here, the geometry incorporates a similar structure to the model of Qureshi (1989), and includes features which correlate with structures identified by Branagan & Pedram (1990) such as the Kulnura Anti-

cline, Yarramalong Syncline, Lapstone Monocline and Kurrajong Fault. The seismic structural contour maps of Mayne *et al.* (1974) provide a good constraint on the geometry of the top of the basal volcanics, and correlate with the depth of volcanics observed in Kurrajong Heights RDH1. The Lapstone Monocline and Kurrajong Fault occur where the thick basal volcanics begin at 70 km along the profile (Figure 4h). In addition, a low density ( $1.00 \text{ t/m}^3$ ) body is added to the end of Line 8 to represent the 1 km or more of ocean present offshore near the edge of the continental shelf. Offshore seismic reflection profile SY81-20 shows a number of tilted fault block closures along the eastern flank of the offshore syncline basement faulting and the displacement of basal volcanics. The sharp boundary and breaks in basal volcanics modelled in Line 8 near the coastline reflect the faulting shown in SY81-20. The offshore syncline and offshore uplift structures are modelled well in this profile. The magnetic map (Figure 3b) indicates a high in the area northwest of Broken Bay, which may be related to an extinct maar volcano, a diatreme or the Gerringong Volcanics. Since it is not possible to distinguish between these possibilities, the source is modelled by a package of volcanics with a density of  $2.88 \text{ t/m}^3$ , which would be compatible with any of the three options.

Profile Lines 9 and 10 (Figure 4i–j), also in the deepest part of the Sydney Basin, have a similar geometry to that of Line 8. The maximum thickness of onshore sediment is approximately 3.3 and 3 km in profile Lines 9 and 10, respectively and over 4 km offshore in both lines. There does not appear to be the need to model any Gerringong Volcanics in Line 9, as no localised gravity high is apparent, there are no surface outcrops, and the aeromagnetic survey map shows neither a high nor a low to suggest the presence of shallow volcanics. However, if the thickness of the basal volcanics were reduced, it would be possible to model Gerringong Volcanics close to the surface and match the gravity response. Seismic structure contours (Mayne *et al.* 1974) suggest the top of the basal volcanics ranges from 2.9 to 3.3 km in the onshore part of the profile and correlate with Dural South No.1, which reached basal volcanics at 3 km.

Line 11 (Figure 4k) is the first profile where the structure of the offshore uplift is much closer to the coast, the offshore syncline appears to be absent, and the faulting described by Ardito (2000, 2003) is more apparent. Offshore, the observed gravity is a strong high, which is modelled with thick basal volcanics to the edge of the continental shelf. Since it is difficult to distinguish seismically between the base of the Gerringong Volcanics and the top of the Dalwood Group, we have assumed a structure and flow pattern based on Campbell *et al.* (2001) and Carr (1998) in that any Gerringong Volcanics would be within the sedimentary packages and separate from the basal volcanics. A more extensive shallow body of Gerringong Volcanics would reduce the thickness of the basal volcanics required in the model on the eastern end of profile Line 11. There is limited information in the area of the Woronora Granite on the top of the volcanics from borehole information and seismic interpretations, so, given the borehole log

for Woronora RDH1 shows no volcanics present above the Woronora Granite (Figure 4k) at 2.2 km depth, it assumed they are most likely absent or minimal. The lateral extent of the basal volcanics decreases in the profiles towards the southern part of the Sydney Basin. This is considered consistent with the tapering off of the Meandarra Gravity Ridge and contraction in basin width. The sediment thickness is approximately 2.2 km onshore and reaches over 6 km offshore on the edge of the continental shelf. A small low-density body was included in the model above the Woronora Granite to represent the Woronora Reservoir and saturated sediments. Detailed gravity modelling, HRE Line1, from Danis (2010) showed a small amount of low-density LFB extended under the basal volcanics to the west of the Woronora Granite (Figure 4k); however, this low-density unit may or may not be related to the Woronora Granite itself.

In profile Line 12 (Figure 4l), the geometry is again similar to Line 11, although low-density LFB is present under the basal volcanics for most of the onshore part of the profile. On the western end of the line, the Bindook Volcanic porphyry is modelled. Gerringong Volcanics are exposed at the surface and are modelled to approximately 1 km deep. Although this exceeds the maximum thickness estimate by Packham (1969), it is not possible to differentiate between basal volcanics and the Gerringong Volcanics, so again we have kept the two bodies separated in the model as per model Line 11. The localised observed gravity low at 40 km along the profile is modelled with an increase in sediment thickness and no basal volcanics. Recently acquired gravity data by Danis (2010) in this area, which is not integrated into the regional map, suggests that the gravity low may not be as pronounced as it is shown in the regional gravity. Danis (2010) modelled the low with HRE Line 1 (location shown on Figure 4l) and showed the presence of some thin basal volcanics at approximately 1 km depth. The gravity low on Line 12 is likely a residual feature of the resolution of the gravity data points used for the regional gravity map.

The Moss Vale profile (Line 13, Figure 4m) shows a significant decrease in sediment thickness in the Sydney Basin from 3 km in Line 12 to 1 km or less. The basal volcanics have almost disappeared in thickness and extent, although a small package is required to model the localised high, believed to be the nose of the Meandarra Gravity Ridge. Both basal volcanics and Gerringong Volcanics are modelled offshore along the edge of the continental shelf as the source of the gravity high. Boreholes along profile Line 11 terminate in the metasediments or conglomerates (Tallong Bore) of the LFB basement at depths of approximately 200 to 900 m, without intersecting basal volcanics. Here, we use a density of  $2.60 \text{ t/m}^3$  to model the shallow LFB basement, and account for the changes in geology. On the western end of the profile outcrops the Lockersleigh Adamellite, the low density body within the basement (modelled with a density of  $2.59 \text{ t/m}^3$  under the low-density LFB) is interpreted to be part of the subsurface extent of either the nearby Uringalla or Glenrock Granite.

For Lines 14 and 15 (Figure 4n–o), the model geometry shows no basal volcanics under the onshore sediments, which are generally less than 500 m thick.

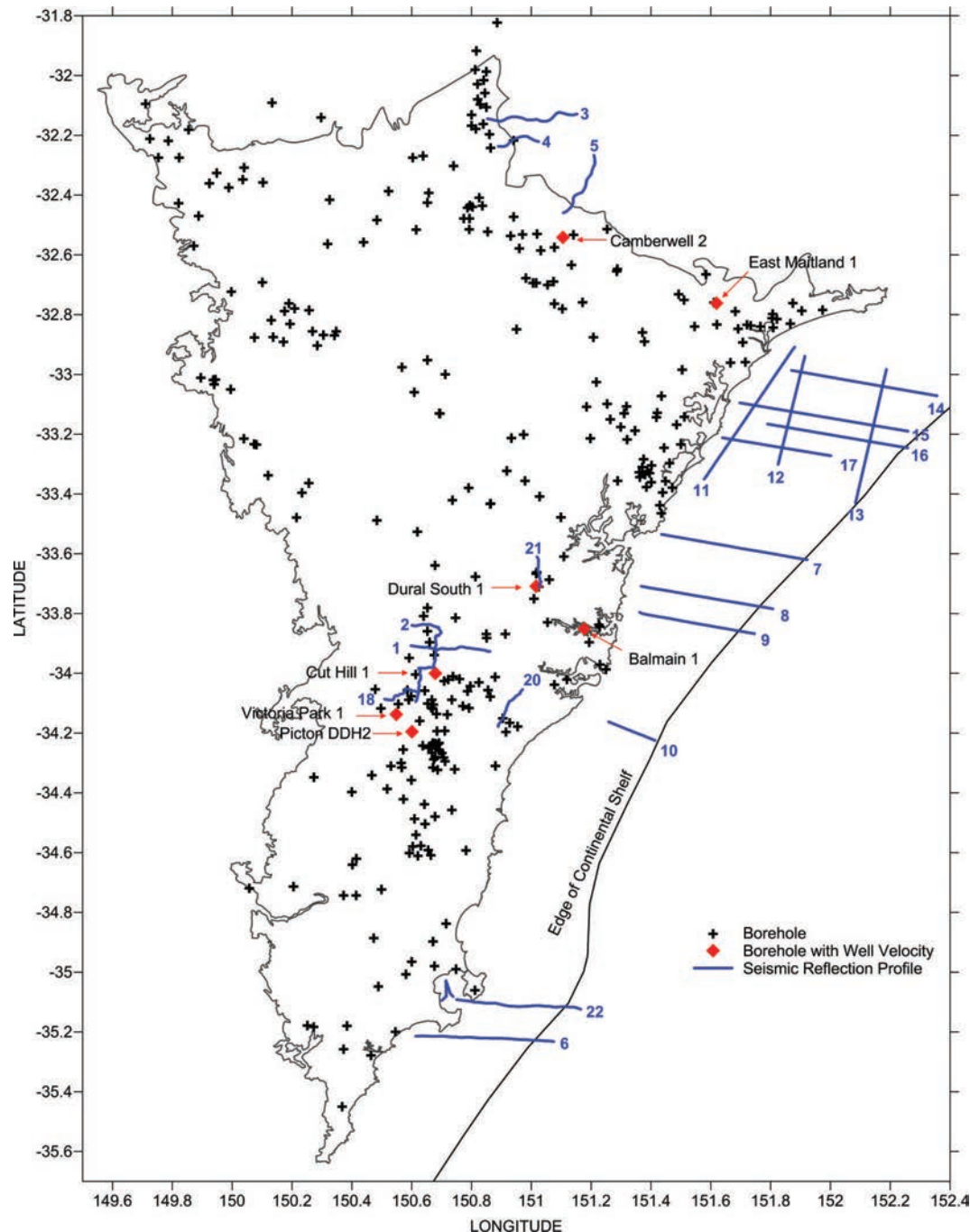


**Figure 6** Location of boreholes and seismic reflection profiles used for the 3D model. Stratigraphic boreholes are crosses; boreholes with well velocities diamonds and seismic reflection profiles are numbered (see Table 3 for details).

Low-density LFB is required to model the regional low and account for the geology encountered in the boreholes. In Line 15 at approximately 30 km along the profile, an increase in the amount of low-density LFB modelled may represent a subsurface portion of the Milton Monzonite. Although profile Line 14 does not extend offshore, an extension of the line offshore would be expected to look similar to Line 15, with basal volcanics and Gerringong Volcanics modelled on the continental shelf. The source of the Gerringong Volcanics is inferred by Campbell *et al.* (2001) to be nearby.

### 3D surface contouring

Figure 7 shows the stacked 3D geological model for the Sydney Basin. During the creation of the LFB 3D surface, it was necessary to add additional points to the data to account for the exposed LFB west of the Sydney Basin. In order to do this, 568 points were added, based on the approximate surface elevation. During editing in AutoCAD for spurious points created from gridding over-interpolation, adjustments were made to 21 points in the LFB (excluding the added data), one point in the top of the basal volcanics, 68 points in the

**Table 5** Construction details for gravity model profiles of Figure 4.

Line name	No. boreholes	Seismic line	Other information
1 Coolah-Scone	6	DPI4	
2 Ulan-Denman	7	DPI5, DPI6	
3 Doyles Creek	9		Seismic structure contours
4 Hunter-Newcastle	8		Seismic structure contours, mapped geology
5 Newcastle	5	SY91-01, SY91-02, SY91-14, SY91-15A	Seismic structure contours
6 Central Coast	7		Seismic structure contours
7 Wolgan	6	SY91-01, SY91-16	
8 Kurrajong	6	SY81-20	Seismic structure contours, mapped geology structures
9 Riverstone	5	SY81-20, SY81-24	Seismic structure contours
10 Sydney	6		Seismic structure contours
11 Wollongong	4	CB87-115, CB87-112, 118, 119, 122	
12 Nepean	5	SY81-34	
13 Moss Vale	4		
14 Ulladulla	3	T4-M41S	
15 Clyde River	4	M4S	

base of the Permian Coal Measures (PCM) (which included 49 points offshore in the Newcastle Syncline), 47 points in the top of the PCM, nine points in the base of the Greta Coal Measures and 19 points in the top of the Greta Coal Measures/base of Shoalhaven Group. Some of the minor adjustments to points in the LFB were based on the results of the detailed field survey of Danis (2010).

The geometry of the Sydney Basin shows a N–S-orientated channel through the basement that runs from the western coalfields to the southern coalfields near Wollongong. The major structural features identified in the structural element map of Krassay *et al.* (2009) and those shown in Figure 2 can be clearly seen in the basement topology (Figure 8). On the western edge of the basin the Illawarra, Sassafras and Boyne Mount Plateaus are clearly observed. In the north, basement shallows over the Mt Coricudgy Anticline (Figure 2) and provides a good structural boundary between the Sydney and Gunnedah Basins. A N–S-orientated basement high runs from the Newcastle/Hunter Coalfield boundary towards Sydney and is referred to by Krassay *et al.* (2009) as the Lochinvar–Kulnura Ridge. East of this ridge, the basement low corresponds well with the Newcastle and Offshore synclines. Offshore, a basement high trends N–E and aligns well with the structure of the offshore uplift. The Cumberland Basin appears to occur where the basement is deepest, in the centre of the Meandarra Gravity Ridge. The termination of the Meandarra Gravity Ridge at the Illawarra Plateau is where the basal volcanics are truncated. The basal volcanics are constrained to the north by the Hunter-Mooki Fault, to the east by the structural highs of the Woronora Plateau and Offshore uplift and to the west by the basement high caused by the surface exposure of the LFB. Offshore, the extent of the basal volcanics and/or shoshonitic activity is difficult to define, and it appears mainly confined by the edge of the continental shelf.

For the coal intervals, gravity modelling is unable to define their extent; instead, the model is reliant on the availability of coal exploration borehole data. In the case of both the Greta and Permian Coal Intervals, the offshore extent of the surface is difficult to define. It is

assumed they extend offshore and would be truncated by the erosional surface of the continental slope. In this model, they are extrapolated from their last known thickness and terminated at the offshore uplift.

### Confidence, reliability, accuracy and precision (CRAP) map

The CRAP map (Figure 9) for the 3D geological model of the Sydney Basin shows that areas of high confidence are generally associated around the Western, Hunter and Southern coalfields. This is expected, as the majority of drill hole information comes from coal exploration boreholes. Limited information is available in the central west of the basin, as expected, owing to limited coal and petroleum resource exploration. Offshore, near Newcastle, detailed seismic reflection work has been undertaken for the exploration of petroleum and gas fields, leading to higher values here. Around Sydney, owing to the nature of the settlement, exploration and drilling is limited, and so the confidence of the data there is generally low.

## DISCUSSION

In the Sydney Basin, previous gravity modelling by Qureshi (1984, 1989) and Leaman (1990a, b) showed several interpretations for the basin's regional structure and depth to basement. Qureshi (1984) suggested that a dense mafic pile existed beneath the Sydney Basin related to rift structure. Leaman (1990b) challenged this idea with models that used variations in basement density and the inclusion of granite bodies. The stratigraphic controls of boreholes which reach basal volcanics required that Leaman (1990b) not preclude the possibility of dense mafic bodies at depth in his models, and he acknowledges that they are present but that they are not as thick as that proposed by Qureshi (1984, 1989). If localised volcanic piles, up to 1 km thick, were included at the basin base, Leaman (1990a) suggests that only the detailed form of the basin would need to change.



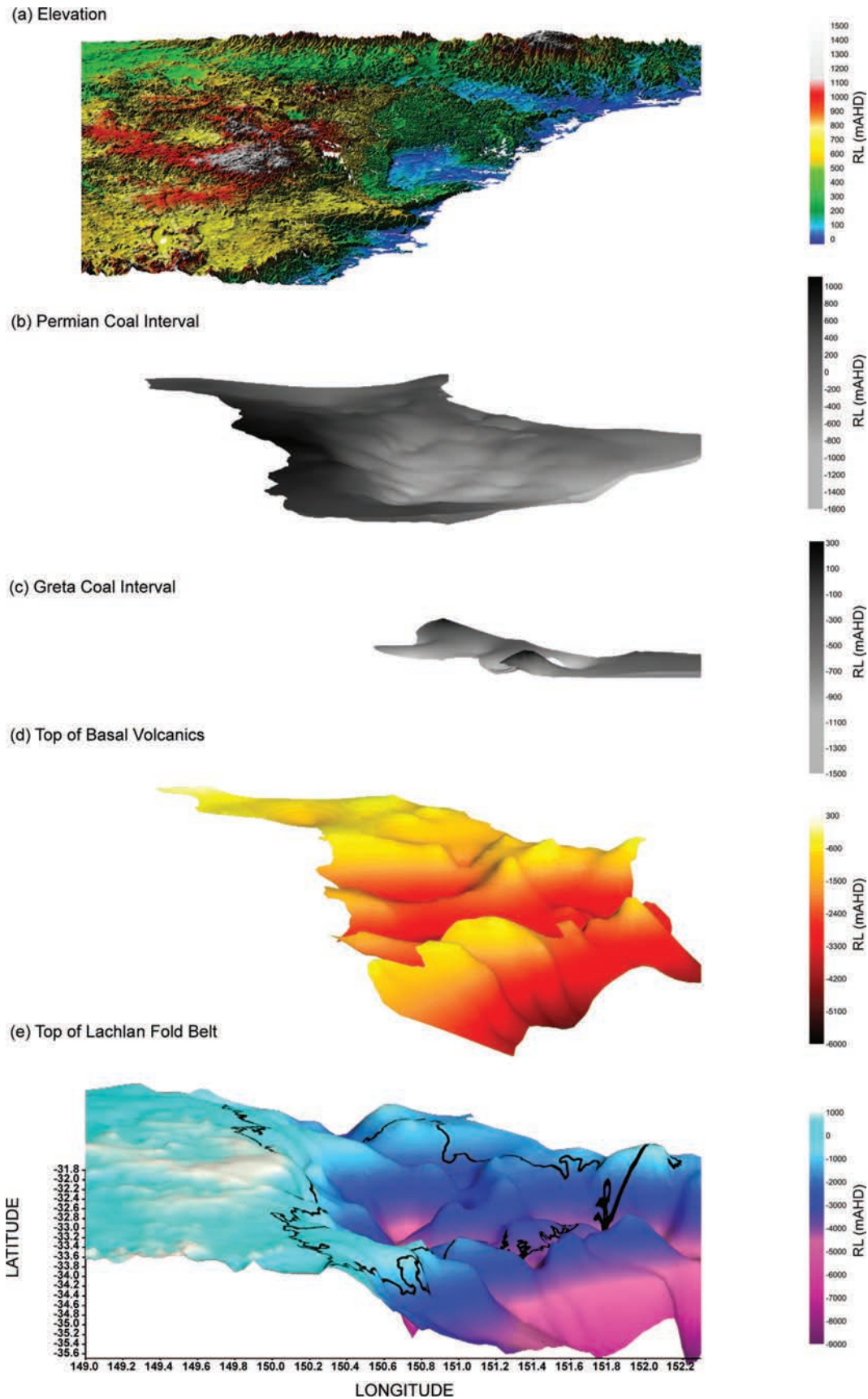


**Figure 7** Stacked model 3D surfaces of the Sydney Basin in mAHD, shown to their approximate extent. (a) Elevation. (b) Top and base of the Permian Coal Interval. (c) Top and base of the Greta Coal Interval. (d) Top of Basal Volcanics. (e) Top of Lachlan Fold Belt basement with Sydney Basin outline. The Permian Coal Interval contains a surface for the top of the Permian where coal first appears and the base where coal is last seen in the Permian stratigraphy. The Greta Coal Interval contains a surface for the top and base of the coal measures. Basement shown on the western limit of the model is surface elevation from the SRTM.



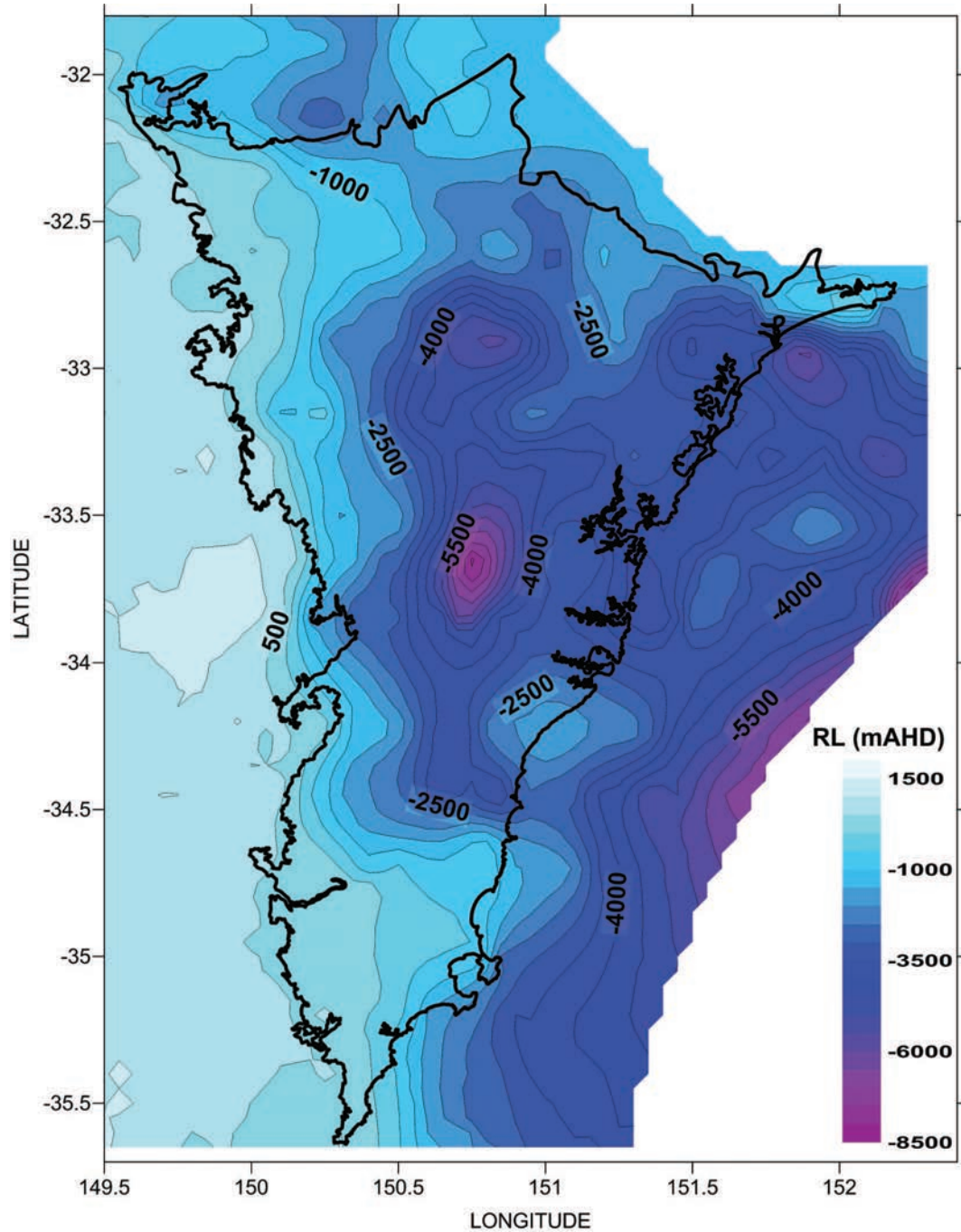


**Figure 8** Top of LFB basement as contoured depth (mAHD) surface showing Sydney Basin outline. Contour interval is 500 mAHD.

The Sydney Basin is dominated by numerous gravity lows onshore in the western boundary, many of which can be directly correlated with exposed or nearly exposed form Paleozoic granitoids (Leaman 1990b). In the models of Leaman (1990a, b), the basin form is more irregular onshore with granite bodies dominating much of the basement. Krassay *et al.* (2009) found that both a Qureshi-type (shallow dense source) model and a Leaman-type (granitic terrain) model gave approximate matches between the gravity data and model results for the work in the Gunnedah Basin. However, the Leaman-type model involving large granite batholiths with

negative density contrast on either side of the Meandarra Gravity Ridge was unstable to small changes in the shape and thickness of granitic bodies. Therefore, a modified Qureshi-type model, using a simple rift-like shape, was Krassay *et al.*'s (2009) preferred model.

The Meandarra Gravity Ridge extends southwards from the Gunnedah Basin into the Sydney Basin and appears to truncate at the Woronora Plateau (Figure 2). As the nature of the basement beneath the Sydney Basin, and the outcrop of geology of the LFB, changes frequently on the scale of the length of the Meandarra Gravity Ridge, Krassay *et al.* (2009) suggested that long,

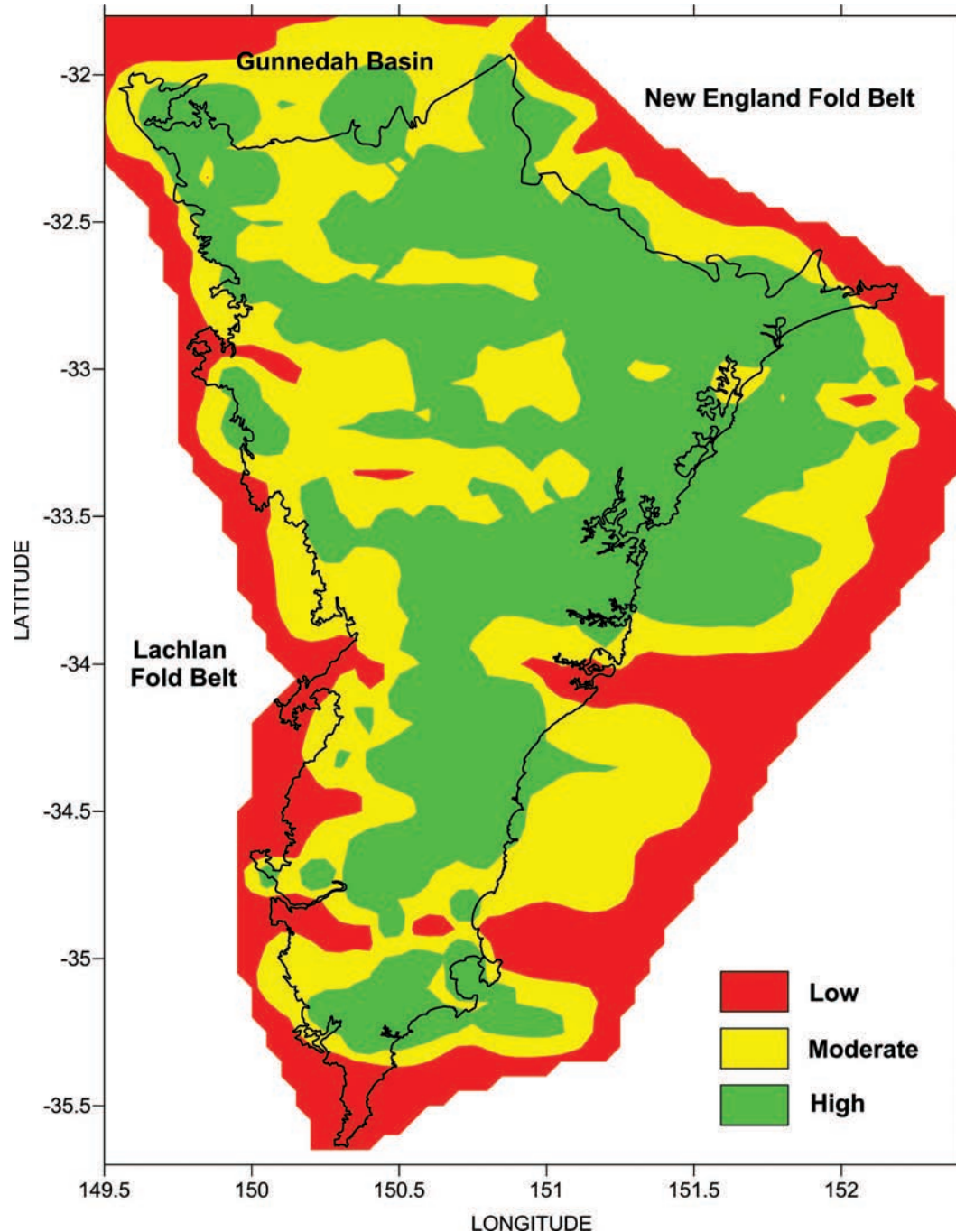


**Figure 9** Confidence Reliability Accuracy and Precision map. This map is an evaluation of the various datasets used and considers all structural layers of the model.

concealed, parallel belts of granite either side of the ridge and the absence of granite beneath it are unlikely. Leaman's solution is not applicable to the regional scale, particularly because significant volumes of mafic material are likely to occur at depth beneath the Sydney Basin (O'Reilly 1990).

The gravity modelling presented in this work takes the modified Qureshi-type model with elements of the Leaman-type model to produce gravity models, which support the interpretation of the Sydney Basin as an extensional rift basin with dense mafic volcanics at

depths. The models are continuous with earlier work in the Gunnedah Basin (Danis *et al.* 2010), as they use the same density parameters and are constrained by boreholes and seismic structural information.

The geometry of the models is considered consistent with an extensional rift basin formation. The models suggest a basement dominated by low-density LFB material, which may relate primarily to granitoids. However, metasediments are not precluded, as south of the Illawarra Plateau, metasediments are encountered in boreholes. Unlike the models of Leaman (1990b), the

**Table 6** Input datasets, maximum distance and weighting factor for the Confidence, Reliability, Accuracy and Precision Map.

Input dataset	Maximum distance (km)	Weighting factor
Gravity Model—Basement	20	2
Gravity Model—Volcanics Onshore	20	0.5
Gravity Model—Volcanics Offshore	20	1
Boreholes—Basement	5	80
Boreholes—Volcanics	5	20
Boreholes—Coal	5	20
Structure Contours—Mayne <i>et al.</i> (1974)	1	5
Magnetics	5	10
Surface Geology	1	5
Seismic Reflection Profiles	5	2
Interpolated Points	5	5

density of the LFB basement in our models remains at an average of 2.70 t/m<sup>3</sup> rather than varying from 2.60 to 2.80 t/m<sup>3</sup>, and the low-density basement/granitoids have densities of 2.59 to 2.60 t/m<sup>3</sup>. The low-density basement/granitoids in each of the 2D profiles of the Sydney Basin could be interpreted as part of a much larger body, on a similar scale to that of the Bathurst Batholith, as there does appear to be some consistency between lines.

Blevin *et al.* (2010) have observed textures in the granites of the Bundandah and Wandandian plutons of the southern Sydney Basin, which indicate emplacement at relatively high crustal levels prior to exhumation. They also suggest the arkosic material represents proximal granite-derived sediments overlying the Woronora granite, indicating that it was exposed at the surface during initial basin sedimentation. This would be consistent with thinning of basal volcanics in the southern Sydney Basin (Figure 4) and its absence on the Sassafras and Boyne Mount Plateaus. Sediment thickness averages 3 km over most of the basin, and basal volcanics range from less than 1 km to over 4 km thick in the central part of the basin around Lines 9 and 10 (Figure 4i–j). The offshore basal volcanic thickness is generally less than 1.5 km.

As mentioned previously, this geological model does not include all individual geological units, as it is designed as a regional model, and combines smaller units with similar physical properties to form larger, significant units, which define the physical structure of the basin. In addition, the complex faulting and folding observed in the basin sediments are not explicitly incorporated in this geological model. This model provides a basic framework, i.e. depth to the basement and depth to top of basal volcanics, from which complex local or regional geological models can be derived. Generally, large-scale faults, folding and monoclines are controlled by the basin architecture, and our models show features comparable with those observed; for example, the uplift and faulting in the Hunter Valley Dome Belt are clearly shown with localised shallower basement.

When comparing our geological model with that of the SEEBASE model (Blevin *et al.* 2007), the total sediment thickness isopach map of the SEEBASE model shows areas of up to 5 km of sediment, which is confirmed in our gravity modelling. It is important to note that the SEEBASE model and our model use different definitions of the term ‘basement’. The SEEBASE model is primarily concerned with the top of economic basement, which is the base of coal- and petroleum-bearing sediments, hence the generally flat nature of the basement, while our model defines basement in terms of crystalline/metamorphic basement representing the top of the LFB. Although the SEEBASE model was constructed to model the basal volcanics and depth to crystalline basement, this information is currently not available. The 3D geological model presented in this work provides the first regional assessment of the basement structure and thickness and extent of the basal rift related volcanics.

The ability to visualise and edit surfaces in 3D allows the introduction of the human iterative step in the transition from a geophysical model to the generation of a geological model. This iterative step ensures the structures being created are geologically reasonable and consistent with available information. The confidence, reliability, accuracy and precision map provides a visual assessment of the overall interpreted quality of the model and highlights areas impacted from limited data.

The regional gravity modelling is also not without some limitations. The detailed gravity work in Danis (2010) highlighted potential limitations in using the regional gravity data particularly in areas with sparse data coverage or poor quality data. The difference in the depths determined from gravity modelling for the top of the basal volcanics and basement was negligible in the basin, but towards the western edge where the basal volcanics began to thin and the LFB exerts more influence, the depth and extent of basal volcanics and basement may vary depending on the resolution of the regional gravity data. For example, on the western end of Line 12, modelling by Danis (2010) showed basal volcanics could extend a further 20 km west of their current truncation (Figure 4l), and the basement could be up to 700 m shallower than modelled from the regional data. Although the regional gravity data have limited resolution in some places, particularly for some small-scale features, the resulting basin scale model provides a reasonable assessment of the structure. The 3D model framework does allow the results of future detailed surveys to be integrated.

The interpolated geometry of the Hunter-Mooki Fault, derived solely from the gravity models, is incorporated into the geological model for the purpose of truncating the basal volcanics and Greta and Permian coal intervals. There is also a level of uncertainty in the offshore section of the model, predominantly where the extrapolation of the coal layers and Gerringong Volcanics is concerned. Seismically, the basement and basal volcanics can be satisfactorily constrained, at least for the purpose of thermal modelling, but the coal cannot, and the Gerringong Volcanics are difficult to distinguish clearly. Because of the uncertainty in the offshore basin, the results of any thermal modelling would need to be carefully considered.



## CONCLUSION

The deep 3D structure of the Sydney Basin is characteristic of an extensional rift basin, where extension, initiated during the Late Carboniferous–Early Permian, developed the approximately north–south-orientated rift structure in the centre of the basin. Previous geological models have estimated over 4 km of sediment thickness in the Sydney Basin, and seismic reflection has outlined the possible extent of the basal volcanics. In our 3D geological model, sediment thickness generally ranges from 2 to 3.5 km, with depths of ~4 km reached in the offshore syncline areas, which is comparable with other geological models. Sediment thickness is greatest in the Cumberland Basin, the central part of the Sydney Basin. In the Newcastle and Hunter Coalfields, sediment thickness averages 3 to 3.5 km and thins to ~1.5 km over the Mt Coricudgy Anticline and the Western Coalfields. South of the Southern Coalfields, sediment thickness is less than 1 km.

The basal volcanics extend over most of the Sydney Basin, truncating in the south on the Illawarra Plateau. Our model confirms the continuation of the Meandarra Gravity Ridge from the Gunnedah Basin into the Sydney Basin, corresponding to a predominant gravity high. The interpretation of the structure and origin of the Meandarra Gravity Ridge by Krassay *et al.* (2009) is consistent with our model. Our models show that rift-related basal volcanics correspond with the north–south-trending gravity high at depths of 2 to 4 km below the surface and reach a maximum thickness of ~4 km.

The architecture and composition of the LFB basement influences not only the distribution (and thickness) of the basal volcanics but also the structures observed in the overlying sediments, e.g. monoclines and dome belts. The LFB basement is an undulating surface with deep channels and structural rises which correspond well to the structural domains shown in Figure 2. Numerous granitic bodies occur in the southern part and on the western edge of the basin, and in the northern half of the basin, granite bodies may be present in the basement as far east as the Hunter-Mooki Fault. Generally, the basement is under a 2 to 4 km-thick package of sediments and volcanics but at its deepest point is at greater than 8 km depth.

This regional-scale geological model of the Sydney Basin, constrained by borehole, seismic and geological information, provides a basic framework for the development of future detailed geological, hydrological and geothermal models. Although it incorporates simplified lithology and structure, the model is geometrically consistent with an extensional rift-basin origin and satisfies geological and structural information.

## ACKNOWLEDGEMENTS

The authors would like to acknowledge the NSW DPI in providing the Hunter-Mooki Seismic Survey data. Critical reviews by B. Musgrave and an anonymous reviewer improved an earlier version of this manuscript. This is contribution no. 690 from the Australian

Research Council National Key Centre for the Geochemical Evolution and Metallogeny of Continents (URL: <<http://www.gemoc.mq.edu.au>>). Craig O'Neill acknowledges support from DP0880801.

## REFERENCES

- ADLER J. D., HAWLEY S., MAUNG J., SCOTT R. D., SINELNIKOV A. & KOUZMINA G. 1998. Prospectivity of the offshore Sydney Basin: A new perspective. *APPEA Journal* **38**, 68–92.
- ARDITTO P. A. 2000. A sequence stratigraphic analysis of the Late Permian succession in the Dural area, central Sydney Basin, New South Wales. *Exploration Geophysics* **31**, 565–578.
- ARDITTO P. A. 2003. An integrated geological and geophysical interpretation of a portion of the offshore Sydney Basin, New South Wales. *APPEA Journal* **43**, 495–514.
- BEMBRICK C. S. & LONERGAN A. D. 1976. Sydney Basin. In: *Economic geology of Australia and Papua New Guinea*, 3, *Petroleum*. Australasian Institute of Mining and Metallurgy, Monograph 7.
- BLEVIN J., HALL L., CHAPMAN J. & PRYER L. 2007. *Sydney Basin Reservoir Prediction Study and GIS*, Project MR705, Confidential Report to the NSW DPI and Macquarie Energy, FrOG Tech Pty Ltd.
- BLEVIN P., CHAPPELL B. & JEON H. 2010. Heat generating potential of igneous rocks within and underlying the Sydney Basin: Some preliminary observations. *Proceedings of the Thirty Seventh Newcastle Symposium 'Advances in the Study of the Sydney Basin'*.
- BRANAGAN D. F. & PEDRAM H. 1990. The Lapstone structural complex, New South Wales. *Australian Journal of Earth Sciences* **37**, 23–26.
- CAMPBELL L. M., CONAGHAN P. J. & FLOOD R. H. 2001. Flow-field and palaeogeographic reconstruction of volcanic activity in the Permian Gurringong Volcanic Complex, southern Sydney Basin, Australia. *Australian Journal of Earth Sciences* **48**, 357–375.
- CARR P. F. 1998. Subduction-related Late Permian shoshonites of the Sydney Basin, Australia. *Mineralogy and Petrology* **63**, 49–71.
- CAUSEBROOK R. 2005. The geological storage potential of the offshore Sydney Basin. *An addendum to 'Geosequestration Investigation—offshore New South Wales' a paper by Sayers et al. 2004*. CO2CRC Geoscience Australia, Canberra, Australia, May 2005. CO2CRC Report Number RPT05-0023.
- CONAGHAN P. J. & JONES J. G. 1975. The Hawkesbury Sandstone and the Brahmaputra: a depositional model for continental sheet sandstones. *Journal of the Geological Society of Australia* **22**, 275–283.
- DANIS C. 2010. EL 6212: Report on the gravity survey and thermal modelling. Report for Hot Rock Energy Pty Ltd and Longreach Oil Ltd.
- DANIS C., O'NEILL C. & LACKIE M. 2010. Gunnedah Basin 3D architecture and upper crustal temperatures. *Australian Journal of Earth Sciences* **57**, 483–505.
- EMERSON D. W. & WASS S. Y. 1980. Diatreme characteristics—evidence from the Mogo Hill intrusion, Sydney Basin. *Australian Society of Exploration Geophysics Bulletin* **11**, 121–133.
- FRÖG TECH 2006. OZ SEEBASE Proterozoic Basins Study, Report to Geosciences Australia by FrOG Tech Pty Ltd.
- GLEN R. A. 2005. The Tasmanides of eastern Australia. In: Vaughan A. P. M., Leat P. T. & Pankhurst R. J. eds. *Terrane processes at the margins of Gondwana*, pp. 23–96. Geological Society, London, Special Publications 246.
- GUO B., LACKIE M. A. & FLOOD R. H. 2007. Upper crustal structure of the Tamworth Belt, New South Wales: constraints from new gravity data. *Australian Journal of Earth Sciences* **54**, 1073–1087.
- HERBERT C. 1972. Palaeodrainage patterns in the southern Sydney Basin. *Record of the Geological Survey of New South Wales* **14**, 5–18.
- HERBERT C. 1989. The Lapstone Monocline-Nepean Fault, A high angle reverse fault system. In: Plimer I. R. ed. *Proceedings of the Twenty Third Newcastle Symposium 'Advances in the Study of the Sydney Basin'*. University of Newcastle.

- HERBERT C. & HELBY R. eds. 1980. *A guide to the Sydney Basin. Geological Survey of New South Wales Bulletin 26, Bulletin No. 26.* Department of Mineral Resources, New South Wales, 603 pp.
- KENT A. J. R. 1994. Geochronology and geochemistry of Palaeozoic intrusive rocks in the Rockvale region, Southern New England Orogen, New South Wales. *Australian Journal of Earth Sciences* **41**, 365–379.
- KRASSAY A. A., KORSCH R. J. & DRUMMOND B. J. 2009. Meandarra Gravity Ridge: symmetry elements of the gravity anomaly and its relationship to the Bowen–Gunnedah–Sydney basin system. *Australian Journal of Earth Sciences* **56**, 355–379.
- LEAMAN D. E. 1990a. Geological Note: The Sydney Basin: Composition of basement. *Australian Journal of Earth Sciences* **37**, 107–108.
- LEAMAN D. E. 1990b. Sydney Basin gravity-magnetic interpretation structures and settings of NSW/P10 for Santos Ltd. (Digs Report No. PGR1990-3.R00018692). Online <<http://digsopen.minerals.nsw.gov.au/>>.
- LEITCH E. C. 1969. *Igneous activity and diastrophism in the Permian of N.S.W.* Geological Society of Australia Special Publication 2, 21–37.
- MAUNG T. U., ADLER D., SHAW R. D. & HAWLEY S. 1997. *Offshore Sydney Basin, New South Wales.* Canberra. Bureau of Resources Sciences, Petroleum Prospectivity Bulletin 1997/1.
- MAYNE S. J., NICHOLAS E., BIGG-WITHER A. L., RASIDI J. S. & RAINE M. J. 1974. Geology of the Sydney Basin—A review. *Bulletin of the Bureau of Mineral Resources Geology and Geophysics Australia*, **149**, 229p.
- MINFO 2008. The mining and exploration magazine of New South Wales Department of Primary Industries. September/October 2008 Issue 88. Online <<http://www.dpi.nsw.gov.au/aboutus/news/minfo>>.
- NSW DPI (2005). Map of NSW coalfields. Online <<http://www.dpi.nsw.gov.au/minerals/resources/coal/coalfields>>.
- O'REILLY S. 1990. Discussion The Sydney Basin: Composition of basement. *Australian Journal of Earth Sciences* **37**, 485–486.
- PACKHAM G. D. ed. 1969. The Geology of New South Wales. Geological Society of New South Wales Incorporated. *Journal of the Geological Society of Australia* **16**, 654 pp.
- QURESHI I. R. 1984. Wollondilly–Blue Mountains gravity gradient and its bearing on the origin of the Sydney Basin. *Australian Journal of Earth Sciences* **31**, 293–302.
- QURESHI I. R. 1989. Positive gravity anomaly over the Sydney Basin. *Exploration Geophysics* **20**, 191–193.
- REYNOLDS J. M. 2003. *An introduction to applied and environmental geophysics.* John Wiley and Sons, London.
- SHEPHERD J. & HUNTINGTON J. F. 1981. Geological fracture mapping in coalfields and the stress fields of the Sydney Basin. *Australian Journal of Earth Sciences* **28**, 299–309.
- TYE S. C., FIELDING C. R. & JONES B. J. 1996. Stratigraphy and sedimentology of the Permian Talaterang and Shoalhaven Groups in the southernmost Sydney Basin, NSW. *Australian Journal of Earth Sciences* **43**, 57–69.
- VEEVERS J. J., CONAGHAN P. J., POWELL C. McA. 1994. Eastern Australia. In: Veevers J. J. & Powell C. McA. eds. *Permian–Triassic Pangean basins and foldbelts along the Panthalassan Margin of Gondwanaland*, pp. 331–353. Geological Society of America, Memoir 184.
- VISHER G. S. 1965. Use of vertical profile in environmental reconstruction. *Bulletin of the American Association of Petroleum Geology* **49**, 41–61.

*Received 16 June 2010; accepted 20 February 2011*

**APPENDIX A** Complete Gravity Modelling Profiles. Density shown of units in t/m<sup>3</sup> not illustrated in Figure 4.

**APPENDIX B** Borehole Location Details.

(available from <http://www.tandfonline.com/ajes>)



# Building 3D geological knowledge through regional scale gravity modelling for the Bowen Basin

Cara Danis<sup>1,3</sup> Craig O'Neill<sup>2</sup> Mark Lackie<sup>2</sup>

<sup>1</sup>Department of Earth and Planetary Sciences, Macquarie University, NSW 2109, Australia.

<sup>2</sup>GEMOC ARC National Key Centre, Department of Earth and Planetary Sciences, Macquarie University, NSW 2109, Australia.

<sup>3</sup>Corresponding author. Email: [cara.danis@mq.edu.au](mailto:cara.danis@mq.edu.au)

**Abstract.** Regional scale gravity modelling is an effective and fast way to gain geological understanding of large scale structures like the Bowen Basin. Detailed deep 3D geological knowledge has become an important component of many types of exploration and resource modelling. Current interest in the Bowen Basin for geothermal exploration highlights the need for a complete basin scale model which is compatible with thermal modelling software. The structure of the Bowen Basin is characteristic of a typical asymmetrical extensional rift basin, with up to 5 km of sediment overlying the basement. By combining gravity modelling, calibrated by boreholes and seismic reflection profiles, we produce geologically reasonable 3D surfaces and structures to create a model of the Bowen Basin. This model is the final part in the completion of the 3D Sydney–Gunnedah–Bowen Basin system geological model and provides both an important framework from which detailed thermal models can be derived and a platform from which to expand with new information.

**Key words:** Bowen Basin, deep 3D structure, gravity modelling, seismic reflection, 3D surfaces.

Received 3 June 2011, accepted 2 December 2011, published online 23 January 2012

## Introduction

The Bowen Basin is part of the vast Sydney–Gunnedah–Bowen Basin (SGBB) system (Figure 1), which formed as a major extensional rift basin in the Late Carboniferous to Early Permian over Palaeozoic basement material (Glen, 2005). Comprised of Permian, Triassic and Jurassic sediments and volcanics the architecture and depositional history of the Bowen Basin is characteristic of its origin but its 3D subsurface architecture and thermal structure is poorly understood on a regional scale. Currently, knowledge of the Bowen Basin's subsurface architecture is confined to interpreted deep crustal seismic reflection profiles, gravity profiles or localised 3D structural models, generally at resource reservoir scale (<25 km × 25 km), and, understanding of the thermal structure has primarily been through extrapolated temperature maps, based on 1D models and estimates of sediment thickness. What is required is a regional scale geological model of the Bowen Basin which can be applied in many different areas, from geothermal exploration to sequestration studies, coal seam gas exploration and petroleum and coal studies.

Integrated gravity modelling is one effective way to build confidence in the knowledge of the 3D subsurface architecture and serves as a platform from which to build geological models. Gravity models consistent with a diverse set of observations, including geology, measured rock properties and borehole depths, allow the development of self-consistent geological models. From these models, an increased understanding of deep basin geology and structure is achieved and they are the ideal framework to develop complex models to investigate other subsurface features such as hydrogeology or thermal profiles.

Gravity modelling is particularly effective in determining the subsurface structure required in thermal models. Thermal models need the thickness, depth and structure of bodies that have similar thermal properties. Commonly these bodies are the sediment, volcanics and defined basement material, all of which, along with distinctive thermal properties, have distinctive densities. Sediment thickness, a critical component of thermal modelling, is efficiently determined with gravity modelling via a consistent density contrast between the sediments and the basement material.

This paper presents regional scale gravity model profiles of the Bowen Basin. We apply bulk lithologies in regional scale gravity model profiles and use geological properties, borehole data, seismic reflection profiles and mapped geology as constraints. These gravity profiles are combined with borehole data and transformed into subsurface geological layers for our 3D geological model. The geological model, developed primarily for high resolution 3D thermal modelling, incorporates surfaces for depth to basement and depth to basal volcanics, determined through the gravity modelling process, and coal layers, determined through borehole interpolation, constrained by knowledge of the subsurface architecture.

## Geological overview

Extension in the Bowen Basin (Figure 1) commenced in the Late Carboniferous to Early Permian (Cadman and Pain, 1998; Elliott, 1989). The Bowen Basin is an elongate north–south trending asymmetrical basin extending from northern New South Wales through into central Queensland and covers an area of approximate 200,000 km<sup>2</sup> (Cadman and Pain, 1998). The Bowen Basin is economically important,

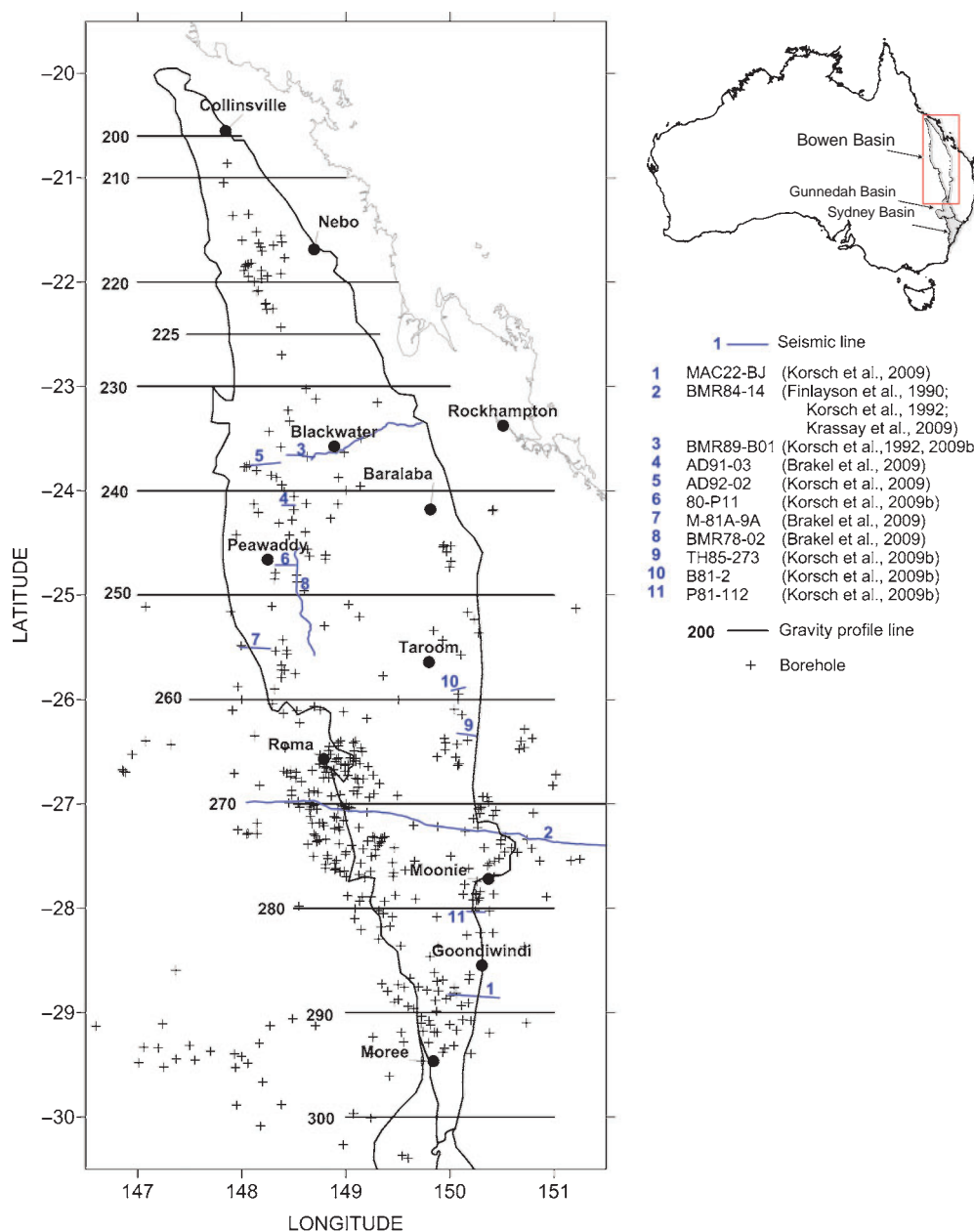


**Fig. 1.** Location of the Bowen Basin, gravity model profiles, boreholes and seismic reflection lines. Seismic reflection line number corresponds to survey line name.

containing vast coal reserves, estimated at more than 30 billion tonnes (DEEDI, 2010) with 57 operating mines (44 open cut and 13 underground) in the 2009–2010 fiscal year (DEEDI, 2011). Sedimentation, estimated at up to 10 km thick (Korsch and Totterdell, 2009), is a repeated sequence of marine and terrestrial deposition resulting in the formation of sandstones, shales, claystones and coal intermingled with extrusive volcanics and the intrusion of plutons. A brief description of the structure, geology and geological history is provided below to present a geological framework from which to interpolate and model the deep 3D structure of Bowen Basin.

The published structural elements and divisions present within the Bowen Basin are shown on Figure 2 based on the works of Cadman and Pain (1998), Brakel et al. (2009), Fielding et al. (2000), Korsch et al. (2009a, b), Krassay et al. (2009) and Waschbusch et al. (2009). The eastern boundary of the basin is marked by a series of north–south orientated Triassic thrust

faults, the Moonie–Goondiwindi and Leichardt–Burunga Faults, extending south of the Auburn Arch. In the north-west, the Comet Ridge separates the major depocentres of the basin, the Taroom Trough and the Denison Trough (Cadman and Pain, 1998). The Hutton–Wallumbilla Fault separates the Comet Ridge from the Roma Shelf and the east dipping Merrivale Fault forms the western limit of the Roma Shelf (Cadman and Pain, 1998). In the central west and south-west, the margins of the Bowen Basin are less defined, with sediments deposited on the St George–Bollon Slope thinning and inter-fingering with sediments of the Galilee Basin on the Nebine Ridge. The Bowen Basin appears continuous with the Gunnedah Basin in the south, however the southern boundary is generally drawn across the basement high near Moree (Tadroz, 1993). Interpretations of the deep seismic reflection surveys (Figure 1) across the Bowen Basin (Finlayson et al., 1990; Korsch et al., 1992) provide information on the geometry of

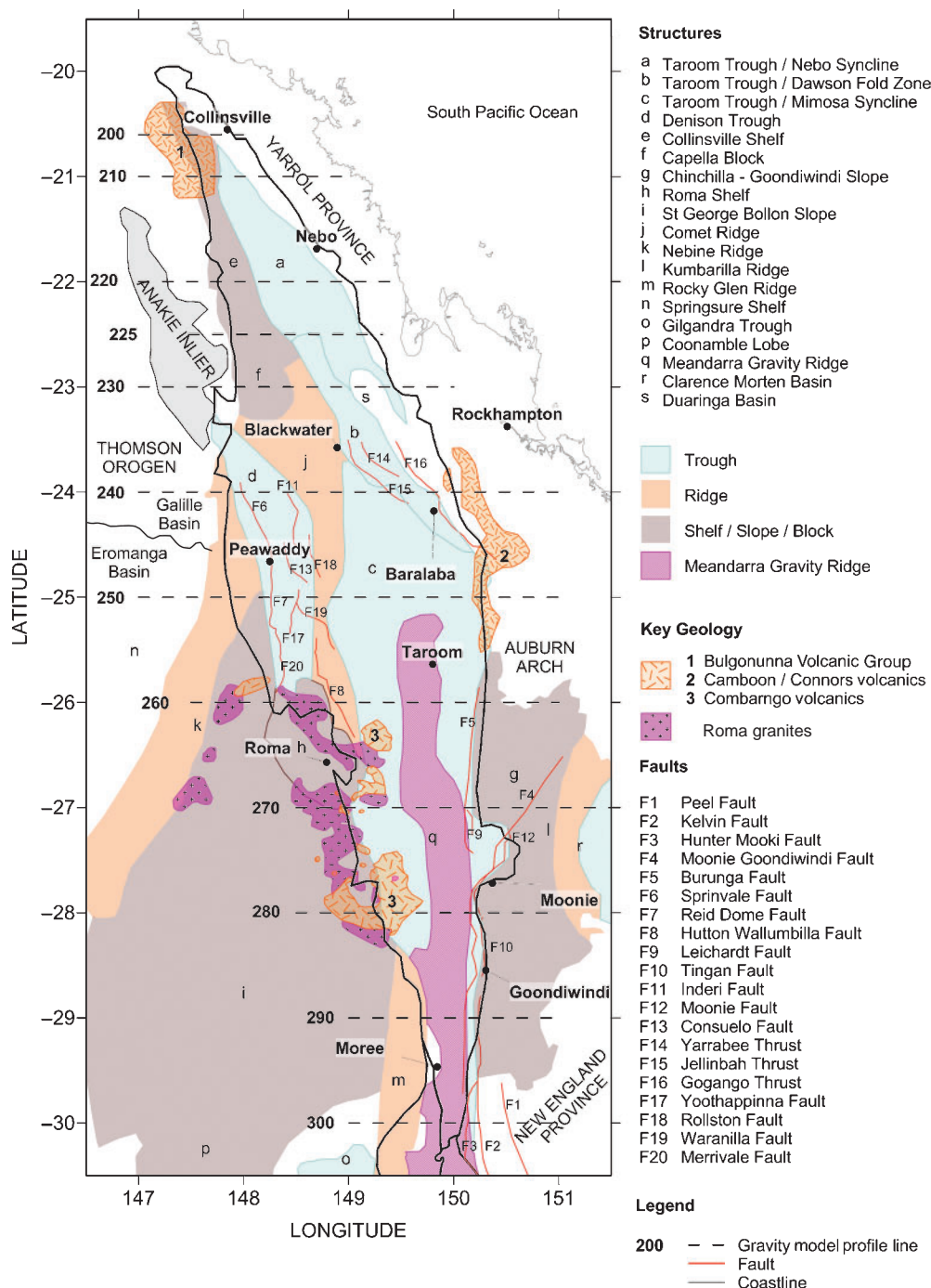


Fig. 2. Structural and tectonic map of the Bowen Basin. Compiled and modified from Cadman and Pain (1998), Brakel et al. (2009), Fielding et al. (2000), Korsch et al. (2009a, b), Krassay et al. (2009) and Waschbusch et al. (2009).

the basin, showing its asymmetrical nature, the orientation of major fault and thrust zones and areas of major sediment deposition.

A collative stratigraphy is presented in Table 1 for the Bowen Basin. A simplified stratigraphy is used for the geological model, with Permian to Cretaceous sediments grouped as a single sedimentary package, and distinction only of the major coal bearing sediment packages in the Jurassic and Permian, which are important for thermal modelling.

In the northern part of the basin, around the Collinsville Shelf and Nebo Syncline, the lower Lizzie Creek, Bulgonunna and Connors volcanics have been noted as the first period of extensional activity in the latest Carboniferous to earliest

Permian by Fielding et al. (1995, 2000) and were deposited before the formation of the Denison Trough. In the Early Permian, a series of extensional basins formed with a series of grabens and half grabens, as a result of crustal extension (Korsch et al., 1993, 2009a, b; Cadman and Pain, 1998), producing the first parts of the Bowen Basin, the Denison and Taroom Troughs. In the Denison Trough, the coal bearing sediment sequences, interbedded with a bimodal suite of basaltic and felsic rocks of the Reid Dome beds (Fielding et al., 1995, 2000), are the earliest deposits, coeval with the thick volcanic piles and volcanoclastic sediments (Korsch and Totterdell, 2009), including the Combarngo volcanics in the west on the flank of the Roma Shelf and

Table 1. Simplified stratigraphy of the Bowen Basin. Modified and compiled from Cadman and Pain (1998), Fielding et al. (2000), Korsch and Totterdell (2009), Mack (1963), Mayers and Lawson (2006) and Simeone and Corbett (2002).

AGE		GROUP	WEST SIDE	Denison Trough	Comet Ridge	Collinsville Shelf	Roma Shelf	Taroom Trough	EAST SIDE											
CRETACEOUS	Early	Rolling Downs Gp	Wallumbilla FM					Wallumbilla FM												
			Bungil FM Mooga SS Orallo FM																	
JURASSIC	Late	Blythesdale Gp	Gubberamunda SST							Westbourn FM Springbok SS Walloon CM Hutton SS Evergreen FM Precipice SS					Gubberamunda SST					
	Middle	Injune Creek Gp / Walloon FM																		Westbourn FM Springbok SS Walloon CM
																				Hutton SS
	Early	Bundamba Gp																		Evergreen FM Precipice SS
TRIASSIC	Late									Moolayember FM Clematis FM					Moolayember FM / Wandoan SS					
	Middle	Mimosa Gp																		Wandoan SS
																				Cahawin FM
PERMIAN	Early	Rewan Gp								Rewan FM						Cahawin FM				
	Late	Black Water Gp	Bandanna FM Black Alley Shale / Winnathoola CM  Peawaddy FM Catherine SS / Ingelara FM	Bandanna CM  Fort Copper CM  Moranbah CM  German Creek FM	Bandanna FM Black Alley Shale / Winnathoola CM Tinowon FM / Wallabella CM	Muggleton FM	Baralaba CM  Gyranda FM  Flat Top FM	Kiangra FM												
									Back Creek Gp	Aldebaran SS Cattle Creek FM Reid Dome beds	Aldebaran SS Collinsville CM Tiverton FM	Blenheim FM Oxtrack FM Buffel FM	Barfield FM	Back Creek FM						
CARBONIFEROUS	Early				Lizzie Creek / Bulgoomuna volcanics	Roma granite Timburly Hills / Kuttung FM	Camboon volcanics	Camboon / Connors volcanics												
																	Kuttung FM			



Camboon volcanics/andesite in the east (Murray, 1994; Cadman and Pain, 1998) of the Taroom Trough.

Rift development in the Denison Trough and volcanism in the Taroom Trough was succeeded by a period of thermal subsidence (Brakel et al., 2009) depositing sediments from marine transgressive-regressive cycles through to the Late Permian. The notable asymmetric basin shape and elongate depocentre (Waschbusch et al., 2009), a feature typical of loaded foreland basins (Busby and Ingersoll, 1995), formed between the early Late Permian and the late Early Triassic in association with the contraction, compression and thrusting events (Fielding et al., 1995).

Towards the end of the Permian, tuffaceous silts and shales were deposited followed by coal sequences. As thrust loading proceeded the basin became overfilled and coal-bearing facies gave way to the terrestrial alluvial strata shortly before the Permian-Triassic boundary (Fielding et al., 1995). At the end of the Permian, granites intruded to the east of the basin and there was movement on the Moonie-Goondiwindi Fault and Leichhardt Fault which continued into the Triassic (Cadman and Pain, 1998). Early in the Middle Triassic the rate of subsidence in the Bowen Basin increased with sediment sourced from areas in the north and east (Day et al., 1983). Extensive erosion occurred in the Middle to Late Triassic (Waschbusch et al., 2009) and movement on the faults on the eastern margin ceased (Cadman and Pain, 1998). Beeston (1986) estimated that during the erosion that followed in the Late Triassic up to 3000 m of strata may have been removed. Closure of the Bowen Basin occurred, followed by the deposition of the unconformably overlying Surat Basin in the Early Jurassic to Early Cretaceous (Waschbusch et al., 2009). A contractional deformational event early in the Late Cretaceous led to limited propagation of thrust faults (Cadman and Pain, 1998) in the central part of the Bowen Basin through to the Surat Basin, which resulted in folding and uplift of Surat sediments over reactivated faults (Korsch and Totterdell, 1996).

### *Basement composition*

The formation of the Bowen Basin occurred over an eroded surface of indurated metasediments of Devonian age bounded to the west by bodies of Late Carboniferous age; granites, schist, gneiss (Cadman and Pain, 1998) and volcanics. Common basement units are the Timbury Hills Formation, Roma granites and Kuttung Formation.

The Timbury Hills Formation has often been indiscriminately applied to a variety of basement rocks in the Roma region, including granite and ignimbritic volcanics, however in general the formation is a collective reference to essentially similar low grade metasedimentary rocks (Murray, 1994). Granitic rocks form a large part of the basement in the Roma Shelf region, collectively referred to as the Roma granites and intrude the Timbury Hills Formation. These granites and the Timbury Hills Formation are nonconformably overlain by the Late Carboniferous Combarngo volcanics, in the Roma Shelf area. The Kuttung Formation, sometimes named as the Cracow Formation, refers to Permo-Carboniferous volcanics and indurated sediments (Cadman and Pain, 1998) and may indiscriminately include the Combarngo volcanics and Camboon volcanics.

The difficulty comes in differentiating between the Late Carboniferous volcanics and volcanics associated with the inception of the Bowen Basin. In the Roma Shelf region the Combarngo volcanics, thought to be related to back arc

extension rifting (Murray, 1990), overlay the basement sediments and Roma granites. On the eastern flank of the Bowen Basin, the exposed volcanic sequence of the Camboon volcanics is assumed to be equivalent to the Combarngo volcanics and presumed by Murray (1990) and Krassay et al. (2009) to extend underneath the Taroom Trough. In most interpretations of the Bowen Basin stratigraphy the early extensional phase has been assumed to be coeval with the volcanic activity associated with the Camboon, Combarngo, Lizzie Creek, Bulgonnuna and Connors volcanics. Work by Fielding et al. (2000) suggests this may not be entirely the case. Along the Connors–Auburn Arch Late Carboniferous to earliest Permian volcanic rocks of broadly extensional affinity are overlain by a mainly sedimentary suite related to later Early Permian extension and no arc-related volcanism can be recognised from the Late Carboniferous or Early Permian (Fielding et al., 2000). Fielding et al. (2000) notes radiometric ages overlap for the seemingly distinctive older predominantly igneous units and younger predominantly sedimentary assemblages. These overlapping ages make a distinction between the basement and rift related volcanics in the Bowen Basin difficult, particularly for the Camboon volcanics. Both Murray (1990) and Fielding et al. (2000) suggest there are two periods of deposition for the Camboon volcanics, which is supported by the radiometric ages. The older Connors, Bulgonnuna, lower Camboon and lower Lizzie Creek volcanics yield ages of 320–300 Ma whilst the igneous rocks from the younger sedimentary suites of the upper Camboon and Lizzie Creek volcanics have ages of 305–280 Ma (Fielding et al., 2000).

For the purpose of this gravity modelling the Camboon, Lizzie Creek, Bulgonnuna and Connors volcanics, Timbury Hills Formation, Kuttung Formation and Roma granites are defined as part of the basement. Where Camboon volcanics outcrop at the surface, they are considered to be lower Camboon and part of the basement and when at depth they are associated with the upper Camboon and part of the extensional rift volcanics. The Combarngo volcanics are also considered associated with extensional rifting.

## **Methodology**

### *Gravity data*

The gravity data used for this work is the National Gravity Database AAGD07, available from Geoscience Australia (GA) from which the continental Australian Onshore/Offshore 2008 Gravity Anomaly Grid of the Australian Region is derived. As vector data, it provides the actual measured gravity values not a gridded interpolation. Vector data is not currently available for the 2009 Gravity Anomaly Grid of the Australian Region, however survey coverage between the 2008 and 2009 data over the Bowen Basin appears unchanged. Previous gravity modelling of the Gunnedah Basin (Danis et al., 2010) and Sydney Basin (Danis et al., 2011) uses this same dataset. The gravity units are in micrometres per second squared ( $\mu\text{ms}^{-2}$ ) and converted to milligals (mGal), with  $1\mu\text{ms}^{-2}$  equivalent to 0.1 mGal, to be consistent with the modelled gravity profiles. In this work no additional corrections have been applied to the gravity data. The spherical Bouguer gravity values were extracted from the database, for the Bowen Basin area, and gridded in Surfer v9 supplied by Golden Software using Kriging at a  $0.01^\circ$  cell spacing, which is  $\sim 100$  m, in the Geodetic datum GDA94 (Figure 3).



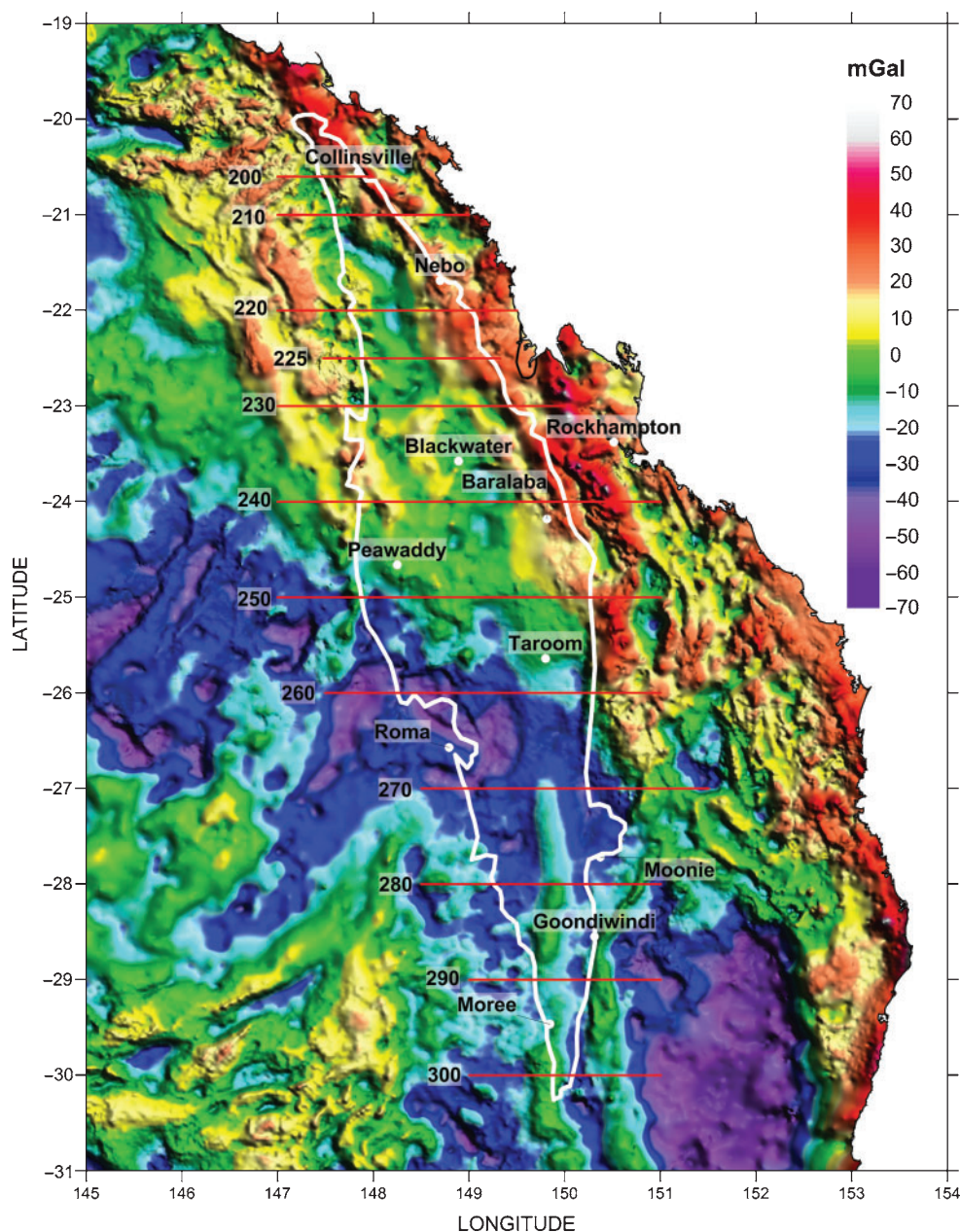


**Fig. 3.** Spherical Bouguer Gravity Anomaly map of the Bowen Basin (white outline in the online version), overlain with gravity model profile locations (red line and black numbers in the online version), and place locations. Gravity units in mGal.

#### *Regional scale 2.5D gravity profiles*

Twelve east–west gravity profiles were extracted from the gridded AAGD07 database using Surfer. Each model profile has an average station spacing of ~1600 m. Profiles were taken east–west along the latitudes of –20.6, –21, –22, –22.5, –23, –24, –25, –26, –27, –28, –29 and –30, as shown in Figure 3. Modelling of the gravity data was performed with the interactive potential field modelling package ModelVision Pro v10.0 supplied by Pitney Bowes Business Insight. ModelVision requires gravity profiles in mGals and a metre coordinate system therefore all profiles were converted from latitude/longitude GDA94 to easting/northing Map Grid of Australia (MGA) coordinate zone 55. The regional gravity correction, which is computed by ModelVision from the gravity data, is a second order polynomial fit.

Models were constructed from an assembly of polygonal bodies, from which the strike length is limited to their approximate geological extent, forming a 2.5D model. These represent the basin sedimentary package, the basal volcanics, the basement, known granites, near surface geology (i.e. Tertiary volcanics) and formations outside of the basin (i.e. Tamworth Belt). As the Bowen Basin models are an extension of previous modelling work in the Gunnedah and Sydney Basins (Danis et al., 2010, 2011) the density values, based on published material averages or measured values (Table 2), have remained constant (Table 3). This ensures the models are consistent with the previous work and suitable for integration with the 3D geological model and subsequent thermal model. These density values may not reflect the true density of every body being modelled but are considered acceptable for a

**Table 2. Summary of density data for the rock samples representative of the Gunnedah and Sydney Basin. Modified from Guo et al. (2007) and Danis et al. (2011).**

Lithology	Density ( $\text{t/m}^3$ )			
	Range	Mean	s.d.	<i>n</i>
Tertiary basalt	2.84–2.98	2.88	0.03	33
Jurassic sandstone	2.12–2.68	2.31	0.14	24
Triassic sandstone	2.32–2.44	2.38	0.03	21
Permian sediments without coal	2.12–2.73	2.37	0.14	53
Permian sediments with coal	1.40–2.73	2.18	0.36	63
All sediments without coal	2.12–2.73	2.36	0.13	116
Coal	1.40–1.50	1.43	0.04	10
Gulgong granite	2.51–2.62	2.59	0.03	13
Weathered basal volcanics <2500 m	2.44–2.89	2.66	0.14	54
<i>Core samples only</i>				
Permian sediments 1200–2400 m	2.53–2.73	2.62	0.07	6
Less weathered basal volcanics 2500–3000 m	2.82–2.97	2.88	0.06	9
Least weathered basal volcanics >3000 m	2.87–2.97	2.92	0.04	5

**Table 3. Summary of density values used for lithologies in the gravity modelling of the Bowen Basin.**

Lithology	Density ( $\text{t/m}^3$ )
Tertiary/exposed Carboniferous volcanics	2.88
Mesozoic to Quaternary sediments	2.31
Surat Basin sediments (<300 m)	2.35
Upper sediments (<300 m)	2.38
Lower sediments (>300 m)	2.54
Basal volcanics	2.95
Granite	2.59
Basement	2.60 or 2.70

regional scale in the absence of available published density values for all bodies.

Table 2 outlines the measured density values of representative lithologies of the Sydney Basin from Danis et al. (2011). The geology of the Bowen Basin consists of Permian to Jurassic sediments, with coal bearing layers, which overly the basal volcanics and basement. In Table 3 the representative lithologies of the Bowen Basin have been assigned the corresponding density values. In addition shallow surface features, i.e. thick alluvial deposits and large river systems, use the average density of  $2.00 \text{ t/m}^3$  (Reynolds, 2003) for sand. For bodies modelled on the edge of the Bowen Basin profiles, such as from the New England Fold Belt, i.e. Tamworth Belt, Texas beds, Whitlow Formation, Bundara Suite and Anakie metamorphics, densities based on Guo et al. (2007) are applied. Where there is significant overlay of sediments from the Surat Basin a density of  $2.35 \text{ t/m}^3$  is used, which is an average density of the Jurassic and Triassic sandstone (Table 2), for the upper 300 m. Where mapped surface geology shows extensive late Mesozoic to Cainozoic sediments a density of  $2.31 \text{ t/m}^3$  for the Jurassic sandstone (Table 2) is applied rather than the density of alluvial sediments.

Gravity model profiles are modelled to 15 km depth and are extended outside the structural outline of the Bowen Basin to ensure minimal edge effects. The removal of a regional gravity field is assumed to eliminate the effects of deeper density variations. The upper 8 km of the models presented in Figure 4 are shown to scale, with vertical exaggeration, to emphasise the delineation of the top of basement and the basin geometry/structure. Models are constrained from stratigraphic depths of boreholes along the profile line, or estimated from boreholes near the profile line which are projected or interpreted. Seismic reflection profiles provide structural information for model

geometry, especially across major faults, and estimates of depth where borehole information is limited. Over 460 borehole logs provide information across the Bowen Basin, for depth of sediment cover, top of basal volcanics, depth to basement and basement composition, 46 of these are used to constrain the gravity models (see Figure 4 for location and Figure 5 for stratigraphic details).

Four additional north–south orientated profiles were modelled through the structures of the Taroom Trough, Comet Ridge and Collinsville Shelf to provide interpolation points between the east–west model lines for the 3D surface interpolation but are not shown in this paper. They are consistent with the east–west profiles and calibrated by boreholes.

### 3D basement structure and lithologic layers

For each gravity profile the depth and location of each model body which defined the basement and basal volcanics was used with the stratigraphic data of 468 boreholes to create 3D surfaces. Depth information from the gravity models and borehole records is converted to metres relative to the Australian Height Datum (mAHD) using the 90 m elevation contour data available from the Shuttle Radar Topography Mission (SRTM) at the United States Geological Survey website ([http://dds.cr.usgs.gov/srtm/version2\\_1/SRTM3/Australia/](http://dds.cr.usgs.gov/srtm/version2_1/SRTM3/Australia/), accessed August 2011).

Using the visualisation, contouring and surface modelling package of Surfer interpolated surfaces are created for the top of basement, the top of basal volcanics, the top and base of Reid Dome beds, the top and base of the Permian coal interval (which is where Permian coal first appears and when it disappears from the stratigraphy) and the top and base of Jurassic coal interval (predominantly the Walloon coal measures) as 0.05 degree grids using Kriging. SRTM data provides the surface topography. Minor editing of the interpolated layers, excluding the surface topography, was undertaken to remove spurious points resulting from over and under interpolation during the gridding process. Figure 6 presents the contoured surfaces in mAHD which, exported as XYZ format, can then be imported into numerous visualisation, animation, geographical information system (GIS), geophysical and thermal modelling programs.

## Results and interpretation

### Gravity modelling

The modelled outcomes for the Bowen Basin (Figure 4) fit well with the observed gravity and the geometry of the models is considered consistent with the structures observed in Figure 2,

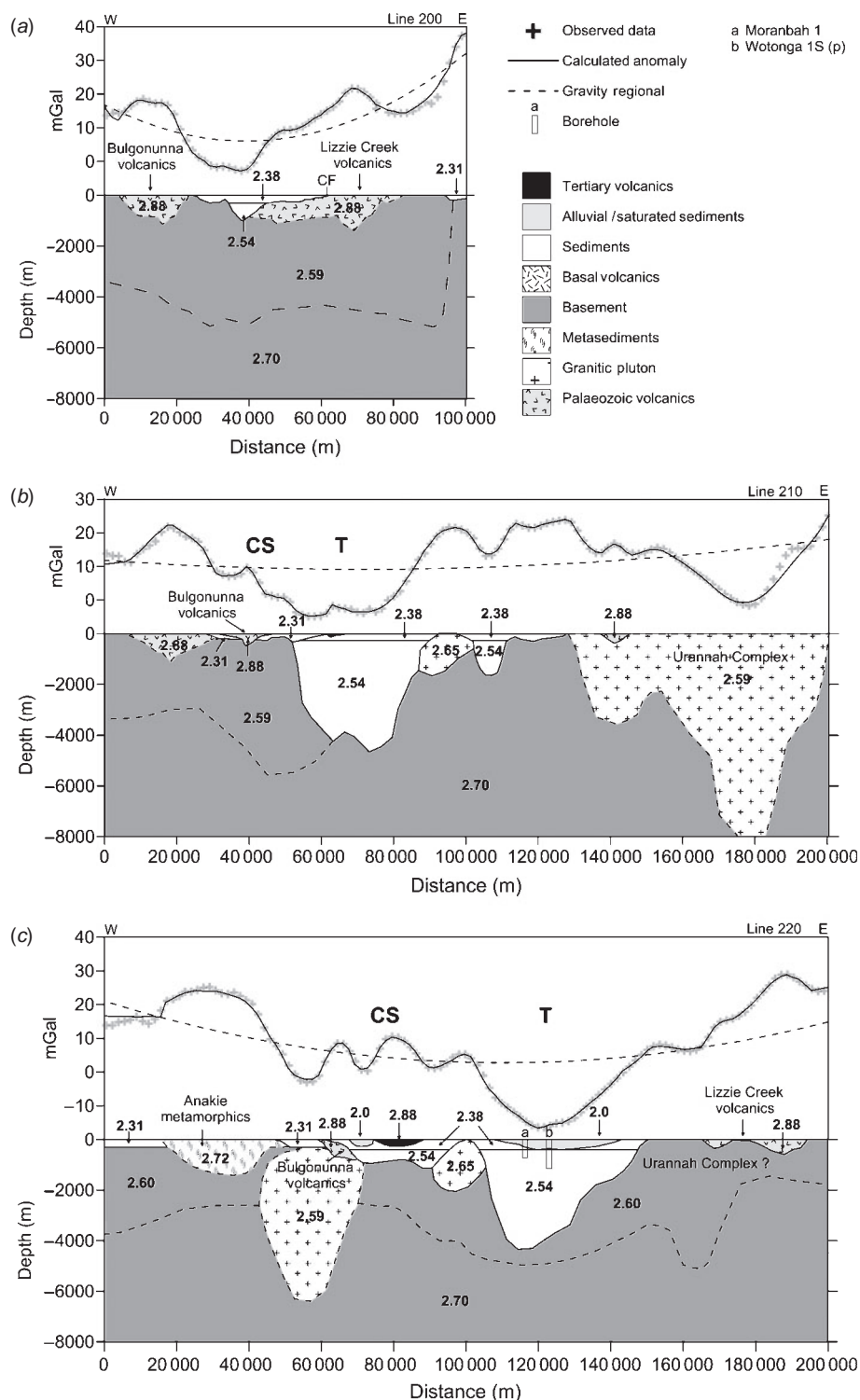


**Fig. 4.** Gravity model profiles with observed gravity points (crosses), regional correction (dashed line), modelled response (solid line) and key structural features. Density of units in  $\text{t/m}^3$ . Calibration boreholes shown as rectangles (see Figure 5 for details). (a) Line 200. (b) Line 210. (c) Line 220. (d) Line 225. (e) Line 230. (f) Line 240. (g) Line 250. (h) Line 260. (i) Line 270. (j) Line 280. (k) Line 290. (l) Line 300. Note vertical exaggeration as indicated by the depth and distance scales. Less constrained model body boundaries shown as dashed lines. i = interpreted borehole location, P = projected borehole location, CF = Collinsville Fault, CS = Collinsville Shelf, T = Taroom Trough, CB = Capella Block, CR = Comet Ridge, DB = Daringa Basin, DT = Denison Trough, SF = Springvale Fault, IF = Inderie Fault, JT = Jellinbah Thrust, GT = Gogango Thrust, NR = Nebine Ridge, CG = Camarvon Gorge, RF = Reid Dome Fault, YF = Yoothappina Fault, LN = Lake Nuga Nuga, MGR = Meandarra Gravity Ridge, RS = Roma Shelf, HWF = Hutton-Wallumbilla Fault, BF = Burunga Fault, LF = Leichardt Fault, MF = Moonie Fault, MGF = Moonie-Goondiwindi Fault, KF = Kelvin Fault, PF = Peel Fault.



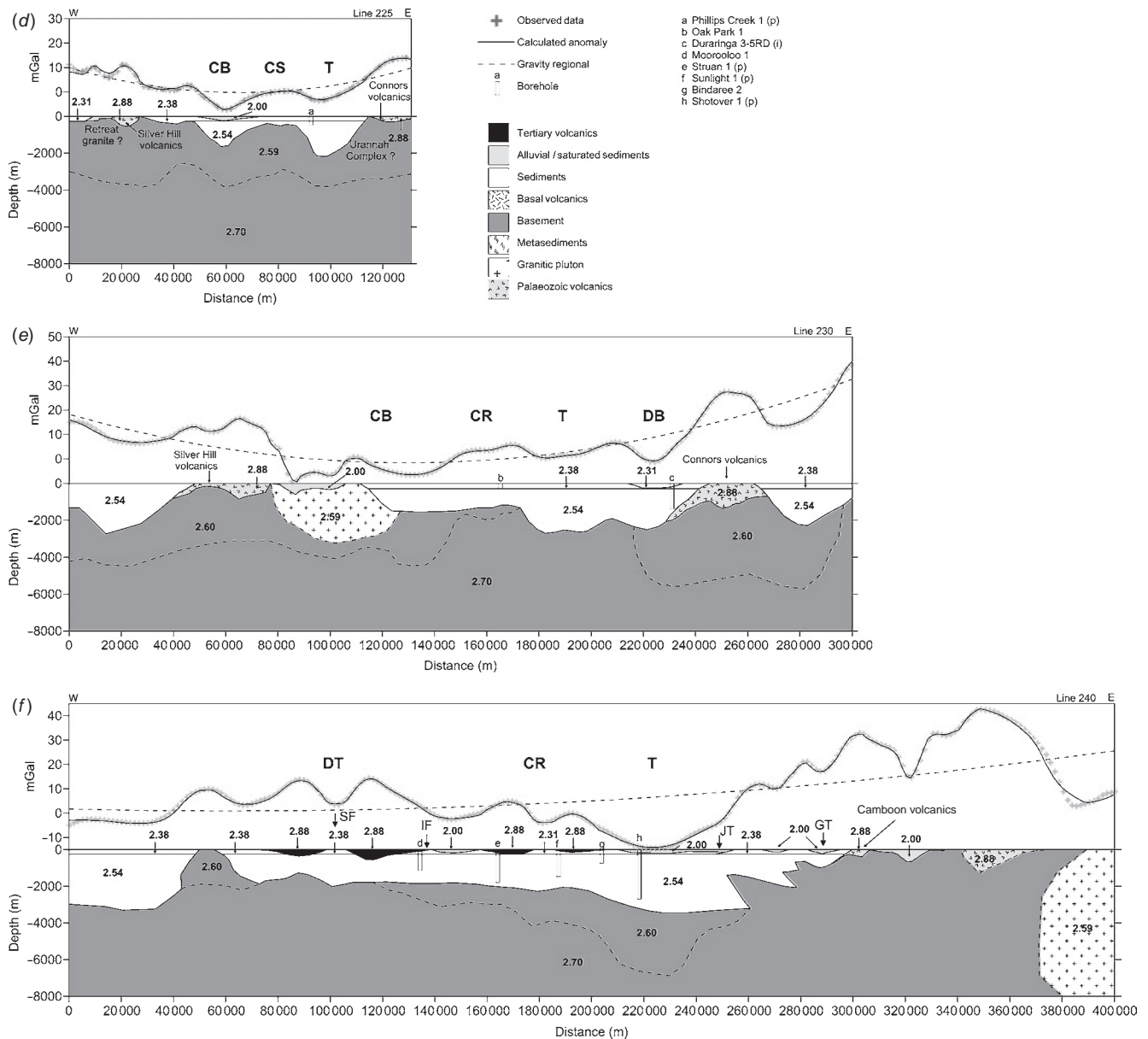


Fig. 4. (continued)

the asymmetrical geometry associated with extensional rift basin formation and the geometry observed from previous work in the Gunnedah Basin (Danis et al., 2010).

In any geophysical modelling the resulting models are always dependent on the input assumptions. Borehole information, seismic reflection data, measured density values and mapped geology are combined with our models of the gravity data to constrain our best estimates of geological reality. Borehole data represents ‘hard’ data, from the direct sampling of the subsurface, and is considered reliable on the metre scale whilst gravity modelling, which is subjective and controlled by density contrasts and imposed constraints, could be considered reliable on the hundreds of metres scale. From previous work in the Gunnedah and Sydney Basins, Danis et al. (2010, 2011) found the variation in depth to basement was generally less than 700 m for gravity models with multiple borehole constraints. Leaman (1990) undertook regional gravity model profiles in the Sydney Basin, using similar density values, and found a difference of around 500 m between his modelled depths and those of nearby boreholes, which were not

used as constraints. With the gravity models of the Bowen Basin using the same density parameters as the Gunnedah and Sydney and Basins, the uncertainty of depth to basement is likely to be similar, where constraints (i.e. boreholes or mapped geology) are used.

The close fit to the observed gravity data in ModelVision is achieved by adjusting the geometries of the bodies to be consistent with constraints or geological reality. Given the geological history of the Bowen Basin, its initial deposition over an eroded surface of indurated metasediments, granites and volcanics, and the formation of half-grabens during rifting it is expected that the geometry of the basement would not be a completely flat surface. The sediments, volcanics and near surface features are always adjusted first to fit the gravity data and constraints before the deeper boundaries between features like the low density basement and basement or granites are adjusted. The boundaries between the low density basement, basement and granites are difficult to define and are modelled, where possible, as smooth surfaces and shown as dashed lines in Figure 4. The overall shape of low density basement bodies

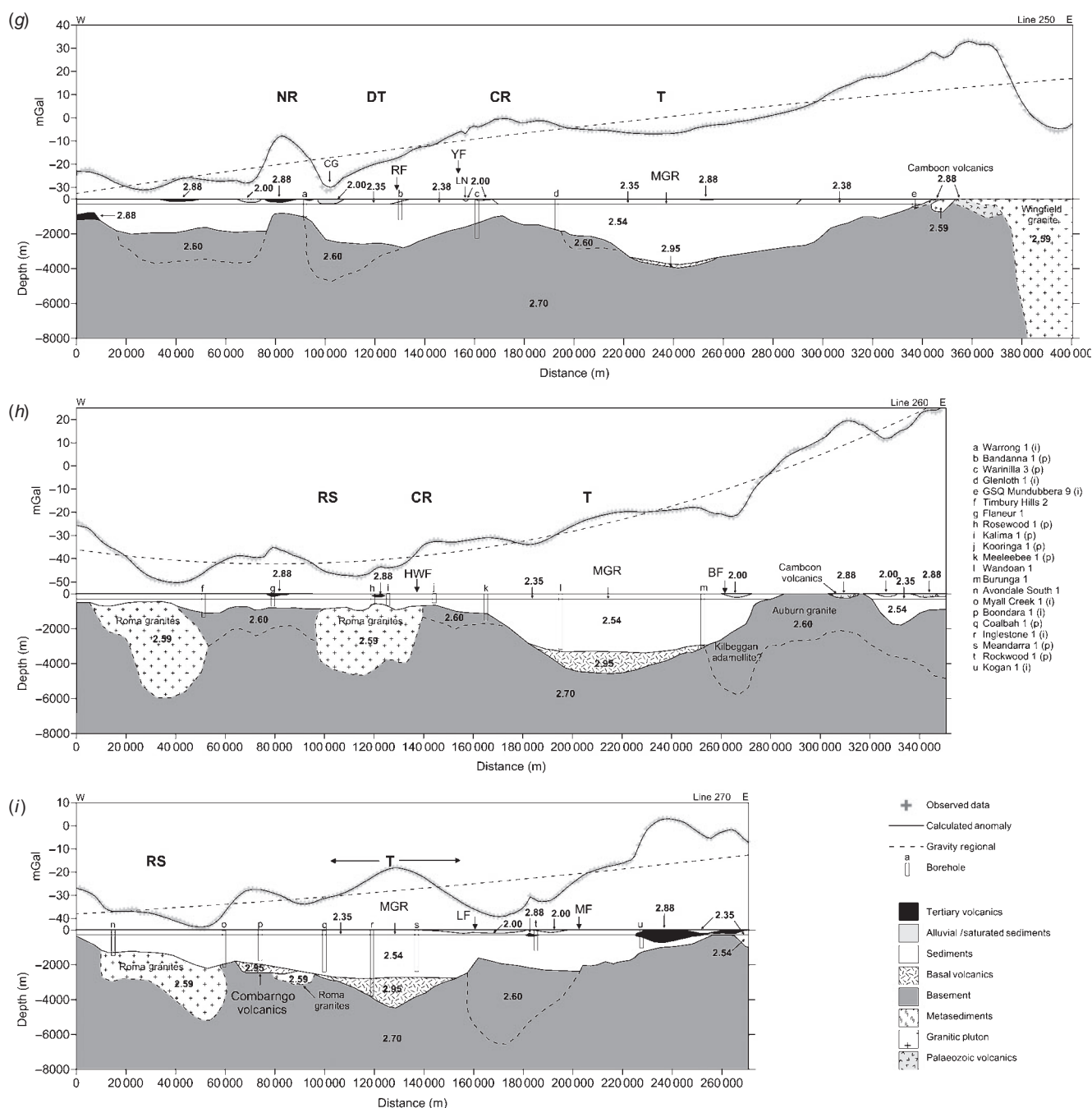


Fig. 4. (continued)

and the granitic intrusions, particularly on the edges of the Bowen Basin, is not considered important as they are all still part of the basement for the 3D geological model and will have limited bearing on subsequent thermal models.

Some near surface features, e.g. Tertiary basalts, alluvial plains and rivers, and some topographic effects, e.g. canyons/gorges, caused difficulties when modelling the profiles and resulted in poor fit of some high frequency anomalies. Some topographic effects were possibly under-corrected in the gravity processing by GA and in this work no additional corrections were done. High frequency anomalies were not removed from the gravity data as most could be replicated using the mapped geological features.

Another possible way to achieve a close fit of the observed gravity data would be to change the assigned density values or increase the thickness of sediment. This often resulted in

modelled responses which did not completely satisfy the constraints (i.e. from boreholes or mapped geology). Outside of the Bowen Basin, changes to the density or thickness of bodies are made to ensure the modelled response is a good fit with the data whilst still being representative of the geology and geometry of the area. Depending on the degree of change, the overall interpretation of the structure of the Bowen Basin may not be significantly altered.

As per our previous modelling in the Gunedah Basin (Danis et al., 2010) and Sydney Basin (Danis et al., 2011) a low density portion ( $2.60 \text{ t/m}^3$ ) of the basement is required to fit several observed long-wavelength gravity lows in the models. The alternative, to increase the sediment thickness, produced models that did not match with the borehole constraints or the mapped geology. This low density portion of the basement may be related to, but not limited



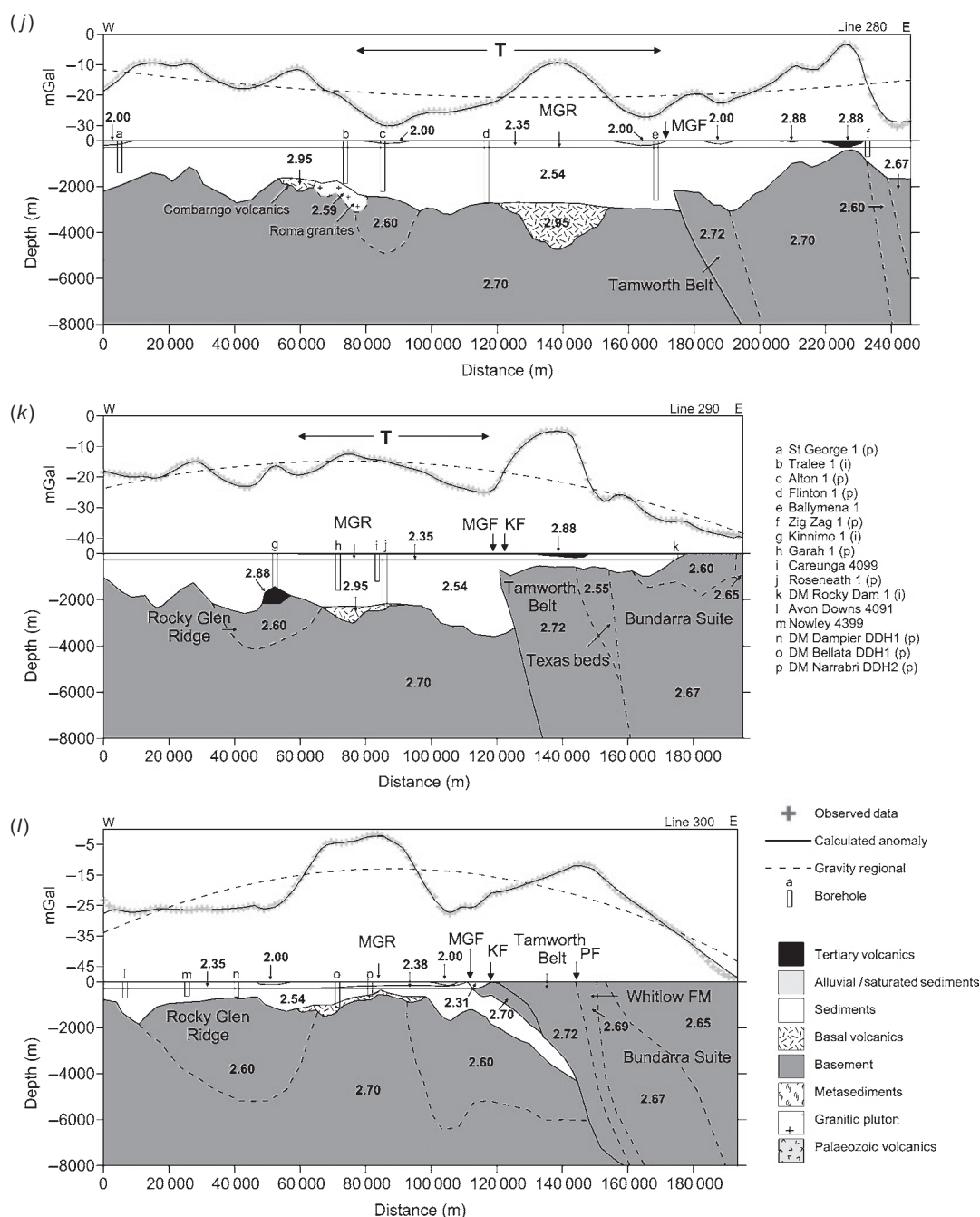


Fig. 4. (continued)

to, granite-rich areas. Therefore where a granite body was identified, from mapped geology or borehole information, near a long-wavelength low our average granite density of  $2.59 \text{ t/m}^3$  (Table 3) was used. However where a granite body was identified, but a gravity low was not apparent, a density of  $2.65 \text{ t/m}^3$  (based on Guo et al., 2007) was used. These are representative density values, to ensure consistent modelling techniques between basins, and may not reflect the true density of every body being modelled.

Across several of the 2.5D profiles there does appear to be some consistency between profiles for low density bodies like the Urannah Complex (Line 210 to Line 230), Bundarra Suite (Line 280 to Line 300) and Roma granites (Line 260 to Line 280), suggesting they may be part of larger scale intrusive complexes. The modelled basement topology generally reflects the structural elements shown in Figure 2, though the extent and location may

vary slightly. The western boundary of the Rocky Glen Ridge, in the Gunnedah Basin, continues north into the Bowen along the St George Bollon Slope, Nebine Ridge, Capella Block and Collinsville Shelf forming, at times, a distinctive structural high. To the east the Yarrol Province, Auburn Arch and Kumbarrilla Ridge form the structural basement high, aided by the Jellinah and Gogango thrusts and Leichardt-Burunga and Moonie-Goonidwindi Faults. Two hundred and seventy-nine boreholes reached basement providing good control on the depth to basement in both the gravity modelling and surface interpolation.

The Taroom Trough is a gravity low observable in profile Lines 200 to Line 250 (Figure 3) before switching to a gravity high for Lines 260 to Line 300 in response to the appearance of the Meandarra Gravity Ridge. In the north of the basin, less than 1 km of sediment is modelled in the trough (Line 200) and in the

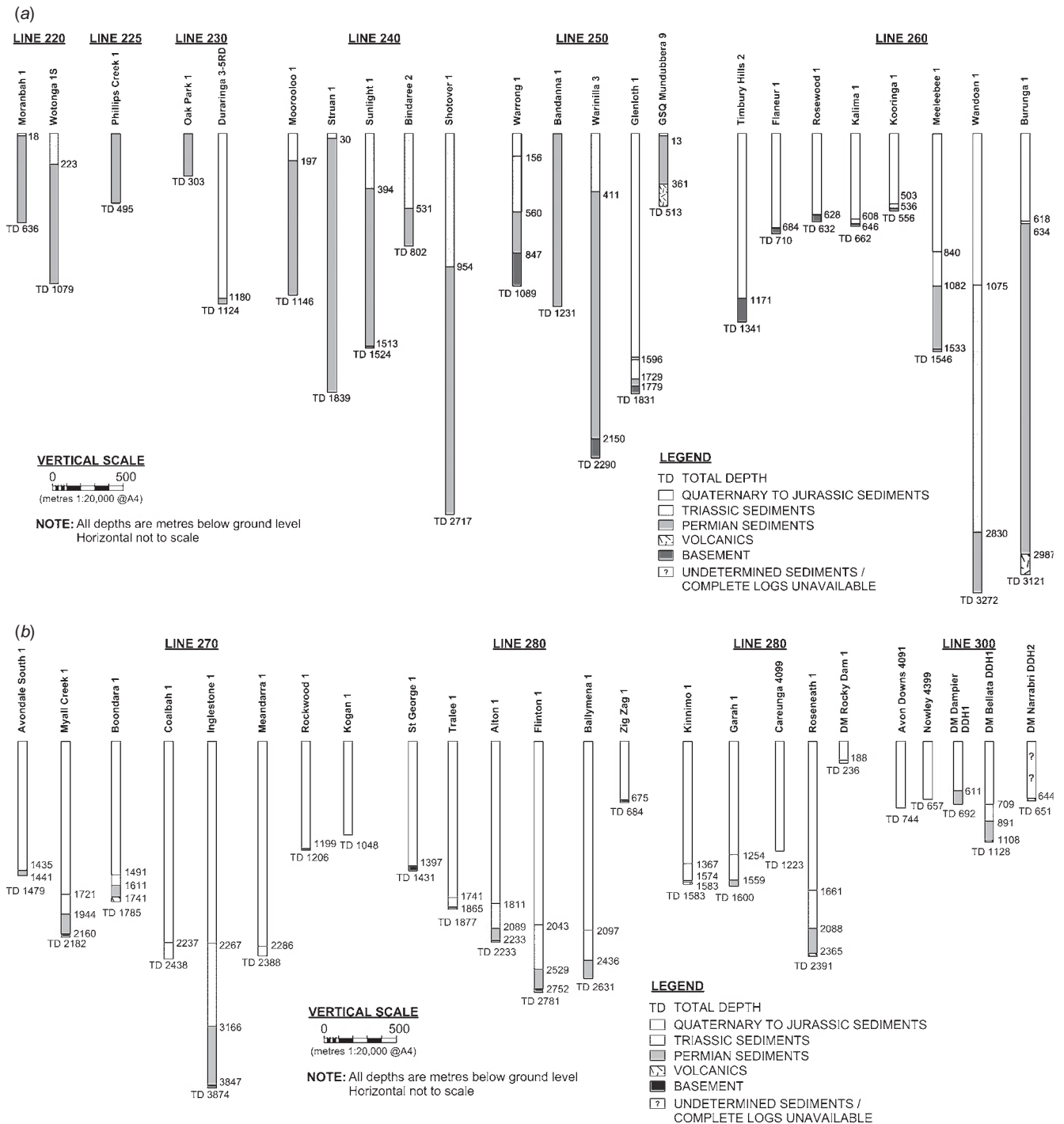


Fig. 5. Stratigraphic sections of boreholes in gravity model profile Lines 220 to 300.

south near the boundary with the Gunnedah Basin (Line 300) around 1 km of sediment is modelled. The Taroom Trough is modelled on average with around 3 km to 4 km of sediment and reaches almost 5 km in the deepest parts (Line 210 and Line 220).

Sediment thickness has been estimated at up to 10 km in the deepest parts of the Taroom Trough by Korsch and Totterdell (2009) based on seismic reflection profile BMR 84.14 (Figure 1) and assumes a velocity of 4000 m/s and a two way travel time of 2.5 s (Korsch et al., 1992). Using different velocities for the conversion of two way travel time, and the choice of reflector, will result in different estimations of sediment thickness. For example; if a velocity of 2000 m/s,

as chosen by Blevin et al. (2007), is used then the estimated sediment thickness of the Taroom Trough could be 5 km. Where our gravity models and the nearby seismic reflection profiles are both constrained by boreholes (i.e. Line 260 and B81–2) the estimated sediment depth is comparable. In the Taroom Trough our gravity model (i.e. Line 270) suggests the velocity chosen for BMR84.14 may not be representative for that area.

The Denison Trough is not as clearly defined by gravity lows as the Taroom Trough. Located west of the Taroom Trough, between the latitudes of  $-23.5$  to  $-25.5$ , it is intersected by profile Line 240 and Line 250. Seismic reflection profiles (i.e. AD92–02) show anticline structures

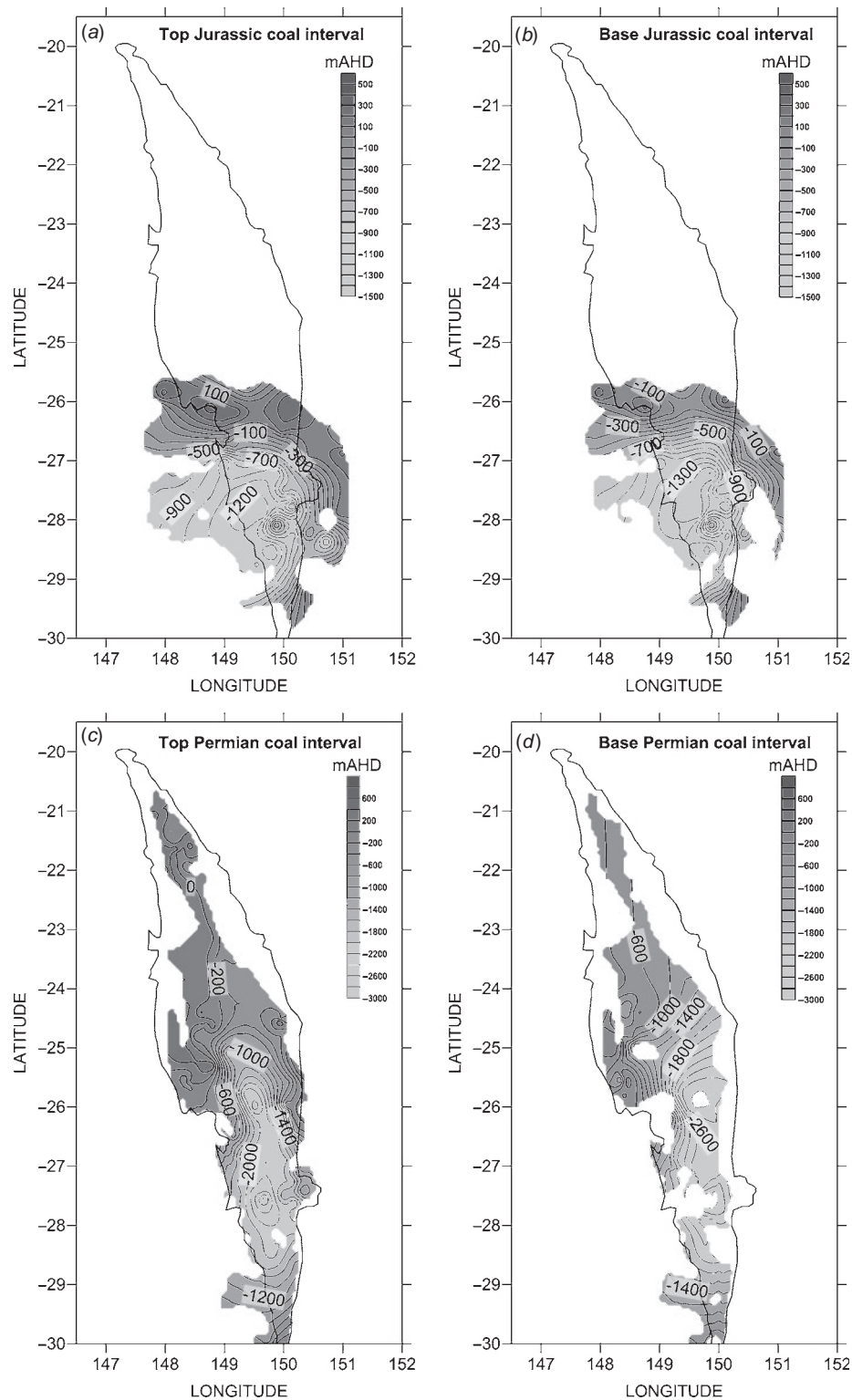


**Fig. 6.** Surface contour maps, in metres Australian Height Datum (mAHD), for the geological layers in the Bowen Basin 3D geological model. The coal interval contains a surface for the top where coal first appears and the base where coal is last seen in the stratigraphy. Surfaces extending outside the limits of the Bowen Basin outline should be considered interpretive only as borehole and modelling information in places is limited. (a) Top of Jurassic coal interval. (b) Base of Jurassic coal interval. (c) Top Permian coal interval. (d) Base Permian coal interval. (e) Top of Reid Dome beds coal interval. (f) Base of Reid Dome beds coal interval. (g) Top of basal volcanics. (h) Top of basement with tectonic subdivisions as per Figure 2.

which developed (Korsch et al., 1992) over half-grabens and Korsch et al. (2009a) estimates up to 4 km of sedimentary fill (assuming a velocity of 4000 m/s). The gravity model profiles indicate almost 3 km of sediments.

The Late Carboniferous volcanics of the Bulgonunna, Lizzie Creek, Connors and lower Camboon appear continuous on the eastern and western boundaries of profile Line 200 through to Line 260. The Meandarra

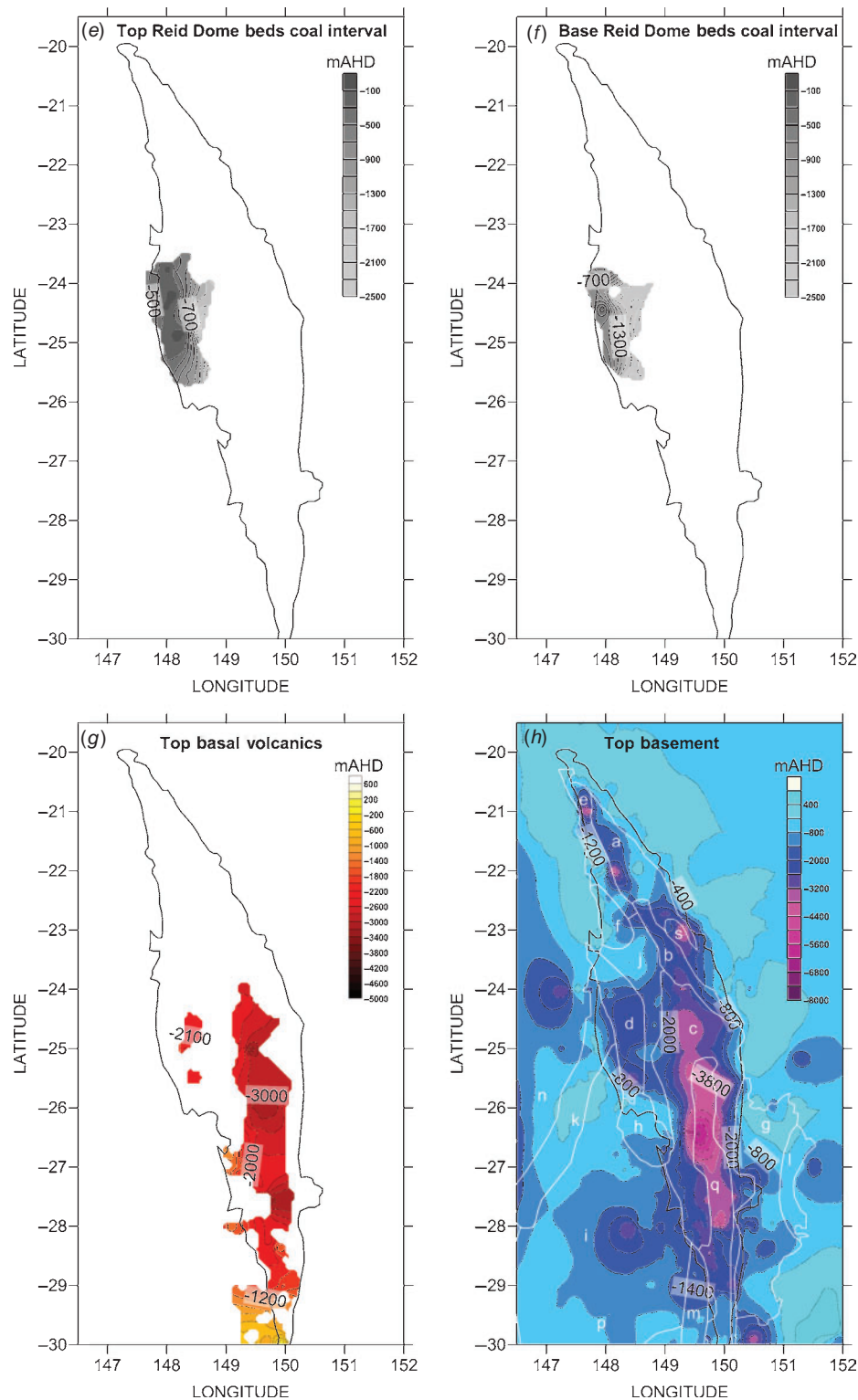


Fig. 6. (continued)

Gravity Ridge, associated with basal rift volcanics (Krassay et al., 2009, Danis et al., 2011) extends north from the Gunnedah Basin to approximately latitude  $-25$ , generally along a gravity high, and gravity modelling suggests basal volcanics do not extend past this point. Fifteen boreholes reached basal volcanics of the Camboon or Combarngo volcanics. Basal rift volcanics are modelled in Line 250 to Line 300 in the Taroom Trough. In the Denison Trough, two boreholes intersect basal volcanics but generally

the interbedded sediments, coal and volcanoclastic sediments of the Reid Dome beds are recorded. The gravity response for profile Line 240 and Line 250 does not suggest basal volcanics are present, especially not a large volume, nor offer a distinctive difference between the signal of the Tertiary volcanics and a signal from deeper volcanics. The 3D interpolated surfaces for the top of the basal volcanics in the Denison Trough is based solely on drill-hole data and constrained by the basement topology.



### Gravity profiles

In the northern most part of the Bowen Basin borehole information is extremely limited, with no boreholes reaching the basement for Line 200 to Line 240. The 1 : 250,000 geological maps which cover the extent of the Bowen Basin are used to constrain surface geology and interpolate for near surface geology. Geological cross-sections, where they pass near the gravity profiles, provide an estimation of subsurface geometry and geology.

In profile Line 200 (Figure 4a) the nearby geological cross-section interpretation (Malone and Pain, 1971) suggests sediments, less than 500 m thick, overlying a basement comprised of Lizzie Creek/Bulgonunna volcanics and adamellite. Gravity modelling suggests that the sediments must be thicker, around 900 m, in order to model the observed gravity low and only the adamellite is continuous under the basin. It is possible to model a very thin layer of Lizzie Creek volcanics extending part way under the basin sediments, but requires a thicker sediment package, a larger adamellite body or a combination of the two.

Model profile Line 210 (Figure 4b) displays the more typical rift basin geometry. In the west the basement high of the Collinsville Shelf is modelled with Bulgonunna volcanics and a granodiorite outcropping on the surface. Sediments in the Taroom Trough, estimated at up to 5 km deep in the geological cross-section of Malone and Pain (1971), were modelled close to this depth at 4.6 km. As per Line 200 the geological cross-section of Malone and Pain (1971) suggests Lizzie Creek volcanics underneath the basin sediments. However, the distinctive gravity low suggests that this is unlikely. At 100 km along the model profile a portion of the lower Cretaceous Gotthardt granodiorite outcrops and is modelled with a density  $2.65 \text{ t/m}^3$  similar to the Bundara Suite (Table 2). The Urannah Complex forms the eastern boundary of the Taroom Trough and Bowen Basin.

The model geometry of Line 220 (Figure 4c) is similar to Line 210, with Bulgonunna and Lizzie Creek volcanics cropping out on the surface on the western and eastern basin margins. The low density basement on the eastern end of the profile is a probable continuation of the graniferous Urannah Complex, and the  $2.65 \text{ t/m}^3$  body is likely the continuation of the Gotthardt granodiorite modelled in Line 210. A Newcrest mining report (No 24084) interprets a buried granite at 50 km along the model profile, which is used to model the long wavelength gravity low between 40 km and 80 km along the profile. An outcrop of the Anakie metamorphic inlier, between 20 km and 40 km along the profile, is modelled with a density of  $2.72 \text{ t/m}^3$ , based on Guo et al. (2007). Underneath the metamorphics, low density basement is modelled. Sediment thickness in the Taroom Trough is modelled at 4.3 km deep. The two boreholes constraining this line do not reach the basement but indicate at least 1 km of sediment is present.

Line 225 (Figure 4d) was modelled to improve the geological information between Line 220 and Line 230 over the transition between the Collinsville Shelf and the Capella Block. It shows a probable continuation of the Urannah Complex in the east and the Retreat granite, which crops out at the start of the profile, may be a continuation of the buried granite suggested in Line 220. The outcrop of Silver Hill volcanics are of Devonian–Carboniferous age. Borehole Phillips Creek 1 indicates at least 500 m of sediment in the Taroom Trough, with the model suggesting up to 2 km of sediment.

In model profile Line 230 (Figure 4e) the structures of the Capella Block, Comet Ridge and Taroom Trough can be observed. The basement high, represented by the Silver Hill

volcanics at 50 km along the profile, and the exposed granite body, mark the western basin boundary and Capella Block. The Comet Ridge represents a reasonably flat modelled basement structure, with ~2 km of sediment before deepening into the Taroom Trough. Sediment in the Taroom Trough is modelled up to 2.7 km deep. Borehole Duaringa 3–5RD, part of the Duaringa Basin, is on the eastern edge of the Taroom Trough and shows at least 1.2 km of sediments, modelling suggest up to 2.5 km of sediment at this point. A geological cross-section by Malone et al. (1971), north of the profile, shows Connors volcanics intruded by granites from the Urannah Complex, therefore for the eastern end of Line 230 low density basement is modelled between 220 km to 290 km along the profile. The  $2.54 \text{ t/m}^3$  sediment body west of the Silver Hill volcanics is presumed associated with the Anakie metamorphic inlier.

The modelled structure of profile Line 240 (Figure 4f) correlates well with the structures observed in seismic lines AD91–03 and AD92–02 for the Denison Trough and BMR89. B01 for the Taroom Trough. The structure of the Jellinbah and Gogango Thrusts in the Dawson Fold Zone are comparable between the seismic reflection profile and the gravity model. Numerous faults are observed between 60 km and 200 km, especially in the Denison Trough, on the structural map (Figure 2), and seismic reflection profiles AD91–03 and AD92–02, generally show a similar stepped basement structure to the model. High frequency anomalies along the profile are best modelled to match surface deposits of Tertiary basalts and quaternary material. Borehole Sunlight 1 is projected onto this line from the south and reached Kuttung Formation at 1.5 km, basement is modelled slightly deeper on the profile. All other boreholes did not reach basement but indicate sediment thickness is at least 1.1 km at Moorooloo 1 in the Denison Trough, 1.5 km to 1.8 km on the Comet Ridge and 2.7 km at Shotover 1 in the Taroom Trough.

Line 250 (Figure 4g) models the distinctive features of the basement structural highs of the Nebine and Comet Ridge and lows of the Denison and Taroom Troughs. Boreholes Warinilla 3 and Glenloth 1 record Timbury Hills Formation basement at 2.1 km and 1.7 km deep respectively on the Comet Ridge. Either side of the Nebine Ridge, a distinctive gravity high, are gravity lows, which have been modelling using low density basement, deep sediments and surface alluvial sediments. In this area the changes in elevation related to the topography of features such as Carnarvon Gorge may be influencing the observed gravity, as no additional topographic corrections have been applied to the data. From borehole Warrong 1 the shallow basement on the Nebine Ridge is confirmed. At ~160 km along the profile a small amount of alluvial sediments is modelled for the localised gravity low of Lake Nuga Nuga. On the eastern boundary, Camboon volcanics crop out on the surface amongst granite bodies and the volcanics are modelled extending underneath the sediments into the Taroom Trough as indicated by borehole GSQ Mundubbera 9. A small amount of basal volcanics are modelled in the base of the Taroom Trough and are presumed to be the start of the Meandarra Gravity Ridge.

Profile Line 260 (Figure 4h) models numerous granite intrusions associated with the Roma granites of the Roma Shelf on the western boundary and the Auburn granite and inferred Kilbeggan adamellite on the eastern boundary. Numerous boreholes on the profile constrain the depth to basement and define basement as either Roma granites or the Timbury Hills Formation. In the Taroom Trough borehole Wandoan 1 indicates at least 3.2 km of sediments and Burunga 1 shows basal Camboon volcanics at 2.9 km.



The modelled structure of profile Line 270 (Figure 4i) is similar to Line 260 with Roma granites on the western boundary and basement shallowing in the east at the Leichardt–Burunga and Moonie–Goondiwindi Faults, reflecting the structures observed in seismic reflection profile BMR84–14. The gravity high at the eastern end of the profile is likely a combination of shallowing basement, thin sediments and the surface Tertiary volcanics observed on geology maps. Borehole Kogan 1 indicates there could be at least 1 km of sediment. Basal volcanics modelled in the Taroom Trough are up to 1.8 km thick and towards the west they are modelled overlying the basement on the Roma Shelf, as indicated by nearby borehole Boondara 1. Boreholes Myall Creek 1 and Avondale South 1 intersect the basement at 2.1 km depth and 1.4 km depth of the Timbury Hills Formation and Roma granites respectively. In borehole Inglestone 1, which is interpreted onto the profile shows basement of Kuttung Formation is logged at 3.8 km depth. Although the borehole does not record basal volcanics it does suggest that the interpreted basement depth for profile Line 270 in this area could be modelled around this depth.

The basal rift volcanics associated with the Meandarra Gravity Ridge become more confined to the basement topology in profile Line's 280 and 290 (Figure 4j, k) as the Taroom Trough begins to shallow at the Bowen Basins southern boundary with the Gunnedah Basin. The modelled structure of both Line 280 and Line 290 is dominated in the east by the Moonie–Goondiwindi Fault uplifting the Tamworth Belt basement and the low density bodies of the Bundara Suite. In Line 280, the Combarngo volcanics are modelled overlying the Roma granites based on boreholes and a continuation of the structure from Line 270. The basement structural high is presumed associated with the northern extension of the Rocky Glen Ridge, observed in Line 290 and Line 300. Borehole Flinton 1 shows on the edge of the Taroom Trough/Meandarra Gravity Ridge that basement is around 2.2 km deep. In profile Line 290 borehole Kinnimo 1 terminated in basalt at 1.5 km, but other nearby deeper boreholes record a Tertiary basalt/dolerite dyke, therefore an intrusion was modelled at 50 km along the profile for the gravity high. The modelled basal rift volcanics are confirmed by borehole Roseneath 1 which encountered basal volcanics at 2.3 km depth. The seismic reflection profiles P81–112 (Line 280) and MAC-22BJ (Line 290), across the Moonie–Goondiwindi Fault, are comparable with the modelled structure.

Profile Line 300 (Figure 4l) shows a modelled structure which is a continued shallowing of the basement and thinning of basal volcanics on the Meandarra Gravity Ridge. The profile is comparable to Line 1 from Danis et al. (2010) which is a NE–SW orientated model profile in the same location. Sediments from the Bowen Basin are modelled to extend down the Moonie–Goondiwindi Fault. Basal rift volcanics are modelled from projected boreholes DM Bellata DDH1 and DM Narrabri DDH2 which intersect basal volcanics at 1.1 km and 650 m respectively.

### 3D surface contouring

Figure 6 shows the contoured surfaces for the top and base of the Jurassic coal interval (Figure 6a, b), the top and base of the Permian coal interval (Figure 6c, d), the top and base of the Reid Dome beds coal interval (Figure 6e, f) the top of basal volcanics (Figure 6g) and the top of the basement (Figure 6h) in mAHD with the Bowen Basin boundary. Editing of spurious points, created by grid over-interpolation, was undertaken on the basement layer.

Areas outside the basin boundary should not be considered reliable as, in the absence of detailed data, interpretive points were added. This ensured the contouring of depths on the edges of the Bowen Basin was consistent with the gravity models and expected geometry. The basement surface is used to control the lateral extent of the basal volcanics and Permian and Reid Dome beds coal intervals. The Jurassic, Permian and Reid Dome beds coal intervals were contoured from borehole data only and are shown to their approximate extent. For each coal interval the depth of the surface is generally shallower near the edge of the Bowen Basin and deeper in the middle, reflecting the architecture of the basin and tectonic history. The coal surfaces are an important part of the geological model as, being thermally insulating, they significantly impact the subsurface thermal field. Figure 6g shows the basal volcanics surface is generally flat with the deepest parts in the centre of the Bowen Basin and the shallowest parts in the south approaching the transition with the Gunnedah Basin.

### Bowen Basin architecture

The geometry of the Bowen Basin shows a predominately N–S orientated channel through the basement, the Taroom Trough, which is deepest between –28 and –24 latitude, and offset to a NW–SE orientated channel between –24 and –20 latitude associated with the Nebo Syncline of the Taroom Trough. The Denison Trough forms a N–S orientated basin between basement structural highs of the Comet Ridge in the east and Nebine Ridge in the west.

The structure of the basement is crucial in that it controls the extent of Permian and Triassic sedimentation and rift related volcanics in the Bowen Basin. In Figure 6h the major structural elements of Figure 2 are overlain on the basement surface and show that structural highs/lows are generally associated with basement highs/lows. The basement surface shows characteristic rift basin architecture with shallow areas defining the basin boundary around the deeper centre. Basement highs are often associated with areas of exposed granite intrusions (i.e. Line 210 to 230, Roma Shelf) or older basement rocks including the pre-rift Camboon volcanics.

In the deep basement channel, in the Taroom and Denison troughs, are the rift related basal volcanics (i.e. Camboon and Combarngo). In the Taroom Trough they are associated with the Meandarra Gravity Ridge, which is predominantly a north–south linear gravity high in the southern part of the Bowen Basin. Some basal rift volcanics are found in the base of the Denison Trough, based on several boreholes, and this is expected given the rift origin. The lateral extent of the basal volcanics is strongly controlled by the basement topology, as shown in Figure 6g, and confined to the deepest part of the Taroom and Denison troughs. This is confirmed by numerous surrounding boreholes that reach basement without passing through basal volcanics. The northern limit of the basal volcanics is controlled by a basement high just north of gravity profile Line 250. Between latitude –27 and –25 the Meandarra Gravity Ridge is not clearly defined, however gravity modelling shows basal volcanics are present and they extended further north than the current interpreted limit of Krassay et al. (2009). In the south, towards the Gunnedah Basin, the basal volcanics are at shallower depths and are thinner in response to a shallowing basement profile.

The gravity profiles do not identify any significant changes in basement structure between latitude –28 and –25 which could account for the changes in the response of the gravity anomaly (Figure 3). One possible interpretation for the gravity low in this

area is the presence and thickness of sediments from the overlying Surat Basin, which are absent further north, along with numerous granite intrusions. Around the Roma area, granites, as shown on profile Lines 270 and 280, most likely account for the deep low gravity response.

## Conclusions

Using regional scale gravity modelling, the characteristic architecture of the Bowen Basin is effectively modelled with constraints from boreholes, mapped geology and seismic reflection profiles. The structure is typical of an asymmetrical extensional rift with the major depocentre, the Taroom Trough, containing up to 5 km of sediment and up to 2 km of basal volcanics. Using representative density values, which are averages of bulk lithologies, the gravity models satisfy both the geological and structural information.

Recent geothermal exploration in the Bowen Basin has highlighted the need for regional 3D geological models which can be used to provide a better understanding of subsurface architecture and thermal profile. Gravity modelling is currently the process best suited to determining the subsurface structure for thermal models as it is a powerful tool for interpreting the depth to basement. The creation of 3D surfaces from the gravity models and borehole data provides a geological framework which can be incorporated into other applications.

The gravity models presented in this work are generally consistent with the current architecture interpretations of the Bowen Basin but differ in part on the estimates of sediment thickness. We find the sediment estimates from seismic profiles which have boreholes reaching basement are comparable to our estimates with gravity modelling. In seismic profiles which do not have boreholes reaching basement the sediment estimate is double that of our gravity models. Changing the velocity of the two way travel time conversion will result in different estimates of sediment thickness. Importantly, this work has provided a valid estimate of sediment thickness for the entire Bowen Basin, which better takes into account the complex geometry, for use in thermal modelling.

The main uncertainty with determining the depth to basement and basal volcanics in the gravity models is the density of bodies. The assumption that the average densities of bulk lithologies are consistent over the entire Bowen Basin creates an inherent level of uncertainty. However, by introducing constraints on the gravity models this level of uncertainty is reduced. More detailed density data for lithologies would permit better gravity models of the subsurface structure of the Bowen Basin and the determination of sediment thickness for thermal models.

The main difficulty with these regional scale gravity models is the complex architectural nature of the Bowen Basin is not always accurately captured and this leads to a more simplified structure in the 3D surfaces. From the thermal modelling perspective this is not considered a significant problem in developing a regional scale thermal model; but it will require refinement for detailed thermal models of resource estimates.

Although regional scale gravity modelling does have some limitations it is an effective and rapid way to gain additional geological knowledge, particularly where boreholes or seismic data are not available, in order to build 3D geological models of complete systems like the Bowen Basin. With a diverse set of observations gravity models can be self consistent, which reduces uncertainty, and ensures confidence in interpretations of subsurface structure. The gravity modelling and 3D surfaces presented in this work do not seek to be a definitive or detailed

assessment of the subsurface structure of the Bowen Basin but rather provide the building blocks from which to develop more detailed models and undertake research in other areas which require a basic geological framework.

## Acknowledgements

This is contribution no. 775 from the Australian Research Council National Key Centre for the Geochemical Evolution and Metallogeny of Continents (<http://www.gemoc.mq.edu.au>), and publication number 7 of the CCFS ARC Centre of Excellence. Craig O'Neill acknowledges support from DP0880801, DP110104145, and FT100100717.

## References

- Beeston, J. W., 1986, Coal rank variation in the Bowen Basin: *Queensland International Journal of Coal Geology*, **6**, 163–179. doi:[10.1016/0166-5162\(86\)90019-4](https://doi.org/10.1016/0166-5162(86)90019-4)
- Blevin, J., Hall, L., Chapman, J., and Pryer, L., 2007, Sydney Basin Reservoir Prediction Study and GIS Project MR705, Confidential Report to the NSW DPI and Macquarie Energy, FrOG Tech Pty Ltd. [Web document]: Accessed 4 December, 2011. Available at <[http://www.dpi.nsw.gov.au/\\_data/assets/pdf\\_file/0006/191814/Sydney\\_Basin\\_Reservoir\\_Study.pdf](http://www.dpi.nsw.gov.au/_data/assets/pdf_file/0006/191814/Sydney_Basin_Reservoir_Study.pdf)>
- Brakel, A. T., Totterdell, J. M., Wells, A. T., and Nicoll, M. G., 2009, Sequence stratigraphy and fill history of the Bowen Basin, Queensland: *Australian Journal of Earth Sciences*, **56**, 401–432. doi:[10.1080/08120090802698711](https://doi.org/10.1080/08120090802698711)
- Busby, C., and Ingersoll, R., 1995, *Tectonics of sedimentary basins*: Blackwell.
- Cadman, S. J., and Pain, L., 1998, Bowen and Surat Basins, Clarence-Moreton Basin, Gunnedah Basin and other minor onshore basins, Queensland, New South Wales and Northern Territory: Australian Petroleum Accumulations Report 11, Bureau of Resources Sciences Canberra.
- Danis, C., O'Neill, C., and Lackie, M., 2010, Gunnedah Basin 3D architecture and upper crustal temperatures: *Australian Journal of Earth Sciences*, **57**, 483–505. doi:[10.1080/08120099.2010.481353](https://doi.org/10.1080/08120099.2010.481353)
- Danis, C., O'Neill, C., Lackie, M., Twigg, L., and Danis, A., 2011, Deep 3D structure of the Sydney Basin using gravity modelling: *Australian Journal of Earth Sciences*, **58**, 517–542. doi:[10.1080/08120099.2011.565802](https://doi.org/10.1080/08120099.2011.565802)
- Day, R. W., Whitaker, W. G., Murray, C. G., Wilson, I. H., and Grimes, K. G., 1983, *Queensland Geology. A companion volume to the 1:2 500 000 scale geological map 1975*: Geological Survey of Queensland Publication 383.
- DEEDI, 2010, Coal, gas and other resources: Queensland Government Department of Employment, Economic Development and Innovation. [Website]: Accessed 31 August, 2011. Available at <<http://mines.industry.qld.gov.au/mining/coal-gas-other-resources.htm>>
- DEEDI, 2011, Coal statistics, coal industry review 2009–2010 production by individual mines – tonnes: Queensland Government Department of Employment, Economic Development and Innovation. [Web document]: Accessed 31 August, 2011. Available at <<http://mines.industry.qld.gov.au/mining/coal-statistics.htm>>
- Elliott, L., 1989, The Surat and Bowen Basins: *Australian Petroleum Explorers Journal*, **29**, 398–416.
- Fielding, C. R., Kassan, J., and Draper, J. J., 1995, Geology of the Bowen and Surat Basins, eastern Queensland, Australasian Sedimentologist Group Field Guide Series No 8: Geological Society of Australia.
- Fielding, C. R., Sliwa, R., Holcombe, R., and Kassan, J., 2000, A new palaeographic synthesis of the Bowen Basin of central Queensland, in J. W. Beeston, ed., *Bowen Basin Symposium 2000*: Proceedings of the Geological Society of Australia, 287–302.
- Finlayson, D. M., Wake-Dyster, K. D., Leven, J. H., Johnstone, D. W., Murry, C. G., Harrington, H. J., Korsch, R. J., and Wellman, P., 1990, Seismic imaging of major tectonic features in the crust of Phanerozoic eastern Australia: *Tectonophysics*, **173**, 211–230. doi:[10.1016/0040-1951\(90\)90219-X](https://doi.org/10.1016/0040-1951(90)90219-X)
- Glen, R. A., 2005, The Tasmanides of eastern Australia, in A. P. M. Vaughan, P. T. Leat, and R. J. Pankhurst, eds., *Terrane Processes at the Margins of Gondwana*: Geological Society London Special Publication, **246**, 23–96.

- Guo, B., Lackie, M. A., and Flood, R. H., 2007, Upper crustal structure of the Tamworth Belt, New South Wales – constraints from new gravity data: *Australian Journal of Earth Sciences*, **54**, 1073–1087. doi:10.1080/08120090701615725
- Korsch, R. J., and Totterdell, J. M., 1996, Mesozoic deformation events in eastern Australia and the impact on onshore sedimentary basins, Mesozoic geology of the eastern Australian plate conference, 23–26 September, Brisbane, 308–318.
- Korsch, R. J., and Totterdell, J. M., 2009, Subsidence history and basin phases of the Bowen, Gunnedah and Surat Basin, eastern Australia: *Australian Journal of Earth Sciences*, **56**, 335–353. doi:10.1080/08120090802698687
- Korsch, R. J., Wake-Dyster, K. D., and Johnstone, D. W., 1992, Seismic imaging of Late Palaeozoic–Early Mesozoic extensional and contractional structures in the Bowen and Surat basins, eastern Australia: *Tectonophysics*, **215**, 273–294. doi:10.1016/0040-1951(92)90357-C
- Korsch, R. J., Johnstone, D. W., and Wake-Dyster, K. D., 1993, Crustal architecture of the New England Orogen based on deep seismic reflection profiling, in P. M. Ashley and P. G. Flood, eds., *Tectonics and Metallogenesis of the New England Orogen*, Alan H. Voisey Memorial Volume: Geological Society of Australia Special Publication 19.
- Korsch, R. J., Boreham, C. J., Totterdell, J. M., Shaw, R. D., and Nicoll, M. G., 1998, Development and petroleum resource evaluation of the Bowen, Gunnedah and Surat Basins, Eastern Australia: *APPEA Journal*, **38**, 199–237.
- Korsch, R. J., Totterdell, J. M., Cathro, D. L., and Nicoll, M. G., 2009a, Early Permian east Australian rift system: *Australian Journal of Earth Sciences*, **56**, 381–400. doi:10.1080/08120090802698703
- Korsch, R. J., Totterdell, J. M., Fomin, T., and Nicoll, M. G., 2009b, Contractional structures and deformation events in the Bowen, Gunnedah and Surat Basins, eastern Australia: *Australian Journal of Earth Sciences*, **56**, 477–499. doi:10.1080/08120090802698745
- Krassay, A. A., Korsch, R. J., and Drummond, B. J., 2009, Meandarra Gravity Ridge, symmetry elements of the gravity anomaly and its relationship to the Bowen–Gunnedah–Sydney basin system: *Australian Journal of Earth Sciences*, **56**, 355–379. doi:10.1080/08120090802698695
- Leaman, D. E., 1990, Sydney Basin gravity-magnetic interpretation structures and settings of NSW/P10 for Santos Ltd. Available via the New South Wales Department of Primary Industries online DIGS database, Report Number PGR1990–3.
- Mack, J. E., 1963, Well Completion Report 15 Union-Kern-AOG Boomi No. 1. Union Oil Development Corporation. Available via the New South Wales Department of Primary Industries online DIGS database, Report Number WCR075.
- Malone, E. J., and Pain, A. G. L., 1971, *Bowen 1 : 250 000 geological sheet SF55–3*: Bureau Mineral Resources, Geology and Geophysics and Geological Survey of Queensland.
- Malone, E. J., Olgers, F., and Kirkegaard, A. G., 1971, *Saint Lawrence 1 : 250 000 geological sheet SF55–12*: Bureau Mineral Resources, Geology and Geophysics and Geological Survey of Queensland.
- Mayers, R., and Lawson, P., 2006, Bindarree 1 Well Completion Report. Origin Energy CSG Limited. Available via the Queensland Government online digital exploration reports (QDEX) system, Report Number 43541.
- Murray, C. G., 1990, Tectonic evolution and metallogenesis of the Bowen Basin, in J. W. Beeston, ed., *Bowen Basin Symposium 1990*: Proceedings of the Geological Society of Australia, 201–212.
- Murray, C. G., 1994, Basement cores from the Tasman Fold Belt System beneath the Great Artesian Basin in Queensland: Geological record 1994/10, Queensland Department of Minerals and Energy.
- Reynolds, J. M., 2003, *An introduction to applied and environmental geophysics*: John Wiley and Sons.
- Simeone, S. F., and Corbett, B. J., 2002, Well Completion Report Mungi 1. Oil Company of Australia Limited. Available via the Queensland Government online digital exploration reports (QDEX) system, Report Number 35252.
- Tadroz, N. Z., 1993, *The Gunnedah Basin, New South Wales*: Geological Survey of New South Wales, Memoir Geology 12, 649 pp.
- Waschbusch, P., Korsch, R. J., and Beaumont, C., 2009, Geodynamic modelling in aspects of the Bowen, Gunnedah, Surat and Eromanga basins from the perspective of convergent margin processes: *Australian Journal of Earth Sciences*, **56**, 309–334. doi:10.1080/08120090802698661



# CHAPTER 6

## 3D GEOLOGICAL MODEL



*Belmore Falls, Robertson NSW*

## Sydney–Gunnedah–Bowen Basin deep 3D structure

Cara Danis

Department of Earth and Planetary Sciences, Macquarie University, NSW 2109, Australia.  
Email: [cara.danis@mq.edu.au](mailto:cara.danis@mq.edu.au)

**Abstract.** Studies of the Sydney–Gunnedah–Bowen Basin (SGBB), one of the largest extensional rift sedimentary basins on the east coast of Australia, lack an understanding of the 3D upper crustal structure. Understanding of the subsurface structure is essential for many areas of resource exploration, development and management, as well as scientific research. Geological models provide a way to visualise and investigate the subsurface structure. The integrated regional scale gravity modelling approach, which uses boreholes and seismic data constraints, provides an understanding of the upper crustal structure and allows the development of a 3D geological model which can be used as the architectural framework for many different applications. This work presents a 3D geological model of the SGBB developed for application in high resolution thermal models. It is the culmination of geological surfaces derived from the interpolation of previous regional scale 2D gravity models and numerous borehole records. The model outlines the basement structure of the SGBB and provides information on depth to basement, depth to basal volcanics and thickness of overlying sediments. Through understanding the uncertainties, limitations, confidence and reliability of this model, the 3D geological model can provide the ideal framework for future research.

**Key words:** architectural framework, deep 3D structure, gravity modelling, Sydney–Gunnedah–Bowen Basin, 3D geological model.

Received 30 August 2011, accepted 2 December 2011, published online 23 January 2012

### Introduction

The Earth's upper crust is host to many important economic resources, from minerals and energy to groundwater, but its subsurface structure is generally poorly understood. To maximise resource returns, monitor resource interplays and develop new resource exploration frontiers, requires a 3D framework geological model of the upper crustal structure. 3D geological models build confidence in the knowledge of subsurface architecture by using a diverse set of observations.

The development of multiple resources in Australia's energy rich sedimentary basins i.e. minerals, energy (coal, coal seam gas, natural gas, geothermal), groundwater and carbon sequestration has highlighted the lack of subsurface information, especially in the vast Sydney–Gunnedah–Bowen Basin (SGBB) (Figure 1). In this basin system the understanding of subsurface structure has been confined to interpreted deep crustal seismic reflection profiles (e.g. Finlayson et al., 1990; Korsch et al., 1992, 1993; Korsch and Totterdell, 2009), gravity modelling (e.g. Qureshi, 1984, 1989; Leaman, 1990) or localised 3D structural models generally constructed at reservoir scale ( $< 25 \text{ km} \times 25 \text{ km}$ ).

The SGBB is  $\sim 1600 \text{ km}$  long and  $200 \text{ km}$  wide and covers an area of over  $260,000 \text{ km}^2$ . Assessing the structure of this sedimentary basin system, from the upper crustal scale, requires a regional scale geological model on the order of  $> 500 \text{ km} \times 500 \text{ km}$ . In order to achieve a detailed regional scale model, first a basic framework was required, i.e. the depth to basement. Then the addition of stratigraphic layers or grouped lithologies, at any level of detail, builds a geological model which has applications in many other areas, such as thermal modelling.

Much of the previous work in the SGBB system has utilised gravity modelling of regional gravity maps i.e. Qureshi (1984,

1989), Leaman (1990) and Krassay et al. (2009) or detailed gravity profiles, i.e. Guo et al. (2007), to assess basin structure and sediment thickness in 2D. Sequestration studies have produced 3D geological models for parts of the SGBB, i.e. Sydney Basin OzSEEBASE model (FrOG Tech, 2006), but they have a defined scope with commercial purposes. The deep architecture of the SGBB system, i.e. depth to basement, can be effectively modelled using gravity because of the consistent density contrast between Permo-Triassic sediments and Palaeozoic basement rocks, provided physical constraints, such as boreholes, are applied.

This paper presents the first internally consistent 3D geological model framework for the SGBB created using integrated gravity models and boreholes with surface interpolation. In essence, the model is a depth to basement model, basement defined here as pre-extensional rift phase Palaeozoic rocks, with the SGBB being a Permian to Triassic (and in some places Jurassic) sedimentary package and rift-related basal volcanics. With this framework, specific stratigraphic units can be added or, as shown in this work, a package of units that represent a particular feature like coal. The ability to add packages of units can be advantageous where it is not practical to model each and every stratigraphic layer. For example, in Danis et al. (2010) and Danis et al. (2011a) the thermally significant coal seams are captured in the geological models of the Gunnedah and Sydney Basins as a package of coal bearing sediments, rather than individual coal seams.

This work presents a collation of the 3D geological model developed from previous gravity modelling work in the Sydney Basin (Danis et al., 2011b), Gunnedah Basin (Danis et al., 2010) and Bowen Basin (Danis et al., 2012). Here, a discussion on the



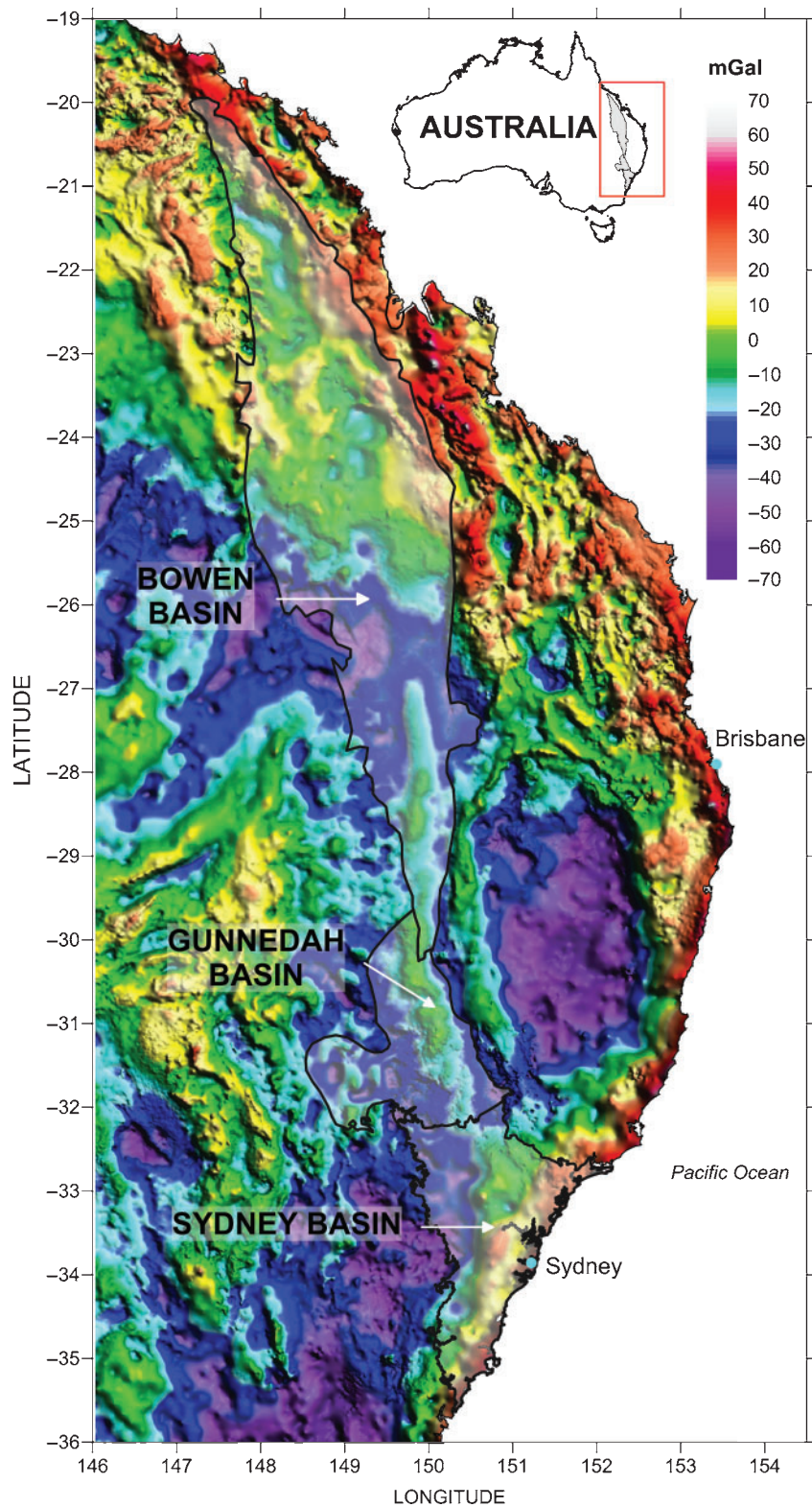


**Fig. 1.** The location of the Sydney–Gunnedah–Bowen Basin system overlain on the 2009 Onshore Gravity Anomaly Grid of Australia. Gravity data is in mGal and available for download from Geoscience Australia.

construction of the 3D geological model and an assessment of overall confidence and reliability is given. The previous papers (Danis et al., 2010, 2011b, 2012) should be referred to for a detailed explanation of the gravity modelling process. Included with this paper is xyz data for the top of the basement and top of the basal volcanics.

### Methodology

A multi-dimensional and integrated modelling approach is essential in defining the upper crustal structure of the SGBB. The 3D geological model is created from a series of interpreted cross sections (e.g. the regional gravity models) which are linked together with boundary surfaces, via interpolation, to

create a series of complex shapes with enclosing volumes. The background material of existing works, i.e. stratigraphy, structure and published models, allow for a conceptual geological model which ensures any data interpolation is self consistent and approaches geological reality.

The first phase involved gravity modelling across the width of each basin component to determine depth to basement, using available borehole and seismic reflection profiles (for approximate depth and geometry) as constraints. Model profiles were created in east–west orientation as well as several approximate north–south orientated profiles as shown in Figure 2. In total 39 profiles were created, 16 in the Bowen Basin, 8 in the Gunnedah Basin and 15 in the Sydney Basin. Refer to Danis et al. (2010, 2011b, 2012) for further explanation and details on the gravity modelling.

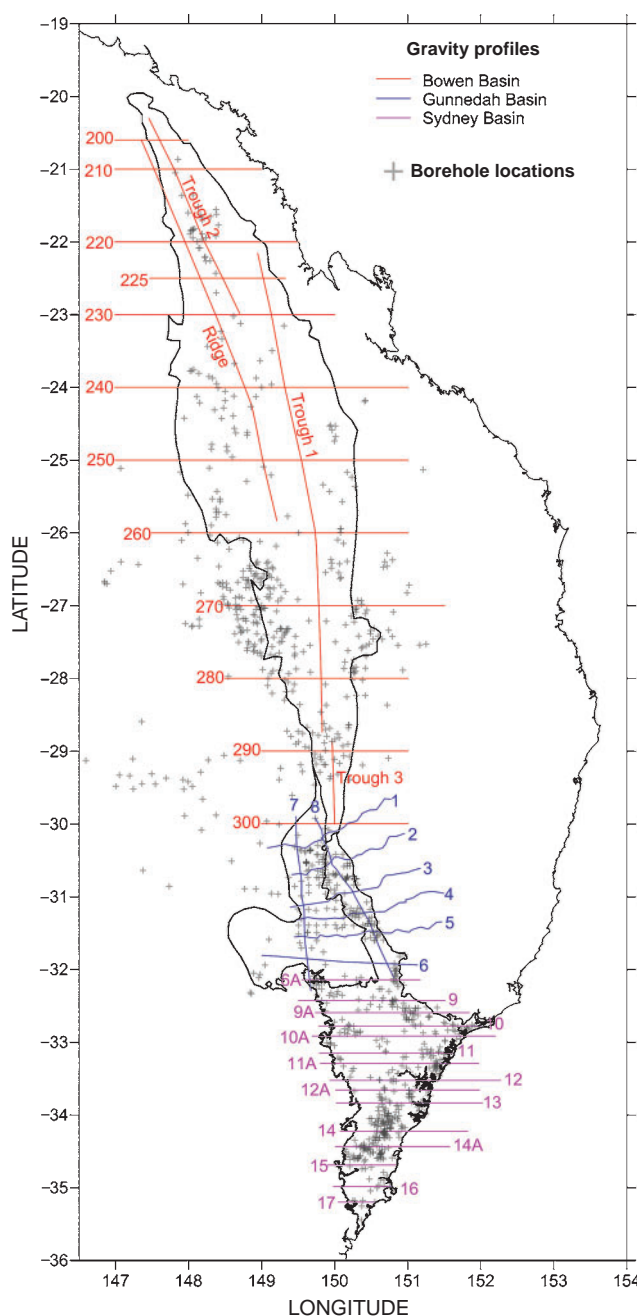


**Fig. 2.** Location of gravity profiles and boreholes in the Sydney–Gunnedah–Bowen Basin.

The second phase involved the extraction of the depth to basement and volcanics surfaces from the gravity models, conversion to a relevant datum i.e. metres Australian Height Datum (mAHD) and interpolation with borehole depths to create geological surfaces. The third phase involved constraining the extent of the basal volcanics and coal bearing formations, using basement structure and boreholes. The final phase is an assessment of the overall confidence and reliability of the model through a Confidence Reliability Accuracy and Precision map.

#### *Extraction and conversion of depth*

The conversion to mAHD is required to ensure all geological information is in the same spatial reference system. The 2D gravity models show depth below ground surface which, as topography is not included, is defined as 0 m. Borehole data is commonly recorded as depth below ground level (m), metres above sea level (mASL) or metres Kelly Bushing (mKB, which relates to the height of the drill rig's rotary table) with the ground elevation generally supplied. Surface elevation data is relative to the height above or below sea level (0 mAHD).

To convert the 2D gravity model profiles, the depth and location of each layer point is collated from the exported model file. First the locations are converted from Eastings and Northings (Zone 55) to Latitude and Longitude. Then the corresponding ground surface elevation is interpolated for the each point using the 90 m elevation data from the Shuttle Radar Topography Mission (SRTM) United States Geological Survey website (URL: < [http://dds.cr.usgs.gov/srtm/version2\\_1/SRTM3/Australia/](http://dds.cr.usgs.gov/srtm/version2_1/SRTM3/Australia/) > accessed 29 Aug 2011). To convert to mAHD the model depth (m) is subtracted from the surface elevation (mAHD).

The same process is applied to depths from borehole records, using either the surface elevation stated in the borehole report or an approximation from the SRTM grid.

#### *Creating 3D surfaces*

To build an acceptable model there needs to be interpolation between the often widely spaced data points and the interpolation process requires geological knowledge to successfully replicate the actual geological environment. Simple geometric algorithms frequently produce unacceptable results, thus iterative methods involving assessments and progressive refinements (Turner, 2006) are required.

In this model, interpolated geological surfaces are created in Surfer, supplied by Golden Software, using the Kriging gridding algorithm, from the borehole and gravity model points for each layer at a 0.05° spacing (~4.7 km). The Kriging gridding process does not produce the ideal surface initially; it requires iteration and progressive refinement in order to approach geological reality i.e. surfaces consistent with actual data and or the conceptual geological model. In this process the model construction relies extensively on actual data, e.g. boreholes and gravity, and adds additional interpreted data points, in line with the conceptual geological model, to areas where subsurface data are less numerous. This is done in order to produce a smoother surface and to extend each layer over the complete model area before truncation to their geological boundaries. In this geological model the majority of interpreted data points do not make up the final geological layer.

During validation and visualisation of the surfaces, they are viewed in 2.5D and 3D, via Surfer and AutoCAD supplied by Autodesk, to check for spurious points, generally a feature of over or under interpolation from the Kriging process, and for

intersections between layers which are not geologically possible. These points were smoothed to reflect either the average height of surrounding points, as for relatively flat areas, or the overall trend of the surface, as for slopes.

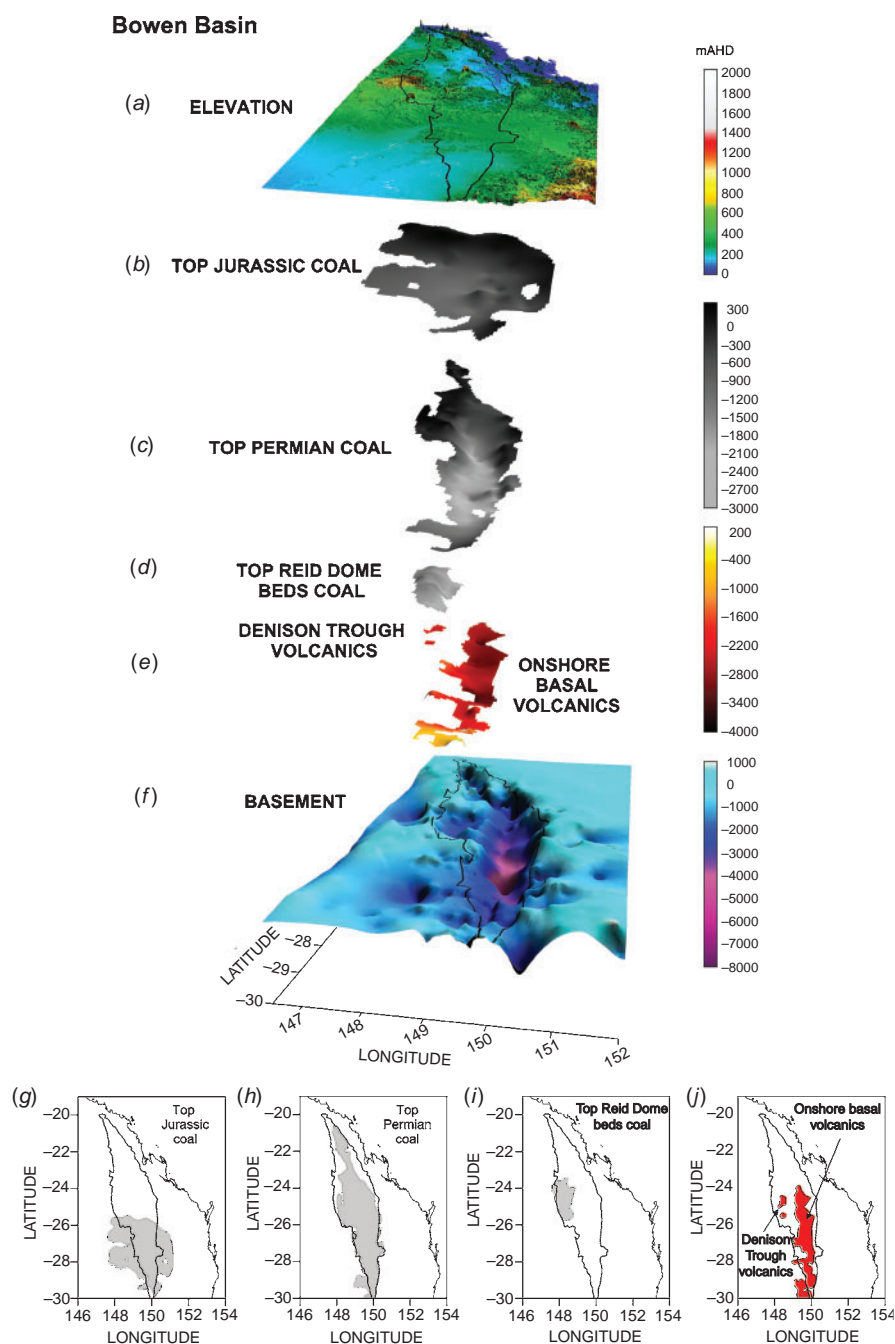
For the geological model of the SGBB surfaces representing the top of the basement, top of basal volcanics and top and base of coal bearing layers were created. Figures 3–5 present 2.5D perspective views of the geological surfaces in the Sydney, Gunnedah and Bowen Basins.

#### Constraining layer boundaries

Complex ‘layer cake’ type conceptual geological models are common in sedimentary environments because of the

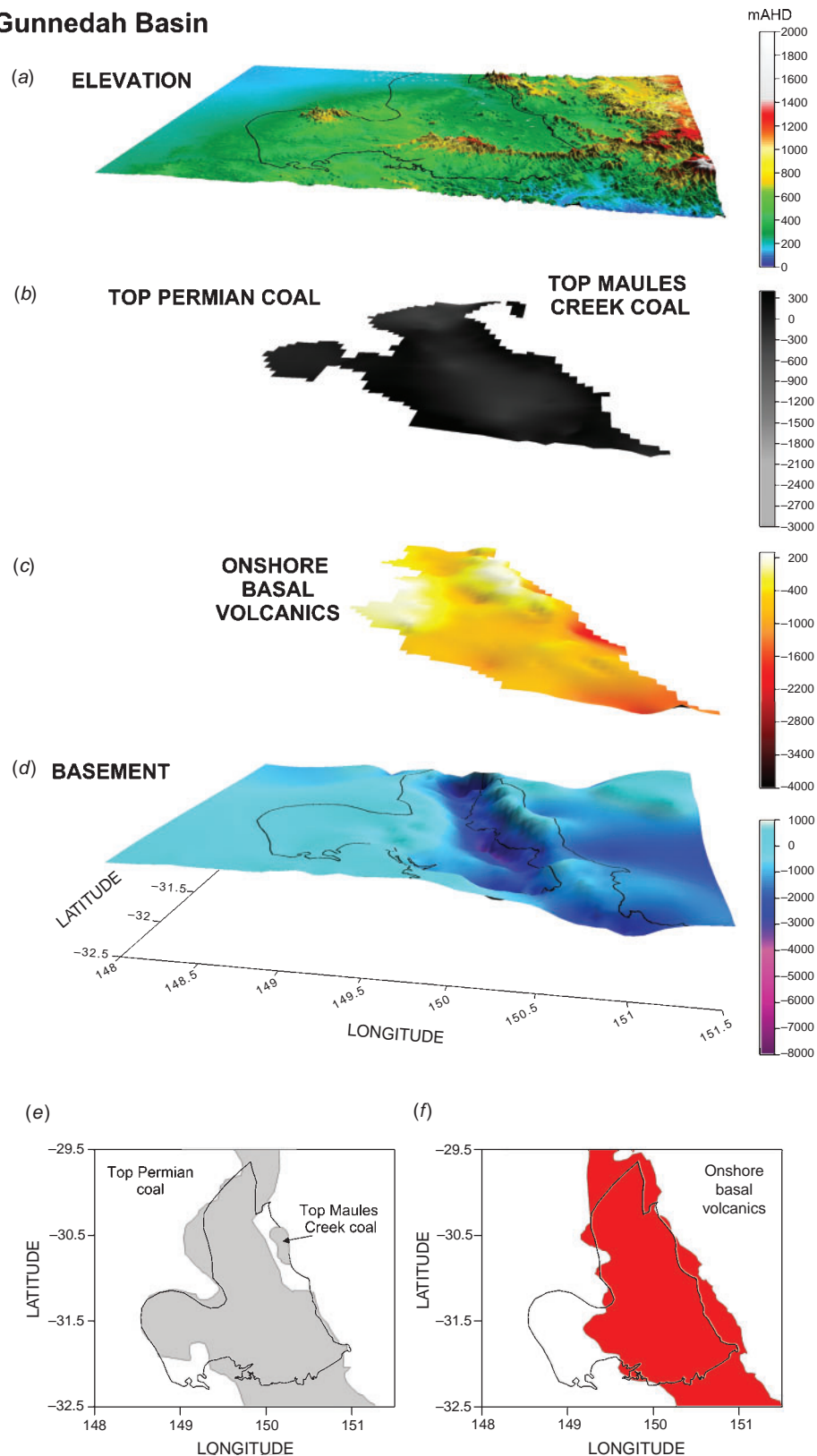
numerous and often inter-fingered sedimentary strata for which surfaces are created. Generally these situations are not explicitly modelled by defining all surfaces, because it is difficult to create all the different facies, but rather as zones subdivided into dominant characteristics, such as basement, or important interfaces, i.e. coal layers, based on the end use of the model.

The geological model of this work was developed for a high resolution 3D thermal model of the SGBB system. It provides the basic geological framework from which to construct the thermal model, by providing boundaries for geological layers which have distinctive thermal properties, e.g. sediments, coal, volcanics and basement. Each geological layer is created as an individual grid



**Fig. 3.** A 2.5D perspective view of the top of the geological surfaces in the Bowen Basin, from Danis et al. (2012). (a) Elevation, (b) Top Jurassic coal, (c) Top Permian coal, (d) Top Reid Dome beds coal, (e) top of the Denison Trough volcanics and onshore basal volcanics and (f) top of the basement. Insert maps (g) to (j) show the plan view of geological surfaces (b) to (e) with Bowen Basin outline.



**Gunnedah Basin**

**Fig. 4.** A 2.5D perspective view of the top of the geological surfaces in the Gunnedah Basin, from Danis et al. (2010). (a) Elevation, (b) Top Permian coal and Top Maules Creek coal, (c) top of the onshore basal volcanics and (d) top of the basement. Insert maps (e) and (f) show the plan view of surfaces (b) and (c) with Gunnedah Basin outline.

over the model space and then truncated to its geological extent, with the exception of the basement which is created for the entire model extent, though outside the SGBB boundary it is interpretive at best.

In the model the intra-basin geological surfaces of the Reid Dome beds coal, Permian coal, Maules Creek coal, Greta coal, Jurassic coal, onshore basal volcanics, offshore basal volcanics and Denison Trough volcanics were initially interpolated over



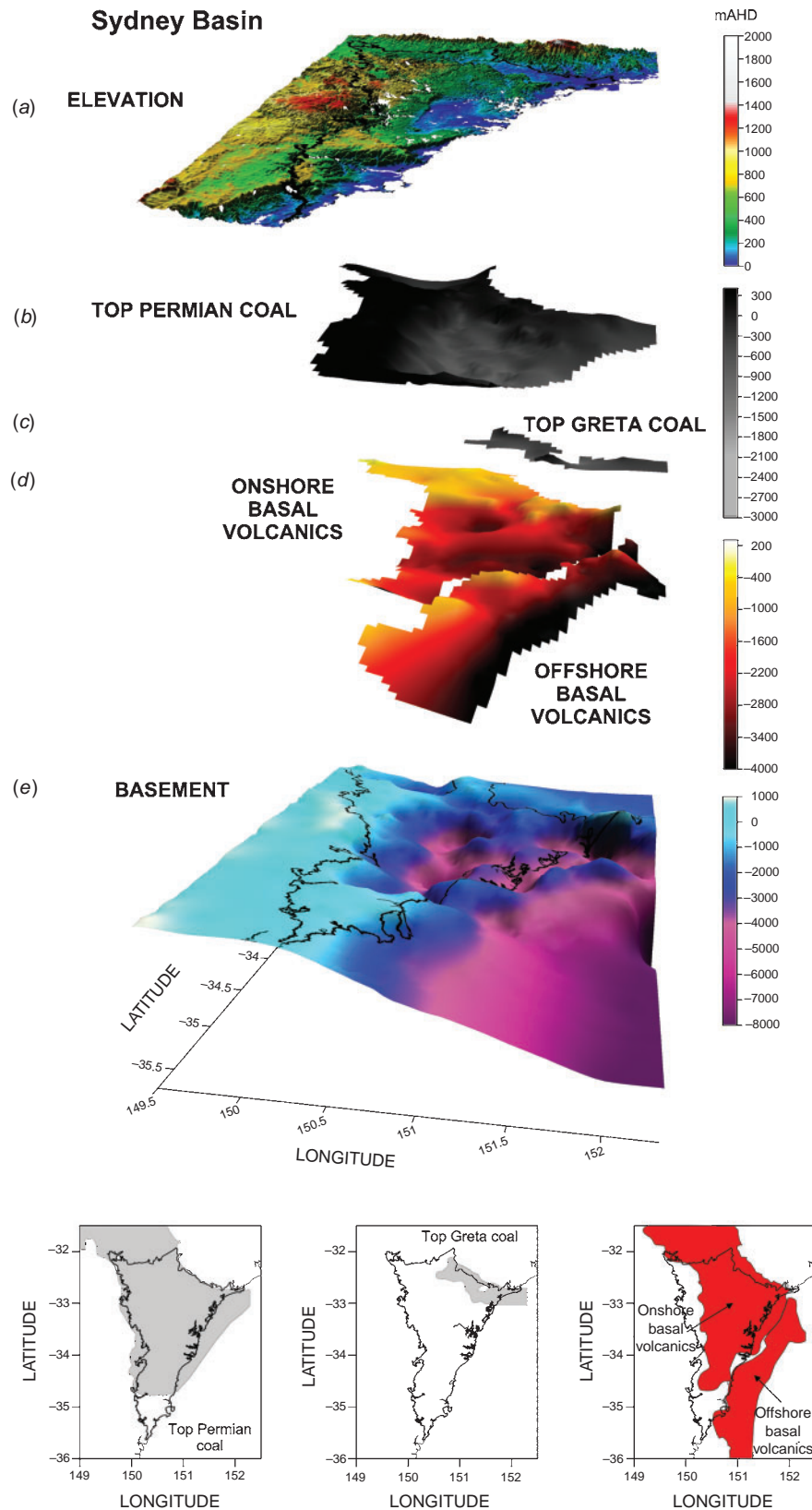


**Fig. 5.** A 2.5D perspective view of the top of the geological surfaces in the Sydney Basin, from Danis et al. (2011b). (a) Elevation, (b) Top Permian coal, (c) Top Greta coal, (d) top of the onshore and offshore basal volcanics and (e) top of the basement. Insert maps (f) to (h) show the plan view of surfaces (b) to (d) with the Sydney Basin outline.

the complete model area, i.e. beyond their data constraints, therefore each surface needed to be truncated to its approximate geological extent. The coal surfaces, excluding

the Jurassic, and the basal volcanics were truncated against the basement layer whilst borehole records are used to estimate the lateral extent of the Jurassic coal surface. In areas

where the basement does not clearly truncate the layers; borehole records, seismic profiles, gravity model profiles or reasonable geological likelihood is used to determine the absence or presence of the layer. In this way layer intersection is used to create the geological boundaries for the surfaces in the model.

As a result of layer intersection, all the model surfaces can be easily converted into the 'block' volumes required for thermal modelling, as they share a common bounding surface which insures no gaps between the layers. This method creates a more realistic geological model for which the extent of each layer can be considered geologically reasonable and lower layers are able to truncate upper layers when necessary i.e. intrusions or erosional surfaces.

#### Confidence reliability accuracy and precision map

One of the challenges in producing geological models is the ability to incorporate and display the uncertainties in the data or the interpretation. The confidence reliability accuracy and precision map is one way to present a quantitative assessment of the overall geological model through an evaluation of the various datasets used in construction. This map is designed to be a quick evaluation tool for the confidence and reliability of the 3D geological model, i.e. highlighting areas where large amounts of data were used versus areas with less that are more subjective to interpretation. The OzSEEBASE model of the Sydney Basin (FrOG Tech, 2006) was the first to show a confidence reliability accuracy and precision map for the evaluation of their model. In Danis et al. (2011b) a confidence reliability accuracy and precision map was developed for the Sydney Basin. The method developed by Danis et al. (2011b) has been applied to evaluate the complete SGBB model. However as the geological model comprises many different datasets, for a quantitative numerical evaluation to be effective at this scale the arbitrary numerical value of the weighting factor and the maximum distance of influence is assigned to each input dataset, as shown in Table 1, needed to be different and new input datasets added.

With the spatial distribution of data in the Bowen Basin greater, due to its larger size, than the Sydney or Gunnedah, the weighting factors for the Gravity Model – Basement Surface, Gravity Model – Volcanics Onshore Surface, Boreholes – Basement, Boreholes – Coal and Seismic Reflection Profiles datasets were increased. The Magnetics dataset was removed, as it only consisted of a few points, and a new dataset Surface Elevation, for areas of basement that are exposed on the surface, was added. The maximum distance of influence was increased for Boreholes – Coal, reflecting their

**Table 1. Input datasets, maximum distance of influence and arbitrary weighting factor for Equation 1 for the confidence reliability accuracy and precision map (Figure 6).**

Input dataset	Max dist (km)	Weighting factor
Gravity model – basement surface	20	50
Gravity model – volcanics onshore surface	20	2
Gravity model – volcanics offshore surface	20	1
Boreholes – basement	5	120
Boreholes – volcanics	5	20
Boreholes – coal	10	25
Structure contours from seismic profiles	1	5
Surface geology	5	5
Surface elevation	4	2
Seismic reflection profiles	5	5
Interpolated points	5	5

importance in creating the coal bearing layers and Surface Geology.

The weighting factor is an arbitrary number related to the type of assigned input data and designed to value its quality, reliability and or quantity. For example borehole data is weighted higher because it is reliable but its quantity is low. Gravity modelling and seismic reflection profiles are weighted lower, not because it's less reliable but because the quantity is high. Setting a maximum distance of influence, related to the type of dataset, ensures datasets with vast quantities of information do not unnecessarily dominate the results and represent a realistic application of the information of the dataset. For example, structural information gathered from a borehole is very location specific and should only be interpreted as applicable to areas very close to the borehole, whilst gravity modelling, which is more regional scale, could be applied over a greater area because of the already inherent level on uncertainty. Using Equation 1 below, from Danis et al. (2011b),

$$p(X, Y) = \sum_{i=0}^n V_i - \frac{d_i^3}{D^3} \times V_i \quad (1)$$

where  $V_i$  is the assigned weighting factor of the data point  $i$  and  $d_i$  is the distance to data from  $(X, Y)$  and  $D$  is the maximum distance considered relevant, a quantitative value of a point at any location of the grid (i.e. the centre of a  $0.05^\circ$  cell) is defined. The total confidence value of each point is the addition of the weighting factors of each nearby dataset. A cubic function is used to give due emphasis to closer data whilst more distant data is weighted appropriately less and if  $d_i > D$  the data is ignored. The values the map produces are subjectively classified as low or medium or high.

Figure 6 represents the total confidence reliability accuracy and precision value of each point in the grid as a contour map over the complete SGBB. The subjective classification of values is designed to specifically highlight areas of maximum and minimal data input, with values 0 to 90 considered low, 90 to 250 moderate and greater than 250 high. In the areas of highs, where there are large volumes of data, the geological model has good physical control and there is confidence that it is well constrained. For the low areas, which represent limited data, the lower confidence highlights the more interpretive areas of the model.

In the Sydney and Gunnedah basins the overall confidence is high due to a large database of boreholes and seismic reflection profiles in a relatively small area. In the Bowen Basin, which covers a much larger area, overall high confidence is clustered around the gravity profile lines and high density areas of boreholes (see Figure 2 for borehole distribution). Outside of the basin boundary for the model the area is shown as low due partly to limited data and being outside the area of interest.

Using the updated maximum distance of influence and weighting factors accounts for the larger scale of the SGBB model compared to the Sydney Basin in Danis et al. (2011b). In Figure 6 the Sydney Basin shows a similar trend in areas of low confidence and high confidence, particularly in the southern part of the Basin, when it is compared with Danis et al. (2011b). In the northern part of the Basin, where there are numerous datasets close together, there is less detail than in Danis et al. (2011b). This is a result of changing the weighting factor of the Gravity Model – Basement Surface dataset. Profiles in the Sydney Basin are very close together (see Figure 2) whilst those in the Bowen Basin are much further apart. For analysis of the complete SGBB the same criteria was applied to each dataset

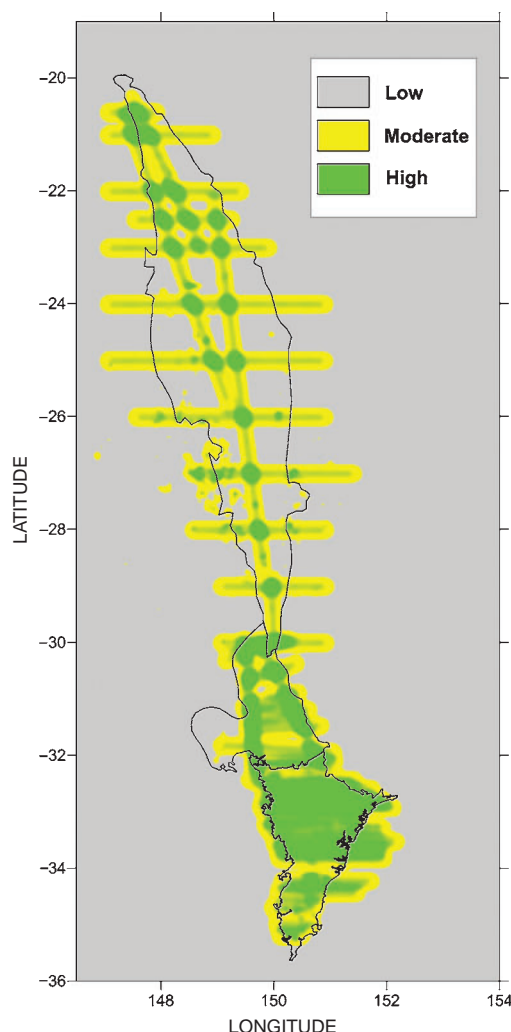


**Fig. 6.** A contour surface of the data points from Equation 1. The confidence reliability accuracy and precision map shows areas of high confidence in green and areas of low confidence in grey in the online version.

however it may be better to have different weighting factors and maximum distances of influence for each basin in the system to better account for the problem of scale and data distribution.

### Geological structure

The process of geological modelling involves the determination of the subsurface spatial variation of selected geological parameters and the evolution of a conceptual model to a 3D model which approaches geological reality. The 3D geological model of the SGBB presented in this work exhibits the architecture typical of formation in an extensional rift environment. It is an approximately north–south orientated asymmetrical basin containing up to 5 km of sediments and volcanics. The basement surface, illustrated in Figure 7, shows architectural features which are comparable with published tectonic maps and the formation environment.

In the basement, a deep centralised channel, generally correlated with the Meandarra Gravity Ridge (i.e. Krassay et al., 2009), is filled with extensional rift related volcanics (i.e. basal volcanics) that are up to several kilometres thick. It is the architecture of the basement which constrains the extent of the basal volcanics along the Meandarra Gravity Ridge, and also in the Denison Trough. The northern and southern limits of basal

volcanics in the Meandarra Gravity Ridge (k in Figure 7) are controlled by respective basement highs, located in the Taroom Trough (c in Figure 7) and the south-eastern edge of the Blue Mts–Illawarra Shelf (x in Figure 7).

The transition between each basin is defined by Herbert and Helby (1980), Tadroz (1993) and Bembrick et al. (1993) as apparent basement highs and these highs are comparable with structurally high basement presented in this 3D model. There is also comparable geometry with most seismic reflection profiles, although the interpreted angular nature of faulted blocks and faults is often smoothed out by the surface gridding interpolation process, however, the overall change in depth is preserved. The published interpreted tectonic lows, as shown in Figure 7, of the Taroom Trough (a, b, c), Denison Trough (d), Macdonald Trough (u), Lake Macquarie Trough - Newcastle Syncline (w) and Cumberland Basin (y) generally correspond to areas of deep basement and thick sedimentation in the model. Published features like the Collinsville Shelf (e), Comet Ridge (g), Rocky Glen Ridge (p) and Blue Mts–Illawarra Shelf (x) also correspond to basement highs.

The shape of the basement, shallow sides with deep centre, determines the lateral extent of the Permian coal layer with the eastern and western margins generally terminating against shallow or exposed basement. In the offshore part of the Sydney Basin the eastern extent of the Permian coal layer remains undefined.

### Model limitations

The 3D geological model presented here is constrained with over 1000 boreholes, 36 gravity model profiles, many seismic reflection profiles and surveys, as well as mapped geology. Although the Confidence Reliability Accuracy and Precision map provides one method of understanding the uncertainties of the model data there are other limitations of the model to be understood.

As noted by Turner (2006) geological models and visualisations are successful in providing improved subsurface investigations when user requirements are accurately identified and addressed. The requirement of this model is thermal modelling (i.e. Danis et al., 2010), thus geological surfaces are created for units with distinctive thermal properties. The model is not a complete ‘layer cake’ of the SGBB sedimentary system, incorporating all stratigraphic units, however this does not preclude it, or parts of it, from being used as the fundamental framework for such models.

The model is constructed as a series of surfaces and as a result the model poorly resolves specific geometric features like faults. This is especially prominent where thrust faults are involved, e.g. Hunter–Mooki, Jellinbah and Gogango, particularly in the Bowen Basin. This is primarily a result of the method of surface interpolation and the underlying construction from gravity modelling. The geological model can represent the overall change in basement depth across a fault area but the interpolation process cannot juxtapose shallower basement over deeper basement, or create angular block geometry. Detailed modelling of faults can be achieved, however for this project, faults were not considered essential. Generally the thermal properties of sediments either side of the fault are similar; what is more important is the termination of coal bearing formations at faults, e.g. the Hunter–Mooki, and significant changes in basement depth which changes sediment thickness.

The basement surface is the most important part of this 3D geological model, therefore the sensitivity of the depth is

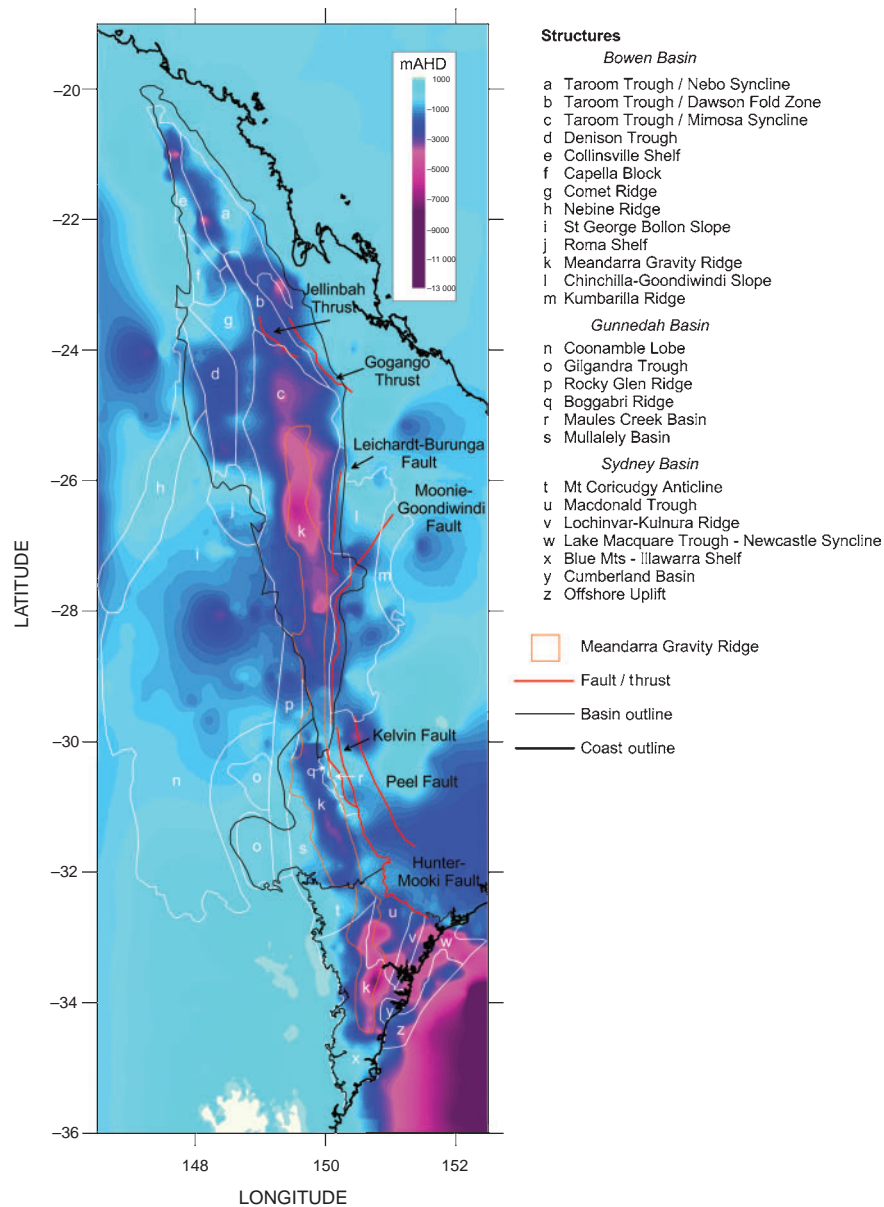


**Fig. 7.** Top of basement as a contoured depth (mAHd) surface showing SGBB outline, tectonic structures (adapted from Adler et al., 1998 and Krassay et al., 2009), the location of major faults and the Meandarra Gravity Ridge.

important. Borehole data represents the fundamental ‘hard’ data from direct sampling of the subsurface and is deemed reliable on the metre scale. Gravity modelling of the depth of basement is subjective and controlled by the density contrasts applied and therefore is reliable on the hundreds of metres scale. Using boreholes to constrain the gravity models limits the variation in density contrast, otherwise models do not fit reality, and the more boreholes available the greater the accuracy of the depth to basement. In the gravity models of Danis et al. (2010, 2011b, 2012) the modelled basement depth varied by less than 700 m when different geologically reasonable density values were used, although the models still conformed to the borehole constraints. To compare, Leaman (1990), who did not use boreholes to calibrate his gravity models, found he had an inconsistency of around 500 m between his modelled depths and the nearby boreholes for his regional gravity models across the Sydney Basin. It should be noted, however, that Leaman (1990) did not use consistent density values across all his profiles for the same geological units. In the SGBB gravity profiles the variation

of basement depth is considered acceptable for the scale of the profiles (200 km × 15 km) and, therefore there can be confidence in the accuracy of the resulting basement layer.

The interpolated geological surfaces of the 3D geological model are well constrained within the boundary of the SGBB. For each layer, constraints are applied from boreholes at the metre scale and gravity models at the 100s of metres scale, thus reducing the level of uncertainty. Inside the SGBB the level of uncertainty of the depth to basement ranges from a few metres to a few hundred metres. Here model confidence is high, particularly in the Sydney and Gunnedah Basins, due to numerous boreholes. Outside the SGBB borehole and geological control is limited, thus the level of uncertainty near the basin boundary is likely be around 1 km but further away from the boundary it will be much higher. Well outside of the basin boundary the depth to basement is more interpretive and should not be considered as reliable (without additional data), as it is constructed purely as part of the surface required to complete block volumes for thermal modelling.



## Conclusions

Understanding the 3D upper crustal structure of the SGBB is essential for resource exploration, development and management. Geological models are important for improving subsurface understanding and visualisation and for providing the fundamental geometric framework for the success of economic resource development and scientific research.

The 3D geological model presented here is the first model of the complete SGBB and is significantly larger than most reservoir scale models. The geological surfaces exhibit features comparable with the current published tectonic and structural interpretations, making it an ideal platform from which to integrate additional stratigraphic layers or important boundaries. This model also serves as the architectural framework in the development of a high resolution 3D thermal model for the SGBB.

The understanding of the upper crustal structure of the SGBB is improved with this model. Particular features, like the Meandarra Gravity Ridge are better constrained. The model shows the deep structure of the SGBB characteristic of an extensional rift basin and the geometry of the basement is comparable with published features. From understanding the uncertainties, limitations, confidence and reliability this 3D geological model is an ideal framework for providing an avenue for the next generation of research.

## Acknowledgements

The author would like to acknowledge A. Danis for the script to complete the confidence reliability accuracy and precision map for the SGBB, which is as an extension of previous work in the Sydney Basin. In addition the author would like to thank M. Lackie, Dave Robson, Ron Hackney and Ray Tracey for critical reviews.

## References

- Adler, J. D., Hawley, S., Maung, J., Scott, R. D., Sinelnikov, A., and Kouzmina, G., 1998, Prospectivity of the offshore Sydney Basin: A new perspective: *APPEA Journal*, **38**, 68–92.
- Bembrick, C. S., Herbert, C., Scheibner, E., and Stuntz, J., 1993, Structural subdivision of the New South Wales portion of the Sydney-Bowen Basin: *Quarterly Notes Geological Survey NSW*, **11**, 1–13.
- Danis, C., O'Neill, C., and Lackie, M., 2010, Gunnedah Basin 3D architecture and upper crustal temperatures: *Australian Journal of Earth Sciences*, **57**, 483–505. doi:10.1080/08120099.2010.481353
- Danis, C., O'Neill, C., and Lee, J., 2011a, Geothermal state of the Sydney Basin: assessment of constraints and techniques: *Australian Journal of Earth Sciences*. doi:10.1080/08120099.2011.606504
- Danis, C., O'Neill, C., Lackie, M., Twigg, L., and Danis, A., 2011b, Deep 3D structure of the Sydney Basin using gravity modelling: *Australian Journal of Earth Sciences*, **58**, 517–542. doi:10.1080/08120099.2011.565802
- Danis, C., O'Neill, C., and Lackie, M., 2012, Building 3D geological knowledge through regional scale gravity modelling for the Bowen Basin: *Exploration Geophysics*, **43**. doi:10.1071/EG11028
- Finlayson, D. M., Wake-Dyster, K. D., Leven, J. H., Johnstone, D. W., Murry, C. G., Harrington, H. J., Korsch, R. J., and Wellman, P., 1990, Seismic imaging of major tectonic features in the crust of Phanerozoic eastern Australia: *Tectonophysics*, **173**, 211–230. doi:10.1016/0040-1951(90)90219-X
- FrOG Tech., 2006, OZ SEEBASE Proterozoic Basins Study, Report to Geoscience Australia by FrOG Tech Pty Ltd.
- Guo, B., Lackie, M. A., and Flood, R. H., 2007, Upper crustal structure of the Tamworth Belt, New South Wales – constraints from new gravity data: *Australian Journal of Earth Sciences*, **54**, 1073–1087. doi:10.1080/08120090701615725
- Herbert, C., and Helby, R., eds., 1980, *A guide to the Sydney Basin*: Geological Survey of New South Wales Bulletin 26, Department of Mineral Resources, New South Wales, 603 pp.
- Korsch, R. J., and Totterdell, J. M., 2009, Subsidence history and basin phases of the Bowen, Gunnedah and Surat Basins, eastern Australia: *Australian Journal of Earth Sciences*, **56**, 335–353. doi:10.1080/08120090802698687
- Korsch, R. J., Wake-Dyster, K. D., and Johnstone, D. W., 1992, Seismic imaging of Late Palaeozoic–Early Mesozoic extensional and contractional structures in the Bowen and Surat basins, eastern Australia: *Tectonophysics*, **215**, 273–294. doi:10.1016/0040-1951(92)90357-C
- Korsch, R. J., Johnstone, D. W., and Wake-Dyster, K. D., 1993, Crustal architecture of the New England Orogen based on deep seismic reflection profiling, in P. M. Ashley and P. G. Flood, eds., *Tectonics and metallogenesis of the New England Orogen*, Alan H. Voisey Memorial Volume: Geological Society of Australia Special Publication 19.
- Krassay, A. A., Korsch, R. J., and Drummond, B. J., 2009, Meandarra Gravity Ridge, symmetry elements of the gravity anomaly and its relationship to the Bowen-Gunnedah-Sydney basin system: *Australian Journal of Earth Sciences*, **56**, 355–379. doi:10.1080/08120090802698695
- Leaman, D. E., 1990, Sydney Basin gravity-magnetic interpretation structures and settings of NSW/P10 for Santos Ltd. (DIGS Report No. PGR1990–3). Available at <http://digsopen.minerals.nsw.gov.au/>
- Qureshi, I. R., 1984, Wollondilly-Blue Mountains gravity gradient and its bearing on the origin of the Sydney Basin: *Australian Journal of Earth Sciences*, **31**, 293–302.
- Qureshi, I. R., 1989, Positive gravity anomaly over the Sydney Basin: *Exploration Geophysics*, **20**, 191–193. doi:10.1071/EG989191
- Tadroz, N. Z., 1993, *The Gunnedah Basin, New South Wales*: Geological Survey of New South Wales, Memoir Geology 12, 649 pp.
- Turner, A. K., 2006, Challenges and trends for geological modelling and visualisation: *Bulletin of Engineering Geology and the Environment*, **65**, 109–127. doi:10.1007/s10064-005-0015-0

# CHAPTER 7

## GEOHERMAL ASSESSMENT TECHNIQUES



*Fire Road, East Kanagloon NSW*

# Geothermal state of the Sydney Basin: assessment of constraints and techniques

C. DANIS<sup>1</sup>, C. O'NEILL<sup>1</sup> AND J. LEE<sup>2</sup>

<sup>1</sup>*GEMOC ARC National Key Centre, Department of Earth and Planetary Sciences, Macquarie University, NSW 2109, Australia.*

<sup>2</sup>*Hot Rock Energy Pty Ltd, NSW 2228, Australia.*

The thermal structure of sedimentary basins is largely dependent on complex three dimension (3D) effects encompassing architecture, geology and groundwater, making it difficult to describe in a one-dimensional (1D) model. New equilibrated down-hole temperature measurements in the Sydney Basin, in conjunction with regional scale thermal modelling using the geodynamics simulation software *Underworld*, can provide an accurate assessment of the thermal structure of the basin. When compared to extrapolation maps, these results highlight important limitations of utilising extrapolation maps as an unaccompanied geothermal exploration tool. The extrapolated temperature method creates a 'temperature-at-depth' map, which propagates and exaggerates near surface variations, and is limited by coverage and number of boreholes that have temperature measurements recorded. Numerical simulations of basin heat flow, using basic material properties, combined with a deep 3D geological model and calibrated by measured equilibrated temperature data are not limited by the borehole coverage but rather the chosen resolution of the model. The *Underworld* thermal model provides a realistic estimation of temperature at depth within the Sydney Basin, a clearer understanding of thermal structure and allows a more comprehensive assessment of potential geothermal targets.

**KEY WORDS:** Sydney Basin, extrapolated temperature, basement temperature, thermal modelling, geothermal exploration

## INTRODUCTION

In sedimentary basins thermal structure is largely dependent on the complex 3D interaction of architecture, geology and heat flow. The thermal structure of the Sydney Basin is yet to be fully explored and more importantly the geothermal state is yet to be accurately defined. With the recent expansion of geothermal exploration in Australia, publically available data is often the first port of call in determining viable exploration targets. To define the geothermal state,

estimates of temperature at depth are required to assess areas of potential geothermal prospectively, however only sparse data is currently available. An existing method, which extrapolates down-hole temperature measurements is one of the few resources providing preliminary estimates of temperature at depth.

The OzTemp interpreted temperature at 5 km depth map (Figure 1; Gerner & Holgate 2010), suggests many parts of the Australian continent



are potentially prospective for geothermal energy. This interpreted temperature at depth map is created using the methodology of Chopra & Holgate (2005) where bottom-hole temperatures are extrapolated in a 1 dimensional (1D) two-layer model to estimate temperature at depth. The OzTemp well database, is an expansion of the Austherm07 database, and contains temperature measurements sourced from petroleum, mineral exploration and groundwater bores (Chopra & Holgate 2005), which were not specifically collected for geothermal exploration. As a result, the database contains primarily non-equilibrated temperature measurements.

The extrapolation method, and its associated database, has limitations that are often not considered when it is used as sole tool for geothermal exploration. The first limitation is an extrapolated temperature map, created from non-equilibrated temperature measurements, i.e. measurements that are not representative of the actual thermal structure, would not show an accurate estimate of temperature at depth. The second and most significant limitation is a 1D two-layer model is potentially too simplistic to accurately capture the thermal structure of the basin.

Newer and more detailed multi-dimensional numerical thermal modelling methods are necessary for defining the thermal state of the Sydney Basin, as the existing methods, no matter how detailed the model, cannot adequately represent the expected temperature fields. In this work we discuss the existing methods of temperature extrapolation with the aim of identifying whether using equilibrated temperature measurements, compared with non-equilibrated measurements, can provide useful preliminary estimates of temperature. The identified areas of potential geothermal prospectively are compared with the OzTemp interpreted map.

One danger in using extrapolated maps as the sole basis for geothermal exploration programs is potential target anomalies may be undervalued, in some geological settings, or missed entirely depending on the distribution of data. By using 2D numerical thermal modelling in *Underworld*, a reliable and representative assessment of the basin-scale thermal structure of the Sydney Basin can be made by calibrating the thermal model against measured equilibrated borehole temperatures.

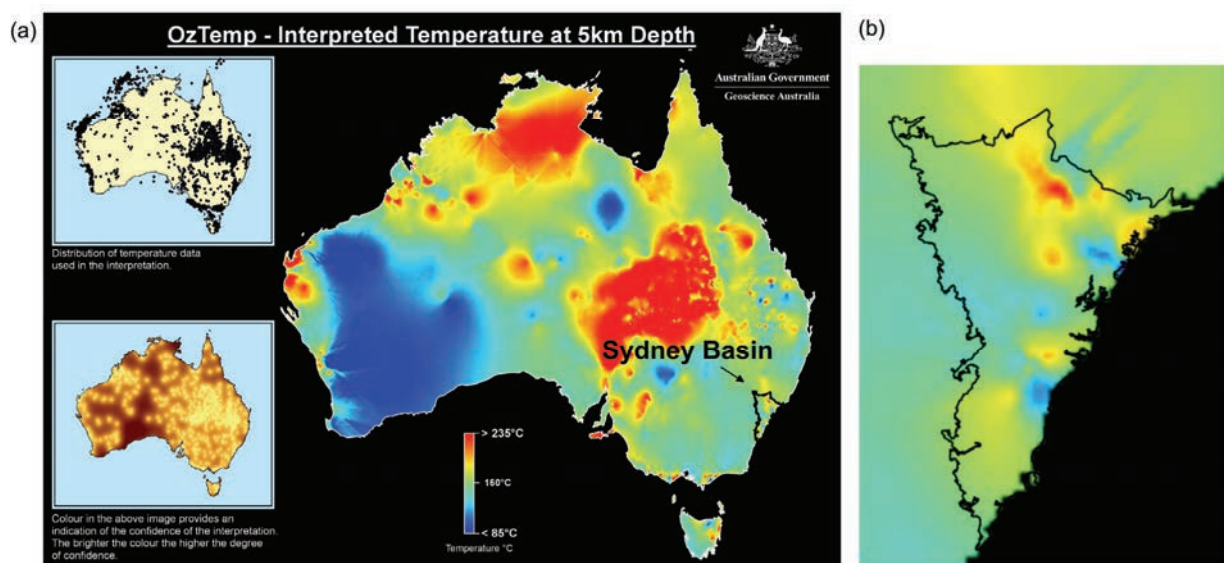


**Figure 1**(a) OzTemp interpreted temperature at 5 km depth, showing location of Sydney Basin and (b) OzTemp for the Sydney Basin, modified from Gerner & Holgate (2010)



## METHODOLOGY

The methodology is divided into three sections, as described below, focusing on the collection of equilibrated down-hole temperature measurements, the 2-layer extrapolation method and the 2D numerical thermal modelling. Existing temperature data were collected from coal and petroleum exploration reports, available online from DIGS (<http://digsopen.minerals.nsw.gov.au/>) or the Sydney Basin Geothermal Data Package (Jaworska 2008) and classed as either equilibrated or non-equilibrated for the extrapolation. Existing groundwater bores provide an opportunity to measure down-hole temperature at depths of 100 m to 300+ m in boreholes that can be classed as equilibrated. Over 30 groundwater boreholes, belonging to the Sydney Catchment Authority, the NSW Office of Water, Ulan Coal Mines Ltd and private landholders were accessed in this study to directly measure down-hole temperatures.

### Down-hole temperature measurements

Two methods for down-hole temperature measurement were used with HOBO™ data loggers from Onset Computer Corporation Ltd. In both these methods the temperature data loggers, a thermistor in a sealed stainless steel unit with the following specifications; an operating range of -20 to 50°C, accuracy of 0.37°C and resolution of 0.1°C at 20°C, were used. The loggers are set to record at 1 second intervals and can store up to 25 000 data points.

Method A required several loggers attached at set intervals (generally 25 to 50 m) on a cable that is slowly lowered to the bottom of the borehole and left undisturbed for a period of 1 hr. Method B used one logger attached at the end of a cable that is slowly lowered down

to the first depth and left stationary for 15 min to 30 mins before being lowered to the next interval and repeated until the bottom of the bore is reached. All recordings were within the groundwater column for maximum thermal coupling, therefore the standing water level of the borehole generally determined the shallowest measurement.

At the end of measurement the loggers are removed, downloaded and the traces analysed for the stable temperature at each depth interval. The stable temperature is determined by the flat-lining of temperatures at each depth interval, as shown in Figure 2. A comparison of repeat measurements using both methods in the same borehole by Danis & O'Neill (2010) found that the measurements were either identical or within the error of the logging unit (0.37°C). The level of water disturbance created in the water column by using Method A over B was not significant enough to affect the temperature results given the accuracy of the sensor and the required corrections for climate variation. Therefore in this work the method applied per borehole was determined by the number of logging units available.

Geophysical down-hole temperature logging by Hydroilex Pty Ltd (Hydroilex), using an AUSLOG A645 system with an accuracy of 0.1°C, was conducted in numerous private groundwater bores and old exploration drillholes in the Sydney Basin and has been generously supplied for this study. The geophysical logging has been conducted according to industry standard practice and is not described here. From the WellCad LAS files, temperature at selected depths was extracted.

### Extrapolated down-hole temperatures

The down-hole temperature data gathered in this study is classified into equilibrated and

non-equilibrated measurements based on the time since drilling of the measurement. As there is a disruption to thermal equilibrium of the bore fluid column caused by the circulation of large volumes of fluid during drilling (Beardsmore & Cull 2001), it can take upwards of 10 to 20 times the drilling time (i.e. up to several months) before a hole is equilibrated to within the accuracy of most equipment (Bullard

1947). In addition production or removal of fluids and the very act of logging a hole also disturbs the bore fluid, although the magnitude is significantly less than for drilling (Beardsmore & Cull 2001).

The existing temperature data from coal and petroleum exploration holes has been collected within several days of the completion of drilling and is classed as non-equilibrated.

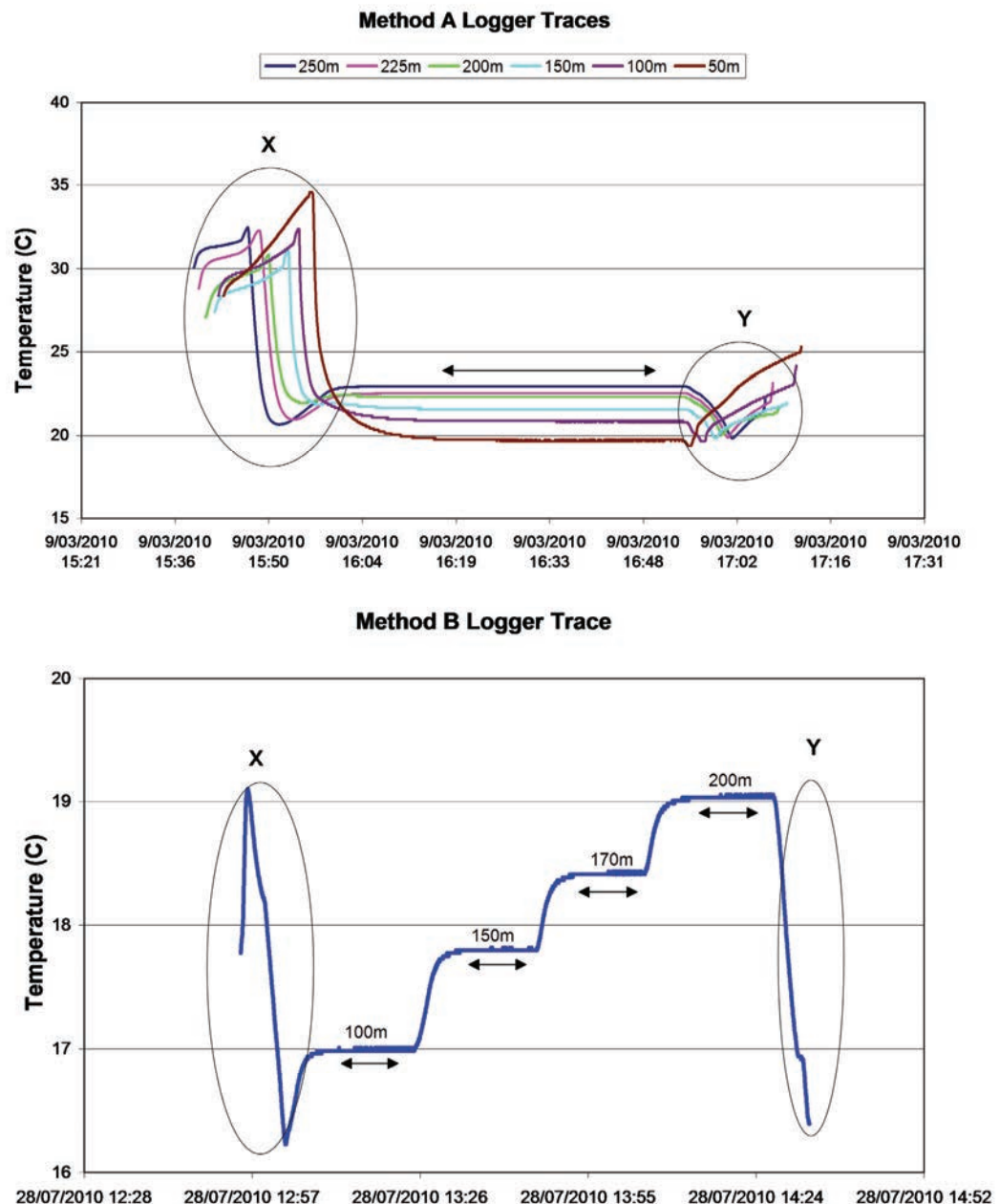


**Figure 2** Example of logger traces for down-hole temperature measurement using methods A and B. Stable temperatures occur when graph flat lines as marked by the arrows, circle X reflects logger prior to and descending into the water column and circle Y reflects logger during extraction and prior to download.

equilibrated if taken one month or greater after drilling, based on the 1 day average drilling time for most boreholes. From the data, 134 results are classed as non-equilibrated and 59 are classed as equilibrated with their distribution across the Sydney Basin shown in Figure 3. All temperature data was corrected for climatic variations, based on Cull (1979) assuming a present surface temperature of 15°C, an ice age surface temperature of 10°C, and that glaciation began 12,000 years ago and ended 8000 years ago, prior to extrapolation.

The extrapolation to depth is based on the 1D two-layer extrapolation models used by Chopra & Holgate (2005), where the geothermal gradient of the sedimentary cover is determined by straight-line interpolation between the surface temperature and the measured temperature at depth of the bore. Then the gradient is extrapolated to estimated basement depth, below which a uniform geothermal gradient of 25°C/km is applied for basement rocks to the required total depth. To calculate the geothermal gradients of the sedimentary cover in this study the temperature measurements are graphed and a linear fit is applied, as shown in Figure 4, to obtain the temperature gradient (m) and the intercept temperature (b). A review of long-term groundwater monitoring in boreholes of Ulan Coal Mines Ltd (UCML) and the Sydney Catchment Authority (SCA) found that below ~70 to 100 m, recorded temperature remains constant between seasons (Figure 5). Therefore, where possible, temperatures from below 100 m ground surface were used to minimise the affects of diurnal/seasonal temperature influences. Where only one temperature measurement was present, as for bottom-hole temperature measurements common in drill stem tests, a surface

temperature average of 15°C is used, based on the yearly average surface temperature for the Gunnedah Basin (Cull 1979), to calculate the geothermal gradient. A geothermal gradient of 25°C/km, as per Chopra & Holgate (2005), was applied for crystalline basement down to 5 km. The thickness of the sedimentary cover was extracted from the 3D geological model of Danis *et al.* (2011) rather than the OzSEEBASE crustal sediment thickness model (FrOG Tech 2006), which is used for the OzTemp interpreted temperature at 5 km depth map (Figure 1).

The extrapolated temperature is calculated at each borehole using the following equation:

$$T = m \times A + b + 25 \times (B - A)$$

where  $T$  = temperature at extrapolation depth in °C,  $m$  = is the temperature gradient from the equation of the linear fit (see Figure 4) in °C/km,  $A$  = thickness of sediment in (km),  $b$  = intercept (surface) temperature from the equation of the linear fit (see Figure 4) °C,  $B$  = extrapolation depth (km),  $25$  = geothermal gradient of crystalline basement (°C/km).

The boreholes of the equilibrated and non-equilibrated datasets of this study with the calculations for extrapolated temperatures at 500 m and 5 km and the bottom-hole or deepest temperature of each borehole are listed in the Appendix (Tables A1, A2). In the OzTemp well database for the Sydney Basin there are 62 boreholes with temperature measurements, all of which can be classified as non-equilibrated, and are contained within our non-equilibrated database. Temperature contour maps (Figure 6) were created from the extrapolated data in Surfer v9 (provided by Golden Software Pty) for the depths of 500 m and 5 km using kriging and a 0.05 degree grid.

### Numerical Thermal Modelling

A series of 2D thermal models were developed using the finite element code *Underworld* (Moresi *et al.* 2007) for 15 east–west model profiles across the Sydney Basin. The geological structure of the thermal models was

taken from the 3D Sydney Basin geological model in Danis *et al.* (2011), which was created from borehole constrained gravity models. An example of the thermal model setup is shown in Figure 7.

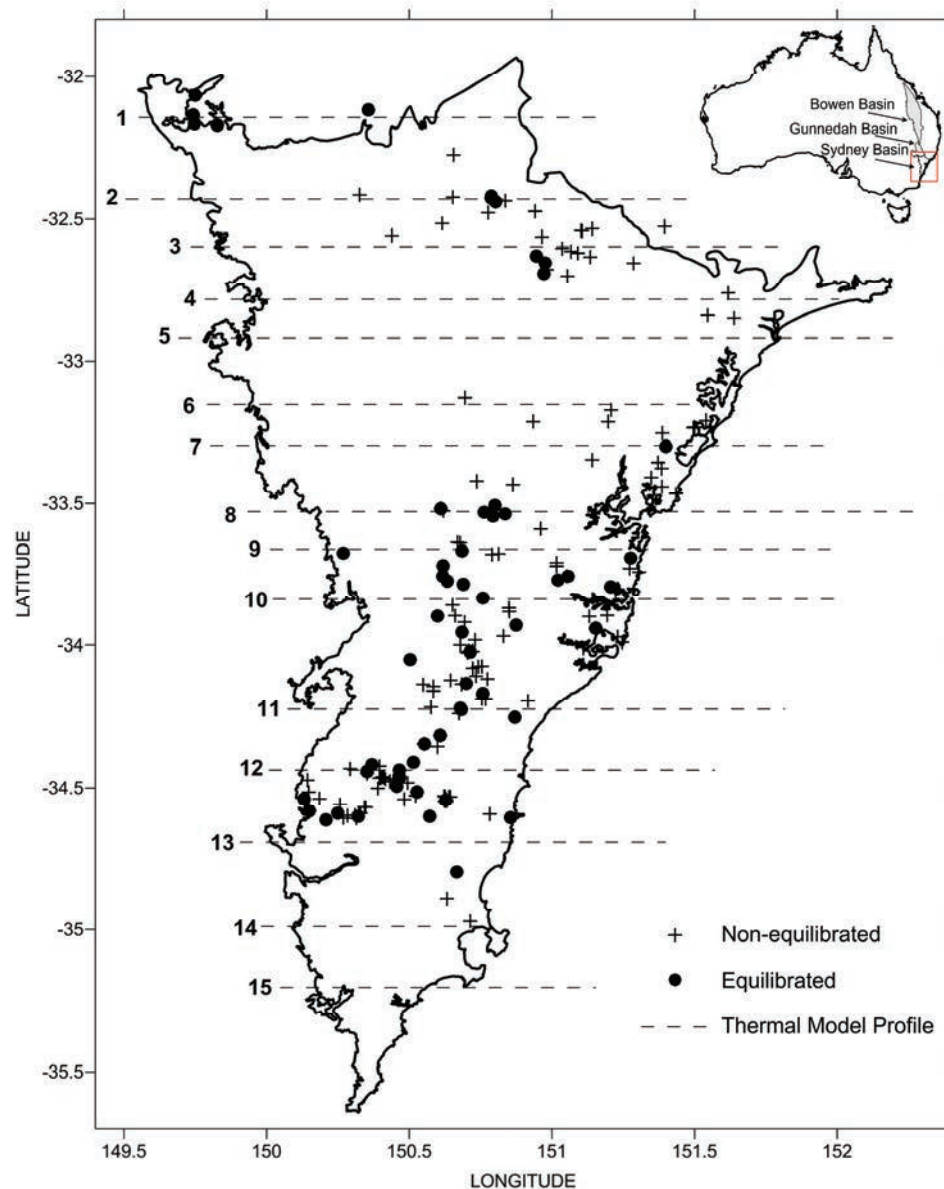


**Figure 3** Sydney Basin showing location of the thermal model profiles and all boreholes with recorded temperature. Circles represent equilibrated-temperature measurements, crosses represent non-equilibrated-temperature measurements.



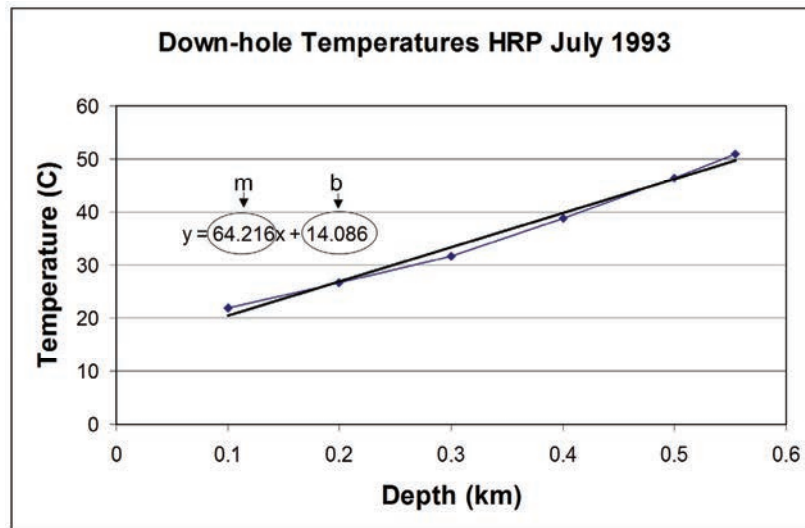


**Figure 4** Measured temperature at depth graph for borehole HPR showing the equation of the linear black line, which is used to calculate the geothermal gradient using  $m$  and  $b$  in Tables 1 and 2.

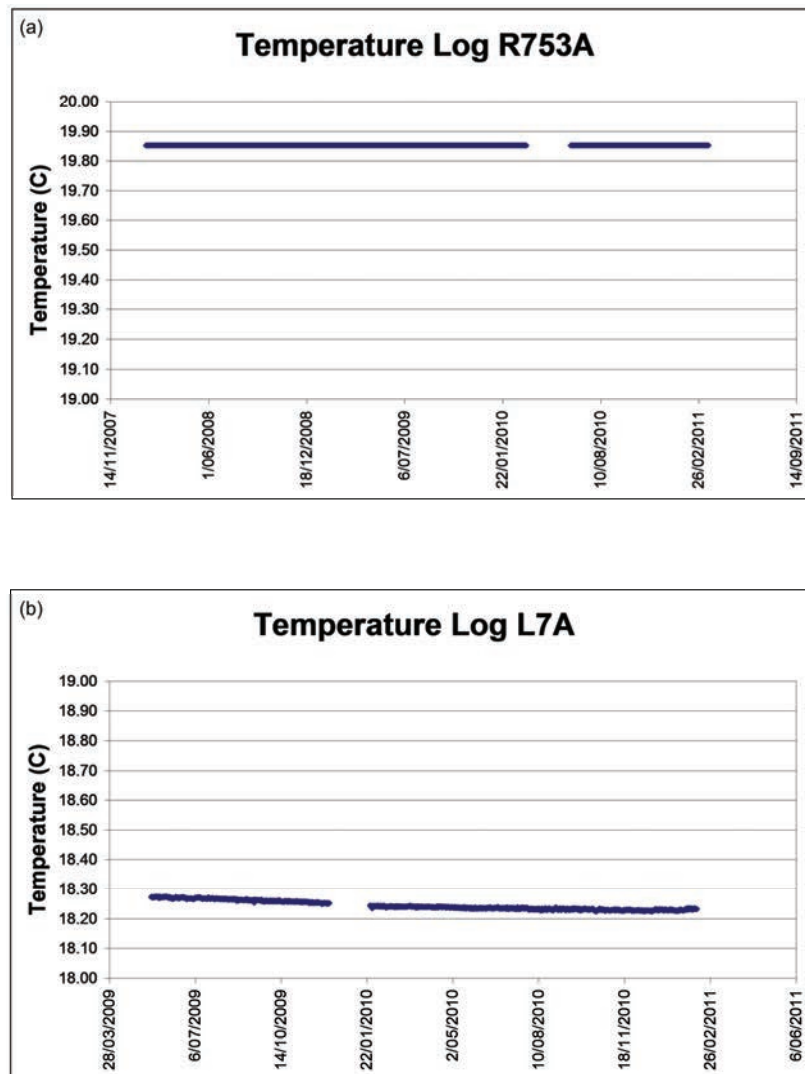


**Figure 5** Temperature logs from long term groundwater monitoring boreholes showing no variation in temperature outside of 0.1 of a degree (a) UCML R753A from January 2008 to September 2009 at 90 m below ground level (b) SCA L7A from May 2009 to February 2011 at 110 m below ground level.

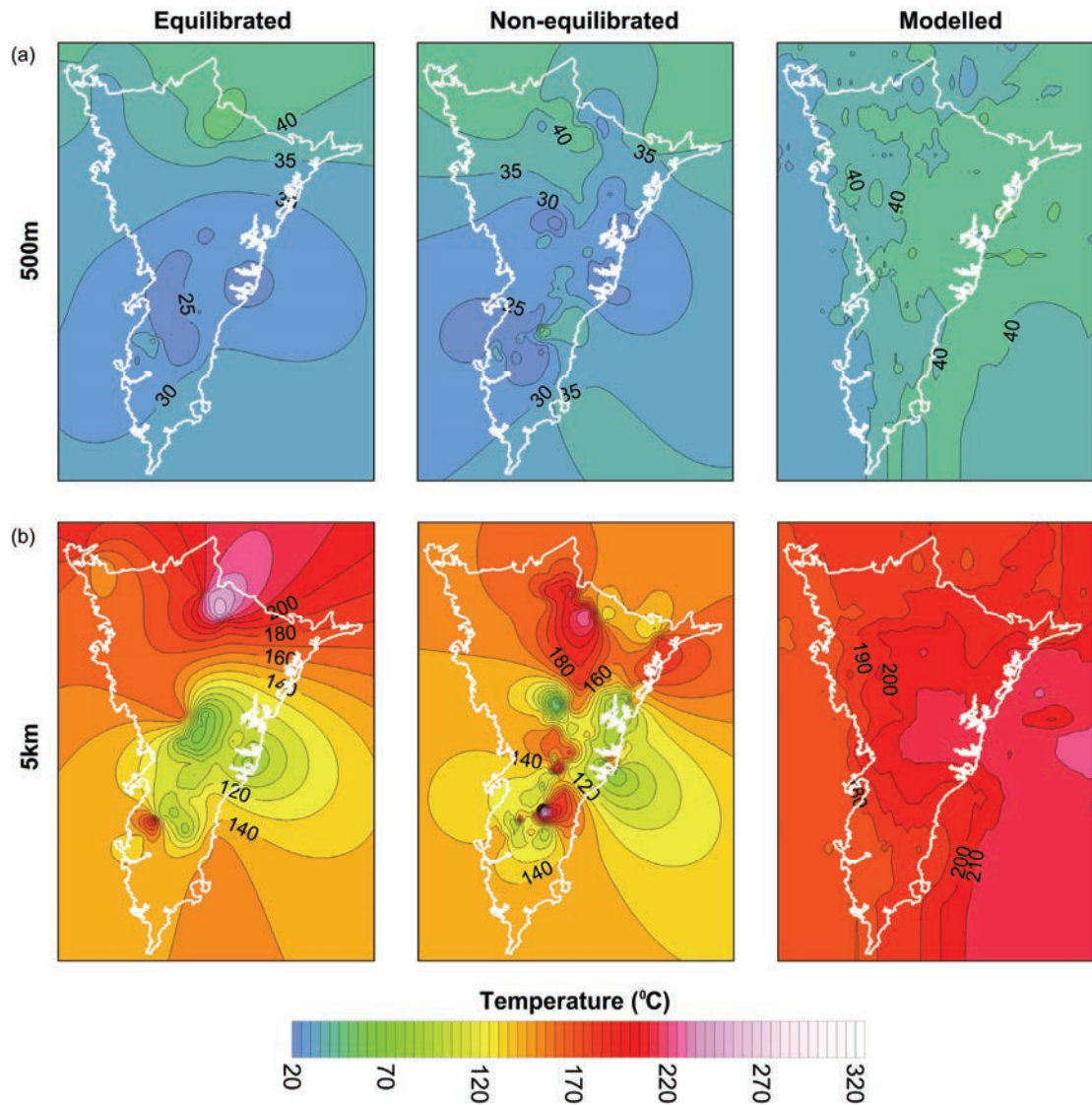


**Figure 6** Temperature contour maps of extrapolated equilibrated and non-equilibrated down-hole temperatures and temperature contour map of numerical model temperatures at (a) 500 m and (b) 5 km.

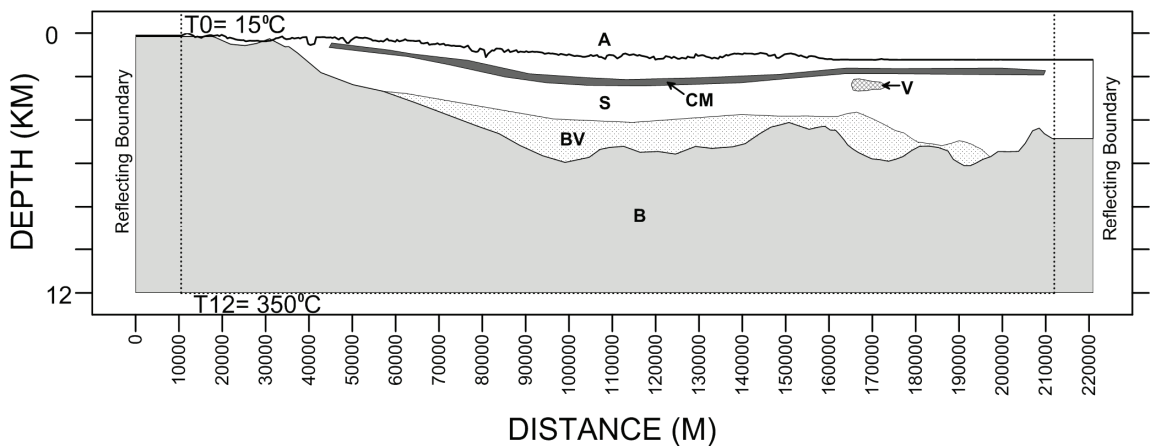


**Figure 7** Schematic of thermal model setup where the top boundary condition  $T_0 = 15^\circ\text{C}$  and the basal boundary condition  $T_{12} = 350^\circ\text{C}$  with reflecting side boundary conditions. The dashed lines represent the limit of the geological model after which an additional 10 km is added to avoid any edge effects. The model is constructed with the following materials A (air), S (sediment), CM (coal measures), V (volcanics), BV (basal volcanics) and B (basement). See Table 1 for thermal properties.

Using *Underworld* we solve the non-steady state heat equation with internal heat sources in two dimensions, given by:

$$\frac{\partial T}{\partial t} = \kappa_m \nabla^2 T + A_m$$

Here T is the temperature, t the time,  $\nabla$  the gradient operator in each orthogonal direction,  $\kappa$  the thermal diffusivity, A the volumetric heat production and m denotes the material. Thermal properties are assigned for each material (Table 1), for the distinct material layers, taken from the 3D geological model of Danis *et al.* (2011).

The *Underworld* models apply a constant top and bottom temperature boundary conditions, with reflecting side boundaries (the

sides are first extended laterally to minimise edge effects with the basin itself). A quasi-material, with a high conductivity, provides direct thermal coupling of the varying topographic surface with the top boundary condition.

The models started with an initial linear temperature profile between the top boundary temperature of 15°C (near the yearly average surface temperature for the Gunnedah Basin; Cull 1979), a basal boundary temperature at 12 km of 350°C and evolve until steady state is reached. The basal temperature was determined from earlier model iterations where the parameter was varied and the resulting geotherms compared to measured equilibrated borehole temperature values.

**Table 1** Thermal Properties of Rock Types used in Underworld. Values derived from Wollenberge *et al.* (1987); Swaine (1990); Clauser & Huenges (1995) and Turcotte & Schubert (2002).

Rock Type	Density (kg/m <sup>3</sup> )	Conductivity (W/m-K)	Heat Production (μW/m <sup>3</sup> )
Basement	2700	3	2
Volcanics	2950	3	0.5
Sediments	2460	2	1.25
Coal Measures	1900	0.3	1.25

The thermal properties for each material, shown in Table 1, are derived from published average value ranges for a particular material type. The coal interval is an aggregate of averages of the percentage of each rock type in the package, of which coal comprises less than 10%. Over the temperature range considered (15 to 180°C), the thermal conductivity of the intrusive crystalline rocks varies to about 80% of their surface value (Clauser & Huenges 1995), and that of sedimentary rocks to ~67% the surface value. We model this by assuming all intrusive rocks

at temperatures above 100°C have conductivities 85% of their surface values (Table 1), whilst all sedimentary above 100°C have a conductivity of 75% their surface value. Clauser & Huenges (1995) did not observe a systematic change in the conductivity of volcanic rocks over this temperature range. Heat production in the basement is derived from representative Lachlan Fold Belt granites in the OZCHEM database (<http://www.ga.gov.au/oracle/index.jsp#geochm>; Budd, 2007). Other heat production values are taken from average values for each lithology

(Table 1; Wollenberg & Smith 1987; Swaine 1990; Turcotte & Schubert 2002).

The 2D thermal field is solved for each of the 15 profiles. The models evolve from the initial conditions until the temperature field and surface heat flow reach a steady-state defined by the heat flux across the system, and internal heat production in each section. The models are preliminary estimates of the thermal structure of the Sydney Basin and as such consider thermal conduction only. They do not take into account advection of heat or the effects of varying surface temperature conditions. The temperature isotherms for all model profiles, overlain with model geometry, are shown in Figure 8. Contoured temperatures maps of the thermal modelling results at 500 m and 5 km (Figure 6), were created using kriging interpolation gridding in Surfer.

Figure 9 shows the results of the model geotherms with temperature measurements in nearby boreholes that are equilibrated. An uncertainty buffer of  $\pm 10^{\circ}\text{C}$ , is applied for the accuracy of the field temperature measurement and the uncertainty of the climate correction. These boreholes provide shallow thermal constraints on the model temperatures and allow calibration of the *Underworld* models.

A comparison between the numerical modelled temperature at 5 km, the extrapolated non-equilibrated temperatures at 5 km and OzTemp interpreted temperature at 5 km for the Sydney Basin is shown in Figure 10.

## RESULTS AND DISCUSSION

The thermal structure of the Sydney Basin is best assessed through numerical modelling, which has the ability to incorporate the effects of architecture and geology. The inherent limitations of temperature extrapolation

preclude it from presenting a comprehensive basin-wide assessment is discussed below.

The non-equilibrated temperature extrapolation map was created to show the methodology used produces comparable results with the OzTemp interpreted map, specifically in terms of anomaly location, even with additional measurements and using the geological model of Danis *et al.* (2011) over the OzSEEBASE model of FrOG Tech (2006). Three distinctive anomalies are observed (Figure 10), one near the north-eastern boundary of the basin (around the Singleton to Muswellbrook area) and two in the southern part of the basin.

To determine whether using equilibrated temperature measurements, instead of non-equilibrated measurements improved the results, temperature contour maps (Figure 6) were created at depths of 500 m and 5 km. What is observed is that the equilibrated temperature map, at 500 m and 5 km, estimates temperatures generally lower than the non-equilibrated map, particularly in the central part of the Sydney Basin where sediment thickness is greatest. Looking specifically at the 5 km map where sediment thickness is greatest, i.e. in the central part of the basin, the equilibrated-temperature map shows temperatures of  $\sim 110^{\circ}\text{C}$ , whilst near the north-eastern edge of the basin, maximum temperatures are over  $250^{\circ}\text{C}$ . The non-equilibrated-temperature map shows temperatures of up to  $160^{\circ}\text{C}$  in the centre of the basin and around  $220^{\circ}\text{C}$  near the north-eastern edge.

The temperature pattern observed on the equilibrated-temperature map was an unexpected feature, which resulted from the vast majority of measurements being collected in shallow (generally less than 500 m deep)



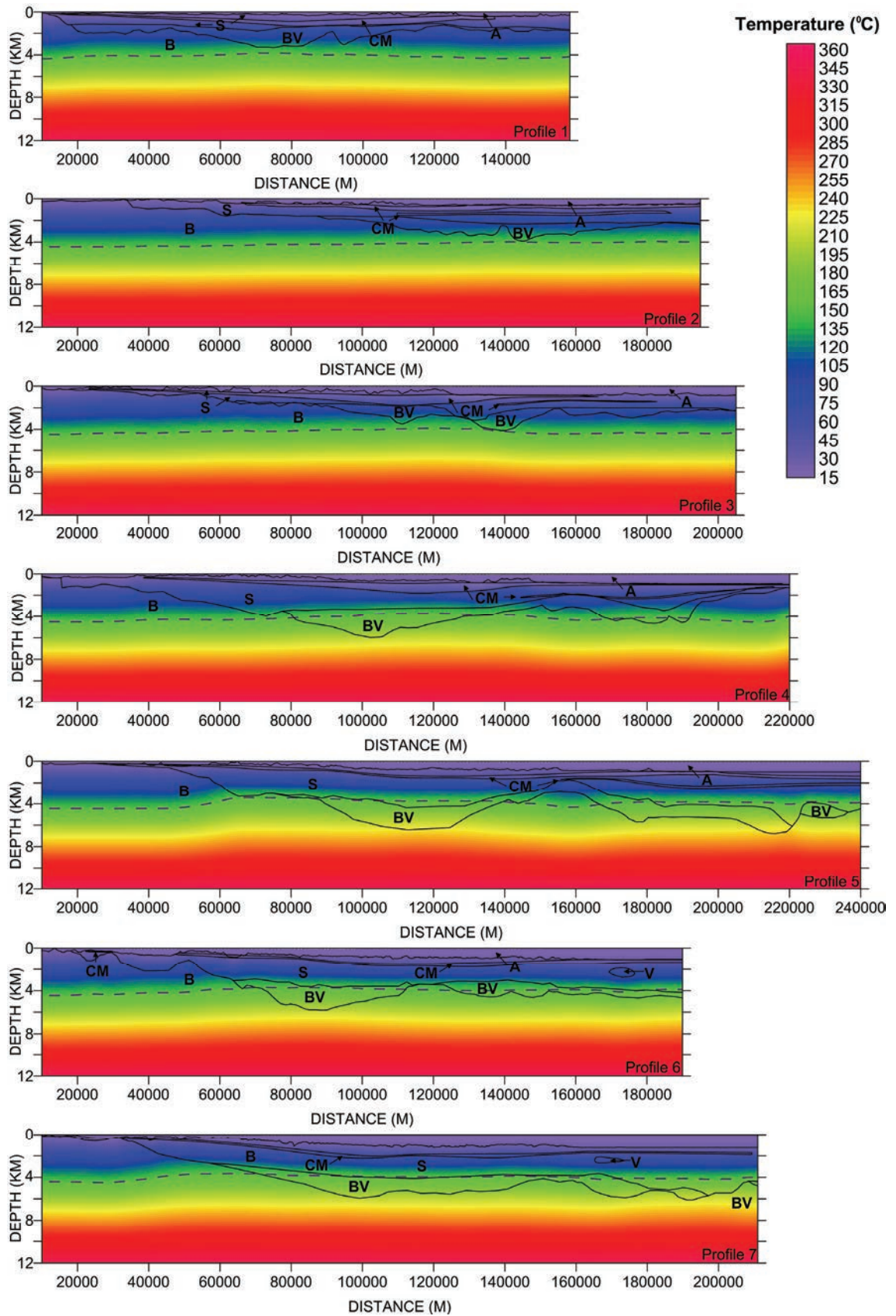


**Figure 8** Modelled temperature field for 2D slices through the Sydney Basin, at the locations shown in Figure 3, with the 150°C temperature contour (dashed line). The model geometry (dark lines) is from the Sydney Basin 3D geological model of Danis *et al.* (2011), with model materials labelled as per Figure 7.

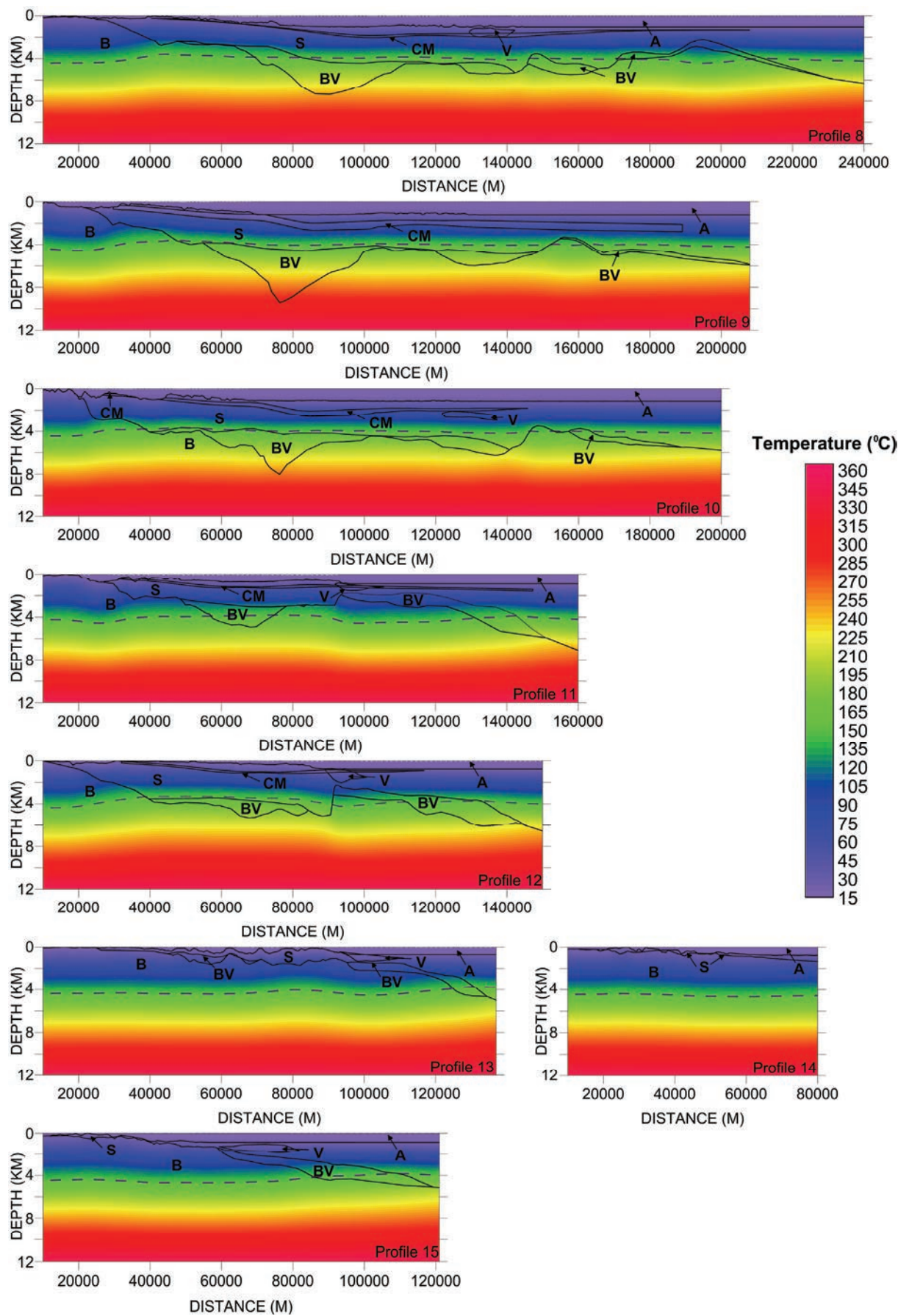
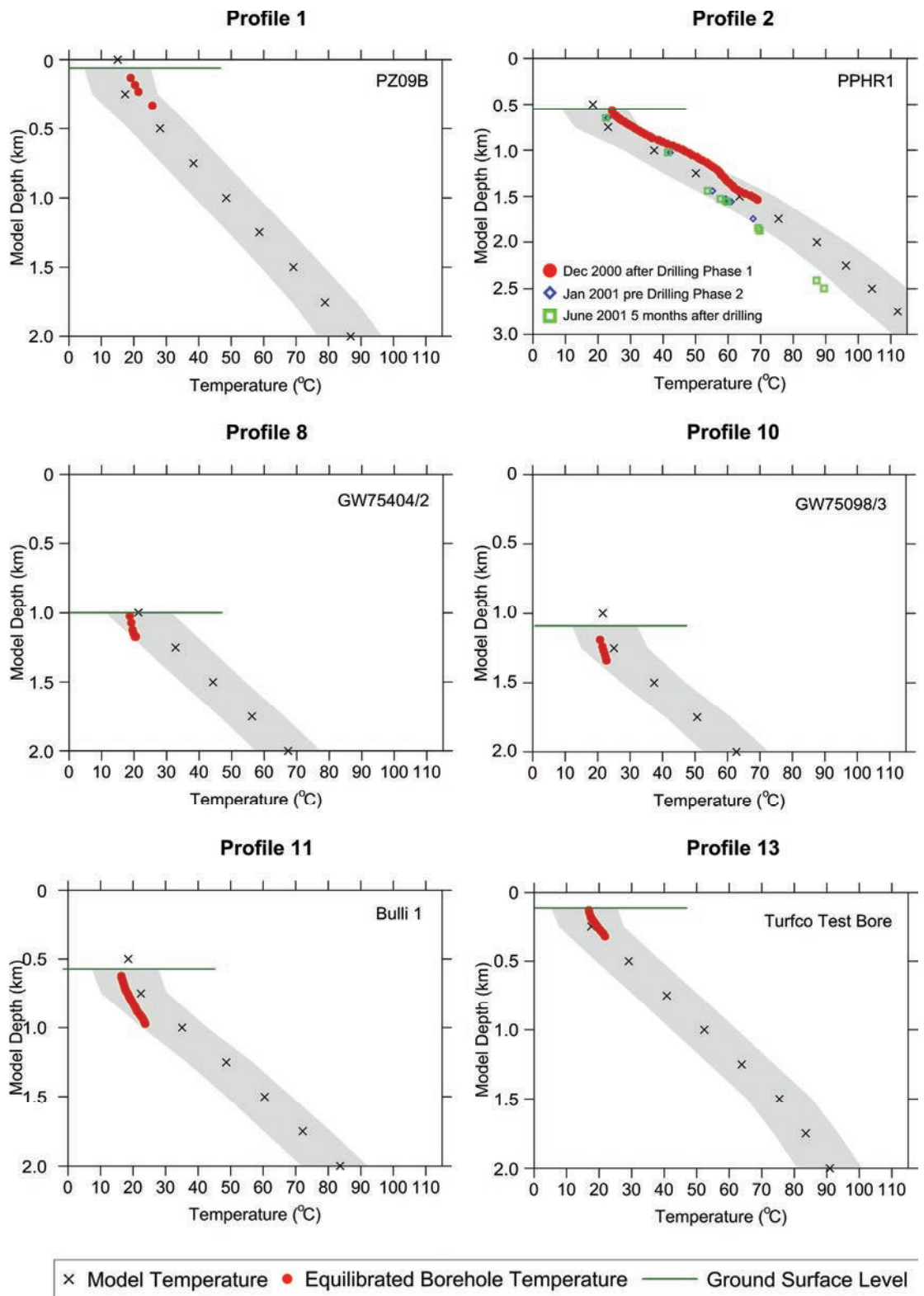
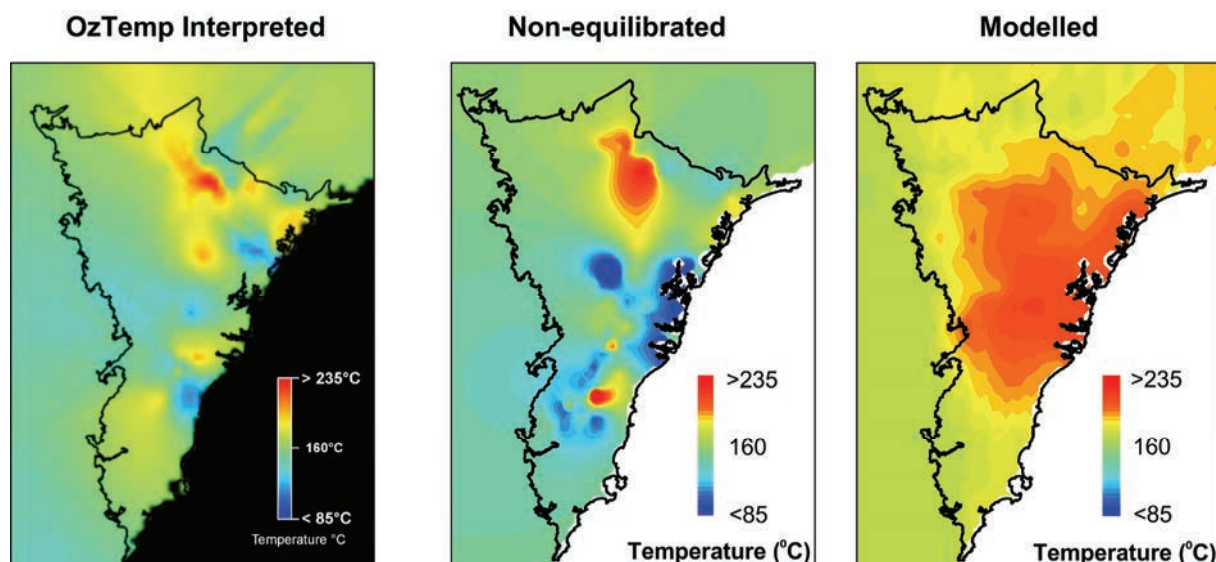


Figure 8 (Continued)



**Figure 9** Geotherm calibration checks using shallow equilibrated borehole temperatures for six selected profiles. Ground surface (green line) varies from model depth zero depending on topography. The equilibrated borehole used is named on each plot. Grey shaded area represents the  $\pm 10^{\circ}\text{C}$  uncertainty for comparing the geotherms and measured temperatures. Note: the June 2001 temperature for PPHR1 in Profile 2 is outside the uncertainty error, this is likely a result of the borehole being cleaned prior to logging thus resulting in a lower than expected temperature; temperatures in Profiles 8 and 10 may be affected by shallow groundwater interactions and Bulli 1 in Profile 11 may not be fully equilibrated.





**Figure 10** Comparison of temperature at 5 km depth between the OzTemp interpreted, non-equilibrated extrapolation and numerical thermal modelled maps.

boreholes located above the major coal-bearing formation. Previous thermal modelling by Danis *et al.* (2010) showed that coal bearing formations provide thermal insulation and the resultant surface heat flux is lower than in areas where they are absent. Therefore on the north-eastern edge of the Sydney Basin estimates of temperature in the equilibrated temperature contour map do appear higher compared to the non-equilibrated-temperature map as a result of heat refraction around the insulating coal measures.

The limitation of the extrapolated temperature method in estimating temperature at depth is clearly demonstrated in Figure 6 with the results of the numerical thermal models. When the extrapolated-temperature maps are compared to the numerical thermal model temperature contour map at 500 m the difference between the extrapolated and modelled temperatures is small, on the order of 10°C to 15°C, but the shape of the contours is different. In the extrapolated-temperature maps the contours are primarily clustered around the centre of the basin, biased by the

distribution of the temperature data (Figure 3), whilst the numerical thermal models cover the entire width of the basin. At 5 km the difference between the extrapolated and modelled temperatures is far more pronounced.

Although the methods of construction are different, a comparison of the estimated temperature at depth can be made between the extrapolated and modelled temperature contour maps. The distinctive 'isolated' anomalies featured in the extrapolated-temperature maps, a result of data clustering, are not expected to be present in the modelled thermal contour map. The modelled temperatures at 5 km show maximum temperatures in the centre of the Sydney Basin, where sediment is thickest, and a temperature range of 170°C to 215°C. The temperature range for the extrapolated-temperature maps is approximately 65°C to 250°C for the equilibrated-temperature map and 50°C to 220°C for the non-equilibrated-temperature map. In the extrapolated-temperature maps areas where sediment is thickest do not always display higher temperatures.



The temperature range and distribution of the extrapolated-temperature maps, which exhibits lows in the centre, and highs on the edge of the basin, is an expected feature that ties in with the effects of insulating coal measures and sediments and the refraction of heat. It is expected that temperatures above a coal measure would be cooler than those below. The problem with the extrapolated-temperature maps is that temperatures are recorded in boreholes that mostly do not penetrate the coal measures, thus when extrapolated in a two-layer model cooler temperatures at depth result. Boreholes that record temperatures below the coal interval are non-equilibrated and are likely responsible for the high temperature anomalies in the central parts of the Sydney Basin on the non-equilibrated-temperature map. In the numerical thermal models, high temperatures occur under areas of greatest sediment thickness, primarily in the central part of the Sydney Basin and under insulating coal measures.

The previous numerical thermal modelling of the Gunnedah Basin (Danis *et al.* 2010) identified basin architecture and the refraction of heat around the insulating coal interval to be a major controlling factor of the thermal profile. In Figure 8 the temperature isotherms of the numerical model profiles of the Sydney Basin, for which geology and basin structure are shown with the 150°C temperature contour marked, illustrate how structure, particularly the coal interval, changes the depth of the 150°C contour. Under the thick package of coal measures and sediment the temperatures are elevated, as shown by the contour line, compared to outside the basin in the Lachlan Fold Belt. In Figure 8 many profiles show the deflection of the 150°C contour on the western edge of the basin (e.g. Profile 8) as a result of the thinning and termination of the coal

measures. This refracted heat would influence measured down-hole temperatures, which if used in a vertical temperature extrapolation, may lead to overestimation of the temperature at depth.

A 1D two-layer extrapolation model poorly takes into account the thermal effects of basin architecture and shallow temperature measurements have a tendency to propagate near surface features to depth and create false anomalies (both highs and lows). However, topography and groundwater, also need to be considered, as these both have an impact of the thermal structure of the basin and in the case of groundwater may affect the temperature measurements used for extrapolation.

In the Sydney Basin, the ground surface elevation ranges from just below sea level, 0 mAHD, to over 1200 mAHD (i.e. Blue Mountains in the west and Liverpool Ranges in the northwest). The numerical thermal model temperature contour map is constructed from the temperatures at 5 km below ground surface level. If temperatures were taken from 5 km below sea level then temperature estimates would be higher in the parts of the basin with the greatest elevation i.e. the effect of an additional 1 km of sediment cover creates temperatures under the Great Dividing Range (and Liverpool Ranges on the northwestern boundary) 15°C higher. From a geothermal exploration viewpoint, defining temperature at depth below actual ground surface is critical for assessing the viability of a drilling program and the effect of variable topography.

The effect of groundwater on thermal structure is not fully assessed in this study; however some observations are significant. Our numerical thermal models consider conduction only and do not model advective

heat transfer by aquifers. For slow flow rates this approximation is valid. Shallow aquifers in the Sydney Basin have been widely studied and utilised (i.e. Hawkesbury Sandstone; Tammetta & Hewitt, 2004) but the nature, extent, volume and flow rate of deeper aquifer systems remain largely unconstrained. Given the decrease in permeability of rocks with pressure, the thermal effects of aquifer heat transport at depth should be less important, but this is an area that deserves greater attention in future geothermal studies. From SCA monitoring data for the Hawkesbury Sandstone (predominantly a semi-confined to confined aquifer system with three main aquifers), this study observed direct rainfall recharge has a delayed temporary decrease in groundwater temperature following a rainfall event particularly in the upper part aquifers as rainfall recharge occurs. Another factor to be considered is groundwater extraction from the aquifer may have an impact on the temperature by creating groundwater gradients that move cooler recharge water at a faster rate than natural flow paths. It is not possible to differentiate between seasonal/diurnal temperature variations and those created from rainfall recharge or pumping, especially in the upper aquifer of the Hawkesbury Sandstone. However repeated measurements in the lower parts of the aquifer showed that, within the accuracy of the logging unit, there are no obvious variations. Therefore, with many equilibrated-temperature measurements taken in groundwater bores of the Triassic Hawkesbury Sandstone aquifer, the use of data from the upper aquifer should be carefully considered in numerical models.

The thermally insulating coal measures appear to have a more significant affect on temperatures measured in Permian aquifers. In these deeper confined aquifers groundwater

flow rates are much slower and the recharge source is more distant thus the effect of groundwater on thermal structure appears minimal. Repeated measurements in Permian aquifers at Ulan over 3 years showed no variation outside of the accuracy of the logging unit.

Our numerical thermal models are calibrated against equilibrated temperature measurements from both Hawkesbury Sandstone and Permian aquifers, as shown in Figure 9. Here a good correlation, i.e. within the  $\pm 10^{\circ}\text{C}$  uncertainty range, occurs between measured temperatures and modelled geotherm temperatures for all profiles, but specifically Profiles 1 and 13, which are in Permian aquifers. Profile 2, also in a Permian aquifer, contains three sets of measurements of which the June 2001 shows a poor correlation with the model geotherm, as a result of the borehole being flushed with water prior to the temperature measurement. The level of disturbance and the introduction of fluids of a lower temperature resulted in a measurement that is lower than the true temperature of the formation. Profiles 8 and 10 are from bores in the Hawkesbury Sandstone aquifer and although they show a reasonable correlation with the model geotherm, groundwater may be influencing the temperatures recorded. Profile 11, from a Permian borehole near the coast, shows a reasonable correlation with the model geotherm, but with the measurements taken about a month after drilling this bore may not be fully equilibrated.

The numerical modelled estimated temperature map (Figure 10) shows that, for the Sydney Basin, temperatures at 5 km are likely to be greater than  $200^{\circ}\text{C}$  for a large portion of the basin. This is directly a result of the thick sediments and insulating coal

measures. A clearer understanding of the thermal structure of the Sydney Basin, achieved with numerical models, suggests portions of the Sydney Basin are highly prospective for geothermal exploration.

## CONCLUSION

Multi-dimensional numerical thermal modelling methods, like *Underworld*, provide a comprehensive assessment tool for defining the thermal state of sedimentary basins. In the Sydney Basin the 2D *Underworld* models provide a realistic estimate of temperature at depth, by accounting for basin architecture, geology and rock thermal properties, and are supported by actual measured equilibrated down-hole temperatures. The numerical modelling estimates temperature at 5 km depth to be greater than 160°C for the Sydney Basin, with temperatures exceeding 230°C for the vast majority of the basin, reflecting areas of thick sediment cover and insulating coal measures.

Temperature extrapolation maps are misused, particularly in geothermal exploration, and their limitations not always considered. These maps produce 'isolated' temperature anomalies at depth, often a function of data type and distribution and propagated shallow surface features. The 1D two-layer extrapolation method is too simplistic and does not account for the geology, architecture and thermal structure of the basin, particularly the influence of refracted heat from insulating coal measures and lateral variations. Our results have shown a comparative replication of the OzTemp interpreted temperature at 5 km map, using non-equilibrated temperatures, and highlight that even with over 70 additional measurements the same 'isolated' anomalies occur. Even considering the best down-hole measurements, i.e. the equilibrated

temperature, the resultant map is not greatly improved and is still unable to provide a comprehensive basin-scale assessment of thermal structure and temperature. When comparing the estimated temperature at 5 km between the two methods, extrapolation vs numerical modelling, the extrapolated-temperature method overall underestimates the temperature, with differences at times exceeding 100°C.

Geothermal exploration requires accurate estimates of temperature at depth for successful programs. The misuse of extrapolated temperature maps as sole exploration tools provide misleading results, which undervalue geothermal prospectively, especially in the Sydney Basin. Numerical thermal modelling, using the average thermal properties of materials, combined with simple assumptions and a detailed 3D geological model provide the solution for an accurate estimation of temperature at 5 km depth and an understanding of the basin-scale thermal structure.

The numerical thermal model of the Sydney Basin has been calibrated with 'real world' data from the equilibrated down-hole temperature measurements collected in this study. Even without deeper (>1 km) boreholes to collect equilibrated temperature measurements, the models are reliable and provide powerful insights into the lateral variations of temperature within a Sydney Basin.

## Acknowledgements

The authors would like to thank Ulan Coal Mines Ltd, the NSW Department of Environment, Climate Change and Water (DECCW) and the Sydney Catchment Authority (SCA) for allowing access to their piezometers for temperature measurements. C Danis would like to thank Greg Russell

(DECCW), Tony Paull (SCA), Katrina Fyfe, Maureen Danis and Greg Jacques for their assistance in collecting temperature measurements. We also acknowledge the NSW Department of Primary Industries for providing the Sydney Geothermal Data Package. Critical reviews by L. Moresi and A. Budd improved an earlier version of this manuscript. This is contribution no. 766 from the Australian Research Council National Key Centre for the Geochemical Evolution and Metallogeny of Continents (<http://www.gemoc.mq.edu.au>).

O'Neill is supported by Discovery Project DP0880801. The authors acknowledge support from Auscope Simulation and Modelling (SAM).

## REFERENCES

- BEARDSMORE G. R. & CULL J. P. 2001. *Crustal heat flow: a guide to measurement and modelling*. Cambridge University Press, 324p.
- BUDD A. R. 2007. Australian radiogenic granite and sedimentary basin geothermal hot rock potential map (preliminary edition), 1: 5 000 000 scale. Geoscience Australia, Canberra.
- BUDD A. R., BARNICOAT A. C., AYLING B. F., GERNER E. J., MEIXNER A. J. & KIRKBY A. M. 2009. A geothermal play systems approach for exploration. *In*: Budd A. R. & Gurgenci H. eds. *Proceedings of the 2009 Australian Geothermal Energy Conference*, Geoscience Australia, Record 2009/35.
- BULLARD E. C. 1947. The time taken for a bore hole to attain temperature equilibrium. *Monthly notices of the Royal Astronomical Society, Geophysics Supplement* **5**, 127–130.
- CHOPRA P. & HOLGATE F. 2005. A GIS analysis of temperature in the Australian crust. World Geothermal Congress, Turkey, 24–29 April 2005, Abstracts.
- CLAUSER C. & HUENGES E. 1995. Thermal conductivity of rocks and minerals. *In: Rock Physics and Phase Relations, A handbook of physical constants*. American Geophysical Union, pp. 105–126.
- CULL J. P. 1979. Climatic corrections to Australian heat-flow data. *BMR Journal of Australian Geology and Geophysics* **4**, 303–307.
- DANIS C. & O'NEILL C. 2010. A static method for collecting temperatures in deep groundwater bores for geothermal exploration and other applications. *Proceedings of Groundwater 2010 the Challenge of Sustainable Management*, 31 October to 4 November 2010, Canberra.
- DANIS C., O'NEILL C. & LACKIE M. 2010. Gunedah Basin 3D architecture and upper crustal temperatures. *Australian Journal of Earth Sciences* **57**, 483–505.
- DANIS C., O'NEILL C., LACKIE M., TWIGG L. & DANIS A. 2011. Deep 3D structure of the Sydney Basin using geophysical modelling. *Australian Journal of Earth Sciences* **58**, 517–542.
- FROG TECH, 2006. OZ SEEBASE Proterozoic Basins Study, Report to Geosciences Australia by FrOG Tech Pty Ltd.
- GERNER E. J. & HOLGATE F. L. 2010. OzTemp – Interpreted Temperature at 5 km Depth Image. Geoscience Australia, Canberra.
- JAWORSKA J. 2008. Sydney Basin Geothermal Data Package (on DVD-ROM), 1<sup>st</sup> edition, New South Wales Department of Primary Industries, Maitland, NSW.
- MORESİ L., QUENETTE S., LEMIALE V., MERIAUX C., APPELBE B. & MULHAUS H.-B. 2007. Computational approaches to studying non-linear dynamics of the crust and mantle.



*Physics of the Earth and Planetary Interiors*  
**163**, 69–82.

SWAINE D. J. 1990. *Trace elements in coal*.  
Butterworth, London. 278 pp.

TAMMETTA P. & HEWITT P. 2004.  
Hydrogeological properties of the  
Hawkesbury Sandstone in the Sydney  
Region. *Australian Geomechanics* **39**, 93–  
108.

TURCOTTE D. L. & SCHUBERT G. 2002.  
*Geodynamics*. Cambridge University Press,  
Cambridge, 456 p.

WOLLENBERG H. A. & SMITH A. R. 1987.  
Radiogenic heat production of crustal rocks:  
An assessment based on geochemical  
data. *Geophysical Research Letters* **14**,  
295–298.

*Received April 2011 ; accepted July 2011.*

## **APPENDIX A** Tables A1 and A2

**Table A1** List of equilibrated boreholes with temperature extrapolation at 500 m and 5 km. Boreholes in italics use the average temperature at depth from repeat measurements.

ID	Latitude	Longitude	Time Since Drilling	Depth (mbgl)	T (°C)	m (°C/km)	b (°C)	Depth to Basement (A)	Temperature @ 500m	Temperature @ 5km
Brindley Park 3	150.35710	-32.11797	9 months	115.650	24.032	41.445	19.404	2.374	40.127	183.437
Bullii 1	150.87018	-34.25414	1 month	401.600	23.717	23.541	14.229	2.521	26.000	135.550
Cadraday 2	150.20841	-34.61344	3 months	107.970	16.245	18.357	14.316	0.668	23.495	134.880
Cooks Cove 1 <sup>#</sup> *	151.15396	-33.94137	25 months	200.000	19.618	8.324	17.894	3.447	22.056	85.417
Dovedale 1	150.13119	-34.53911	~1 month	88.150	16.343	32.464	13.497	0.427	29.187	141.687
Elanora GC	151.27562	-33.69159	1-10 years	141.500	19.883	17.430	17.380	4.598	26.095	107.573
Frank Attard 1	150.50382	-34.04931	29 yrs	310.860	19.294	16.857	13.829	3.103	22.258	113.564
GBD1	150.97173	-32.69178	~1 yr	240.000	26.783	42.417	15.958	2.980	37.167	192.864
GBD2	150.94618	-32.62935	~1 yr	300.000	32.200	71.745	14.603	2.629	50.476	262.475
GBD3	150.97712	-32.65382	~6 months	378.210	36.694	52.109	17.853	2.967	43.908	223.290
GW273190 <sup>#</sup> *	150.62767	-34.54375	~2 months	230.000	20.161	13.658	16.951	5.247	23.780	82.444
GW40946 <sup>#</sup> *	150.63352	-33.77297	~5 yrs	200.000	18.809	19.217	14.891	3.848	24.500	117.637
GW40953 <sup>#</sup> *	150.60846	-34.31812	~5 yrs	170.000	19.099	16.071	16.359	3.467	24.395	110.403
GW40954/2 <sup>#</sup> *	150.75649	-34.17152	~5 yrs	200.000	19.618	19.123	15.711	3.449	25.273	120.439
GW40969 *	150.75799	-34.17008	~5 yrs	140.000	16.892	17.637	13.507	2.940	22.326	116.860
GW41064 *	150.52717	-34.51396	~3 yrs	140.000	14.867	10.963	13.605	2.940	19.087	97.338
GW41065 *	150.62767	-34.54375	~3 yrs	160.000	15.372	15.998	12.263	5.084	20.262	91.498
GW7093/4 <sup>#</sup> *	150.61780	-33.75578	>1 yr	150.000	18.405	7.280	17.255	5.100	20.895	51.886
GW7095/3 *	150.61876	-33.71976	>1 yr	155.000	17.510	16.796	15.022	5.138	23.420	97.871
GW75098/3 <sup>#</sup> *	150.68985	-33.78416	>1 yr	250.000	22.715	13.000	19.487	6.211	25.987	69.957
GW75142 <sup>#</sup> *	150.59974	-33.89738	~4 yrs	240.000	19.652	17.364	15.485	4.244	24.167	108.076
GW75185 *	150.26902	-33.67464	>2 yrs	175.000	18.856	29.458	13.713	0.184	28.442	139.533
GW75401/2 *	150.83539	-33.53774	>1 yr	175.000	20.403	13.546	18.034	6.087	24.807	73.310
GW75402/2 <sup>#</sup> *	150.76231	-33.53229	>1 yr	175.000	20.284	12.380	18.138	6.256	24.328	64.185
GW75403 *	150.79995	-33.50728	>1 yr	145.000	19.741	11.126	18.153	6.107	23.716	58.420
GW75404/2 <sup>#</sup> *	150.79331	-33.54512	>1 yr	195.000	20.527	12.688	18.018	6.256	24.362	65.992
Highlands GC	150.46511	-34.43741	4 yrs	170.300	15.769	17.344	12.820	2.976	21.492	115.035
Hunter Randwick Park	150.80267	-32.43970	~1 yr	554.500	50.956	64.216	14.086	2.491	46.194	236.757
Jamie Inglis 1	150.68540	-33.95468	3 months	310.000	23.625	17.929	18.359	4.259	27.324	113.240

# Boreholes with averaged logged temperatures

\* Boreholes logged by author

mbgl = meters below ground level

Table A1 (Continued)

ID	Latitude	Longitude	Time Since Drilling	Depth (mbgl)	T (°C)	m (°C/km)	b (°C)	Depth to Basement (A)	Temperature @ 500m	Temperature @ 5km
Jason Gazal 1	150.51487	-34.40948	3 months	187.000	15.833	11.935	13.597	3.264	19.565	95.949
Liverpool Catholic Club	150.87491	-33.92919	>5 yrs	270.000	22.758	16.117	18.424	3.685	26.483	110.689
M&M Vella 1	150.68472	-33.66655	2 months	180.770	21.810	13.111	19.440	6.432	25.996	67.965
Mardi 1	151.39976	-33.29953	1 month	149.510	20.321	22.472	16.936	3.242	28.172	133.740
Muirfield GC	151.02102	-33.76926	18 months	145.000	19.425	16.168	17.099	3.567	25.183	110.593
Pennant Hills GC1	151.05710	-33.75600	16 yrs	178.520	19.660	20.005	16.091	3.492	26.094	123.646
Phillips 1	150.36941	-34.41725	7 months	163.650	18.205	14.109	15.911	2.535	22.966	113.301
PPG8	150.78794	-32.42086	~2 yrs	693.200	50.955	48.952	16.742	2.398	41.218	199.190
PPHR1	150.78794	-32.42686	4 months	1945.500	89.504	35.402	22.154	2.408	39.855	172.200
PZ07A#*	149.74794	-32.16467	> 5yrs	250.000	27.396	51.683	13.750	1.370	39.592	175.319
PZ09B *	149.74244	-32.13470	> 5yrs	280.000	25.741	36.816	15.265	1.757	33.673	161.032
PZ14A *	149.82754	-32.16986	> 5yrs	290.000	25.635	29.051	16.538	1.396	31.064	147.192
PZ26A#*	149.75019	-32.06556	> 5yrs	230.000	26.056	50.879	14.266	1.969	39.706	190.209
R. Mason 1	150.69989	-34.13478	9 months	199.170	21.631	14.070	19.149	3.873	26.184	101.813
Rockdale South 1	150.35249	-34.44167	7 months	120.870	16.936	55.018	10.276	2.449	37.785	208.780
Rowsthorne 1	150.45690	-34.49438	1 month	201.730	17.369	19.081	13.522	2.874	23.063	121.511
Russell Jarvie 2	150.61067	-33.51903	1 month	219.000	18.245	34.045	11.000	3.953	28.023	171.757
Shellharbour Links GC	150.85562	-34.60571	~1 month	200.000	21.981	31.846	15.595	1.584	31.518	151.438
Slade Bore	150.55311	-34.34755	18 yrs	148.140	17.530	13.229	15.499	3.438	22.114	100.027
Southlands 1	150.24993	-34.58946	22 yrs	98.150	15.650	27.258	12.867	1.021	26.496	140.172
St Alloysius Oval Bore	151.20640	-33.79345	16 months	220.260	20.640	13.003	17.758	4.094	24.260	93.642
Summer Dell Farm 1	150.32103	-34.60128	2 months	169.460	18.176	38.959	11.447	1.497	30.927	157.345
The Lanes 1	150.71370	-34.02326	7 months	301.730	23.113	13.549	18.988	4.083	25.763	97.239
Travis 2	150.46679	-34.46348	~3 months	232.360	19.146	18.471	14.739	2.954	23.975	120.450
Turco Test Bore 2	150.66720	-34.79485	3 months	197.360	21.798	34.161	15.088	0.618	32.169	145.748
Twin Creeks 1	150.75865	-33.83412	30 months	215.320	22.451	14.014	19.591	5.916	26.598	79.596
Wilton 1	150.68232	-34.22736	5 months	179.350	19.155	20.042	15.516	4.048	25.537	120.448
Wilton 2	150.67981	-34.22198	4 months	193.330	19.352	19.919	15.514	4.024	25.474	120.070
Winter Hill Run 1	150.15007	-34.58171	11 months	162.850	17.146	31.704	12.104	0.481	27.827	140.327

# Boreholes with averaged logged temperatures

\* Boreholes logged by author

mbgl = meters below ground level

**Table A2** List of non-equilibrated boreholes with temperature extrapolation at 500m and 5km.

ID	Latitude	Longitude	Depth (mbgl)	T (°C)	m (°C/km)	b (°C)	Depth to Basement (A)	Temperature @ 500m	Temperature @ 5km
Appin 1	150.76739	-34.19054	680.00	43.520	41.941	15.000	3.302	35.971	195.947
Appin 2	150.75429	-34.18915	628.00	33.531	29.509	15.000	3.477	29.755	155.676
Appin 3	150.76769	-34.18843	652.40	38.525	36.060	15.000	3.301	33.030	176.507
Austral TNC16	150.58391	-34.14499	101.75	18.016	12.514	16.742	3.310	22.999	100.419
Badgerys Creek 1	150.26919	-34.60683	156.98	18.205	42.697	11.497	1.075	32.846	155.520
Belford Dome 1	151.28586	-32.65481	1154.28	44.042	22.996	23.017	1.839	34.515	144.332
Berkshire Park 1	150.79052	-33.67981	1089.96	44.017	26.622	15.000	7.434	28.311	152.058
Big Adder Hill 1	150.77603	-32.47714	655.00	49.725	47.787	18.588	2.355	42.482	197.261
Boomerang Creek 1	151.20722	-33.17408	1050.00	37.559	27.120	9.077	3.581	22.637	141.669
Bowral C.C. TB1	150.41598	-34.46837	224.56	18.878	15.151	15.446	2.701	23.022	113.847
Camberwell 1	151.10180	-32.54052	1905.00	61.561	24.209	16.094	2.379	28.199	139.212
Camberwell 2	151.10559	-32.54128	1165.10	44.602	22.438	18.240	2.332	29.459	137.264
Campa 1	150.31044	-34.59716	168.52	17.710	25.592	13.018	1.469	25.814	138.888
Cape Three Points	151.43447	-33.46508	451.10	23.107	17.971	15.000	4.004	23.986	111.859
Cardrona 1 (GW72207)	150.34373	-34.56805	108.20	16.752	10.117	15.622	1.893	20.681	112.453
Castlereagh 1	150.66949	-33.63676	1012.00	41.769	26.452	15.000	5.681	28.226	148.248
Cecil Park 1	150.84963	-33.86853	697.69	39.517	35.140	15.000	4.075	32.570	181.318
Cecil Park 2	150.85033	-33.88187	689.46	37.296	32.339	15.000	4.023	31.170	169.522
Comfort Hill 1	150.25697	-34.55815	113.36	16.717	13.185	15.231	1.276	21.824	125.155
Cook Cove 1	151.15396	-33.94137	217.65	20.695	10.969	18.172	3.462	23.657	94.602
Cook Cove 2	151.15321	-33.94379	163.28	19.686	4.352	18.967	3.451	21.143	72.719
Coonemia 1	150.71319	-34.97135	796.75	47.844	41.223	15.000	0.525	35.612	148.519
Cromer Golf Club PB4	151.27304	-33.72866	103.25	19.750	13.189	18.379	4.481	24.974	90.449
Cryon Park 1	150.18543	-34.53840	75.00	16.036	52.624	11.941	0.669	38.253	155.409
Currockbilly 1	150.39551	-34.42381	191.97	17.327	29.963	11.123	2.626	26.105	149.156
Cut Hill 1	150.67907	-34.00004	994.00	40.098	25.556	14.642	4.110	27.420	141.927
Cut Hill 3	150.73130	-33.98223	716.00	50.626	49.757	15.000	4.283	39.879	246.040
Cut Hill 3A	150.73130	-33.98223	825.80	40.512	31.606	15.962	4.283	31.765	169.257
D.Smith 1	150.31473	-34.60807	136.91	15.161	8.360	13.977	1.438	18.157	115.041
DM Baerami Creek									
DDH02	150.43943	-32.55760	359.00	33.867	43.993	17.952	1.024	39.949	162.401

mbgl = meters below ground level



Table A2 (Continued)

ID	Latitude	Longitude	Depth (mbgl)	T (°C)	m (°C/km)	b (°C)	Depth to Basement (A)	Temperature @ 500m	Temperature @ 5km
DM Surveyors Creek 1	151.54564	-32.84017	490.00	32.005	23.527	20.124	3.928	31.888	139.338
DM Warkworth DDH12	151.03630	-32.60310	500.00	46.240	52.636	18.189	3.124	44.507	229.534
DM Warkworth DDH13	151.09110	-32.61900	210.00	26.851	32.252	19.675	2.511	35.801	162.883
DM Warkworth DDH17	151.06650	-32.61320	280.00	30.559	33.301	20.737	2.866	37.388	169.525
DM Whybrow DDH2	150.98229	-32.67746	610.00	47.236	52.847	15.000	3.014	41.424	223.933
Downs 1	150.28325	-34.59881	162.11	16.497	13.791	14.265	1.261	21.161	125.127
Duncans Creek 1	150.66058	-33.89651	1257.00	53.641	30.280	14.732	4.529	29.872	163.646
Dunsmore 1	150.44338	-34.47462	185.58	18.444	13.298	15.950	2.917	22.599	106.816
Dural South 1	151.01615	-33.70843	3061.72	93.331	24.010	22.114	3.625	34.119	143.525
East Maitland 1	151.61766	-32.76098	3017.52	84.997	13.903	37.554	3.024	44.506	128.999
Eddie Ross 1	150.58394	-34.16072	108.99	17.299	7.593	16.460	3.271	20.256	84.517
Elgin 1	150.32940	-34.59078	151.50	17.069	12.363	15.204	1.617	21.386	119.769
Elgin 2	150.32360	-34.58881	175.76	17.910	33.114	11.630	1.593	28.187	149.560
Elizabeth Macarther 01V	150.73442	-34.10850	585.53	31.524	25.879	15.717	3.667	28.657	143.940
Erina Oval	151.38619	-33.43987	159.91	19.906	15.663	17.304	3.744	25.136	107.344
Gary Chapman 1	151.11042	-34.00987	160.25	19.651	8.936	18.234	2.947	22.702	95.889
Glenelg 1	150.49388	-34.48207	210.00	20.361	15.430	17.121	3.068	24.836	112.756
Glenlee 4	150.75496	-34.07399	654.38	32.525	22.317	18.185	3.746	29.344	133.133
Glenlee 6	150.74212	-34.07523	877.66	40.918	23.543	18.338	3.779	30.110	137.833
Goulburn River 1	150.65345	-32.42365	564.00	46.052	52.430	15.490	2.243	41.705	202.024
Goulburn Valley 2	150.32610	-32.41620	410.00	41.632	40.632	24.552	0.983	44.868	164.924
Griffiths 1	150.41050	-34.46338	96.60	13.541	18.106	11.811	2.745	20.864	117.884
GW040945	150.60846	-34.31812	200.00	19.506	22.528	15.000	3.849	26.264	130.486
GW040954/2	150.60846	-34.31812	200.00	20.681	23.766	15.952	3.849	27.835	136.203
GW040969	150.52717	-34.51396	200.00	16.691	16.837	13.266	2.937	21.685	114.291
GW041064	150.63051	-34.53976	145.00	14.473	11.162	12.840	2.993	18.421	96.419
GW041067	150.63094	-34.54657	175.00	24.024	13.182	21.757	2.906	28.348	112.417
GW041068	150.62405	-34.54750	160.00	12.869	3.713	12.255	2.891	14.111	75.724
GW40972	150.62193	-34.52893	170.00	15.519	18.671	12.279	3.133	21.615	117.451
GW40973	150.62569	-34.52983	145.00	14.723	13.030	12.821	3.120	19.336	100.470

mbgl = meters below ground level

Table A2 (Continued)

ID	Latitude	Longitude	Depth (mbgl)	T (°C)	m (°C/km)	b (°C)	Depth to Basement (A)	Temperature @ 500m	Temperature @ 5km
GW40992	150.63899	-34.53128	130.00	14.638	11.710	13.134	3.107	18.989	96.844
GW40993	150.64364	-34.53064	130.00	14.678	11.103	13.295	3.115	18.847	95.005
Hawkesbury Bunnerong 1	151.23006	-33.97023	1122.00	53.585	30.358	16.084	3.607	31.263	160.413
Hawkesbury Everleigh 1	151.19387	-33.89588	1295.00	60.658	31.917	14.410	3.849	30.369	166.035
Hawkesbury Lisarow 1	151.38463	-33.37579	975.00	47.537	35.838	10.772	3.518	28.691	173.897
Hawkesbury Munnorah 1	151.49944	-33.23289	260.00	25.247	39.155	14.992	3.618	34.570	191.199
Hawkesbury Munnorah 2	151.50017	-33.23417	269.00	23.539	32.255	13.957	3.632	30.085	165.308
Hawkesbury Munnorah 3	151.49526	-33.23518	245.00	26.260	21.469	20.871	3.614	31.606	133.109
Higher Macdonald 1	150.93394	-33.21370	627.89	41.753	42.608	15.000	2.966	36.304	192.219
Hopewood Farm 1	150.39580	-34.46440	211.51	16.627	20.504	12.254	2.658	22.506	125.302
Howes Swamp 1	150.69477	-33.13120	2567.33	90.541	28.203	19.570	4.716	33.672	159.675
Hunter Llanillo 1	150.83654	-32.43603	765.80	64.511	64.653	15.000	2.354	47.327	233.351
Hunter Randwick Park 1	150.80267	-32.43970	699.80	47.517	42.207	21.263	2.491	42.367	189.119
Hurdle Ridge 1	150.35233	-34.44843	190.66	17.169	11.452	14.891	2.478	20.617	106.323
Jerry Plains	150.94115	-32.47314	1595.32	60.901	28.837	15.648	2.775	30.067	151.296
Jiliby 1	151.38656	-33.25435	615.09	37.035	31.896	16.659	3.181	32.607	163.593
John Barnfield 1	150.96076	-33.58976	266.11	21.464	19.975	17.709	4.514	27.697	120.027
John Kinross 1	150.39015	-34.50086	107.20	15.821	11.584	14.610	2.448	20.402	106.767
John Reid Castle Hill 1	151.01703	-33.72019	255.54	21.203	15.984	17.099	3.614	25.091	109.512
Johnillo 6	150.64491	-34.12252	696.80	33.327	17.613	19.902	3.773	28.709	117.034
Johns 1	150.46285	-34.46430	171.05	16.398	14.510	13.928	2.939	21.183	108.099
Kay Park 1	150.68342	-34.13603	802.80	38.911	24.567	16.984	3.863	29.268	140.311
Kirkham 1	150.70490	-34.02576	2560.93	71.096	16.970	28.090	4.078	36.575	120.346
Knight 1	151.05402	-32.70095	746.30	53.652	51.435	15.622	2.857	41.340	216.150
Kulnura 1	151.19729	-33.21388	2212.00	79.954	29.364	15.000	3.752	29.682	156.376
Kurrajong Heights 1	150.61962	-33.52688	2782.52	78.327	15.618	30.156	4.211	37.965	115.645
Lake Nepean 1	150.59905	-34.35732	333.80	43.019	71.628	20.543	3.940	56.357	329.262
Lepington Pastoral Co 2	150.69419	-33.91908	334.77	24.365	16.058	19.176	4.613	27.205	102.925
Loder 1	151.13448	-32.63370	2062.58	51.041	16.193	20.324	2.057	28.421	127.208
Long Reef GC1	151.30554	-33.74069	101.97	20.628	20.194	18.572	4.673	28.669	121.115

mbgl = meters below ground level

Table A2 (Continued)

ID	Latitude	Longitude	Depth (mbgl)	T (°C)	m (°C/km)	b (°C)	Depth to Basement (A)	Temperature @ 500m	Temperature @ 5km
Lower Portland 1	150.86356	-33.43268	889.41	40.631	29.975	15.605	5.142	30.593	166.186
Mangrove Creek 4	151.14118	-33.34708	130.87	20.301	16.163	18.186	4.144	26.268	106.570
Martindale 1&1A	150.61529	-32.51596	1178.97	56.275	35.009	15.000	1.942	32.505	159.437
Mooney 1	150.43252	-34.47728	150.52	16.578	39.625	10.283	2.809	30.096	176.364
Moonshine 7	150.67514	-34.24071	585.00	32.544	29.012	14.798	4.091	29.304	156.211
Mt Broughton 4	150.34833	-34.56905	183.30	17.126	7.473	15.742	1.924	19.479	107.022
Mummorah DDH1	151.54000	-33.21000	1621.00	73.888	35.422	16.630	3.617	34.341	179.322
Narellan 1	150.72224	-34.02103	1250.20	58.638	33.212	13.925	4.074	30.531	172.384
Narellan 3	150.70940	-34.01951	1030.00	50.664	48.724	-1.254	4.105	23.108	221.128
North Bulli No. 1	150.72322	-34.08106	402.60	23.797	21.572	15.131	3.784	25.917	127.158
North Castlereagh 1	150.67805	-33.63871	1319.67	54.669	30.700	11.872	5.961	27.222	170.850
Northbridge GC 1	151.22320	-33.81221	200.76	20.034	14.351	17.173	4.214	24.349	97.303
Ourimbah Soccer Oval 1	151.37189	-33.35521	97.55	18.095	8.622	17.244	3.362	21.555	87.184
Paddy Clifton 2	151.34823	-33.40831	183.71	20.705	7.572	19.161	3.552	22.947	82.256
Pennant Hills GC extension	151.05129	-33.75611	254.00	21.037	14.637	17.277	3.494	24.596	106.064
Pinegrove 1	150.96506	-32.56246	510.70	43.665	52.328	17.539	2.669	43.703	215.489
PPHR1	150.78794	-32.42686	442.90	40.161	49.249	17.020	2.408	41.645	200.407
RDH Mummorah 1	151.54000	-33.21000	1621.69	73.889	35.491	16.638	3.617	34.384	179.580
Riverstone 1	150.81305	-33.67695	1537.00	45.766	20.017	15.000	6.998	25.009	105.129
Rosalind Park 07	150.77391	-34.11871	610.67	33.236	24.215	17.551	3.429	29.659	139.859
Russell Jarvie 2	150.61067	-33.51903	225.20	18.325	26.114	12.623	3.953	25.680	142.027
Shoalhaven Ex-ser 1	150.63206	-34.88945	202.11	21.027	18.779	17.332	0.389	27.412	139.912
Siena 1	150.40622	-34.46005	101.13	16.857	53.208	11.598	2.758	38.202	214.388
Singleton 1	151.14114	-32.53342	1296.10	51.659	28.284	15.000	2.103	29.142	146.908
Spring Hill 1	150.52284	-34.52703	218.65	17.802	30.225	10.618	2.869	25.731	150.608
St Michaels GC 1	151.24621	-33.99078	205.00	19.602	6.055	18.224	3.547	21.252	76.031
Steve McGrath 1	150.83045	-33.96842	215.83	22.466	17.255	18.754	3.913	27.382	113.445
Stockyard Mt 1	150.78249	-34.59308	1071.37	48.456	31.636	15.971	1.252	31.789	149.280
Tahmoor Sports Ground 1	150.57614	-34.21922	175.70	18.941	18.796	15.511	3.165	24.909	120.878
Tennessee Orchard TO1	150.55135	-34.34840	291.84	20.732	22.006	14.036	3.427	25.039	128.776

mbgl = meters below ground level

Table A2 (Continued)

ID	Latitude	Longitude	Depth (mbgl)	T (°C)	m (°C/km)	b (°C)	Depth to Basement (A)	Temperature @ 500m	Temperature @ 5km
Trinity Collage	151.13100	-33.89916	181.36	19.349	15.380	16.409	3.595	24.099	106.822
Tugolong Vineyard 1	150.14766	-34.51522	133.50	17.488	19.405	14.899	0.544	24.602	136.855
Upper Colo	150.73609	-33.42084	426.70	13.321	2.073	12.376	5.008	13.413	22.564
Varrowille 2	151.39542	-32.52581	1017.10	53.159	31.421	21.782	1.650	37.493	157.378
Victoria Park 1	150.54868	-34.13728	1261.00	44.088	19.519	19.962	3.043	29.722	128.281
Wallacia 1	150.65237	-33.85877	1118.00	48.472	29.940	15.000	4.362	29.970	161.548
Winchmore Hill 1	150.14334	-34.47266	91.39	15.386	21.787	13.408	0.490	24.335	136.835
Windy Hill 1	151.63846	-32.84990	909.90	49.523	37.941	15.000	3.909	33.971	190.589
Wingecaribbee 1	150.48239	-34.53967	176.55	16.083	24.717	11.529	2.640	23.888	135.782
Winter Hill Run 2	150.15007	-34.58171	214.91	18.137	30.378	11.409	0.481	26.495	138.995
Woodside 1	150.40090	-34.46471	190.00	17.880	2.310	17.413	2.675	18.568	81.721
Moronora 1	150.91567	-34.19630	2313.13	71.633	19.105	28.327	2.321	37.880	139.646
Wybong 1	150.65483	-32.27345	760.00	53.312	42.333	17.824	1.599	38.991	170.537
Yaraandoo 3	150.29242	-34.43272	136.15	15.712	12.885	13.986	2.038	20.429	114.298

mbgl = meters below ground level



# CHAPTER 8

## IMPLICATIONS OF DISTURBANCE AND THERMAL RECOVERY FOR GEOTHERMAL MEASUREMENTS



*Glenbrook Lagoon, Glenbrook NSW*

# **The implication of fluid disturbance and thermal recovery on bottom-hole temperatures for the collection of equilibrated measurements and the need to understand borehole history: a case study on PZ14A, Ulan Coal Mine, NSW Australia.**

**C. DANIS**

*GEMOC ARC National Key Centre, Department of Earth and Planetary Sciences, Macquarie University, NSW 2109, Australia.*

The existing groundwater borehole network in Australia is an excellent resource from which to collect equilibrated bottom-hole temperature measurements, due to its vast area of coverage and history of monitoring data. Equilibrated temperature measurements are critical for the calibration of detailed thermal models for the assessment of thermal structure and geothermal potential. The disturbance of fluid in a bore, as observed in PZ14A, can have a significant affect on thermal structure and result in non-equilibrated temperatures being recorded. To mitigate these issues careful planning, repeated measurements, consideration of groundwater level trends and an understanding of the history of a borehole is required to ensure an equilibrium state is present or determine when thermal recovery to an equilibrium state is likely to be achieved. PZ14A displays a disturbance over approximately 6 months which required a thermal recovery of almost two years.

**KEY WORDS: Sydney Basin, thermal recovery, groundwater, geothermal exploration, temperature measurement.**

## **INTRODUCTION**

The collection of equilibrated down-hole temperature measurements is vital for the calibration of detailed thermal models to assess thermal structure and geothermal potential. High resolution 3D thermal models are effective in producing representative estimates of thermal structure that correlate with real world data. Currently, in Australia, temperature at depth data is available from Geoscience Australia, in the OzTemp database (Holgate & Gerner 2010). The majority of these measurements are from non-equilibrated boreholes for which a Horner plot correction has been applied to approximate the

equilibrated temperature. The problem with this method is that it has been shown (i.e. Deming 1989) to depend strongly on assumptions that may not be justified, and in general most empirical corrections only work within the geothermal field in which they have been derived.

With equilibrated measurements essential, the difficulty is finding boreholes which are in an equilibrium state. Temperature measurements are common in exploration boreholes but these are non-equilibrated results and the bores are often filled in a few days after completion. Groundwater boreholes are constructed for long term use and monitoring, thus they can reach an equilibrium state and be accessed. The existing

groundwater bore network offers huge potential for collecting equilibrated measurements, but an understanding the history of these boreholes, as well as careful choice of measurement method, is still required for valuable results.

Bore fluid disturbance is a major cause of change to thermal equilibrium, either by drilling, pumping or logging, all of which take different amounts of time for thermal equilibration to return. The mixing of fluid in a borehole, which at different depths is different temperatures, results in the temperature measured no longer being representative of the surrounding host rock. The history of activities undertaken in a borehole give guidance in determining whether or not equilibrium is present. For example, during the drilling process large volumes of fluid are circulated within the borehole and as a result the length of time the borehole needs to be left undisturbed to reach equilibrium is, according to

Beardsmore & Cull (2001) upwards of 10 to 20 times the drilling time. Another process that causes disturbance is the removal or addition of fluids through activities such as pumping, cleaning or aquifer leakage. The act of logging a borehole for temperature also causes disturbance, although the magnitude is significantly less (Beardsmore & Cull 2001).

In this work the implication of disturbance to the groundwater column, by aquifer mixing, on bottom-hole temperature is assessed through a case study on groundwater monitoring piezometer PZ14A of Ulan Coal Mines Ltd (UCML) located in western New South Wales (Figure 8.1). This work presents an observation of changes in bottom-hole temperature, as a result of sudden borehole failure detected by repeated monitoring, and thermal recovery over a period of three years.

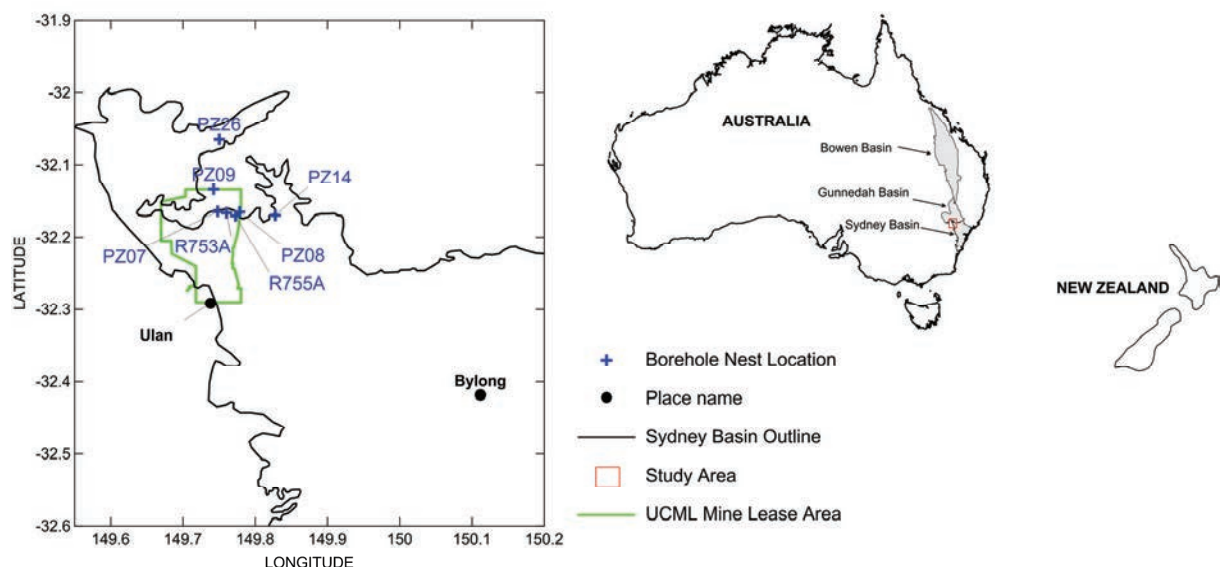


**Figure 8.1** Location of the Ulan Coal Mine (UCML) in the Sydney Basin, western New South Wales, Australia. Study area is shown on the country map as the red rectangle and the major basin systems Bowen, Gunnedah and Sydney are shown. Borehole nest locations are shown, local towns and the mine lease area is in green.

### Background Geology of PZ14A

UCML is located in the north western part of the Sydney Basin (Figure 8.1) near the boundary with the Gunnedah Basin. PZ14, which is located approximately 2 km west of the mine boundary lease area on private property, is the groundwater monitoring nest of three boreholes PZ14A, PZ14B and PZ14C constructed in September 2006. The geology of the area consists of Jurassic and Triassic sediments overlying coal bearing sediments of Permian age. Refer to Herbert & Helby (1980)

or Tadroz (1993) for detailed geological histories of the area.

PZ14A is screened in the Permian Ulan coal seam aquifer (Figure 8.2), whilst PZ14B is screened in the Triassic aquifer and PZ14C is screened in the Jurassic aquifer. The boreholes are constructed from 200 mm diameter steel casing with a slotted steel casing section of 120 mm in the aquifer zone. Cement grout is used to seal the unscreened section of the borehole from Jurassic and Triassic sediments and their aquifers.

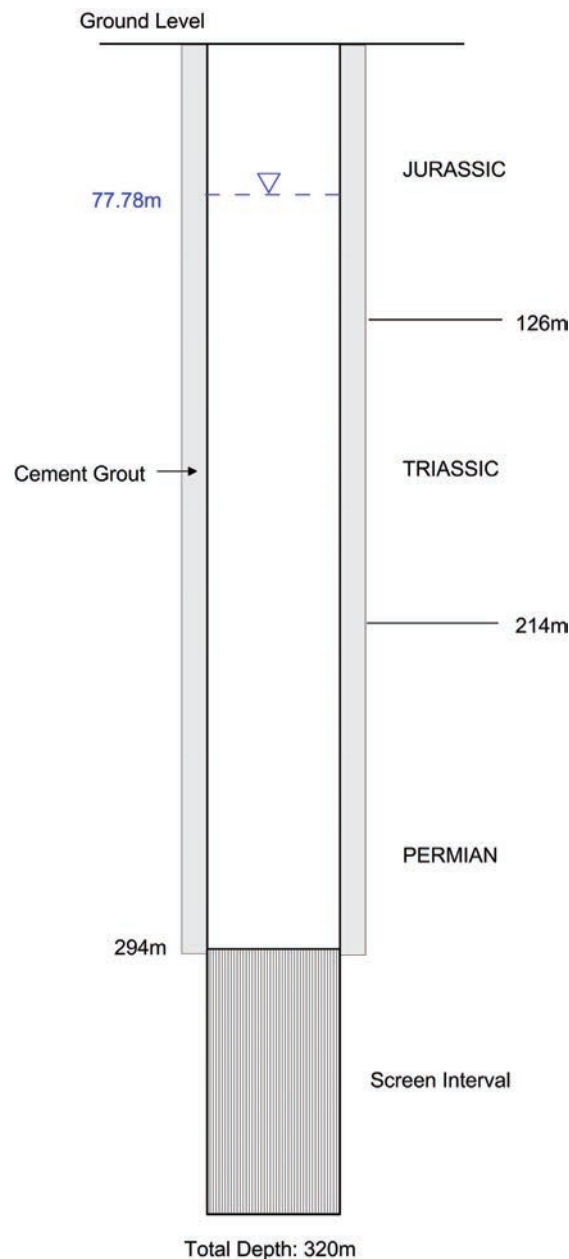


**Figure 8.2** PZ14A borehole construction details showing depth below ground level for the Jurassic, Triassic and Permian sediment boundaries. Bore screen interval is 294 – 320 m. Groundwater level (blue dashed line) as at December 2008.

## Measurements History

Down-hole temperature measurements were undertaken in PZ14A and other boreholes of UCML during March 2009. Due to casing construction issues no temperature measurements were taken within the screened section of any boreholes. From the measurement results it was noted that the results of PZ14A appeared inconsistent with those of nearby boreholes of comparable depths. For example, the temperature in PZ14A at 200 m below ground level was 20.3°C, whilst nearby in borehole PZ07A at 200 m the temperature was 24.2°C. Topography could be a cause of the difference; however the difference in elevation between these two boreholes is approximately 50 m and therefore unlikely to be significant. A comparison of the groundwater levels of these two bores, which are screened in the same Permian aquifer unit, showed PZ14A had risen 29 m since December 2008 whilst PZ07A had fallen only a few metres over the same period. The general trend of groundwater levels in the Permian aquifers around UCML is for decreases in groundwater level as a result of mine dewatering.

In June 2009 repeat measurements were taken which showed all boreholes, with the exception of PZ14A were consistent with the previous results. Temperature in PZ14A had increased slightly but the groundwater level in PZ14A had also continued to rise, whilst all other bores fell slightly. Therefore, at this point PZ14A was suspected to have failed, most likely due to casing and or cement grout failure, causing one or more of the upper aquifers leak into the bore column. This would cause mixing of the aquifers and disturb the temperature. Thus the down-hole temperature measurements of PZ14A were not in equilibrium with the host rock. The thermal

recovery of PZ14A was monitored over the next few years to observe the length of time for the temperature to stabilise and return to equilibrium.

## METHODOLOGY

Down-hole temperature measurements were collected using HOBO™ temperature data loggers from Onset Computer Corporation Ltd attached to an electronic dip meter which is lowered down the borehole and stopping at specific intervals for approximately 15 minutes. The stable temperature is determined by the flat-lining of temperatures at each depth interval. This method of temperature collection is described in detail by Danis & O'Neill (2010) and Danis *et al.* (2011). For the temperature measurements presented in this work, no climate corrections are applied.

In addition, groundwater level measurements were also recorded using an electronic dip meter and in September 2010 groundwater samples were collected, by Australian Laboratory Services Ltd (ALS), from PZ14A, PZ14B and PZ14C. These samples were analysed for major anions and cations (sodium, potassium, calcium, and magnesium), sulphates, chlorine and alkalinity (carbonate and bicarbonate) to determine whether the Jurassic or Triassic aquifer had mixed with PZ14A. The groundwater sample results are compared to the previous sampling results from September 2009 (Tammetta 2009).

## RESULTS AND DISCUSSION

### Temperature Measurements

Down-hole temperature measurements were collected between March 2009 and March 2011 for PZ14A, as shown in Table 8.1 and



**Table 8.1** Measured temperature PZ14A between March 2009 and March 2011 for various depths in meters below ground level (mbgl)

Depth (mbgl)	March 2009	June 2009	November 2009	March 2010	June 2010	September 2010	March 2011
40			19.00	19.09		19.03	
70					19.28	19.27	
90		19.38	19.57	19.66	19.66	19.56	
110					20.04	20.01	
130					20.62	20.51	
140		19.57	20.33	20.71		20.70	
150	19.84						
190		20.14	21.19	21.57		21.53	
200	20.33						
240			22.33	23.20	23.29	23.30	23.40
265				24.32			
290		21.38	24.45	25.67	25.87	25.91	26.01

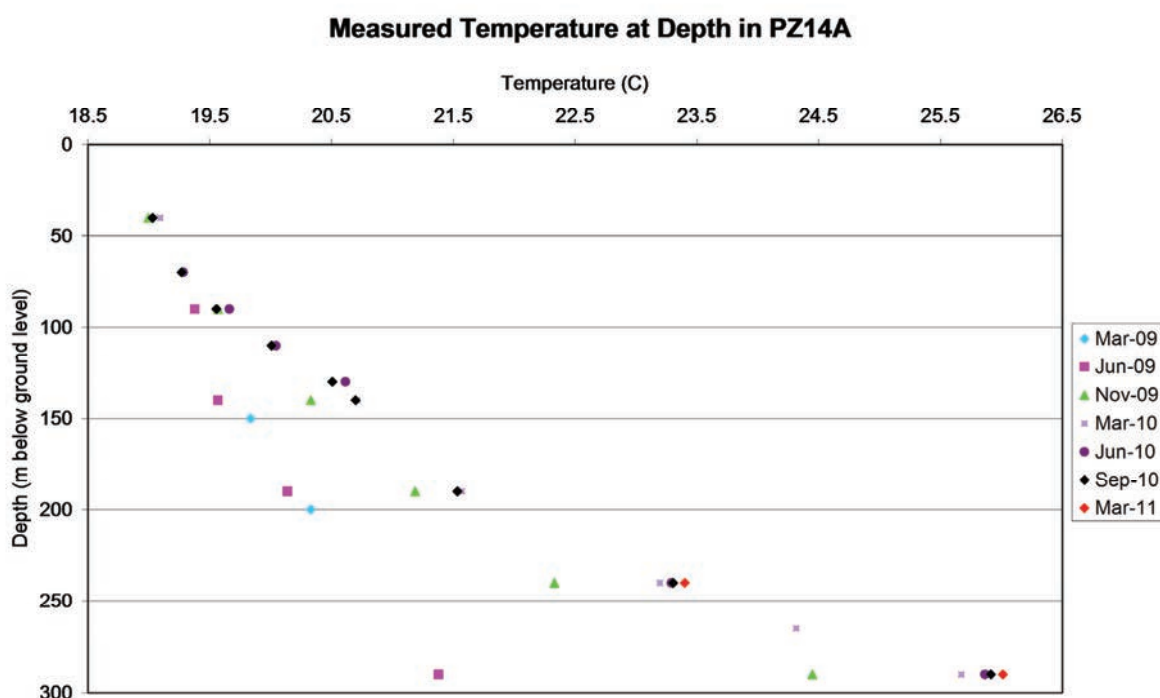


**Figure 8.3** Results of measured temperature at depth in PZ14A from March 2009 to March 2011.

Figure 8.3, at various depths below the ground level. The results of Table 8.1 show that over the monitoring period the recorded temperatures increased, with the greatest rises observed at 290 m. Temperatures between 40

m and 110 m are not assessed as they are affected by diurnal and seasonal climatic variations. At 140 m the temperature has increased 1.13°C between June 2009 and September 2010, whilst at 190 m the

temperature increased 1.43°C over the same period. At 290 m, just above the screened Permian aquifer, temperature increased by 4.63°C over the monitoring period.

The most rapid changes in temperature are observed between the June and November 2009 and November 2009 and March 2010 measurements coinciding with a stabilising of the groundwater level (Figure 8.4). The Jurassic and Triassic groundwater levels have remained stable since the installation of the

bore, whilst the Permian groundwater level shows typical decline from mine dewatering up until December 2008 then a rapid rise of 44 m between December 2008 and September 2009. Temperature measurements show a difference of 1.05°C at 190 m between June and November 2009 and 0.38°C and November 2009 to March 2010. At 290 m the difference is 3.07°C and 1.22°C for the same periods.

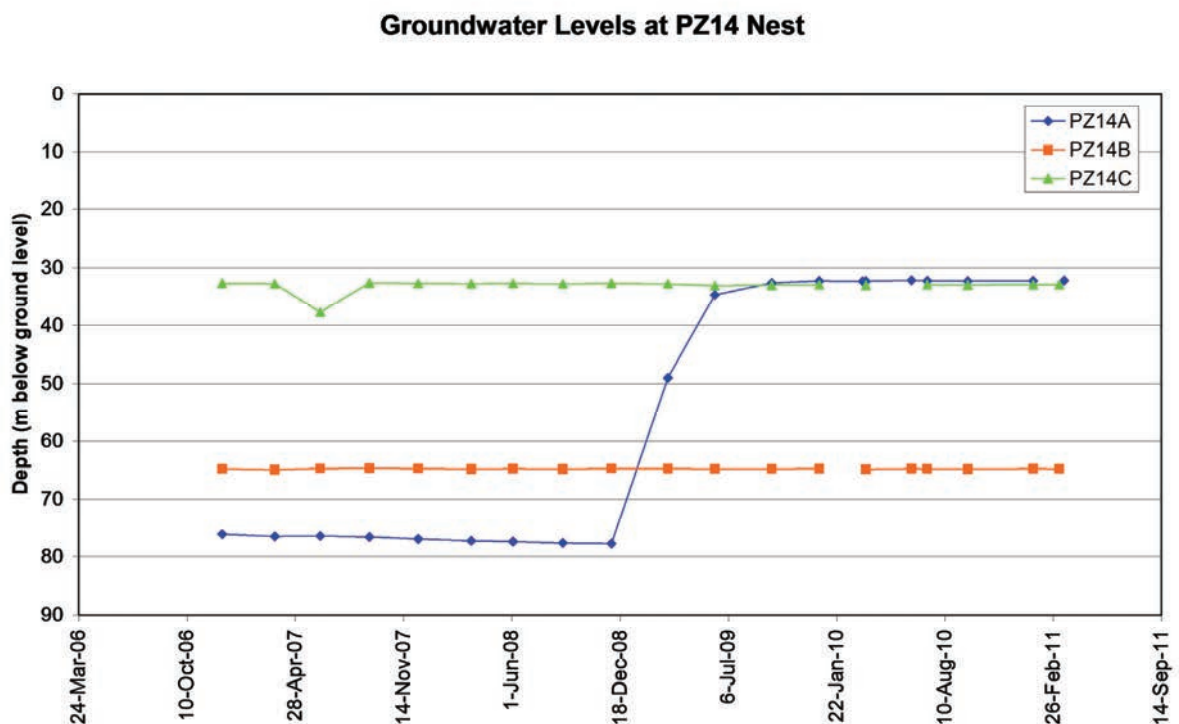


**Figure 8.4** Measured groundwater levels at the borehole nest PZ14. PZ14A is screened in the Permian Ulan Seam, PZ14B is screened in the Triassic Sandstone and PZ14C is screened in the Jurassic Sandstone

### Groundwater Chemistry

To determine which aquifer, the Jurassic or the Triassic, has mixed with the groundwater of PZ14A a piper plot (Figure 8.5) compares the September 2010 chemistry results with those from September 2009 of all Jurassic, Triassic and Permian Ulan Seam aquifers of UCML. Previous sampling results, reported by Tammetta (2009), show the three different

aquifers plot in distinct groups and are characteristically different from each other. The Permian Ulan Seam aquifer tends to be more dominant in calcium and chlorine, whilst the Triassic is more sodium and bicarbonate dominant and the Jurassic is more sodium and chlorine dominant.

The September 2010 sample from PZ14A will reflect the characteristics the upper aquifer

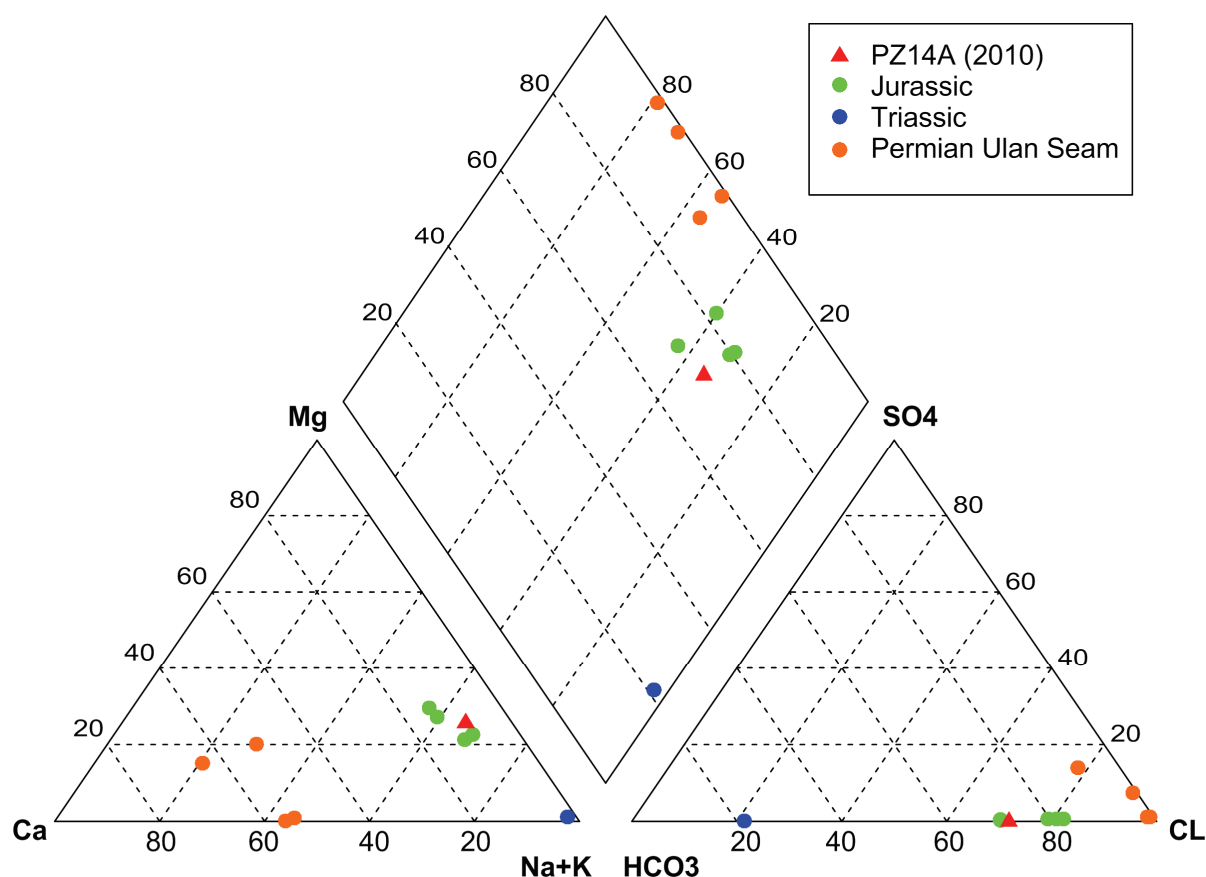


**Figure 8.5** Piper plot of groundwater chemistry results for PZ14A from September 2010 and all Jurassic, Triassic and Permian Ulan Seam aquifers from September 2009. Modified from Tammetta (2009, 2010).

which has mixed. From Figure 8.5, the groundwater chemistry of PZ14A shows a close affinity with the Jurassic Sandstone. The groundwater level also shows an affinity with the groundwater level of the Jurassic aquifer of PZ14C.

## CONCLUSION

The groundwater levels and down-hole temperature measurements show that PZ14A suffered a structural failure sometime between December 2008 and March 2009 which led to the upper Jurassic aquifer entering the bore and mixing into the groundwater column. As a result the temperature measured in March 2009 was significantly lower than other nearby boreholes. The amount of disturbance to

PZ14A was significant, over approximately 6 months, and the thermal recovery period was almost two years.

These results show PZ14A, which should have been equilibrated based on time since drilling, had non-equilibrium conditions from fluid disturbance. The changes in groundwater level were the first indication of a problem but without a history of groundwater level measurements, to indicate the norm for the bore, this would most likely not have been identified. The difference in temperature between March 2009 and March 2011 was almost 5°C and if the March 2009 temperature had been applied to thermal models the estimated temperature would have been significantly lower.

With careful planning, consideration of groundwater level trends and borehole history, ground water boreholes can provide a valuable source of equilibrated bottom-hole temperature measurements.

## REFERENCES

- BEARDSMORE G. R. & CULL J. P. 2001. *Crustal heat flow: a guide to measurement and modelling*. Cambridge University Press, 324p.
- DANIS C. & O'NEILL C. 2010. A static method for collecting temperatures in deep groundwater bores for geothermal exploration and other applications. *Proceedings of Groundwater 2010 the Challenge of Sustainable Management*, 31 October to 4 November 2010, Canberra.
- DANIS C., O'NEILL & LEE, J. 2011. Geothermal state of the Sydney Basin: assessment of constraints and techniques. *Australian Journal of Earth Sciences* (in press).
- DEMING D. 1989. Application of bottom-hole temperature corrections in geothermal studies. *Geothermics* **18**, 775-786.
- HERBERT, C. & HELBY, R. (editors), 1980. A guide to the Sydney Basin. Geological Survey of New South Wales Bulletin 26, Bulletin No. 26. Department of Mineral Resources, New South Wales, 603 pp.
- HOLGATE F.L. & GERNER E.J. 2010. OzTemp well temperature data.  
<<http://www.ga.gov.au/energy/geothermal-energy-resources.html>> (accessed 14 September 2011)
- TADROZ N.Z. (Editor) 1993. The Gunnedah Basin, New South Wales. Geological Survey of New South Wales, *Memoir Geology* **12**, 649pp.
- TAMMETTA P. 2009. North monitoring network quarterly and annual sampling report September 2009. Available from Ulan Coal Mines Ltd, Coffey Geotechnics Report Number GEOTLCOV23873AB-AA.
- TAMMETTA P. 2010. North monitoring network quarterly and annual sampling report September 2010. Available from Ulan Coal Mines Ltd, Coffey Geotechnics Report Number GEOTLCOV23873AB-AE.

# CHAPTER 9

## UNCERTAINTY IN 3D GEOTHERMAL MODELS



*Govetts Leap, Blackheath NSW*



# An assessment of subsurface temperatures and uncertainty in 3D geothermal models of the Sydney-Gunnedah basin system

C. DANIS<sup>1</sup>, S. QUENETTE<sup>2</sup>, C. O'NEILL<sup>1</sup> J. MANSOUR<sup>3</sup> AND L. MORESI<sup>4</sup>

<sup>1</sup>*GEMOC ARC National Key Centre, Department of Earth and Planetary Sciences, Macquarie University, NSW 2109, Australia.*

<sup>2</sup>*Monash eResearch Centre, Monash University, VIC 3800, Australia.*

<sup>3</sup>*Victorian Partnership for Advanced Computing, VIC 3053, Australia.*

<sup>4</sup>*School of Geosciences, Monash University, VIC 3800, Australia.*

Inferences on subsurface temperatures in geothermal studies, based on sparse datasets and modelling, contain many sources of significant uncertainty. By understanding and constraining the largest sources of uncertainty in simulations we can determine more valid and representative estimates of thermal structure and subsurface temperature. By being able to adapt our model parameters we can better understand variance in the expected responses in subsurface temperature, when identifying geothermal anomalies. Reliable observables are, inevitably, necessary over large areas for better calibration, otherwise assumptions about the inherent heterogeneity add to the levels of uncertainty in a model. Traditional Monte Carlo approaches to understanding uncertainty are not as useful and far too time consuming, when the fundamental problem is a massively parallel forward geothermal model, as is the case here. Here we outline an approach to understanding the sensitivity in model parameters in a forward modelling suite of a basin-scale geothermal problem, which allows the fundamental controlling parameters in the problem to be identified and constrained. By using real world observables, such as down-hole temperatures, we can reduce and understand the uncertainty of our 3D models, and constrain the parameter range of both the fundamental physical properties of the basin's lithologies, and the relevant boundary conditions.

**KEY WORDS:** Sydney-Gunnedah Basin, Underworld, subsurface temperature, 3D geothermal models.

## INTRODUCTION

The study of heat flow in the Earth's upper crust is critical in understanding the occurrence of mineral deposits, petroleum accumulations and geothermal anomalies. Historical approaches have been to assess the upper crustal heat flow using extrapolated temperatures and heat flow measurements (i.e. Somerville *et al.* 1994) and 1D models (i.e. Chopra & Holgate 2005). In any assessment or model of subsurface conditions the ability to identify and quantify the

uncertainties involved will determine the quality and reliability of the results. Using new multidimensional large scale geodynamic models the assumptions which lead to uncertainties can be assessed and thus the parameters optimised to 'best-fit' with real world observables.

Research in Australia over the last 15 years has indicated the potential for significant geothermal energy resources but the ability to accurately define these regions of high crustal temperatures requires a combination of detailed

geological structure, heat flow measurements, rock thermal conductivities and temperature at depth measurements. Currently extrapolated bottom-hole temperature data (e.g. Gerner & Holgate 2010) with some heat flow measurements and geochemistry data are used to create maps, which have their own inherent limitations, which for many years provided sole estimates of heat flow and temperature, at a continental scale, that have guided geothermal resource exploration programs. Geothermal resource exploration in Australia is limited by scarce/inaccurate thermal datasets (extracted mostly from shallow drill-holes), oversimplified interpretations and under-constrained thermal models (Musson *et al.* 2009). Estimates of heat flow, thermal conductivity at depth, heat production, and temperature at depth are limited in the Sydney-Gunnedah basin system (Figure 9.1). However, these parameters are critical for thermal modelling, and without observables,

assumptions regarding these terms can lead to critical uncertainties in modelling results.

In thermal models the primary unconstrained parameters are the temperature boundary conditions, particularly the basal temperature used for the forward model, as well as material properties such as heat production and thermal conductivity. Thermal conductivity has also been shown to vary with temperature for many rock types (Clauser & Huenges 1995), but the magnitude of this effect has not been demonstrated in geothermal models.

3D geodynamic models in systems such as *Underworld* are advantageous as they approach the problem of assessing thermal structure from the upper crustal scale (>500 x 500 km), as opposed to the small scale (<25 x 25 km) reservoir models used in resource modelling, and allow modelled components, like heat flow, to fully interact with detailed geological structures

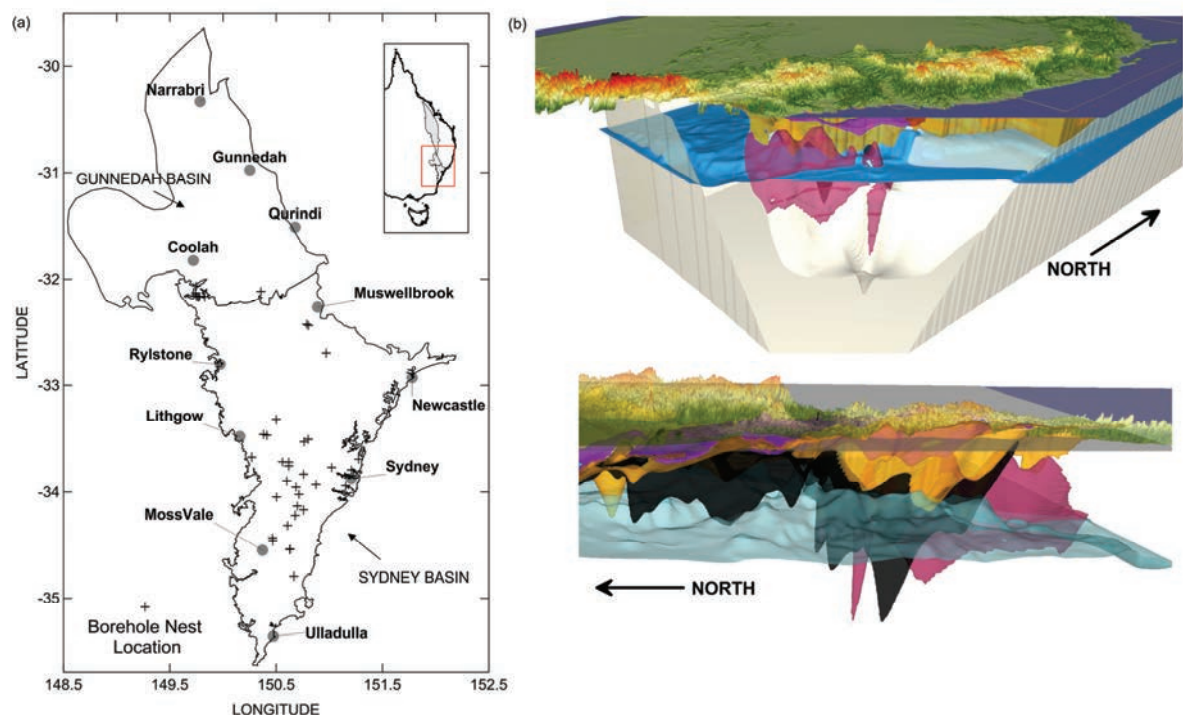


**Figure 9.1** Sydney-Gunnedah Basin model area showing (a) location of equilibrated drill holes, and (b) 3D geological model views from *Underworld*, with surface elevation, coal layers, volcanics and basement.

and physical rock properties. There are many software tools, or “codes”, that provide numerical approximations of subsurface temperature for linear heat flow problems using a mixture of finite difference and finite element numerical approaches but are often constrained by the computing platforms they are associated with. At large scales with models of increased rheological complexity, another approach to obtaining solutions to the forward heat flow problem is required.

Presented in this work is our 3D Sydney-Gunnedah Basin thermal model which covers a volume area of over 600 km by 300 km to a depth of 12 km and is an order of 10 to 100 times larger than typical reservoir scale models. In this contribution we focus on applying *Underworld-GT*, a toolbox in *Underworld*, to solve the non-linear approach to the heat flow equation, for temperature dependent conductivity, to assess the subsurface temperatures and uncertainties. *Underworld-GT* has the ability to scale to 1000s of processes, incorporate different material properties, i.e. heat flow, conductivity, density, for different 3D model layers. In this model the varied parameters and the resulting temperatures can be quantitatively compared to any real world observables thus providing an understanding of sensitivity which allows the quantification of uncertainty.

The Sydney-Gunnedah Basin model exhibits distinct challenges in calibration – the process of tuning unknown model parameters such that the model matches real world observables as closely as possible. The most basic approach is to manually adjust the parameters and visually inspect the agreement between the observables and the computer model. However at hundreds of observation points this method is tedious, subjective and fails to capitalise on the potential statistical

relevance of the observation space. Furthermore, given the model scale and complexity, the calibration needs to also quantify the effect of computational resolution. Done completely manually such an activity is also time consuming.

The uncertainties involved with the parameters used for thermal models are often under-explored but of high importance. For example, in geothermal exploration if the target temperature is 150°C then the thermal conductivities of the materials insulating the heat source can significantly change the estimated depth of this temperature. One method to produce optimum parameters and thus reduce uncertainties involves utilising a stochastic approach. By varying relevant input parameters over valid ranges the sensitivity and fit of these values (Vogt *et al.* 2010) is assessed. The very nature of geological models posed with a relatively small set of observables and non-linear rheology leads to the difficulties in obtaining unique optimum parameters (global minimas in the response surface of the objective function). This is due to complex response surfaces, for example, with the presence of multiple local minima. Hence the development of global optimisation techniques such as simulated annealing (Kirkpatrick *et al.* 1983) and domain specialisations of derivative free methods (i.e. Sambridge 1999a, 1999b) Such methods utilise Bayesian oriented approaches to inference, and ultimately use the posterior parameter distribution to quantify uncertainty.

However, we are interested in models that already use notable numbers of computer processors and memory, and take the assumption that sampling of thousands of models is impractical. Rather, in this contribution, we offer a process of ascertaining model confidence incrementally; leveraging

properties of a model described by geological architecture, large numbers of drill holes with profiles, non-linear heat flow and associated geophysical material properties and the assumption that such systems are only weakly / moderately non-linear in the objective function space. We do not attempt to fully automate this process but rather to keep the process simple.

### **Sydney-Gunnedah Model Background**

The Sydney-Gunnedah Basin thermal model is comprised of a 3D geological model of the subsurface structure, determined through integrated gravity modelling of Danis *et al.* (2010, 2011a), with four main material types forming the surfaces. These material types relate to groups of lithologies with similar thermal properties and represent sediments which are non coal bearing (generally sandstone and shale dominated), coal measures which are inter-bedded with sediments (generally dominated by sandstone and shale), volcanics which formed during basin extension (and are bimodal) and the Lachlan basement which is a combination of Palaeozoic metasediments, granites and volcanics. For the coal measures the average percentage of coal compared to sandstone and shale sediments was determined, using borehole records, of which coal generally comprises 10% and sandstone and shale are approximately equal (at 45% each). This percentage is important for estimating thermal conductivity, density and heat production for this material.

For the model domain all the surface data is in metres Australian Height Datum (mAHD) and the Map Grid of Australia (MGA) Zone 56 is the coordinate reference system of the Eastings and Northings. This allows smooth integration with the data of the real world

observables. The real world observables, for calibration of this model, are derived from equilibrated temperature at depth measurements collected in Danis *et al.* (2011b). They provide over 300 observation points in more than 40 locations across the Sydney Basin, as shown in Figure 9.1. In addition, the densities of the materials are derived from measured samples presented in Danis *et al.* (2011a).

### **METHODOLOGY**

We present a method to assess heat flow on basin to continental scale 3D geological models, which against many drill hole observables provides the ability to quantify uncertainty. This requires; (1) the ability to assume a 3D geological model at this scale, (2) the ability to solve for heat flow and subsurface temperatures at and beyond the resolution required, and (3) the ability to create & assess ensembles.

#### **Lithologies, material properties, and the implementation of temperature dependent conductivities**

The Sydney-Gunnedah model material types are outlined in Table 9.1 with density, derived from Danis *et al.* (2010, 2011a), conductivity and heat production from published averages (Turcotte & Schubert 2002; Swaine 1990; Wollenberg & Smith 1987), with the exception of the Basement which is derived from Lachlan Fold Belt granites in the OZCHEM database (Champion *et al.* 2007). Model boundary conditions, i.e. surface boundary temperature and basement boundary temperature are the same as Danis *et al.* (2010, 2011a) with 15°C for surface and a basement boundary temperature of 350°C.

**Table 9.1.** Thermal properties of each model material, non temperature dependent conductivity

Model Material	Density (t/m <sup>3</sup> )	Conductivity (W/m-K)	Heat Production (μW/m <sup>3</sup> )
Sediments	2.46	2.00	1.25
Coal Measures	1.90	0.30	1.25
Basal Volcanics	2.95	3.00	0.50
Lachlan Basement	2.70	3.00	2.00

**Table 9.2.** Thermal properties of each model material, temperature dependent conductivity

Model Material	Density (t/m <sup>3</sup> )	K <sub>0</sub> (W/m-K)	K <sub>crit</sub> (W/m-K)	T <sub>crit</sub> (°C)	Heat Production (μW/m <sup>3</sup> )
Sediments	2.46	2.00	1.50	300	1.25
Coal Measures (Jurassic, Greta, Reid Dome, Maules Creek)	1.90	0.30	0.20	300	1.25
Permian Coal Measures (PCM)	1.90	1.20	0.20	300	1.25
Basal Volcanics	2.95	3.00	2.25	300	0.50
Basement (under fault)	2.70	3.00	2.25	300	2.00
Lachlan Basement	2.70	3.00	1.50	300	2.00

The initial material properties of Table 9.1 form the basis from which to determine the material properties in Table 9.2 for the model when temperature dependent conductivity is applied. Clauser & Huenges (1995) compile a large database of thermal conductivity measurements on various rocks under different temperature conditions. While there is a large variation in conductivity for different rock types, they also demonstrate significant decreases in thermal conductivity for increasing temperatures for many lithologies. For instance, crystalline basement rocks - such as granites - show a significant decrease in conductivity from ambient temperature up to around 400°C, dropping from around 3.5 W/mK to around <2 W/mk. After around 500°C the decrease in thermal conductivity is minimal. Insulating sediments such as shales decrease from room temperature conductivities of around 2.5 W/mK, less than <1.5 W/mK at

400°C, before plateauing out. However, some units, such as basaltic volcanics, show no systematic change in thermal conductivity over the same range. The behaviour of these rocks can be encapsulated by a piecemeal thermal conductivity function, with a linear trend between two temperatures (e.g. 0 to 300°C for crystalline basement rocks), and a constant value for thermal conductivity past a critical temperature. The relevant parameters for this function are T<sub>0</sub> and K<sub>0</sub>, the surface temperature and conductivity; and T<sub>Crit</sub> and K<sub>Crit</sub>, the critical temperature and conductivity beyond which the conductivity is held constant. The thermal conductivity decreases linearly between T<sub>0</sub> and T<sub>Crit</sub>, and stays at a constant value (K<sub>Crit</sub>) for temperature beyond T<sub>Crit</sub>. The thermal properties of Table 9.2 form the initial model in which the sensitivity of each model material is tested.



## The ability to solve heat flow and subsurface temperatures at or beyond the resolution required

*Underworld* (Moresi *et al.* 2007) is a 3D parallel geodynamic modelling framework, capable of deriving viscous / viscoplastic thermal, chemical and thermochemical models. Based on the StGermain approach (Quenette *et al.* 2007), it is highly adaptable software but yet designed specifically for high performance computing platforms. *Underworld* includes and specialises the Lagrangian Particle-In-Cell Finite Element Method, of which *Ellipsis* and *Ellipsis 3D* (Moresi *et al.* 2003, O'Neill *et al.* 2006) were the prototypes. It uses PETSc optimised numerical solvers (Balay *et al.* 1997, 2011), the MPI interface (Gropp & Lusk, 1996), and is regularly used at 100s and 1000s of processes for complex geodynamics-oriented simulations. *Underworld-GT* is the toolbox specialisation of *Underworld* that provides easier to use interfaces to the heat and fluid flow equations. *Underworld* also provides gLucifer, which enables the rendering of visualisations whilst computing.

### Thermal equations

We solve the steady state heat equation with internal heat sources in three dimensions, given by:

$$\nabla \cdot (K \nabla(T)) = -A$$

Eq.9.1

Here  $T$  is the temperature,  $K$  is a variable thermal conductivity, and  $A$  is the volumetric heat production. Thermal conductivity is given by:

$$K = K_m(T)$$

Eq.9.2

where  $m$  is the lithology, is dependent on both position and temperature and is specified

below. Note that this temperature dependence introduces non-linearity to dynamics. Heat generation ( $A = A_m$ ) is piecewise constant and defined per material. The equation for the thermal conductivity of each lithology ( $m$ ) is given by

$$K_m(T) = K_0 - \frac{(T - T_0)(K_0 - K_{crit})}{(T_{crit} - T_0)}$$

Eq.9.3

if  $T_0 < T < T_{crit}$  ; if  $T \geq T_{crit}$  then

$$K_m(T) = K_{crit}$$

Eq.9.4

Here  $T$  is the temperature and  $K$  the thermal conductivity.  $K_0$  and  $K_{crit}$  denote the thermal conductivity at surface temperature and at  $T_{crit}$ , respectively.  $T_{crit}$  is the temperature above which the thermal conductivity is held constant,  $T_0$  is the surface temperature. We use a constant temperature top and bottom boundary condition with reflecting side boundary conditions where the side boundary condition is far enough away from the region of interest so that it does not impact the results.

### Finite Element Method (FEM)

Linear hexahedral elements are used in the finite element discretisation of the heat flow equation over the geometric domain. However a novel approach, conceptually identical to the Particle-In-Cell (PIC) methods of the 1950s (Harlow 1955) is used through the construction of finite element integrals from the values on the material “particles”. This approach was first developed as the material point method (Sulsky & Brackbill 1991; Sulsky & Schreyer 1996) with additional work on improved integration schemes by Moresi *et al.* (2003). In our application, we choose to enforce PIC integration points to the linear FEM Gauss points on the basis this steady-state thermal

problem is a non-Lagrangian model. However, this method allows both sub-element scale representation of heterogeneity and the ability to capture arbitrary geology geometry, whilst maintaining a regular quadrilateral mesh for computation.

The problem stiffness matrix derives from a standard Galerkin weighted residual formulation. Solution to the linear equation system is obtained through the GMRES Krylov method provided by PETSc, with block jacobi preconditioning. The weak non-linearity introduced through the thermal conductivity is accounted for through fixed point iteration, and only a few cycles are generally required.

### **Import geometry into *Underworld***

Geodynamics-oriented problems are usually discretised into normalised domains (e.g. -0.5 to 0.5 length in each direction). *Underworld-GT* has piloted the ability to import stratigraphic layers in the form of ascii data, or GoCAD and Geomodeler voxel sets into *Underworld*. In the Sydney-Gunnedah model the surface of each geological unit, in the form of ascii data {easting, northing, depth mAHD}, was imported in stratigraphic order to create unit volumes from the shapes.

To create the surfaces between the points provided in the ascii file a consistent method, based on Smoothed Particle Hydrodynamics (SPH) (Monaghan 1992), to interpolate model input data points. SPH based interpolation provides a number of key benefits such as ease of implementation and computational efficiency. Further to this, data points can be (to a large extent) arbitrarily located, and only need be specified where a surface (or region) is defined. Data decomposition for parallel simulations is also straightforward, and comes at no additional cost. Where data points describe region volumes for some quantity,

SPH is simply used to provide a continuous definition of this quantity, from which values on Gauss (or PIC) points may be set for any given simulation resolution.

For data provided to represent region surfaces, we interpret 3D data points as 2D points which carry a height value. A 2D SPH interpolation is then formed to define a 'height field' for each surface dataset. These 'height fields' may then be used to specify the top and bottom limits for each material layer. Where provided data does not span domain laterally, material 'islands' are created. Surfaces are constrained to be one-to-one within this workflow.

### **Synthetic drill hole measurements**

For each real world observable drill hole there can be one bottom hole temperature measurement or a string of temperature measurements along the drill hole profile. To incorporate this information into the model, for comparison with model values synthetic drill holes are created, using a feature in *Underworld-GT*. These synthetic drill holes contain the location of the measured temperature as a depth below the ground surface, or depth in an absolute reference frame such as mAHD, the elevation above the surface and azimuthal and drill hole inclination.

The interpolation functions used are the finite element method shape functions as per the computation. The results are provided as both a text file of {eastings, height, northings, temperature} as well as a geotherm plot. This decreases the time and effort to assess a resultant model either quantitatively or qualitatively with regard to geological observables.

### **Quantify computational effects on the results**

*Underworld-GT* has approximately linear memory to at least 1000 cores of 3 gigabytes of memory each on the NCI Vayu supercomputer facility (National Computational Infrastructure 2009). Hence a weak scaling approach of doubling unknowns whilst doubling the number of cores is used to ensure the modelled problem is equivalent as resolution is increased. The following model is used to appraise each resolution:

$$ave_r = \frac{1}{O} \cdot \sum_{O=1}^O (|t_{r-1,O} - t_{r,O}|)$$

Eq.9.5

for  $r$  in  $R$  where  $O$  is the number of drill hole observation points.  $R$  is the set of resolutions where

$$r - 1_i \cdot r - 1_j \cdot r - 1_k = \frac{1}{2} \cdot r_i \cdot r_j \cdot r_k$$

Eq.9.6

such that each trial resolution is doubled in problem size to the prior. The initial resolution

$$e_1 = r_{1,i} \cdot r_{1,j} \cdot r_{1,k}$$

Eq.9.7

is chosen such that the run utilises approximately 90% of the memory proportioned to a processor. The equivalent min and max is also considered.

### **Creation of ensembles towards best fit parameters & quantifying uncertainty**

The calibration to optimal parameter configuration minimizes misfits between the modelled solution for subsurface temperatures, and actual down-hole temperature logs. However our model faces two fundamental issues with giving a priority choice to an automated optimisation approach - it is not necessarily clear how non-linear the objective function space is, and the high resolution models already consume vast computational resources per model such that the many

thousands of models required for a stochastic approach is not clearly practical. Hence we aim to utilise concepts of exiting techniques, but cast them into a practical parametric human iterative manner. The assumption, which is ultimately proven valid, is that the objective / appraisal function space is sufficiently weakly non-linear that any one 1D parameter investigation is representative.

We followed these steps:

1. Quantify computational effects.
2. Using the thermal parameters of the initial model as starting values undertake a parameter reduction. On the assumption that the objective function is weakly non-linear, the parameters can be varied independently, and the reduction can be based on a measure of the misfit. The steepest gradients in a modelled observable, such as temperature, with varying parameter choices, denotes the region most sensitive to small parameter perturbations.
3. Establish a parametric based ensemble (ie. a collection of models with varying parameters), described by each free parameter between a specified range and number of steps. The number of steps per parameter is chosen to limit the ensemble to a few hundred models.
4. Assess and order the ensemble based on the objective function.
5. Repeat step 3-4 whilst:
  - (a) any one dimensional parameter projection of the objective function has not yet reached a minimum across all ensembles, then
  - (b) for each perceived global minima in the set 'within the threshold on the present ensemble', and finally
  - (c) for each parameter optimal is within some tolerance of the average of that parameter in

the set ‘within the threshold on the present ensemble’.

Step 5 dictates how the search is performed and clearly utilises concepts from many existing techniques. The minimisation is exhibited through the ‘within the threshold on the present ensemble’. However, rather than choosing a single optimal model, an ensemble of models that fall within a chosen tolerance is taken. We then guide the iterative development of the reduced ensemble to capture multiple possible optimums by equally considering all models in the ensemble as possible global minimas and repeating the process for each of these. If automated each model within the ensemble threshold could be a base point to repeat the process, ultimately only continuing on the ensembles with the best outcomes. Also, a consistent and autonomous method to predicting appropriate ranges and the ability to randomly generate many models in step (3) for non-trivial objective functions spaces. However, as stated, the process can be executed within a sequence of parametric runs.

The result is the reduced ensemble of all the models in the final ensemble below the threshold. This ensemble is a spectrum of models that represent the optimal parameters, and is described by optimal, ave and stdev for each free parameter.

### **Observed drill hole profiles and the objective function**

We choose to constrain our model results with over 300 drill hole temperatures (varying spatially laterally and with depth) from over 40 drill hole location in the Sydney-Gunnedah Basin (see Figure 9.1). This gives us a good spatial distribution of control points, which possess a strong coverage of shallow depths and near-surface lithologies. The drill hole

temperatures are assigned an qualitative confidence; either ‘Well trusted,’ ‘Possibly ok,’ or ‘Don’t trust’, which is used to qualify the certainty of the observations themselves. The ‘Don’t trust’ are not used in the assessment, and the ‘Well trusted’ have a higher weighting than the ‘Possibly ok’.

Equation 9.8 describes the objective function used. It is more complicated than the simple temperature difference used in the computational assessment.

$$obj = \frac{1}{4} \cdot \left[ \frac{ave_T}{C_{aveT}} + \frac{stdev_T}{C_{stdevT}} + \frac{ave_P}{C_{aveP}} + \frac{stdev_P}{C_{stdevP}} \right]$$

Eq.9.8

Where  $ave_T$  and  $stdev_T$  is the average and standard deviation of temperature misfits between the model observation for all ‘Well trusted’ observation points. Similarly,  $ave_P$  and  $stdev_P$  are for all ‘Possibly ok’ observation points. Here we are giving the trusted drill holes just as much weighting as the possibly ok because we know there are not enough trusted ones to use solely. To avoid bias from outlying points the standard deviation is also considered in the objective function. For example, where a drill hole profile has a different gradient to the modelled the outliers bias the results, when just using an average, compared to a gradient that matches the model. This objective function exposes more information than the average and relates to the shape of the drill hole profile.

A variant is to use the root mean rather than the average, however the variance in the resultant ensembles is not significant. The approach to scaling was to take the minimum “average” and minimum “standard deviation” of all the models from all the ensembles thus far.

## **RESULTS AND DISCUSSION**

With the ability to easily change parameters in *Underworld*, tests on the sensitivity of the model parameters; conductivity, heat production and basal boundary temperature were conducted for the 8 geological units and the results compared to the known measured temperature values. Through the iteration process the fundamental controlling parameters were identified and where possible an optimal value was selected. These optimum values then form the 'best fit' model.

### Quantify computational effects on the results

Figure 9.2 shows the improvement in certainty of computational results with increasing model resolution. As the resolution is increased, the difference in temperature at an observation point (in average and at maximum) trends towards a reduced variance in model values compared to the observation points. The observation points are all the temperature values from the drill holes.

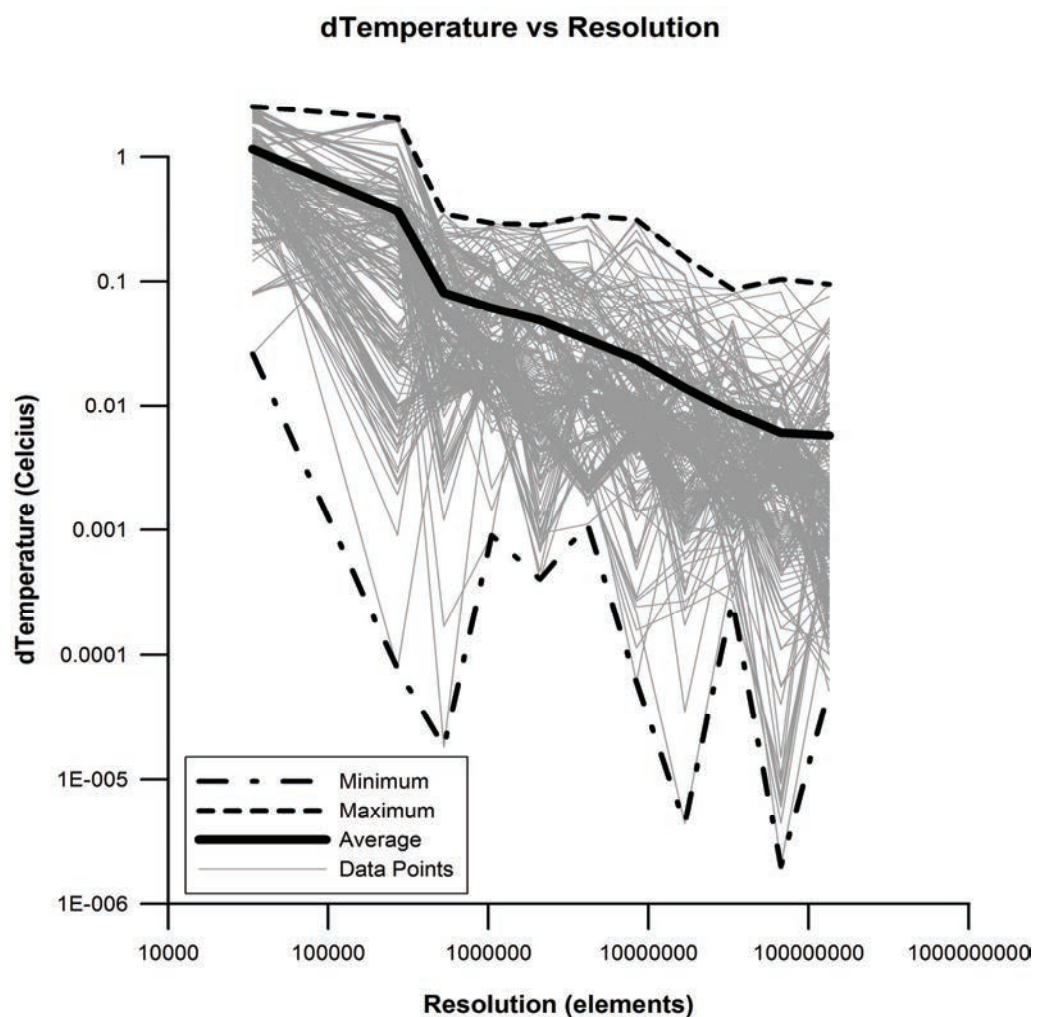


**Figure 9.2** The difference in temperature (°C) between two consecutive weak scaling resolutions for every observation point. The black lines represent the average (solid), minimum (upper dashed) and maximum (lower dashed).

The lowest resolution ( $r_1 = 48, 88, 64$  (total elements in the Eastings [E], Northings [N], and vertical [v] directions), had a total of 270,000 elements. This configuration allows a

$10 \times 10 \times 1$  (E, N, v) aspect ratio and the constraint of 3GBs of memory per core on the NCI Vayu supercomputer facility. The highest



resolution ( $r_{10}$ ) had a total of 134 million elements. We deemed the resolution at which;

$$ave_r \approx 0.01^\circ C \text{ and } max_r \approx 0.1^\circ C$$

the point at which computational effects on model observations were sufficiently bounded. Hence our reference resolution was at  $r_7 = 192$  (E), 348 (N), 252 (v), where;

$$ave_{r_7} \approx 0.015^\circ C \text{ and } max_{r_7} \approx 0.16^\circ C.$$

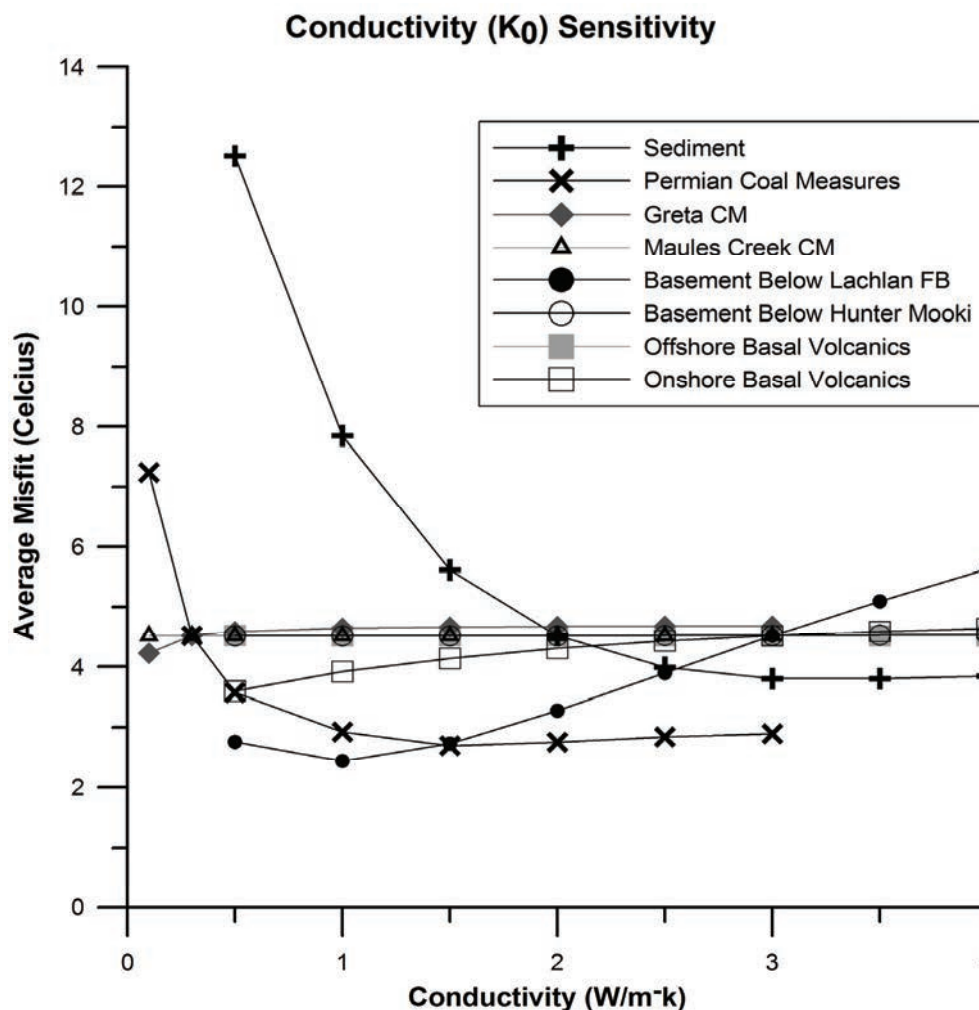
The resolution in the refined region of the mesh is 1406 m x 1422 m x 14 m (E, N, v).

### Sensitivity study & parameter reduction

Figures 9.3 to 9.7 show the sensitivity analysis of the eight geological units, which comprise

the model, to each parameter; conductivity (Figure 9.3, 9.6 and 9.7), heat production (Figure 9.4) and the surface and basal temperature (Figure 9.5). These figures highlight during the iteration process the reduction of misfits in some parameters can lead to increases in others but in general there are two geological units most sensitive to change as well as the basement temperature.

We use 16 conductivity parameters, 8 for  $K_0$  and 8 for  $K_{crit}$ , 8 heat production parameters and 8 for  $T_{crit}$ . Collectively they show the areas where there is most sensitivity to each of the parameters and we use this to reduce the number of parameters in the calibration.



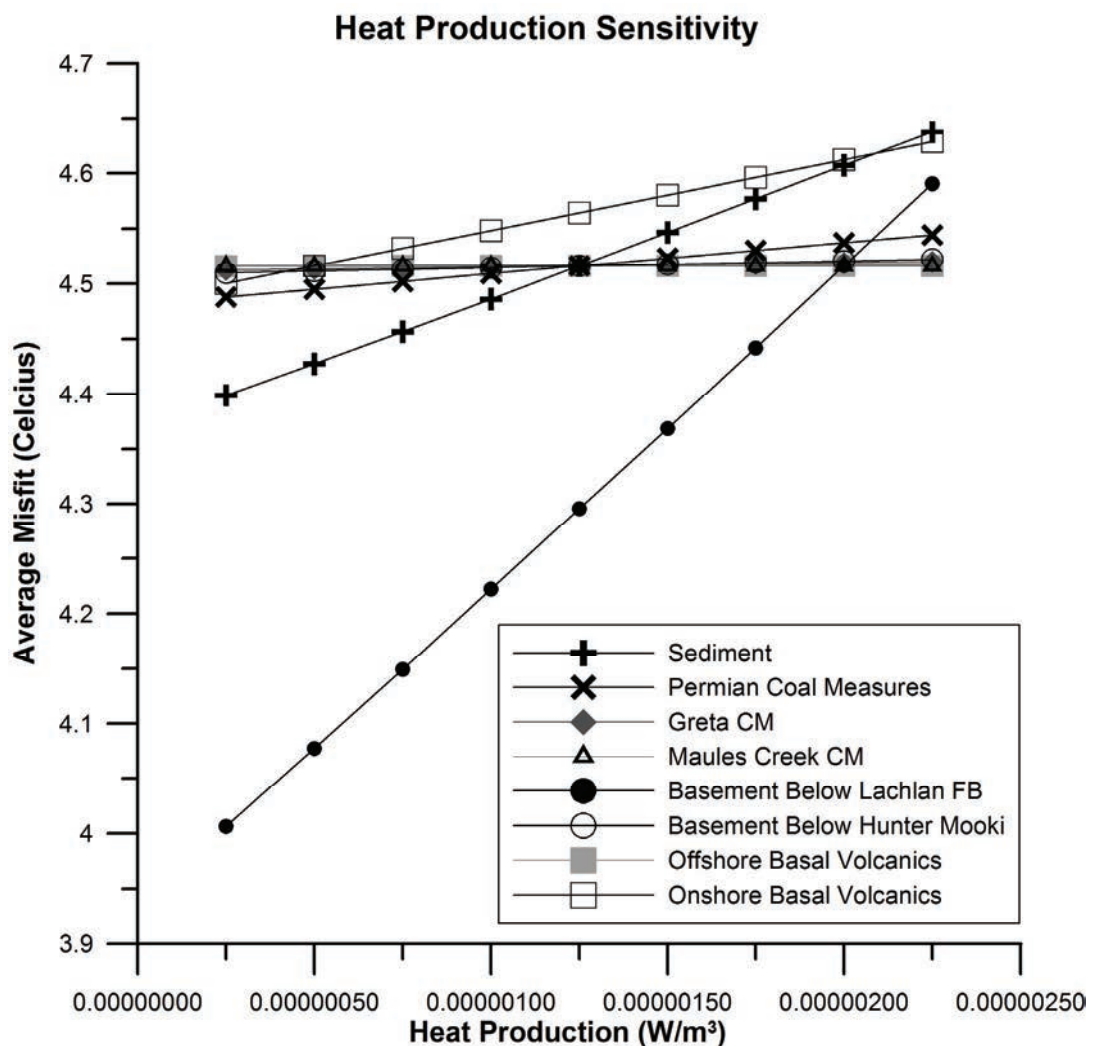
**Figure 9.3** The difference in temperature, as an average across all observation points, between observed and model scenarios when varying only the set of conductivity ( $K_0$ ) parameters.

Figure 9.3 shows the sensitivity of the 8 conductivity ( $K_0$ ) parameters in the model.  $K_{\text{Crit}}$  here is set to  $K_0$  to ensure equivalence to the linear conductivity model. The model is most sensitive to the insulation of the sediment unit, especially when  $K_0$  is less than 1.5. However, given the sedimentary unit is relatively well served by observables, this most sensitive band is not relevant to the calibration and we fix the sediment  $K_0$  to 2. Consequently, of greater interest are the gradients of the basement below the Lachlan Fold Belt (green line) and within the PCM (purple line).

In the likely ranges of greater than 2 and less than 1.5 respectively, they exhibit the

strongest sensitivities. Together these two have the least amount of constraining information, but the strongest impact. Within the likely bands, the remaining geological units are relatively inconsequential.

Similarly, the heat production sensitivities are shown in Figure 9.4. The sediment unit (blue line) again shows a strong impact on the model, however we constrain its value based on observation. Also, once again, the Lachlan basement exhibits the most sensitivity. The Onshore volcanics unit (light blue line) exhibit an effect however; ultimately we also removed it from the search space.



**Figure 9.4** The difference in temperature, as an average across all observation points, between observed and model scenarios when varying only the set of heat production parameters.

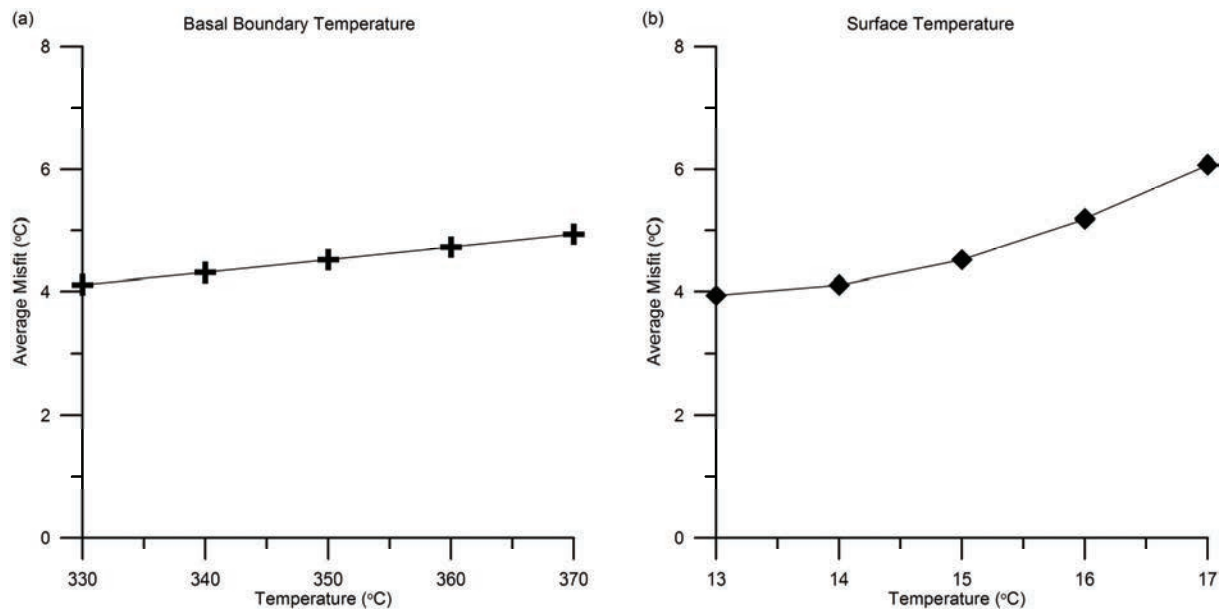


**Figure 9.5** The difference in temperature, as an average across all observation points, between observed and model scenarios when varying only (a) the basal boundary temperature and (b) the surface temperatures.

Despite the surface temperature being a strong controlling parameter, as shown by Figure 9.5b, we assume a constant temperature to the surface of 15°C which is based on the yearly average surface temperature for the Gunnedah Basin from Cull (1979).

Figure 9.5a shows a relatively linear response to basal temperature over a wide range. We constrain this to a narrower window based on the extrapolation of an average continental geotherm to 12 km, but this remains a free parameter. A temperature of 350°C at 12km is possible, by applying a low basement thermal conductivity however the thermal conductivity required would not be plausible for crystalline basement rocks at this depth.

Figures 9.6 and 9.7 provide the sensitivities for the geophysical parameters associated with the non-linear temperature dependent conductivity model. Within a reasonable range based on Table 9.2,  $T_{crit}$  (the temperature at which the non-linear behaviour begins) has marginal effect on the system. However,  $K_{crit}$  for the Lachlan basement at  $K_0$  of 1.5 and 3, both have an increasing effect on the error. This suggests that only the basement is hot enough to behave in a temperature dependent manner, and for higher values of  $K_0$ , could be a strong control on the outcome.

From the sensitivity study we at this point have reduced the free parameters to  $K_0$  and  $K_{crit}$  of the Lachlan basement,  $K_0$  of the PCM, and the basal temperature.

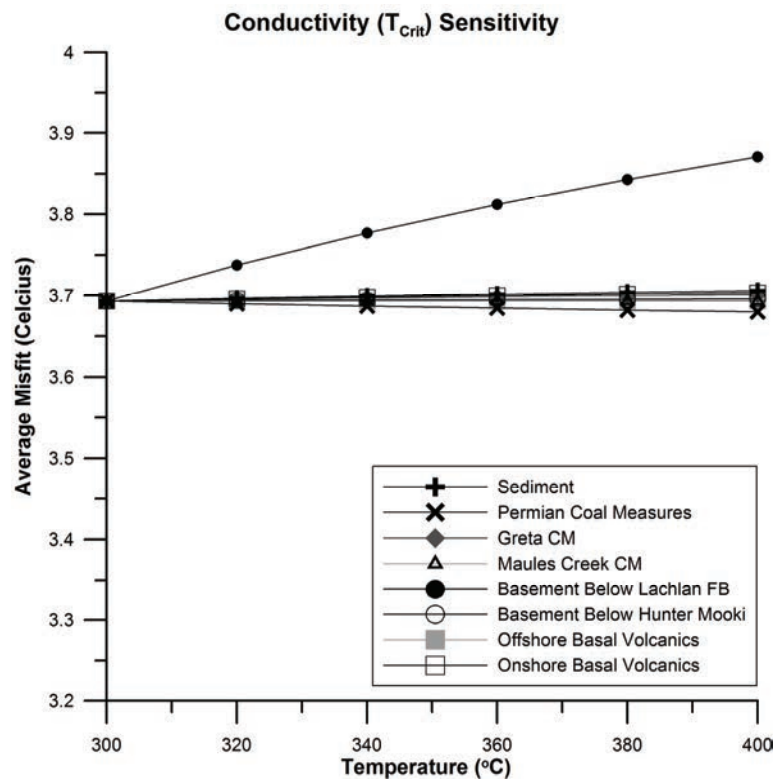


**Figure 9.6** The difference in temperature, as an average across all observation points, between observed and model scenarios when varying only the set of  $T_{crit}$  parameters for when Lachlan  $K_0=3$  and Permian Coal Measures  $K_0=1$ .

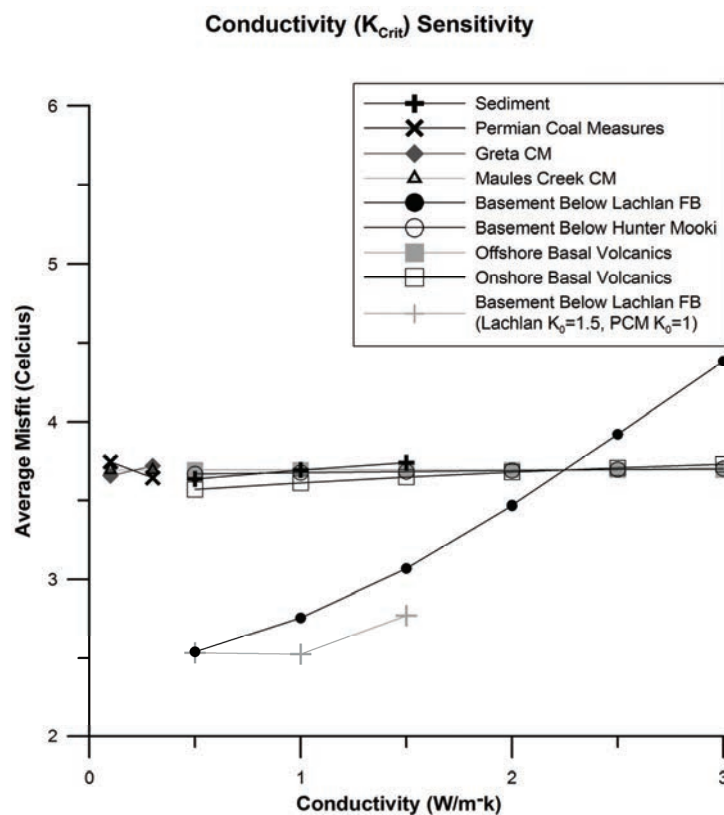


**Figure 9.7** The difference in temperature, as an average across all observation points, between observed and model scenarios when varying only the set of conductivity ( $K_{crit}$ ) parameters for when Lachlan  $K_0=3$  and Permian Coal Measures  $K_0=1$ .

### Model objective function

Using the objective function, Figure 9.8 demonstrates some important qualities of the objective function space. Projected onto any given parameter the objective function is non-linear, but has a clear minimum within the projection and parameter bounds. Figure 9.8 also demonstrates the impact of the objective function over a simple temperature misfit. Where the average or the standard deviation is used to reduce the set of differences between the observation and simulation, the minima point is at vastly differing  $K_0$  values. Our model has observation points that have varying

proximity to the geologic units, and thus any one parameter change may improve some cohort of observation points but worsen others. Hence a good temperature fit is where both the average and standard deviation is low. Furthermore, our objective function biases the fitness towards ‘Well trusted’ drill holes, weighting the appraisal to the fitness of drill holes we have more certainty on. Figure 9.9 shows a least squares regression of temperature at the observed points versus a random simulation. The set of outlying data points from the regression line all belong the HRP drill hole, a drill hole labelled ‘Don’t trust’.

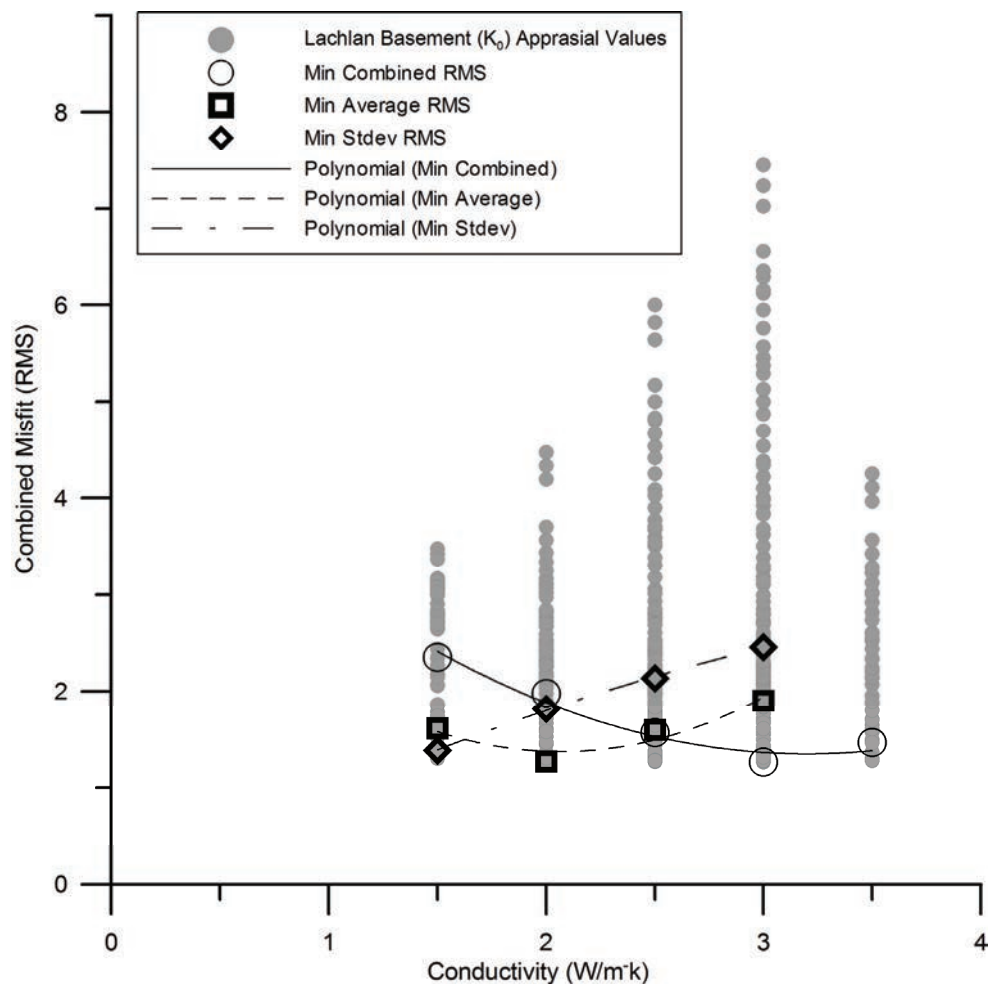


**Figure 9.8** The appraisal values for the spectrum of  $K_0$  values within a set of ensemble iterations, given our appraisal function. The solid black line shows the minima for this appraisal function, and its projection on  $K_0$ . The non-solid lines show the minima and projection on  $K_0$  when the appraisal function is merely the average and standard deviation of the observed-simulated difference.



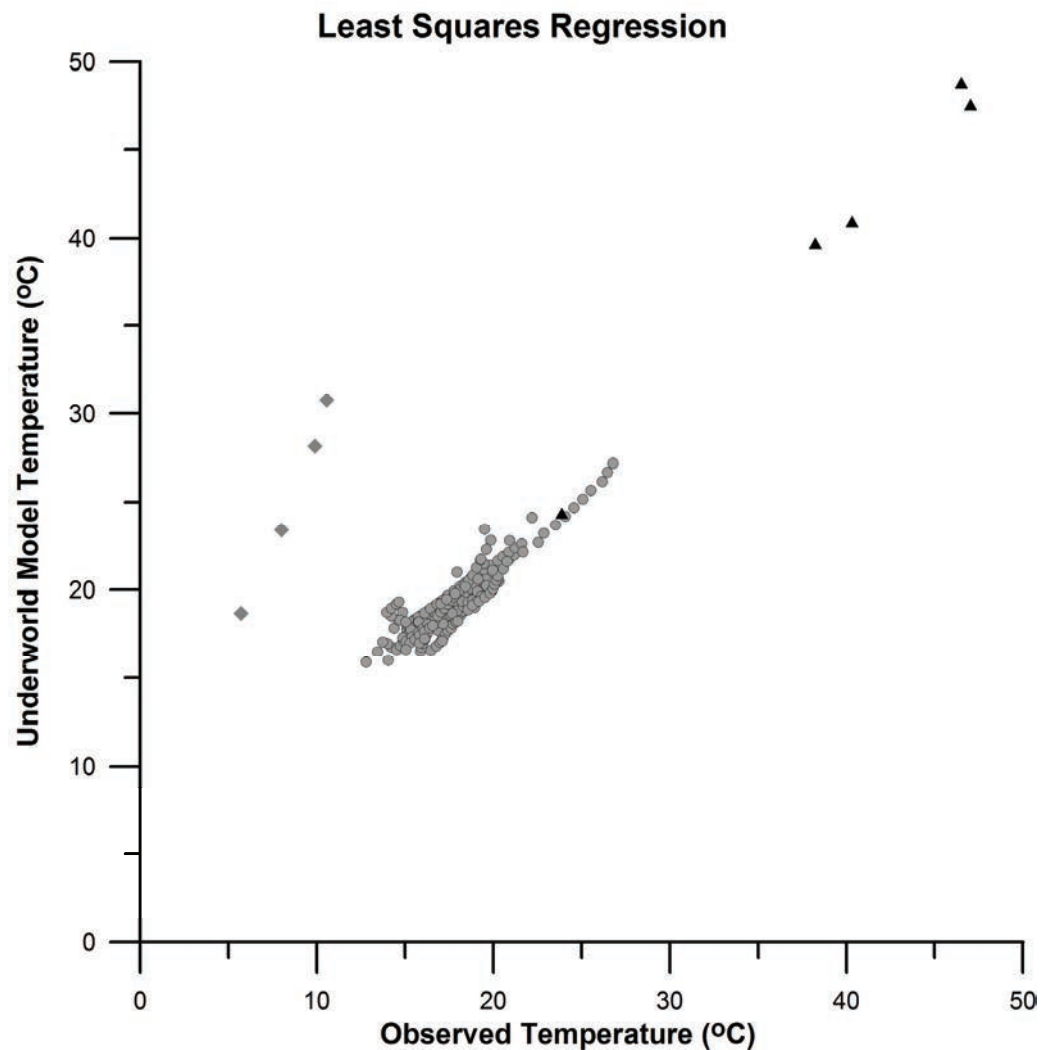


**Figure 9.9** A least squares regression of a selection of observation points for observed temperature compared to the *Underworld* modelled temperature. Grey diamonds represent observation points from drill hole HRP and black triangles represent observation points from drill hole PPG8.

HRP's observation points are omitted from the appraisal function as the boreholes temperature measurements were found, after further investigation, to be affected by disturbance. This disturbance resulted from flushing of the borehole with fresh water prior to temperature logging. Danis & O'Neill (2010) found the effect of disturbance to the temperature of the groundwater in a borehole, approximation of the temperature of the surrounding rock formation, can significantly alter the measured temperature over a long period of time.

The method of temperature measurement is crucial in ensuring representative temperatures however it is often not described in many borehole reports. The data used in the appraisal function is from two sources; from the author using the methodology described in Danis & O'Neill (2010) and from geophysical logging undertaken by private parties. As a result the specific details of the logging operation by the private parties may not be documented and although the boreholes are technically equilibrated, based on length of time since drilling, there is no guarantee they have not suffered disturbance like HRP.

Lateral comparisons of temperature at the same depth with nearby boreholes are not always a representative way to determine if the measurement is trustworthy because of distance and the dimensional effects of geology and architecture.

A further six boreholes are characterised as 'Don't trust' but are not removed from the appraisal functions as their regressions were not overly concerning.

### **Optimal parameters**

Using the approach articulated in the section '*Creation of ensembles towards best fit parameters and quantifying uncertainty*', with an ensemble threshold of 0.1 on the objective (appraisal) function, optimal parameters are reached for the two geological units with the most uncertainty, the PCM and Lachlan basement, and for the basal temperature (Table 9.3). They have the least amount of constraining information but the strongest potential to impact the uncertainty of the model. The parameters for the 'best fit' model are shown in Table 9.4 and incorporate the optimised values for parameters of greatest uncertainty.

In the PCM the  $K_{\text{crit}}$  and  $T_{\text{crit}}$  are not reached, because of the depth of the unit, therefore only  $K_0$  is optimised. The results show for the PCM  $K_0$  is best at 1.2 and probably has an insulating effect closer to that of the sediments ( $K_0 = 2$ ) than the other coal measures ( $K_0 = 0.3$ ). This association may be related to fact that the majority of the PCM is sediments with only a small percentage of coal (10%) in the package, finer variations in the coal proportion are not possible within the resolution of the geological units. The Lachlan basement exhibits strongest potential to generate uncertainty, from either its conductivity, heat production. Both  $K_0$  and  $K_{\text{crit}}$

are the main free parameters for the Lachlan basement which have been optimised. The results show  $K_0$  is close to the anticipated published values. The results of the optimal basal temperature suggest that at 12 km, 345°C represents the best 'regional' basal constraint, in that it produces the best fit with down-hole temperature measurements in the near surface. This is subject to the caveat that the basal temperature may well change over the scale of a basin. If the optimization were done autonomously, the numbers could be further refined.

The residual (smallest objective function from Figure 9.9) was 1.28 as compared to 1, confirming that there isn't sufficient heterogeneity in the model and/or the geometry is moderately incorrect to gain further certainty on the optimal parameters. This may be because there are several inherent assumptions in the geothermal model which provide an existing level of uncertainty.

Some of these assumptions include the supposition that the basement is homogenous, both in geology and thermal parameters, which we know is not true but is a necessary generalisation on the scale of the model. It is possible to introduce heterogeneity if enough real world observables exist to constrain those assumptions, which currently in this model there are not. Secondly we have assigned a qualitative trust assessment of the temperatures from our drill holes, all of which constrain the near surface features and have a climate correction applied, which introduces possible uncertainty. And finally this model assumes conductive effects only, which may not be entirely valid, particularly around near surface aquifers.

**Table 9.3** Optimised parameters for Lachlan basement, PCM and basal temperature for our ensemble threshold of 0.1

Parameter	Optimal	Average	Stdev
Lachlan basement $K_0$	3.0	3.63	0.492
Lachlan basement $K_{\text{Crit}}$	1.5	1.58	0.297
PCM $K_0$	1.2	1.18	0.111
Basal Temperature (°C)	345	343.85	4.160

**Table 9.4** Parameter values of the 'Best Fit' model

<i>Surface Boundary Temperature</i>	15°C	
<i>Basal Boundary Temperature (at 12km)</i>	345°C	
Parameter	$K_0$ (W/m-K)	$K_{\text{crit}}$ (W/m-K)
Sediments	2.00	1.50
Coal Measures (Jurassic, Greta, Reid Dome, Maules Creek)	0.30	0.20
Permian Coal Measures (PCM)	1.20	0.20
Basal Volcanics	3.00	2.25
Basement (under fault)	3.00	2.25
Lachlan Basement	3.00	1.50

## CONCLUSION

Estimating subsurface temperature through geothermal modelling contains many significant sources of uncertainty, especially when sparse datasets are involved. Estimates of thermal structure and subsurface temperature should only be considered valid if the uncertainties have been clearly identified and attempts made to constrain them. In our basin scale model for the Sydney-Gunnedah Basin we have identified the largest sources of uncertainty to be the parameters governing temperature-dependent thermal conductivity, particularly in the basement and Permian coal measures; as well as the basal temperature condition, and unconstrained heterogeneities in the basement rocks.

The results show that the best regional basal temperature constraint, which correlates well to down-hole temperature values, is 345°C (at 12 km) with a standard deviation of 4.16°C. Temperature dependent thermal conductivity for the Lachlan basement and Permian coal measures is difficult to optimize further without more constraints from observables. However these results show that even with the inherent uncertainties of insufficient heterogeneity the standard deviation is low. For the Lachlan basement  $K_0$  is optimal at 3 W/m-K, which is comparable with published values, and  $K_{\text{Crit}}$  is optimal at 1.5 W/m-K. The Permian coal measures have several down-hole temperature measurements which allow  $K_0$  to be optimal at 1.2 W/m-K. The traditional approach of multiple models, i.e. Monte Carlo, to understand uncertainty is overtly time consuming for large scale

massively parallel forward models. Through Underworld simulations we have demonstrated that it is possible to constrain the sources of uncertainty and optimise model parameters using down-hole temperature measurements. Reliable observables are essential, and by adapting our model parameters to produce

results which match these observables we can better understand the variance expected in the responses in subsurface temperature. This variance is crucial for understanding the sensitivity and robustness of modelled geothermal anomalies.

## REFERENCES

- CHOPRA P. & HOLGATE F. 2005. A GIS analysis of temperature in the Australian crust. World Geothermal Congress, Turkey, 24-29 April 2005, Abstracts.
- CLAUSER C. & HUENGES E. 1995. Thermal conductivity of rocks and minerals, in *Rock Physics and Phase Relations, A handbook of physical constants*. American Geophysical Union, 105-126.
- BALAY S., EIJKHOUT V., GROPP W.D., MCINNES L.C. & SMITH B.F. 1997. Efficient Management of Parallelism in Object Oriented Numerical Software Libraries. In: E. Arge, A.M. Bruaset & H.P. Langtangen (Editors) *Modern Software Tools in Scientific Computing*. Birkhauser Press, 163-202.
- BALAY S., BUSCHELMAN K., GROPP W.D., KAUSHIK D., KNEPLEY M.G., MCINNE, L.C., SMITH B.F. & ZHANG H. 2011. Portable, extensible toolkit for scientific computation. <<http://www.mcs.anl.gov/petsc>> (accessed 14 September 2011).
- CHAMPION D.C., BUDD A.R. & WYBORN L.A.I. 2007. OZCHEM National Whole Rock Geochemistry Database. <<http://www.ga.gov.au/meta/ANZCW0703011055.html>> (accessed 14 September 2011).
- DANIS C. & O'NEILL C. 2010. A static method for collecting temperatures in deep groundwater bores for geothermal exploration and other applications. *Proceedings of Groundwater 2010 the challenge of sustainable management*, 31 October to 4 November 2010, Canberra.
- DANIS C., O'NEILL C. & LACKIE M. 2010. Gunnedah Basin 3D architecture and upper crustal temperatures. *Australian Journal of Earth Sciences* **57**, 483-505.
- DANIS C., O'NEILL C., LACKIE M., TWIGG L. and DANIS A. 2011a. Deep 3D structure of the Sydney Basin using geophysical modelling. *Australian Journal of Earth Sciences* **58**, 517-542.
- DANIS C., O'NEILL C. & LEE J. 2011b. Geothermal state of the Sydney Basin: assessment of constraints and techniques. *Australian Journal of Earth Sciences* (in press)
- GERNER E.J. & HOLGATE F.L. 2010. OzTemp – Interpreted Temperature at 5km Depth Image. Geoscience Australia, Canberra.
- GROPP W.D. & LUSK E. 1996. User's guide for mpich a portable implementation of MPI, ANL-96/6.
- HARLOW F. 1955. Machine calculation method for hydrodynamics problems. Los Alamos Scientific Laboratory Report LAMS-1956.
- KIRKPATRICK S., GELATT C.D. VECCHI M.P. 1983. Optimization by simulated annealing. *Science* **220**, 671-680.
- MONAGHAN J.J. 1992. Smoothed particle hydrodynamics. *Annual Review of Astronomy and Astrophysics* **30**, 534-574.

- MORESI L., DUFOUR F. & MULHAUS H.-B. 2003. A Lagrangian integration point finite element method for large deformation modeling of viscoelastic geomaterials. *Journal of Computing Physics*, **184**, 476–497.
- MORESI L., QUENETTE S., LEMIALE V., MERIAUX C., APPELBE B., & MULHAUS H.-B. 2007. Computational approaches to studying non-linear dynamics of the crust and mantle. *Physics of the Earth and Planetary Interiors* **163**, 69-82.
- MUSSON A., HARRISON B., GORDON K., WRIGHT S. & SANDIFORD M. 2009. Thermal thinking: optimal targeting for Australian geothermal explorers. In: Budd A.R. and Gurgench H. (Editors) *Proceedings of the 2009 Australian Geothermal Energy Conference*, Geoscience Australia, Record 2009/35.
- NATIONAL COMPUTATIONAL INFRASTRUCTURE 2009. <<http://nci.org.au>> (accessed 14 September 2011).
- O'NEILL C., MORESI L., MULLER R.D., ALBERT RA., & DUFOUR F. 2006. Ellipsis 3D: A particle-in-cell finite element hybrid code for modelling mantle convection and lithospheric deformation, *Computers and Geosciences* **32**, 1769-1779.
- QUENETTE S., MORESI L., SUNTER P.D. & APPELBE W.F. 2007. Explaining StGermain: an aspect orientated environment for building extensible computational mechanics modelling software. HIPS Workshop, Parallel and Distributed Processing Symposium, Proceedings of the 19<sup>th</sup> IEEE International.
- SAMBRIDGE M. 1999a. Geophysical inversion with a neighbourhood algorithm, I, Searching a parameter space. *Geophysics Journal International* **138**, 479-494.
- SAMBRIDGE M. 1999b. Geophysical inversion with a neighbourhood algorithm, II, Appraising the ensemble. *Geophysics Journal International* **138**, 727-746.
- SULSKY D. & BRACKBILL J.U. 1991. A numerical method for suspension flow. *Journal of Computational Physics* **96**, 339-368.
- SULSKY D. & SCHREYER H.L. 1996. Axisymmetric form of the material point method with applications to upsetting and Taylor impact problems. *Computer Methods in Applied Mechanics and Engineering* **139**, 409-429.
- SWAINE DJ. 1990. Trace elements in coal. Butterworth, London.
- TURCOTTE D.L. & SCHUBERT G. 2002. Geodynamics. Cambridge University Press, Cambridge.
- VOGT D.M., WOLF A. RATH V., PECHING R. & CLAUSER C. 2010. Reducing temperature uncertainties by stochastic geothermal reservoir modelling. *Geophysics Journal International* **181**, 321-333.
- WOLLENBERG HA. & SMITH AR. 1987. Radiogenic heat production of crustal rocks: An assessment based on geochemical data. *Geophysical Research Letters* **14**, 295-298.



# CHAPTER 10

## THERMAL STRUCTURE AND GEOTHERMAL POTENTIAL



*Kowmung River, Blue Mt National Park South NSW*

## THERMAL STRUCTURE AND GEOTHERMAL POTENTIAL

This chapter presents the results of three *Underworld* high resolution 3D thermal models, using the optimised material and subsurface parameters (Chapter 4: section 4.8.3, Tables 4.8, 4.9 and 4.10; Chapter 9), to assess the thermal structure and geothermal potential of the Sydney-Gunnedah-Bowen Basin. In Chapter 5 (i.e. Danis *et al.* 2010) the 2D thermal models of the Gunnedah Basin showed subsurface architecture and geology, particularly the coal measures, have a significant influence on thermal structure. This influence is also observed in the 3D models of this chapter, as discussed in section 10.1. An assessment of the geothermal potential of the SGBB system, outlined in section 10.2, uses the key industry indicator, as defined by Goldstein *et al.* (2008) and Budd *et al.* (2008) of temperatures greater than 150°C at 5 km depth below the surface, to define areas of geothermal potential. Figure 10.1 shows the location of the thermal cross-sections and observation boreholes in the SGBB.

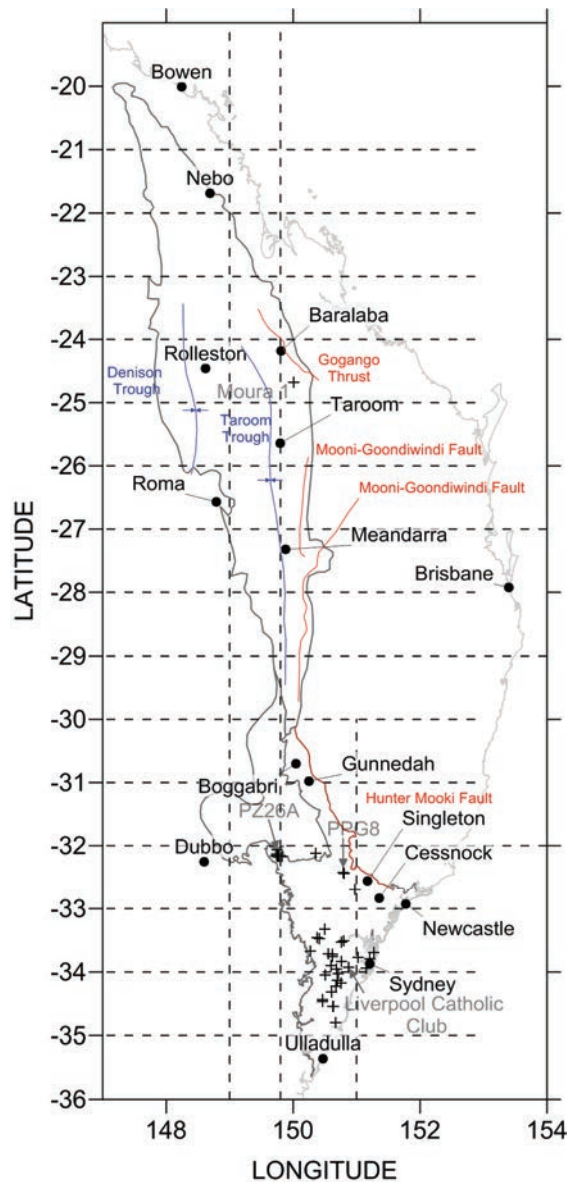


**Figure 10.1** Location of thermal cross-sections (dashed lines) and observation boreholes (crosses) in the Sydney-Gunnedah-Bowen Basin. Denison and Taroom troughs shown (blue lines) with major faults (red lines).

## 10.1 Thermal Structure of the SGBB

The 3D thermal models use optimised material and subsurface parameters as there is limited data on the temperature at depth, heat flow and material conductivity for the SGBB system. Chapter 9 identified the aspects of the model where there is uncertainty and showed how it can be constrained using observable temperatures at depth.

The observed borehole temperature data has been compared to the geotherms from the 'best fit' model, with some examples of the results shown in Figure 10.2. A good fit of the data is considered when the majority of the observed points fall within a 5% error of the modelled values and the shape of the geotherm is similar. An acceptable fit is considered when the observed points are within 10% of the modelled values and a poor fit is when the observed points are outside of this range. During calibration improving the fit in one area often reduced it in another and thus it was biased towards the 'well trusted' boreholes.

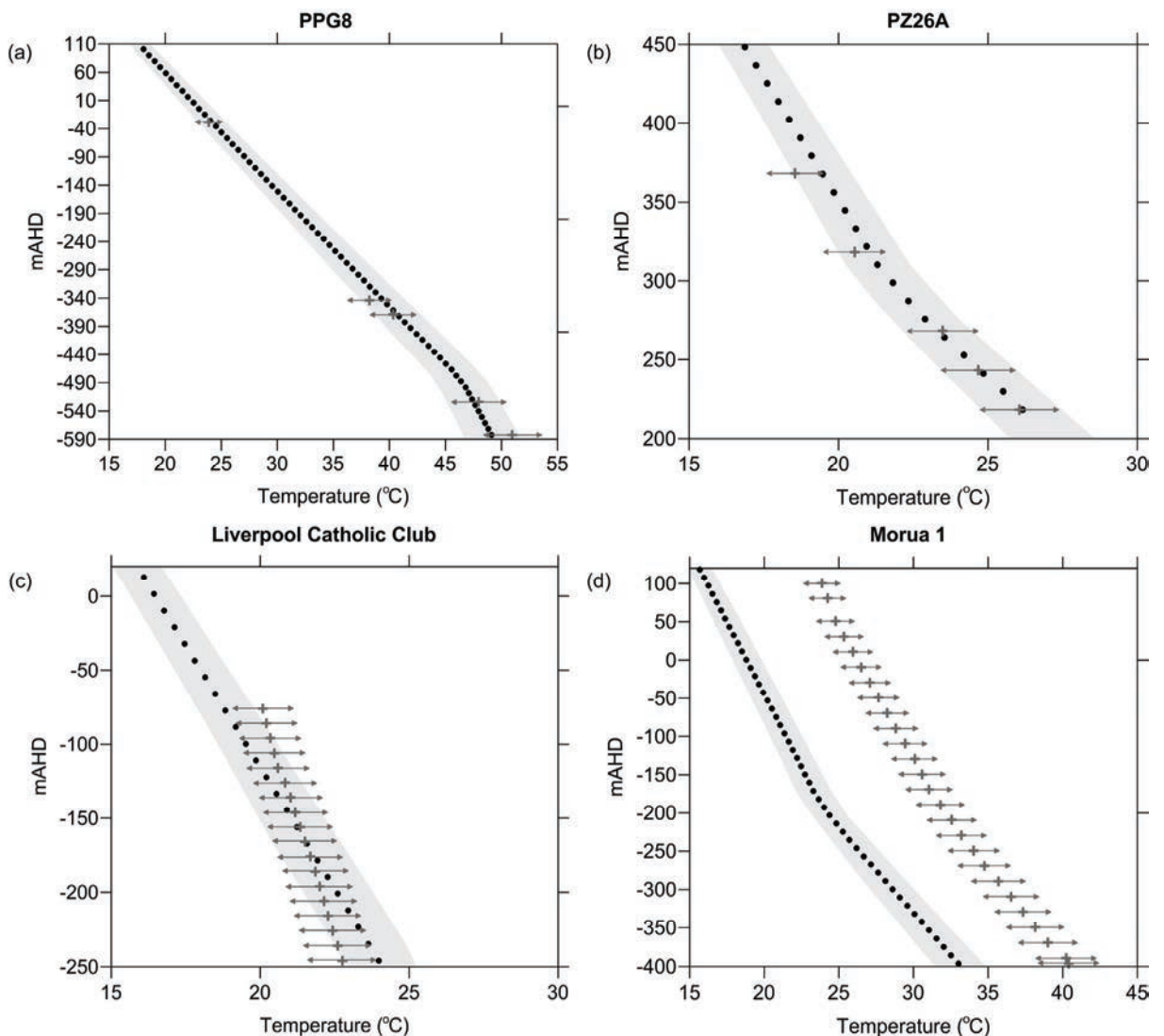


**Figure 10.2** Model values compared to observed temperature at depth measurements for at borehole location a) PPG8, b) PZ26A, c) Liverpool Catholic Club and d) Moura 1. Grey shaded area is 5% error on modelled values. Grey arrows indicate 5% error on observed temperatures.

Figure 10.2 presents geotherm plots of the modelled data with observed data at four locations, three of which are from 'well trusted' boreholes (PPG8, PZ26A and Liverpool Catholic Club) and one (Figure 10.2d) from an un-trusted borehole. These plots illustrate examples of good model fit (e.g. Figure 10.2a, b) where the majority of observed points fall within 5% error of the modelled values and the shape of the geotherm is similar. 23 of the 40 calibration boreholes comply with these criteria and are considered a good fit with the 'best fit' model.

In figure 10.2c the majority of the observed temperatures fall within 5% of the modelled values but the overall shape of the geothermal is not consistent with the model. This is an acceptable fit of the data but highlights that the thermal structure is being influenced, most likely by the advective effects in the shallow aquifers. There are 5 boreholes which show this trend and all are located in shallow Hawkesbury Sandstone aquifers. The remaining 12 boreholes are considered poor fits to the model data as the observed values fall outside the 10% error, as shown in Figure 10.2d, but interestingly the shape of the geotherm for most of them is still relatively similar to the model. All but HRP1 and Moura 1, which are in Permian strata, are in shallow aquifers.

Moura 1, as shown in Figure 10.2d, was the only borehole identified in the Bowen Basin (Figure 10.1) which appeared to match the criteria for an equilibrated temperature measurement, though it is uncertain if it is truly equilibrated since the fit with the model data is poor. This borehole was not used to calibrate the model but rather as an observation point to assess the application of regional 'best-fit' material and subsurface parameters for the Bowen Basin. From Figure 10.2d the observed temperatures are approximately 5°C higher than the model values and well outside the 5% error range. This suggests either the borehole may not be truly equilibrated or the thermal model is not representative in this part of the basin because of the inherent model assumptions and uncertainties. The assumption of basement homogeneity, both in geology and thermal properties, is a false but necessary simplification for the scale of the SGBB model. Therefore, it is important to remember this uncertainty when assessing the thermal structure.

Three models were run, using the material properties defined in Tables 4.8, 4.9 and 4.10 of Chapter 4, with the main difference for each model being the conductivity ( $K_0$ ) of the coal measures. The models are run with a resolution equivalent to a 3000 m by 17 m by 3000 m cell size on 512 nodes of the NCI Vayu supercomputer. Model 1 uses  $K_0 = 1.2$  for the Permian coal measures (PCM) and  $K_0 = 0.3$  for all other coal measures. Model 2 uses  $K_0 = 1.2$  for all coal measures and Model 3 uses  $K_0 = 1.2$  for the PCM and  $K_0 = 2$  for all other coal measures. In each of these model runs the fit between the model values and observed temperatures did not significantly change.

Figure 10.3 presents a series of East-West and North-South thermal cross-sections through the SGBB showing the model geometry (i.e. surface elevation, coal measures, basal volcanics and basement surface) with the 150°C temperature isotherm for Model 1. In the northern part of the Bowen Basin (Figure 10.3a to c) basal volcanics are absent in the Taroom Trough and the isotherm is around -5000 mAHD. The coal measure (the Permian) causes a minor perturbation of the isotherm, to around -4000 mAHD, in Figures 10.3b and 10.3c in the deep parts of the Taroom Trough, where sediment thickness



is approximately 3 km. In the central part of the Bowen Basin (Figures 10.3d and 10.3e) the introduction of a second coal measure (the Jurassic) results in a further shallowing of the isotherm up to -2600 mAHD (e.g. Figure 10.3d).

In the southern Bowen Basin (Figure 10.3f) there is one coal measure and the basement is shallower and basal volcanics are thin. Here the isotherm is around -5000 mAHD. In the Gunnedah Basin, Figures 10.3f and 10.3g, the Meandarra Gravity Ridge correlates with the occurrence of basal volcanics and the eastern extent of the coal measures are truncated by the Hunter-Mooki Fault. This basin is relatively shallow, with up to 2 km of sediment cover in parts, and the isotherm is stable at around -4900 mAHD.

In the Sydney Basin (Figures 10.3h to 10.3j) sediment thickness ranges from less than 500m to up to 3.5 km with thick basal volcanics. The isotherm ranges from approximately -5000 mAHD (Figure 10.3j) where sediment is thinnest to -4500 mAHD (Figure 10.3i) where sediment is thickest. Figures 10.3k and 10.3l present two North-South cross-sections; one through the western part of the Bowen Basin, including the Denison Trough, and the other through the central Sydney Basin. These cross-sections show the isotherm shallowing significantly where two coal measures, particularly in the Denison Trough area (Figure 10.3k), are present.

Figures 10.4 to 10.9 present a comparison of selected cross-sections, for each of the three models, in the deep parts of the Bowen Basin and the north-eastern part of the Sydney Basin. The  $K_0$  value is related to the composition ratio of coal to sediments.  $K_0 = 0.3$  represents 50% coal to 50% sediment in Model 1,  $K_0 = 1.2$  represents 10% coal to 80% sediment in Model 2 and  $K_0 = 2$  represents 100% sediment with no coal. In this way the range of temperatures observed covers the possible outliers. In Model 1  $K_0 = 0.3$ , for the Reid Dome Beds coal measures, the depth of the isotherm is significantly reduced, and in places produces very steep localised gradients, compared to the results of Models 2 and 3.

This is particularly observed in the Denison Trough of Figures 10.4 and 10.5 where there is the addition of Permian coal measures. In Model 1 the isotherm is around -1100 mAHD (Figure 10.4a) and -800 mAHD (Figure 10.5a), in Model 2 it is around -2100 mAHD (Figure 10.4b) and -3000 mAHD (Figure 10.5b) and in Model 3 it is around 3000 mAHD (Figure 10.4c) and -3700 mAHD (Figure 10.5c). There is a significant difference in depth of the isotherm in the Denison Trough between the models but in the Taroom Trough, where only PCM is present, the depth of the isotherm between each model is relatively consistent at -4100 mAHD.



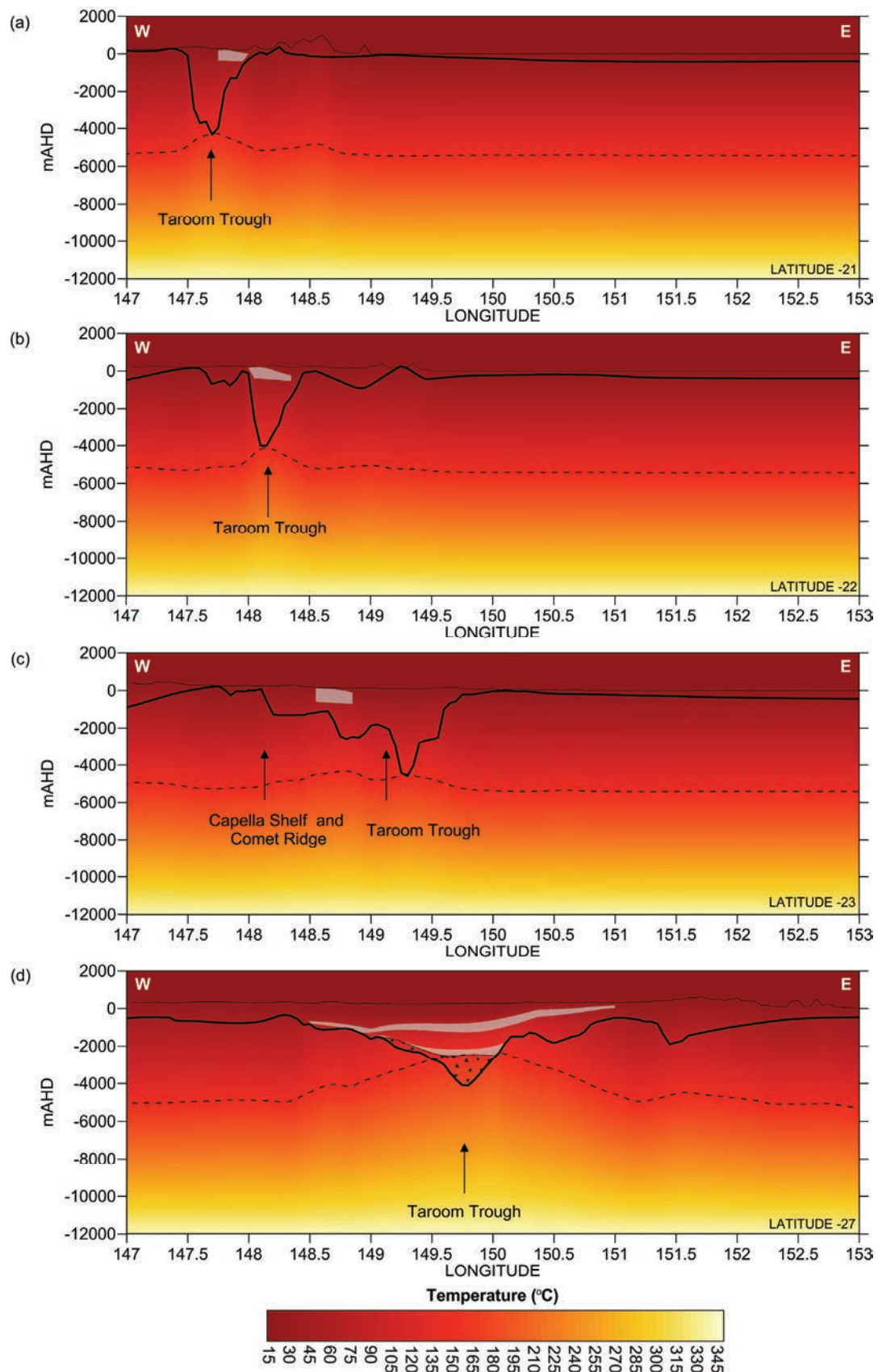


**Figure 10.3** Thermal profiles in the Sydney-Gunnedah-Bowen Basin for Model 1 East-West for Latitude a) -21, b) -22, c) -23, d) -27, e) -29, f) -30, g) -31, h) -32, i) -34, j) -35 and Longitude k) 149 and l) 151. Basement geometry (thick black line), coal measures (grey shading), basal volcanics (black triangles), surface elevation (black line) and 150°C temperature isotherm (dashed line). Depth in metres Australian Height Datum (mAHD). Refer to Figure 10.1 for profile locations.

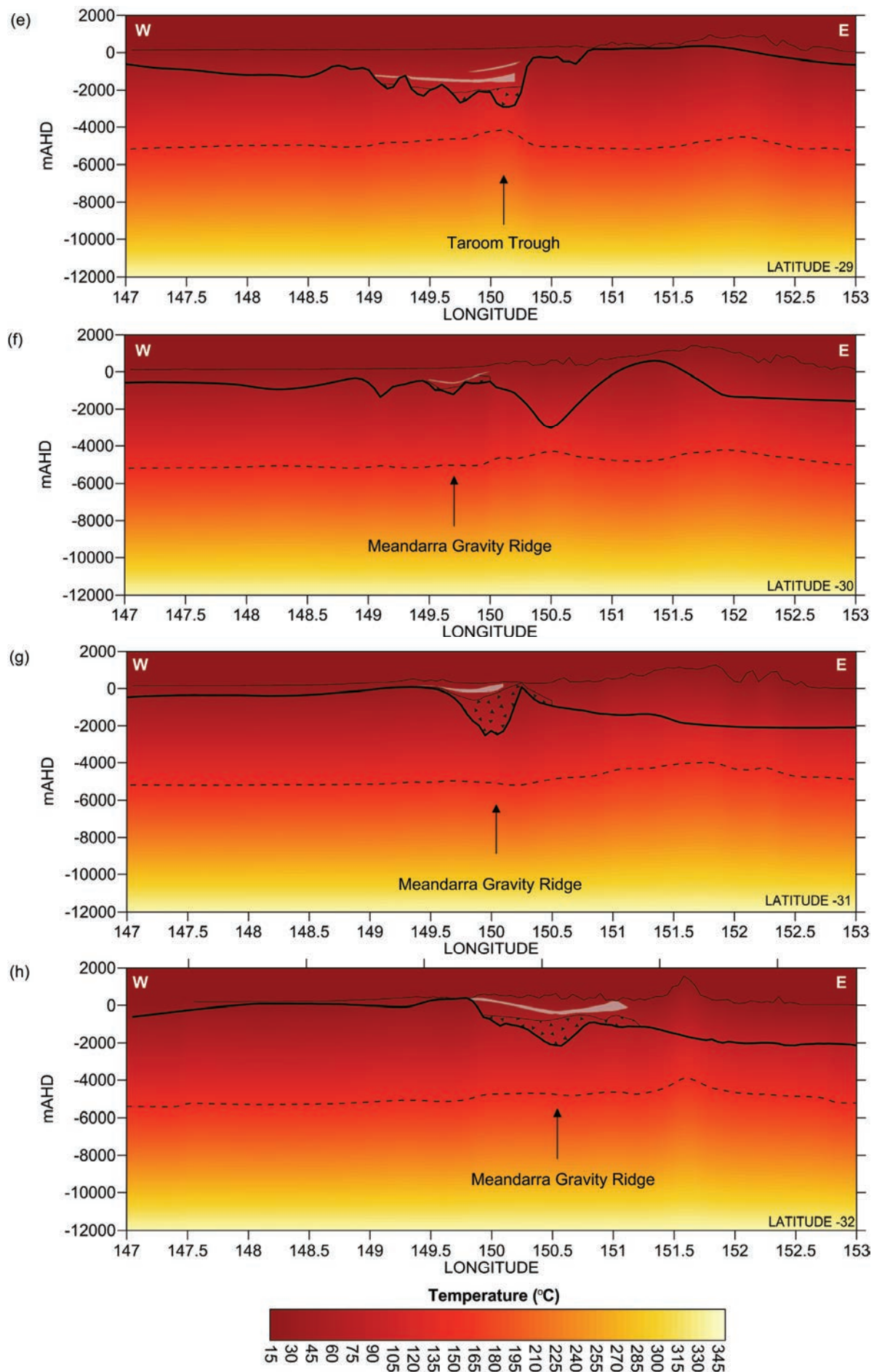


Figure 10.3 (Continued)

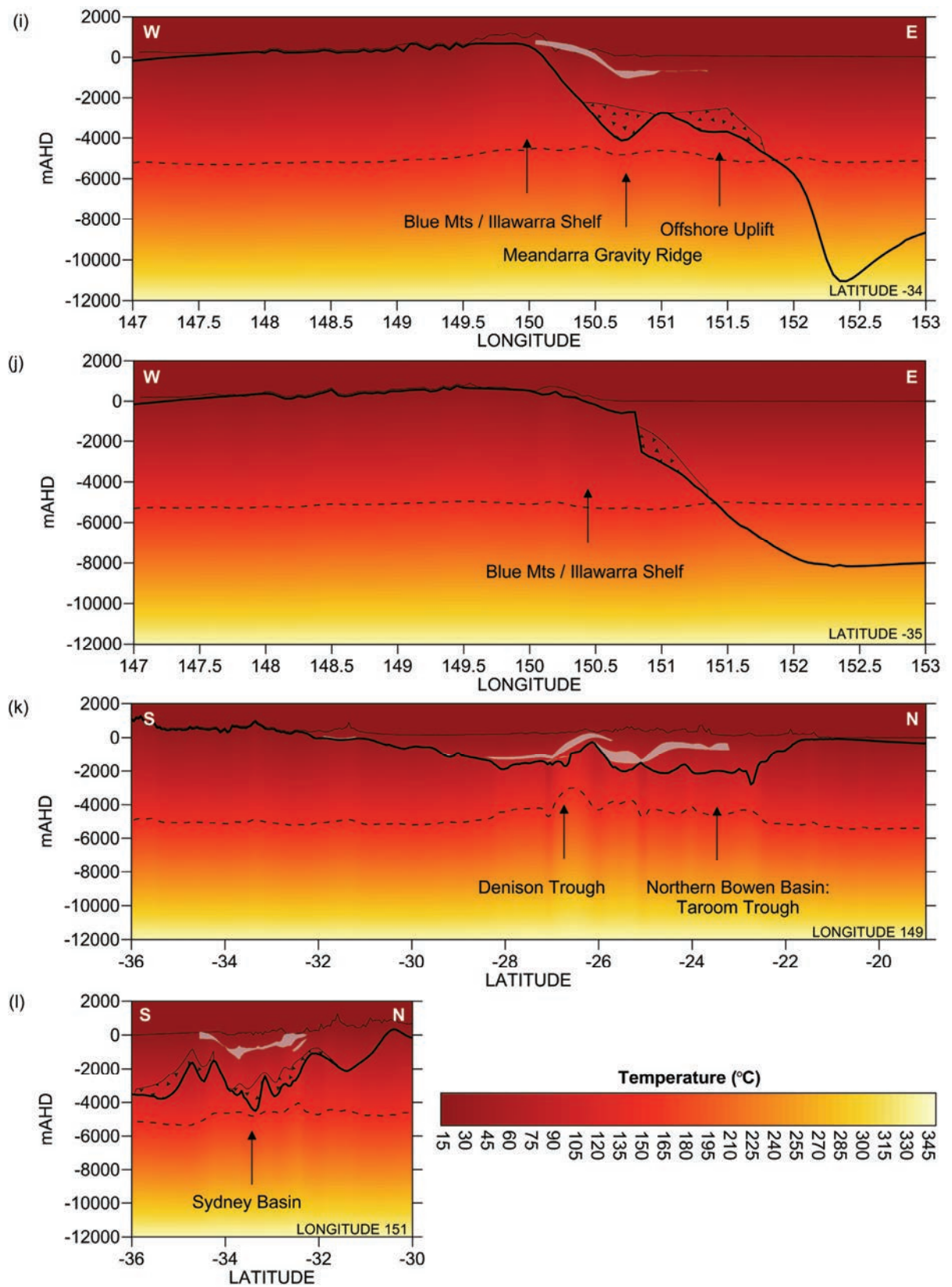
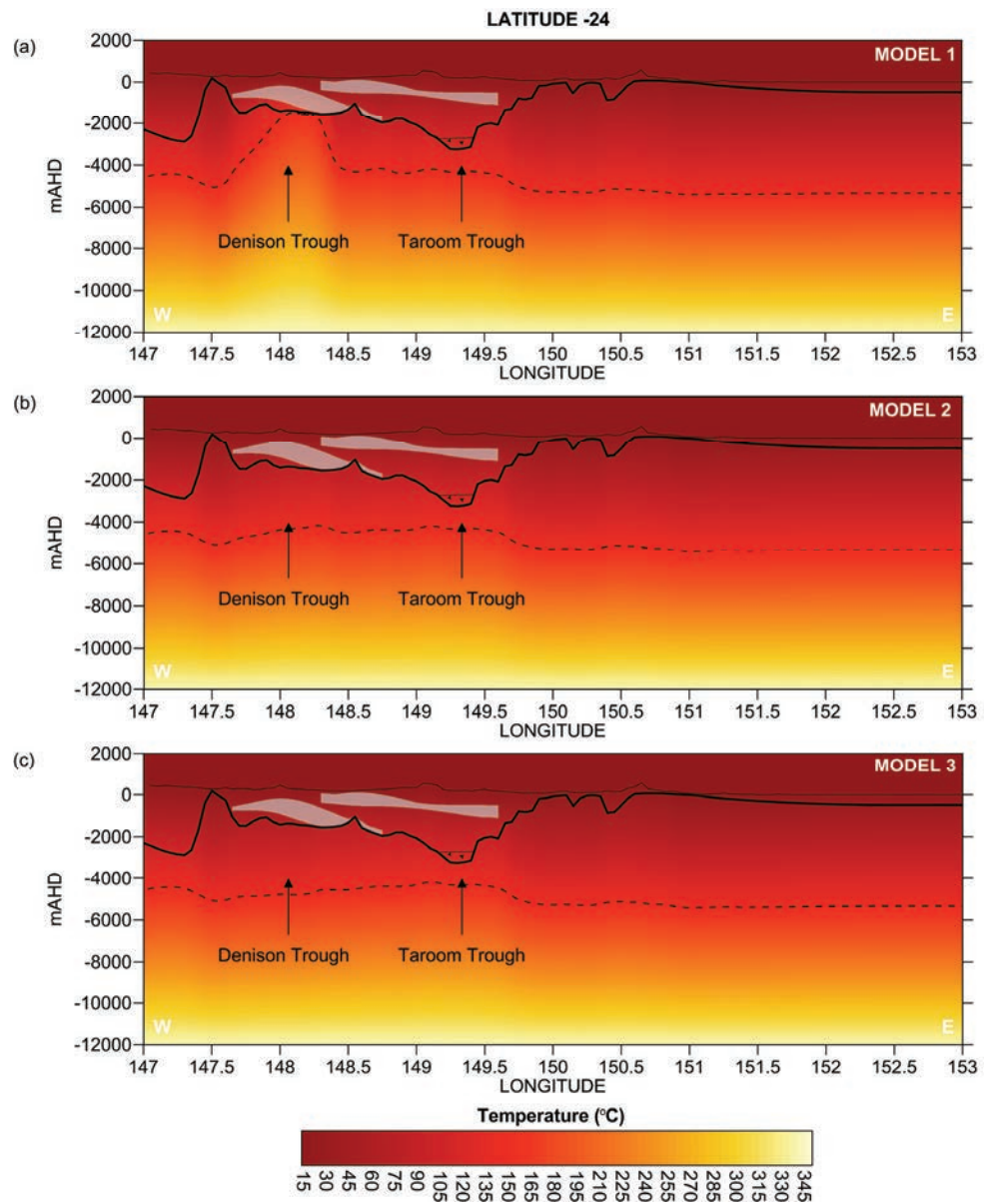
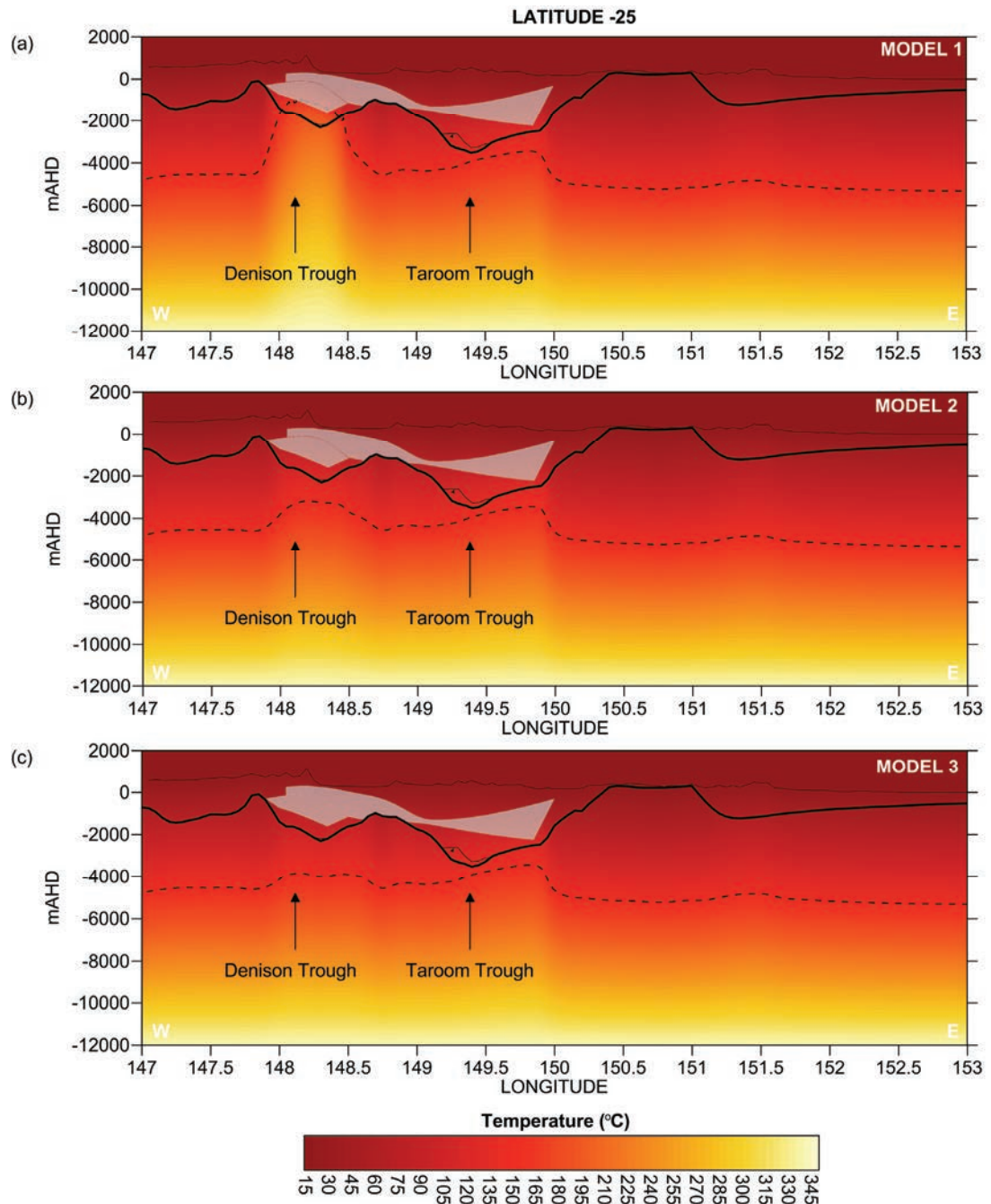


Figure 10.3 (Continued)





**Figure 10.4** East-West thermal cross-section for Latitude -24 in the northern Bowen Basin for a) Model 1, b) Model 2 and c) Model 3. Depth in metres Australian Height Datum (mAHD). Geometry as per Figure 10.3, see Figure 10.1 for location.



**Figure 10.5** East-West thermal cross-section for Latitude -25 in the northern Bowen Basin for a) Model 1, b) Model 2 and c) Model 3. Depth in metres Australian Height Datum (mAHD). Geometry as per Figure 10.3, see Figure 10.1 for location.

In Figure 10.6, in the Taroom Trough, the depth of the isotherm is reasonably consistent between each model, at around -2600 mAHD in Model 1, -2800 mAHD in Model 2 and -3000 mAHD in Model 3, despite the presence of two coal measures. The perturbation of the isotherm is less intense than in Denison Trough (Figure 10.4) and this is most likely due to the shallow nature of the Jurassic coal measures. It is the PCM which exerts the most influence on the thermal structure. The isotherm shows a distinctive trend of shallowing towards the east in Figure 10.6b and 10.6c. The truncation of the PCM, at its thickest point, against a rapidly shallowing basement results in heat refraction to the east and thus a shallowing of the isotherm. Heat refraction, around terminating coal measures, was first



shown in the 2D thermal profiles of Chapter 5 and 7 and continues to be an important feature in the thermal structure of the SGBB.

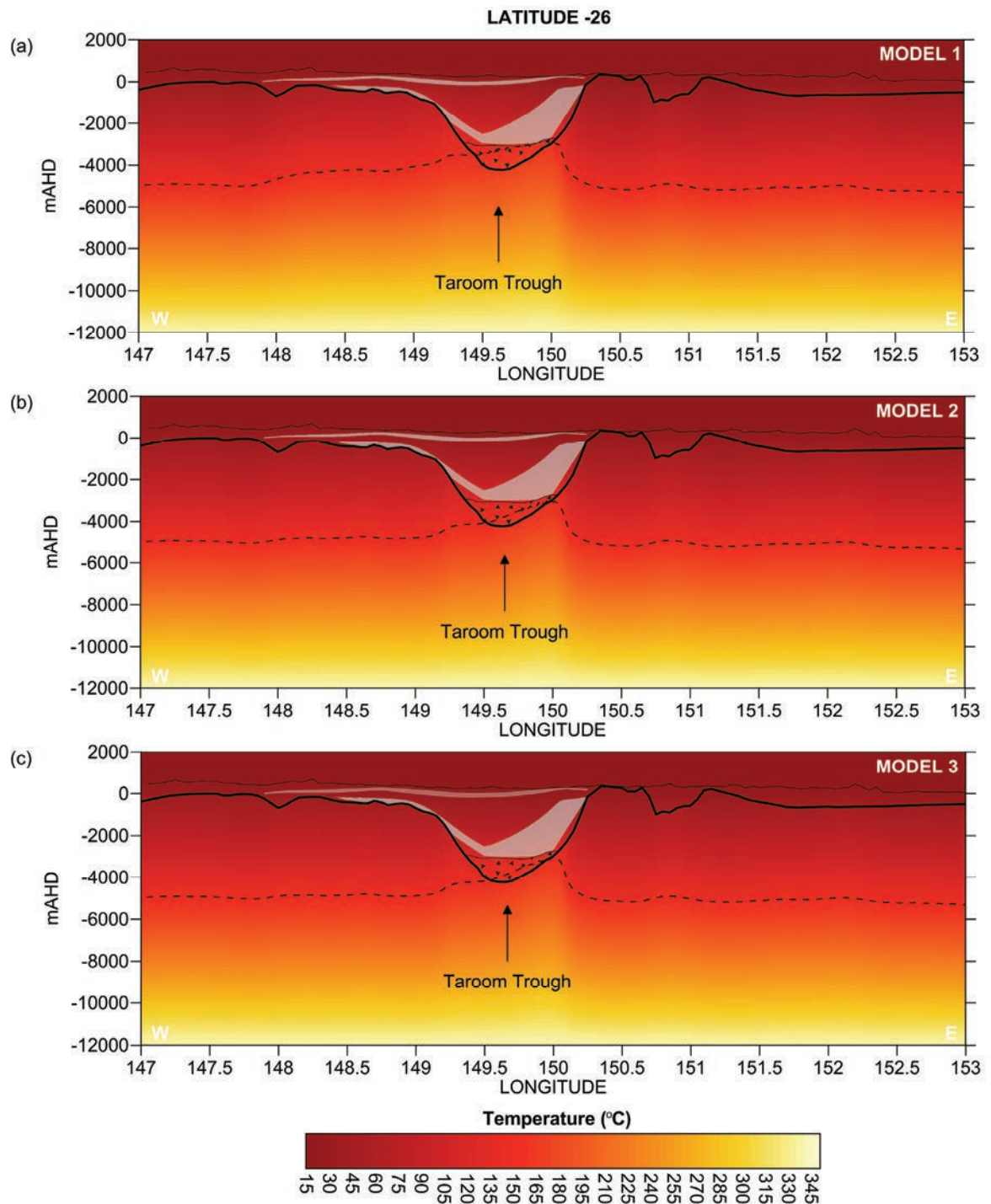


**Figure 10.6** East-West thermal cross-section for Latitude -26 in the central Bowen Basin for a) Model 1, b) Model 2 and c) Model 3. Depth in metres Australian Height Datum (mAHD). Geometry as per Figure 10.3, see Figure 10.1 for location.

Heat refraction is also observed in Figure 10.7, along with asymmetrical shallowing of the isotherm. In Model 1 the isotherm is around -3800 mAHd in (Figure 10.7a) compared to -4000m in Models 2 and 3 (Figure 10.7b and 10.7c). The Jurassic coal measures are deeper, compared to Figure 10.6, but with a thinner PCM the overall depth of the isotherm is greater than in Figure 10.6.

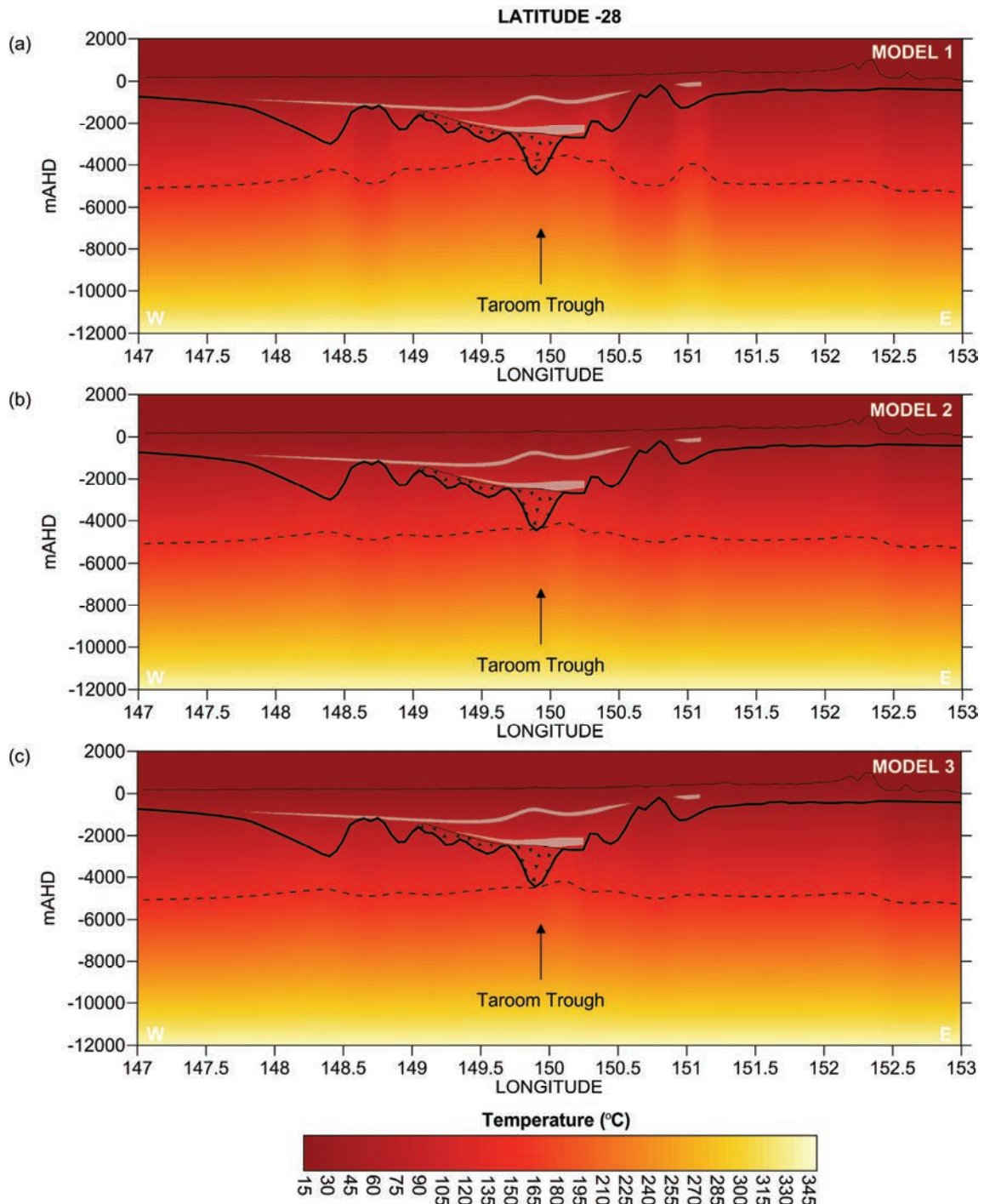


**Figure 10.7** East-West thermal cross-section for Latitude -25 in the southern Bowen Basin for a) Model 1, b) Model 2 and c) Model 3. Depth in metres Australian Height Datum (mAHd). Geometry as per Figure 10.3, see Figure 10.1 for location.

Figure 10.8 presents a cross-section through the north-eastern part of the Sydney Basin and includes the deep offshore area of the Newcastle Syncline. Sediment thickness is approximately 3.5 km onshore and reaches up to 6 km offshore and overlies thick onshore and offshore basal volcanics. Two coal measures are present, the upper being the PCM and the lower being the Greta. There is significant perturbation of the isotherm around the Greta coal measures in the offshore part of the basin, similar to the results of the Denison Trough profile, in Figure 10.8b. In Figure 10.8b and 10.8c there is a slight elevation of the isotherm on the western edge of the basin, most likely a result of the PCM, thick sediment cover and thick basal volcanics.

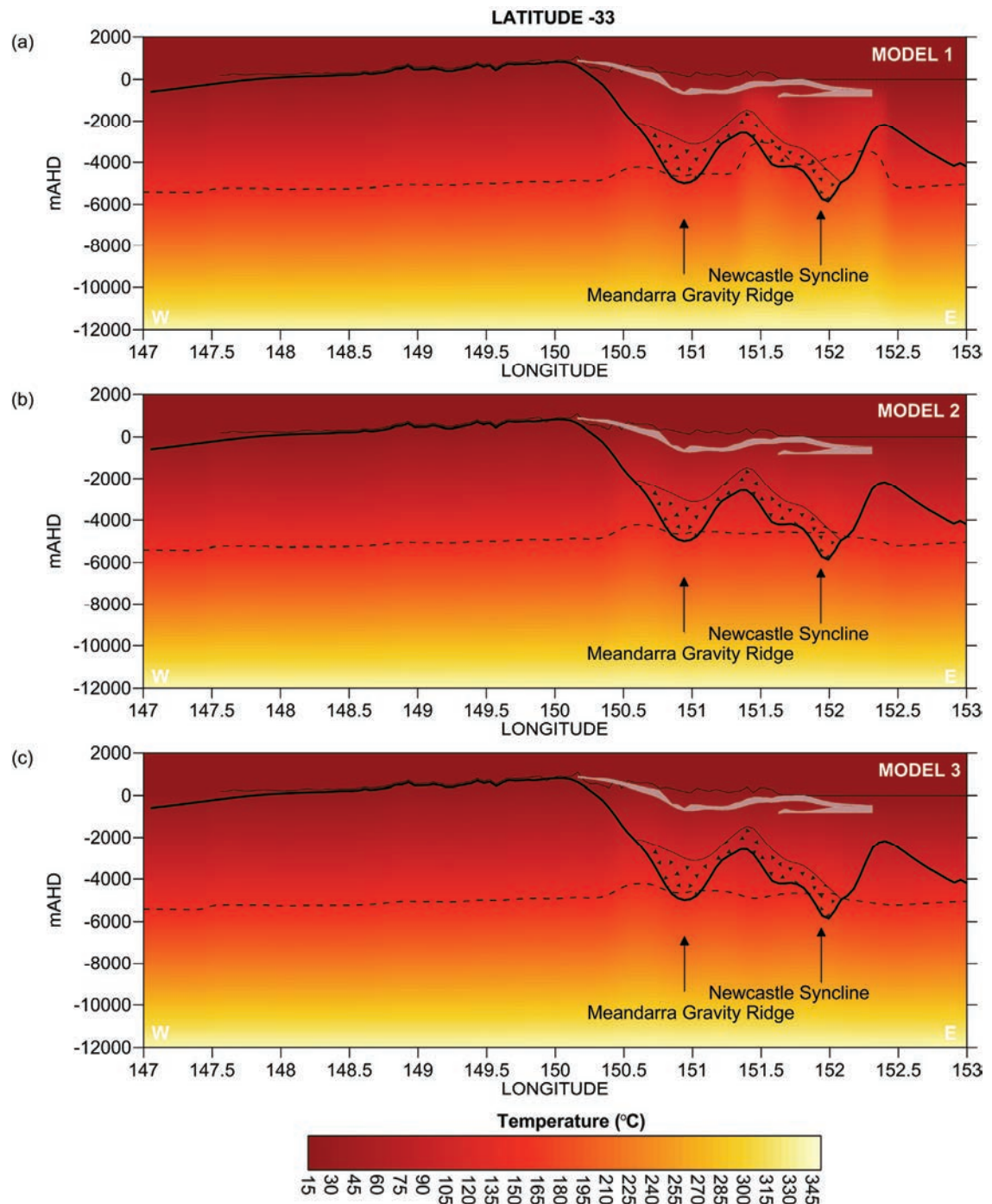


**Figure 10.8** East-West thermal cross-section for Latitude -33 in the Sydney Basin for a) Model 1, b) Model 2 and c) Model 3. Depth in metres Australian Height Datum (mAHD). Geometry as per Figure 10.3, see Figure 10.1 for location.



The North-South cross-section (Figure 10.9) is an additional example of the difference in depth of the isotherm between the three different models. This profile runs through the central part of the Bowen and Gunnedah Basin. In the deep part of the central Bowen Basin, under around 3 to 4 km of sediment, and several km of basal volcanics, temperatures are expected to be elevated. The isotherm is shallowest at around -2600 mAHd in Model 1 but much deeper, at around -3700 mAHd for Models 2 and 3, in the Bowen Basin. Despite the insulating coal measures and thick basal volcanics the isotherm in the Gunnedah Basin remains relatively stable around -4800 mAHd. Heat refraction is observed in Figure 10.9b, in the central Bowen Basin, with the isotherm shallowest towards the north reflecting the termination of the Jurassic coal measures, combined with the thickest part of the PCM.

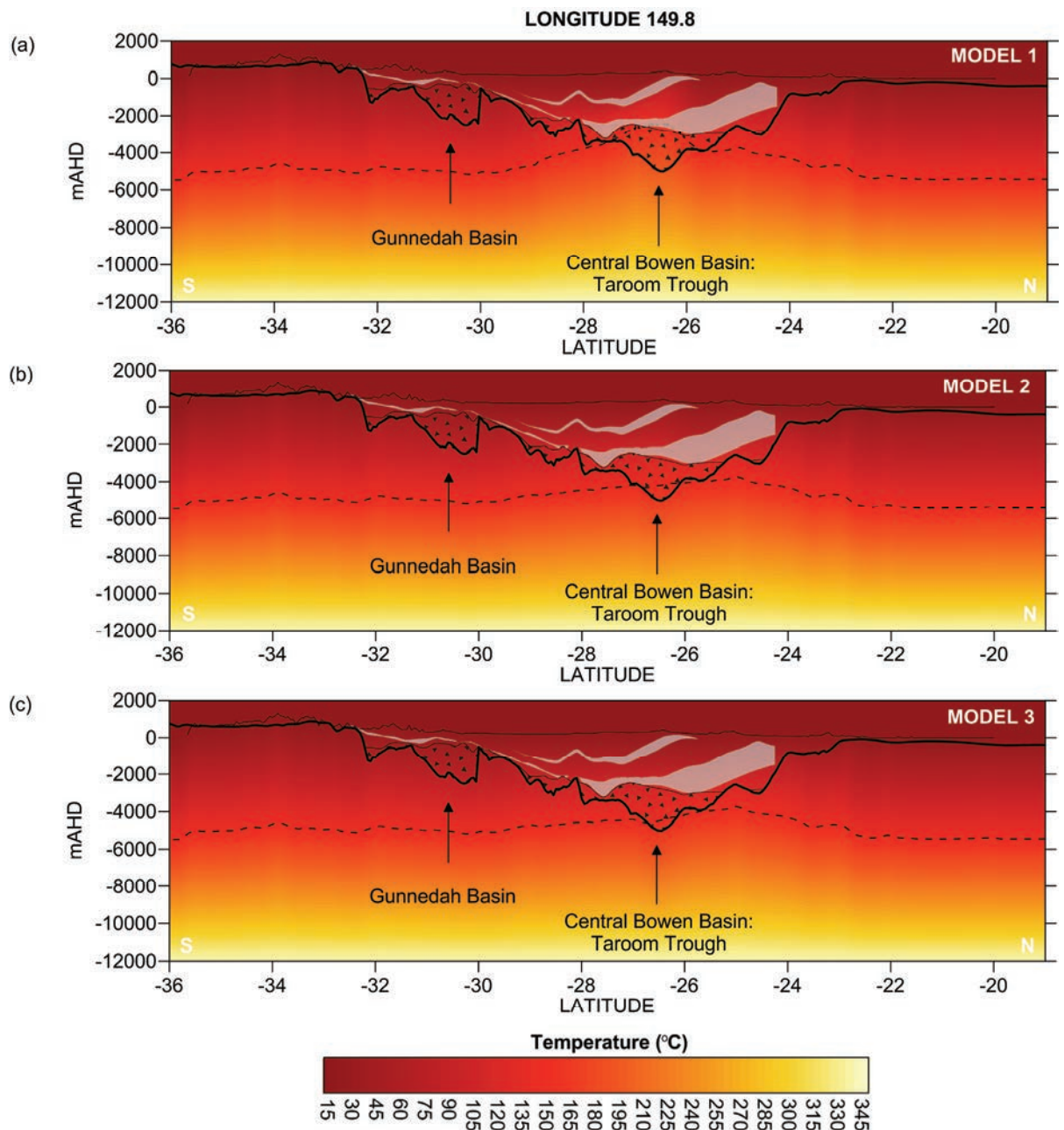


**Figure 10.9** North-South thermal cross-section for Longitude 149.8 through the central part of the Gunnedah and Bowen basins for a) Model 1, b) Model 2 and c) Model 3. Depth in metres Australian Height Datum (mAHd). Geometry as per Figure 10.3, see Figure 10.1 for location.

The thermal structure of the SGBB, from the results of these three models, is strongly dominated by the architecture of the basin and its geology and the thermal properties of the coal measures. The geometry is important as it determines areas of heat refraction from the termination of coal measures. On the eastern margin thrust faults rapidly uplift the basement and truncate the coal measures when they are thickest. Basement geometry is important for thermal structure but this suggests fault geometry, could also be important.

Sediment accumulation in the deep depocentres (i.e. Taroom and Denison troughs), thick basal volcanics and multiple coal measures all influence the thermal structure. In addition basement heterogeneity, especially high heat producing granites, and the advective effects of aquifers will also influence thermal structure, although they have not been assessed in this research. It is likely that some boreholes used in the calibration of the model may be affected by the advective effects of shallow aquifers, or indeed other affects such as pumping or rainfall recharge. These are likely to be the boreholes which show values within 5% of the modelled values and are mostly from the Hawkesbury Sandstone aquifer. Boreholes which measure temperatures in deeper Permian aquifers (i.e. PZ26A) do fit well with the model values and suggest the deeper thermal structure may not be as affected by advection.

In Model 1,  $K_0 = 0.3$  for the Jurassic, Reid Dome Beds and Greta coal measures produces significant perturbations of the isotherm with steep thermal gradients, especially when PCM is also present, but the heat refraction is difficult to observe. As the coal to sediment ratio is unlikely to be 50:50 this model is not the most appropriate representation of the thermal structure of the SGBB. Heat refraction is clearly observed in both Model 2 and Model 3. The thermal structure of these models is very similar, with the main difference being  $K_0$  for the non Permian coal measures but Model 2 is most likely representative of the SGBB.

## 10.2 Geothermal Potential

Detailed large scale thermal modelling provides an avenue to direct geothermal exploration programs to areas of highest geothermal potential, based on reliable and representative estimates of temperature at depth. The research of this project uses the criteria of 'temperatures greater than 150°C at 5 km depth below the surface' to determine areas of geothermal potential, although the ability to commercialise the geothermal potential of the SGBB is ultimately dependent on a series of other factors, which are not assessed in this project.

Figure 10.10 presents the contour depth maps of the 150°C temperature isotherm in metres below ground surface for each of three models of the SGBB. The thermal cross-sections showed that the isotherm can be significantly elevated where multiple coal measures are present, i.e. the Denison Trough. Figure 10.10a shows that for Model 1 the minimum depth to the isotherm is around 800 m in the Denison Trough and 1800 m in the Taroom Trough and in the areas surrounding, the depth quickly increases to 3600 m. For the majority of the SGBB the depth of the isotherm is generally greater than 4000 m. In Model 2 (Figure 10.10b) the depth to the isotherm for the majority of the SGBB is around



4500 m. The shallowest depths observed in the Denison and Taroom troughs of between 4000 m to 3000 m.

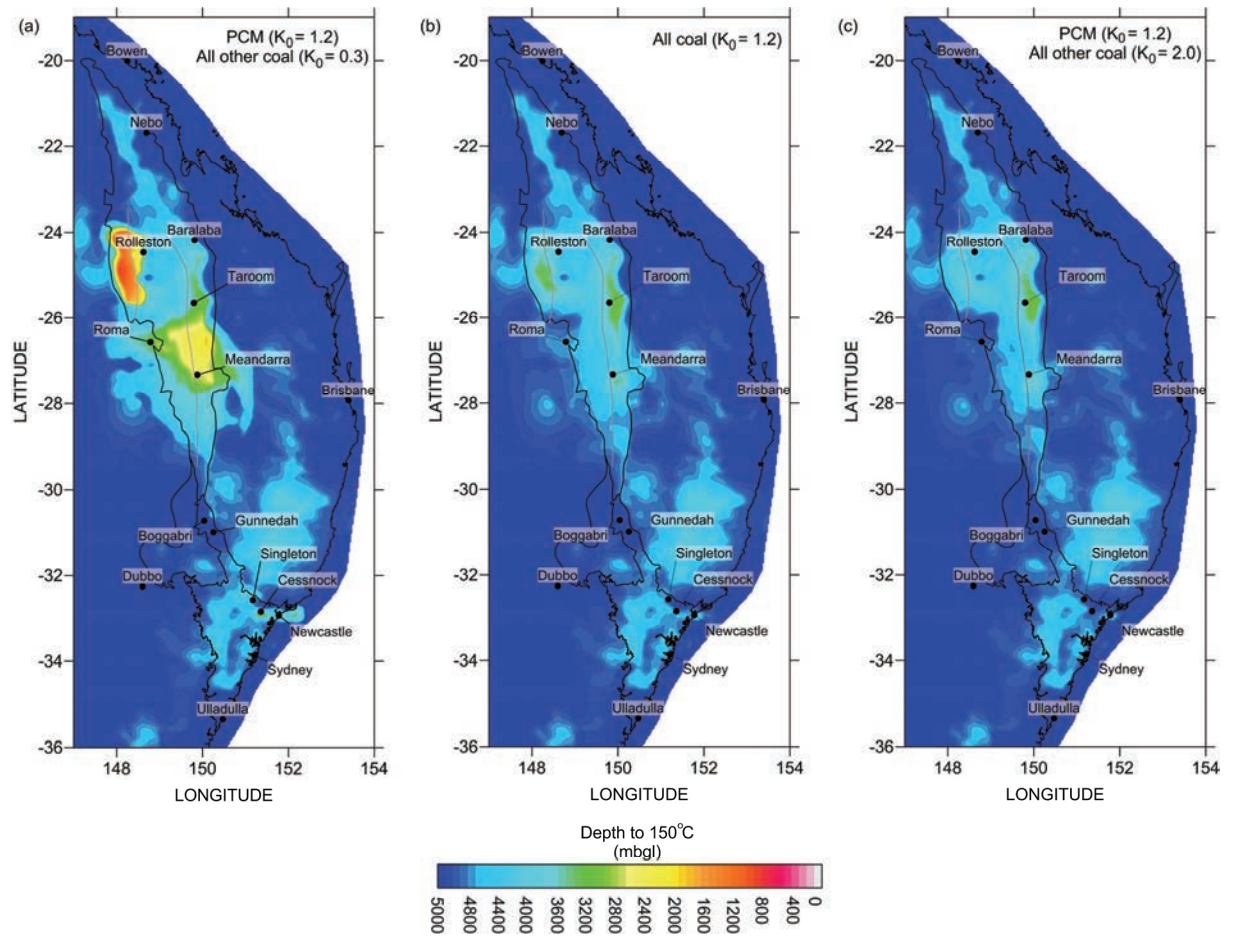


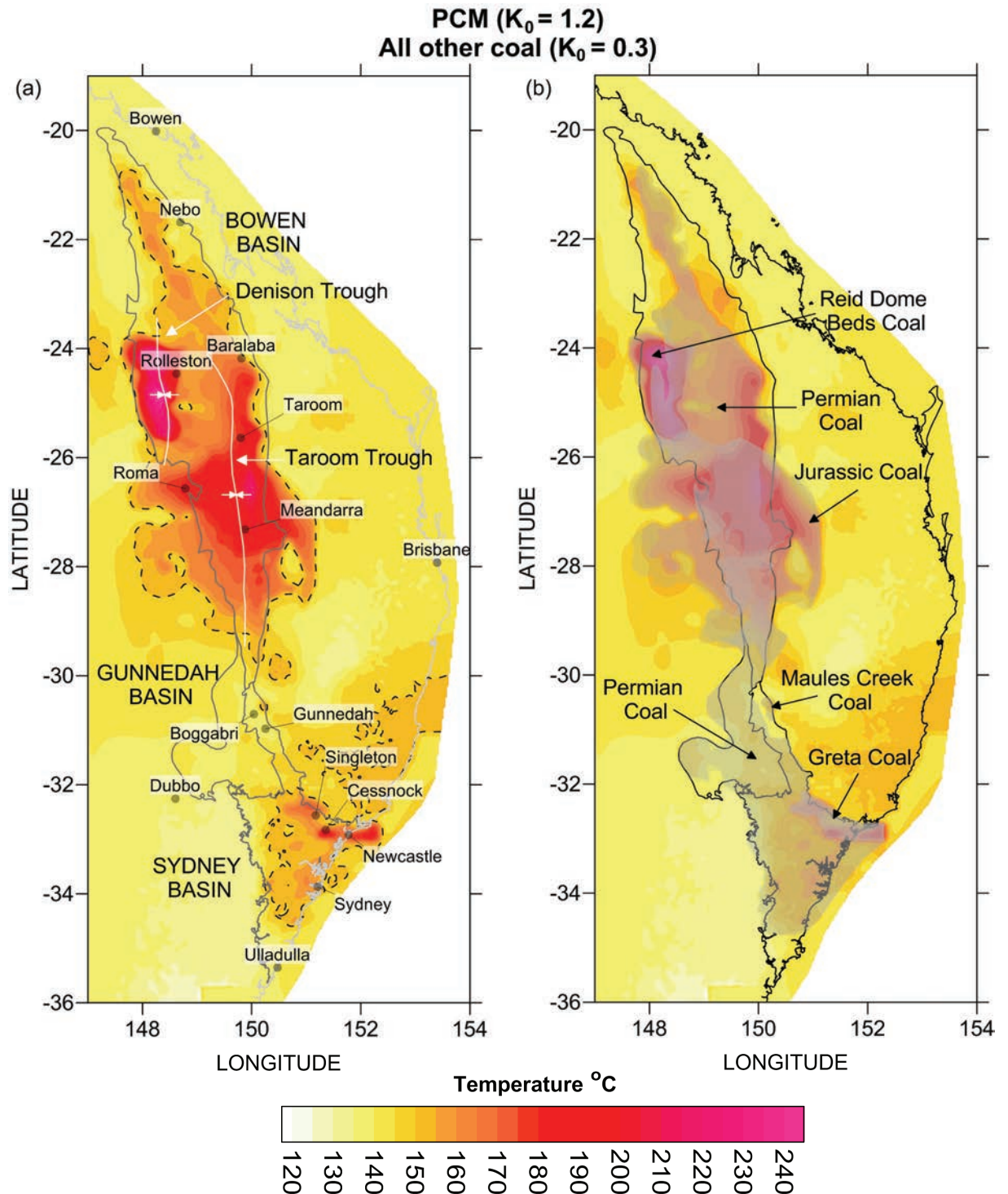
**Figure 10.10** Depth of the 150°C temperature isotherm in metres below ground level (mbgl) for the Sydney-Gunnedah-Bowen Basin system from a) Model 1, b) Model 2 and c) Model 3. Denison and Taroom troughs shown (grey lines) as per Figure 10.1.

For Model 3 the isotherm, for the majority of the SGBB, is around 4600 m with the shallowest depths observed in the Taroom Trough of between 3600 m to 3000 m.

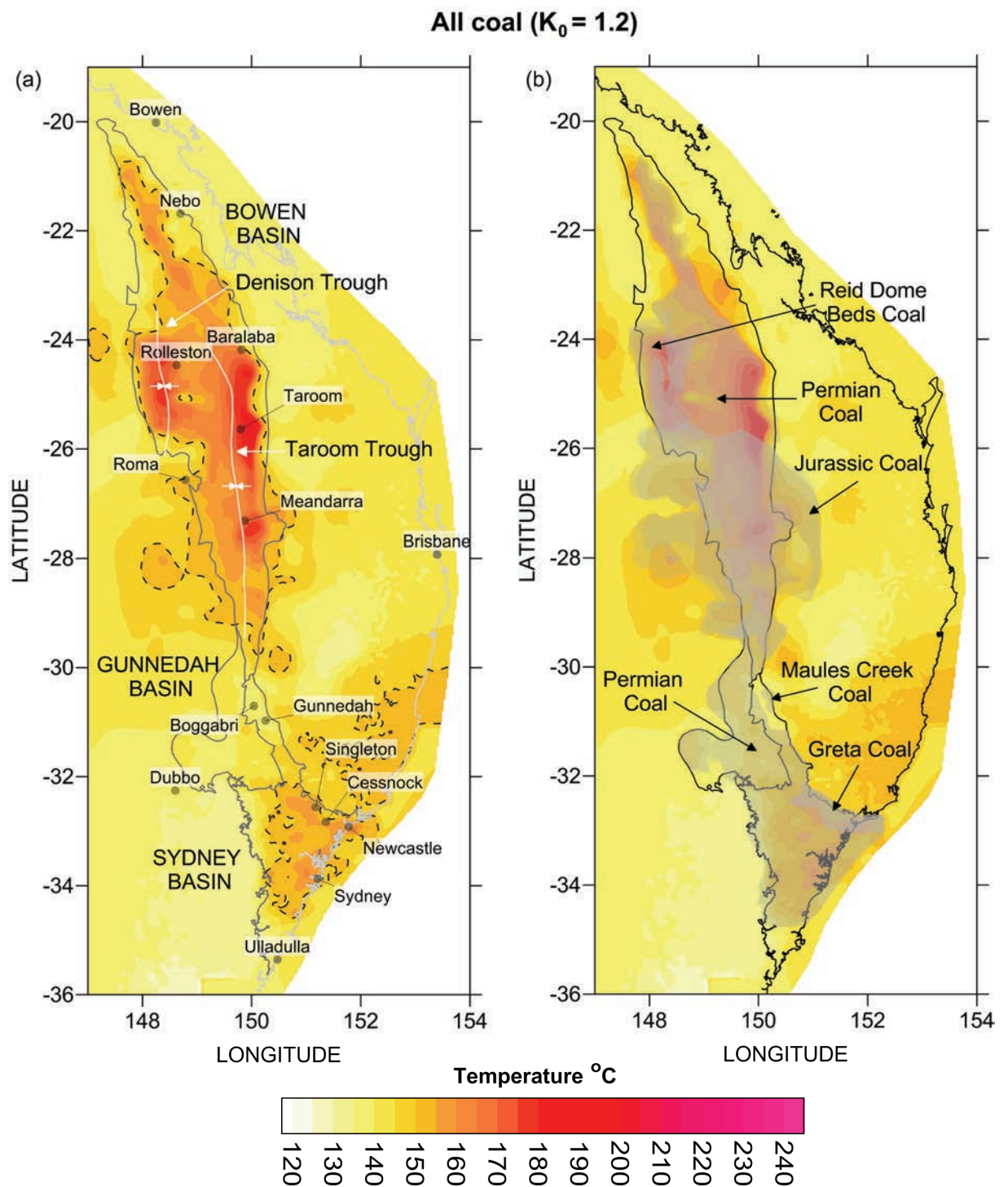
With Model 1 not considered representative of the thermal structure of the SGBB, the depth of the 150°C isotherm, as an indicator of geothermal potential, is assessed from Models 2 and 3. For the majority of the SGBB the isotherm occurs at depths below 4000 m but there are parts where the depth is as shallow as 3000 m. These results conclude that there is a significant portion of both the Sydney and Bowen basins which have temperatures above the required 150°C at depths 5 km or less. The Gunnedah Basin however, appear to be only a few areas where this occurs.

Figure 10.11 to 10.13 present the estimated temperature at 5 km below the ground surface for each of the three models, with a corresponding overlay of the location and extent of the coal measures. With 5 km considered the current economic limit of drilling a map showing the estimated temperature at this depth is a valuable tool for identifying potential geothermal anomalies for geothermal exploration. In Model 1 (Figure 10.11) the temperature at depth ranges from 140°C to almost 240°C, with the highest

temperatures under areas with multiple coal measures. For Model 2 (Figure 10.12) the maximum temperature is around 155°C in the Sydney Basin, 145°C in the Gunnedah Basin and 190°C in the Bowen Basin. For Model 3 (Figure 10.13) the maximum temperatures at depth is around 185°C in the Sydney Basin, 150°C in the Gunnedah Basin and 185°C in the Bowen Basin. In Model 2 a greater proportion of the Bowen Basin is over 160°C than for Model 3, but in the north-eastern part of the Sydney Basin a greater proportion is over 160°C in Model 3 than in Model 2.



**Figure 10.11** Estimated temperature at 5 km below ground level for the Sydney-Gunnedah-Bowen Basin for Model 1 showing a) the 150°C isotherm (dashed line) and b) coal measures (grey shading).



**Figure 10.12** Estimated temperature at 5 km below ground level for the Sydney-Gunnedah-Bowen Basin for Model 2 showing a) the 150°C isotherm (dashed line) and b) coal measures (grey shading).



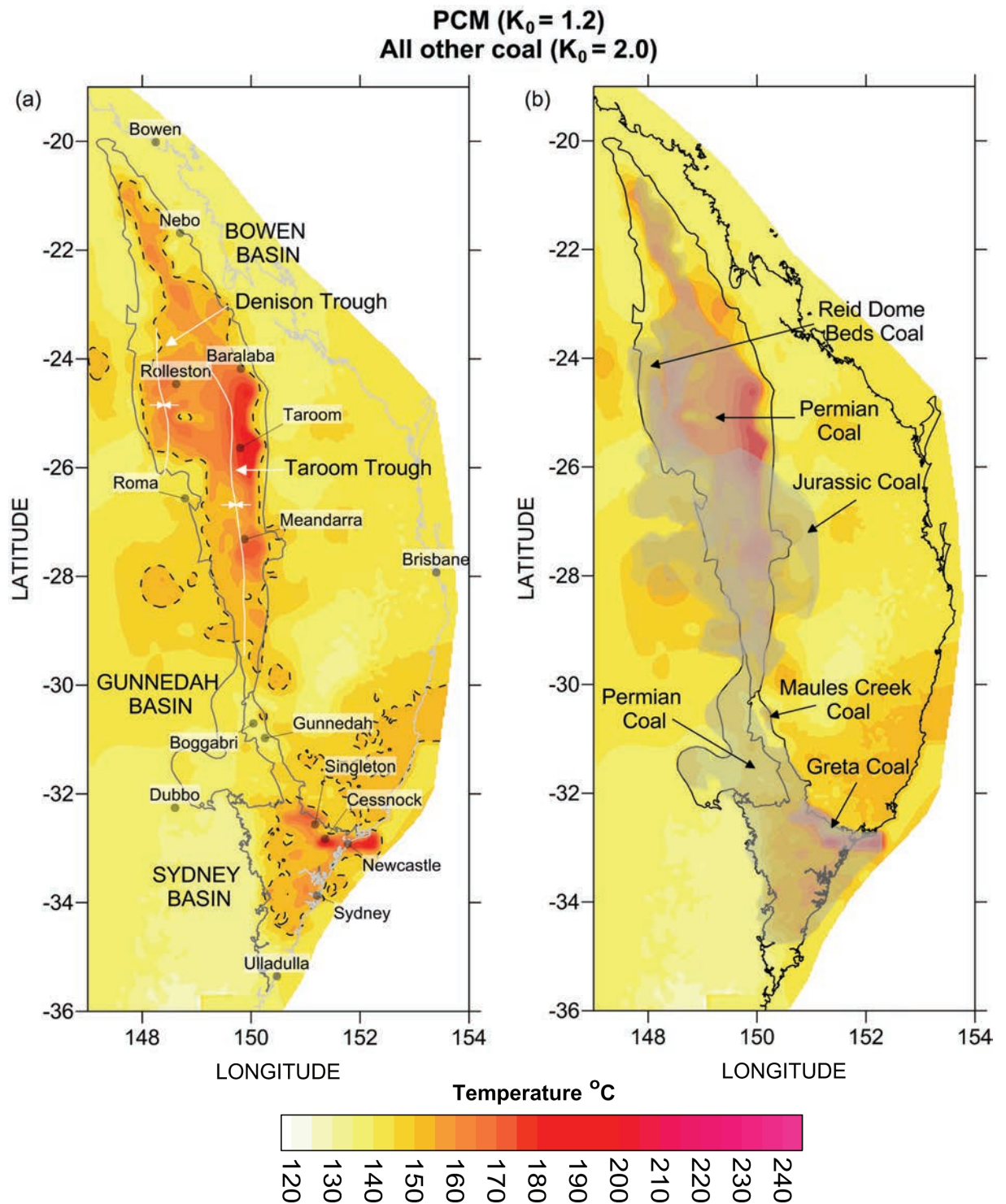


**Figure 10.13** Estimated temperature at 5 km below ground level for the Sydney-Gunnedah-Bowen Basin for Model 3 showing a) the 150°C isotherm (dashed line) and b) coal measures (grey shading).

In Figures 10.11 to 10.13 heat refraction around the terminating edges of coal measures produces localised elevated temperatures at depth. For example, in the Sydney Basin, the north-eastern part is elevated as a result of the termination of the PCM by the Hunter-Mooki Fault. In the Bowen Basin the Leichardt-Burunga Fault and Gogango Thrust truncate the PCM on the eastern edge of the basin between Taroom and Baralaba. At Meandarra and near Rolleston, heat refraction is the result of the termination of the Jurassic coal measures and PCM and this, combined with basin geometry, results in elevated temperatures in these areas.

With both Models 2 and 3 very similar the differences observed in the temperature at depth is a result of the sensitivity of the coal measures to the  $K_0$  values. The thermal cross-sections (Figures 10.4 to 10.9) clearly demonstrate how changing the  $K_0$  values can influence the thermal structure. In this research the average percentage of coal in the coal measures has been calculated at 10% (see Chapter 4 section 4.1.1) and  $K_0 = 1.2$  is optimised based on this percentage. Figure 10.14 is an example of what the estimated temperature at depth could be if all the coal measures were given the  $K_0 = 2$  of sediments. Here the estimated temperature barely exceeds  $150^{\circ}\text{C}$  for most parts of the SGBB but, as there is limited calibration data at depth, the values of this model still match those of the observable temperatures. However, this is less likely to be representative of the true thermal structure of the SGBB.

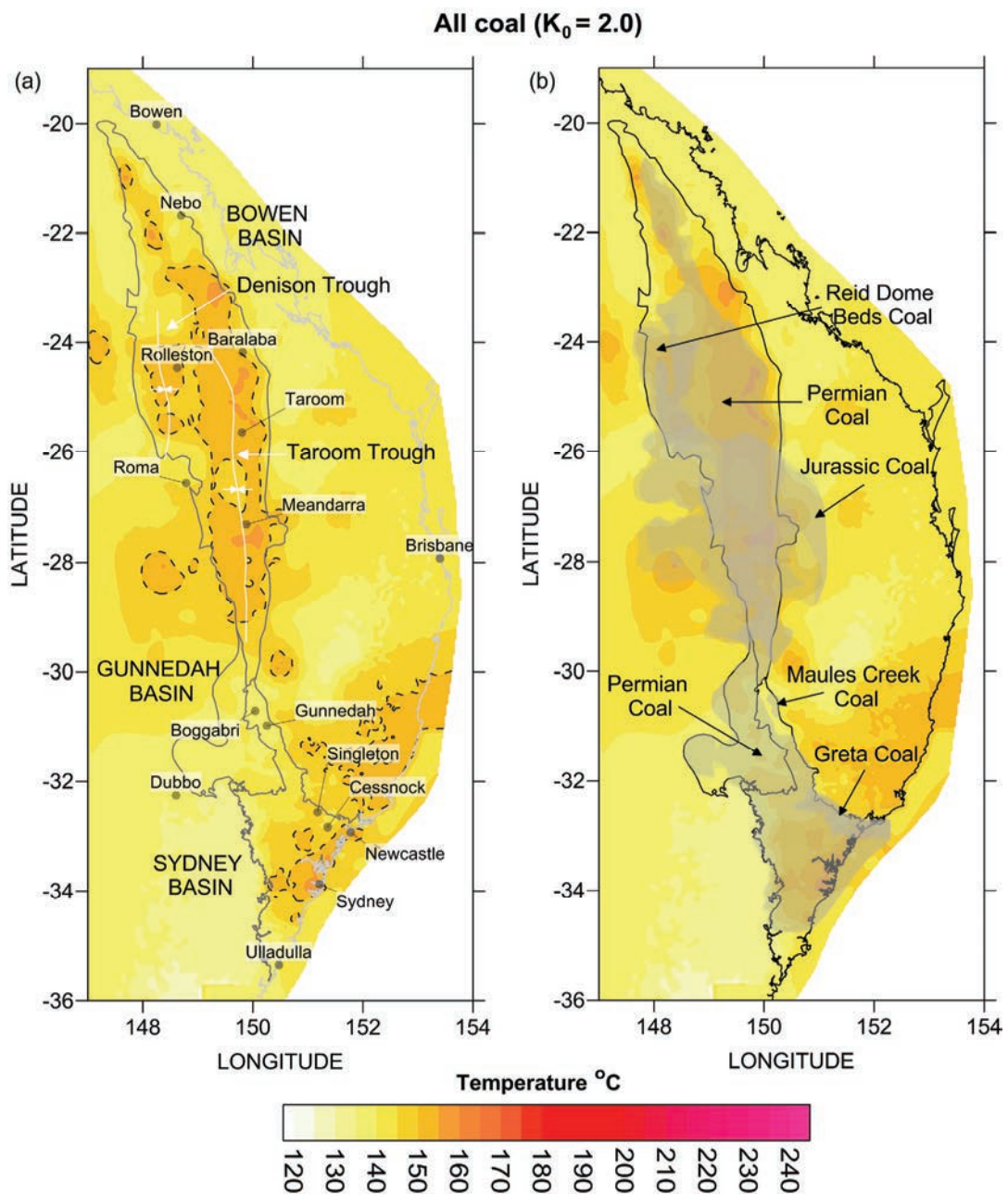


**Figure 10.14** Estimated temperature at 5 km below ground level for the Sydney-Gunnedah-Bowen Basin for all coal measures with  $K_0 = 2$  showing a) the  $150^{\circ}\text{C}$  isotherm (dashed line) and b) coal measures (grey shading).



The series of models using different  $K_0$  values highlights the sensitivity of the thermal structure to the coal measures. As a result, depending on the material parameters utilised, the areas identified for geothermal potential will vary. Considering both Models 2 and 3, and based on the 150°C isotherm at 5 km depth, there are significant areas in both the Sydney and Bowen basins for which there is a potential for geothermal anomalies.

### 10.3 Summary

From analysis of the thermal structure and an assessment of the estimated temperature at 5 km depth the SGBB does have the potential for geothermal anomalies. The model results show the thermal properties of the coal measures do have a significant impact on thermal structure and associated estimates of temperature at depth. For the Jurassic, Greta and Reid Dome Beds coal measures, some of which start out shallow and then deepen significantly, a low  $K_0$  value produces steep thermal gradients which are not likely to represent the true thermal structure or geological composition. The optimisation process for the material properties of the coal measures is limited by the lack of data at depth and as a result all three of the models match the observed measured temperatures but produce significantly different thermal profiles and estimates of temperature at depth.

The thermal structure of the SGBB is strongly controlled by architecture, geology and the thermal properties of the coal measures and is best represented by Model 2 with  $K_0 = 1.2$ ,  $K_{\text{crit}} = 0.20$  applied to all coal measures to produce results that are reliable for assessing thermal structure and geothermal potential. In the Bowen Basin, where limited calibration data exists, the basin architecture and sediment thickness is similar to the Sydney Basin thus the thermal structure is expected to be comparable, but with slightly higher temperatures due to the presence of additional coal measures. With additional data it would be possible to further refine the material parameters as the 'optimal model' lies somewhere between Model 2 and Model 3.

The high resolution 3D thermal models presented in this chapter suggest the maximum estimated temperature at 5 km depth is likely to be at least 180°C. Therefore, areas which have the potential for geothermal anomalies are considered to be the north-eastern part of the Sydney Basin and the central part of the Bowen Basin. The Gunnedah Basin is not considered to have any significant geothermal anomalies.

The next chapter, Chapter 11, provides concluding remarks on the aims and outcomes of the research of this project and outlines some areas of potential future work.

# CHAPTER 11

## CONCLUSIONS



*Sunset, Cooks Gap NSW*

## CONCLUSION

This project applies innovative techniques to improve the understanding the geometry, thermal structure and geothermal potential of the largest sedimentary basin on the east coast of Australia, the Sydney-Gunnedah-Bowen Basin. The work presented in this thesis can be used as a background framework that can be applied to resource development, specifically geothermal, and management and future scientific investigations. This concluding chapter outlines the research aims, outcomes and limitations and identifies areas for future work.

### **The 3D Geological Model**

The integrated approach to gravity modelling (i.e. utilising constraints of borehole, seismic and mapped geology) provides an ideal technique for determining the depth to basement, the primary building block of the geological model. By design the key lithological groups, i.e. basement, sediment and volcanics, not only have distinctive density contrasts, they have distinctive thermal properties, thus building geological model for application in thermal modelling is relatively simple. Chapter 6 outlined the process of the model construction as well as the limitations of the geological model. In developing a model over such a large area simplification was often necessary and some smaller scale features, e.g. faults, are lost. There is also a substantial amount of geological information, such as stratigraphic layers, which has not been integrated into the model, however the inclusion of specific strata is a relatively simple process as demonstrated with the addition of the coal bearing layers.

This 3D geological model firstly provides the necessary platform for high resolution thermal modelling but it also provides a reference framework, particularly for areas where there has been limited investigation, from which to build more detailed models. Good correlation with published tectonic features, comparable geometry to seismic reflection profiles, depth constraints at over 1000 borehole locations and application of mapped geological makes this 3D geological model self consistent. Geological features, such as trends in low density basement which could be related to buried granite bodies or subsurface extensions of exposed granites, are of interest to various different resource exploration groups and to incorporating known granite bodies would be a valuable contribution of future works.

### **The Limitations of Extrapolated Temperature Maps**

Early work on thermal structure of the upper crust in Australia focused on a continental wide assessment (i.e. Somerville *et al.* 1994) using borehole bottom-hole temperature in an extrapolation method with heat flow measurements and geochemistry. This style of approach has inherent limitations which have been discussed extensively in Chapter 7. The main aim of assessing the extrapolated temperature maps, using both equilibrated and non-equilibrated temperature data, was to determine the implications, if any, for geothermal exploration. This work has shown extrapolation maps fail to adequately account for the architecture and geology of the SGBB and the temperature at depth is often undervalued compared to thermal modelling. The implication of this on geothermal exploration has been areas of potential anomalies are often poorly identified.

### **Equilibrated Temperature Measurements**

A major component of the fieldwork of this project was the collection of equilibrated down-hole temperature measurements within the Sydney Basin. Finding and gaining access to equilibrated boreholes is difficult, especially to those which are greater than 200 m deep. Measurements were collected from the groundwater monitoring networks of the Sydney Catchment Authority, NSW Office of Water and Ulan Coal Mines Ltd with addition geophysical logging data supplied by Hydroilex. An outcome of this process was identifying that borehole history, repeat measurements and measurement technique are critical in collecting value measurements. This was highlighted by the case of thermal recovery from disturbance in PZ14A as described in Chapter 8. The main benefits of this work are equilibrated temperatures are now available for the Sydney Basin and these can be used as effective calibration points for the thermal model.

### **Developing the High Resolution Thermal Model in Underworld**

Multidimensional numerical thermal models are ideal for developing an understanding of the thermal structure in complex environments, however, historically they have been small scale. The model developed in the research appears to be one of the first to model, in high resolution, at an upper crustal scale. The SGBB model, at over 1600 km long, 400 km wide and 12 km deep is on the order of 10 to 1000 time larger than most thermal models. At high resolution, approximately 1400 m by 10 m by 1400 m, the model requires massively parallel computer architectures. The geological model developed in this project is the framework and the thermal properties of the materials were initially based off published or measured values before being optimised, as described in Chapter 9, to the 'best-fit' value calibrated by using the measured equilibrated temperature. The main outcome of this research has been the process of testing the sensitivity of the model and identifying the main uncertainties. These are the conductivity of the Permian coal at  $K_0$  and the basement at  $K_0$  and  $K_{\text{crit}}$ , the basal temperature boundary condition and the lack of heterogeneity in the basement. Because of the size of the model a traditional Monte Carlo approach to reduce uncertainty would be too time consuming, thus the approach presented here favours a human iterative system to guide the reduction of the ensemble. The inherent assumption of basement homogeneity, both in geology and thermal properties, leads to uncertainty but it is a necessary simplification for the scale of this model and the introduction of heterogeneity is limited by the data available on these parameters. The isolation of granites and the ability to tailor their heat production to measured values would produce more accurate thermal profiles and is a goal for future work. Another necessary part of future work is the collection of additional data across the Gunnedah and Bowen basins specifically, but not limited to, temperature at depth and the thermal properties of the coal measures. From the assessment of the thermal structure in Chapter 10 the thermal properties of the coal measures strongly influence the thermal structure and more research is needed in this area.

### **Estimated Temperature at 5 km and Geothermal Potential**

The preliminary 2D thermal models of the Gunnedah and Sydney basins suggest that the estimated temperature at 5 km depth below the surface could range from 160°C on the basin edge to up to 200°C in the centre for the Sydney Basin and around 100°C to 165°C for the top of the basement in the Gunnedah Basin. These models, which compared reasonably well with the observed

temperatures, used the average published thermal properties of representative materials and a basal temperature boundary condition of 350°C at 12 km but the sensitivity and uncertainty of these results was unclear. The 3D thermal models, using the optimal material parameters and subsurface boundary condition, showed estimated temperature at depth was strongly defined by the thermal properties of the coal. In Chapter 10 three models were run using different conductivity values for the coal layers which produced maximum temperatures of 240°C (Model 1) and 185°C (Models 2 and 3) at 5 km depth but each models fit with the observable temperature data did not change. Models 1 and 3 tested the estimated minimum and maximum temperature range by considering the effects of 50% coal or no coal in the coal measures. Model 2 is the preferred 'optimum' model, where  $K_0 = 1.2$  and  $K_{\text{crit}} = 0.2$  is the optimised value to apply to all the coal measures in the region, as this produces the best assessment of thermal structure from the available data. The maximum estimated temperature at 5 km depth is likely to be at least 180°C and therefore there is geothermal potential in the SGBB. The most likely areas for geothermal anomalies are in the north-eastern part of the Sydney Basin and in the central part of the Bowen Basin. From these results the main outcome is a more reliable estimate of thermal structure and temperature at depth that can provide a more targeted approach to geothermal exploration in the SGBB.

### **Concluding Remarks**

The thermal structure of the Sydney-Gunnedah-Bowen Basin is controlled by its architecture and geology. The coal measures of the Jurassic and Permian strongly influence the thermal structure and elevation of temperature in the basement. High resolution 3D thermal models provide an efficient means of assessing thermal structure and can identify, test and constrain uncertainties using real world data. The geothermal potential of the SGBB is tied to reliable estimates of temperature at depth. Thermal modelling identifies the Sydney and Bowen basins as prospective for geothermal with temperatures reaching at least 180°C under 3 to 4 km of insulating sediment.

*When we experiment, we try things and when we fail we start to ask why and that is when we learn best. This is the essence of true science.*

C. Danis



# REFERENCES



*Kanangra Walls, Kanangra NSW*

## REFERENCES

- ADLER J.D., HAWLEY S., MAUNG J., SCOTT R.D, SINELNIKOV A. & KOUZMINA G. 1998. Prospectivity of the offshore Sydney Basin: A new perspective. *APPEA Journal* **38**, 68-92.
- AITCHISON J.C. & FLOOD P.G. 1992. Implications of radiolarian research for analysis of subduction complex terranes in the New England Orogen, NSW, Australia. *Palaeogeography, Palaeoclimatology, Palaeoecology* **96**, 89-102.
- ARDITTO P.A. 2003. An integrated geological and geophysical interpretation of a portion of the offshore Sydney Basin, New South Wales, *APPEA Journal* **43**, 495-514.
- BAKER J.C., FIELDING C.R., DE CARITAT P. & WILKINSON M.M. 1993. Permian evolution of sandstone composition in a complex back-arc extensional to foreland basin: the Bowen Basin, Eastern Australia. *Journal of Sedimentary Petrology* **63**, 881-893.
- BARNICOAT A. & ERNST R. 2010. Geothermal energy in Australia. Presentation to the International Partnership for Geothermal Technology. Available online: <[http://internationalgeothermal.org/Documents/Geothermal\\_Overview.pdf](http://internationalgeothermal.org/Documents/Geothermal_Overview.pdf)> (accessed 2 June 2011).
- BEARDSMORE G.R. & CULL J.P. 2001. Crustal heat flow: a guide to measurement and modelling. Cambridge University Press.
- BEARDSMORE G.R. & HILL A. 2010. Australia – country updated. Proceedings World Geothermal Congress, 25-29 April 2010, Bali Indonesia.
- BEESTON J.W. 1986, Coal rank variation in the Bowen Basin: *Queensland International Journal of Coal Geology* **6**, 163-179.
- BEMBRICK C.S. & LONERGAN A.D. 1976. Sydney Basin. In: Economic geology of Australia and Papua New Guinea, 3, Petroleum. *Australasian Institute of Mining and Metallurgy*, Monograph 7.
- BEMBRICK C.S. HERBERT C. SCHEIBNER E. & STUNTZ J. 1993. Structural subdivision of the New South Wales portion of the Sydney-Bowen Basin. *Quarterly Notes Geological Survey NSW* **11**, 1-13.
- BLEVIN J., HALL L., CHAPMAN J. & PRYER L. 2007. Sydney Basin Reservoir Prediction Study and GIS, Project MR705, Confidential Report to the NSW DPI and Macquarie Energy, FrOG Tech Pty Ltd.
- BRADLEY G. 1993. Evolution and hydrocarbon prospectivity of the Offshore Sydney basin – NSW/P10. In: Swarbrick G.J. & Morton D.J. eds. *Proceedings of the NSW Petroleum Symposium, Petroleum Exploration Society of Australia*, NSW Branch, Sydney.
- BRAKEL A.T., TOTTERDELL J.M., WELLS A.T. & NICOLL M.G. 2009. Sequence stratigraphy and fill history of the Bowen Basin, Queensland: *Australian Journal of Earth Sciences* **56**, 401-432.
- BRANAGAN D.F. & PACKHAM G.H. 2000. Field Geology of New South Wales. Department of Mineral Resources New South Wales, Sydney.
- BROWN R.D., ELLIOT L.G. & MOLLAH R.J. 1983. Recent exploration and petroleum discoveries in the Denison Trough, Queensland. *APEA Journal* **23**, 120-135.
- BRUCE M.C., NIU Y., HARBORT, T.A. & HOLCOMBE R.J. 2000. Petrological, geochemical and geochronological evidence for a Neoproterozoic ocean basin recorded in the Marlborough terrane of the northern New England Fold Belt. *Australian Journal of Earth Sciences* **47**, 1053-1064.

- BUDD A.R. 2007. Australian radiogenic granite and sedimentary basin geothermal hot rock potential map (preliminary edition), 1: 5 000 000 scale. Geoscience Australia, Canberra.
- BUDD A., HOLGATE F., GERNER E. & AYLING B. 2007. In search of the next hot spot, Project to boost exploration for bountiful renewable energy. *AUSGEO News* **87**, 1-5. <[http://www.ga.gov.au/image\\_cache/GA10519.pdf](http://www.ga.gov.au/image_cache/GA10519.pdf)> (accessed 2 June 2011).
- BUDD A., HOLGATE F., GERNER E. & AYLING B. 2008. Pre-competitive geoscience for geothermal exploration and development in Australia: Geoscience Australia's Onshore Energy Security Program and the Geothermal Project. *GRC Transactions* **32**, 347-350.
- BURBURY J. 1986. Report on reprocessing and reinterpretation of seismic data, PEL 260, Sydney Basin for AGL Sydney Ltd. DIGS Report No. SS148 <<http://digsopen.minerals.nsw.gov.au>>.
- BURNS K.L., WEBER C., PERRY J. & HARRINGTON H.J. 2000. State of the geothermal industry in Australia. Proceedings World Geothermal Congress, Kyushu-Tahoku Japan May 28 – June 10, 2000.
- CADMAN S.J. & PAIN L. 1998. Bowen and Surat Basins, Clarence-Moreton Basin, Gunnedah Basin and other minor onshore basins, Queensland, New South Wales and Northern Territory: Australian Petroleum Accumulations Report 11, Bureau of Resources Sciences Canberra.
- CAPRARELLI G. & LEITCH E.C. 1998. Magmatic changes during the stabilisation of a cordilleran fold belt: the Later Carboniferous-Early Triassic igneous history of eastern New South Wales, Australia. *Lithos* **45**, 413-430.
- CAPRARELLI G. & LEITCH E.C. 2001. Geochemical evidence from Lower Permian volcanic rocks of northeast New South Wales for asthenospheric upwelling following slab breakoff. *Australian Journal of Earth Sciences* **48**, 151-166.
- CAUSEBROOK R. 2005. The geological storage potential of the offshore Sydney Basin. An addendum to "Geosequestration Investigation – offshore New South Wales" a paper by Sayers et al 2004. CO2CRC Geoscience Australia, Canberra, Australia, May 2005. CO2CRC Report Number RPT05-0023.
- CAWOOD P.A. 1982. Structural relations in the subduction complex of the New England Fold Belt, eastern Australia. *Journal of Geology*, **90**, 381-392.
- CAWOOD P.A. & LEITCH E.C. 1985. Accretion and dispersal tectonics of the Southern New England Fold Belt, eastern Australia. In: Howell D.G. ed. Tectonostratigraphic Terranes of the Circum-Pacific Region. Circum-Pacific Council for Energy and Mineral Resources, Houston, 1, 481-492.
- CAWOOD P.A., LEITCH E.C., MERLE R.E. & NEMCHIN A.A. 2011. Orogenesis without collision: Stabilizing the Terra Australis accretionary orogen, eastern Australia. *Geological Society of America Bulletin* DOI: 10.1130/B30415.1.
- CHAPPELL B.W. & STEPHENS W.E. 1988. Origin of intra-crustal (I-type) granite magmas. *Transactions of the Royal Society of Edinburgh, Earth Sciences* **79**, 71-86.
- CHAPPELL B.W. & WHITE A.J.R. 1974. Two contrasting granite types. *Pacific Geology* **8**, 173-174.
- CHAPPELL B.W., WHITE A.J.R. & HINE R. 1988. Granite provinces and basement terranes in the Lachlan Fold Belt southeastern Australia. *Australian Journal of Earth Sciences* **35**, 505-521.
- CHOPRA P. & HOLGATE F. 2005. A GIS analysis of temperature in the Australian crust. World Geothermal Congress, Turkey, 24-29 April 2005, Abstracts.

- CLAUSER C. & HUENGES E. 1995. Thermal conductivity of rocks and minerals, *In: Rock Physics and Phase Relations, A handbook of physical constants*, pp. 105-126, American Geophysical Union.
- COLLINS W.J. 1998. Evaluation of petrogenetic models for Lachlan Fold Belt granitoids: implications for crustal architecture and tectonic models. *Australian Journal of Earth Sciences* **45**, 483-500.
- CONAGHAN P.J. & JONES J.G. 1975. The Hawkesbury Sandstone and the Brahmaputra: a depositional model for continental sheet sandstones. *Journal of the Geological Society of Australia* **22**, 275-283.
- CRAWFORD A.J., CAMERON W.E. & KEAYS R.R. 1984. The association boninite low-Ti andesite-tholeiite in the Heathcote greenstone belt, Victoria; ensimatic setting for the early Lachlan Fold Belt. *Australian Journal of Earth Sciences* **31**, 161-174.
- CROOK K.A.W. 1980. Fore-arc evolution in the Tasman Geosyncline: the origin of southeast Australian continental crust. *Journal of the Geological Society of Australia* **26**, 215-232.
- CULL J.P. 1979. Climatic corrections to Australian heat-flow data. *BMR Journal of Australian Geology and Geophysics* **4**, 303-307.
- DANIS C., O'NEILL C. & LACKIE M. 2010. Gunnedah Basin 3D architecture and upper crustal temperatures. *Australian Journal of Earth Sciences* **57**, 483-505.
- DANIS C., O'NEILL C., LACKIE M., TWIGG L. & DANIS A. 2011. Deep 3D structure of the Sydney Basin using gravity modelling. *Australian Journal of Earth Sciences* **58**, 517-542.
- DAY R.W., MURRAY C.G. & WHITAKER W.G. 1978. The eastern part of the Tasman Orogenic Zone. *Tectonophysics* **48**, 327-364.
- DAY R.W., WHITAKER W.G., MURRAY C.G., WILSON I.H. & GRIMES K.G. 1983. Queensland Geology. A companion volume to the 1: 2500 000 scale geological map (1975). *Geological Survey of Queensland Publication* **383**.
- DEMING D. 1989. Application of bottom-hole temperature corrections in geothermal studies. *Geothermics* **18**, 775-786.
- DEEP ENERGY 2009. Lake Frome: Arrowine Basin, Geothermal exploration technical overview. Company Overview at the 2009 Geothermal Energy Conference, Brisbane, 10-13 November.
- DIREEN N.G., LYONS P., KORSCH R.J. & GLEN R.A. 2001. Integrated geophysical appraisal of crustal architecture in the eastern Lachlan Orogen. *Exploration Geophysics* **32**, 141-153.
- DIRKS P.H., HAND M., COLLINS W.J. & OFFLER R. 1992. Structural-metamorphic evolution of the Tia Complex, New England fold belt: thermal overprint of an accretion-subduction complex in a compressional back arc setting. *Journal of Structural Geology* **14**, 669-688.
- ELLIOTT L. 1989. The Surat and Bowen Basins. *Australian Petroleum Exploration Journal* **29**, 398-416.
- E. S. P. EXPLORATION PTY LTD 1982. PEP 9 Annual report: permit year 2, 1<sup>st</sup> October 1981 – 30<sup>th</sup> September 1982, Volume 1. Offshore seismic survey, Sydney Basin. DIGS Report No. SS116 <<http://digsopen.minerals.nsw.gov.au>>.
- FERGUSON C.L., CARR P.F., FANNING C.M. & GREEN T.J. 2001. Proterozoic-Cambrian detrital zircons and monzonite ages from the Anakie Inlier central Queensland: Grenville and Pacific-Gondwana signatures. *Australian Journal of Earth Sciences* **48**, 857-866.

- FIELDING C.R., KASSAN J. & DRAPER J.J. 1995. Geology of the Bowen and Surat Basins, eastern Queensland: Australasian Sedimentologist Group Field Guide Series No 8, *Geological Society of Australia*.
- FIELDING C.R., SLIWA R., HOLCOMBE R. & KASSAN J. 2000. A new palaeogeographic synthesis of the Bowen Basin of central Queensland. *In: Beeston J.W. ed. Bowen Basin Symposium 2000*, Proceedings of the Geological Society of Australia, 287-302.
- FIELDING C.R., SLIWA R., HOLCOMBE R. & JONES J.T. 2001. A new palaeogeographic synthesis for the Bowen, Gunnedah and Sydney basins of eastern Australia. *In: Berecher T. & Hill K. eds. PESA Eastern Australasian Basins symposium*. Australasian Institute of Mining and Metallurgy, Melbourne, 269-279.
- FINLAYSON D.M., WAKE-DYSTER K.D., LEVEN J.H., JOHNSTONE D.W., MURRAY C.G., HARRINGTON H.J., KORSCH R.J. & WELLMAN P. 1990. Seismic imaging of major tectonic features in the crust of Phanerozoic eastern Australia: *Tectonophysics* **173**, 211-230.
- FLODD R.H. & SHAW S.E. 1977. Two S-type granite suites with low initial  $^{87}\text{Sr}/^{86}\text{Sr}$  ratios from the New England Batholith, Australia. *Contributions to Mineralogy and Petrology* **61**, 163-173.
- FORSTER A. & MERRIAM D.F. 1999. *Geothermics in Basin Analysis*. Kluwer Academic, Plenum Publishers.
- FROG TECH 2006. OZ SEEBASE Proterozoic Basins Study, Report to Geosciences Australia by FrOGTech Pty Ltd.
- GERNER E.J. & HOLGATE F.L. 2010. OzTemp – Interpreted Temperature at 5km Depth Image. Geoscience Australia, Canberra.
- GLEN R.A. 2005. The Tasmanides of eastern Australia. *In: Vaughan A.P.M., Leat P.T. & Pankhurst R.J. eds. Terrane Processes at the Margins of Gondwana*, pp 23-96. Geological Society, London, Special Publications 246.
- GLEN R.A. & BECKETT J. 1997. Structure and tectonics along the inner edge of a foreland basin: the Hunter Coalfield in the northern Sydney Basin, New South Wales. *Australian Journal of Earth Sciences* **44**, 857-877.
- GOLDSTEIN B.A., HILL A.J., BUDD A.R. & MALAVAZOS M., 2008. Status of geothermal exploration and research in Australia. *GCR Transactions* **32**, 79- 86.
- GRAY D.R. & WILLMAN C.E. 1991. Deformation in the Ballarat Slate Belt, central Victoria, and implications for crustal structure across southeast Australia. *Australian Journal of Earth Sciences* **38**, 171-201.
- GRAY D.R. & FOSTER D.A. 1997. Orogenic concepts – application and definition: Lachlan Fold Belt, eastern Australia. *American Journal of Science* **297**, 859-891.
- GRAY D.R., FOSTER D.A. & BUCHER M. 1997. Recognition and definition of orogenic events in the Lachlan Fold Belt. *Australian Journal of Earth Sciences* **44**, 489-501.
- GUO B., LACKIE M.A. & FLODD R.H. 2007. Upper crustal structure of the Tamworth Belt, New South Wales: constraints from new gravity data. *Australian Journal of Earth Sciences* **54**, 1073-1087.
- HERBERT C. 1972. Palaeodrainage patterns in the southern Sydney Basin. *Record of the Geological Survey of New South Wales* **14**, 5-18.



- HERBERT C. 1989. The Lapstone Monocline-Nepean Fault, A high angle reverse fault system. *In: Plimer I.R. ed. Proceedings of the Twenty Third Newcastle Symposium "Advances in the Study of the Sydney Basin"*. University of Newcastle.
- HERBERT C. & HELBY R. (Editors) 1980. *A guide to the Sydney Basin*. Geological Survey of New South Wales Bulletin 26, Bulletin No. 26. Department of Mineral Resources, New South Wales.
- HERRIN J.M. & DEMING D. 1996. Thermal conductivity of US coals. *Journal of Geophysical Research* **101**, 25381-25386.
- HOFFMANN K.L., TOTTERDELL J.M., DIXON O., SIMPSON G.A., BRAKEL A.T., WELLS A.T. & MCKELLAR J.L. 2009. Sequence stratigraphy of Jurassic strata in the lower Surat Basin succession, Queensland. *Australian Journal of Earth Sciences* **56**, 461-477.
- HOT ROCK LTD 2009. Geothermal exploration is hotting up. Company Overview from the 2009 Australian Geothermal Energy Conference, Brisbane, 10-13 November 2009.
- HOUSEMAN G.A., CULL J.P., MUIR P.M. & PATTERSON H.L. 1989. Geothermal signatures and uranium ore deposits on the Stuart Shelf of South Australia. *Geophysics* **54**, 158-170.
- JENKINS R.B., LANDENBERGER B. & COLLINS W.J. 2002. Late Palaeozoic retreating and advancing subduction boundary in the New England Fold Belt, New South Wales. *Australian Journal of Earth Sciences* **49**, 467-489.
- JONES J.G. & McDONNELL K.L. 1981. Papua New Guinea analogue for the late Permian environment of northeastern New South Wales. *Palaeoecology* **34**, 191-205.
- JONES J.G., CONAGHAN P.J., McDONNELL K.L., FLOOD R.H. & SHAW .S.E. 1984. Papuan Basin analogue and a foreland basin model for the Bowen-Sydney Basin. *In: Veevers J.J. ed. Phanerozoic Earth History of Australia*. Oxford University Press, Oxford.
- KEAY S., COLLINS W.J. & McCULLOCH M.T. 1997. A three-component Sr-Nd isotopic mixing model for granitoid genesis, Lachlan fold belt, eastern Australia. *Geology* **25**, 307-310.
- KILGOUR B. 2002. National Geoscience Datasets. [Digital Datasets] Canberra: Geoscience Australia. <[https://www.ga.gov.au/products/servlet/controller?event=GEOCAT\\_DETAILS&catno=32407](https://www.ga.gov.au/products/servlet/controller?event=GEOCAT_DETAILS&catno=32407)> (accessed 21 September 2011).
- KORSCH R.J., WAKE-DYSTER K.D. & JOHNSTON D.W. 1992. Seismic imaging of Late Palaeozoic-Early Mesozoic extensional and contractional structures in the Bowen and Surat basins, eastern Australia. *Tectonophysics* **215**, 273-294.
- KORSCH R.J., WAKE-DYSTER K.D. & JOHNSTON D.W. 1993. Crustal architecture of the New England Orogen based on deep seismic reflection profiling. *In: Ashley P.M. & Flood P.G. eds. Tectonics and Metallogensis of the New England Orogen: Alan H. Voisey Memorial Volume*. Geological Society of Australia Special Publication 19.
- KORSCH R.J., BARTON T.J., GRAY D.R., OWEN A.J. & FOSTER D.A. 2002. Geological interpretation of the deep seismic-reflection transect across the boundary between the Delamerian and Lachlan Orogen, in the vicinity of the Grampians, Western Victoria. *Australian Journal of Earth Sciences* **49**, 1057-1075.
- KORSCH R.J., TOTTERDELL J.M., CATHRO D.L. & NICOLL M.G. 2009a. Early Permian Rift System. *Australian Journal of Earth Sciences* **56**, 381-401.

- KORSCH R.J., TOTTERDELL J.M., FOMIN T. & NICOLL M.G. 2009b. Contractional structures and deformational events in the Bowen, Gunnedah and Surat Basins, eastern Australia. *Australian Journal of Earth Sciences* **56**, 477-501.
- KRASSAY A.A., KORSCH R.J. & DRUMMOND B.J. 2009. Meandarra Gravity Ridge: symmetry elements of the gravity anomaly and its relationship to the Bowen-Gunnedah-Sydney basin system. *Australian Journal of Earth Sciences* **56**, 355-379.
- LANFORD R. P & PATCHETT A. 2005. Carbon dioxide storage: potential of coal measures in the Sydney and Gunnedah Basins, New South Wales; and the Bowen, Surat and Galilee Basins, Queensland. CO2CRC Report Number RPT07-0752.
- LEAMAN D.E. 1990. Sydney Basin gravity-magnetic interpretation structures and settings of NSW/P10 for Santos Ltd. DIGS Report No. PGR1990-3 <<http://digsopen.minerals.nsw.gov.au/>>.
- LEITCH E.C. 1969. Igneous activity and diastrophism in the Permian of New South Wales. *Special Publication of the Geological Society of Australia* **2**, 21-37.
- LEITCH E.C. 1974. The geological development of the southern part of the New England Fold Belt. *Journal of the Geological Society of Australia* **21**, 133-156.
- LEITCH E.C. 1993. The floor of the Gunnedah Basin north of the Liverpool Range. In: Tadroz N.Z. ed. *The Gunnedah Basin*. New South Wales, Geological Survey of New South Wales, Sydney, *Memoir Geology* **12**, 335-348.
- MALONE E.J., OLGERS F., MOLLAN R.G. & JENSEN A.R. 1967. Geological map Bowen Basin Queensland. Bureau of Mineral Resources, Geology and Geophysics.
- MAUNG T.U., ADLER D., SHAW R.D. & HAWLEY S. 1997. Offshore Sydney Basin, New South Wales. Canberra. *Bureau of Resources Sciences, Petroleum Prospectivity Bulletin* **1997/1**.
- MAYNE S.J., NICHOLAS E., BIGG-WITHER A.L., RASIDI J.S., & RAINE M.J. 1974. Geology of the Sydney Basin – A review. *Bulletin of the Bureau of Mineral Resources Geology and Geophysics Australia* **149**, 229p.
- METTLER TOLEDO AG. 1994. Operating Instructions – Density determination software for Mettler Toledo AG balances, Switzerland.
- MINFO, 2008. The mining and exploration magazine of New South Wales Department of Primary Industries. September/October 2008 Issue 88.  
<<http://www.dpi.nsw.gov.au/aboutus/news/minfo>>
- MOFFIT W.H. 1961. Final report on the reflection seismograph survey of the Wallacia area, NSW, Australia for Australian Oil and Gas Corporation Ltd Sydney. Petty Geophysical Engineering Company. DIGS Report No. SS004 <<http://digsopen.minerals.nsw.gov.au/>>.
- MORESI L., DUFOUR F. & MULHAUS H.-B. 2003. A Lagrangian integration point finite element method for large deformation modeling of viscoelastic geomaterials. *Journal of Computing Physics* **184**, 476–497.
- MORESI L., QUENETTE S., LEMIALE V., MERIAUX C., APPELBE B. & MULHAUS H.-B. 2007. Computational approaches to studying non-linear dynamics of the crust and mantle. *Physics of the Earth and Planetary Interiors* **163**, 69-82.
- MURRAY C.G. 1994. Basement cores from the Tasman Fold Belt System beneath the Great Artesian Basin in Queensland, Geological Record, Queensland Department of Minerals and Energy, 1994/10.

- MURRAY C.G., FERGUSON C.L., FLOOD P.G., WHITAKER W.G. & KORSCH, R.J., 1987. Plate tectonic model for the Carboniferous evolution of the New England fold Belt. *Australian Journal of Earth Sciences*, **36**, 423-449.
- MUSSON A., HARRISON B., GORDON K., WRIGHT S. & SANDIFORD M. 2009. Thermal thinking: optimal targeting for Australian geothermal explorers. In: Budd A.R. & Gurgenci H. eds. *Proceedings of the 2009 Australian Geothermal Energy Conference*. Geoscience Australia, Record 2009/35.
- POGSON D.J. & WATKINS J.J.C. 1998. Bathurst 1:250 000 Geological Sheet SI/55-8: Explanatory notes. Geological Survey of New South Wales, Sydney.
- O'REILLY S. 1990. Discussion The Sydney Basin: Composition of basement. *Australian Journal of Earth Sciences* **37**, 485-486.
- QURESHI I.R. 1984. Wollondilly-Blue Mountains gravity gradient and its bearing on the origin of the Sydney Basin. *Australian Journal of Earth Sciences* **31**, 293-302.
- QURESHI I.R. 1989. Positive gravity anomaly over the Sydney Basin. *Exploration Geophysics* **20**, 191-193.
- RENYOLDS J.M. 2003. *An introduction to applied and environmental geophysics*. John Wiley and Sons, London.
- ROBERTS J. & ENGEL B.A. 1987. Depositional and tectonic history of the southern New England Orogen. *Australian Journal of Earth Sciences* **34**, 1-20.
- RUTLAND R.W.R. 1976. Orogenic evolution of Australia. *Earth Science Reviews* **12**, 161-196.
- SEISMOGRAPH SERVICES LTD 1965. Final report on the central Sydney Basin Vibroseis and seismic survey for Shell Development Australia Pty Ltd. DIGS Report No. SS038  
<<http://digsopen.minerals.nsw.gov.au>>.
- SCHEIBNER E. 1973. A plate tectonic model of the Palaeozoic tectonic history of New South Wales. *Journal of the Geological Society of Australia* **20**, 405-426.
- SCHEIBNER E. & BASDEN H. (Editors) 1998. Geology of New South Wales – synthesis. Volume 2: Geological evolution. *Memoir of the Geological Survey of New South Wales* **13**.
- SCHEIBNER E. & VEEVERS J.J. 2000. Tasman Fold Belt System. Billion-year earth history of Australia and neighbours in Gondwanaland. In: Veevers J.J. ed. *Billion-year earth history of Australia and neighbours in Gondwanaland*. GEMOC Press, Sydney, 154-234.
- SHAW S.E., FLOOD R.H. & LANWORTHY P.J. 1989. Age and association of the Rylstone Volcanics: new isotopic evidence. In: Symposium Proceedings, *Advances in the Study of the Sydney Basin* **23**, 45-51. University of Newcastle, Newcastle.
- SHAW S.E., CONAGHAN P.J. & FLOOD R.H. 1991. Late Permian and Triassic igneous activity in the New England Batholith and contemporaneous tephra in the Sydney and Gunnedah Basins. In: Symposium Proceedings, *Advances in the Study of the Sydney Basin* **25**, 44-51. University of Newcastle, Newcastle.
- SHEPHERD J. & HUNTINGTON J.F. 1981. Geological fracture mapping in coalfields and the stress fields of the Sydney Basin. *Australian Journal of Earth Sciences* **28**, 299-309.
- SOMERVILLE M., WYBORN D., CHOPRA P., RAHMAN S., ESTRELLA D. & VAN DER MEULEN T. 1994. Hot dry rock feasibility study, Energy Research and Development Corporation (ERDC) Report, 94/243, Canberra, ACT.

- SWAINE D.J. 1990. *Trace elements in coal*. Butterworth, London.
- TADROZ N.Z. (Editor) 1993. The Gunnedah Basin, New South Wales. Geological Survey of New South Wales, *Memoir Geology* **12**, 649pp.
- TOTTERDELL J.M., MOLONEY J., KORSCH R.J. & KRASSAY A.A. 2009. Sequence stratigraphy of the Bowen-Gunnedah and Surat Basins in New South Wales. *Australian Journal of Earth Sciences* **56**, 433-461.
- TURCOTTE D.L. & SCHUBERT G. 2002. *Geodynamics*. Cambridge University Press, Cambridge.
- VEEVERS J.J. (Editor) 1984. *Phanerozoic Earth History of Australia*. Oxford University Press.
- VEEVERS J.J. 2000. Impact on Australia and Antarctica of the collisional merging of Gondwanaland and Laurussia in Pangea. In: Veevers J.J. ed. *Billion-year earth history of Australia and neighbours in Gondwanaland*. GEMOC Press, Sydney, 283-291.
- VOGT D.M., WOLF A. RATH V., PECHING R. & CLAUSER C. 2010. Reducing temperature uncertainties by stochastic geothermal reservoir modelling. *Geophysics Journal International* **181**, 321-333.
- WATKINS J.J. 1998. Geochemistry of the Carboniferous intrusions. Bathurst 1:250 000 Geological Sheet SI/55-8. 2<sup>nd</sup> Edition. Explanatory Notes. Geological Survey of New South Wales, Sydney, 262-264.
- WASCHBUSCH P., KORSCH R.J. & BEAUMONT C. 2009. Geodynamic modelling in aspects of the Bowen, Gunnedah, Surat and Eromanga basins from the perspective of convergent margin processes: *Australian Journal of Earth Sciences* **56**, 309-334.
- WILLIAMS I.S. & CHAPPELL B.W. 1998. Crustal evolution in southeastern Australia: a zircon view-point. The Bruce Chappell Symposium: granites, island arcs, the Mantle and ore deposits. Record of the Australian Geological Survey Organisation, 1998/33.
- WITHNALL I.W., 1995. Pre-Devonian rocks of the southern Anakie Inlier. In: Withnall I.W., Blake P.R. & Crouch S.B.S. eds. *Geology of the southern part of the Anakie Inlier, central Queensland*. *Queensland Geology*, **7**, 20-66.
- WITHNALL I.W., GOLDING S.D., REES I.D. & DOBOS S.K. 1996. K-Ar dating of the Anakie Metamorphic Group: evidence for the extension of the Delamerian Orogeny into central Queensland. *Australian Journal of Earth Sciences* **43**, 567-572.
- WOLLENBERG HA. & SMITH AR. 1987. Radiogenic heat production of crustal rocks: An assessment based on geochemical data. *Geophysical Research Letters* **14**, 295-298.
- WYBORN D. & CHAPPELL B.W. 1986. The petrogenetic significance of chemically altered plutonic and volcanic units. *Geological Magazine* **123**, 619-628.
- WYNNE P. & BACCHIN M. 2009. Index of Gravity Surveys (Second Edition). Geosciences Australia, Record 2009/07.